

CERN LIBRARY GENEVA



P00018701

CERN/SPSC 86-18
SPSC/P 200 Add.2
06.05.1986

INFN/AE-86/4

March 1986

C₁

THE LEPTON ASYMMETRY ANALYSER

LAA

BCFL Collaboration

C. Alberini, G. Bari, M. Basile, J. Berbiere, G. Cara Romeo,
R. Casaccia, L. Cifarelli, F. Cindolo, A. Contin, G. D'Ali,
C. Del Papa, G. Iacobucci, I. Laakso, G. Maccarrone,
T. Massam, R. Meunier, F. Motta, R. Nania, F. Palmonari,
G. Prisco, F. Rohrbach, P. Rotelli, G. Sartorelli, A. Scarsella,
G. Susinno, L. Votano, M. Willutzky and A. Zichichi

ABSTRACT

This volume contains four years of research work on a new method to identify the "up-like" or "down-like" nature of heavy-flavour states produced at Collider energies, and on the possibility of studying - at these extreme energies - the phenomenology of lepton-jet physics.

THE LEPTON ASYMMETRY ANALYSER

LAA

BCFL Collaboration

C. Alberini, G. Bari, M. Basile, J. Berbiers, G. Cara Romeo,
R. Casaccia, L. Cifarelli, F. Cindolo, A. Contin, G. D'Ali,
C. Del Papa, G. Iacobucci, I. Laakso, G. Maccarrone,
T. Massam, R. Meunier, F. Motta, R. Nania, F. Palmonari,
G. Prisco, F. Rohrbach, P. Rotelli, G. Sartorelli, A. Scarsella,
G. Susinno, L. Votano, M. Willutzky and A. Zichichi

ABSTRACT

This volume contains four years of research work on a new method to identify the "up-like" or "down-like" nature of heavy-flavour states produced at Collider energies, and on the possibility of studying - at these extreme energies - the phenomenology of lepton-jet physics.

CONTENTS

I - <u>Introduction .</u>	page 1
I.1 - Physics.	page 3
I.2 - Physicists.	page 6
II - <u>List of the original works (published and unpublished).</u>	page 9
III - <u>The original works .</u>	page 13
IV - <u>Conclusions.</u>	page 631
IV.1 - The cross-sections for Heavy Flavour production.	page 633
IV.2 - The ratio of "leading" versus total cross-sections.	page 634
IV.3 - Three-body versus more than three- body decays of the Heavy Flavours.	page 634
IV.4 - Lepton-jet physics and UA1 hermeticity.	page 634
IV.5 - The phenomenology in addition to the Heavy Flavour Physics.	page 635
IV.6 - Note on past experience with Committees.	page 636

I - INTRODUCTION

I - INTRODUCTION

I.1 - Physics

This volume contains all papers (published and unpublished) by our group on the problem of having a powerful lepton detector to study the lepton asymmetry in the two, outgoing proton and outgoing antiproton, hemispheres at the CERN ($p\bar{p}$) Collider. The basic purpose of the detector, coupled with a central one, is to study the lepton asymmetry, its p_T dependence and the phenomenology of jet-lepton physics. This volume starts with the most recent work, (March 1986) paper n° 1, and ends with our first contribution in this field of research (paper n° 11): the interest of our group in the study of some specific aspects of Collider Physics started at the end of 1981.

Paper n° 11 (March 1982) discusses a new method to detect the possible production of the "top" quark. This new method is based on the "leading" effect and on the charge asymmetry produced by the semileptonic decay of heavy-flavoured baryons.

In paper n° 10 (January 1983) we extended our "top" study to the general problem of Heavy Flavour production at Collider energies. A review of theory versus experiment is presented. It gives the correct basis which allows comparison of known facts with theoretical expectations. It is pointed out that, in the field of charm production (a heavy flavour extensively studied in hadronic machines), the only theory available (QCD) has failed to agree with all known results. Furthermore, the "leading" production mechanism of Λ_c^+ has been experimentally discovered, but theoretically "predicted" a posteriori. This is a warning for present QCD predictions, especially in the field of "leading" Heavy Flavour production at extreme energies, such as those of the CERN and Fermilab Colliders. In fact the "leading" effect remains unexplained by QCD. The paper emphasizes the need for a careful experimental study of the "leading" production of Heavy Flavours and shows how this could be experimentally accomplished.

In paper n° 9 (June 1983) the CERN ($p\bar{p}$) Collider data are studied in terms of possible evidence for a new Heavy Flavour.

Paper nº 8 (August 1983) contains a review lecture where the physics of new flavours is discussed with the purpose of showing its relevance and its basic role in subnuclear physics.

Paper nº 7 (May 1984) is the experimental proposal to construct and install the basic instrument to study the physics of Heavy Flavours at the CERN ($p\bar{p}$) Collider. This basic instrument is the Lepton Asymmetry Analyser (LAA). The proposal is a detailed study of its installation in conjunction with UA2, a "central detector" which would allow an additional research field to be investigated: the lepton-jet physics.

Paper nº 6 (June 1984) contains the answers to the questions raised by the Referees appointed by the CERN-SPS Committee.

Paper nº 5 (August 1984) emphasizes the interest of our group in the hadronic physics to be studied at the Collider, in addition to the heavy flavour physics. With reference to our published papers it is shown that we have found evidence that, at Collider energies, the "leading" effect must be as dominant as it is at ISR energies.

Paper nº 4 (August 1984) is a review lecture describing how the new flavours can be looked for at ($p\bar{p}$) Collider machines. Some detailed problems are discussed, such as the multibody decays of the heavy flavours and the new results on the generalized Cabibbo angles for higher family transitions.

Paper nº 3 (September 1984) contains a series of answers to the Referees' new questions. In particular, the problem of the lepton asymmetry with various hypotheses is discussed, together with the problem of the asymmetry in the background. In connection with this, it should be emphasized that this "background" asymmetry is an important check of QCD.

Paper nº 2 (March 1986) describes the results obtained during the test run at the Collider. The data show that the trigger rates we had calculated agree very well with the results of the test run. The success of the test run allowed UA1 to make use of our trigger and proved that our proposed set-up can indeed be a powerful detector for lepton-jet physics and for the measurement of the lepton asymmetry whose background is a basic QCD test. These results support the great scientific value of the Lepton Asymmetry Analyser in conjunction with the UA1 central detector.

Paper n° 1 (March 1986) contains all data presented at the open session of the CERN-SPS Committee (Geneva, 18 March 1986) and at the open session of the INFN-Committee n° 1 (Bologna, 24 March 1986). The physics interest is reviewed and the detailed study of the LAA version in LSS5 with UA1 as central detector is presented. The paper also contains the detailed plan for installation of the various LAA components in such a way as to match the SPS schedule and the UA1 needs.

Let us close this summary by emphasizing the relevance of having at the CERN ($p\bar{p}$) Collider a powerful instrument able to measure the lepton asymmetry in both hemispheres, its p_T dependence and its background (a crucial QCD test), and to study the phenomenology of lepton-jet physics.

The detailed list of the original works which have brought us to the present LAA project is given in section II.

1.2 - Physicists

The LAA group is part of a large Collaboration: LAA - ZEUS - GRAN SASSO.

Know-how in all fields of the technology used for the three experiments is shared among all members of the Collaboration.

In case of need, emergency help is foreseen among all physicists of the Collaboration, whose affiliations follow.

LAA - ZEUS - GRAN SASSO COLLABORATION

Bologna : C. Alberini, G. Bari, M. Basile, G. Cara Romeo, A. Castelvetti, L. Cifarelli, A. Contin, C. Del Papa, D. Galli, G. Iacobucci, R.R. Janik, G. Maccarrone, T. Massam, F. Motta, R. Nania, V. O'Shea, F. Palmonari, E. Perotto, G. Prisco, G. Rinaldi, G. Sartorelli, M. Willutzky

Brown Univ. (USA): P. Allan, R. Brick, M. Widgoff

CERN : F. Rohrbach, A. Zichichi

Firenze : G. Barbagli, E. Borchini, P. Burlamacchi, G. Cirri, A. Cordero, S. De Gennaro, A. Del Puglia, L. Lombardini, G.R. Maccii, P. Pelfer, B. Tesi, M. Zoli

Frascati INFN/LNF : S. Bianco, G. Anzivino, R. Casaccia, F. Cindolo, M. Enorini, F. Fabbri, I. Laakso, S. Qian, A. Rindi, F. Sgamma, G.C. Susinno, L. Votano, A. Zallo

Houston (USA) : K. Lau, F. Lipps, J. Pyrlík, W. Sheldon, H. Wald, R. Weinstein

L'Aquila : G. Di Sciascio, R. Scrimaglio

- Lecce : G. Rocco Semeraro, P. Rotelli, A. Scarsella
- Milano : E. Acerbi, G. Baccaglioni, F. Groppi, A. Kotarba,
G. Liguori, S. Pensotti, P.G. Rancoita, L. Rossi,
C. Simeoni, M. Stanziani
- MIT (USA) : Chang Zhao, Cheng Sheng Mao, D. Goloskie,
E.S. Hafen, P. Haridas, I.A. Pless, Shi Wei Wang,
Ying Rong Wu
- Moscow (USSR) : B.V. Berezinski, A.S. Chudanov,
V.L. Dadykin, V.B. Korchaguin, P.V. Korchaguin,
A.S. Malguin, O.G. Ryazkaya, A.L. Tziabuk,
U.P. Talockin, G.T. Zatsepin, V.F. Yakushev
- Palermo : G. D'Ali', S. De Pasquale
- Peking Academia Sinica (CHINA)
- Rome - ENEA : N. Sacchetti, M. Ricci, M. Spadoni, G. Pasotti,
R. Bruzzese
- Saclay - CEN : P.O. Lagage, R. Meunier
- Tokyo (JAPAN) : Y. Hatano, T. Kitamura, A. Misaki, K. Mitsui,
S. Mori, I. Nakamura, N. Ogita, T. Saito,
H. Sasaki, M. Shibata, G. Takahara, Y. Takahashi,
T. Wada, Y. Yamamoto
- Torino : C. Aglietta, G. Badino, L. Bergamasco,
C. Castagnoli, A. Castellina, G. Cini, M. Dardo,
M.I. Ferrero, W. Fulgione, P. Galeotti, C. Morello,
G. Navarra, L. Periale, O. Saavedra,
G.C. Trinchero, P. Vallania, S. Vernetto

II - LIST OF THE ORIGINAL WORKS
(PUBLISHED AND UNPUBLISHED)

II - LIST OF THE ORIGINAL WORKS
(PUBLISHED AND UNPUBLISHED)

- II-1. "The lepton asymmetry analyser : LAA"
 Proposal-P200-Addendum 1
 Open presentation CERN SPSC, March 18, 1986 and
 INFN Bologna, March 24, 1986.
- II-2. "The lepton asymmetry analyser : LAA"
 CERN SPSC 86-3, SPSC/P200 Addendum 1, March 3,
 1986.
- II-3. LAA Proposal: Memorandum to the chairman of the SPSC,
 September 4, 1984.
- II-4. "New flavours: how they can be looked for at the ($p\bar{p}$)
 Collider with the Lepton Asymmetry Analyser"
 Proc. of the XXII Course of the Ettore Majorana
 International School of Subnuclear Physics: "Quarks,
 Leptons and their Constituents" (Plenum Press Inc.,
 New York-London), Erice, August 5-15, 1984.
- II-5. LAA Proposal: Memorandum to the Chairman of the
 SPSC, August 2, 1984.
- II-6. LAA Proposal: Memorandum to the SPSC referees
 (Prof. A. Donnachie and Prof. R. Klanner), June 28, 1984.
- II-7. "The lepton asymmetry analyser : a proposal"
 CERN SPSC 84-33, SPSC/P200, May 16, 1984.
- II-8. "The problem of new heavy flavours: top and superbeauty"
 Proc. of the XXI Course of the Ettore Majorana
 International School of Subnuclear Physics: "How far are
 we from the Gauge Forces" (Plenum Press Inc.,
 New York-London), Erice, August 4-13, 1983.

II-9. "A study of possible new heavy-flavour production at the CERN ($p\bar{p}$) Collider"
Lettere al Nuovo Cimento, vol.37, p.255, June 18, 1983.

II-10. "New flavours: experiment versus theory. From charm to the 4th family"
Proc. of the 3rd Topical Workshop on Proton-Antiproton Collider Physics (CERN-83-04), Roma, January 12-14, 1983.

II- 11. "Search for open top at the CERN ($p\bar{p}$) Collider"
Il Nuovo Cimento, vol.68A, p.65, March 1, 1982.

III.- THE ORIGINAL WORKS

III-1. "The lepton asymmetry analyser : LAA"
Proposal-P200-Addendum 1
Open presentation CERN SPSC, March 18, 1986 and
INFN Bologna, March 24, 1986.

1 - The lepton asymmetry analyser:
LAA Addendum 1

Open presentation CERN SPSC, March 18, 1986

BCFL Collaboration

K. Alberini, G. Bari, M. Basile, J. Berbiere, G. Cara Romeo,
R. Casaccia, L. Cifarelli, F. Cindolo, A. Contin, G. D'Ali,
C. Del Papa, G. Iacobucci, I. Laakso, G. Maccarrone,
T. Massam, R. Meunier, F. Motta, R. Nania, F. Palmonari,
G. Prisco, F. Rohrbach, P. Rotelli, G. Sartorelli, A. Scarsella,
G. Susinno, L. Votano, M. Willutzky and A. Zichichi

ABSTRACT

The problem of establishing the existence of new flavours is discussed.

A method is proposed which allows to determine the "up-like" or the "down-like" nature of the new flavour: i.e. the lepton asymmetry.

The Lepton Asymmetry Analyser is an instrument which, apart from any theoretical model expectation, serves the purpose of searching for a lepton asymmetry and its p_T dependence.

To measure the sign of the asymmetry means to establish the "up-like" or "down-like" nature of the new flavour. The p_T dependence is function of the new flavour mass.

The LAA coupled to a powerful central detector, like UA1, allows the study of lepton-jet physics and of its associated phenomenology.

THE PRESENT STATUS OF OUR KNOWLEDGE OF QUARKS AND LEPTONS MAY BE SUMMARIZED AS FOLLOWS:

FAMILIES :	1 st	2 nd	3 rd
QUARKS :	$\begin{pmatrix} u \\ d \end{pmatrix}$	$\begin{pmatrix} c \\ s \end{pmatrix}$	$\begin{pmatrix} ? \\ b \end{pmatrix}$
LEPTONS :	$\begin{pmatrix} \nu_e \\ e \end{pmatrix}$	$\begin{pmatrix} \nu_\mu \\ \mu \end{pmatrix}$	$\begin{pmatrix} \nu_\tau \\ \tau \end{pmatrix}$

THERE ARE GOOD REASONS TO BELIEVE THAT OUR KNOWLEDGE IS FAR FROM BEING COMPLETE AND THUS THE SEARCH FOR NEW FLAVOURS AND THE STUDY OF THEIR FAMILY STRUCTURE IS ONE OF THE KEY PROBLEMS IN SUBNUCLEAR PHYSICS.

QUARK MASSES

- WHEN WE STARTED CHOOSING MASS VALUES FOR NEW FLAVOURS THE CHOICE WAS BASED ON SIMPLE EXTRAPOLATIONS OF KNOWN FACTS:

$$\frac{m_{\text{up-like}}}{m_{\text{down-like}}} \sim 4$$

$$\frac{m_{\text{family } +1}}{m_{\text{family}}} \sim 10$$

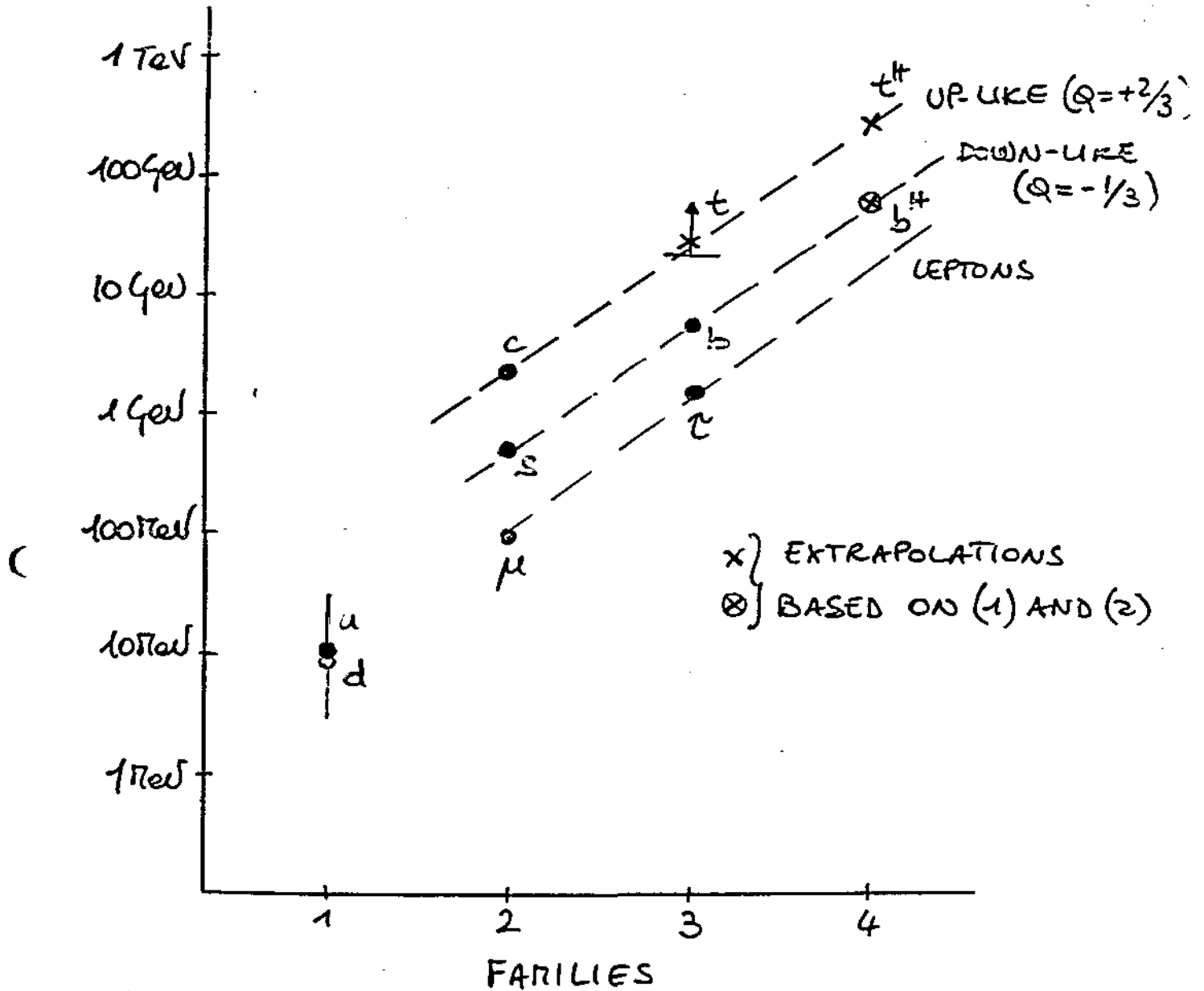
- UA1 HAS EVIDENCE FOR TOP QUARK AT

$$m_t = 40 \pm 15 \text{ GeV}/c^2$$

WE HAVE TAKEN TWO VALUES:

- i) THE LOWEST ESTIMATE FOR TOP: $m_t = 25 \text{ GeV}/c^2$
- ii) THE HIGHEST ESTIMATE FOR BEAUTY^{HEAVY}: $m_b = 55 \text{ GeV}/c^2$

NOTE: UA1 CAN MEASURE MASSES, BUT CANNOT MEASURE FLAVOUR NATURE (UP-LIKE OR DOWN-LIKE)



$$(1) \frac{m_c}{m_s} = \frac{m(\text{"up-like"})}{m(\text{"down-like"})} \sim 4$$

$$(2) \frac{m_b}{m_s} = \frac{m(\text{FAMILY } N+1)}{m(\text{FAMILY } N)} \sim 10$$

TWO "THEORETICAL" ARGUMENTS FAVOUR THE NEED FOR NEW FLAVOURS

- THE ABJ ANOMALY CANCELLATION REQUIRES:

NUMBER OF LEPTONS \equiv NUMBER OF QUARKS

I.E. A SIXTH QUARK IS NEEDED.

ITS NATURAL LOCATION WOULD BE THE UP-LIKE MEMBER OF THE 3rd FAMILY: THE "TOP" QUARK.

- ACCORDING TO SUPERSYMMETRY A VERY HEAVY QUARK (MASS IN THE FEW 10^2 G_{W/C^2} RANGE) IS NEEDED IN ORDER TO PRODUCE RADIATIVELY A GLUINO WITH A MASS SUCH AS TO AVOID A CONFLICT WITH EXISTING LOWER UNITS.

NONE OF THE PRESENTLY KNOWN QUARKS IS HEAVY ENOUGH FOR THIS PURPOSE.

THE MAXIMUM NUMBER OF QUARKS ALLOWED BY SUPERSYMMETRY IN ORDER TO HAVE A CONSISTENT THEORY (FOR EXAMPLE THE UNIFICATION UNIT NOT ABOVE THE PLANCK MASS) IS 8.

THE UP-LIKE QUARK OF THE 4th FAMILY SHOULD BE:

- THE HEAVY QUARK NEEDED BY SUPERSYMMETRY
- THE LAST QUARK EVER TO BE DISCOVERED.

THIS IS THE NEED FOR THE 4th FAMILY.

APART FROM ALL THESE PREMISES, THE INTEREST IN STUDYING LEADING PRODUCTION OF NEW FLAVOURS IS OF GREAT VALUE FOR THE COLLIDER PHYSICS PROGRAMME.

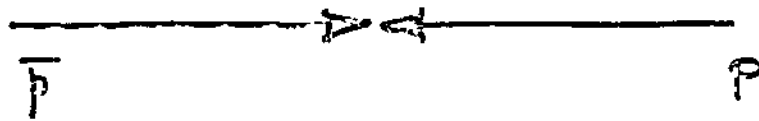
PROPOSAL FOR A NEW METHOD

DUE TO THE LEADING BARYON PRODUCTION MECHANISM, EXTENDED TO THE HEAVIEST BARYON AND ANTI BARYON STATES, A CHARGE ASYMMETRY OF THE LEPTONS ORIGINATING FROM THEIR DECAY CAN BE OBSERVED IN A SELECTED REGION OF PHASE-SPACE.

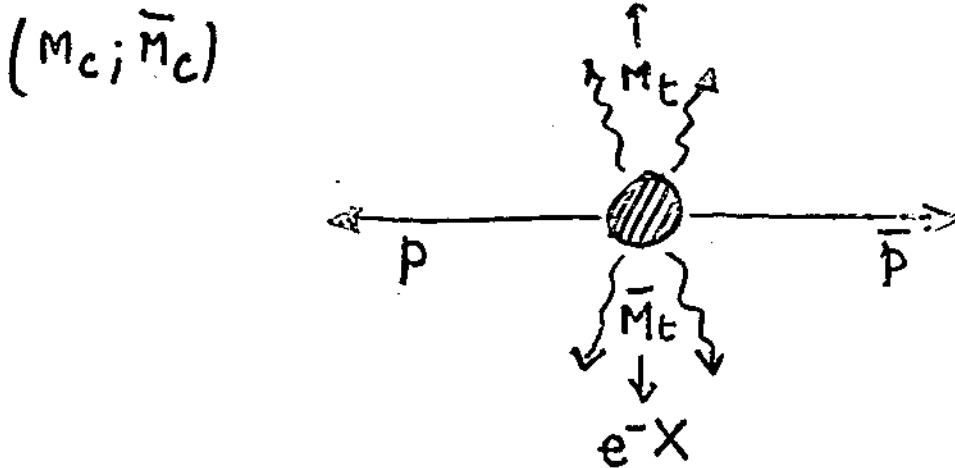
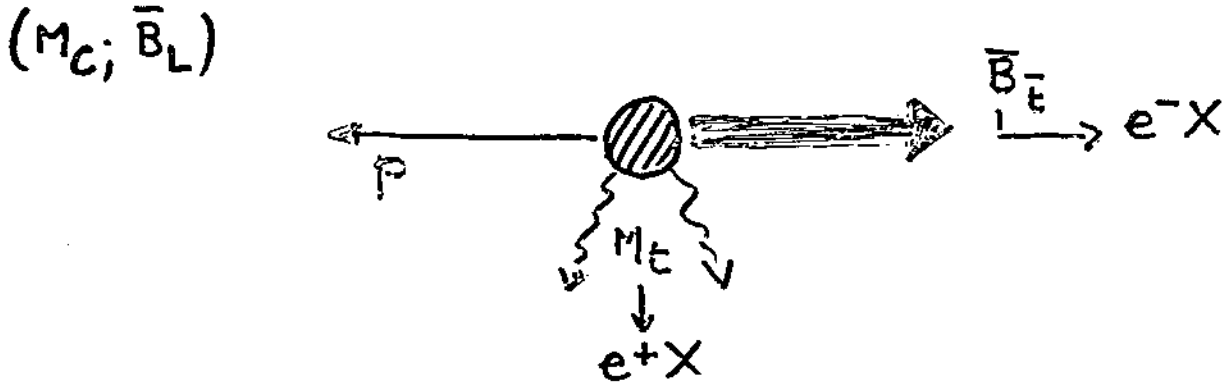
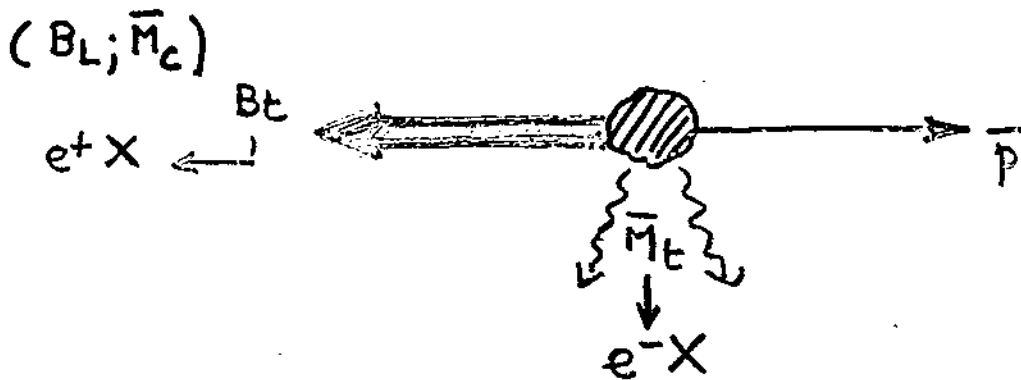
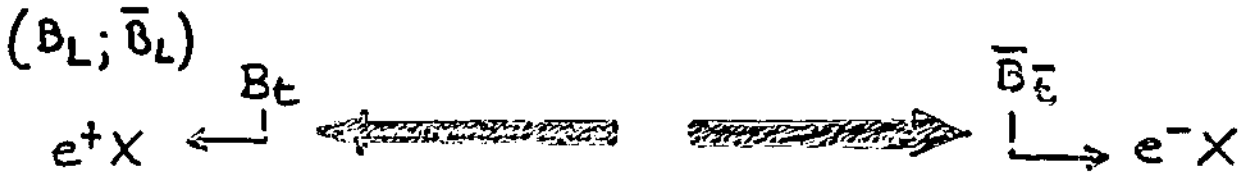
THE SIGN OF THIS ASYMMETRY WILL DETERMINE THE UP-LIKE OR DOWN-LIKE NATURE OF THE PARENT FLAVOURS.

THE ASYMMETRY WILL SHOW AN ENERGY (P_T) DEPENDENCE CHARACTERISTIC OF THE MASSES OF THE DECAYING STATES.

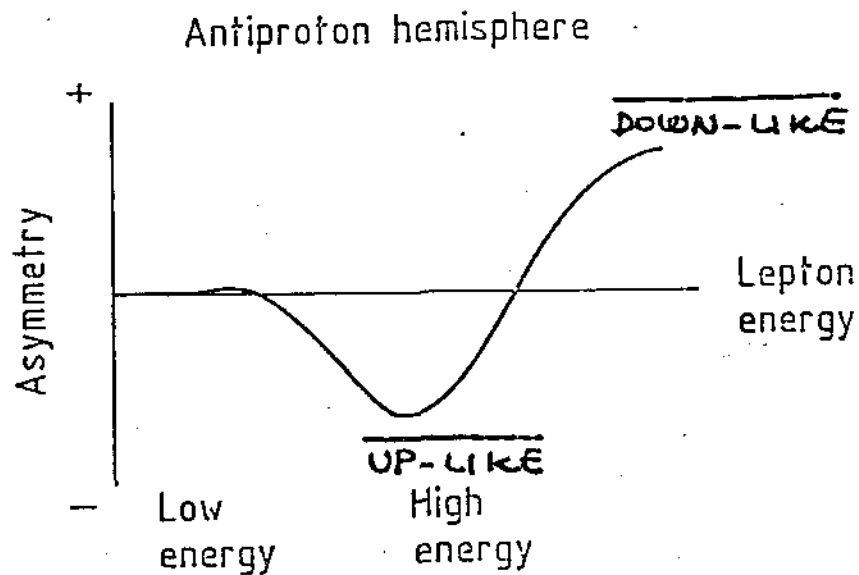
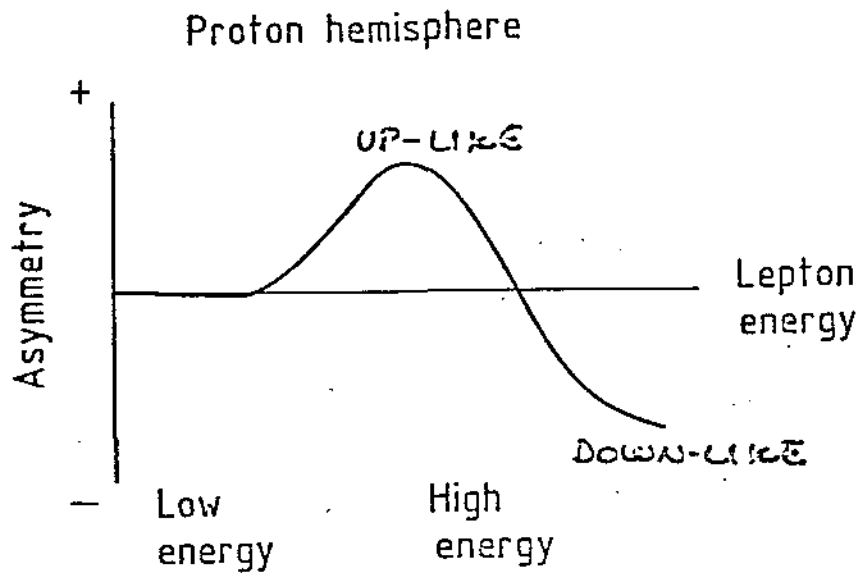
INITIAL STATE



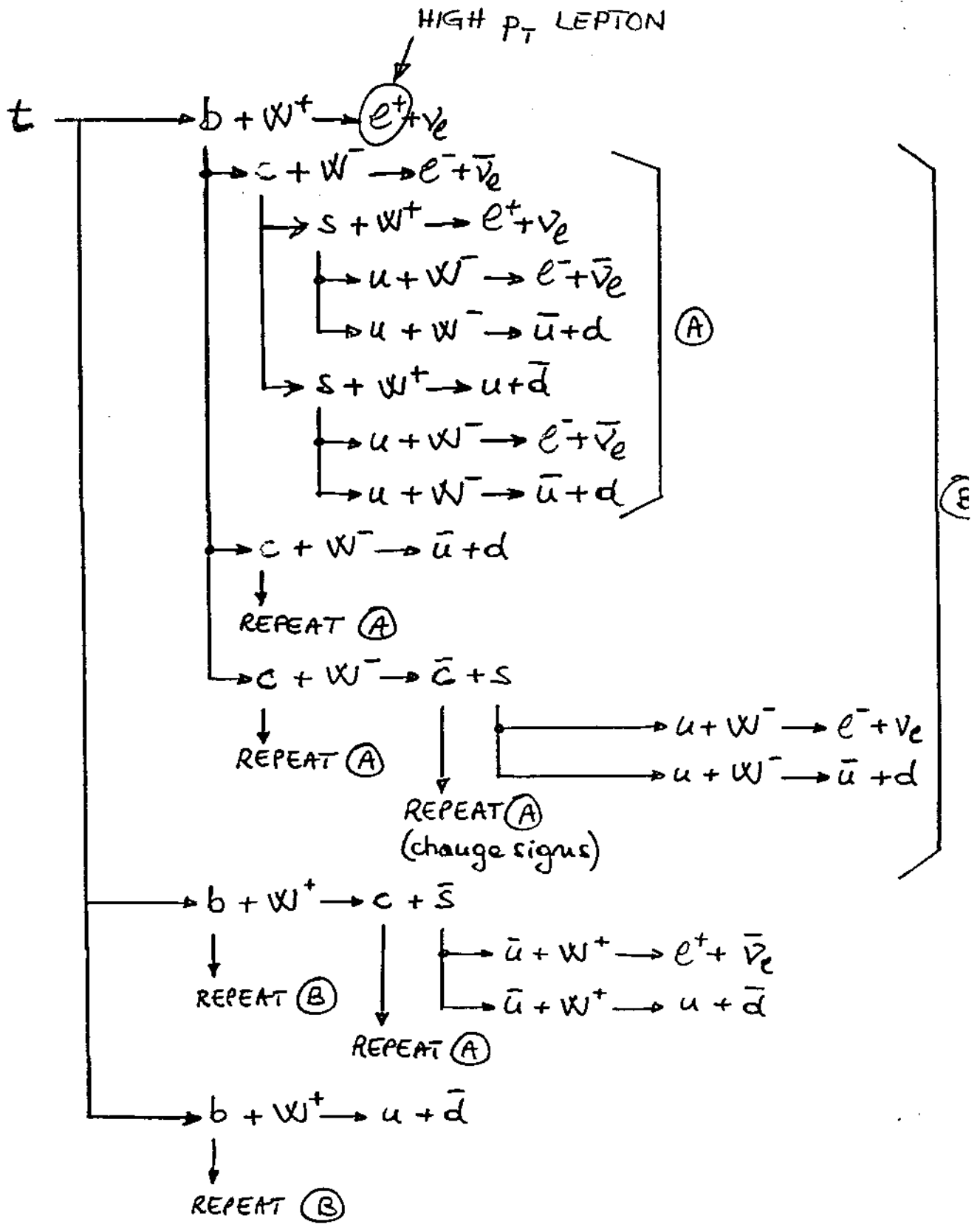
FINAL STATES



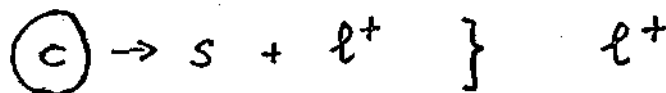
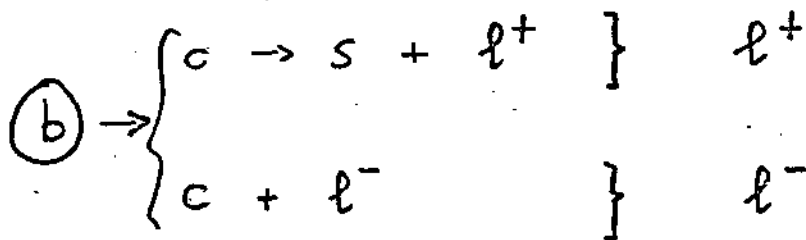
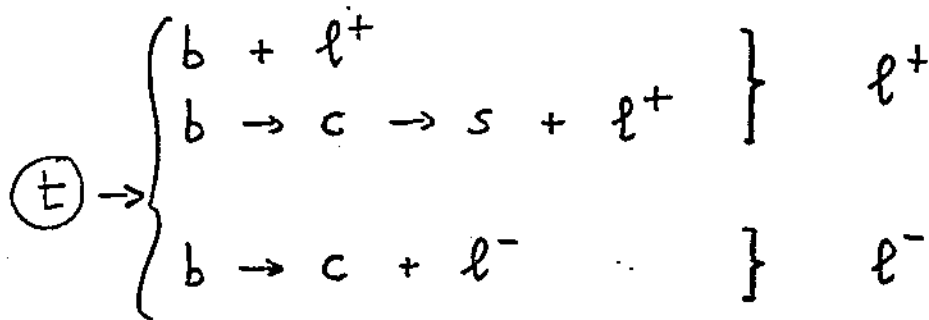
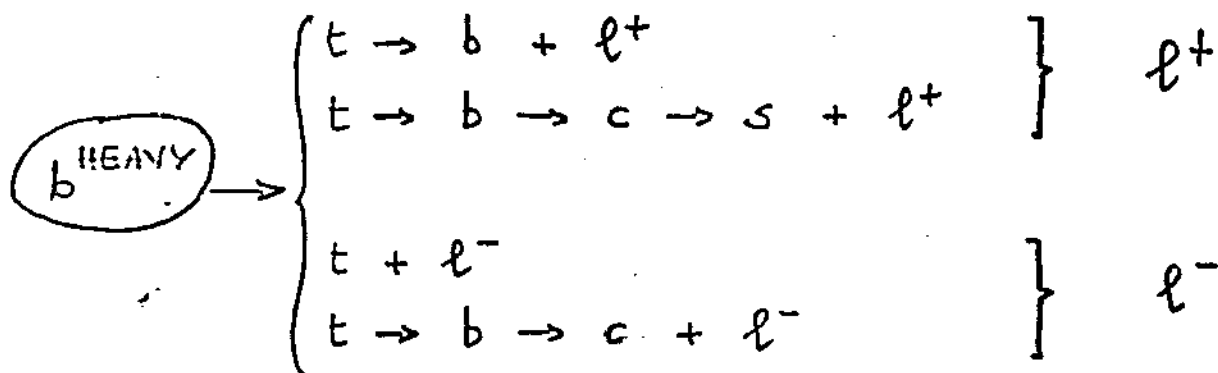
$$\text{ASYMMETRY} = \frac{l^+ - l^-}{l^+ + l^-}$$



THE ADVANTAGE OF HAVING TWO DETECTORS, ONE IN EACH HEMISPHERE IS SHOWN ABOVE: THE ASYMMETRY HAS OPPOSITE SIGNS IN THE TWO HEMISPHERES.



THE LEPTONS ORIGINATING FROM THE DECAY OF THE VARIOUS FLAVOURS ARE SUMMARIZED BELOW.



FOR THE CORRESPONDING ANTI-FLAVOURS THE CHARGE SIGN OF THE LEPTON IS REVERSED.

DEFINITION OF THE ASYMMETRY

$$A^0 = \frac{N(\mu^+) - N(\mu^-)}{N(\mu^+) + N(\mu^-)}$$

WHERE:

$N(\mu^\pm) = N(\mu^\pm; P_T, \theta_{cut}) \equiv$ NUMBER OF μ^\pm PRODUCED WITH TRANSVERSE MOMENTUM P_T IN THE ANGULAR RANGE θ_{cut}

$$N(\mu^\pm) = L \left[\sum_f m_f^\pm(\mu^\pm) \right]$$

WHERE:

$m_f(\mu^\pm)$ (WITH $f = b^H, t, b, c$) IS THE CONTRIBUTION FROM THE DIRECT PRODUCTION OF b^H, t, b, c STATES, EACH ONE DECAYING IN ALL ALLOWED CHAINS AS SPECIFIED IN THE PREVIOUS GRAPH.

L

IS THE INTEGRATED LUMINOSITY

$m_f(\mu^+)$ AND $m_f(\mu^-)$ CAN BE EXPRESSED IN TERMS OF

- σ_f^T TOTAL CROSS SECTION FOR THE PRODUCTION OF OPEN (f, \bar{f})
- $\rho_{\pi f}, \rho_{\bar{\pi} \bar{f}}, \rho_{B f}, \rho_{\bar{B} \bar{f}}$ RATIO BETWEEN THE INCLUSIVE CROSS SECTION FOR PRODUCING MESONS, ANTI-MESONS, BARYON ANTI-BARYONS AND THE TOTAL CROSS-SECTION
- $BR_{\pi f}, BR_{\bar{\pi} \bar{f}}, BR_{B f}, BR_{\bar{B} \bar{f}}$ SEMILEPTONIC BRANCHING RATIOS OF THE VARIOUS STATES WITH FLAVOUR f'
- $\epsilon_{\pi f}(\mu_{f'}^\pm), \epsilon_{\bar{\pi} \bar{f}}(\mu_{\bar{f}'}^\pm), \epsilon_{B f}(\mu_{f'}^\pm), \epsilon_{\bar{B} \bar{f}}(\mu_{\bar{f}'}^\pm)$ ACCEPTANCE FOR μ^\pm FROM THE SEMILEPTONIC DECAY OF THE FLAVOUR f' PRODUCED IN THE DECAY CHAIN OF THE STATE WITH FLAVOUR f . THIS ACCEPTANCE IS A FUNCTION OF THE μP_T AND OF THE ANGULAR RANGE OF THE DETECTOR.

ACCORDINGLY, FOR THE CASE OF TOP WE HAVE:

$$m_t(\mu^+) = \sigma_t^T \left\{ \begin{aligned} & p_{Hc} [BR_{Ht} \epsilon_{Ht}(\mu_t^+) + BR_{Hc} \epsilon_{Hc}(\mu_c^+)] + \\ & p_{H\bar{c}} [BR_{H\bar{b}} \epsilon_{H\bar{c}}(\mu_b^+)] + \\ & p_{Bt} [BR_{Bt} \epsilon_{Bt}(\mu_t^+) + BR_{Bc} \epsilon_{Bc}(\mu_c^+)] + \\ & p_{B\bar{c}} [BR_{B\bar{b}} \epsilon_{B\bar{c}}(\mu_b^+)] \end{aligned} \right\}$$

$$m_t(\mu^-) = \sigma_t^T \left\{ \begin{aligned} & p_{Ht} [BR_{Hb} \epsilon_{Ht}(\mu_b^-)] + \\ & p_{H\bar{c}} [BR_{H\bar{c}} \epsilon_{H\bar{c}}(\mu_{\bar{c}}^-) + BR_{H\bar{c}} \epsilon_{H\bar{c}}(\mu_{\bar{c}}^-)] + \\ & p_{Bt} [BR_{Bb} \epsilon_{Bt}(\mu_b^-)] + \\ & p_{B\bar{c}} [BR_{B\bar{c}} \epsilon_{B\bar{c}}(\mu_{\bar{c}}^-) + BR_{B\bar{c}} \epsilon_{B\bar{c}}(\mu_{\bar{c}}^-)] \end{aligned} \right\}$$

THE ANALOGOUS EXPRESSIONS FOR $m_b(\mu^\pm)$, $m_c(\mu^\pm)$ CAN BE EASILY DERIVED.

FROM THE ABOVE FORMULAS IT CAN BE SEEN THAT IN ORDER TO EVALUATE THE LEPTON ASYMMETRY A^0 ONE NEEDS TO KNOW:

- ① - THE TOTAL CROSS SECTION $\Rightarrow \sigma^T$
- ② - THE DECAY BRANCHING RATIOS $\Rightarrow BR$
- ③ - THE PRODUCTION DISTRIBUTIONS OF THE BARYON AND MESON STATES, AND THE LEPTON DISTRIBUTIONS IN THE DECAY $\Rightarrow \epsilon$
- ④ - THE RELATIVE FRACTION OF BARYONS AND MESONS $\Rightarrow \rho$

EXTRAPOLATIONS OF THE TOTAL CROSS SECTIONS

THE TOTAL CROSS-SECTIONS FOR HEAVY FLAVOURS AT THE (p \bar{p}) COLLIDER ($\sqrt{s} = 540 \text{ GeV}$) ARE TAKEN FROM QCD PERTURBATIVE CALCULATIONS:

$$\sigma_c \sim 2000 \mu\text{b}$$

$$\sigma_b \sim 10 \mu\text{b}$$

$$\sigma_t \sim 0.1 \mu\text{b} \quad \text{WITH } m_t = 25 \text{ GeV}/c^2$$

FOR HIGHER MASSES WE EXTRAPOLATE USING THE FORMULA

$$\sigma(m) \sim \frac{1}{m^2} f\left(\frac{s}{m^2}\right)$$

TO THE FOLLOWING VALUES:

$$\sigma_t \sim 0.05 \mu\text{b} \quad \text{WITH } m_t = 35 \text{ GeV}/c^2$$

$$\sigma_b \sim 0.01 \mu\text{b} \quad \text{WITH } m_b = 55 \text{ GeV}/c^2$$

WE WILL TRY TO ESTIMATE THE PRODUCTION CROSS SECTION FOR VERY HIGH FLAVOUR MASSES USING THE QCD FLAVOUR EXCITATION PREDICTION! FROM V. BARGER, F. HALZEN AND M.Y. KEUNG :

$$\sigma_t (m_t = 20 \text{ GeV}/c^2) \approx 0.15 \mu\text{b} \text{ AT } \sqrt{s} = 540 \text{ GeV}$$

(SEE FIGURE ON PAGE 35)

FOR THE EXTRAPOLATION WE TAKE USE OF DIMENSIONALITY AND SCALING :

$$\sigma(m) \sim \frac{1}{m^2} f\left(\frac{s}{m^2}\right)$$

IN ORDER TO CHECK DIMENSIONALITY AND SCALING WE HAVE USED :

STRANGENESS DATA TO PREDICT CHARM

STRANGENESS AND CHARM DATA TO PREDICT BEAUTY

THE RESULTS ARE SHOWN IN FIGURES ON PAGES 33 AND 34

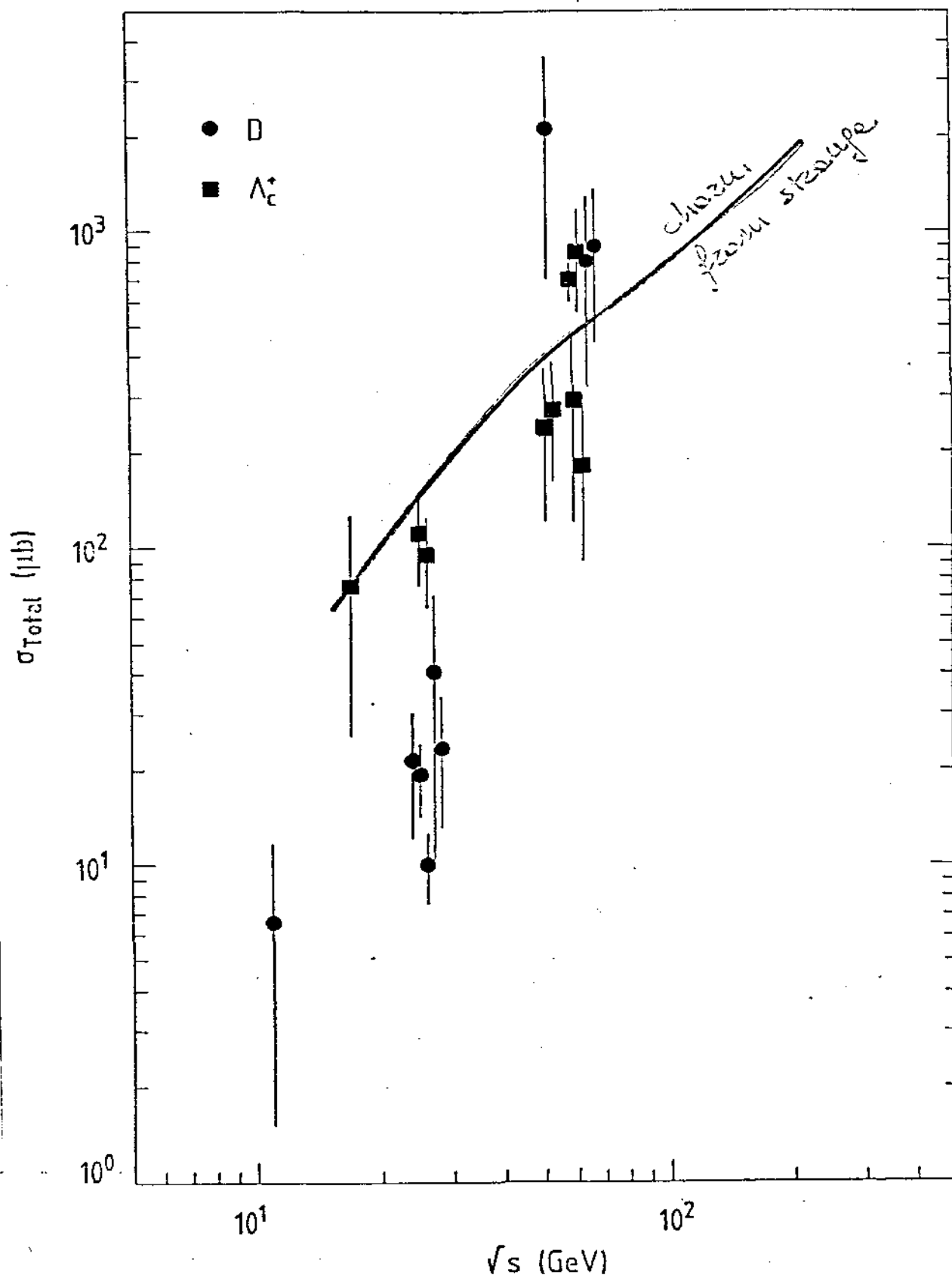
$pp \rightarrow \text{charm}$


FIG. 6

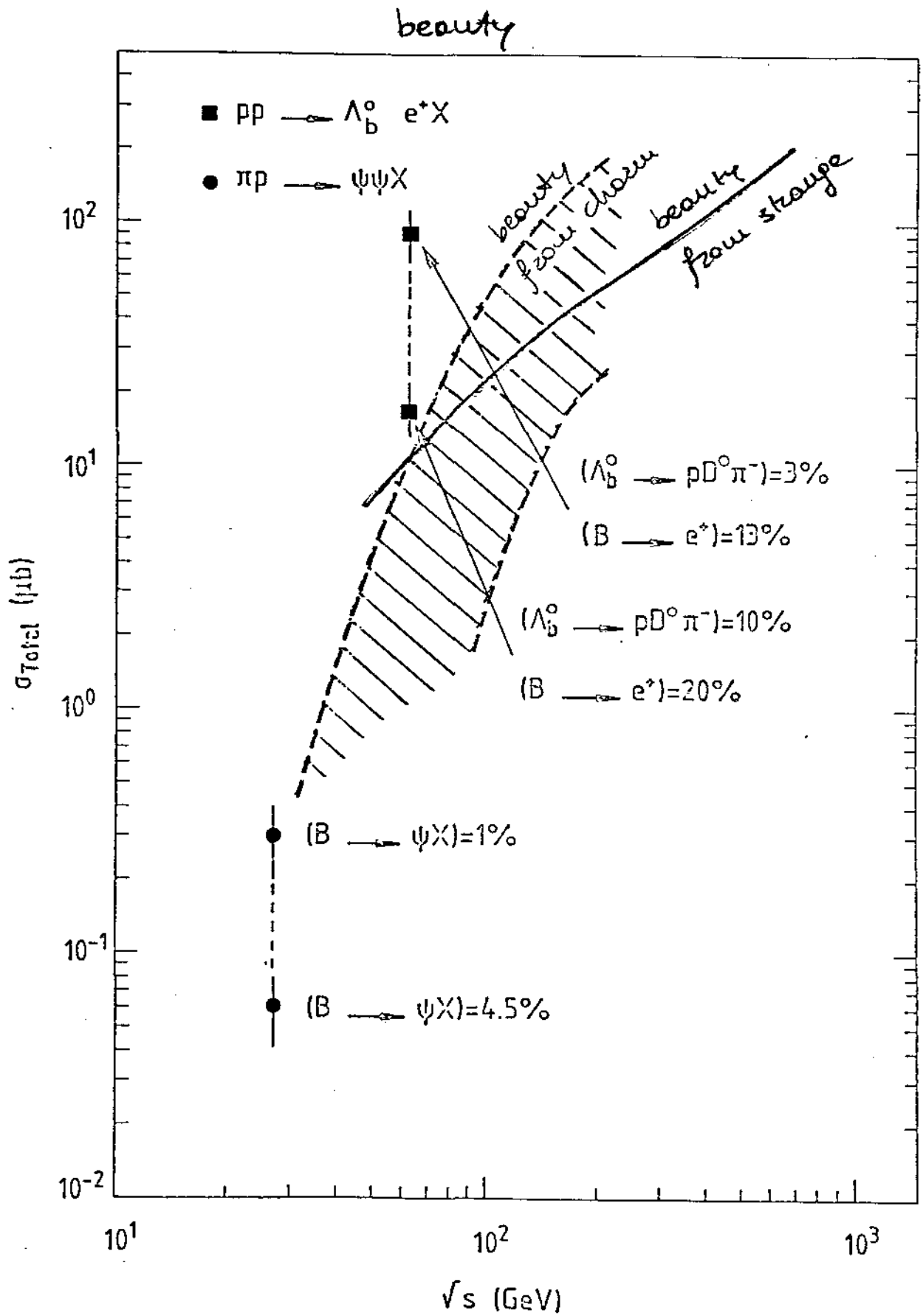
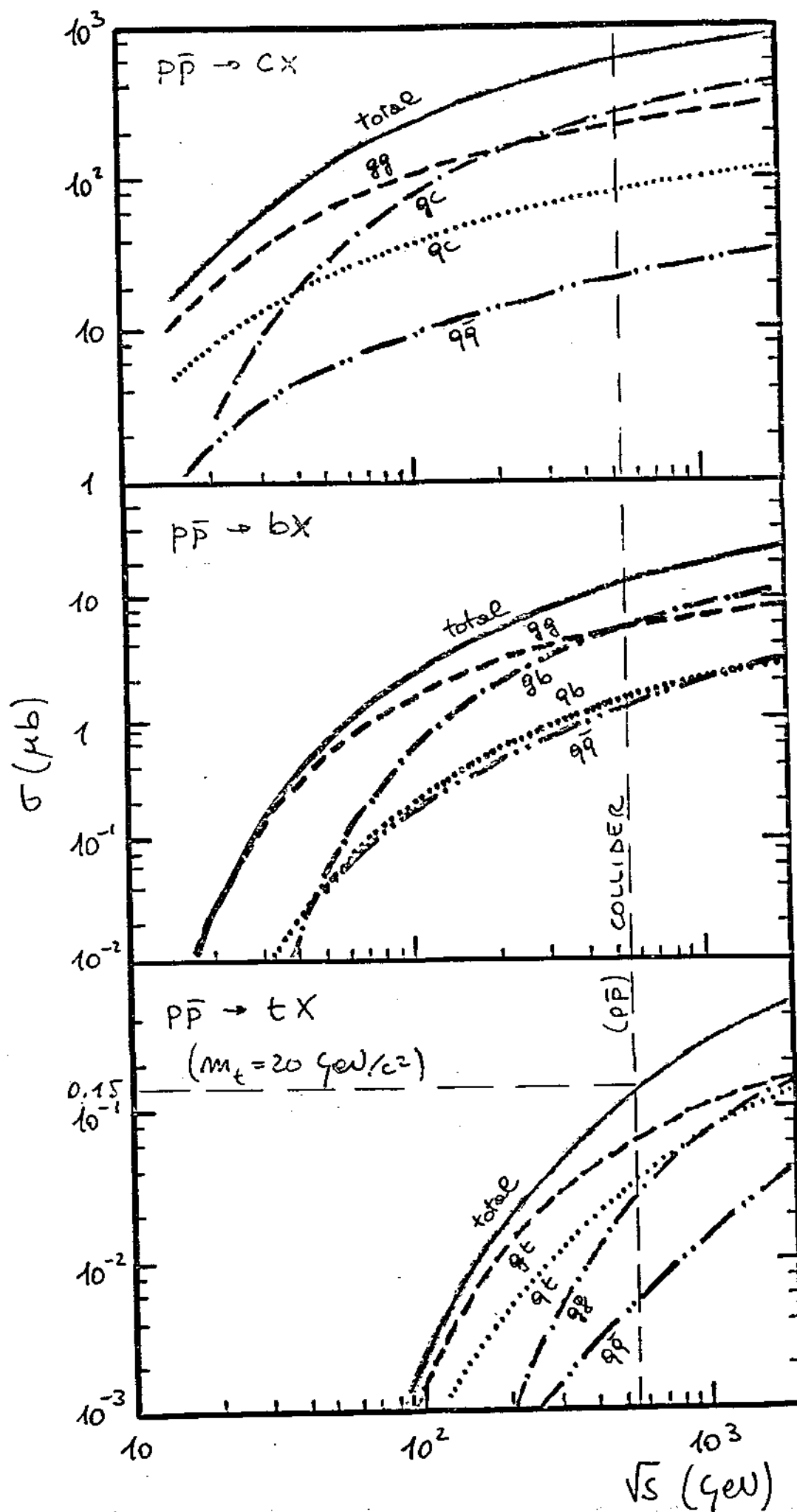


FIG. 7



THE DECAY BRANCHING RATIOS

WE USE THE KNOWN SEMILEPTONIC BRANCHING RATIOS FOR CHARM

$$\frac{(D \rightarrow \ell^\pm)}{(D \rightarrow \text{ALL})} \approx 0.085$$

$$\frac{(\Lambda_c^+ \rightarrow \ell^\pm)}{(\Lambda_c^+ \rightarrow \text{ALL})} \approx 0.045$$

FOR ALL OTHER HEAVIER PARTICLES WE ASSUME A CONSERVATIVE VALUE

$$\text{BR}(\ell^\pm) = 0.1$$

• RECENT DATA FROM CLEO: $\frac{(M_b \rightarrow \ell^\pm)}{(M_b \rightarrow \text{ALL})} \approx 0.13$

- FOR QUARK MASSES GREATER THAN THE BEAUTY MASS $\text{BR}(\ell^\pm)$ SHOULD BE EVEN GREATER, APPROACHING THE VALUE 0.25 WHICH IS EXPECTED FROM THE QUARKS COLOURS AND LEPTONS COUNTING.

$$BR(\text{LEPTONS/TOTAL}) =$$

$$= \frac{\sum_{i=1}^n \text{LEPTON FAMILIES}}{\sum_{i=1}^n \text{LEPTON FAMILIES} + 3 \times \sum_{i=1}^n \text{QUARK FAMILIES}} =$$

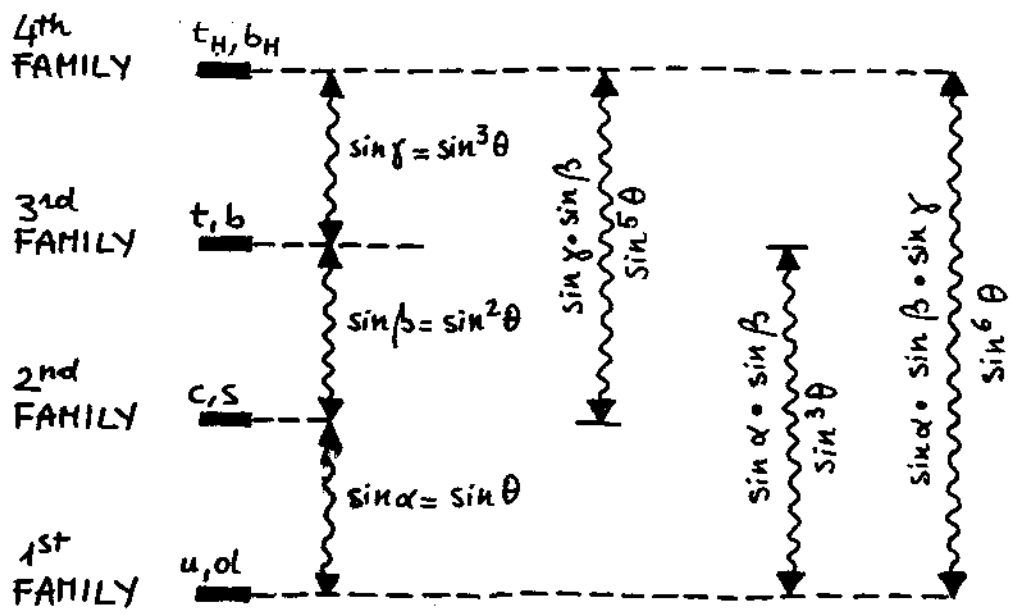
$$= 25\%$$

INTO ONE LEPTONIC CHANNEL:

$$BR = 25\% \times \frac{1}{N}$$

WHERE $N = n$. OF FAMILIES.

SCHEMATIC DIAGRAM ILLUSTRATING FOR A QUARK THE TRANSITION FACTORS BETWEEN TWO FAMILIES.



MODEL SUGGESTED BY THE BEAUTY LIFETIME

THE LEPTON DECAY DISTRIBUTIONS

DATA FROM CLEO ON THE SEMILEPTONIC DECAY OF BEAUTY MESONS, M_b : $\pi_b \rightarrow X \ell \nu$.

- $M_X \sim M_D \simeq 2.0 \text{ GeV}/c^2$

(i.e. THE MASS RECOILING WITH RESPECT TO THE LEPTONS IS VERY NEAR TO THE D MASS
(SEE FIGURE ON PAGE 41))

- MEAN CHARGED MULTIPLICITY OF THE DECAY = 4.
(OF WHICH 2.5 ARE, ON AVERAGE, CONTRIBUTED BY THE D DECAY)

THESE RESULTS SUGGESTS THAT EVEN AT THE HIGH MASS VALUE OF M_b , THE SEMILEPTONIC DECAY PROCEEDS VIA A 3-body DECAY, WITH A MASS DIFFERENCE VERY NEAR TO THE VALUE:

$$\Delta m = \text{mass}_{\text{beauty}} - \text{mass}_{\text{charm}}$$

DATA ON THE HADRONIC DECAY OF BEAUTY MESONS SHOW THAT THE MEAN CHARGED MULTIPLICITY IS 6.

$$\begin{aligned} \pi_b &\rightarrow D + 4 \text{ charged} + 2 \text{ neutrals} \\ &\hookrightarrow 2.5 \text{ charged} \end{aligned}$$

i.e.

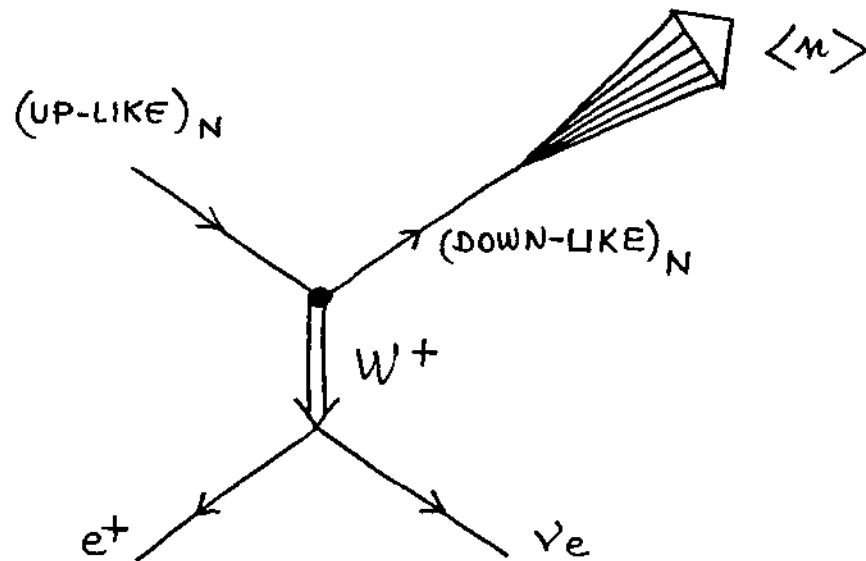
$$\pi_b \rightarrow D + 6\text{-body}$$

IN THE FOLLOWING WE WILL MAKE THE ASSUMPTION:

- THE TOTAL MULTIPLICITY OF SEMILEPTONIC DECAYS IS 3 AND THE DECAY IS K_{e3} -LIKE FOR MESONS AND PHASE-SPACE FOR BARYONS.
- THE TOTAL MULTIPLICITY OF HADRONIC DECAYS IS
 - ~ 3 FOR CHARM
 - $\sim (n_{\text{charm}} + 6)$ FOR -beauty
 - top
 - heavy beauty

(THIS IS A CONSERVATIVE HYPOTHESIS - HIGHER VALUES OF MULTIPLICITY FOR THE HADRONIC DECAY PRODUCE HIGHER VALUES FOR THE ASYMMETRY - SINCE THE HADRONIC DECAYS OF TOP AND HEAVY BEAUTY CAN BE EXPECTED TO PRODUCE MORE PARTICLES THAN BEAUTY)

EXAMPLE OF A SEMILEPTONIC DECAY

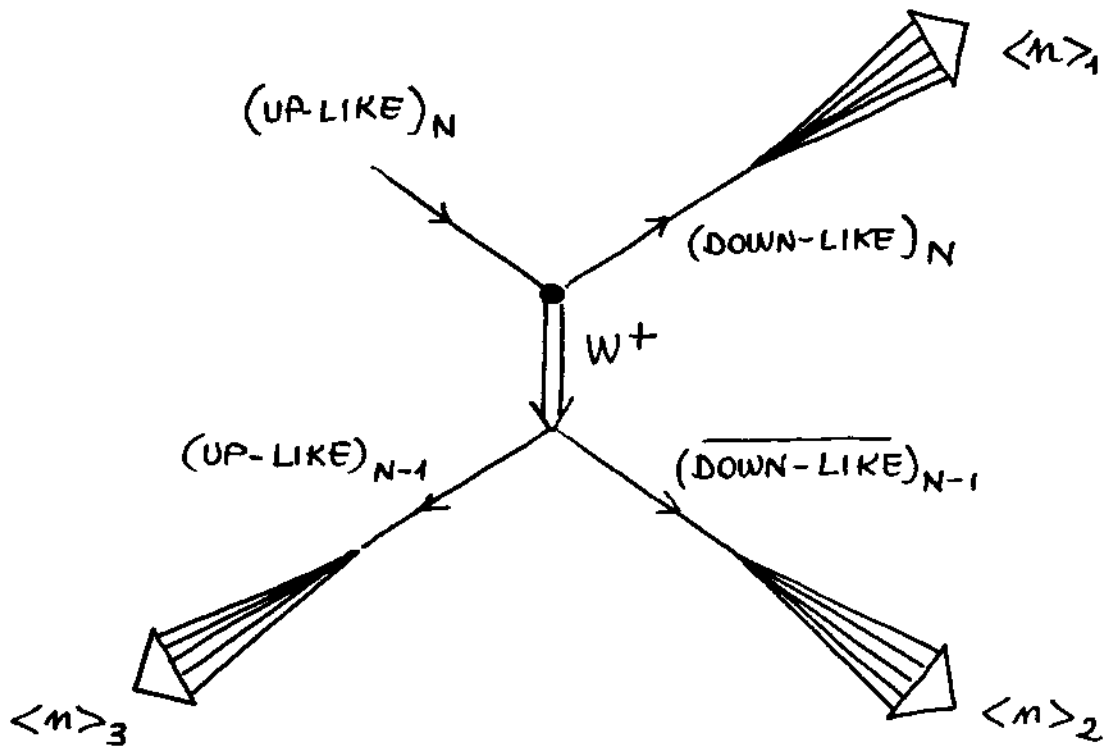


DECAY OF UP-LIKE QUARK INTO DOWN-LIKE QUARK.

NOTICE THAT THE MULTIPLICITY $\langle n \rangle$ IS PRODUCED BY THE HADRONIZATION PROCESS.

AS THE W^+ IS VIRTUAL, THE "DECAY VERTEX" IS A THREE-BODY DECAY.

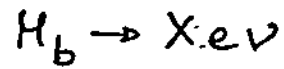
EXAMPLE OF A HADRONIC DECAY



THE TOTAL MULTIPLICITY IS THE RESULT OF 3 HADRONIZATION PROCESSES, EACH ONE GIVING A MULTIPLICITY $\langle n \rangle_i$.

N INDICATES THE FAMILY NUMBER.
LEPTONS ORIGINATING FROM SECONDARY DECAYS OF THE HADRONIZATION ARE LOW p_T PARTICLES.

RECOILING MASS IN THE DECAY:



THESE DATA SHOW THAT THE "PARTICLE"
RECOILING HAS $M(X) \approx 2 \text{ GeV}/c^2$ MASS, i.e. CHARM

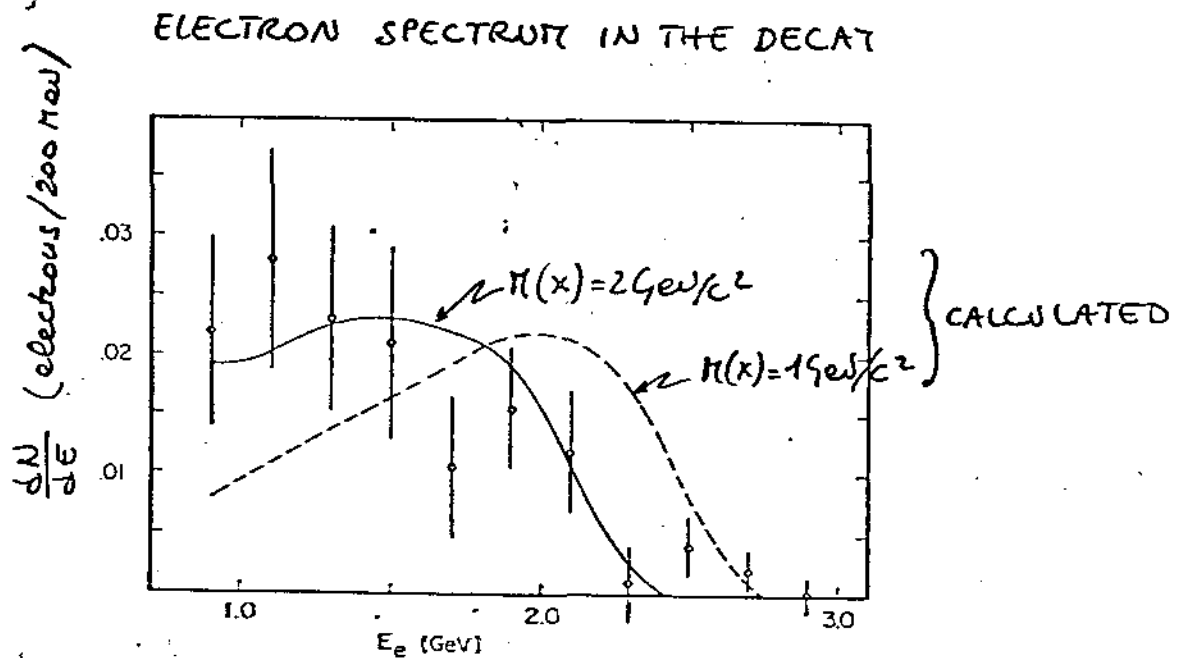
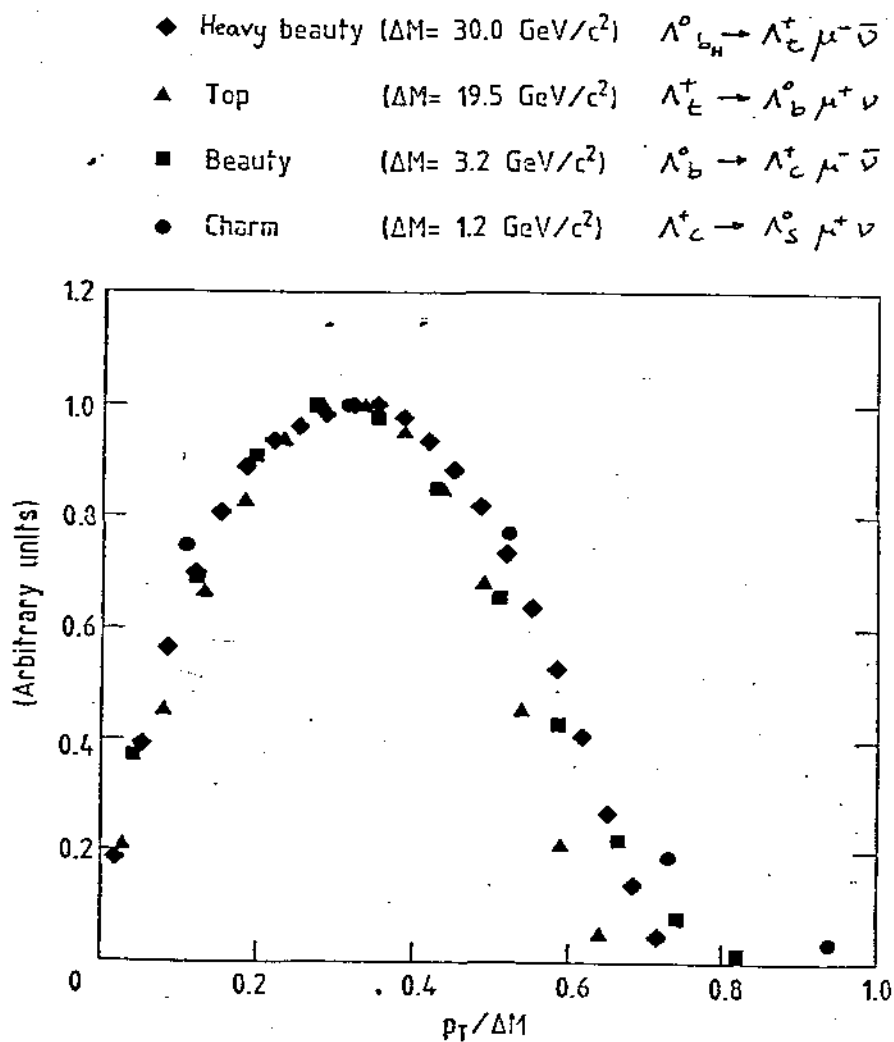


Fig. 9 Experimental results for the electron spectrum, CUSB, Re
B compared with calculation of the spectrum for the decay $B \rightarrow e\nu X$,
for $M(X) = 1 \text{ GeV}$ (b-u) and $M(X) = 2 \text{ GeV}$ (b-c).

	Mass of the decaying Flavour (GeV/c ²)		Mass difference between the primary flavour and its decay ΔM (GeV/c ²)
Heavy beauty	55	}-----	30
Top	25	}-----	20
Beauty	5	}-----	3
Charm	2	}-----	1.5
Strangeness	0.5		

The data obtained from Monte Carlo simulation show that the lepton spectra obtained in the (up-like \leftrightarrow down-like) transition are characterised by the same trend -
Notice: the abscissa is $p_T/\Delta M$.



EXPERIMENTAL FINDINGS VERSUS THEORETICAL PREDICTIONS

CHARM PRODUCTION IN (pp) INTERACTIONS

THE CONCLUSION OF THIS SHORT REVIEW ON THE "CHARM" FLAVOUR PRODUCTION IN (pp) INTERACTIONS IS THEREFORE AS FOLLOWS:

- i) THE CROSS-SECTION VALUES FOUND ARE AT LEAST AN ORDER OF MAGNITUDE ABOVE THE "THEORETICAL" PREDICTIONS OF PERTURBATIVE QCD;
- ii) THE X-DISTRIBUTION FOR Λ_c^+ , I.E. THE LEADING EFFECT, WAS THEORETICALLY UNPREDICTED;
- iii) WITH "NEW" MODELS (ESSENTIALLY FLAVOUR EXCITATION AND NON-PERTURBATIVE QCD) BOTH CROSS-SECTION VALUES AND X-DISTRIBUTIONS CAN BE "THEORETICALLY" DERIVED.

NOTICE:
THESE MODELS CAME LATER.

ALL THIS SHOULD BE QUITE A WARNING FOR QCD PREDICTION ON HEAVY-FLAVOUR PRODUCTION AT EXTREME ENERGIES SUCH AS THOSE OF THE CERN $p\bar{p}$ COLLIDER

⊙ FURTHER REMARKS

FOR THE BENEFIT OF THOSE WHO HAVE STRONG FAITH IN QCD, IT COULD BE INTERESTING TO RECALL FEW FACTS ON THE ONLY HEAVY FLAVOUR SO FAR EXTENSIVELY STUDIED.

THE PHOTOPRODUCTION WAS CONSIDERED A SIMPLER CASE FOR QCD. THEREFORE ITS PREDICTIONS SHOULD HAVE BEEN IN AGREEMENT WITH EXPERIMENTAL FINDINGS.

A SUMMARY OF QCD PROBLEMS IN CHARM PHOTOPRODUCTION PHYSICS FOLLOWS:

- a) IT IS IMPOSSIBLE TO PREDICT LARGE PHOTOPRODUCTION CROSS-SECTIONS OF THE HEAVY FLAVOURS BY MEANS OF PERTURBATIVE QCD;
- b) THE p_T DEPENDENCE OF INELASTIC ($c\bar{c}$), FOR OPEN AND HIDDEN STATES, CANNOT BE ACCOUNTED FOR BY QCD;
- c) THE A -DEPENDENCE CANNOT BE A^1 (PERTURBATIVE QCD PREDICTS A^2).

COMPARISON BETWEEN THEORETICAL MODELS
AND EXPERIMENTAL RESULTS ON HEAVY FLAVOURS
PRODUCTION.

Table II

	experiment	models		
		diffractive	flavour excitation	fusion
Leading effect	yes	yes	yes	no <small>NO</small>
threshold behaviour	steeper than $\ln^2 s$	$\ln s$ <small>NO</small>	steeper than $\ln^2 s$	\gg steeper than $\ln^2 s$
mass dependence	?	$1/m^2$	stronger than $1/m^2$	\gg stronger than $1/m^2$
cross section	large	large	large	small <small>NO</small>
A^α dependence	$\alpha < 2/3$ (*)	$\alpha = 2/3$	$\alpha = 1$ <small>NO</small>	$\alpha = \dots$

(*) The p_T dependence is derived from data on strangeness.

DOES ANY MODEL REPRODUCE DATA? NO

PRODUCTION DISTRIBUTIONS OF BARYONS AND MESONS.

FROM ISR : LONGITUDINAL MOMENTUM DISTRIBUTIONS:

(FIGURES 45, 46, 47)

BARYONS : $\frac{d\sigma}{dx} = \text{const.}$

(FIGURE 48)

MESONS : $E \frac{d\sigma}{dx} \propto (1-x)^3$

TRANSVERSE MOMENTUM DISTRIBUTION:

BARYONS & MESONS : $\frac{d\sigma}{dp_T} \propto p_T e^{-2.5p_T}$

RELATIVE YIELD OF MESONS AND BARYONS.

$$\left(\text{AT ISR : } \frac{L}{T} = \frac{\text{INCLUSIVE CROSS-SECTION FOR BARYONS}}{\text{TOTAL CROSS-SECTION}} = \frac{1}{16} \text{ s} \right.$$

$$\left. \frac{1}{8} \text{ c} \right.$$

$$\frac{\text{LEADING}}{\text{TOTAL}} = \frac{L}{T} = \text{FREE PARAMETER } (1/20 \rightarrow 1/4)$$

SEMILEPTONIC BRANCHING RATIOS.

FROM (e^+e^-) DATA : $B_{SL}(\text{beauty meson}) = 0.13$

$B_{SL} = 0.1$ FOR ALL FLAVOURS

DECAY DISTRIBUTIONS.

FROM (e^+e^-) DATA : SEMILEPTONIC DECAYS : 3-BODY PHASE SPACE
FOR BARYONS
 k_{e3} FOR MESONSHADRONIC DECAYS : PHASE SPACE WITH
MULTIPLICITY 3 FOR CHARGED
6 FOR OTHERSCROSS SECTION.FROM QCD EVALUATION : $\sigma(p\bar{p} \rightarrow tX) = 0.15 \mu\text{b}$ WITH $m_t = 20 \text{ GeV}$
[V. BARGER et al. (1981)]FROM DIMENSIONALITY AND SCALING : $\sigma \sim \frac{1}{m^2} f\left(\frac{s}{m^2}\right)$

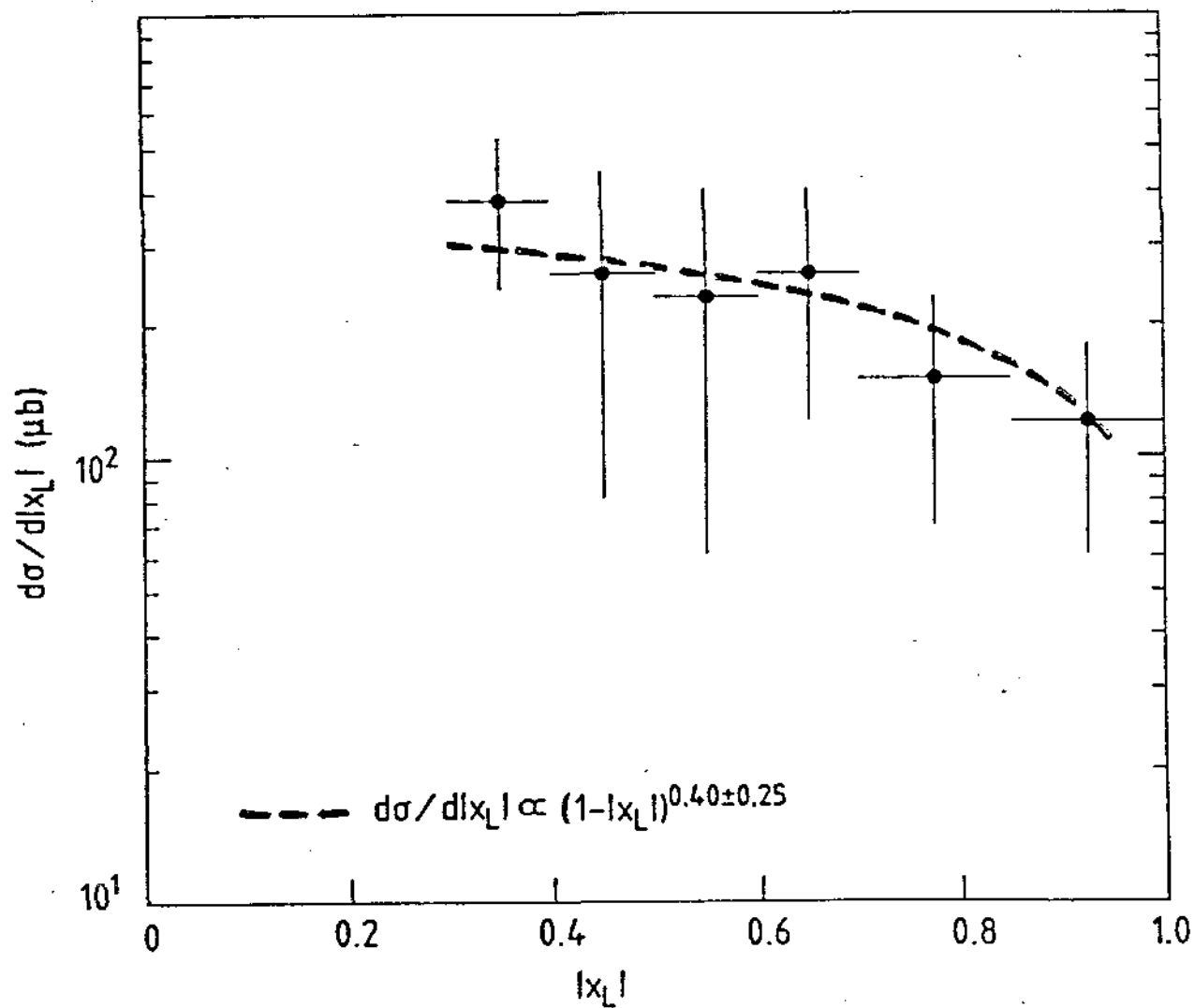
$\sigma_c = 2000 \mu\text{b} \quad \sigma_t(m_t = 35 \text{ GeV}/c^2) = 0.05 \mu\text{b}$

$\sigma_b = 10 \mu\text{b} \quad \sigma_{bH}(m_{bH} = 55 \text{ GeV}/c^2) = 0.01 \mu\text{b}$

$\sigma_t(m_t = 25 \text{ GeV}/c^2) = 0.1 \mu\text{b}$

LEADING EFFECT IN Λ_c^+ PRODUCTION

pp $\rightarrow \Lambda_c^+ \bar{D} + \text{anything}$ $\sqrt{s} = 63 \text{ GeV}$



LEADING EFFECT IN Λ_b^0 PRODUCTION
$$pp \rightarrow \Lambda_b^0 \pi_B^+ + \text{anything}$$

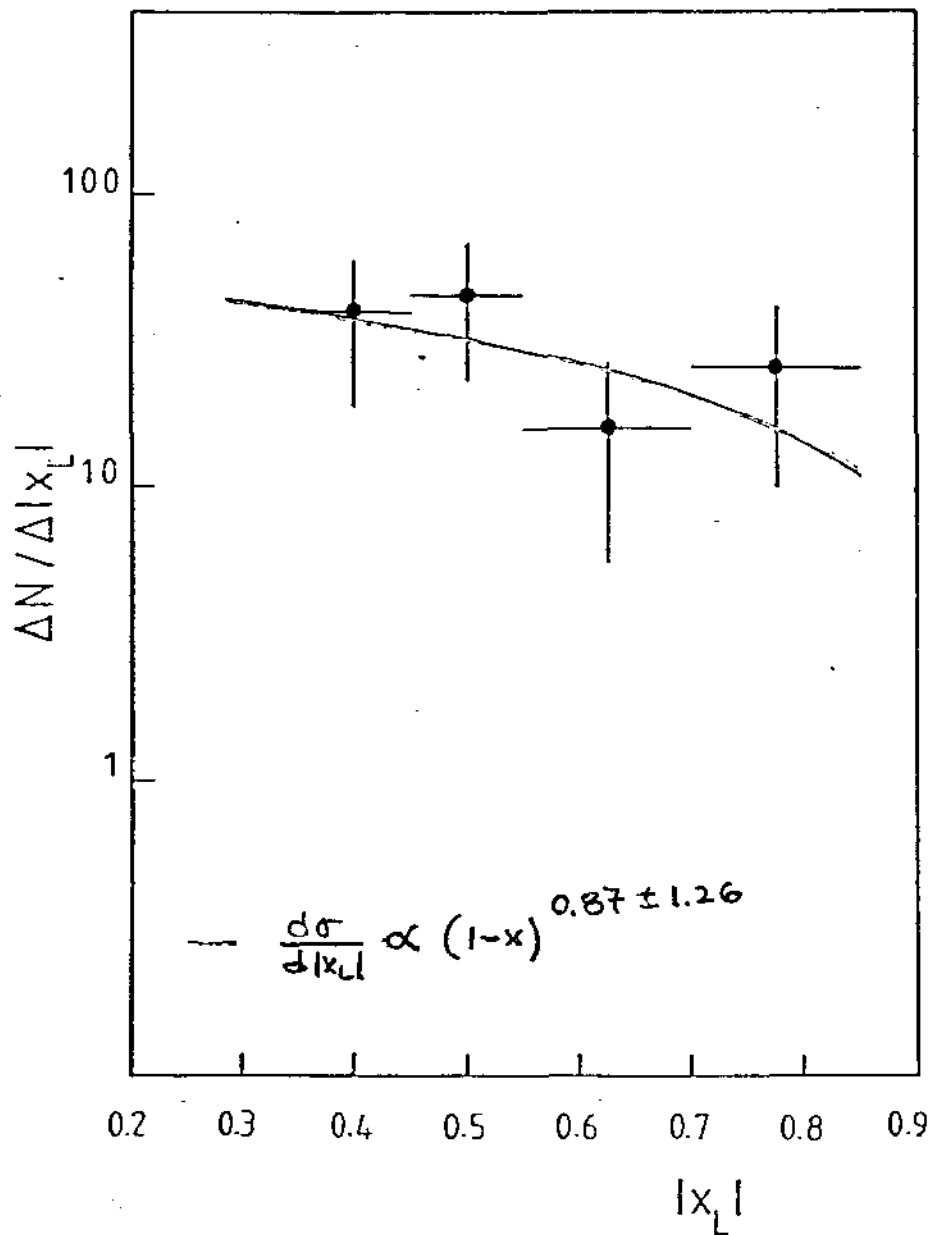
$$\sqrt{s} = 63 \text{ GeV}$$


Fig. 1

STRANGENESS, CHARM AND BEAUTY BARYONS
COMPARISON AT $\sqrt{s} = 63 \text{ GeV}$.

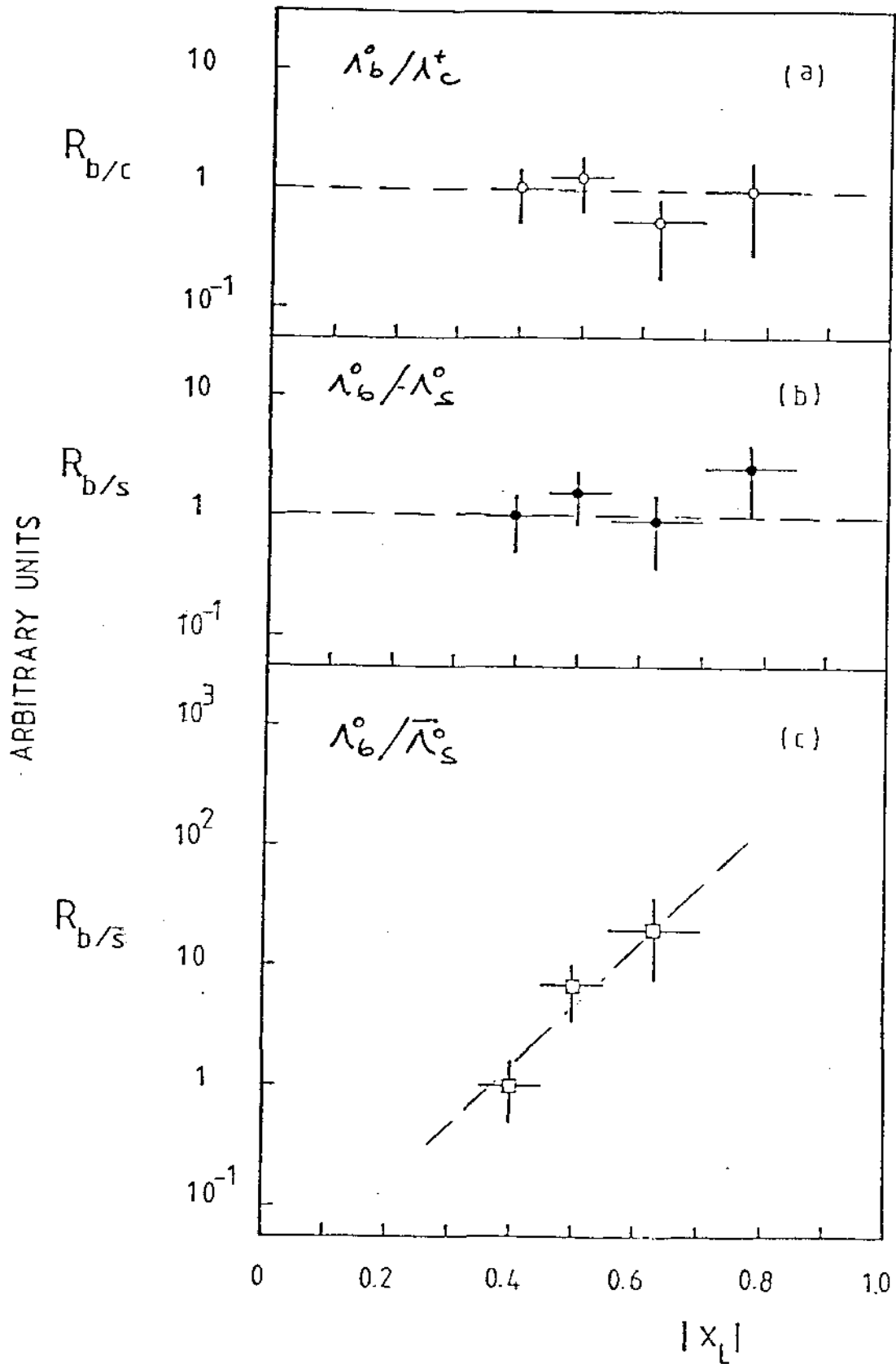
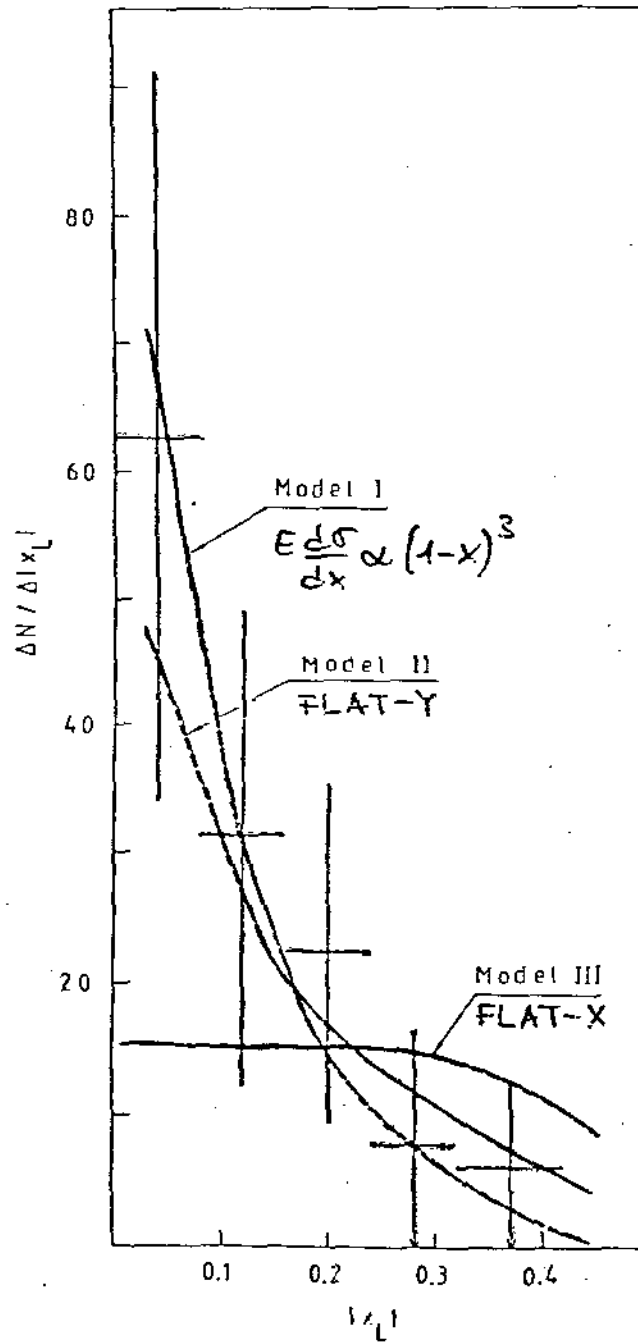
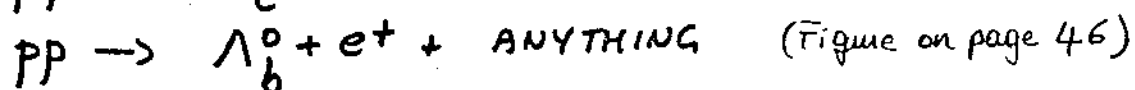
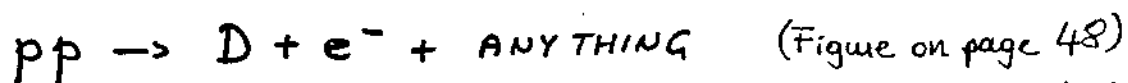


Fig. 2

EXPERIMENTAL x_L DISTRIBUTION OF D^0 

THE PRODUCTION DISTRIBUTIONS OF BARYON AND MESON STATES.

ISR RESULTS ON THE REACTIONS :



INDICATE FOR THE LONGITUDINAL MOMENTUM DISTRIBUTION

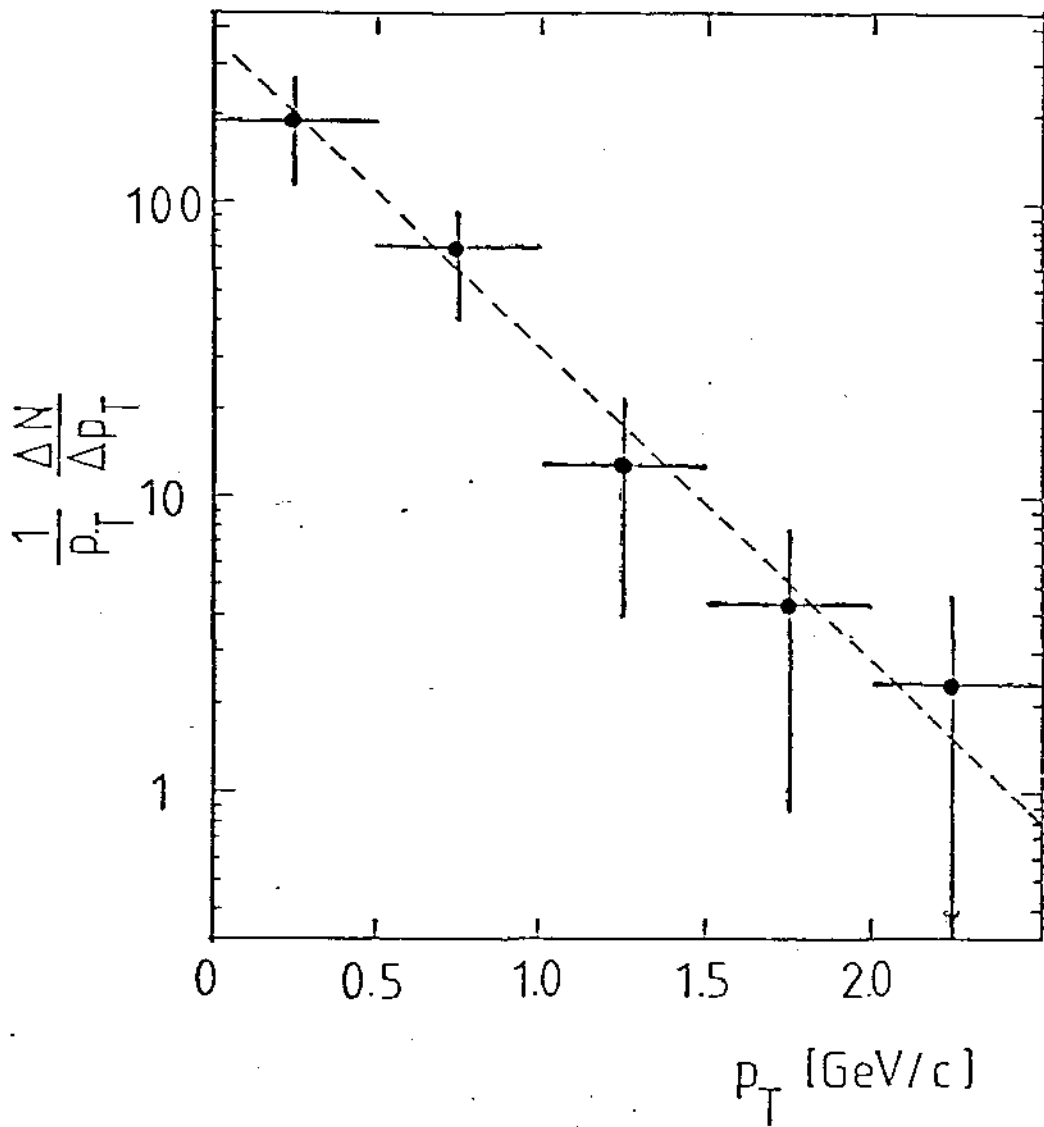
$$\left(\frac{d\sigma}{dx} \sim \text{CONST FOR HEAVY FLAVOURED BARYONS} \right. \\ \left. (\text{i.e. A RATHER FLAT } x\text{-DISTRIBUTION}) \right)$$

$$\left(E \frac{d\sigma}{d|x|} \sim (1-|x|)^3 \text{ FOR HEAVY FLAVOURED MESONS} \right. \\ \left. (\text{i.e. A SOFTER } x\text{-DISTRIBUTION}) \right),$$

AND, FOR THE TRANSVERSE MOMENTUM DISTRIBUTION :

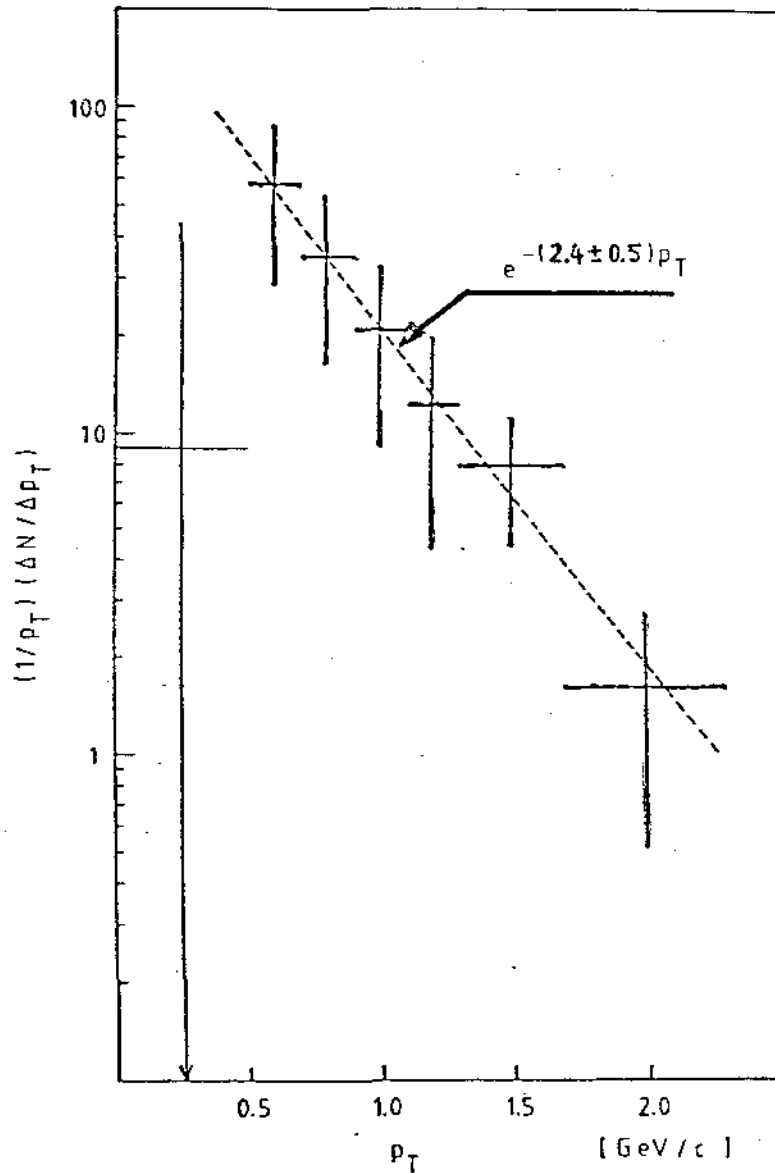
$$\left(\frac{d\sigma}{dp_T} \sim p_T \cdot e^{-2.5 p_T} \text{ FOR BOTH BARYONS AND} \right. \\ \left. \text{MESONS.} \right. \\ \left. (\text{Figures on pages 50 and 51}) \right)$$

THESE DISTRIBUTIONS WILL BE ASSUMED ALL ALONG THE FOLLOWING DISCUSSION.

EXPERIMENTAL p_T DISTRIBUTION OF Λ_c^+ 

$$\frac{1}{p_T} \frac{\Delta N}{\Delta p_T} \propto e^{-b p_T}$$

$$b = 2.5 \pm 0.4$$

EXPERIMENTAL p_T DISTRIBUTION OF D^0 

$$\begin{array}{l} \text{IN} \\ \text{OUT} \end{array} \quad \begin{array}{l} e^{-(3.06 \pm 0.25) p_T} \\ e^{-(3.75 \pm 0.26) p_T} \end{array}$$

$$\langle p_T \rangle \cong 900 \text{ MeV}/c^2$$

THE RELATIVE YIELD OF MESONS AND BARYONS

IN (PP) COLLISIONS THE FOLLOWING REACTIONS DOMINATE (L = LEADING, C = CENTRAL PRODUCTION):

$$(L) P_1 P_2 \rightarrow \bar{\pi}_{\text{CENTRAL}} + (B_{\text{LEADING}})_1 + \text{ANY} \equiv \{ \bar{\pi}_C; B_{L_1} \}$$

$$(L) P_1 P_2 \rightarrow \bar{\pi}_{\text{CENTRAL}} + (B_{\text{LEADING}})_2 + \text{ANY} \equiv \{ \bar{\pi}_C; B_{L_2} \}$$

$$(C) P_1 P_2 \rightarrow \bar{\pi}_{\text{CENTRAL}} + \pi_{\text{CENTRAL}} + \text{ANY} \equiv \{ \bar{\pi}_C; \pi_C \}$$

IN (P \bar{P}) COLLISIONS, DUE TO THE PRESENCE OF AN ANTI-FLAVOURED ANTI-BARYONIC STATE, OTHER LEADING REACTIONS CAN OCCUR:

$$(L) P_1 \bar{P}_2 \rightarrow \bar{\pi}_{\text{CENTRAL}} + (B_{\text{LEADING}})_1 + \text{ANY} \equiv \{ \bar{\pi}_C; B_{L_1} \}$$

$$(L) P_1 \bar{P}_2 \rightarrow \pi_{\text{CENTRAL}} + (\bar{B}_{\text{LEADING}})_2 + \text{ANY} \equiv \{ \pi_C; \bar{B}_{L_2} \}$$

$$(L) P_1 \bar{P}_2 \rightarrow (B_{\text{LEADING}})_1 + (\bar{B}_{\text{LEADING}})_2 + \text{ANY} \equiv \{ B_{L_1}; \bar{B}_{L_2} \}$$

$$(C) P_1 \bar{P}_2 \rightarrow \pi_{\text{CENTRAL}} + \bar{\pi}_{\text{CENTRAL}} + \text{ANY} \equiv \{ \pi_C; \bar{\pi}_C \}$$

THE INDICES (1,2) ARE REDUNDANT IN THE (P \bar{P}) CASE AND WILL BE OMITTED FROM NOW ON.

THE RELATIVE YIELDS FOR THE PRODUCTION OF CENTRAL MESONS/ANTIMESONS AND OF LEADING BARYONS/ANTIBARYONS, ARE THEREFORE:

$$\left. \begin{aligned} \rho_M &= [\sigma\{M_C; \bar{B}_L\} + \sigma\{M_C; \bar{M}_C\}] / \sigma^T \\ \rho_{\bar{M}} &= [\sigma\{\bar{M}_C; B_L\} + \sigma\{\bar{M}_C; M_C\}] / \sigma^T \end{aligned} \right\} 1 - \frac{\text{LEADING}}{\text{TOTAL}}$$

$$\left. \begin{aligned} \rho_B &= [\sigma\{\bar{M}_C; B_L\} + \sigma\{B_L; \bar{B}_L\}] / \sigma^T \\ \rho_{\bar{B}} &= [\sigma\{M_C; \bar{B}_L\} + \sigma\{B_L; \bar{B}_L\}] / \sigma^T \end{aligned} \right\} \frac{\text{LEADING}}{\text{TOTAL}}$$

WITH

$\sigma^T = \text{TOTAL CROSS SECTION} =$

$$= \sigma\{\bar{M}_C; B_L\} + \sigma\{M_C; \bar{B}_L\} + \sigma\{\bar{M}_C; M_C\} + \sigma\{B_L; \bar{B}_L\}$$

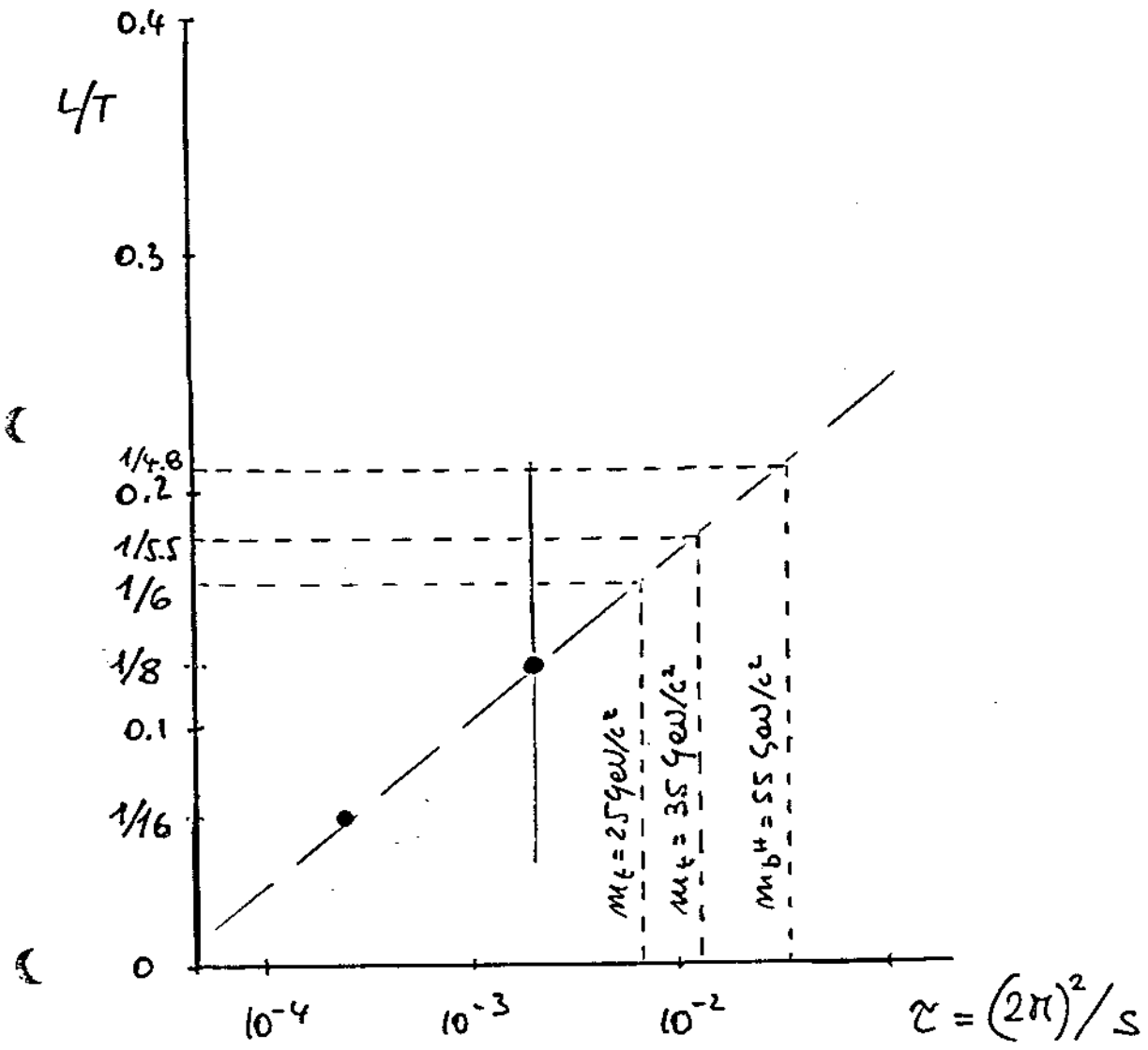
AT THE ISR, THE RATIO LEADING/TOTAL IS:

$$\sim 1/16 \quad \text{FOR STRANGENESS}$$

$$\sim 1/8 \quad \text{FOR CHARM}$$

IN OUR DISCUSSION WE WILL STUDY THE BEHAVIOUR OF THE LEPTON ASYMMETRY A° AS A FUNCTION OF THE RATIO LEADING/TOTAL 1.37

\sqrt{s}	2π	$\frac{\text{LEADING}}{\text{TOTAL}}$	$\tau = \frac{(2\pi)^2}{s}$
60 GeV (ISR)	(strange) 1 GeV	1/16	$\sim 2.5 \times 10^{-4}$
	(charm) 3 GeV	1/8	$\sim 2 \times 10^{-3}$
600 GeV (SP \bar{P} S)	(beauty) 10 GeV	1/16	$\sim 2.5 \times 10^{-4}$ as strange at ISR
	30 GeV	1/8	$\sim 2 \times 10^{-3}$ as charm at ISR
	10^2 GeV	1/4	$\sim 2.5 \times 10^{-2}$



THE LEPTON ASYMMETRY IN AN IDEAL EXPERIMENT.

WITH THE ABOVE MENTIONED ASSUMPTIONS
WE HAVE EVALUATED THE LEPTON ASYMMETRY
FOR

a-) $m_t = 25 \text{ GeV}/c^2$ $m_b = 55 \text{ GeV}/c^2$

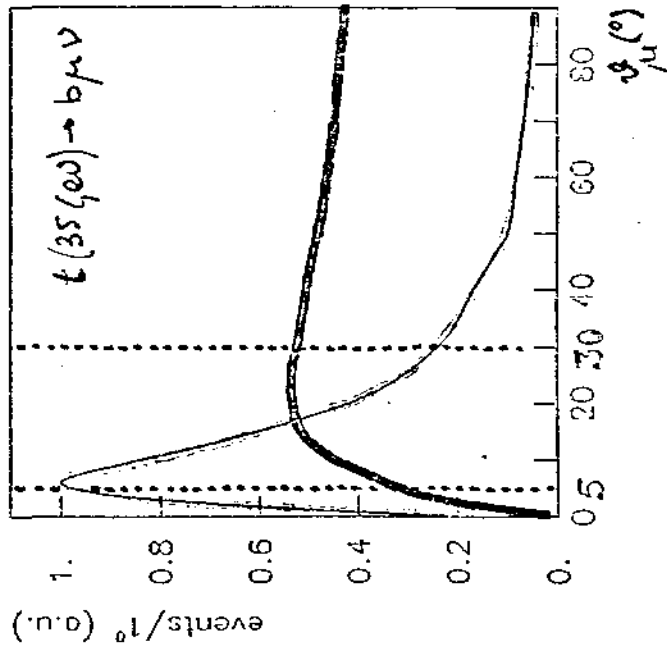
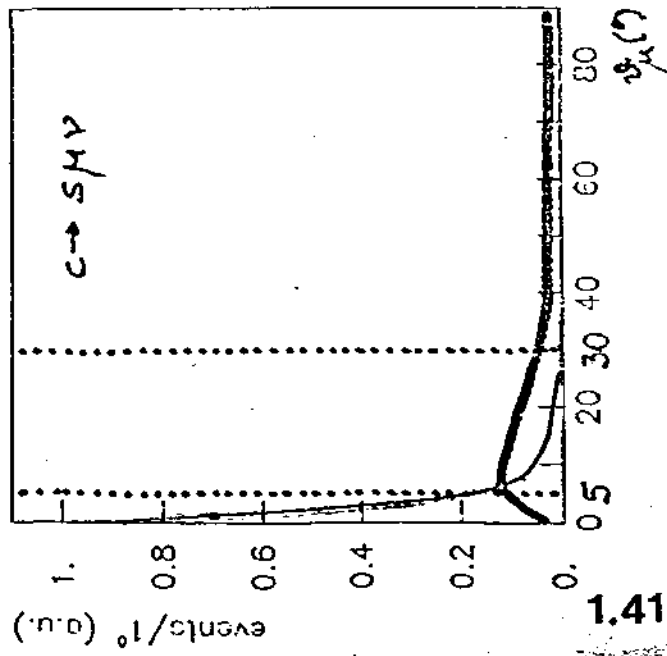
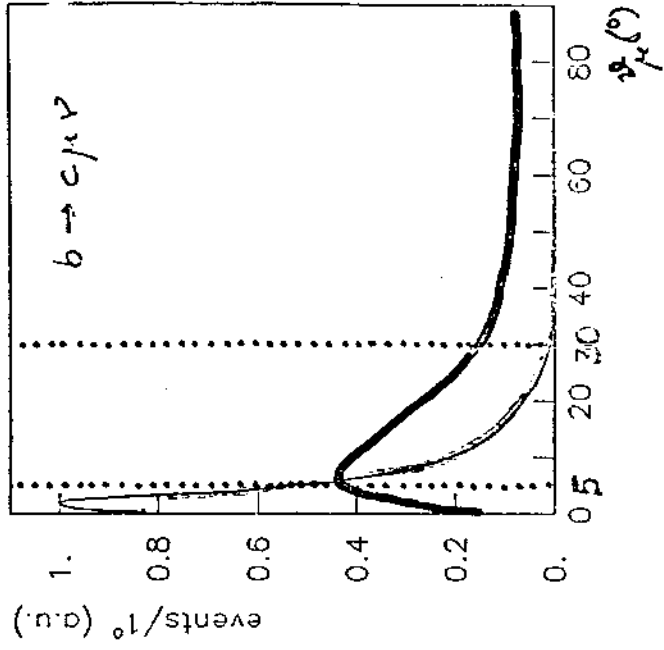
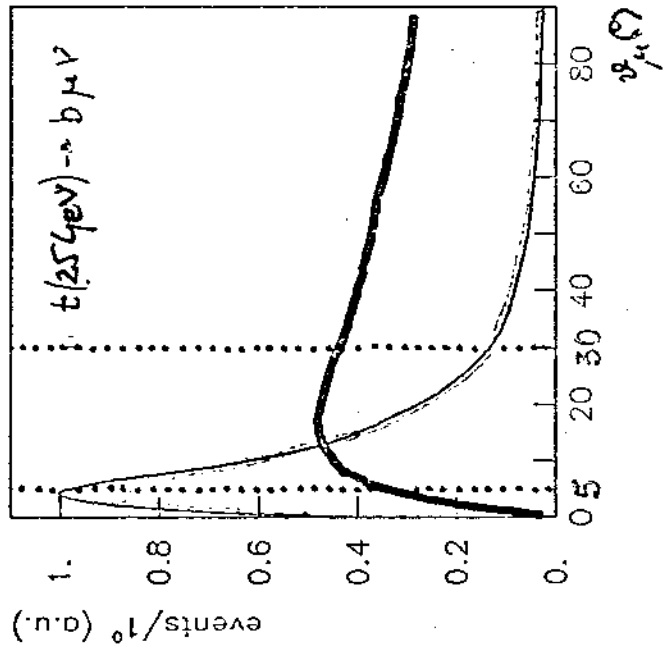
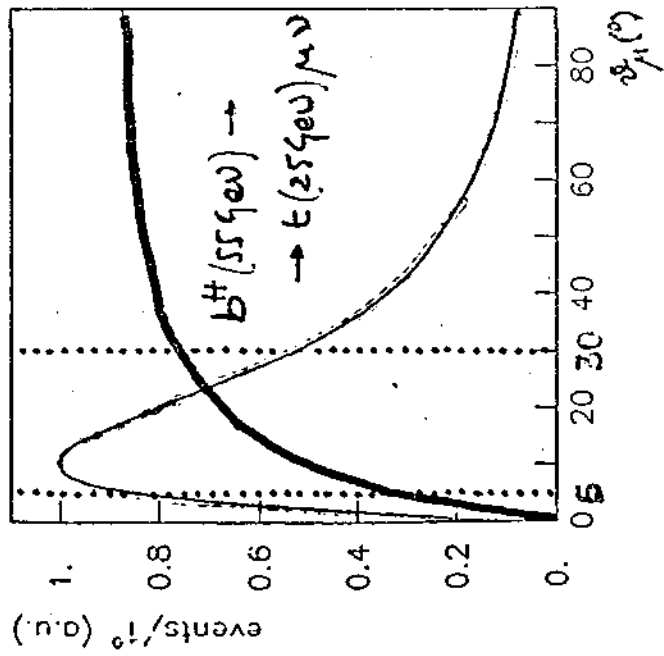
b-) $m_t = 35 \text{ GeV}/c^2$

AS MEASURED BY AN IDEAL EXPERIMENT
CAPABLE OF DETECTING MUONS IN THE
AZIMUTHAL AND POLAR INTERVALS

$$0^\circ \leq \theta \leq 30^\circ$$

$$0 \leq \phi \leq 360^\circ.$$

IN THE FOLLOWING TRANSPARENCIES SOME
OF THE RESULTS FROM THIS MONTE CARLO
SIMULATION ARE SHOWN.



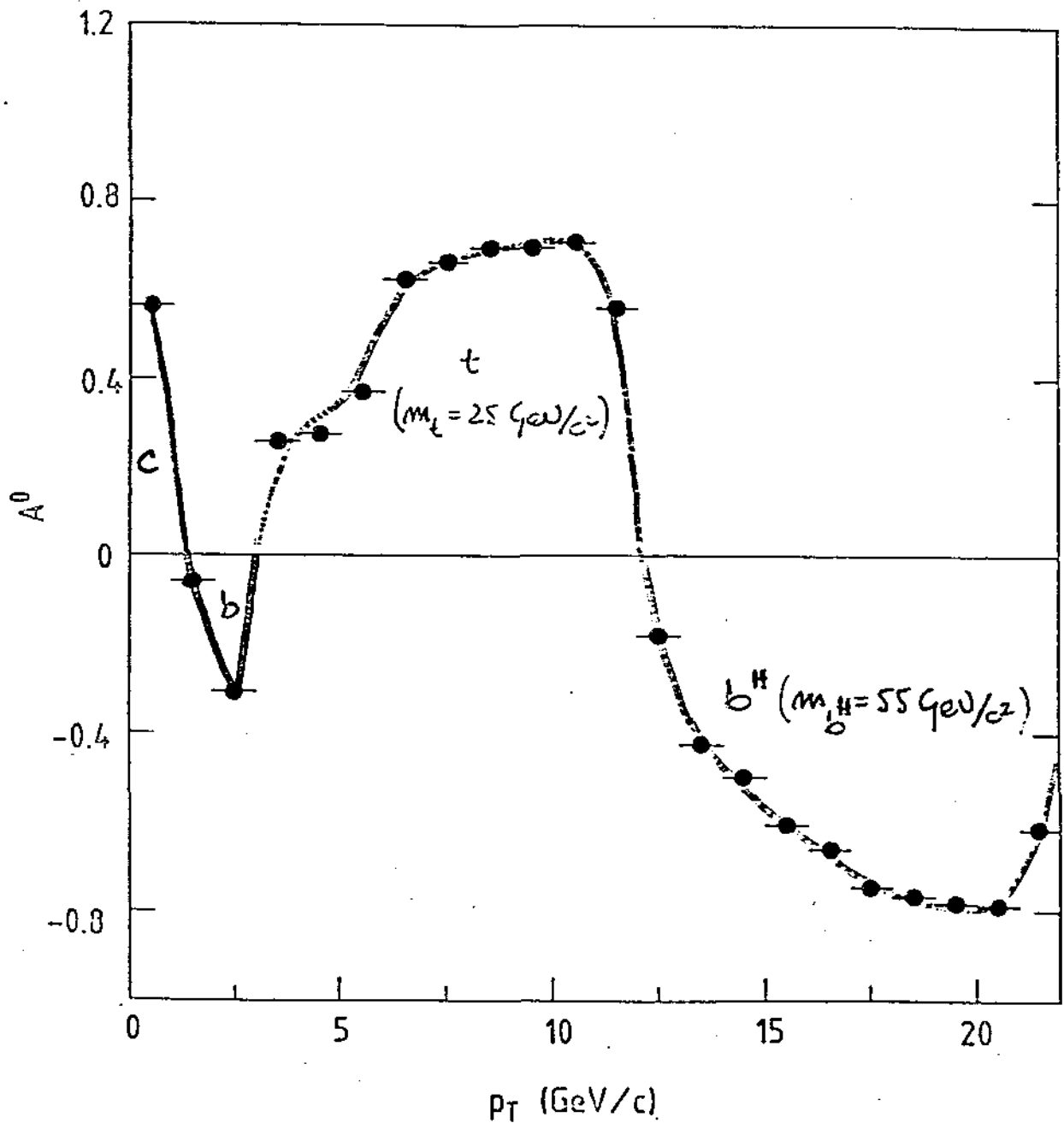
ANGULAR DISTRIBUTION OF MUONS FROM PRIMARY DECAYS OF BARYONS AND MESONS

— BARYONS
 — MESONS
 (... ACCEPTANCE OF THE PROPOSED APPARATUS)

THE SPECTRA FROM BARYONS AND MESONS ARE NORMALIZED TO 0.25 (LEADING/TOTAL) = 0.25

THE LEPTON ASYMMETRY A^0 COMPUTED IN THE
CONDITIONS SPECIFIED BELOW :

$$s_{\text{cut}}^{\text{MAX}} = 30^\circ, (\text{Leading/Total}) = 0.25$$



THE PEAK POSITIONS DEPEND ON THE MASS
DIFFERENCES IN THE DECAY

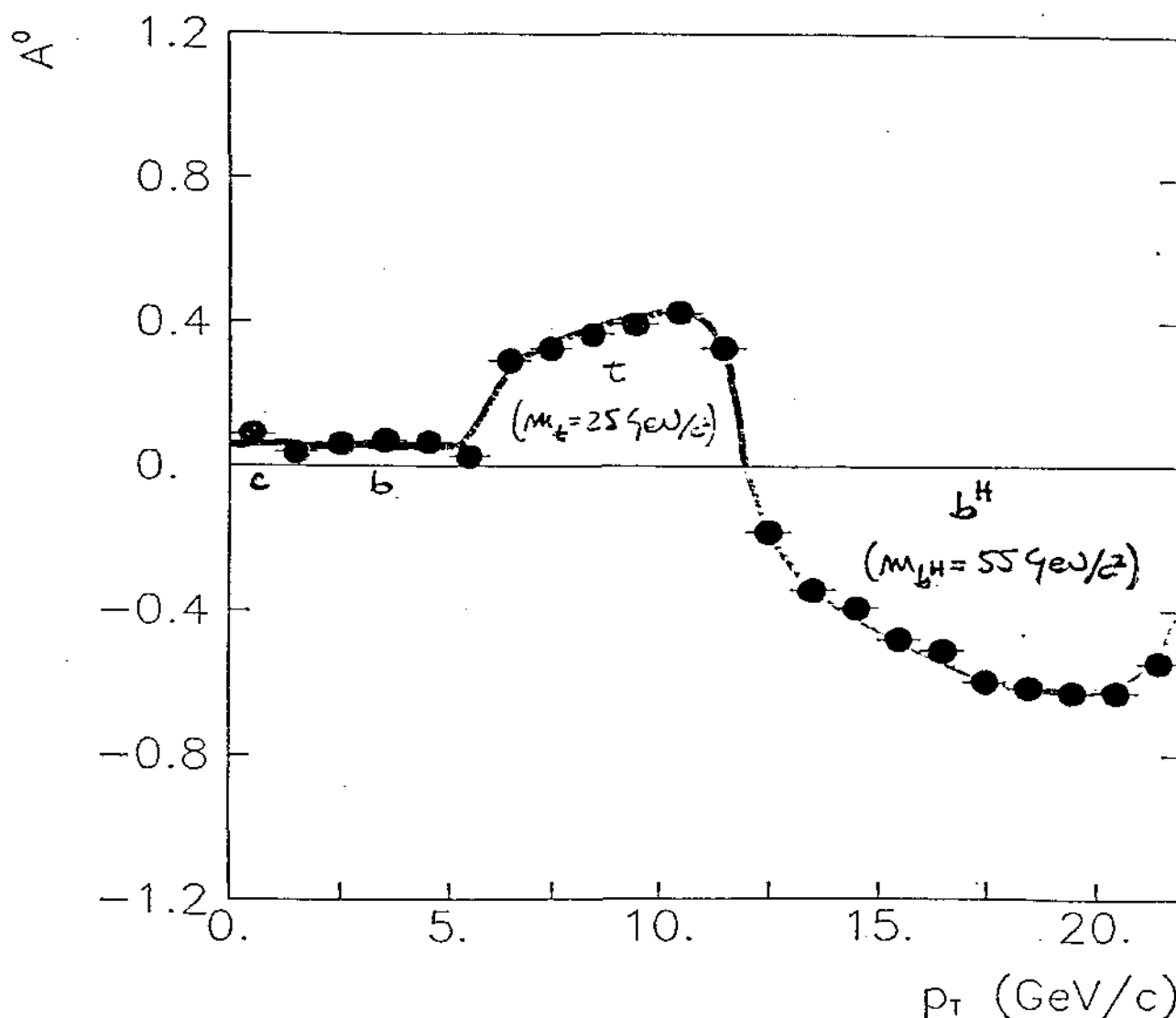
THE EXPERIMENTAL LEPTON ASYMMETRY

IN ORDER TO EVALUATE THE LEPTON ASYMMETRY
IN A REAL EXPERIMENT, TWO FACTORS
NEED TO BE TAKEN INTO ACCOUNT:

- 1- THE DETECTOR ACCEPTANCE
- 2- THE BACKGROUND LEVEL AS DETERMINED
BY PHYSICS AND BY THE APPARATUS
REJECTION POWER.

THE EFFECT OF THE ANGULAR CUT
 THE LEPTON ASYMMETRY A° COMPUTED IN THE
 ANGULAR REGION DEFINED BY THE APPARATUS

$$5^\circ \leq \theta \leq 30^\circ$$



THE EFFECT OF THE LOWER CUT IN THE ANGULAR
 COVERAGE OF THE APPARATUS IS TO MAKE DISAPPEAR
 THE ASYMMETRY DUE TO CHARM AND BEAUTY.
 THE LEPTON ASYMMETRY REMAINS SUPERB FOR
 HEAVIER FLAVOURS.

- ③ BACKGROUND DUE TO MUONS PRODUCED BY π AND K DECAY:

EXTRAPOLATION OF UA1 DATA

$$\bar{c} \frac{d^3\sigma}{dp^3} = A p_0^m / (p_0 + p_T)^m \quad \left[\text{FOR } \frac{h^+ + h^-}{2}, |y| < 2.5 \right]$$

$$(A = 0.37 \text{ mb c}^2 \text{ GeV}^{-2}; p_0 = 1.49 \text{ GeV}/c; m = 9.87)$$

INTEGRATED IN THE RAPIDITY INTERVAL:

$$1.3 \leq y \leq 3.1$$

USING A K/π RATIO OF $\approx 1/2$.

THE EXTRAPOLATED HADRON RATES HAVE BEEN MULTIPLIED BY THE DECAY PROBABILITY IN THE APPARATUS.

- ④ BACKGROUND FROM PROMPT MUON SOURCES OTHER THAN HEAVY FLAVOURS, i.e. W^\pm, Z^0 .

THIS BACKGROUND IS RELEVANT ONLY FOR $p_T \gtrsim 20 \text{ GeV}/c$ AND CAN BE ELIMINATED BY IDENTIFYING THE W^\pm OR Z^0 'S.

THE ASYMMETRY CAN BE DEFINED EXPERIMENTALLY AS:

$$A^{\text{exp}} = \frac{N^T(\mu^+) - N^T(\mu^-)}{N^T(\mu^+) + N^T(\mu^-)}$$

WHERE: $N^T(\mu^\pm)$ = TOTAL NUMBER OF μ^\pm SEEN IN THE APPARATUS.

SUBTRACTING THE BACKGROUND FROM A^{exp} WE HAVE:

$$A_{\text{exp}}^{\circ} = \frac{[N^T(\mu^+) - N_b^{\text{calc.}}(\mu^+)] - [N^T(\mu^-) - N_b^{\text{calc.}}(\mu^-)]}{[N^T(\mu^+) - N_b^{\text{calc.}}(\mu^+)] + [N^T(\mu^-) - N_b^{\text{calc.}}(\mu^-)]}$$

WHERE: $N_b^{\text{calc.}}(\mu^\pm)$ = NUMBER OF CALCULATED μ^\pm FROM BACKGROUND

IN THE DETERMINATION OF A_{exp}° TWO ERRORS ON BACKGROUND

CONTRIBUTES:

$\Delta [N_b^{\text{calc.}}(\mu^+) + N_b^{\text{calc.}}(\mu^-)]$ ABSOLUTE BACKGROUND LEVEL
(assumed $\sim 20\%$)

$\Delta \left[\frac{N_b^{\text{calc.}}(\mu^+) - N_b^{\text{calc.}}(\mu^-)}{N_b^{\text{calc.}}(\mu^+) + N_b^{\text{calc.}}(\mu^-)} \right]$ CHARGE ASYMMETRY ON THE
BACKGROUND
(assumed $\sim 10\%$)

↑
in the following

t ($m_t = 25 \text{ GeV}/c^2$)

AND

b^H ($m_{b^H} = 55 \text{ GeV}/c^2$)

$5. \leq \theta < 30.$

$\Delta p_T / p_T = 20. \%$

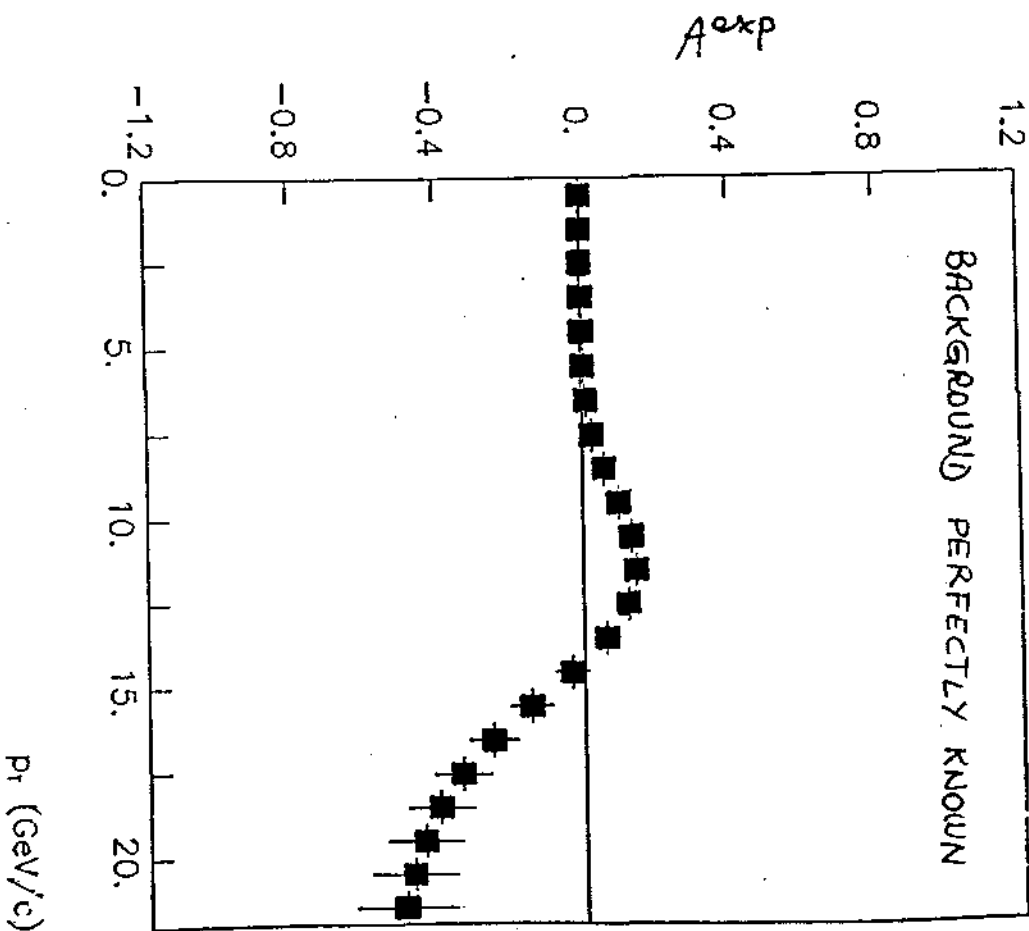
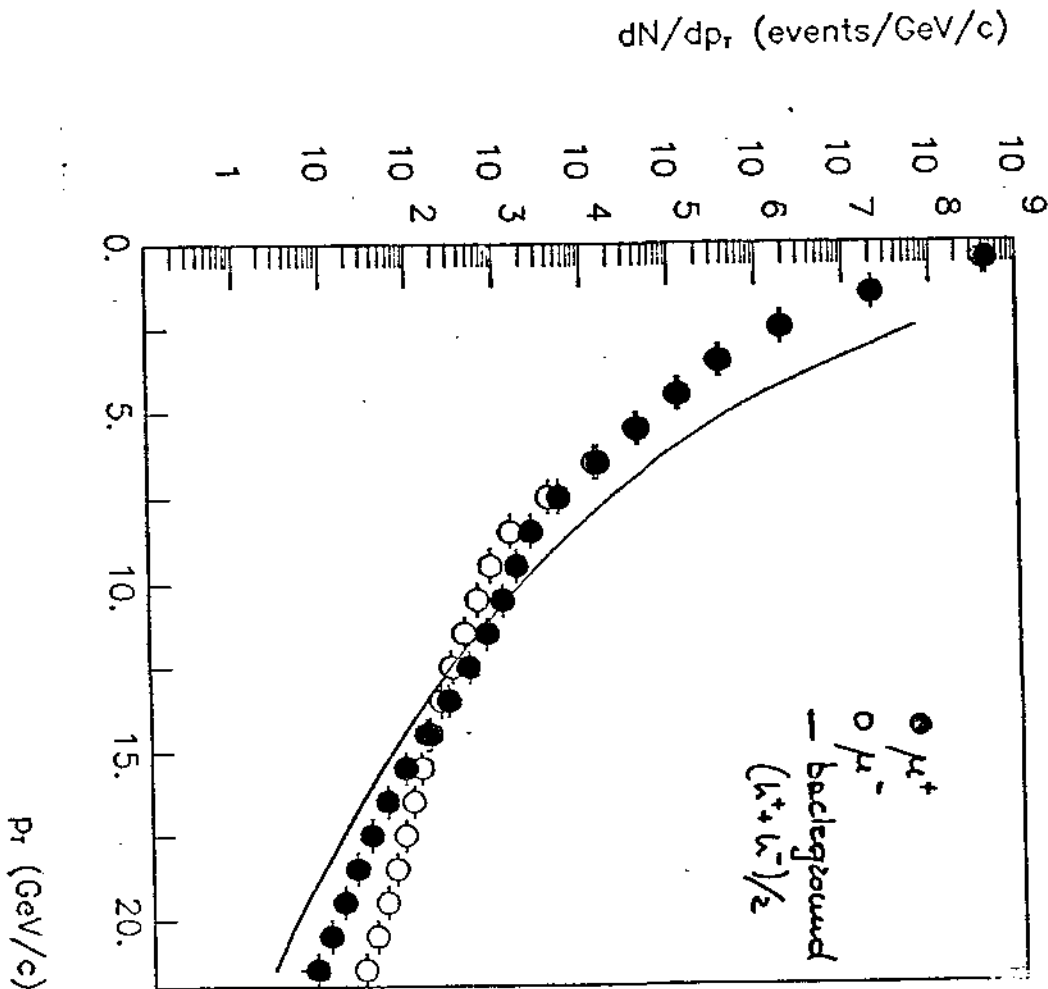
(LEADING/TOTAL) = .25

$\sigma_{b^H} = .0100 \mu\text{b}, \sigma_t = .1000 \mu\text{b}$

PRODUCTION BARYONS = $x - \text{fluct.}$, MESONS = $(1-x)^2$

$$\int L dt = 10 \text{ pb}^{-1}$$

DECAY 3-body



t ($m_t = 25 \text{ GeV}/c^2$) AND b^H ($m_{b^H} = 55 \text{ GeV}/c^2$)

$5. \leq \eta < 30.$

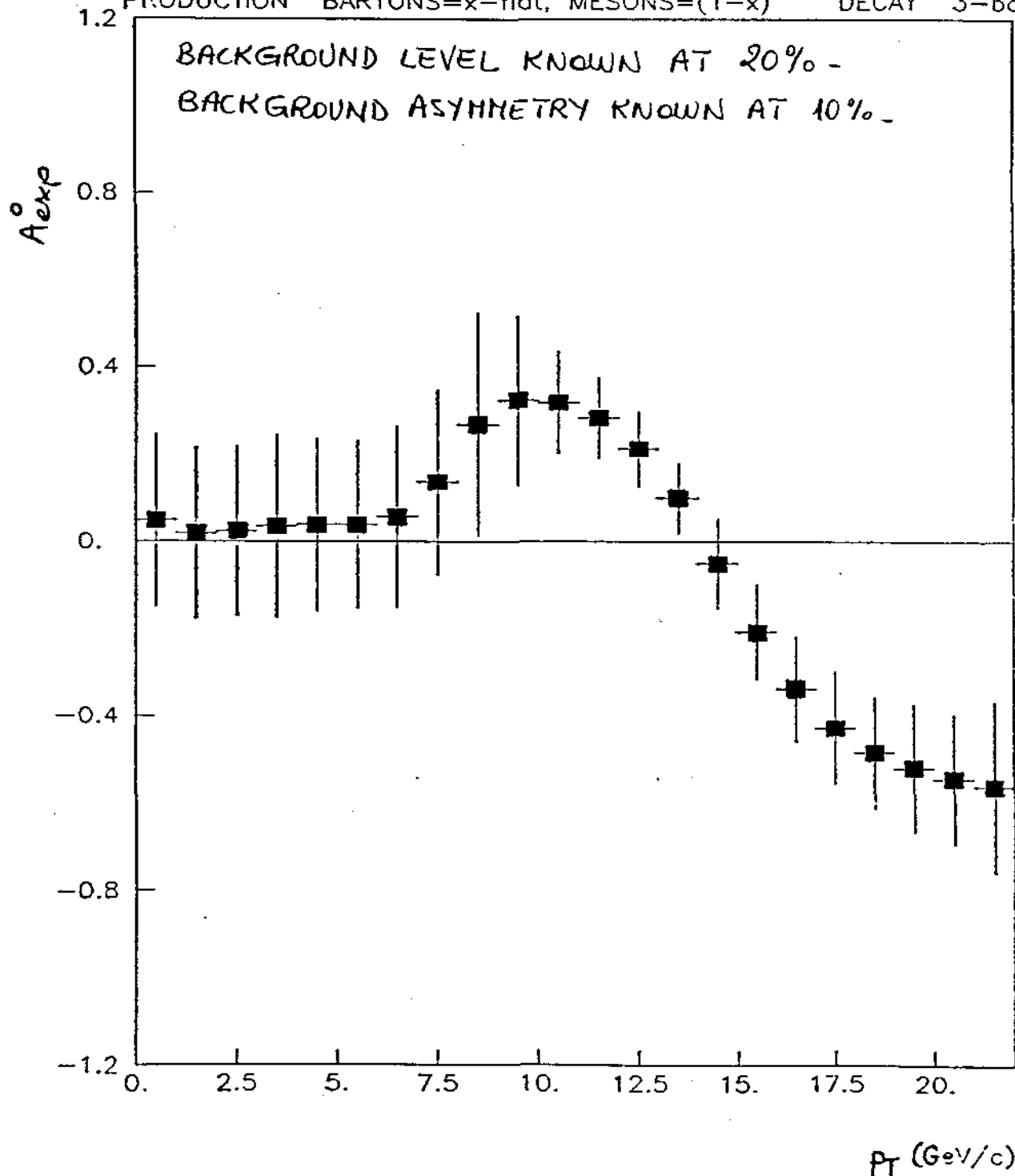
$\Delta p_T/p_T = 20\%$

(LEADING/TOTAL) = .25

$\sigma_{b^H} = .0100 \mu\text{b.}$ $\alpha_t = .1000 \mu\text{b}$

$\int L dt = 10 \text{ pb}^{-1}$

PRODUCTION BARYONS = x -flat, MESONS = $(1-x)^3$ DECAY 3-body



$t (m_T = 35 \text{ GeV}/c^2)$

$5. \leq \eta < 30.$

$\Delta p_T / p_T = 20. \%$

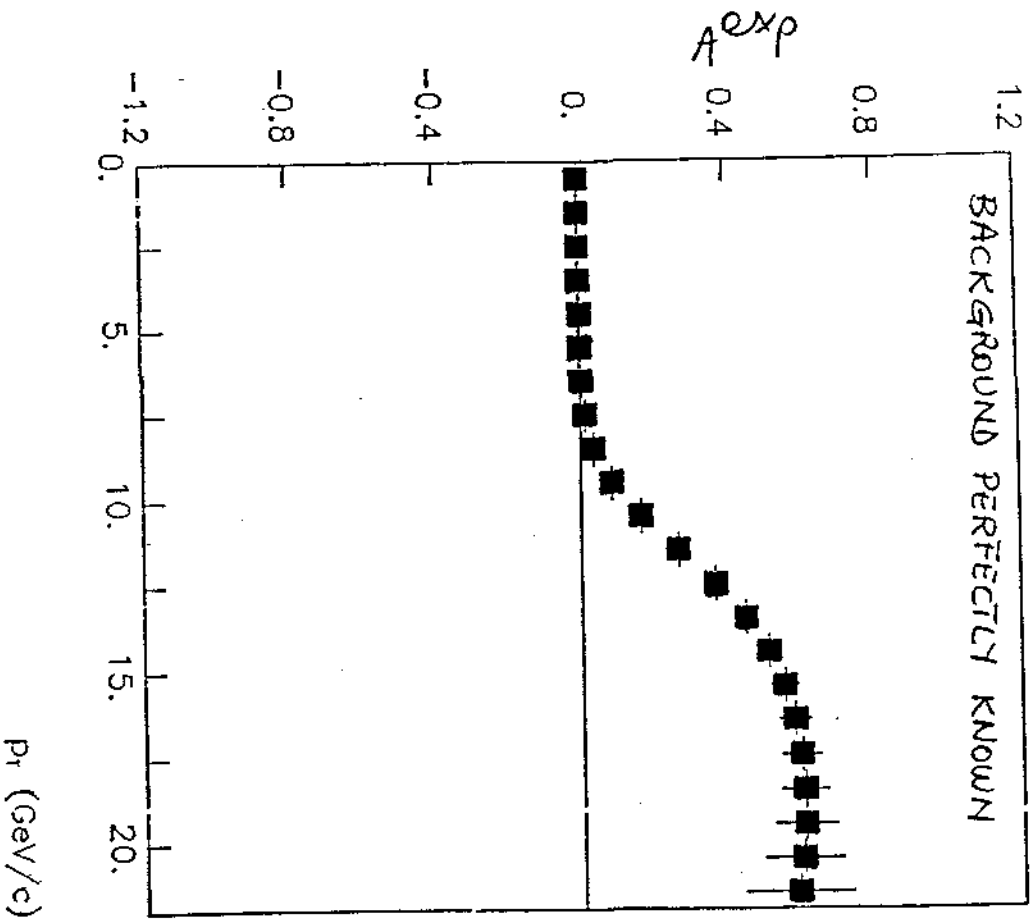
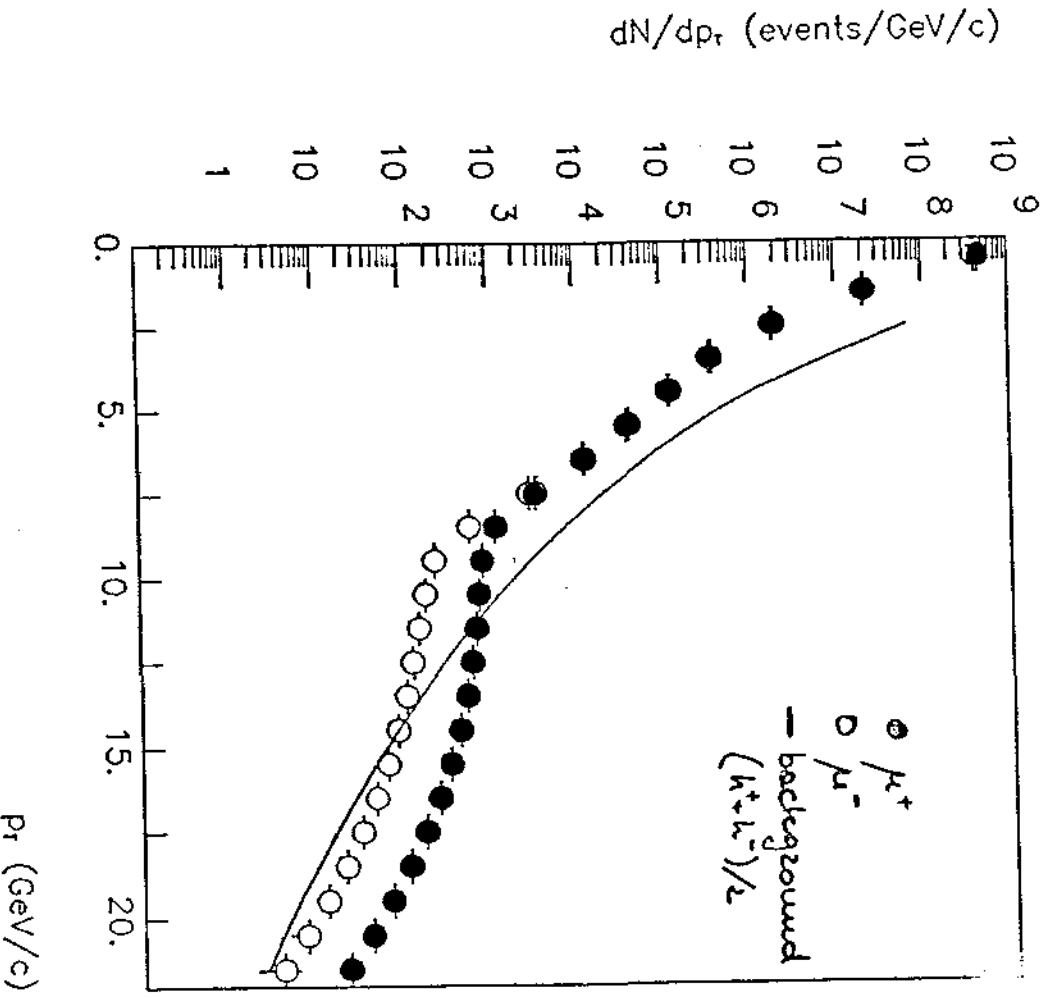
(LEADING/TOTAL) = .25

$\sigma_1 = .0500 \mu\text{b}$

PRODUCTION BARYONS = $x - \text{flat}$, MESONS = $(1-x)^2$

$\int L dt = 10 \text{ pb}^{-1}$

DECAY 3-body



$$t (m_t = 35 \text{ GeV}/c^2)$$

$$5. \leq \vartheta < 30.$$

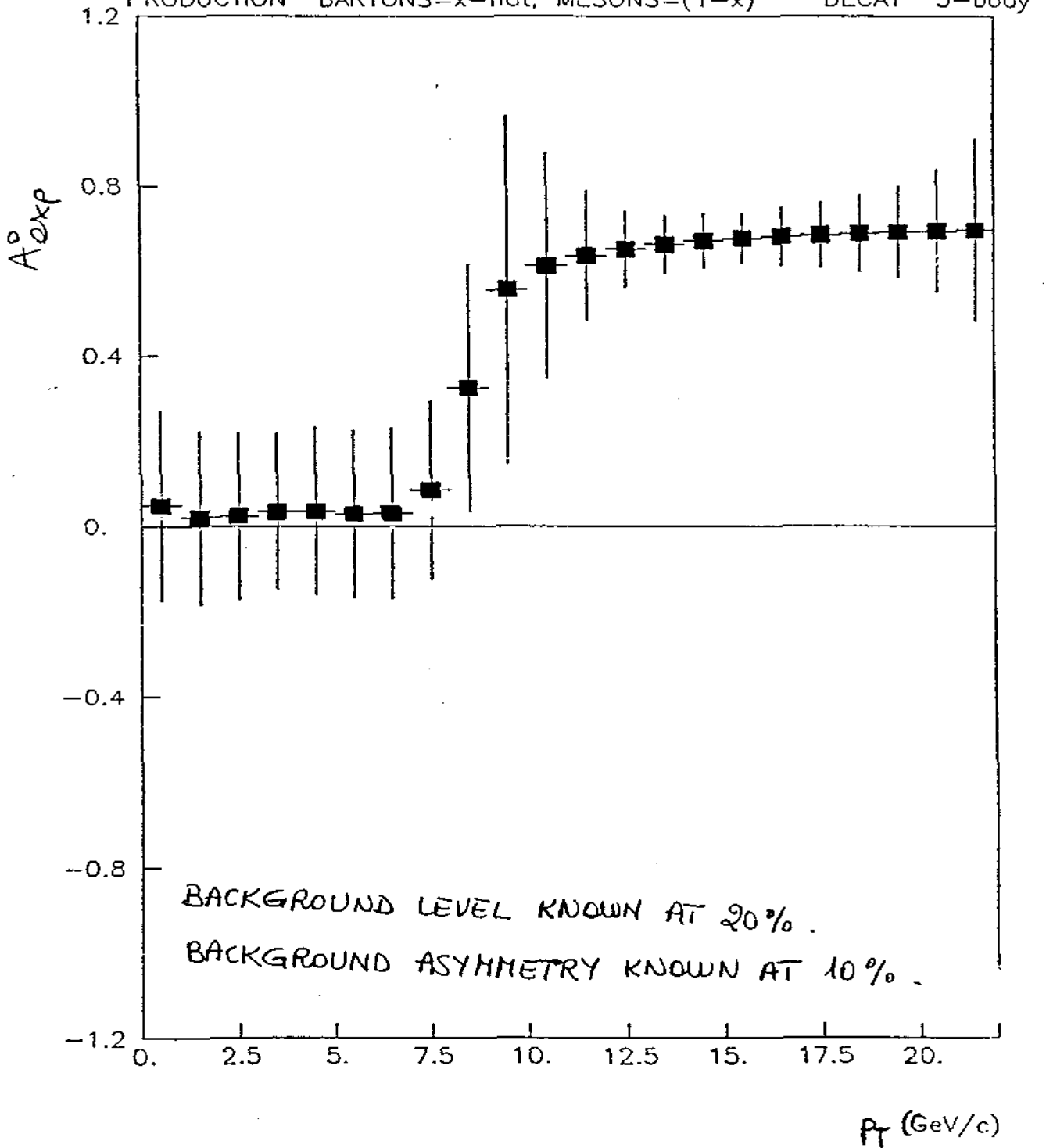
$$\Delta p_T / p_T = 20. \%$$

$$(\text{LEADING/TOTAL}) = .25$$

$$\sigma_t = .0500 \mu\text{b}$$

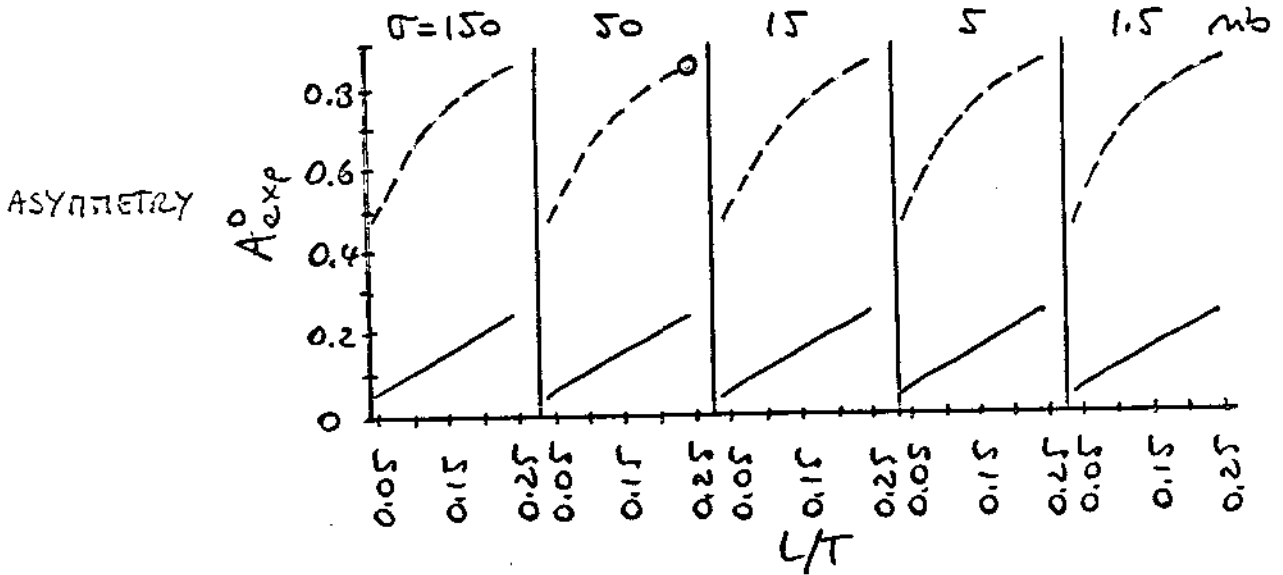
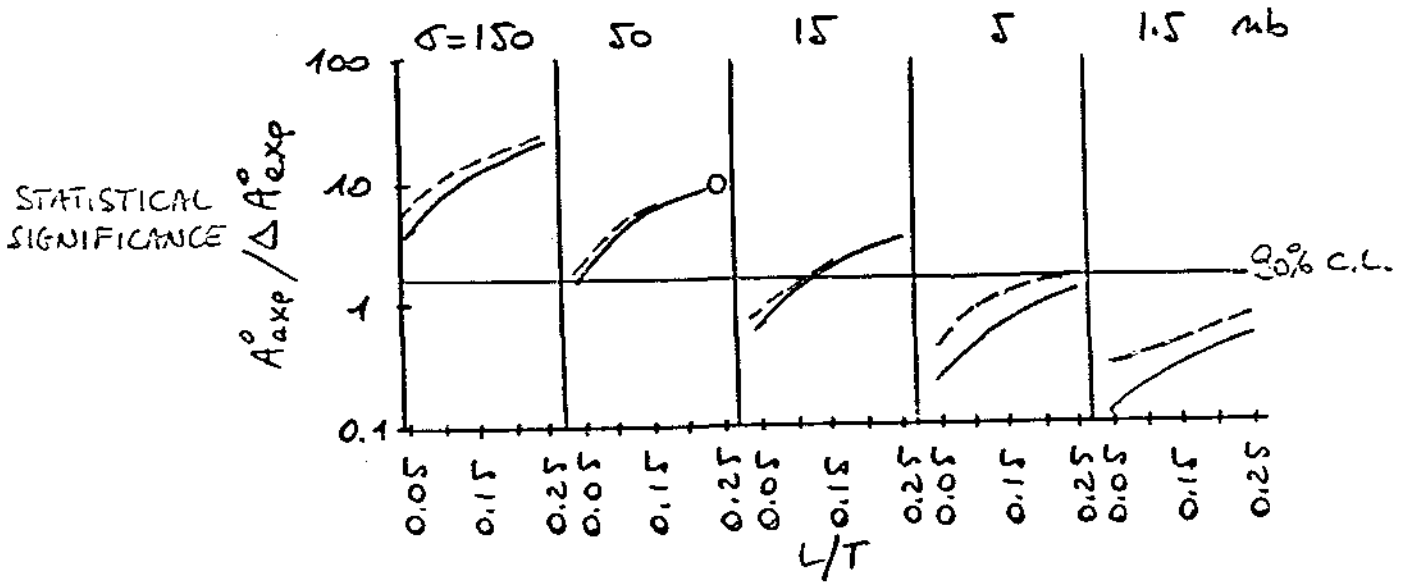
$$\int \mathcal{L} dt = 10 \text{ pb}^{-1}$$

PRODUCTION BARYONS = x -flat, MESONS = $(1-x)^3$ DECAY 3-body



TOP ($m_t = 35 \text{ GeV}/c^2$) A_{exp}^0

ASYMMETRY AND STATISTICAL SIGNIFICANCE AS FUNCTION OF CROSS SECTION, LEADING/TOTAL AND PRODUCTION DISTRIBUTIONS.



BARYONS

MESONS

$$\int L dt = 10 \text{ pb}^{-1}$$

$$\Delta P_T / P_T = 20\%$$

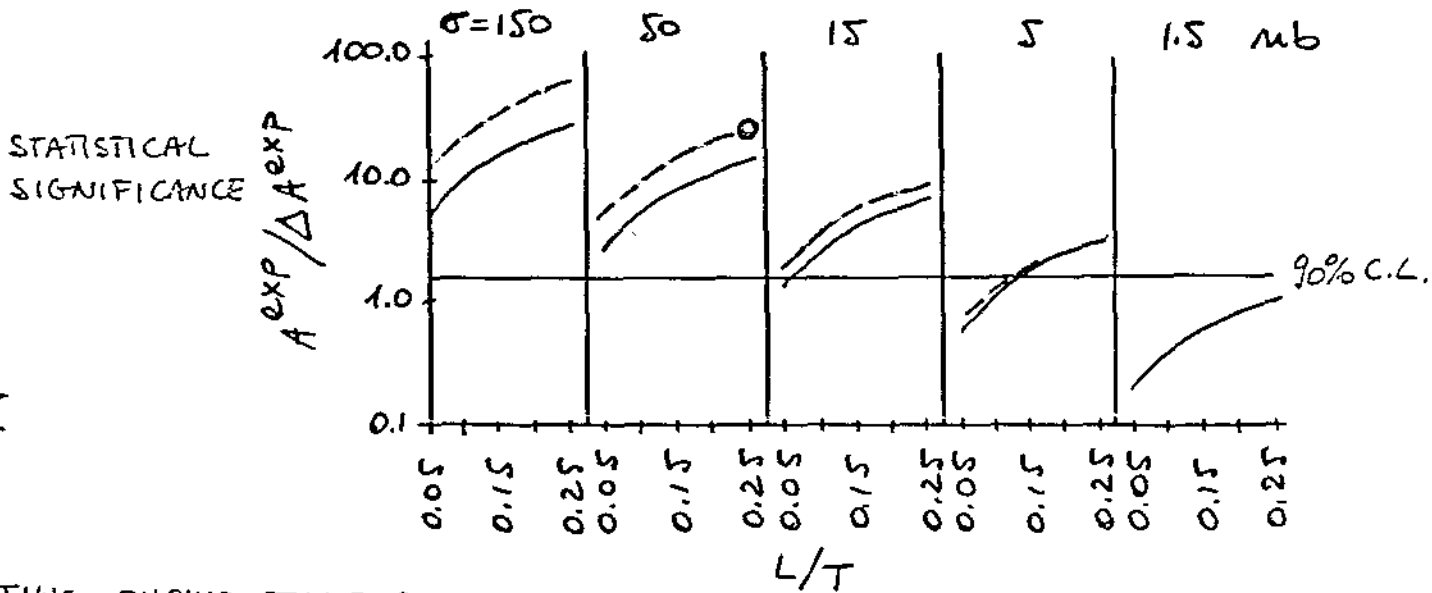
$$\frac{d\sigma}{dx} = \text{const.}$$

$$E \frac{d\sigma}{dx} \propto (1-x)^3$$

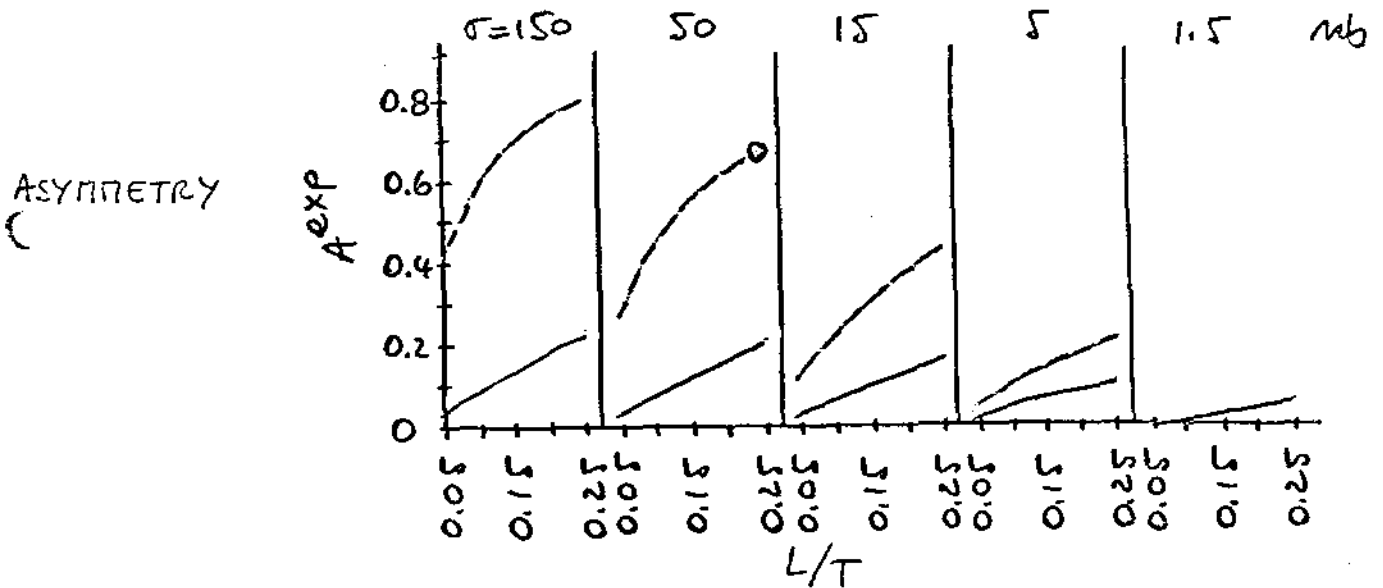
$$\frac{d\sigma}{dx} \propto (1-x)$$

68 TOP ($m_t = 35 \text{ GeV}/c^2$) A^{exp}

ASYMMETRY AND STATISTICAL SIGNIFICANCE AS FUNCTION OF CROSS SECTION, LEADING/TOTAL AND PRODUCTION DISTRIBUTIONS.



THIS SHOWS THAT BETTER KNOWLEDGE OF THE BACKGROUND IS ESSENTIAL TO IMPROVE THE KNOWLEDGE OF ASYMMETRY.



BARYONS

RESONS

$$\int L dt = 10 \text{ pb}^{-1}$$

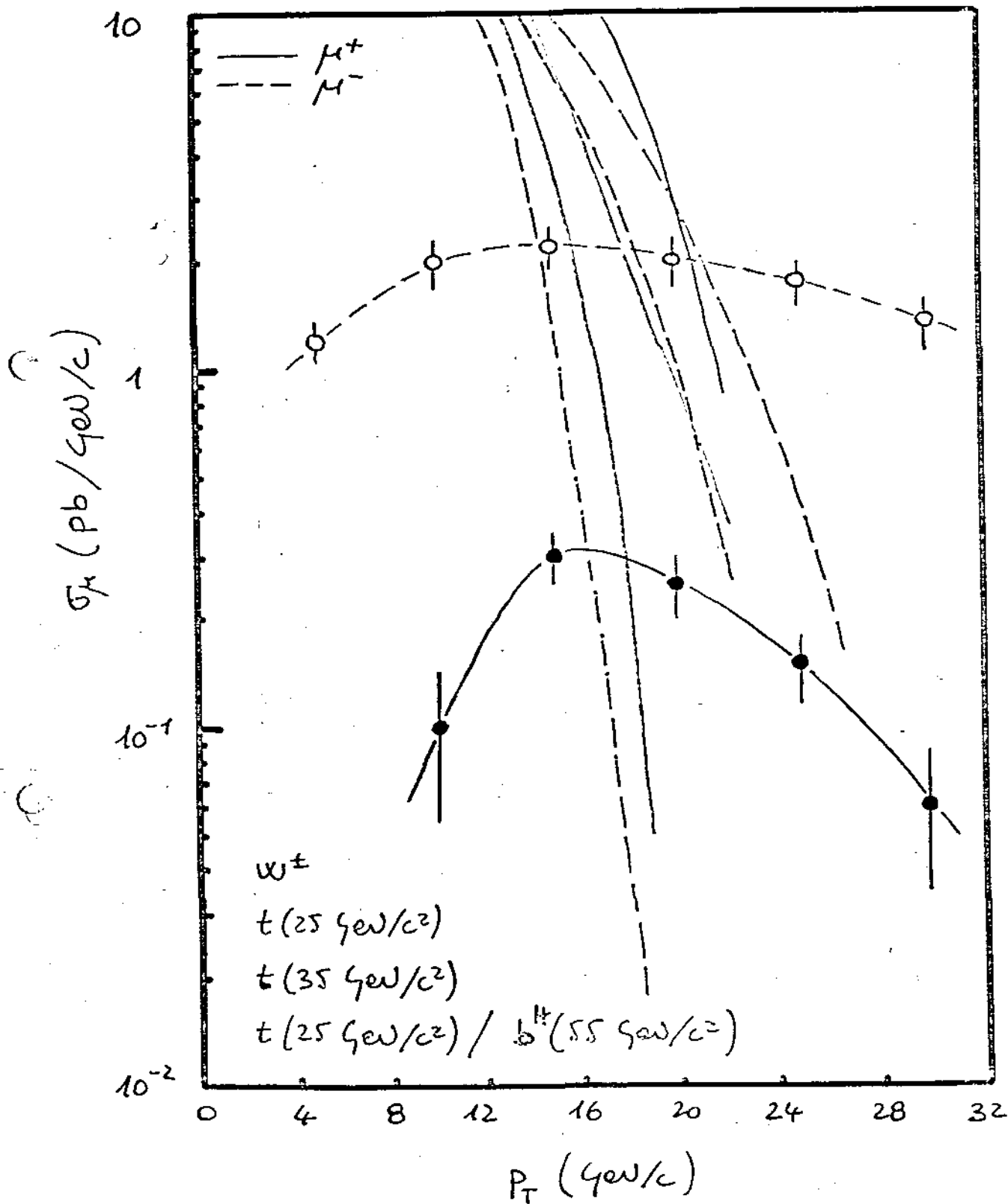
$$\Delta p_T / p_T = 20\%$$

$$\frac{d\sigma}{dx} = \text{const.}$$

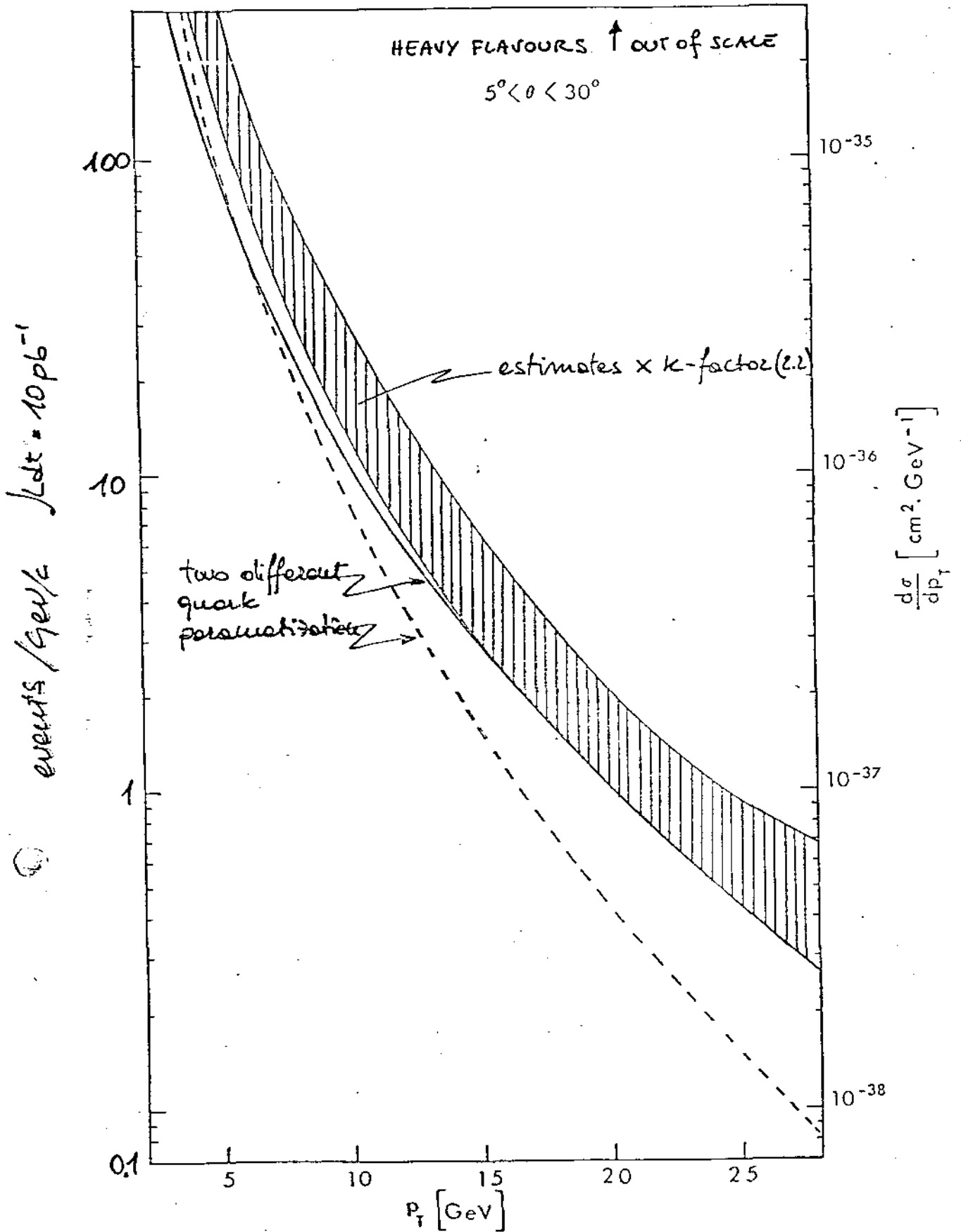
$$\frac{Ed\sigma}{dx} \propto (1-x)^3$$

$$\frac{d\sigma}{dx} \propto (1-x)$$

π ONS FROM $W^\pm \rightarrow \mu^\pm \nu$ IN THE SOLID
 ANGLE DEFINED BY THE APPARATUS



DRELL - YAN



NEGUGIBLE WITH RESPECT TO μ FROM HADRON

1.54 DECAY.

THE BEST WAY TO KNOW THE ASYMMETRY IN THE BACKGROUND MUONS DUE TO A CHARGE ASYMMETRY IN THE PARENT HADRONS (MORE π^+/κ^+ IN THE PROTON HEMISPHERE, MORE π^-/κ^- IN THE ANTI-PROTON HEMISPHERE) IS TO MEASURE THE TOTAL HADRON FLUX IN OUR APPARATUS.

THIS HAS TO BE DONE ALSO TO KNOW THE ABSOLUTE LEVEL OF THE BACKGROUND IN THE EXPERIMENTAL CONDITIONS.








DATA ALREADY EXISTING FROM UA1 (IF STATISTICALLY SUFFICIENT) CAN BE USED TO THIS PURPOSE.

CALORIMETERS LEAKAGE ("SHOWER MUONS")

THE SHOWER DEVELOPMENT MONTECARLO USED IN OUR STUDIES CONNECTED WITH THE ORIGINAL LAA PROPOSAL (CALORIMETER + IRON ABSORBER \Rightarrow $\approx 10 \lambda_0$) GAVE AS RESULT A CONTRIBUTION FROM "SHOWER MUONS" APPROXIMATELY EQUAL IN ABSOLUTE RATE TO THE "DIRECT" HADRON DECAY TO THE BACKGROUND MUONS, BUT DEPRESSED IN ENERGY BY A FACTOR 0.3. AS A RESULT THE CONTRIBUTION OF "SHOWER MUONS" TO THE BACKGROUND WAS VERY SMALL.

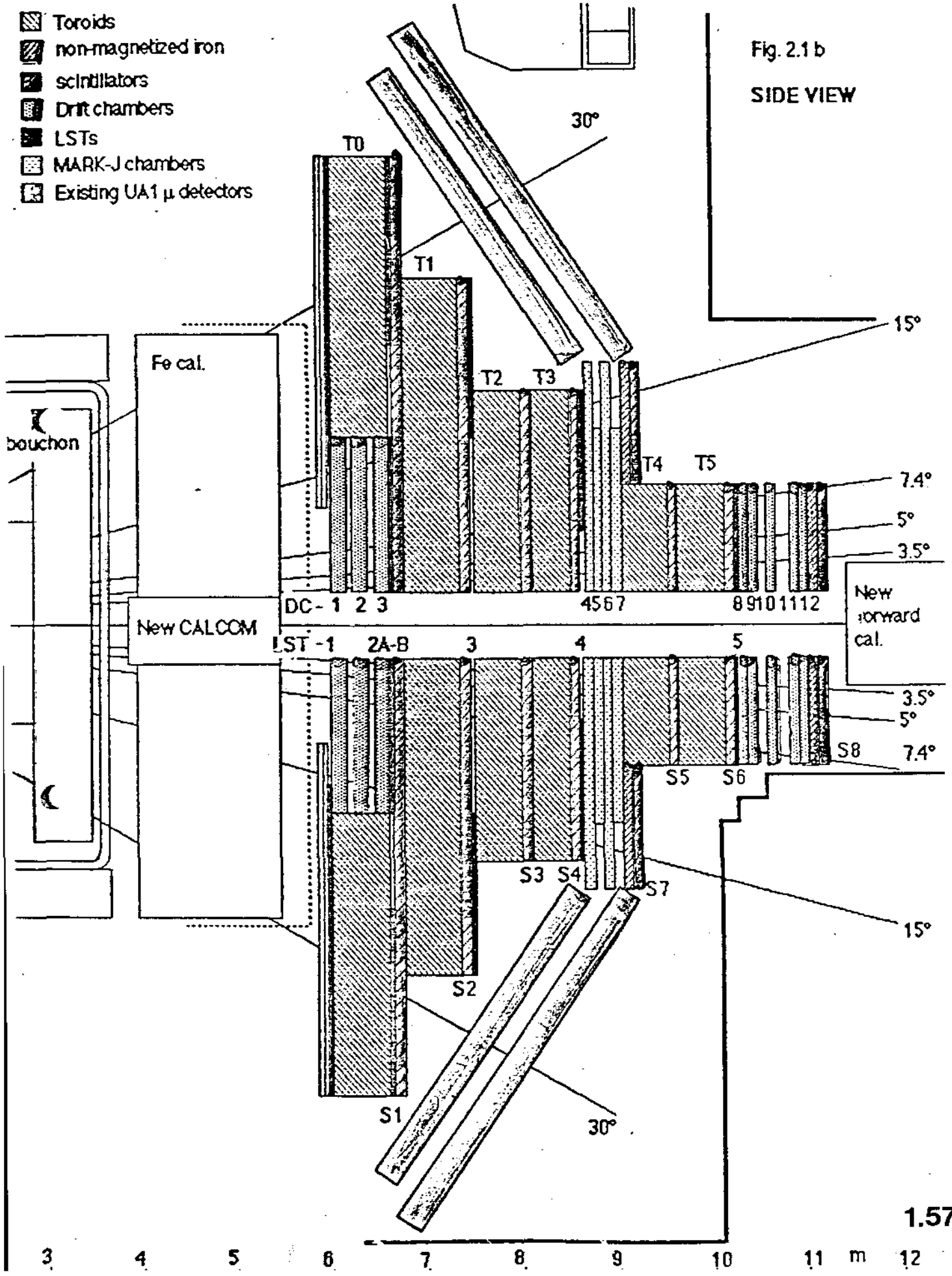
IN THE UAM CONFIGURATION, WE HAVE APPROXIMATELY THE SAME AMOUNT OF INTERACTION LENGTHS (i.e., 10) AS IN OUR ORIGINAL PROPOSAL, SO WE EXPECT THE SAME RATE OF "SHOWER MUONS".

IN ANY CASE, A FULL SHOWER DEVELOPMENT MONTECARLO (GEANT / GHEISHA CHAIN) ALREADY UNDER DEVELOPMENT HAS TO BE RUN.

-  Toroids
-  non-magnetized iron
-  scintillators
-  Drift chambers
-  LSTs
-  MARK-J chambers
-  Existing UA1 μ detectors

crane cabin

Fig. 2.1b
SIDE VIEW









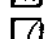
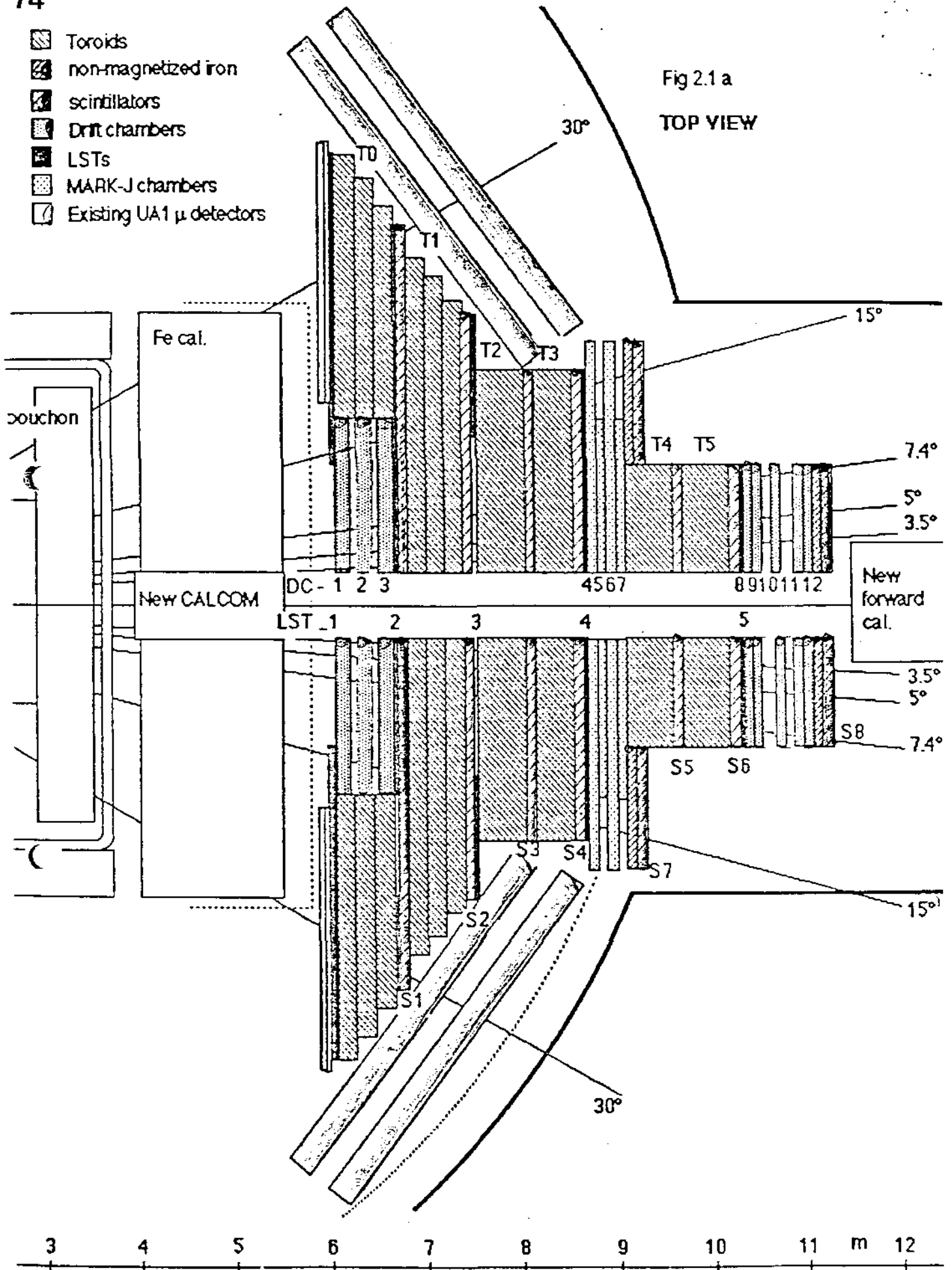
-  Toroids
-  non-magnetized iron
-  scintillators
-  Drift chambers
-  LSTs
-  MARK-J chambers
-  Existing UA1 μ detectors

Fig 2.1 a
TOP VIEW



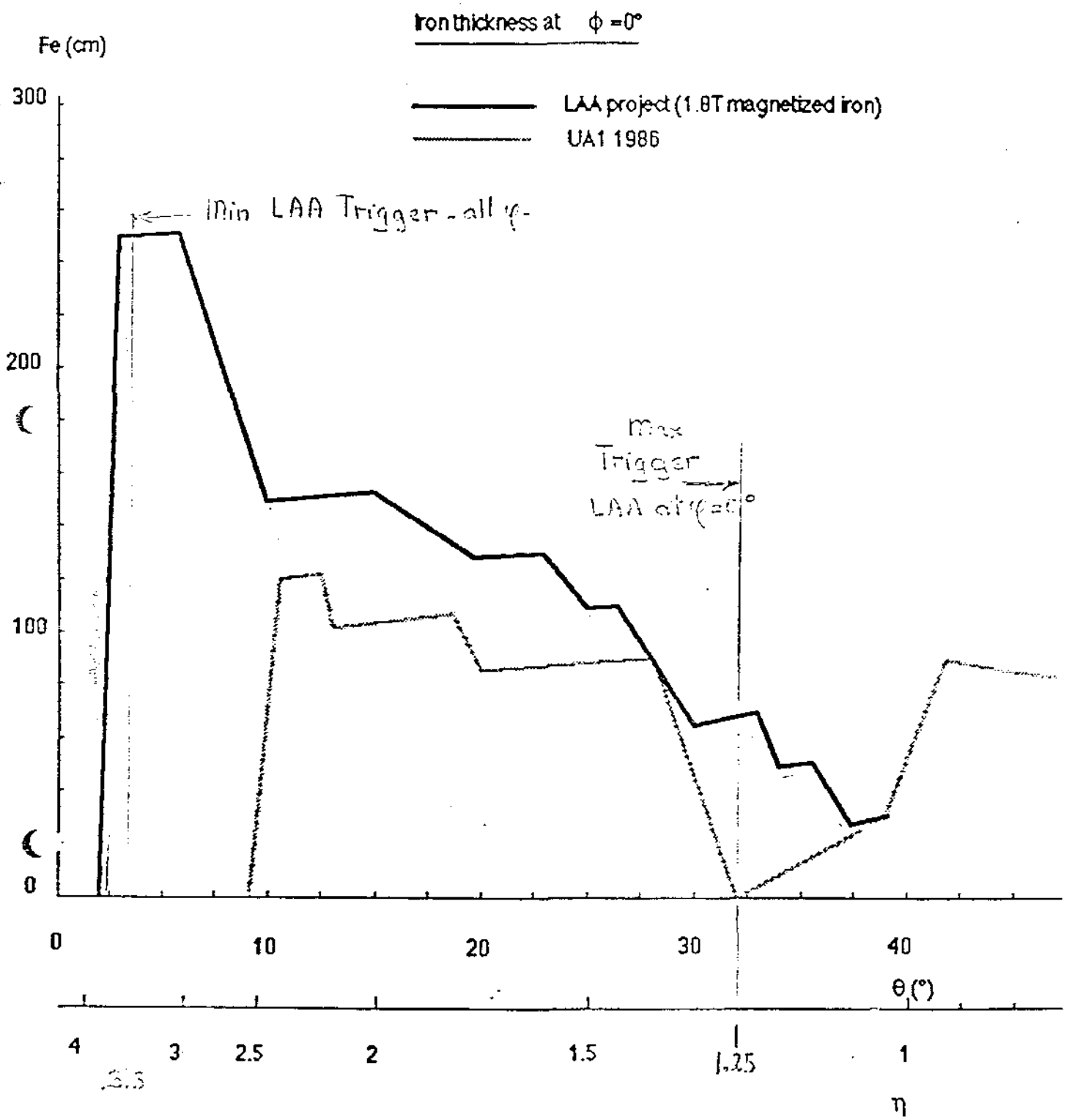
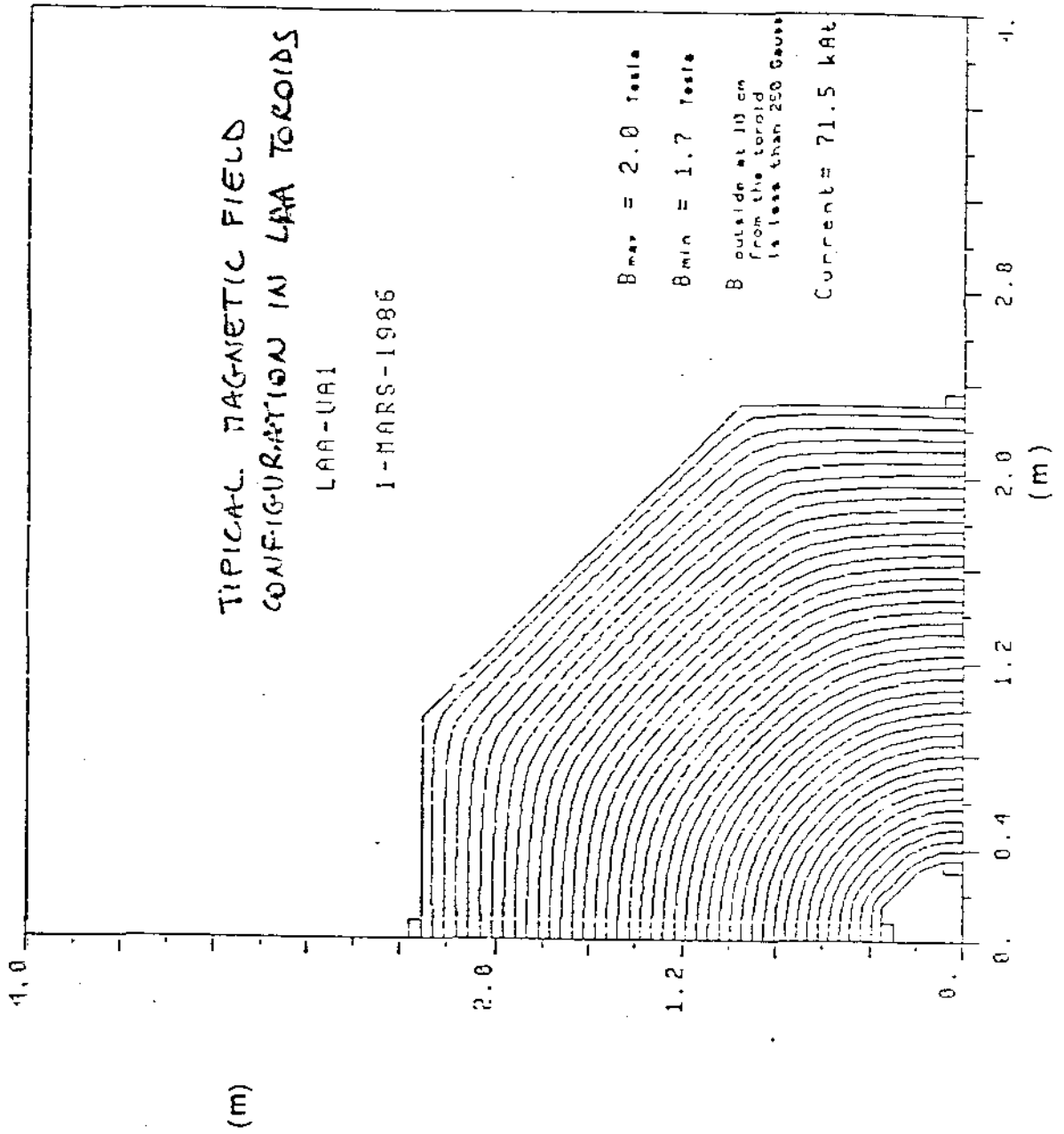


Fig. 23



Drift chambers DC1, DC2, DC3

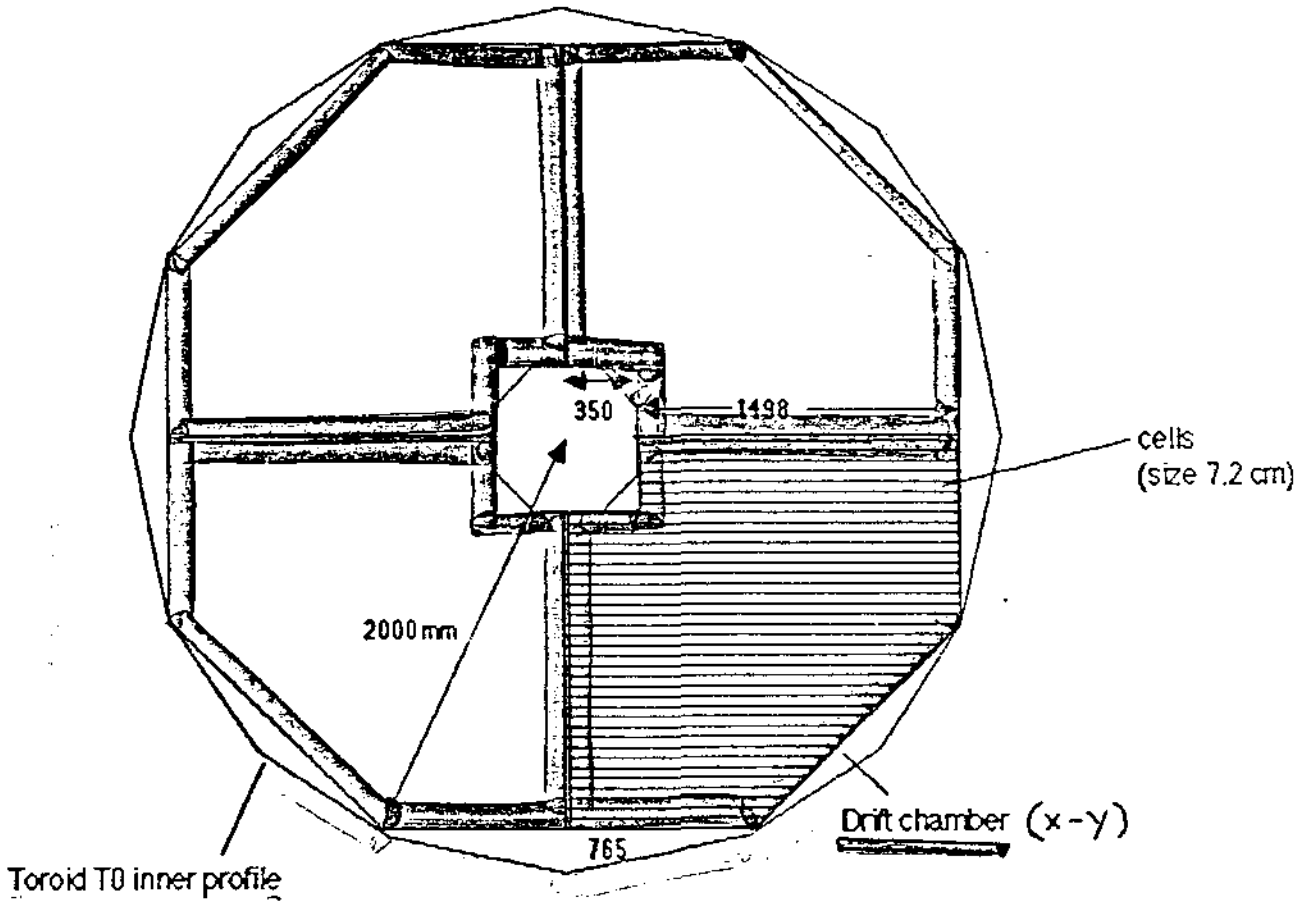


Fig. 2.5

- Front chambers -

Drift chambers DC8 to DC12

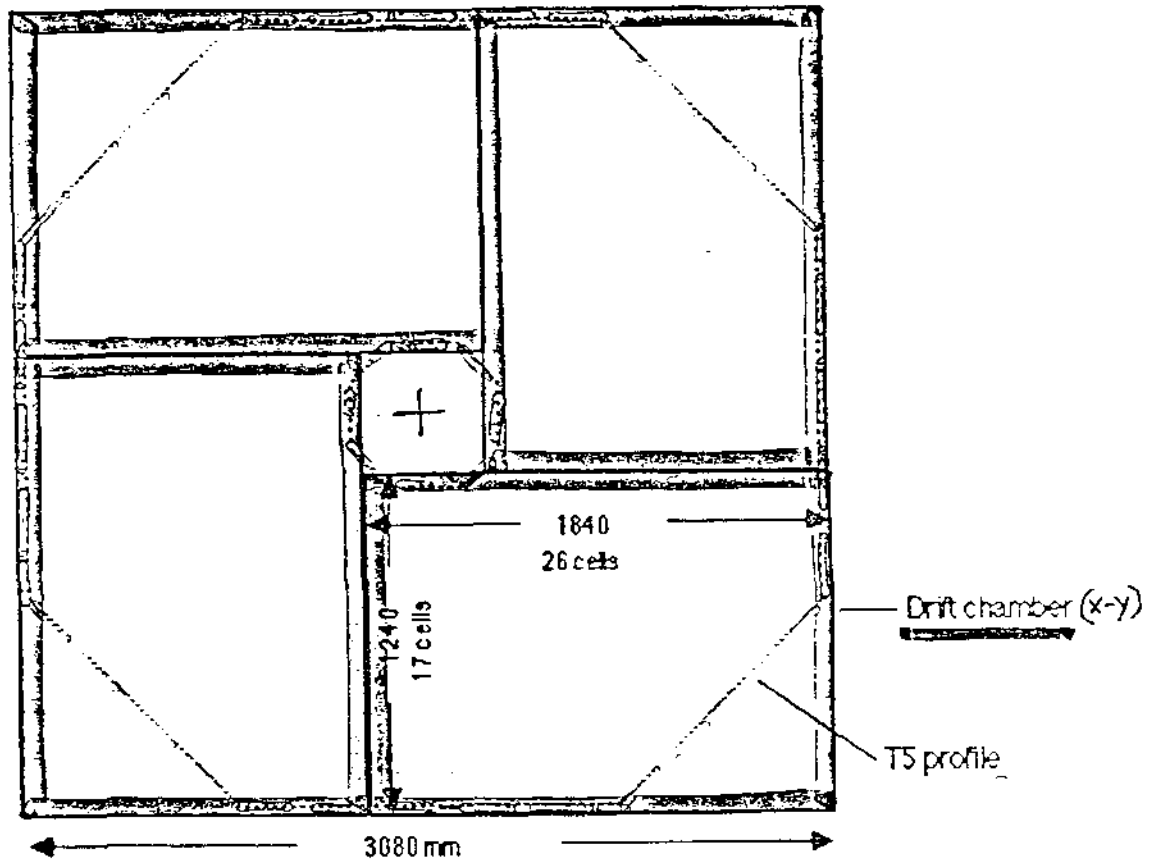
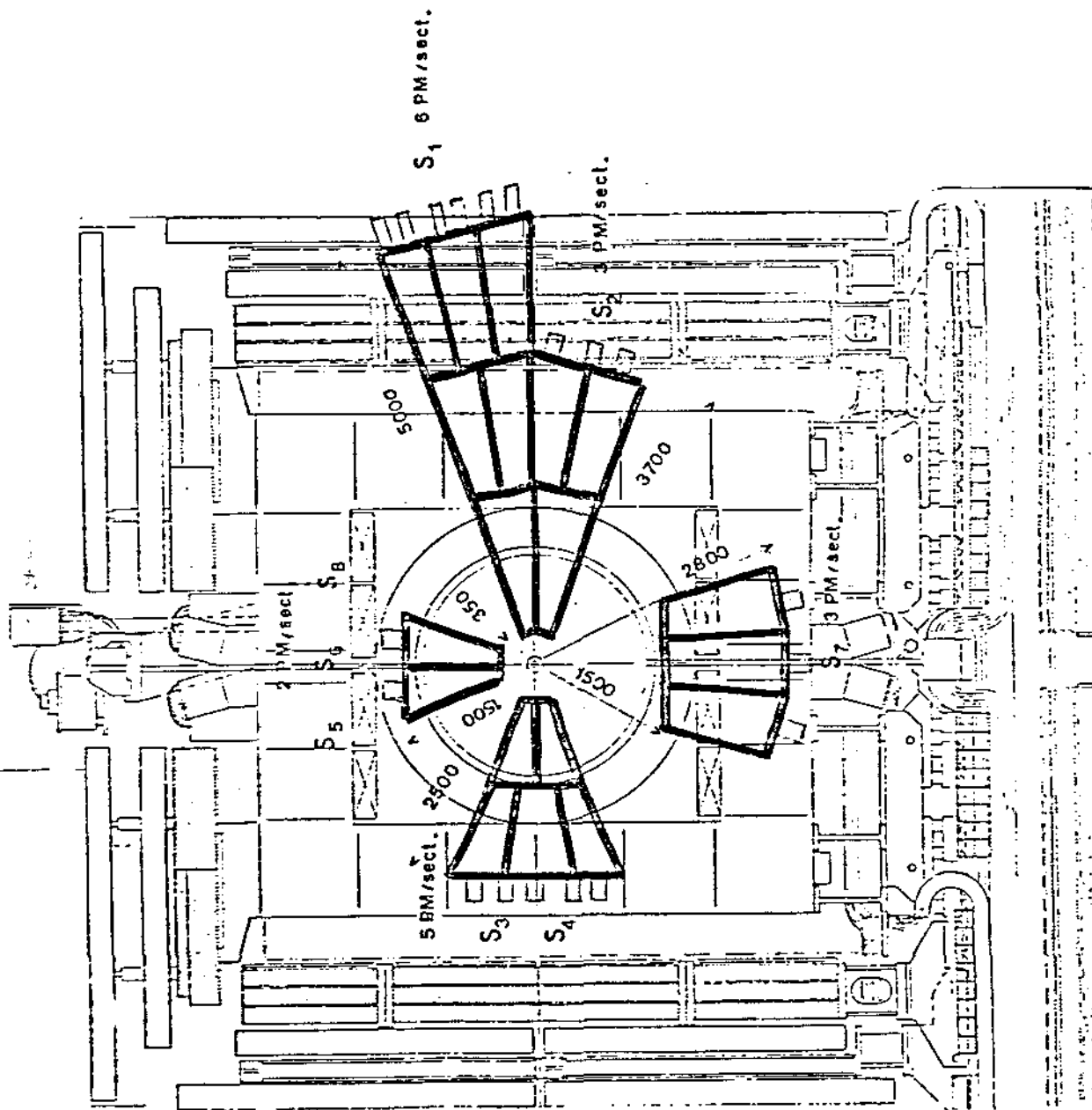


Fig. 2.6

- Back chambers -



Front View

Fig. 2.4

- S planes -

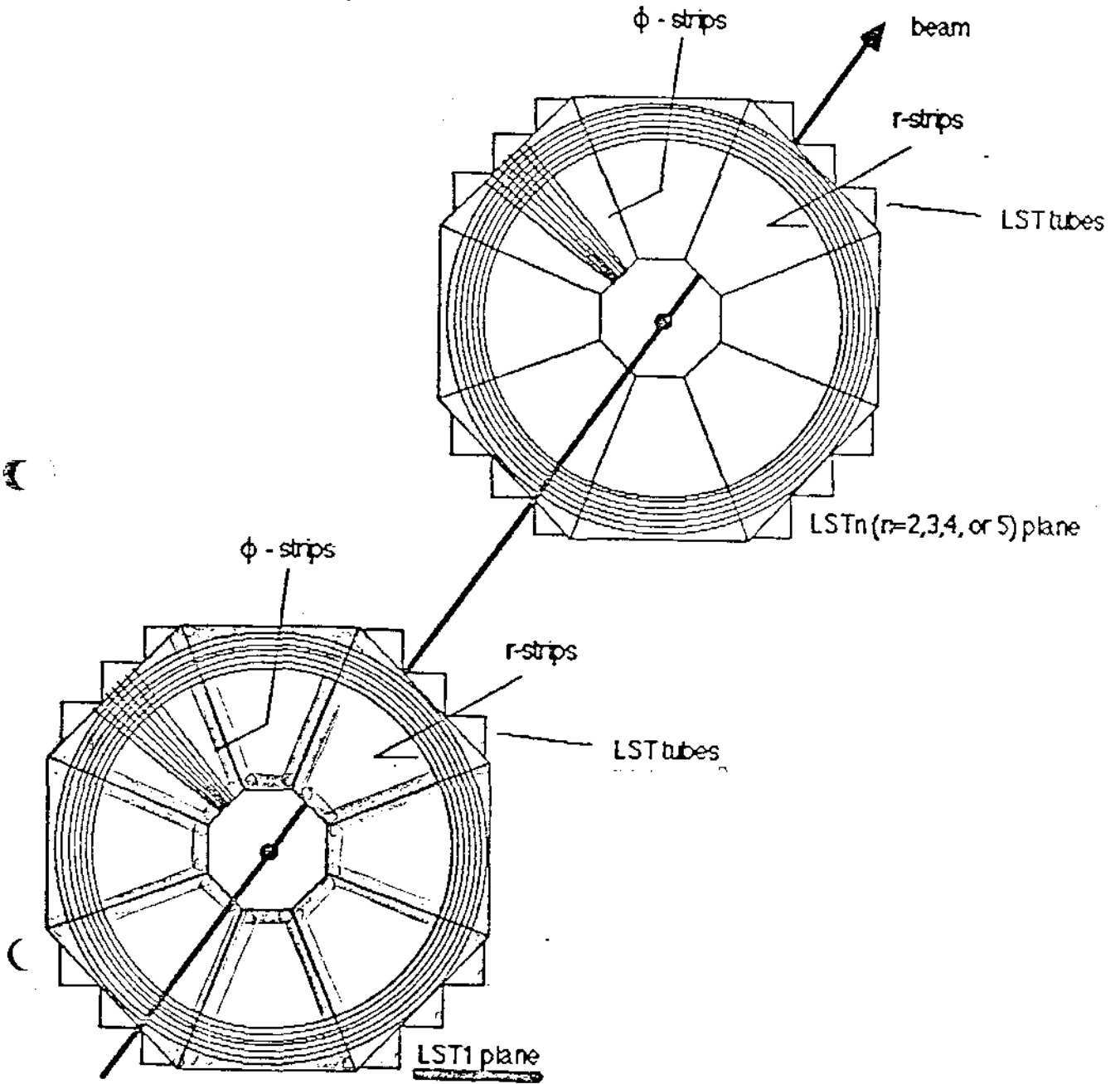


Fig. 3.2

- 23 -

Table 2.1. Toroids.

Magnetized iron:

	sectors	internal radius [mm]	external radius [mm]	length [mm]	weight [t]	B minimum [T]
T0	16	2000	5000	600	303	1.82
T1	16	357	3700	600	196	1.63
T2	16	379	2500	500	74	1.68
T3	16	379	2500	400	59	1.68
T4	8	379	1624	500	28	1.73
T5	8	379	1624	500	28	1.73

B maximum is always 2.0 T.

Total weight = 1376 t

Non-magnetized iron:

	sectors	internal radius [mm]	external radius [mm]	length [mm]	weight [t]
F0	8	1634	2600	100	9.1
F1	8	379	1732	100	6.4

Table 2.II. Scintillation counters.

	sectors	internal radius [mm]	external radius [mm]	surface [m ²]	PMTs per sector	PMTs total
S1	16	357	5000	64.3	6	96
S2	16	357	3700	41.6	3	48
S3	8	379	2500	17.3	5	40
S4	8	379	2500	17.3	5	40
S5	8	379	1624	7.0	2	16
S6	8	379	1624	7.0	2	16
S7	8	1634	2500	11.6	3	24
S8	8	379	1732	8.1	2	16

Each scintillator is 2 cm thick and less than 2 m in length.

Total surface (both sides) = 348.5 m²

Total weight of scintillator = 7200 Kg

Total number of PMTs = 592

- 25 -

Table 2.III. Limited Streamer Tubes.

	sectors	internal radius [mm]	external radius [mm]	surface [m ²]	r-strips per sector	r-strip size [mm]
LST1	16	1550	5000	69.1	256	13.2
LST2A	8	379	2000	10.9	128	11.7
LST2B	16	3050	5000	48.1	128	14.9
LST3	16	2000	3700	29.7	128	13.0
LST4	8	1000	2500	14.9	128	10.8
LST5	8	379	1624	7.1	128	9.0

Total area (both sides) = 359.6 m²

Total number of strips (both sides) = 24688

Table 2.III. Limited Streamer Tubes.

	sectors	internal radius [mm]	external radius [mm]	surface [m ²]	r-strips per sector	r-strip size [mm]
LST1	16	1550	5000	69.1	256	13.2
LST2A	8	379	2000	10.9	128	11.7
LST2B	16	3050	5000	48.1	128	14.9
LST3	16	2000	3700	29.7	128	13.0
LST4	8	1000	2500	14.9	128	10.8
LST5	8	379	1624	7.1	128	9.0

Total area (both sides) = 359.6 m²

Total number of strips (both sides) = 24688

TOROIDS

IRON } PRELIMINARY CONTACTS WITH
 COILS } ANSALDO (Genova, Italia)

ESTIMATES :

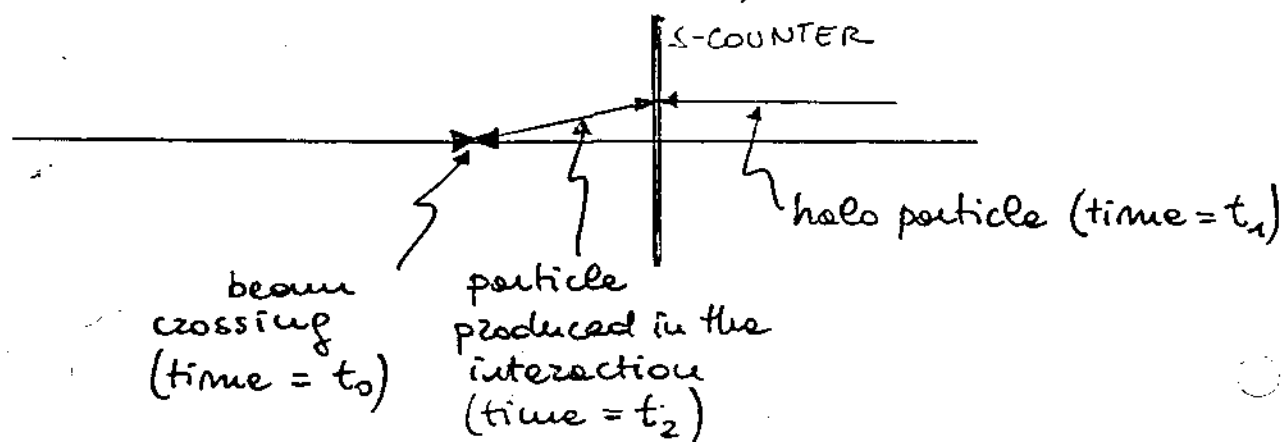
DELIVERY TIME : 10 ÷ 12 months

TOTAL COST :

Comprehensive of : PROJECT
 CONSTRUCTION
 TEST
 TRANSPORT

10 TOROIDS
 160 PIECES
 1376 t

- REJECT BEAT HALO BY TITING (WITH RESPECT TO SPS SYNCHRONIZATION TIME)



$$[t_2 - t_0] - [t_1 - t_0] \sim 20 \div 40 \text{ nsec} \quad \left(\begin{array}{l} \text{depending on the} \\ \text{position of the S-COUNTER} \end{array} \right)$$

(NOTE: t_0 IS KNOWN WITH A PRECISION OF ~ 0.5 nsec.)

- FOLLOW A PARTICLE THROUGH THE IRON
IN LAA TEST RUN, EACH SCINTILLATOR INSIDE THE
MAGNETIZED IRON REDUCED THE TRIGGER RATE BY
A FACTOR ~ 80 .

SCINTILLATOR COUNTERS

SCINTILLATOR

NE102A or Home-made.

TENDERS TO BE DONE (MAJOR
CONSTRAINT: DELIVERY TIME)

LIGHT-GUIDES

PROBABLY FROM POLIVAR (Pomezia,
Italy) -A UV ABSORBER WILL BE USED
AT THE END OF LIGHT-GUIDE TO
KILL CHERENKOV LIGHT.

ELECTRONICS

PILS XP2262 (PHILIPS)
UNDER TEST

14 STRIPS

160 SECTORS

592 COUNTERS

LIMITED STREAMER TUBES

TUBES	PLASTIC	Commercially available
	COATING	} Three options:
	WIRING	
		• both in FRASCATI (ITALIA)
		• Coating in FRASCATI, wiring in CERN
		• both in HUSTON (TEXAS)

(2) STRIPS A MACHINE SIMILAR TO THAT USED IN BARI FOR ALEPH WILL BE USED TO CUT THE STRIPS. STRIPS ARE 35 μ m COPPER FILM ON VETRONITE.

HEAD ELECTRONICS AMPLIFIER/DISCRITINATOR with parallel read-out.

360 m^2

24688 strips

SUMMARY ON LST MODULES

	LENGTH (m)						
	8	6	4	2.5	2	1.5	1
LST 1	112	216	512				
LST 2A			352				
LST 2B	192	64	240				
LST 3		56	344				
LST 4				320			48
LST 5					80	192	
TOTAL	304	336	1448	320	80	192	48

TOTAL N. OF LST MODULES : 2728

⊙ TOTAL LENGTH : 11 536 m

TOTAL N. OF WIRES : 21 824

TOTAL GAS VOLUME : 9.23 m³

MECHANICS

FINAL CELL DESIGN BY JUNE 1986.
SAME PRINCIPLE AS THOSE USED IN
THE LAA TEST RUN.

ELECTRONICS

AN ELECTRONIC CHAIN IS UNDER
TEST: AMPLIFIER/DISCRIMINATOR BY
AUREL (ITALY); FASTBUS TDC'S FROM
CERN (LTD: CERN/EP Electronic Note
85-06, November 1985).

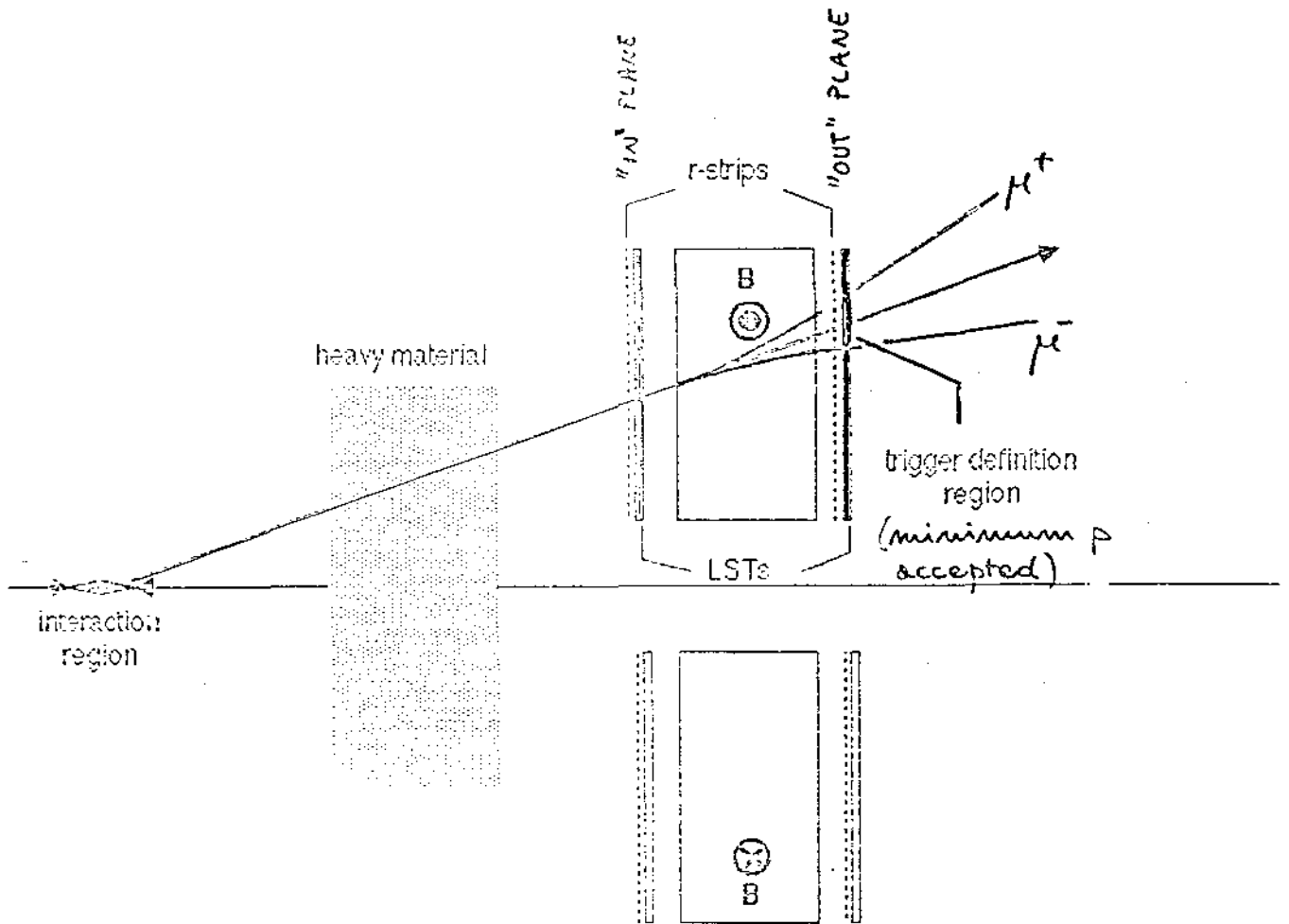
64 chambers
142 m²

LAA

TRIGGER

AND

TRIGGER RATES



Principle of the trigger.

LST READ OUT STRIPS INFORMATION USED TO DEFINE MINIMUM MOMENTUM CUT DEPENDING ON μ PRODUCTION ANGLE, WITH MULTIPLE SCATTERING TAKEN INTO ACCOUNT.

TRIGGER LOGIC

- LST Z-STRIPS DEFINE THE RADIAL TRAJECTORY OF THE MUON.
- LST ϕ -STRIPS ESTABLISH THAT THIS TRAJECTORY IS COPLANAR WITH THE BEAM.

THE Z-STRIPS ARE ARRANGED SO THAT THE STRIP NUMBER IS PROPORTIONAL TO THE ANGLE SUBTENDED AT THE INTERACTION REGION. A MATRIX

(COINCIDENCE TO IMPOSE A p_T CUT IS POSSIBLE AND REPRESENTS A BASIC PART OF THE TRIGGER.

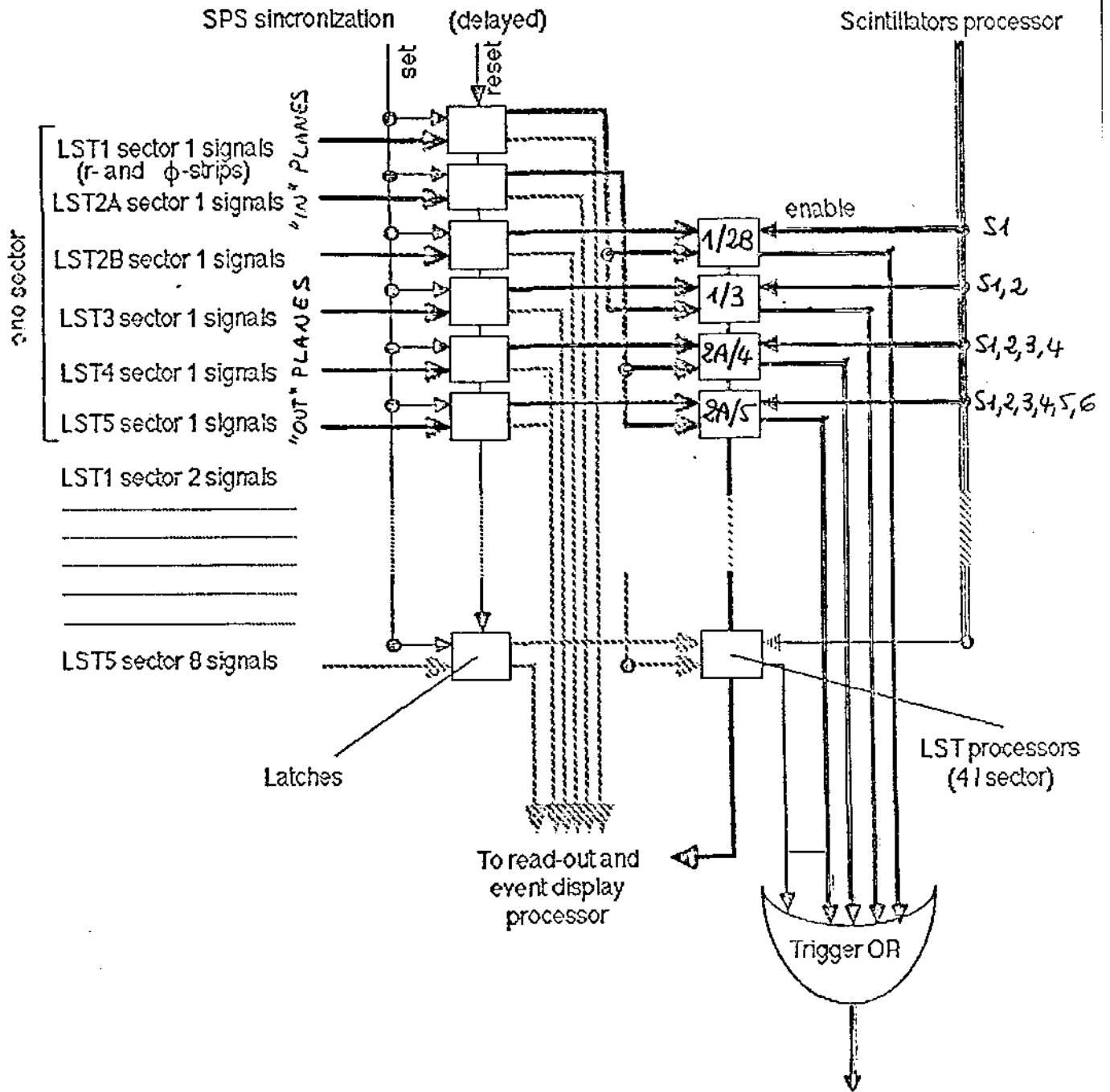
FOR TRIGGER PURPOSES, THE APPARATUS WILL BE DIVIDED INTO 8 ϕ -SECTORS TREATED INDEPENDENTLY AND IN PARALLEL.

THE TRIGGER LOGIC WILL BE BASED ON:

- SCINTILLATION COUNTER PROCESSORS
(TO DETERMINE THE HIT OCTANT)
- LST Z-STRIP PROCESSORS
(TO APPLY p_T CUT, ADJUSTABLE FOLLOWING THE WANTED TRIGGER RATE)
- LST ϕ -STRIP PROCESSORS
(TO REJECT TRACKS WHICH ARE NOT IN THE RIGHT PLANE, i.e. LOW MOMENTUM, HIGHLY SCATTERED MUONS)

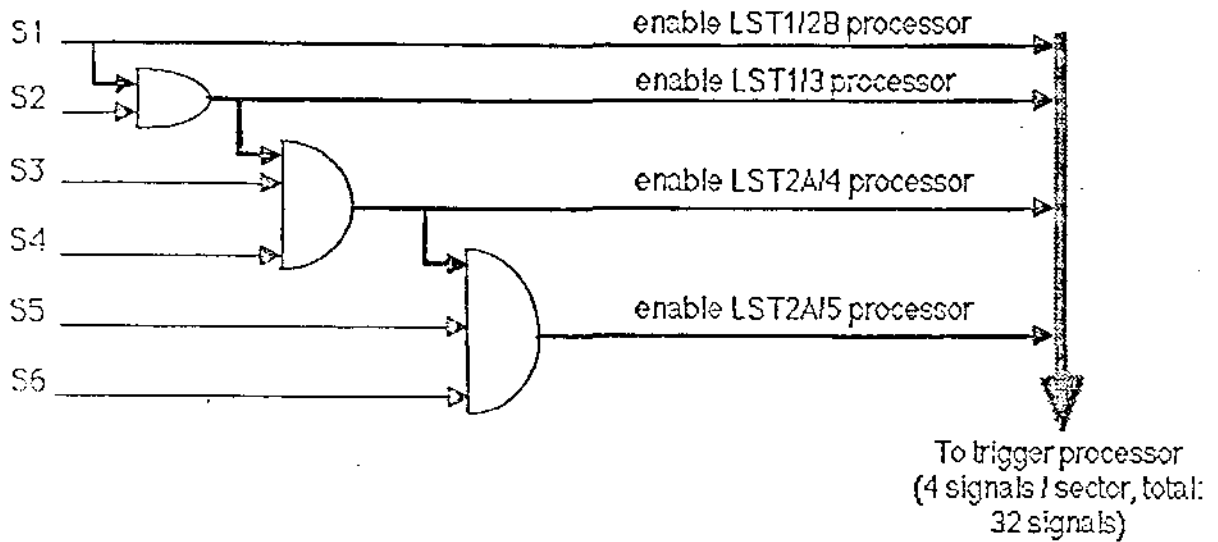
LST TELESCOPES	ANGULAR RANGE OF TRIGGER
1 and 2B	$\theta > 25^\circ$
1 and 3	$15^\circ \leq \theta \leq 26^\circ$
2A and 4	$7.5^\circ \leq \theta \leq 16^\circ$
2A and 5	$\theta < 7.5^\circ$

Trigger processor



Scintillators processor (one sector)

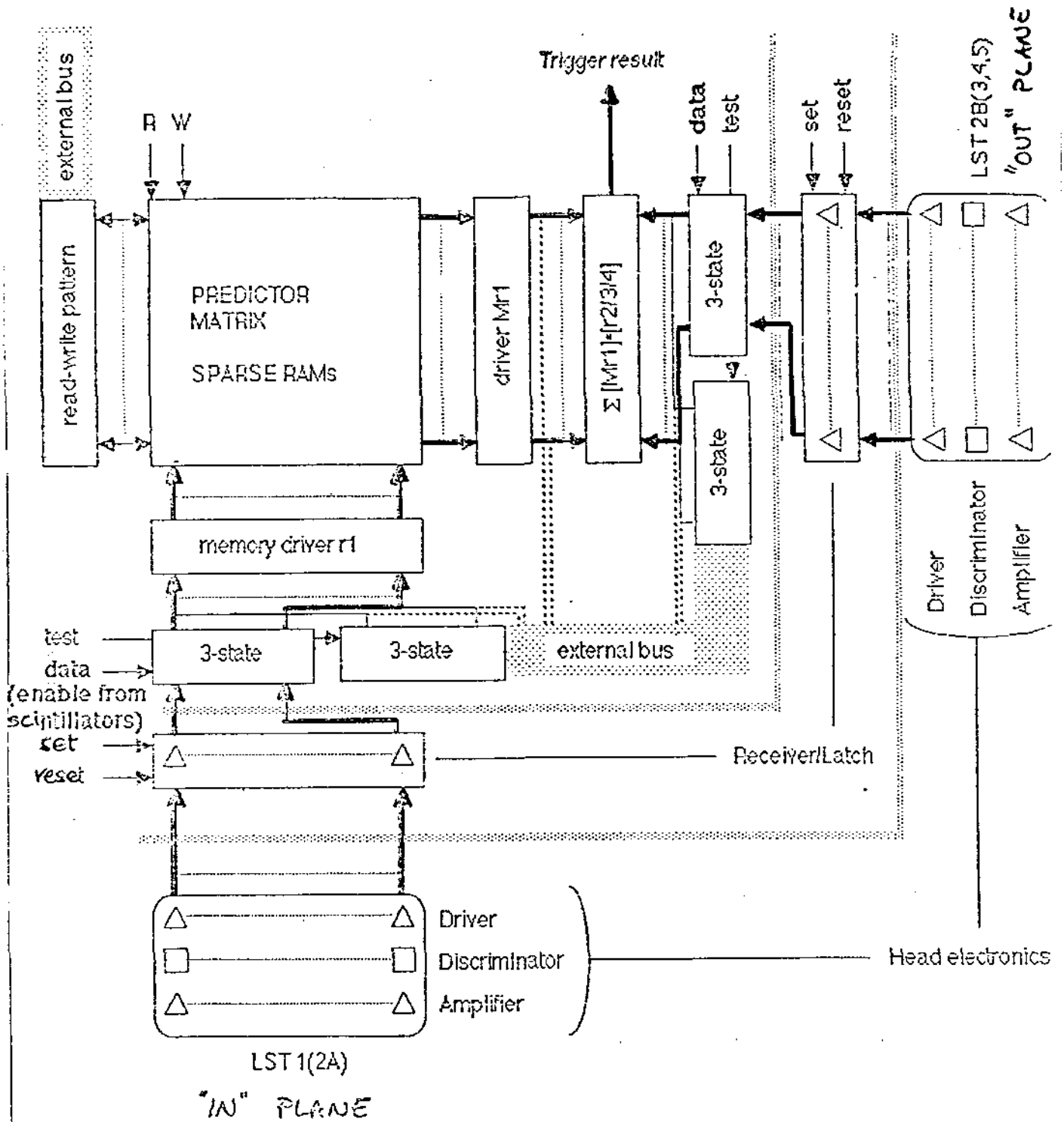
Scintillator



Scintillators signals from one sector are discriminated and then ORed.
A small number of ADCs and TDCs is used for monitor and calibration
multiplexing to the counters signals.

PROVIDES A FIRST DETERMINATION OF THE
OCTANT TRAVERSED BY THE μ AND
ENABLES THE LST PROCESSORS

LST processor (r-strips)



REQUIRES THE COINCIDENCE BETWEEN ONE CIRCULAR Z-STRIP OF THE 1st LST PLANE WITH A SUITABLE NUMBER OF STRIPS IN THE FOLLOWING LST PLANES

TRIGGER ELECTRONICS AND LST READ-OUT.

SCINTILLATOR PROCESSORS

STANDARD MIT ELECTRONICS

LST PROCESSORS

3 fundamental modules have to be designed:

- "IN" PLANE READ-OUT
- PREDICTOR MEMORIES
- "OUT" PLANE READ-OUT AND TRIGGER

Goal: a modular electronics for easy testing and operation

Preliminary contacts with:

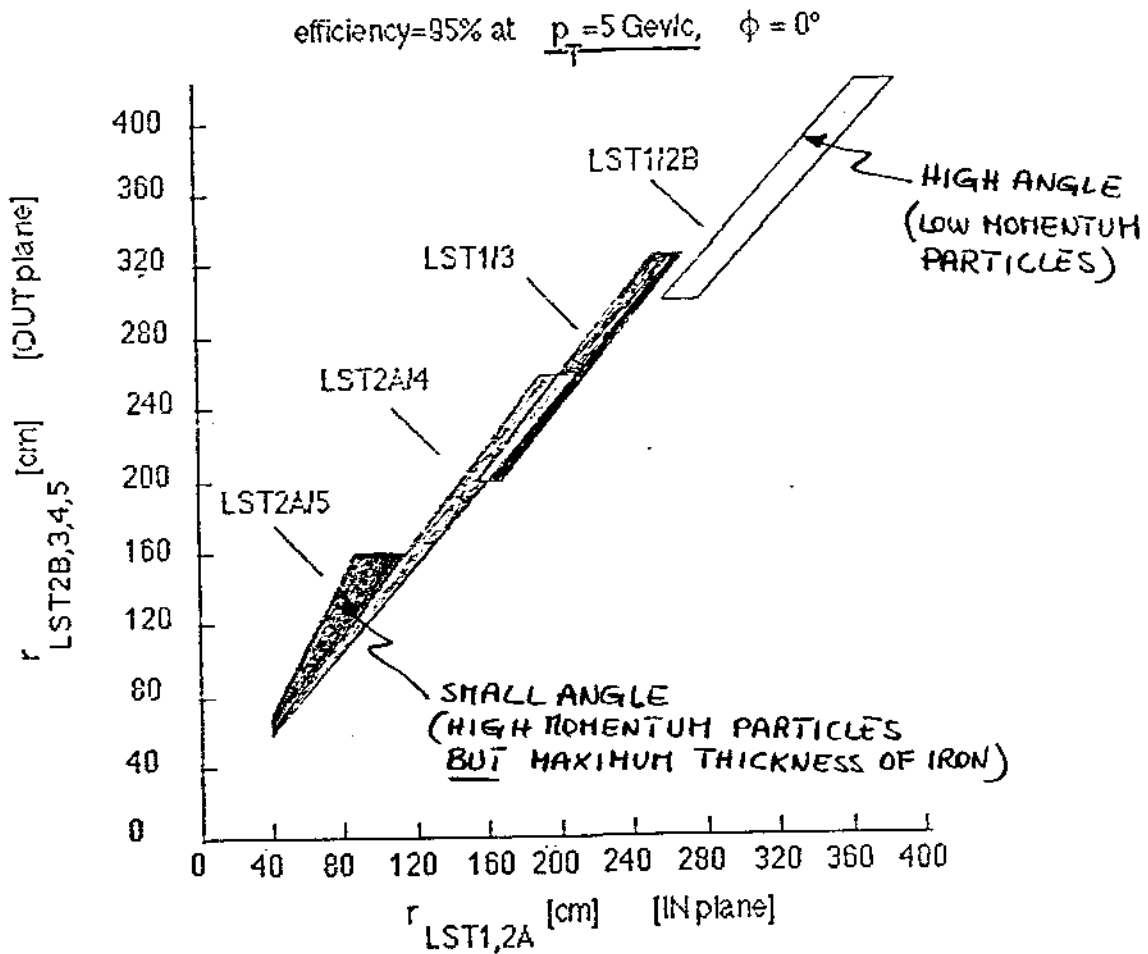
EUROBIT SPA (Rome, Italia)

for the development of the

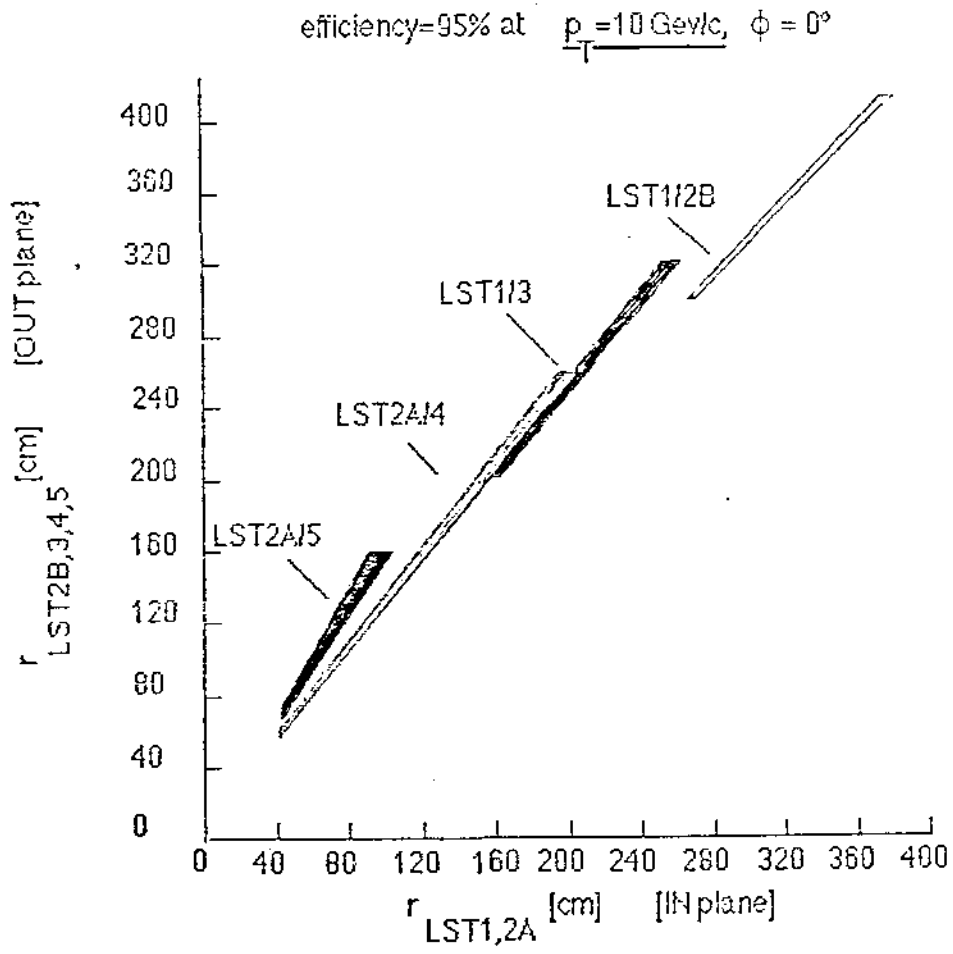
processors and their construction.

98+9E LST processors (r, ϕ)

RADIAL SPREAD ON LST m ($m=2B, 3, 4, 5$) PLANE(S)
VS RADIAL COORDINATE IN THE 1ST LST PLANE (1, 2A)

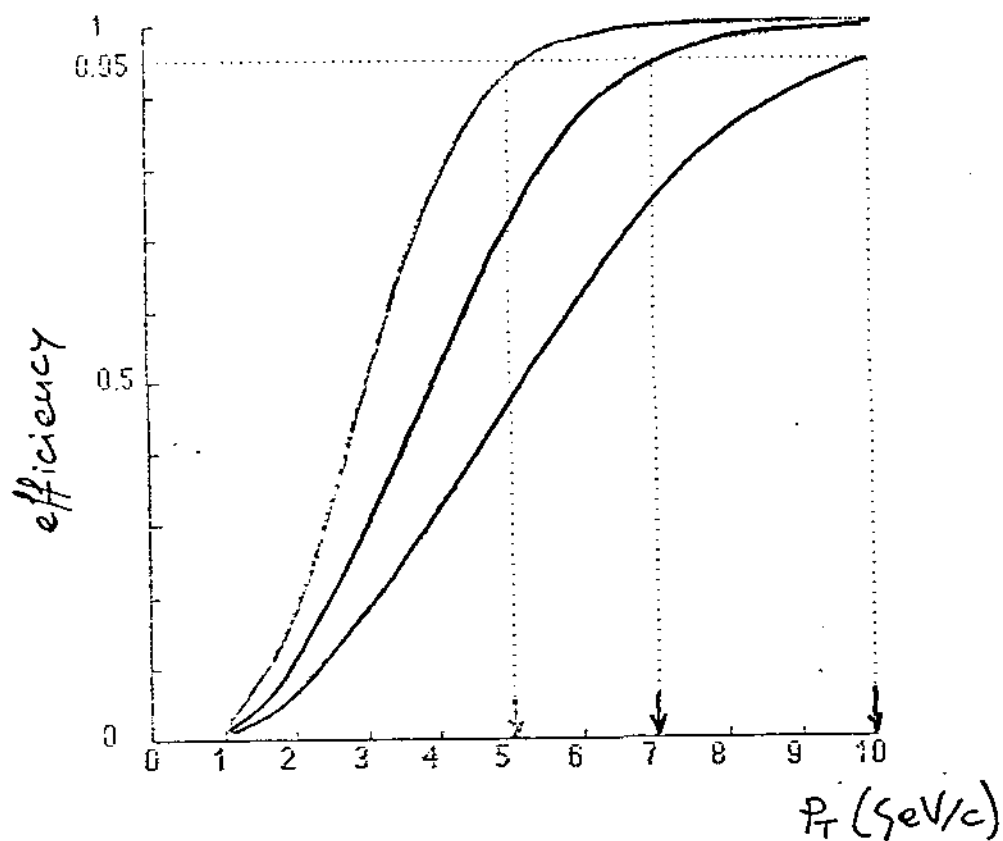


THE SIZE OF THE SPREAD IS COMFORTABLY
HIGHER THAN THE SIZE OF THE LST 2-STRIPS
⇒ POSSIBILITY OF ADJUSTMENT OF THE p_T CUT



Efficiency curves for :

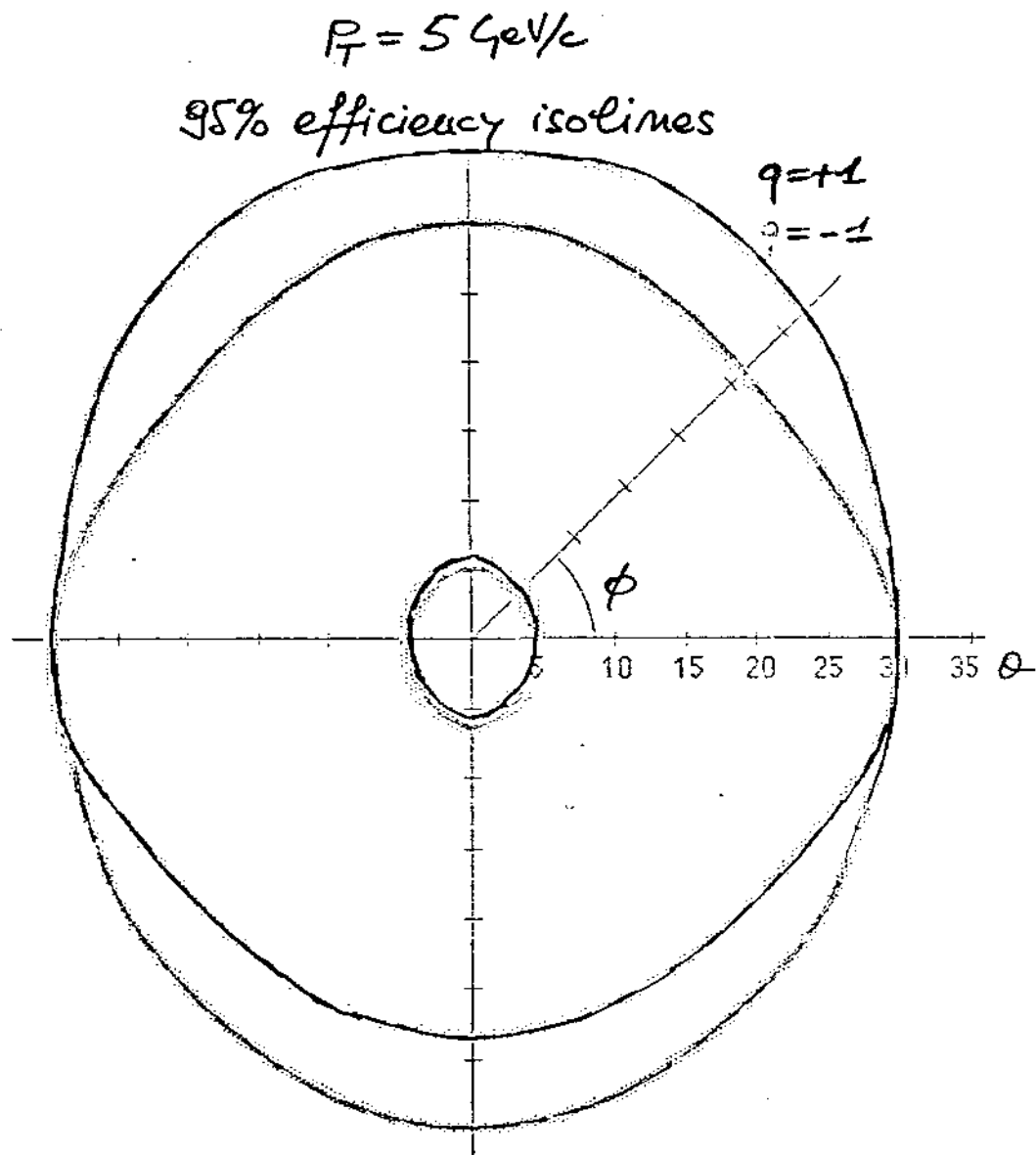
- positive μ 's
- $\theta = 8^\circ$
- $\phi = 0^\circ$



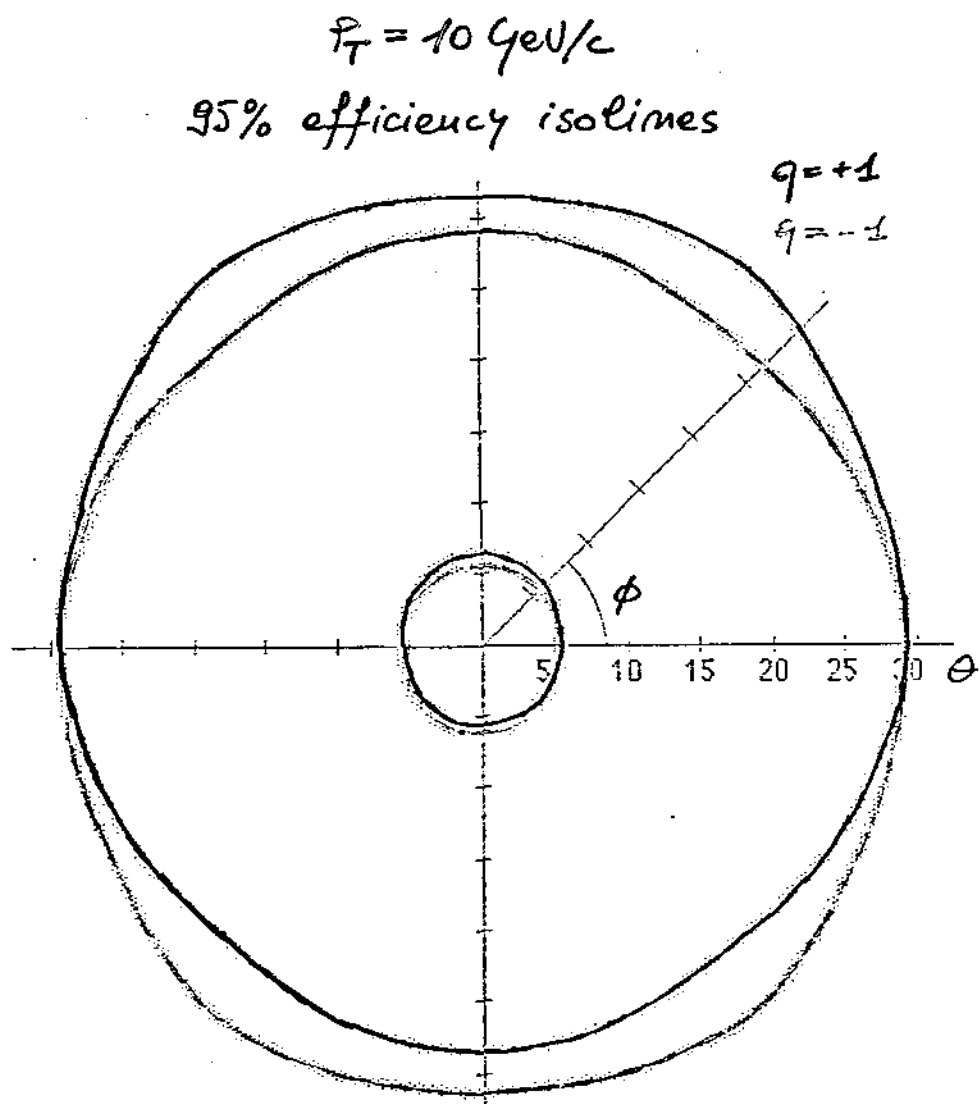
THE CURVES CORRESPOND TO 3 TRIGGER CONFIGURATIONS GIVING 95% EFFICIENCY

AT:

$$\left. \begin{array}{l} P_T = 5 \text{ GeV/c} \\ P_T = 7 \text{ GeV/c} \\ P_T = 10 \text{ GeV/c} \end{array} \right\} \text{ RESPECTIVELY}$$



THE LINES SHOW THE LIMITS OF THE APPARATUS FOR TRACKS WITH $p_T = 5 \text{ GeV}/c$ IN THE TRIGGER CONFIGURATION GIVING AN EFFICIENCY OF 95% AT $p_T = 5 \text{ GeV}/c$.



EXPECTED FIRST LEVEL TRIGGER RATES

CALCULATED ON THE BASIS OF THE PRODUCTION OF
BACKGROUND MUONS FROM π and K DECAYS

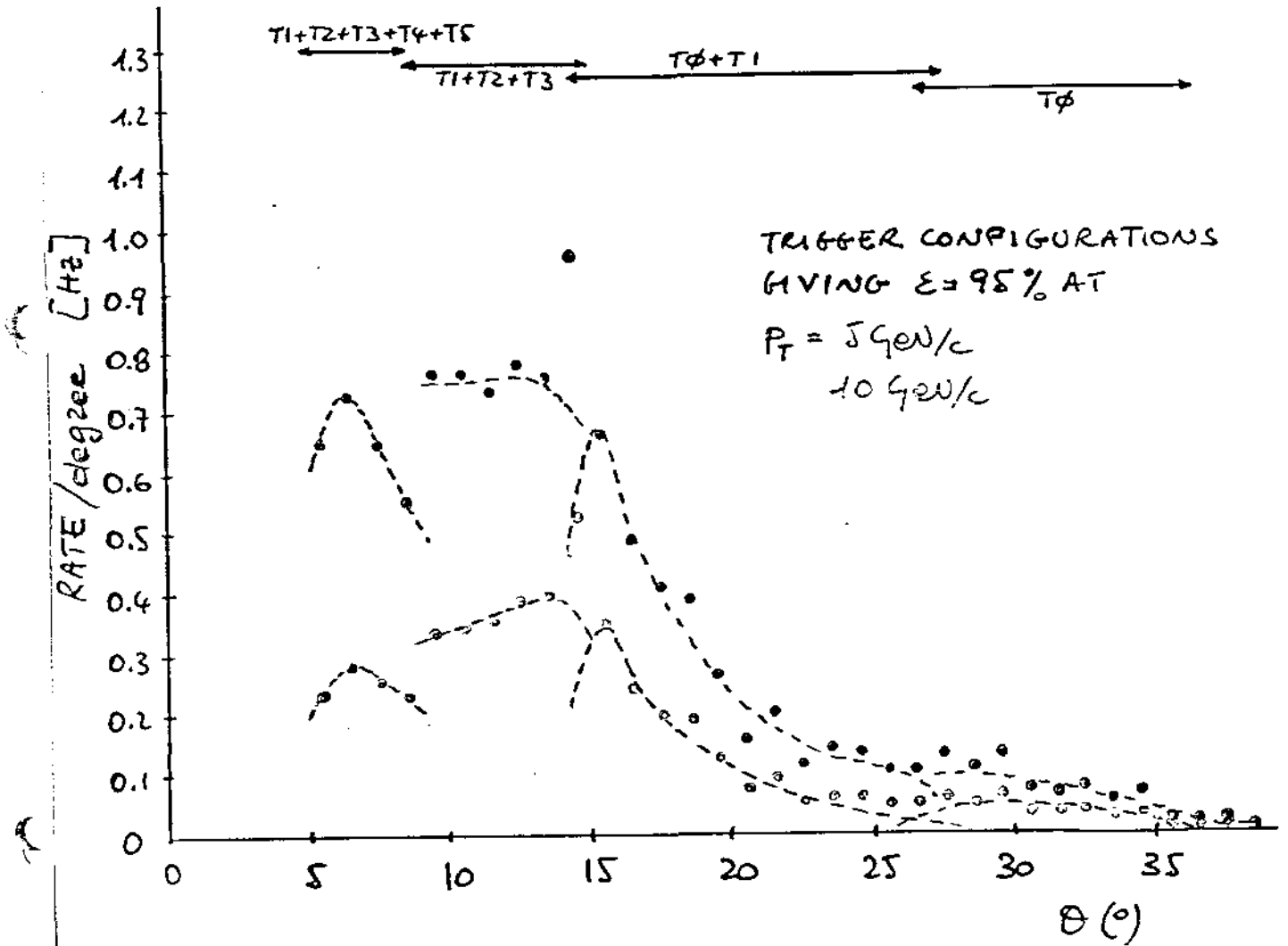
USING:

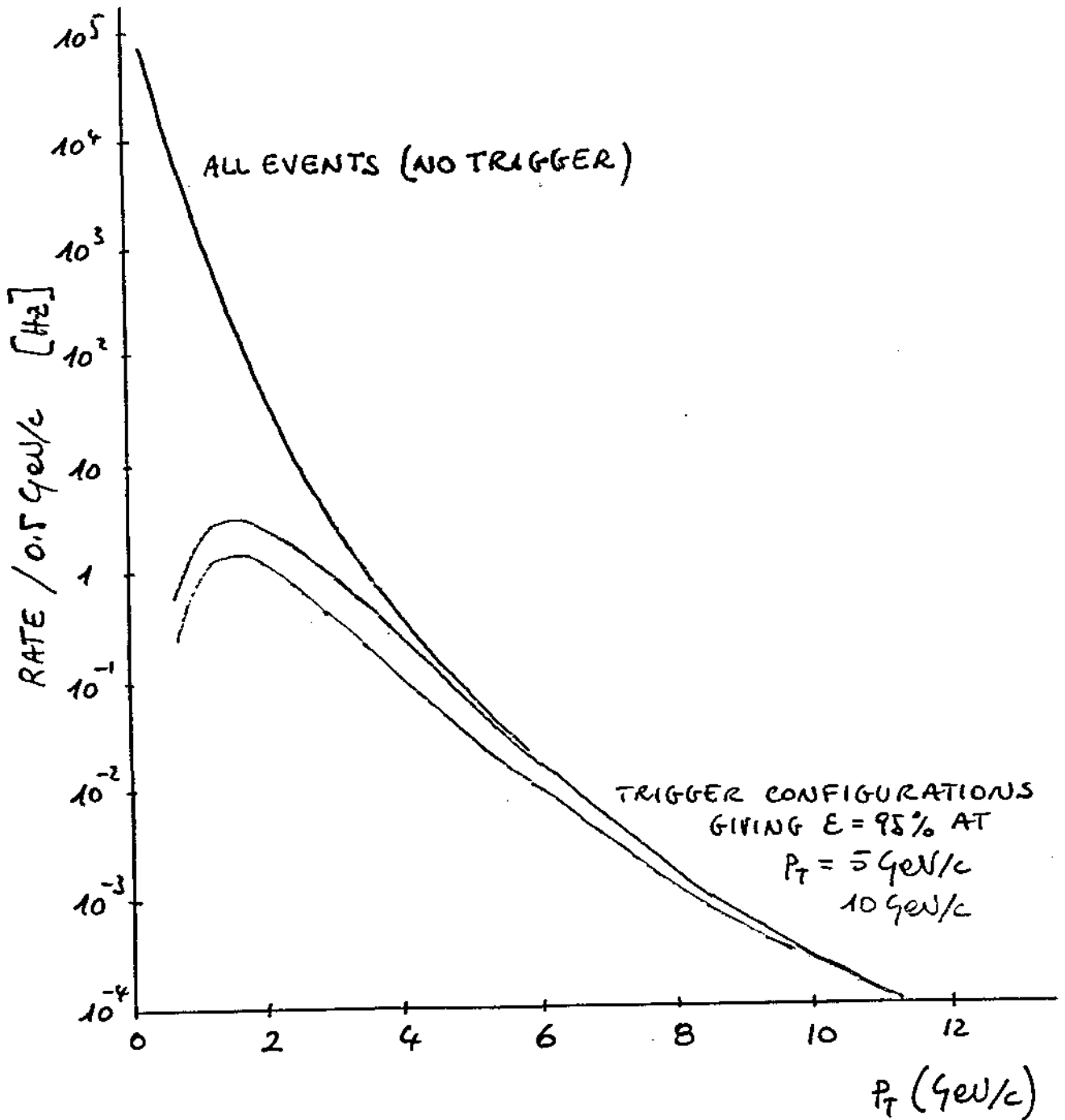
- THE UA1 FIT TO THE INVARIANT CROSS-SECTION
FOR THE PRODUCTION OF HADRONS AT $\sqrt{s} = 630$ GeV.
- THE η DISTRIBUTION OF HADRONS MEASURED BY UA5.
- (- A $\pi:K$ RATIO OF 2:1 .
- A DECAY PATH OF 340 cm .
- THE BEOL LUMINOSITY $L = 4 \times 10^{30} \text{ cm}^{-2} \text{ sec}^{-1}$

FIRST LEVEL TRIGGER RATES

$\epsilon = 95\% \text{ AT}$	charge sign	Rate [Hz]	both sides
$P_T = 5 \text{ GeV}/c$	positive	6.4	11.1
	negative	4.7	
$P_T = 7 \text{ GeV}/c$	positive	4.2	7.4
	negative	3.2	
$P_T = 10 \text{ GeV}/c$	positive	2.9	5.1
	negative	2.2	

A SECOND LEVEL TRIGGER CAN BE APPLIED USING THE DRIFT CHAMBER INFORMATION IN ORDER TO REFINE THE P_T TRIGGER.

BACKGROUND TRIGGER RATE AS FUNCTION OF θ .

BACKGROUND TRIGGER RATE AS FUNCTION OF P_T .

MONTE CARLO SIMULATION
(GEANT)

TO STUDY THE BEHAVIOUR OF THE APPARATUS.

IN PARTICULAR:

- WHAT PARTICLES DO IN THE UA1 LST PLANES AND μ CHAMBERS WHEN COUPLED TO LAA IRON TOROIDS

(

- STUDY OF HIT DISTRIBUTIONS ON LAA LST TRIGGER PLANES

THE U-GRADED UA1, WITH THE NEW CALORIMETERS, WAS CONSIDERED IN THE SIMULATION.

(

110 μ^\pm

$23^\circ \leq \theta \leq 30^\circ$

$\phi = 0^\circ$

$p_T = 2.5 \text{ GeV}/c$

$\uparrow \bar{B}$ LAA TOROID

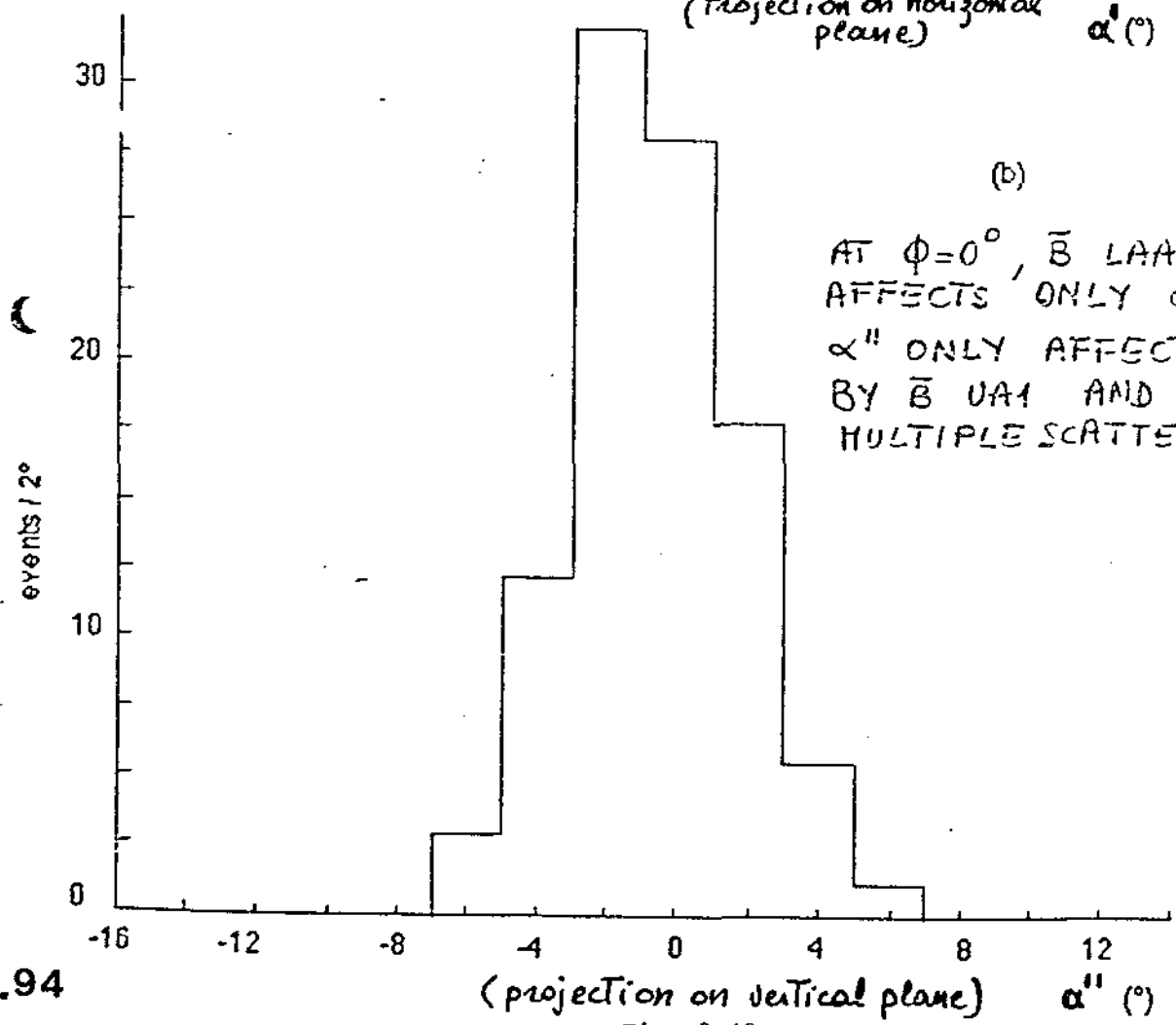
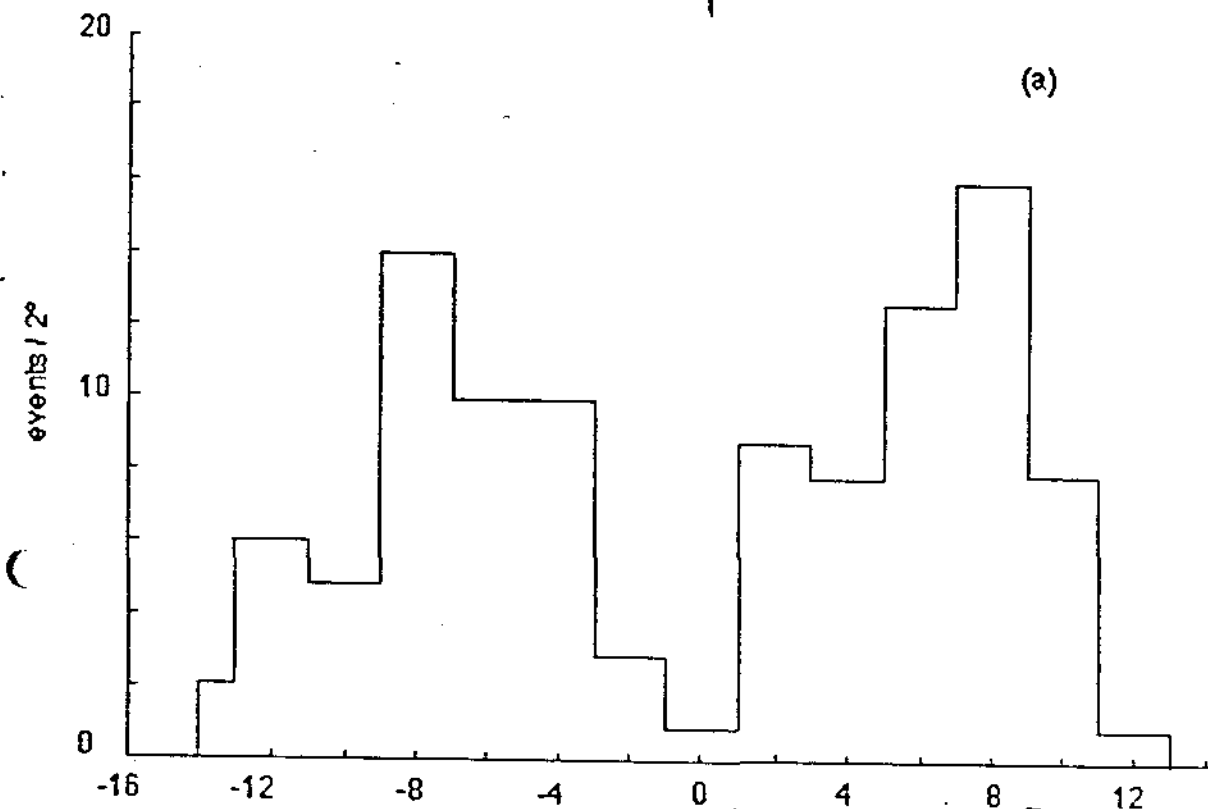
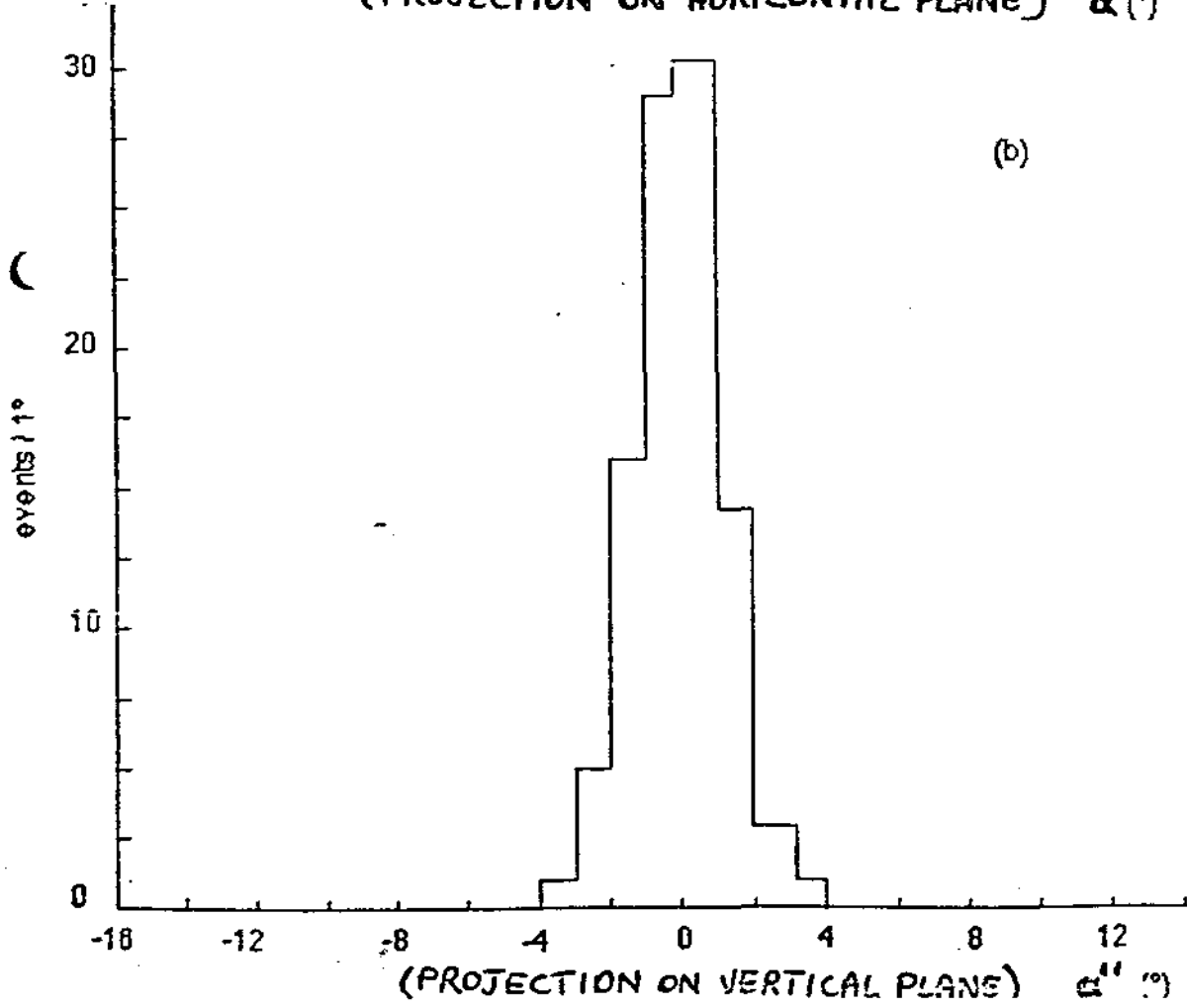
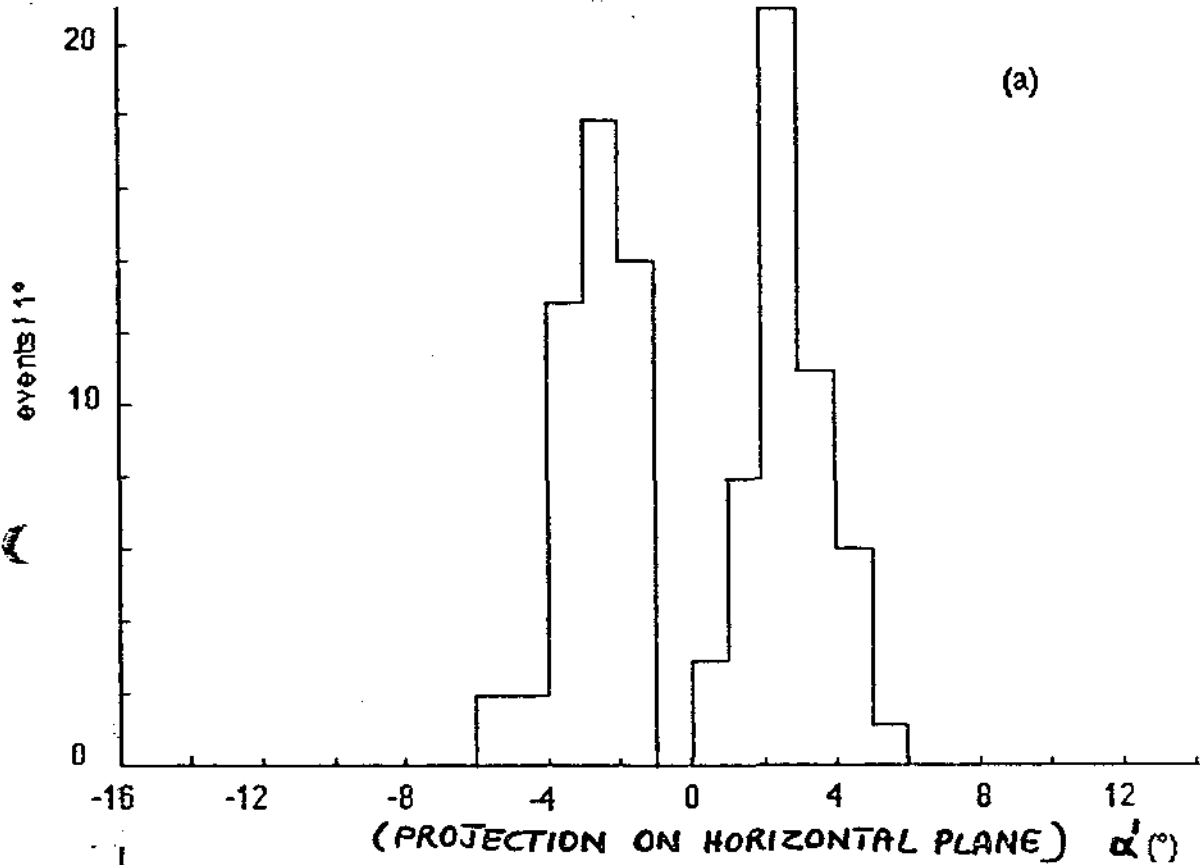


Fig. 3.10

μ^\pm $23^\circ \leq \theta \leq 30^\circ$ $\phi = 0^\circ$ $p_T = 5 \text{ GeV}/c$

111



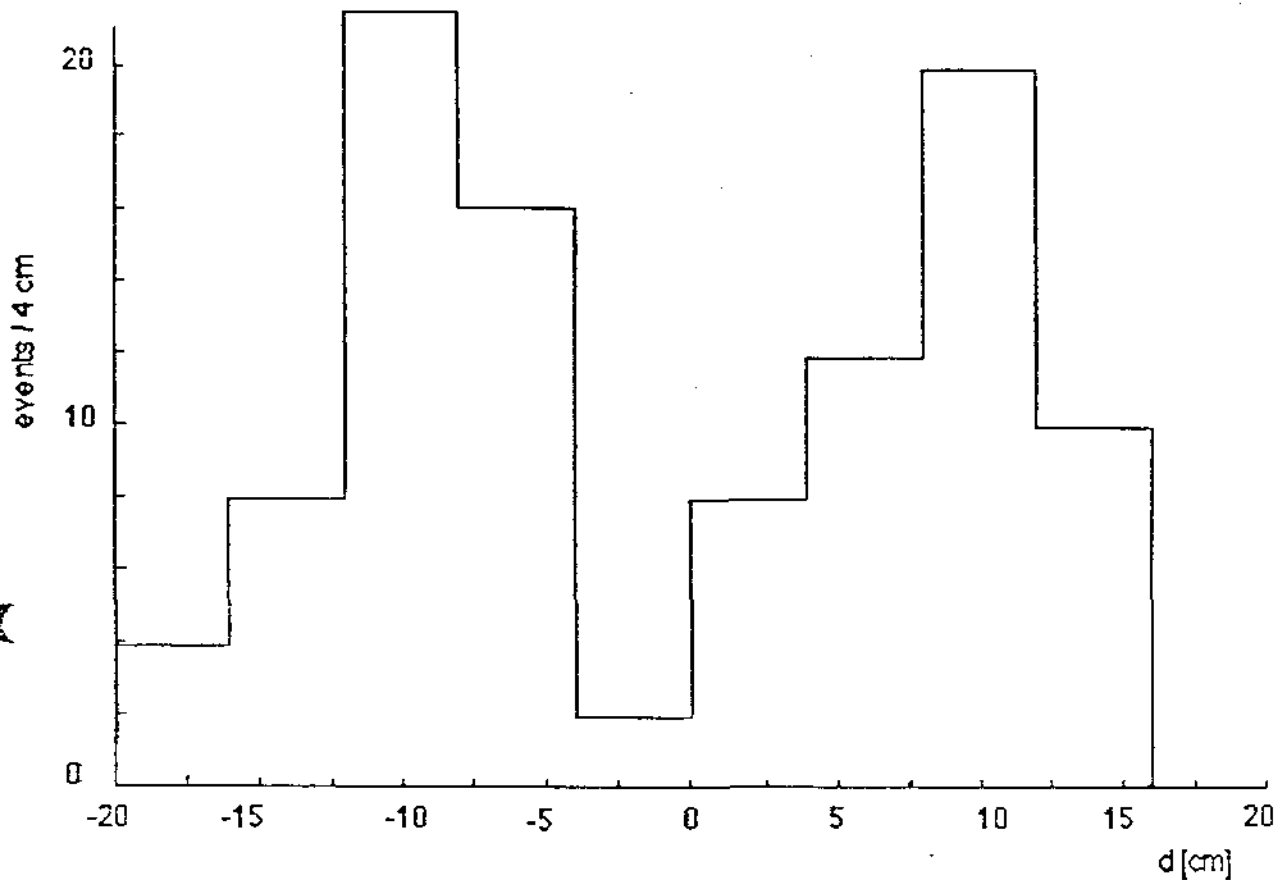


Fig. 3.12

 μ^{\pm} $23^{\circ} \leq \theta \leq 30^{\circ}$ $\phi = 0^{\circ}$ $p_T = 2.5 \text{ GeV}$

↑ \vec{B} LAA TOROID

← \vec{B} UA1

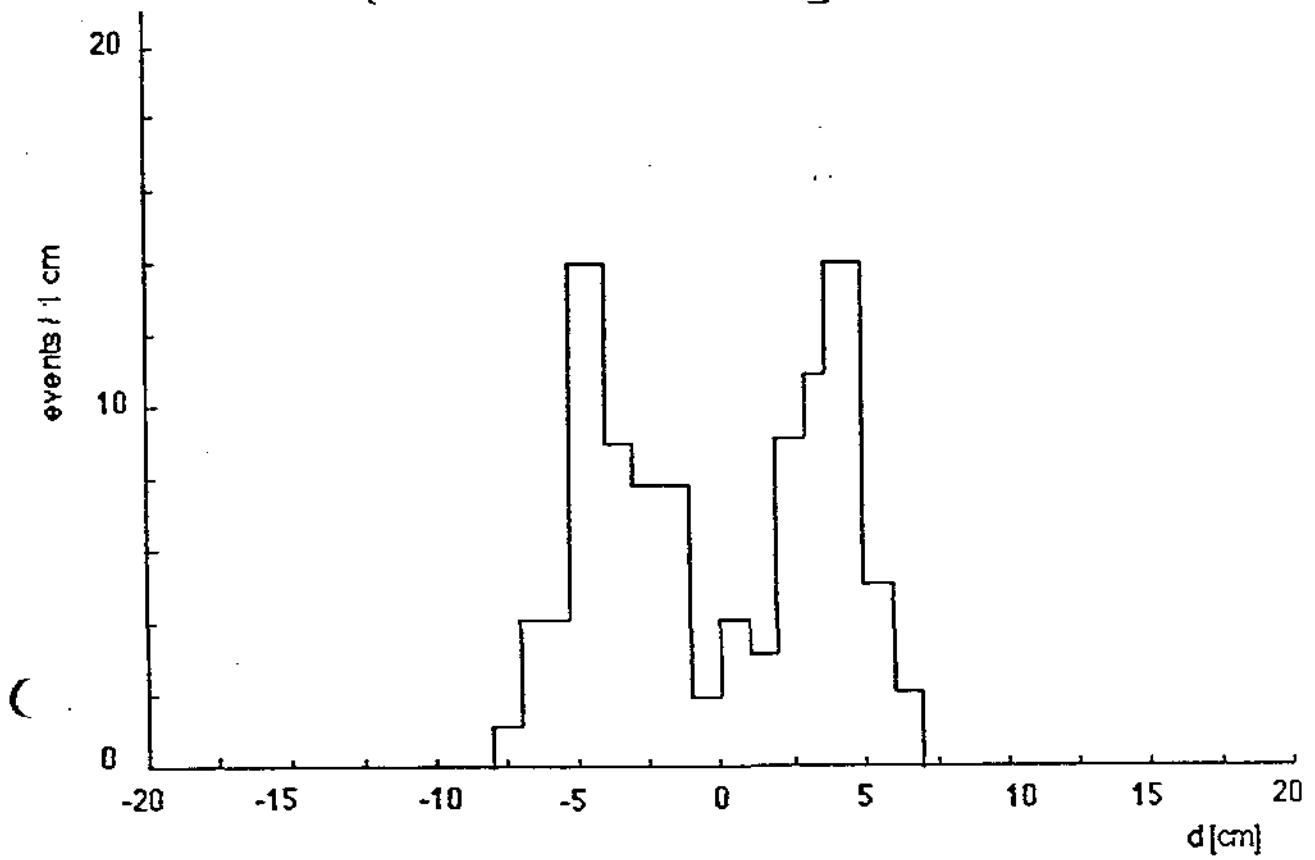
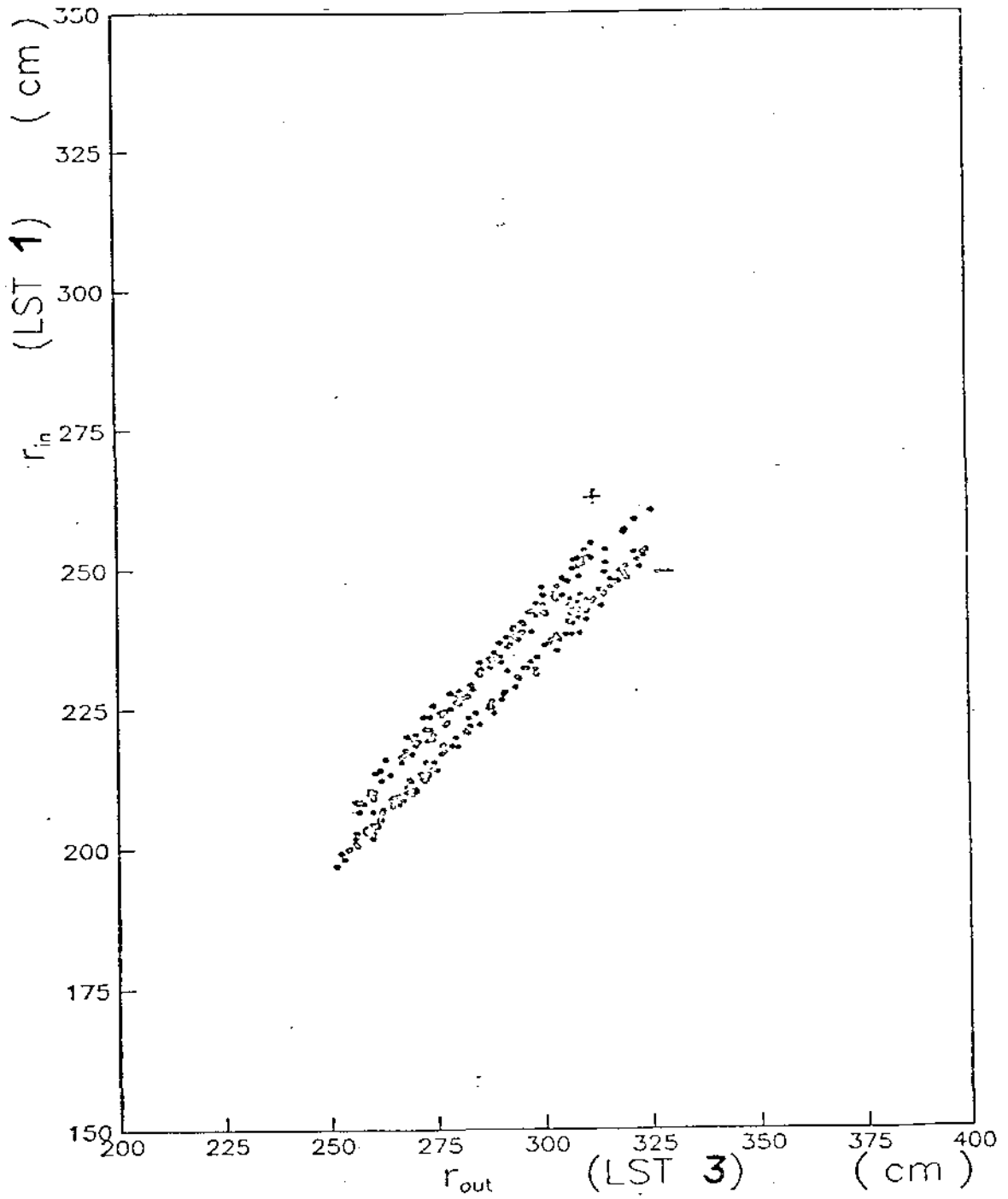


Fig. 3.13

$$p_{\perp}^{\pm} \quad 23^{\circ} \leq \theta \leq 30^{\circ} \quad \phi = 0^{\circ} \quad p_T = 5 \text{ GeV}/c$$

RADIAL DISTANCE CORRELATION
FOR HITS ON LAA LST PLANES

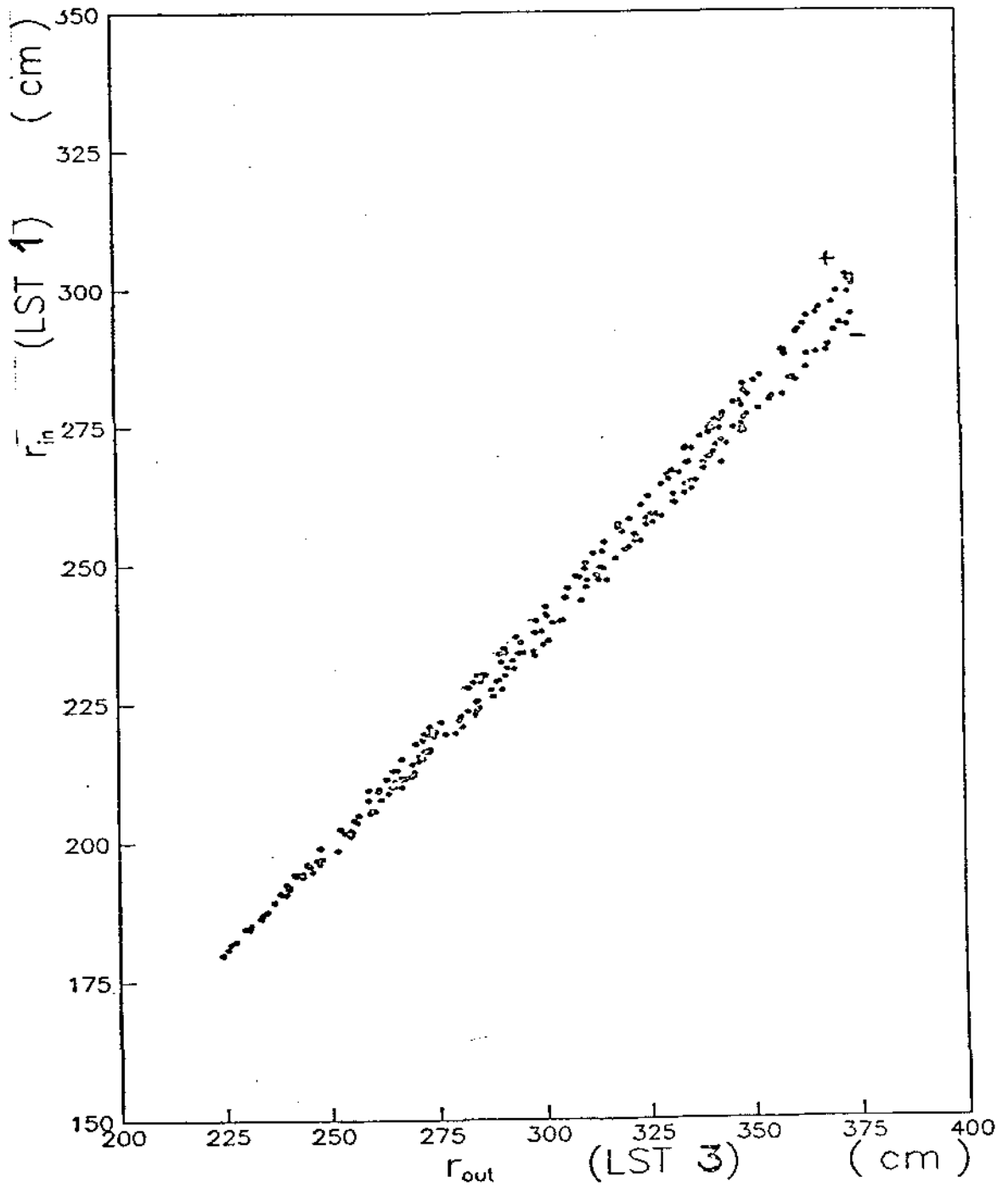


$\mu \approx 16^\circ < \theta < 23^\circ$ $\phi = 0^\circ$ $P_T = 5.6 \text{ GeV}/c$

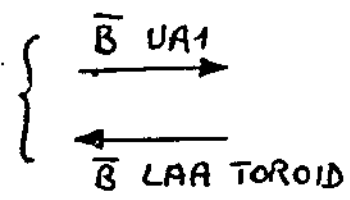
\uparrow \bar{B} LAA TOROID

\leftarrow
 \bar{B} UA1

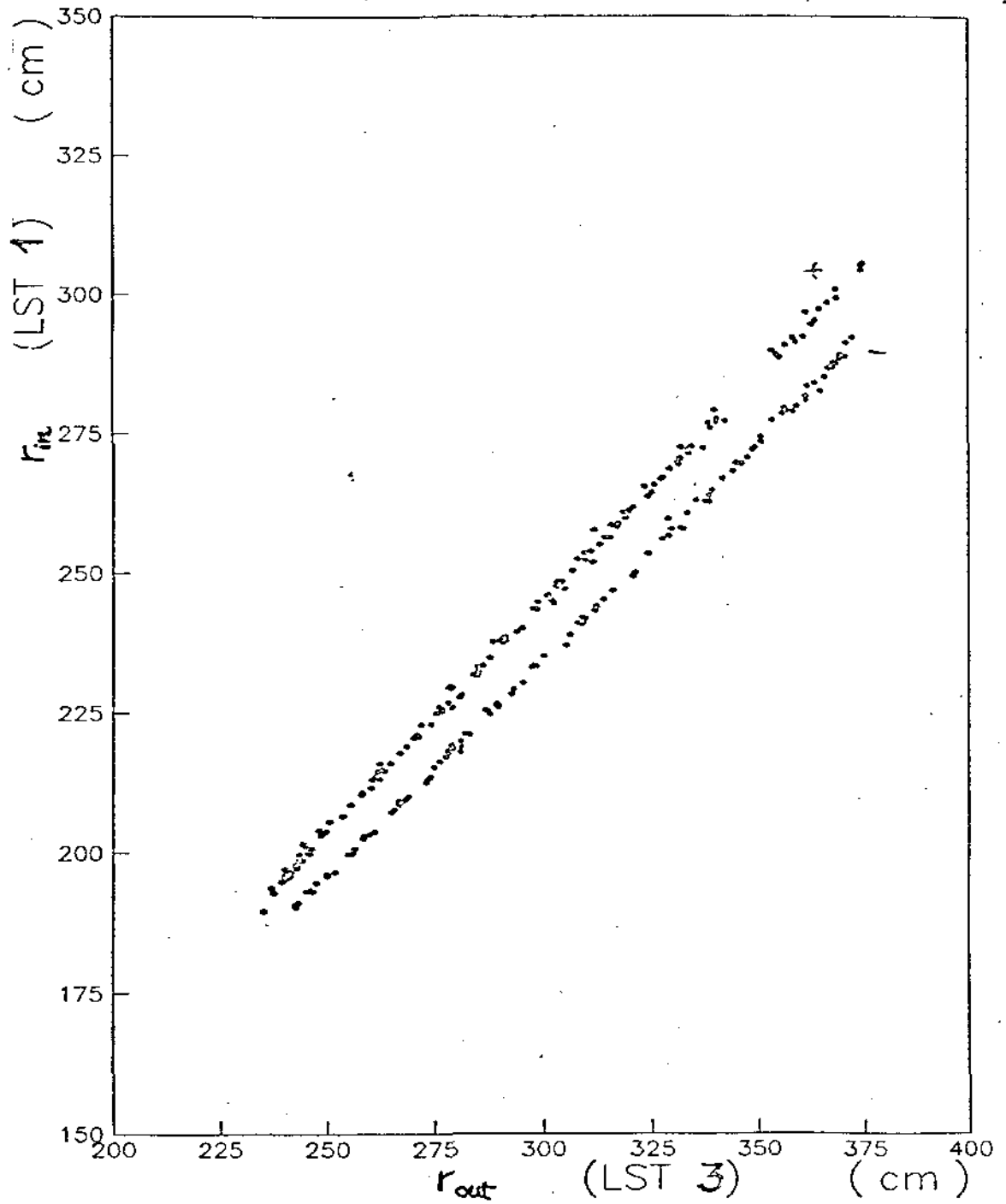
FOR HITS ON LAA LST PLANES



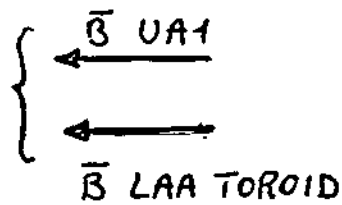
$\mu \approx 16^\circ < \theta < 30^\circ$ $\beta = 90^\circ$ $P_T = 5.6 \text{ GeV}/c$



RADIAL DISTANCE CORRELATION
FOR HITS ON LAA LST PLANES



μ^\pm $16^\circ < \theta < 30^\circ$ $\phi = 270^\circ$ $P_T = 5.6 \text{ GeV}/c$



DATA ACQUISITION SYSTEM

HARDWARE } TO BE AS COMPATIBLE AS POSSIBLE
 SOFTWARE } WITH UA1 SYSTEM BASED ON VMEbus
 "DISTRIBUTED INTELLIGENCE" FOR DATA
 ACQUISITION AND REDUCTION

MONITOR VMEbus BASED SYSTEM TO MONITOR:

- HIGH VOLTAGES
- THRESHOLDS ON SCINTILLATION
 COUNTERS AND LST
- TRIGGER ELECTRONICS

COMPUTER A COMPUTER FOR PROGRAM DEVELOPMENT,
 TEST OF (PARTIAL) DATA ACQUISITION,
 etc.... WILL BE NEEDED BY ~ DEC. 1986.

(POSSIBLY: NORD-500 OR EQUIVALENT)

LAA

TEST

RUN

PURPOSE OF THE TEST RUN

- TO PROVE WE ARE ABLE TO TRIGGER WITH HIGH EFFICIENCY ON μ_e PRODUCED IN pp INTERACTIONS IN THE REGION NEAR THE BEAM PIPE

- TO CHECK OUR MONTE CARLO SIMULATION IN ORDER TO EXTRAPOLATE THE TRIGGER RATES MEASURED IN THE TEST RUN TO THE FULL SET-UP

SET UP COVERAGE

THE LONGITUDINAL AXES OF THE SPECTROMETERS
POINT TO THE VERTEX AT

$$\theta = 7.5^\circ$$

COVERAGE :

(PSEUDORAPIDITY

$$|\eta| = 2.5 \div 2.9$$

AZIMUTH

$$\phi = -10^\circ \div 10^\circ$$

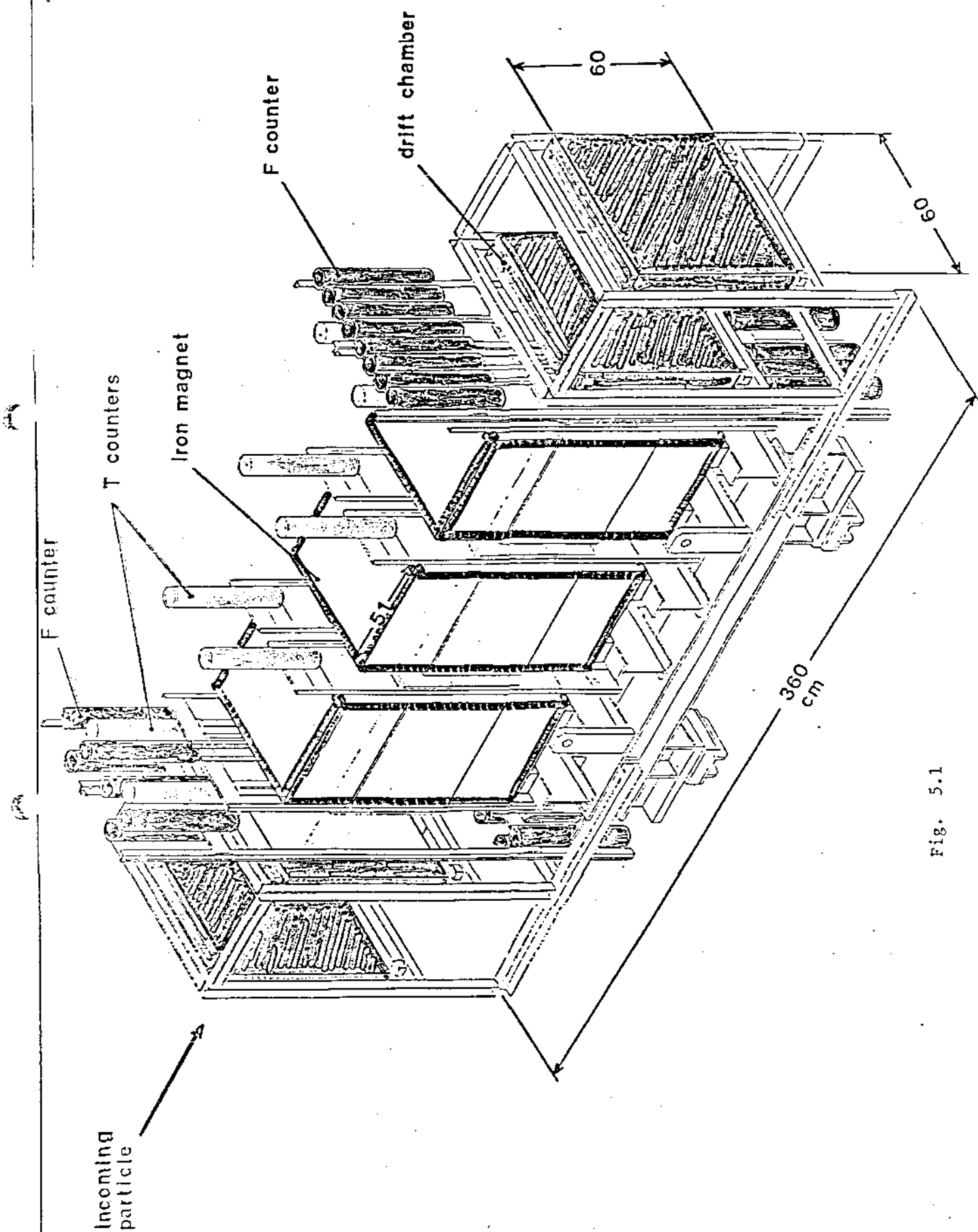


Fig. 5.1

OUTGOING
PROTON
BERM

10 m.
from
interaction
point

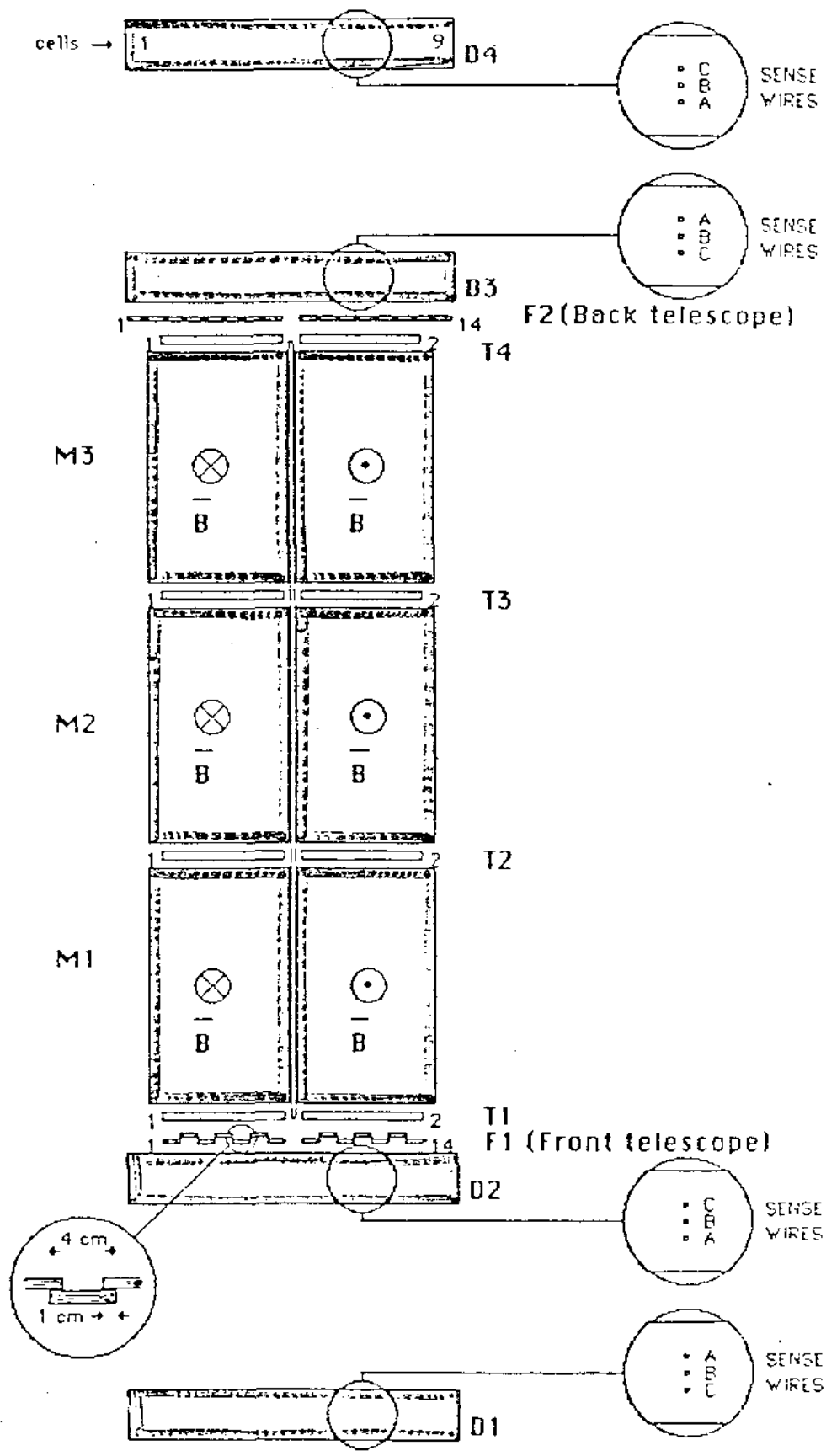


Fig. 5.3

THE SET-UP

2 SPECTROMETERS IN THE FORWARD AND BACKWARD U/A REGIONS.

EACH SPECTROMETER CONSISTS OF:

— 3 IRON MAGNETS (FOR A TOTAL THICKNESS OF 153 cm)

THICKNESS	:	51 cm	} EACH
CROSS-SECTION	:	60 x 100 cm ²	
VERTICAL WINDOW	:	5 x 50 cm ²	
FIELD	:	1.7 Tesla	

— 4 PLANES OF SCINTILLATION TOF COUNTERS

(T1 → T4)

2 COUNTERS / PLANE, i.e. 8 COUNTERS

28 x 58 x 2 cm ³	} EACH
2 PHOTOMULTIPLIERS	

USED FOR TRIGGER AND TIME-OF-FLIGHT PURPOSES

— 2 PLANES OF SCINTILLATION FINGER COUNTERS
(F1 → F2)

14 COUNTERS / PLANE, i.e. 28 COUNTERS

4 × 50 × 2 cm³ } EACH
1 PHOTOMULTIPLIERS

MOUNTED VERTICALLY AND PLACED IN SUCH A WAY AS TO BE ALIGNED ALONG THE LINES POINTING TO THE INTERACTION VERTEX

(USED FOR TRIGGER PURPOSES

— 4 DRIFT CHAMBERS
(D1 → D4)

60 × 60 cm²
9 CELLS OF ± 3.5 cm
3 STAGGERED WIRES / CELL } EACH
Argon / Ethane (60/40%)
SPATIAL RESOLUTION ~ 300 μm

USED FOR TRACK RECONSTRUCTION

FIELD LINES

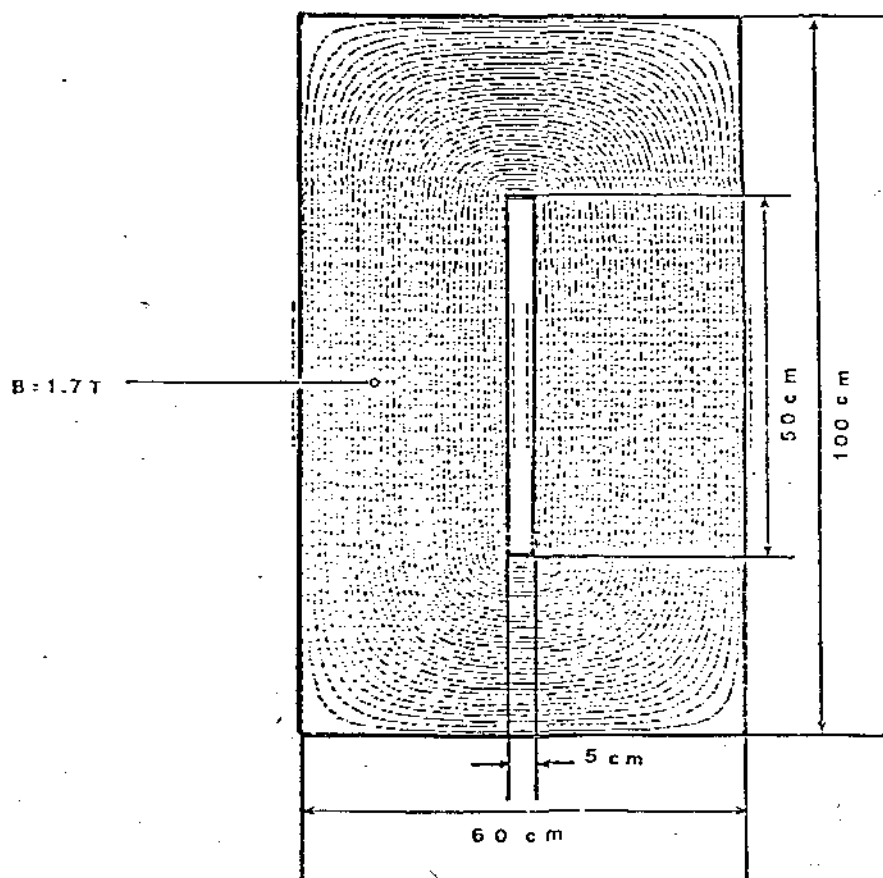


Fig. 5.2

EXPECTED RATES FROM π, K DECAY

MONTE CARLO CALCULATION TO ESTIMATE THE FLUX OF DECAY MUONS FROM PRIMARY INTERACTIONS IN LAA TEST SET-UP.

- $\frac{dN_{ch}}{d\eta}$ PSEUDORAPIDITY DISTRIBUTION (UA5) OF HADRONS

- $E \frac{d^3\sigma}{dp^3} \propto \frac{P_0^m}{(P_0 + P_T)^m}$ WITH $\begin{cases} p_0 = 1.49 \text{ GeV}/c \\ n = 9.87 \end{cases}$

FIT TO THE INVARIANT CROSS-SECTION FOR THE PRODUCTION OF HADRONS WITH $|\eta| < 2.5$ (UA1)

- $\pi : K$ RATIO = 2 : 1
- DECAY LENGTH = 290 cm
- MOMENTUM CUT (DUE TO RANGE) : 5 GeV/c

(TAKING INTO ACCOUNT IN THE SIMULATION :

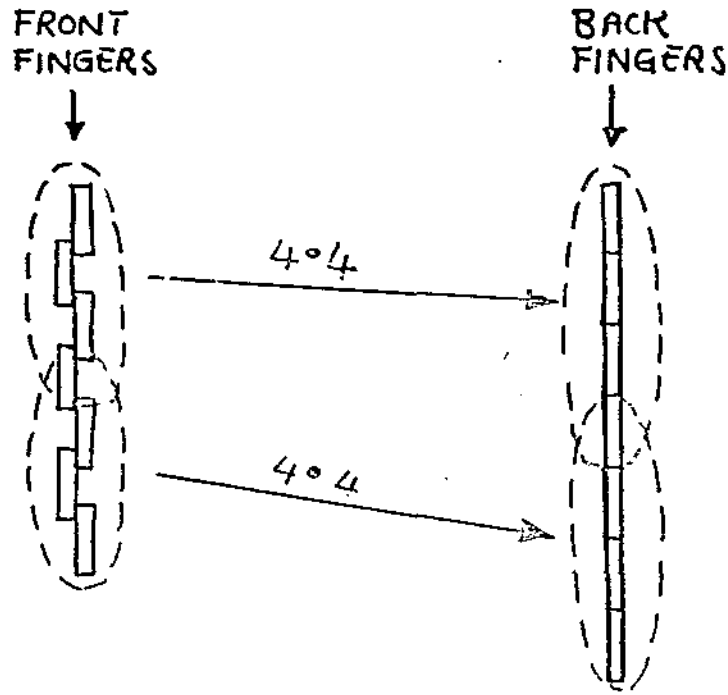
- THE HARDWARE TRIGGER GEOMETRICAL REQUIREMENTS OF LAA TEST
- THE EFFICIENCY OF UA1 MINIMUM BIAS TRIGGER

WE FIND :

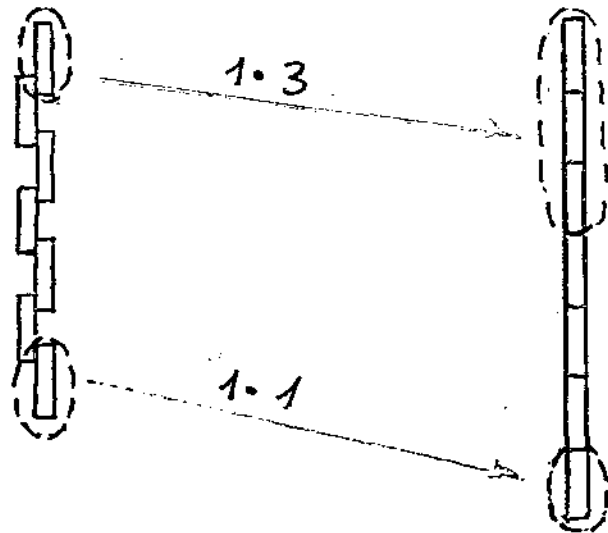
$$\boxed{\text{RATE/SIDE} = (0.15 \pm 0.01) \text{ Hz}} \quad \text{MAGNET OFF}$$

$$(L = 2 \times 10^{29} \text{ cm}^{-2} \text{ sec}^{-1}, \sqrt{s} = 630 \text{ GeV})$$

(HALF OF SPECTROMETER)



- FINGER CONFIGURATION (1) : 4.4 COINCIDENCES



- FINGER CONFIGURATION (2) : 1.3 COINCIDENCES
- FINGER CONFIGURATION (3) : 1.1 COINCIDENCES

WHEN MAGNET IS ON,
 CONFIGURATIONS (1) → (2) → (3) SELECT
 INCREASING p, i.e. PT, PARTICLES

TRIGGERS

(a)	T COUNTERS	(B = 0)
(b)	(a) • UA1 MINIMUM BIAS	(B = 0)
(c)	(b) • FINGERS (1)	(B = 0)
(d)	(b) • FINGERS (1)	(B = 1.7T)
(e)	(b) • FINGERS (2)	(B = 1.7T)
(f)	(b) • FINGERS (3)	(B = 1.7T)

COLLIDER SYNCHRONIZATION SIGNAL IN COINCIDENCE

MEASURED RATES

$$L = 2 \times 10^{29} \text{ cm}^{-2} \text{ sec}^{-1}$$

● TRIGGER (a) RATES:

OUTGOING \bar{p} SIDE :	0.11 ± 0.01 Hz
OUTGOING p SIDE :	0.30 ± 0.02 Hz

- IN OUTGOING \bar{p} SIDE, THE HALO ACCOMPANYING THE p BEAM IS ELIMINATED BY TIMING IN T COUNTERS

- IN OUTGOING p SIDE, THIS HALO REACHES THE SPECTROMETER IN TIME WITH PARTICLES PRODUCED IN $p\bar{p}$ INTERACTIONS

⇒ ADD TO OUR TRIGGER UA1 MINIMUM BIAS SIGNAL (WHICH ACCEPTS 85% OF THE TOTAL CROSS-SECTION)

● TRIGGER (b) RATES:

OUTGOING \bar{p} SIDE :	0.11 ± 0.01 Hz
OUTGOING p SIDE :	0.16 ± 0.01 Hz

REDUCTION OF HALO CONTRIBUTION ON p SIDE

TO BE COMPARED WITH MONTE CARLO

RATE/SIDE :	0.15 ± 0.01 Hz
-------------	--------------------

RATE IN FINGER COUNTERS

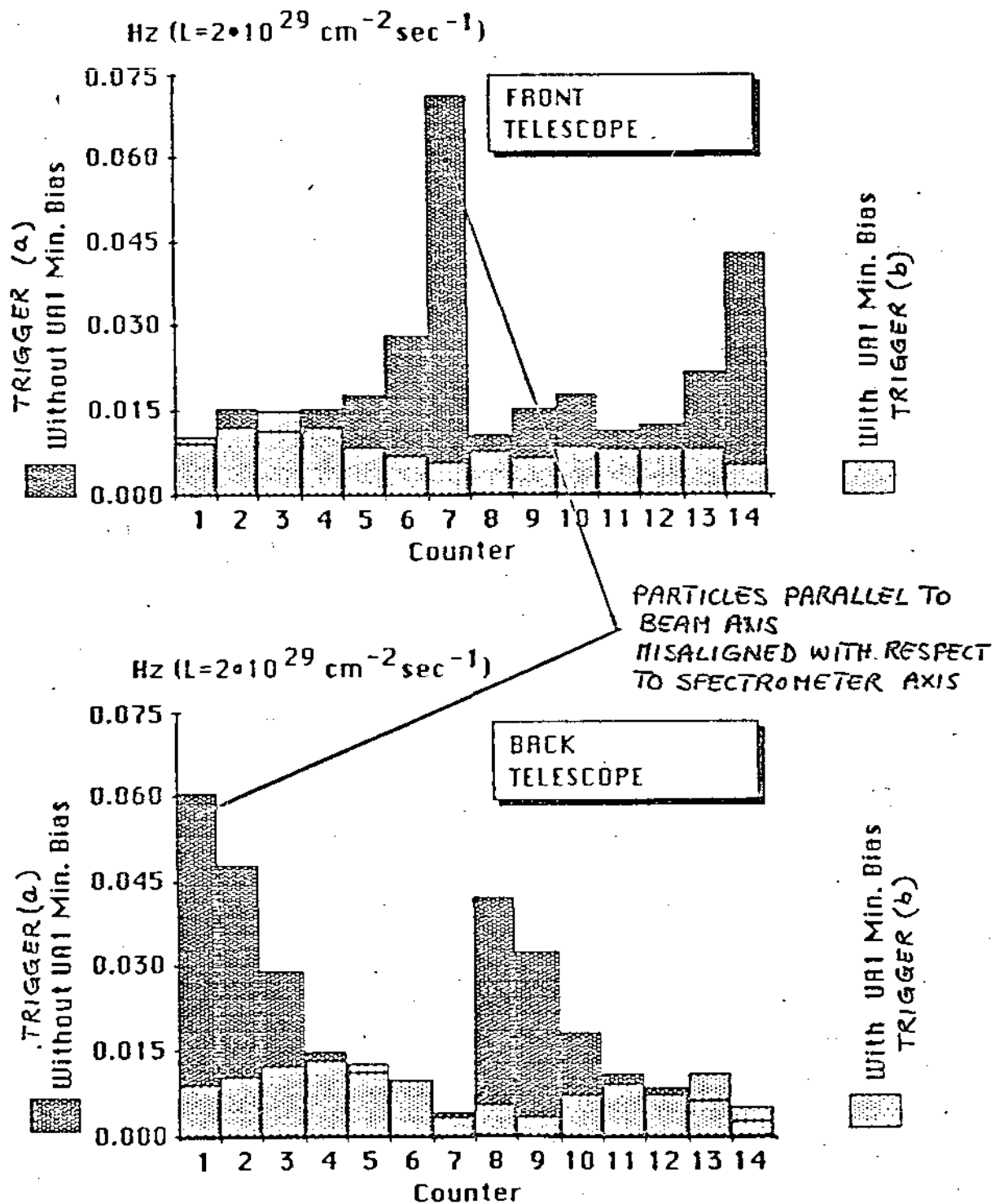


Fig. 5.6

Extrapolation of halo rate in UA1:

1.8 Hz/m² at 1.5 m from the beam

1.115

TRIGGER RATE SUMMARY
(Hz)

TRIGGER	MONTE CARLO ESTIMATE PER SIDE	OUTGOING \bar{p} SIDE	OUTGOING p SIDE	TOTAL
(a)	—	0.11	0.30	0.41
(b)	0.15	0.11	0.16	0.27
(c)	—	0.065	0.085	0.15
(d)	0.0093	0.015	0.020	0.035
(e)	0.0042	0.0065	0.0075	0.014
(f)	—	0.0018	0.0023	0.0041

WITH $B=1.7T$, THE FINAL TRIGGER RATE CAN BE REDUCED BY MEANS OF THE FINGER COUNTERS, i.e. BY CHOOSING AN APPROPRIATE p_T W_T , REJECTING LOW MOMENTUM HIGHLY DEFLECTED PARTICLES.

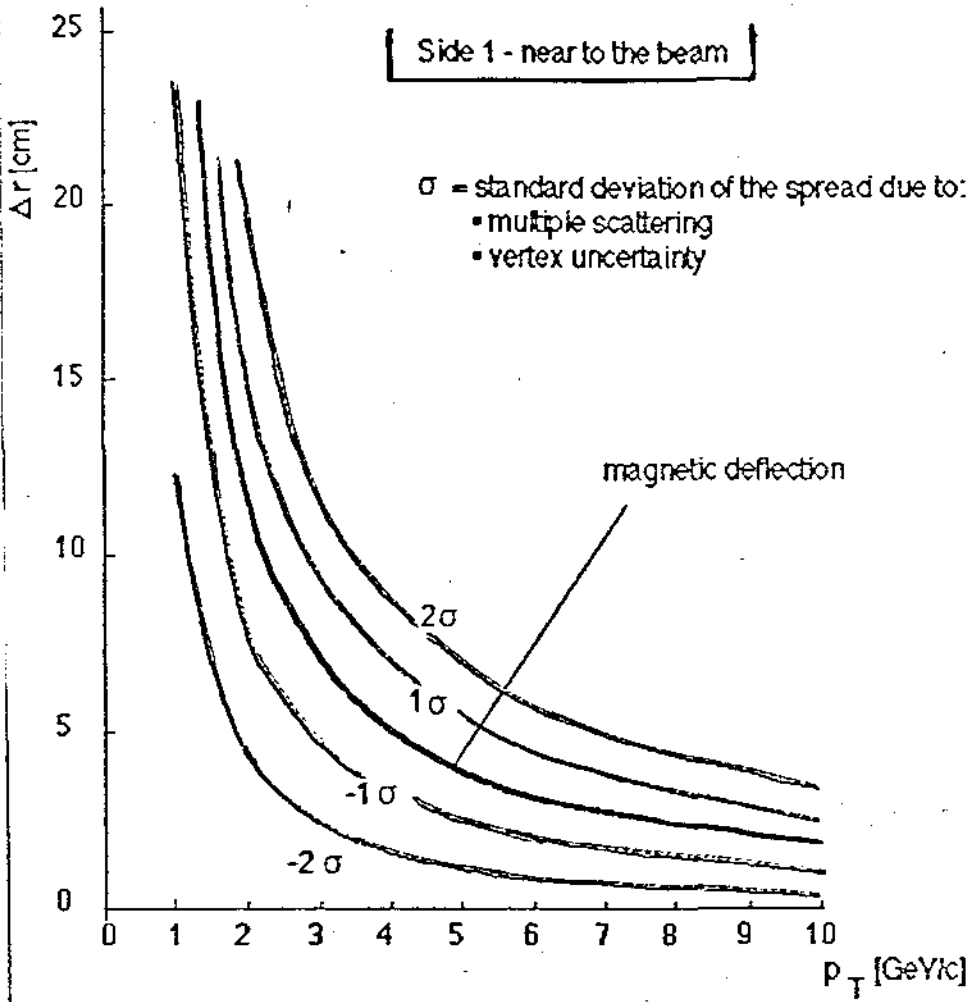


Fig. 5.7

TRIGGER EFFICIENCY

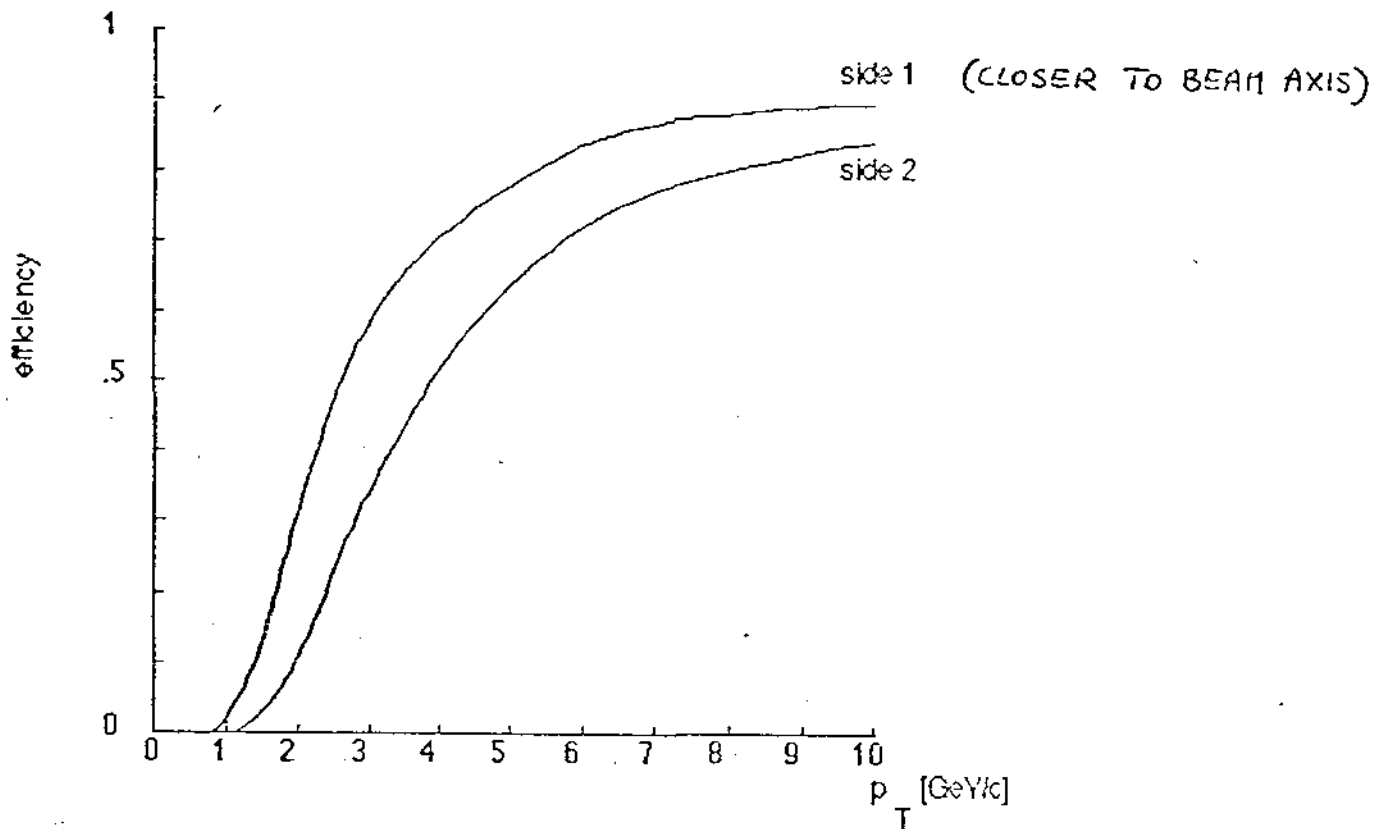


Fig. 5.8

TRIGGER (d):

T COUNTERS • FINGERS (1) • (B=1.7 T)

↑
(4•4 COINCIDENCES)

	DATE	LUMINOSITY (nb ⁻¹)	MAGNET CURRENT (Amp)	N. OF TRIGGERS
LAA Test	29/10/1985 → 21/12/1985	223	+ 20 - 20 0	1.33 × 10 ⁷ 1.08 × 10 ⁷ 2.45 × 10 ⁷
LAA • UA1 it	12/12/1985 → 13/12/1985	10	+ 20	1.75 × 10 ³

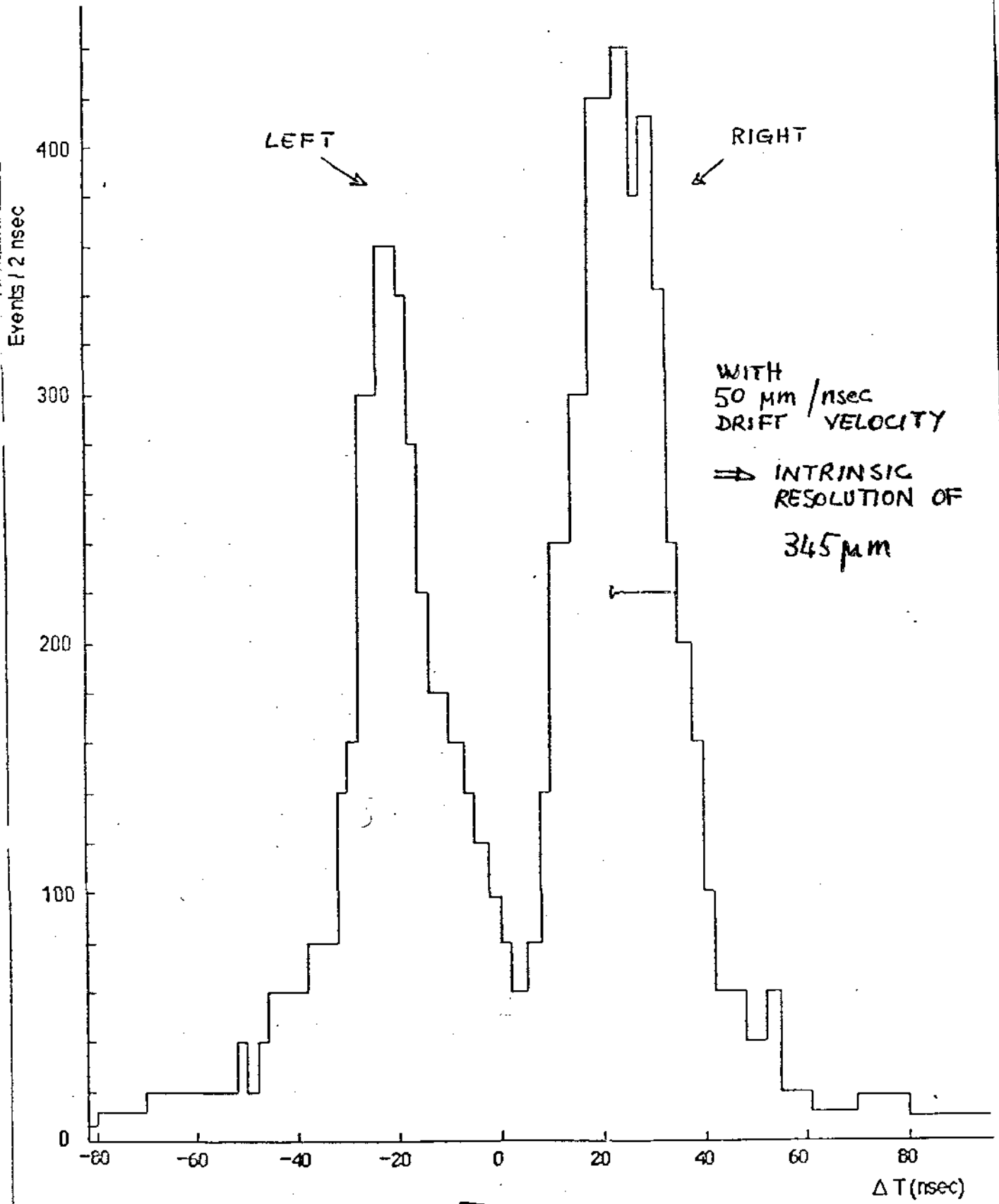
SUMMARY OF
LAA TEST RUN
DATA TAKING

OFF LINE ANALYSIS

DATA HAVE BEEN COLLECTED WITH TRIGGER (d):

T COUNTERS • UA1 MIN. BIAS • FINGERS (1) • (B = 1.7 T)
↑
(4•4 COINC.)

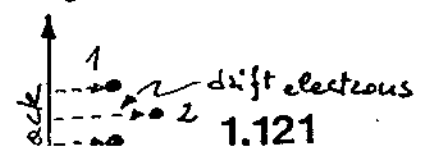
DUE TO THE SHORT INSTALLATION TIME, IT WAS NOT POSSIBLE TO PUT MUCH CARE ON DRIFT CHAMBERS ALIGNMENT \Rightarrow SETTING ERROR OF THE ORDER OF 1 mm.



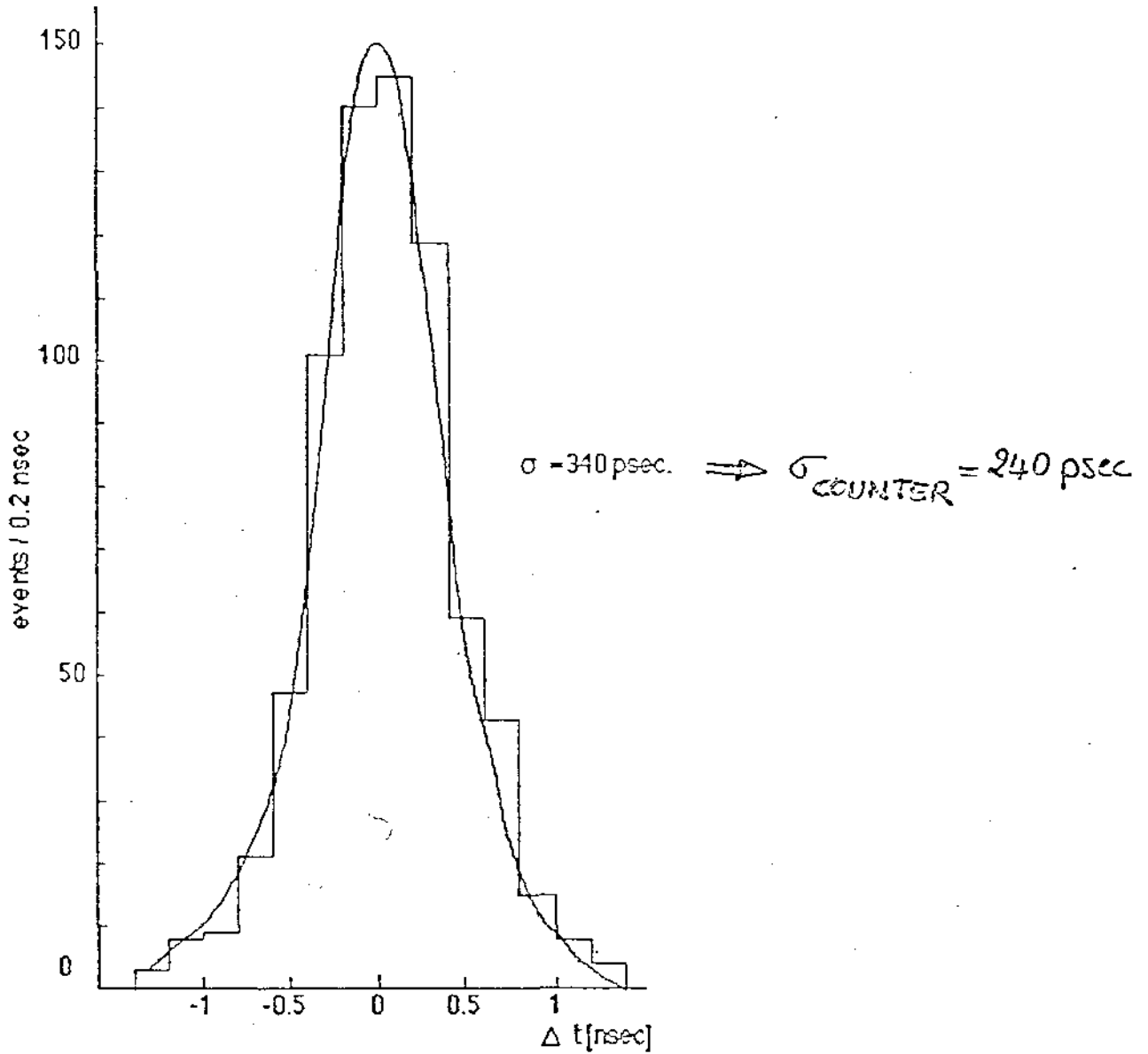
$$\Delta T = \left(\frac{T_1 + T_3}{2} \right) - T_2$$

Fig. 5.9

T_1, T_2, T_3 Time signals of staggered wires



TIME-OF-FLIGHT DISTRIBUTION IN T COUNTERS



$$\Delta t = \left(\frac{t_1^U + t_1^D}{2} \right) - \left(\frac{t_2^U + t_2^D}{2} \right)$$

FOR A PAIR OF T COUNTERS 1, 2
Fig. 5.4

WITH: U (D) = PHOTOMULTIPLIER
UP (DOWN)

RECONSTRUCTED MOMENTUM
DISTRIBUTION (corrected for energy loss)

$\langle p \rangle \approx 13 \text{ GeV}/c$

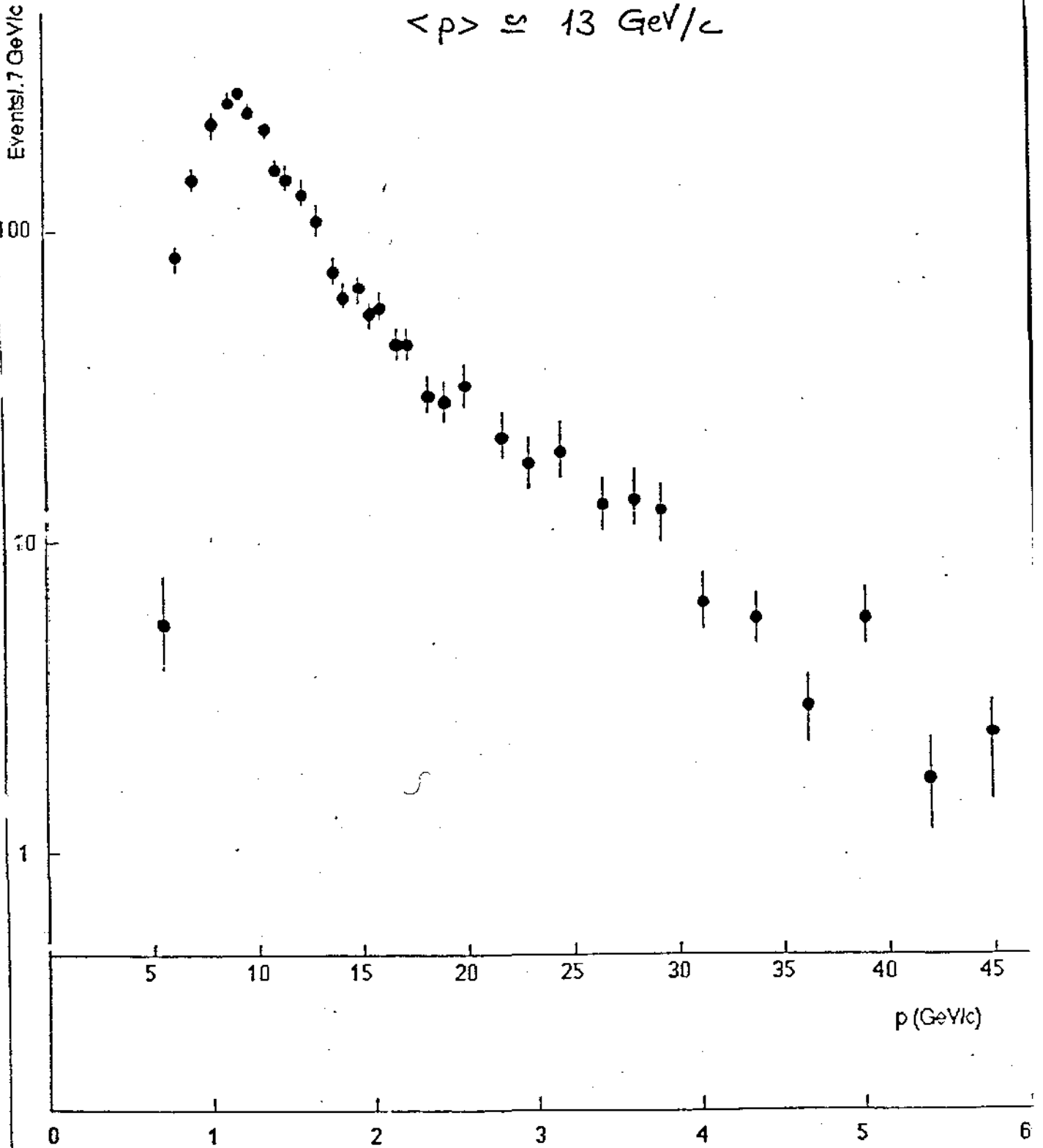


Fig. 5.10

$P_T \text{ (GeV}/c)$

$\langle \theta \rangle = 7.5^\circ$

1.123

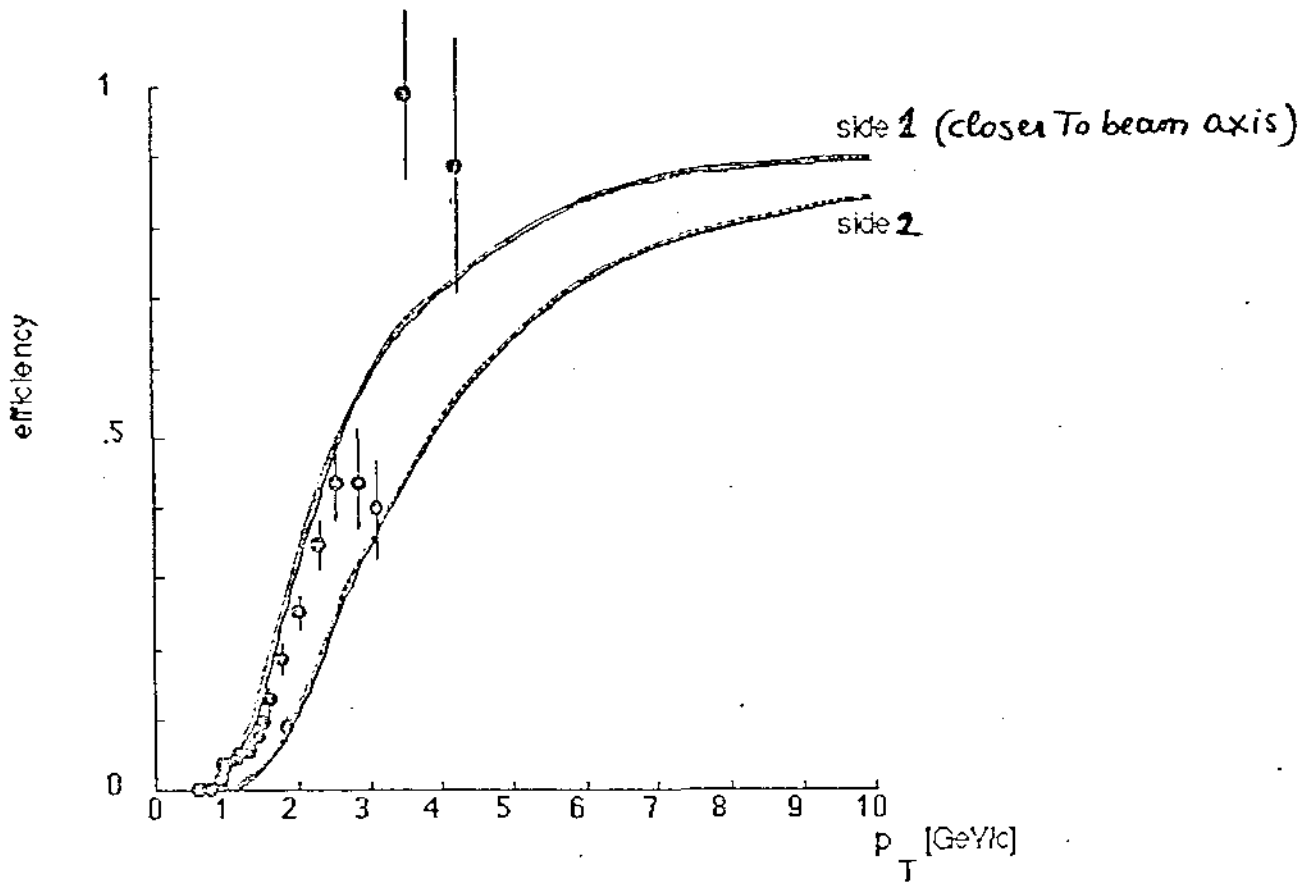


Fig. 5.11

RATIO $\frac{\text{EXPERIMENTAL } p_T \text{ DISTRIBUTION}}{\text{MONTE CARLO}}$

COMPARED WITH THE EXPECTED TRIGGER (d)
EFFICIENCY

LAA IN UA1 TRIGGER LOGIC

INSERT LAA TEST IN UA1 TRIGGER LOGIC
IN ORDER TO PROCEED FURTHER AND TO STUDY
THE COMPLETE EVENTS, AS SEEN BY UA1.

10 nb⁻¹ INTEGRATED LUMINOSITY COLLECTED TO
THIS PURPOSE.

A SAMPLE OF EVENTS, RECONSTRUCTED BOTH IN
UA1 AND IN LAA SPECTROMETER, HAS BEEN
SELECTED TO BE SCANNED BY EYE USING THE
EVENT DISPLAY FACILITY OF UA1 MEGATEK.

TWOFOLD PURPOSE :

- TO CHECK THE GENUINITY OF THE TRACKS
TRIGGERED BY LAA TEST, i.e. THEIR
PRODUCTION BY TRUE p \bar{p} INTERACTIONS.
- TO CHECK THE CONSISTENCY OF THE MOMENTA
MEASURED BY UA1 AND THE LAA TEST
SET-UP.

SCANNING :

116 events

SEARCH FOR TRACKS HAVING MOMENTA ABOVE ~ 5 GeV/c AND WHOSE EXTRAPOLATION FROM UA1 CENTRAL DETECTOR POINTS TO LAA TEST SET-UP.

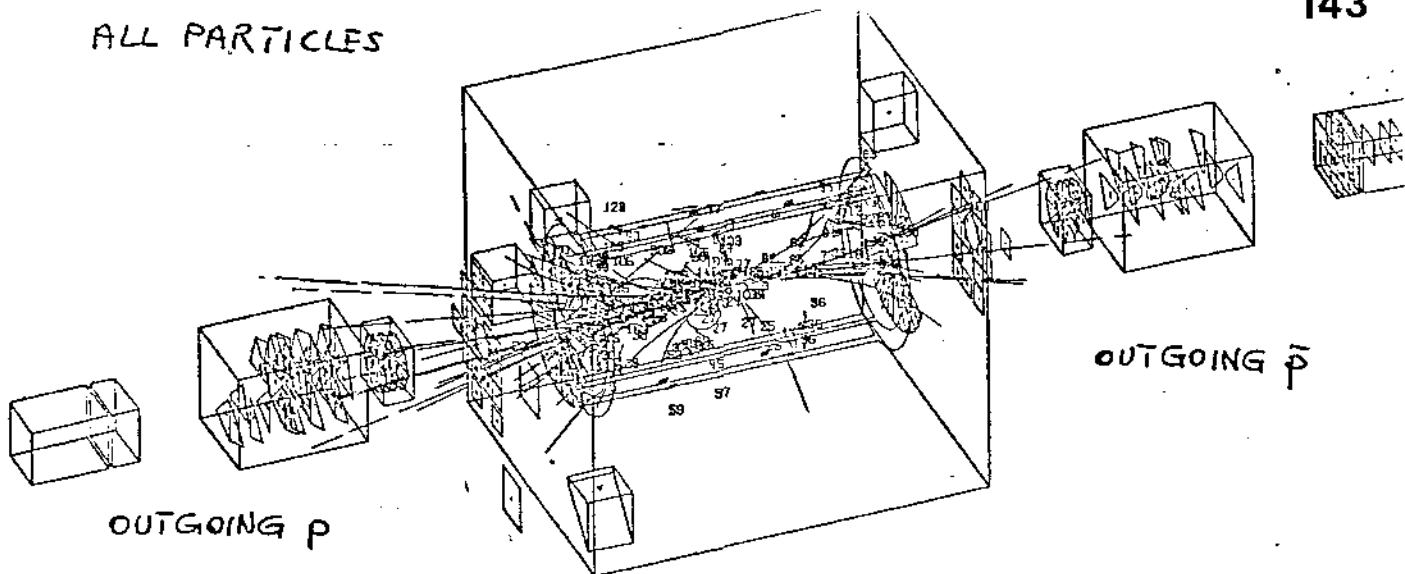
WE FOUND :

- o 1 DOUBLE INTERACTION EVENT
- o 3 EVENTS WITH A STRONG UNBALANCE OF TRACKS BETWEEN INCOMING p AND \bar{p} HEMISPHERES (PROBABLY DUE TO BEAM-GAS INTERACTIONS)
- o 1 ALMOST EMPTY EVENT (<10 RECONSTRUCTED TRACKS)
- o 2 EVENTS WHERE THE LAA TRIGGER TRACK WAS CLEARLY IDENTIFIED AS A HALO TRACK

THE REMAINING EVENTS (94%) WERE INDEED $p\bar{p}$ INTERACTIONS.

IN ORDER TO CHECK THE MOMENTUM MEASUREMENT OF LAA TEST WITH UA1, WE HAVE TAKEN 54 EVENTS WHERE A TRACK WAS UNAMBIGUOUSLY POINTING TO LAA SET-UP.

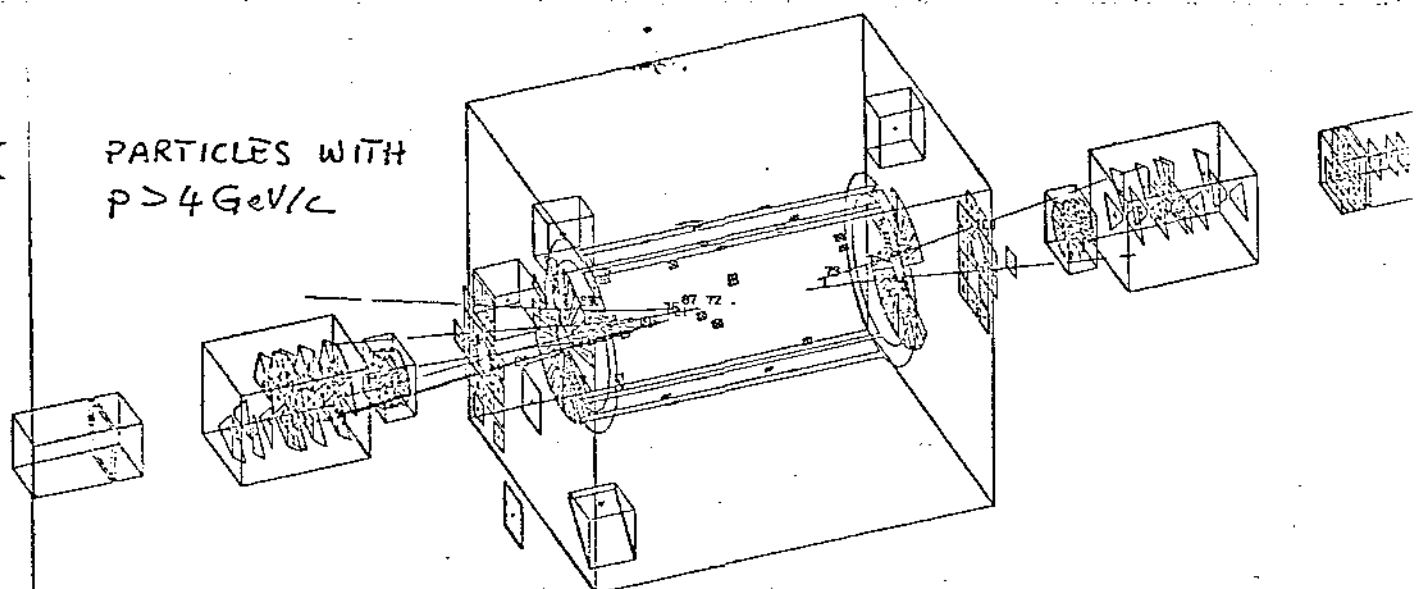
ALL PARTICLES



OUTGOING p

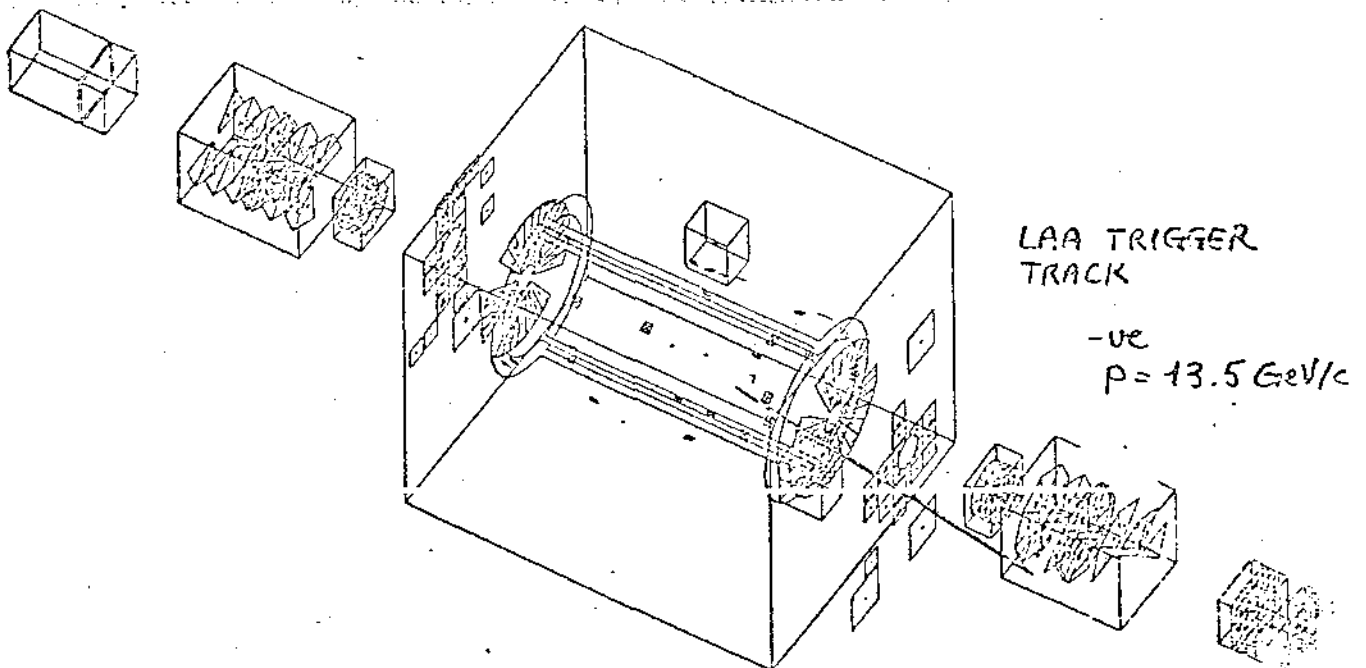
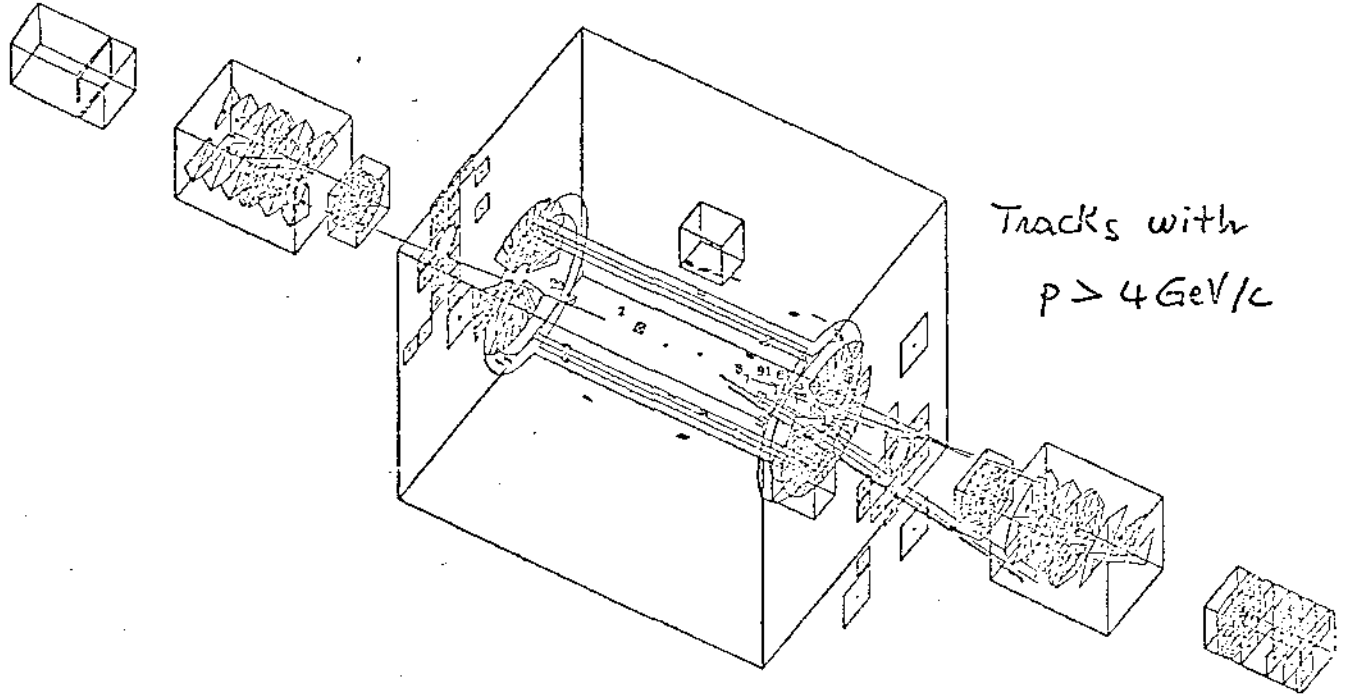
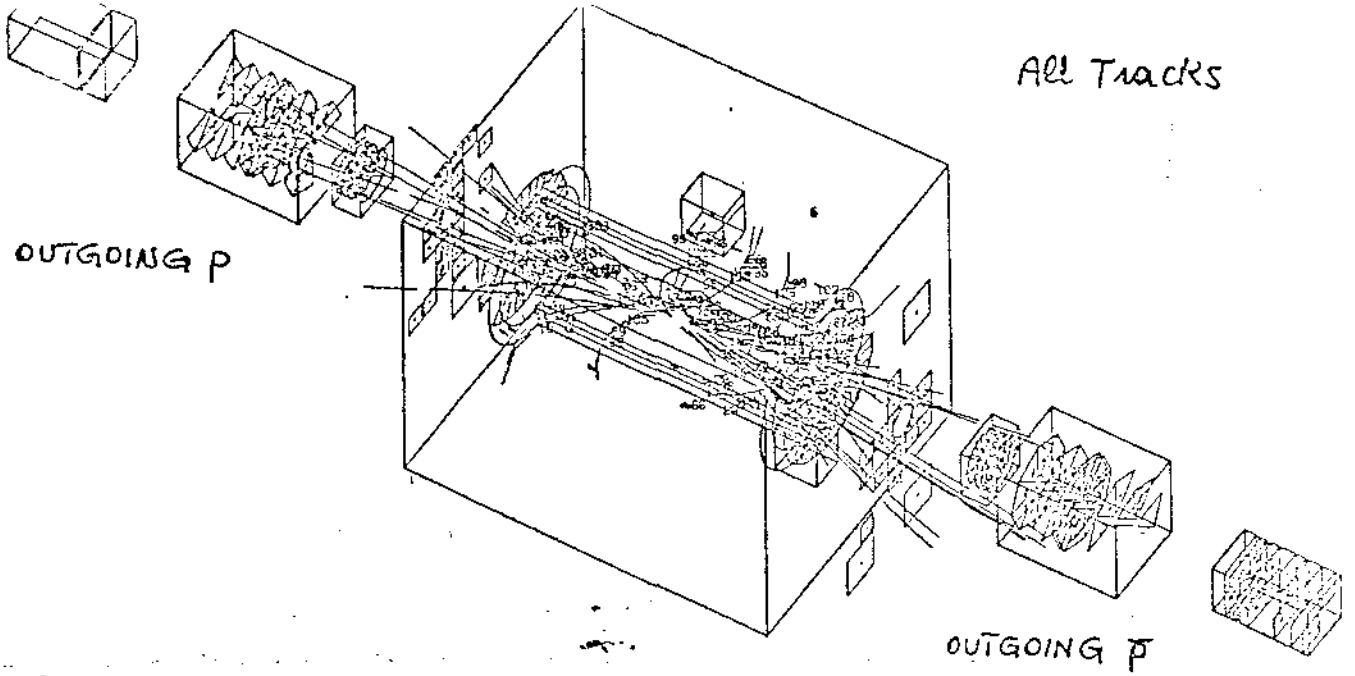
OUTGOING \bar{p}

PARTICLES WITH $p > 4 \text{ GeV}/c$

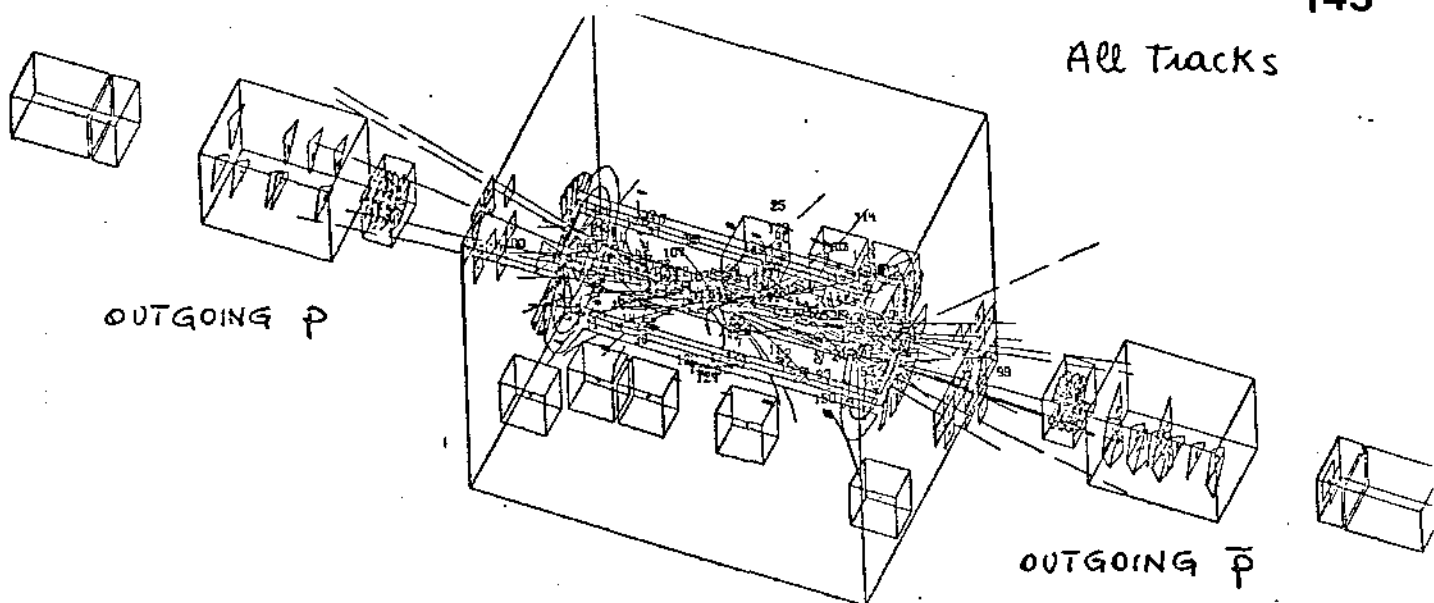


LAA TRIGGER TRACK

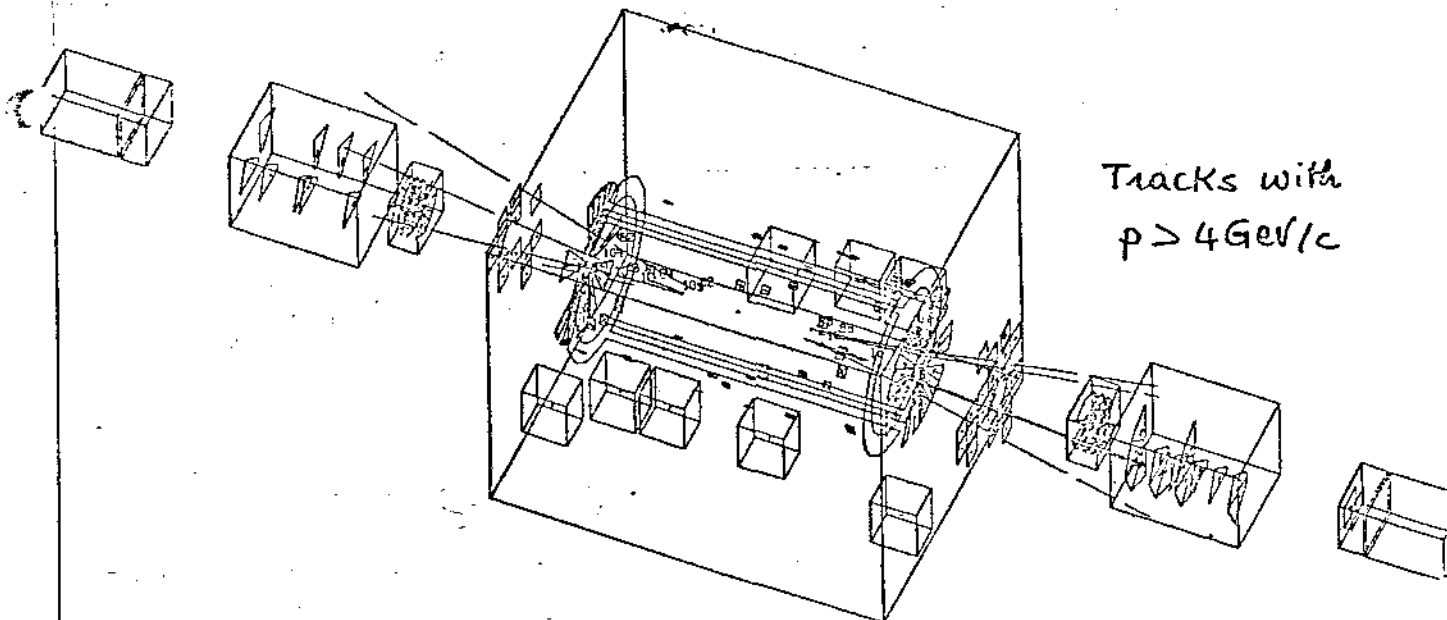
+ve
 $p = 12 \text{ GeV}/c$
 $\eta = -2.7$



All Tracks

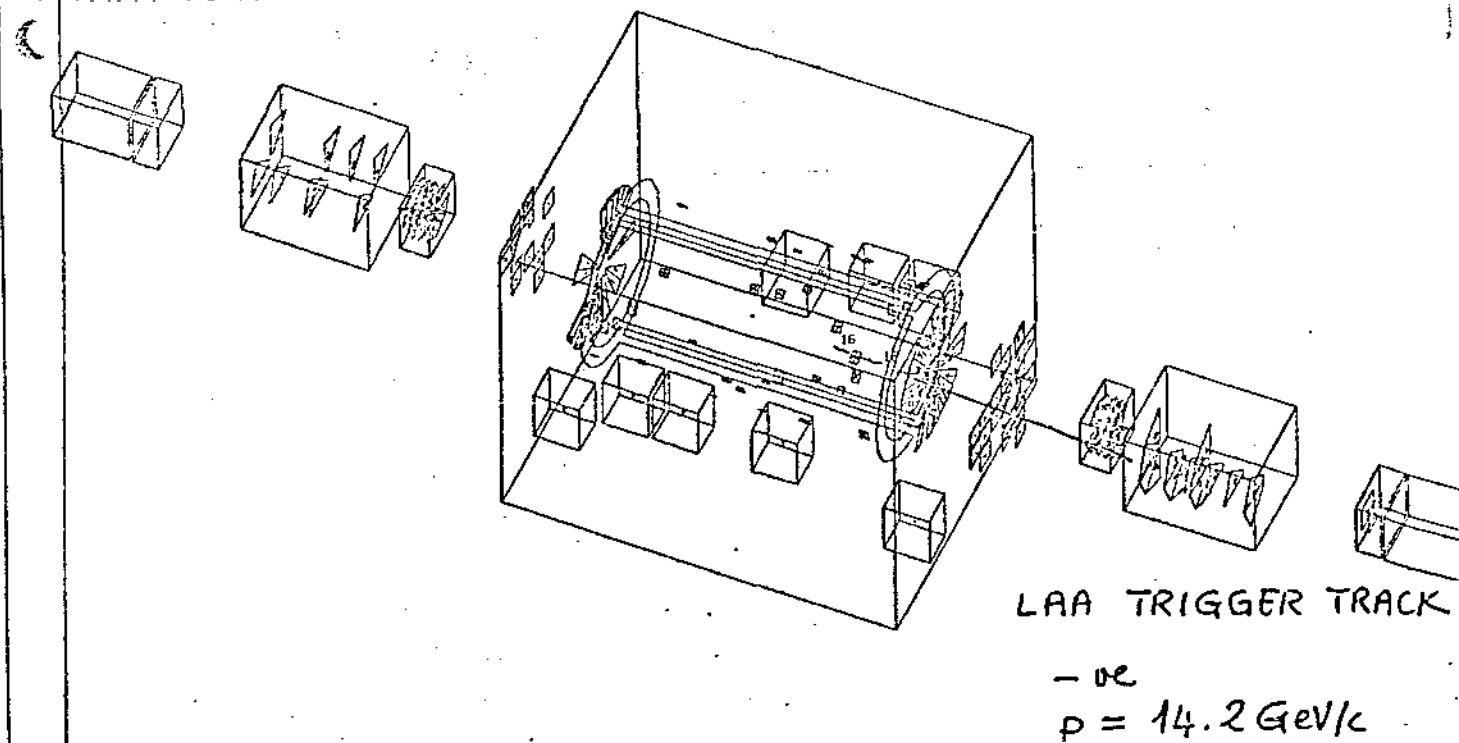


Tracks with $p > 4 \text{ GeV}/c$

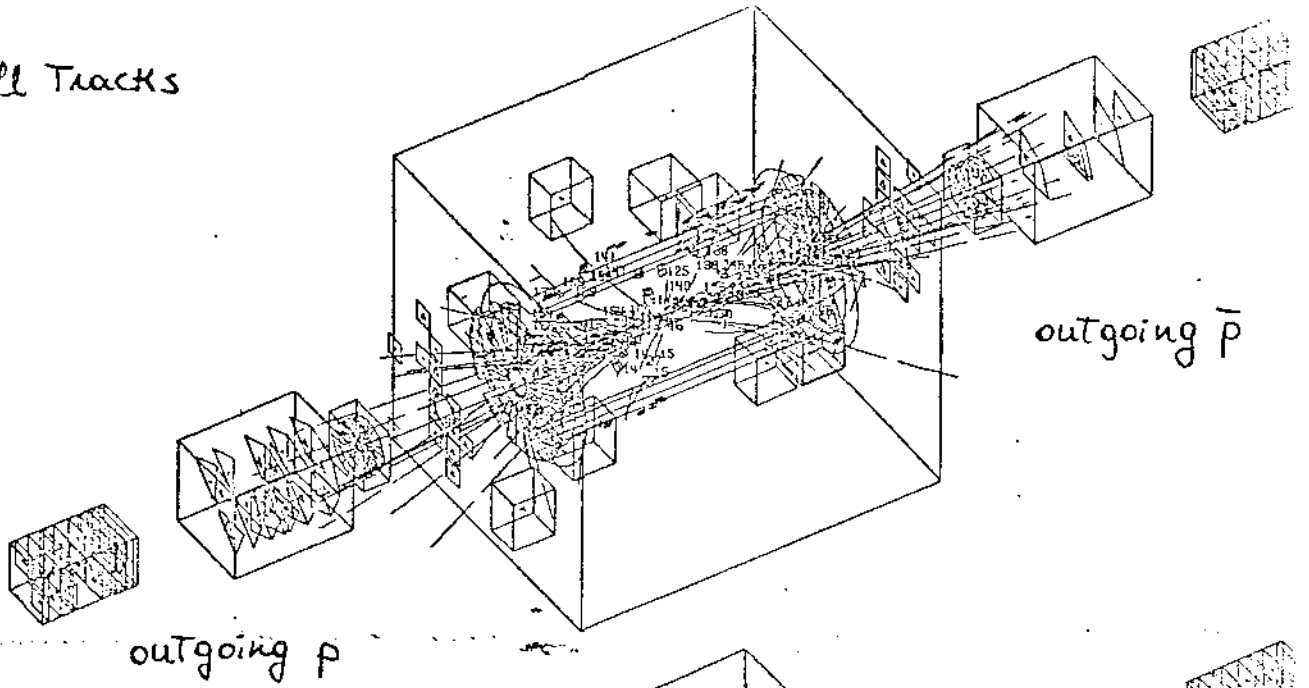


LAA TRIGGER TRACK

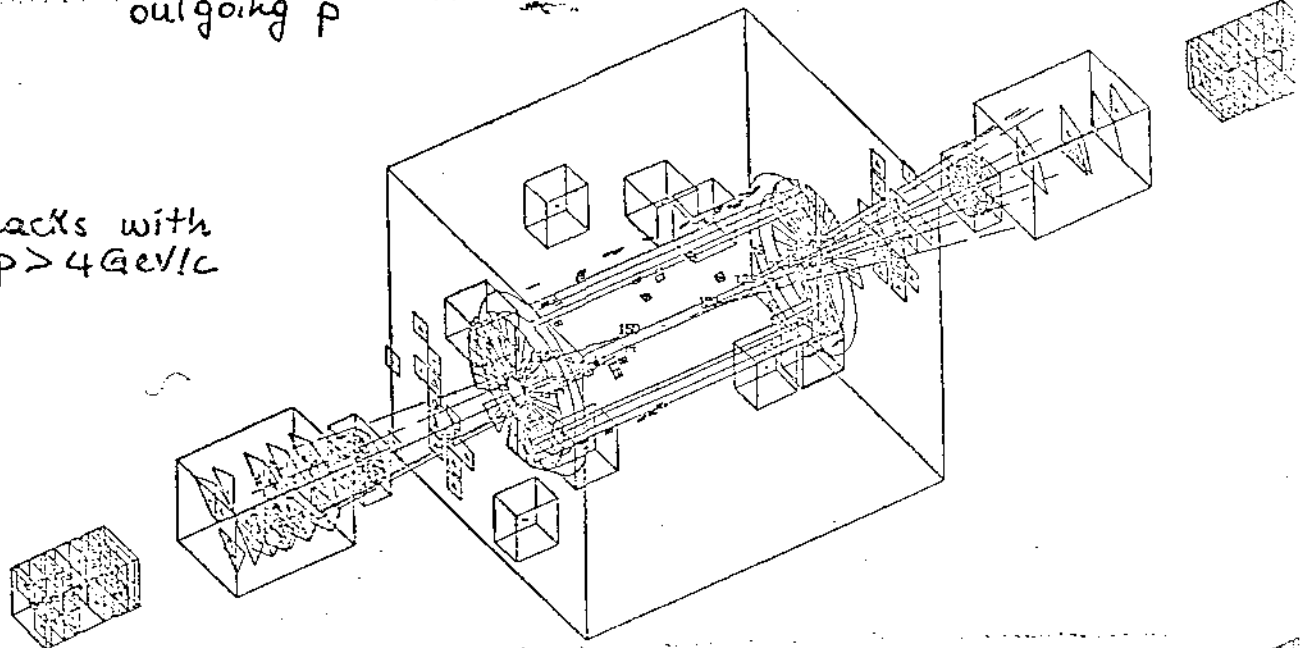
- ν_e
 $p = 14.2 \text{ GeV}/c$



All Tracks

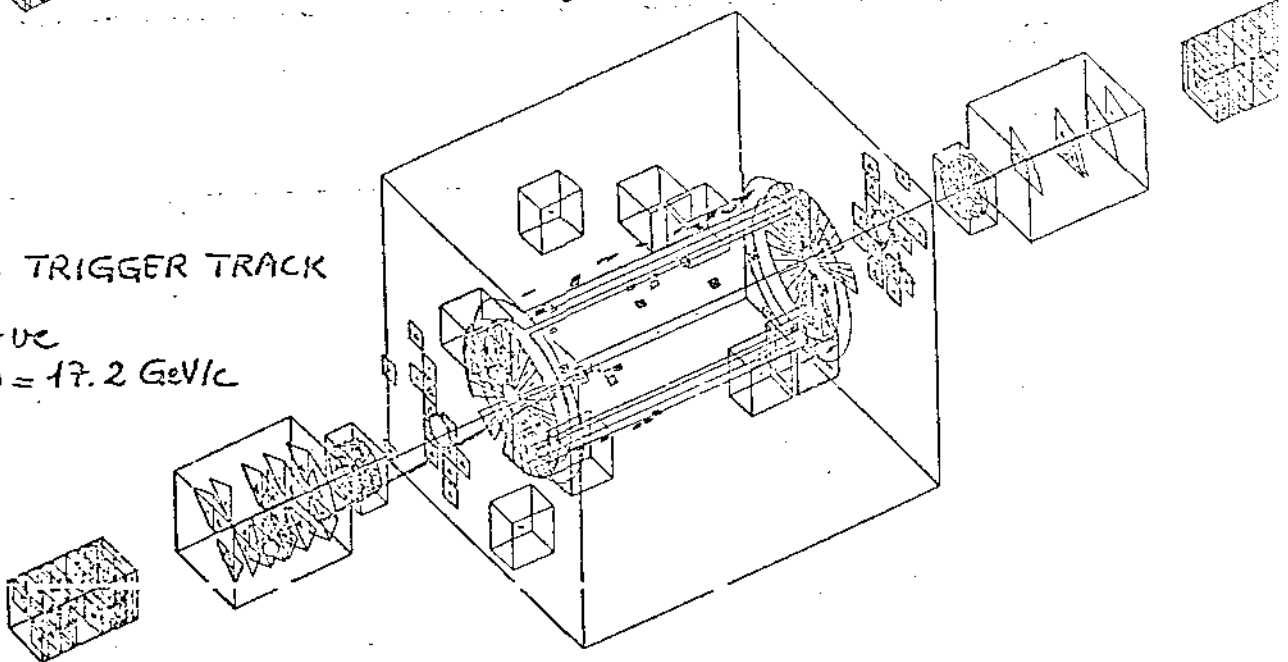


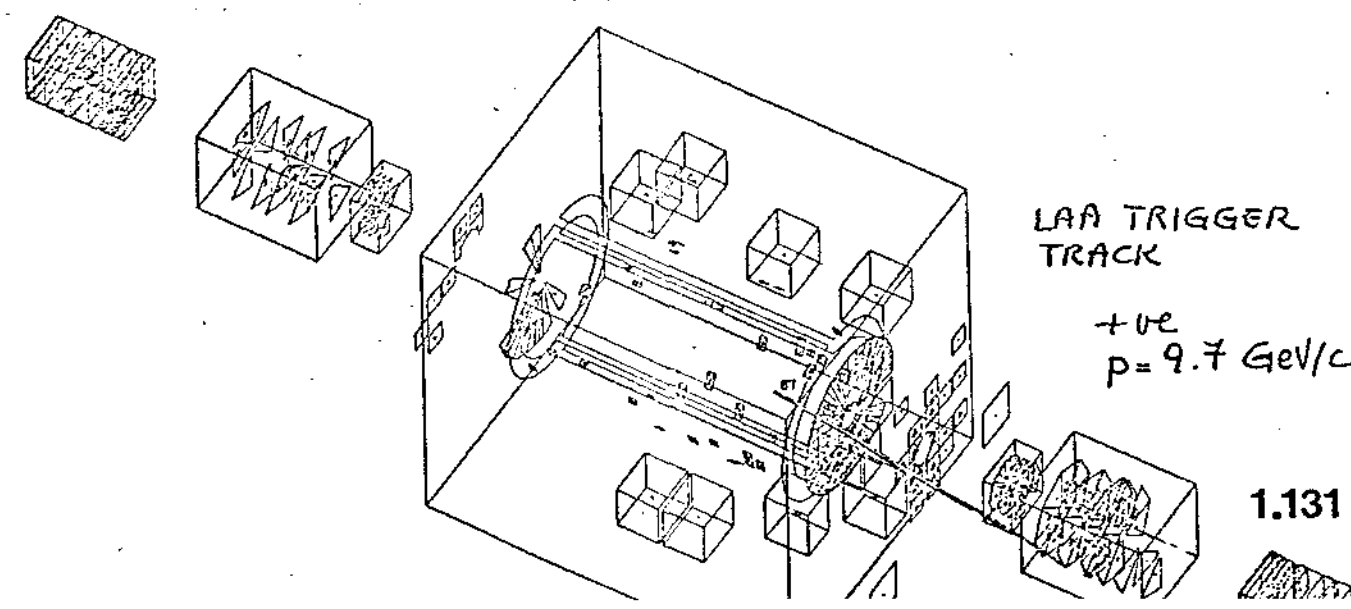
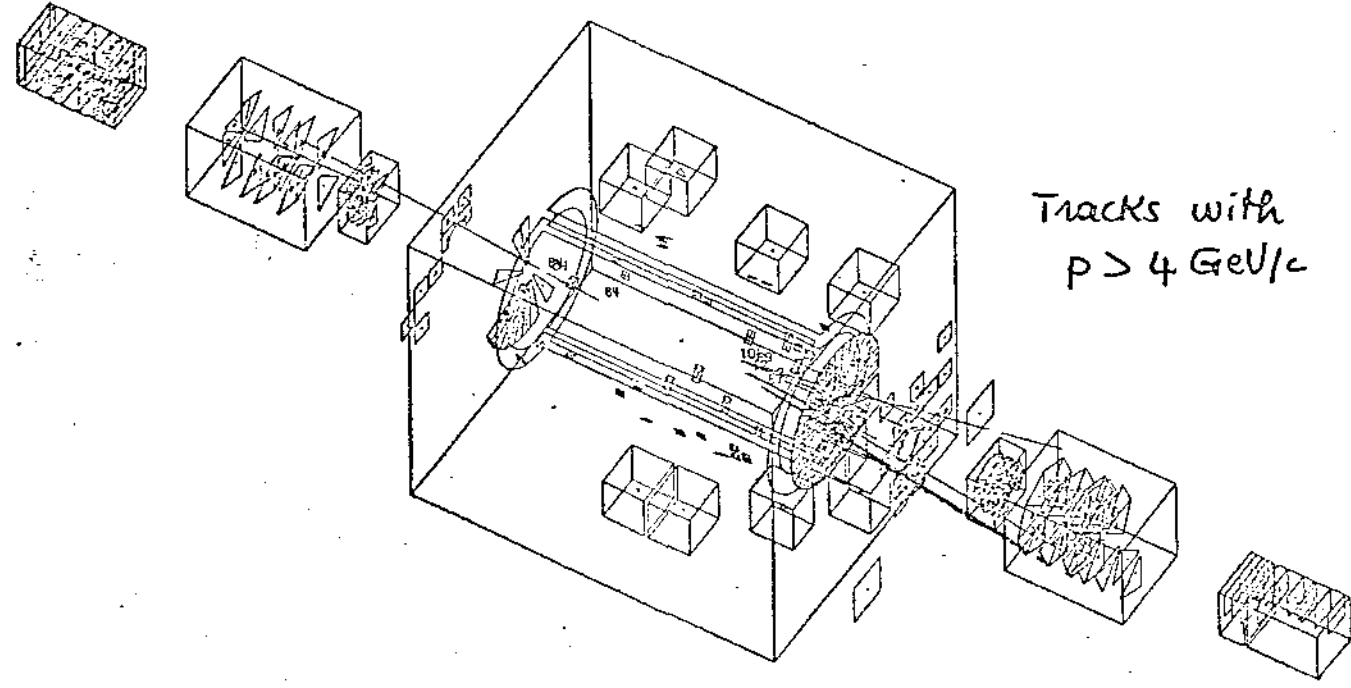
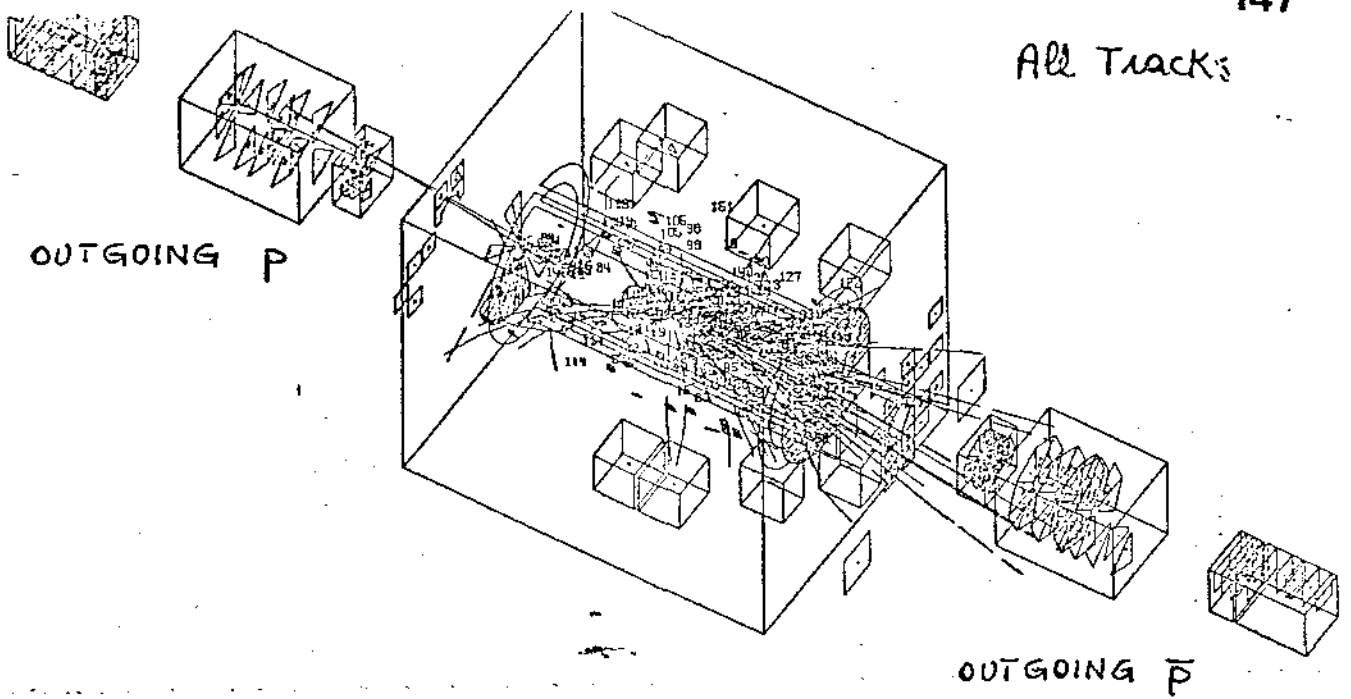
Tracks with $p > 4 \text{ GeV}/c$

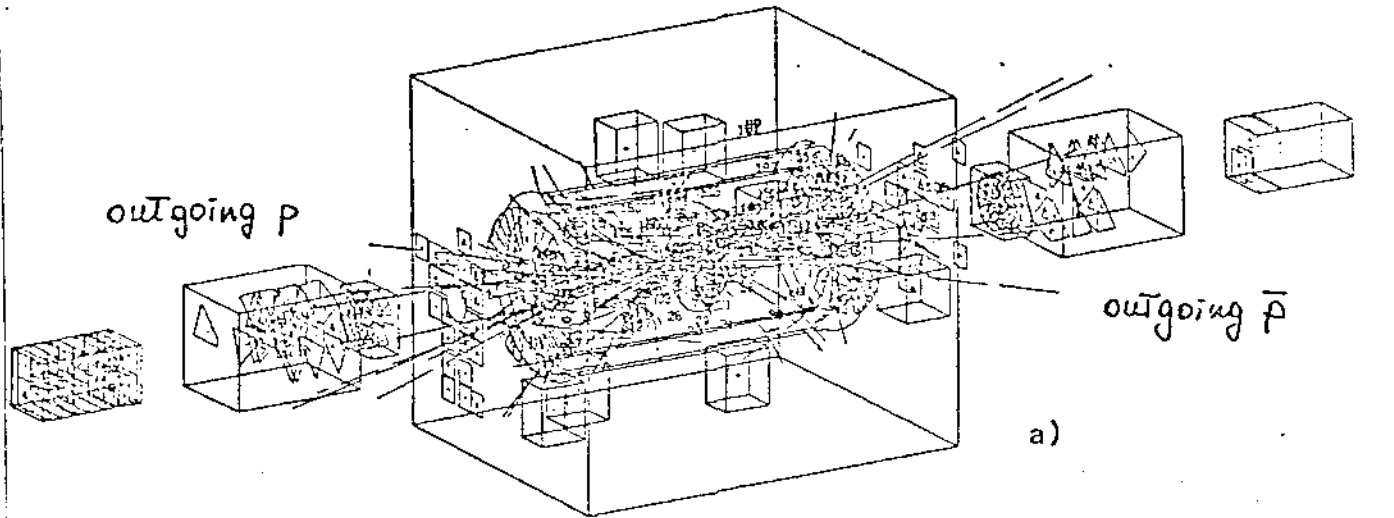


LAA TRIGGER TRACK

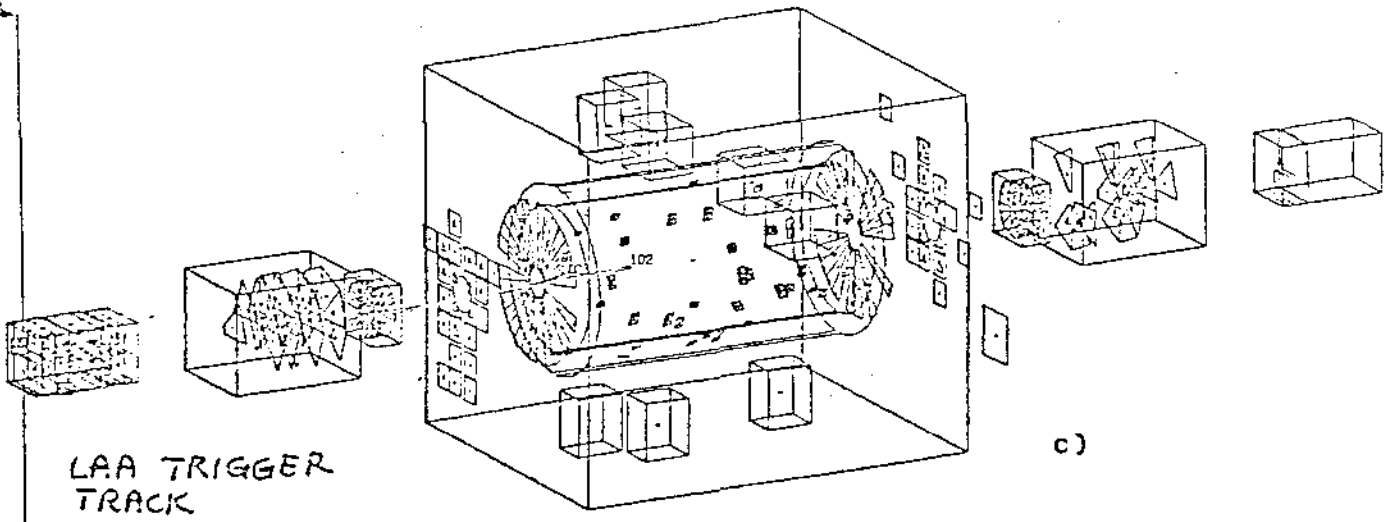
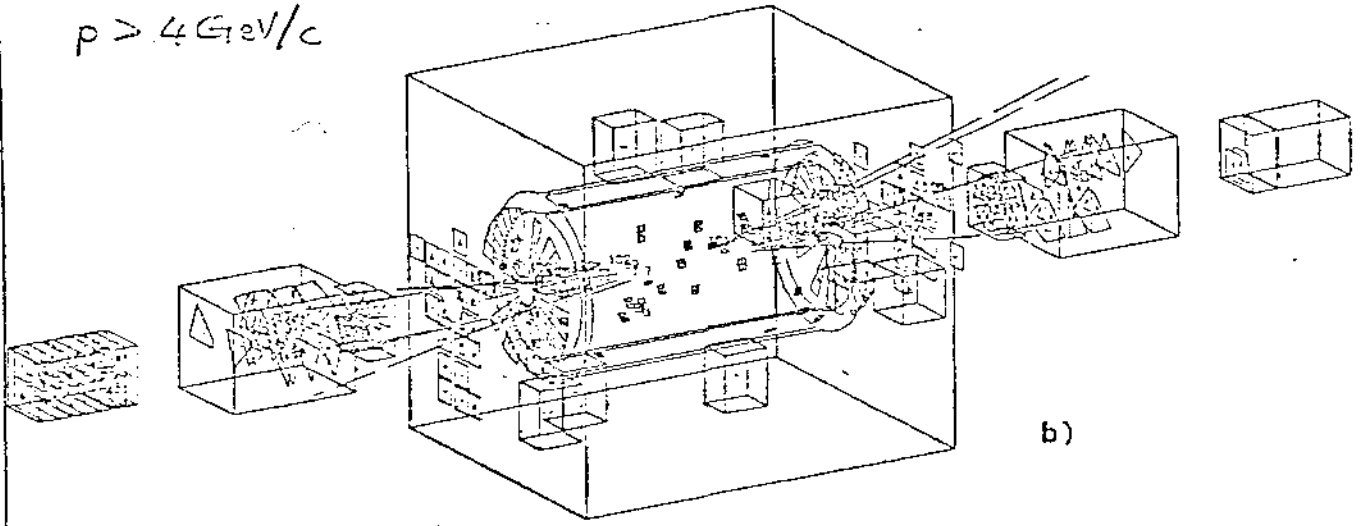
+ve
 $p = 17.2 \text{ GeV}/c$







TRACKS WITH
 $p > 4 \text{ GeV}/c$



LAA TRIGGER
TRACK

- ν_e
 $p = 10.4 \text{ GeV}/c$

Fig. 5.12

$$\frac{(1/P_{UA1} - 1/P_{LAA})}{1/P_{UA1}}$$

DISTRIBUTION

PLAA CORRECTED FOR ENERGY LOSSE
IN UA1 FORWARD CALORIMETER
AND IN LAA IRON MAGNET

$$\langle P_{LAA} \rangle = \langle P_{UA1} \rangle \approx 13 \text{ GeV}/c$$

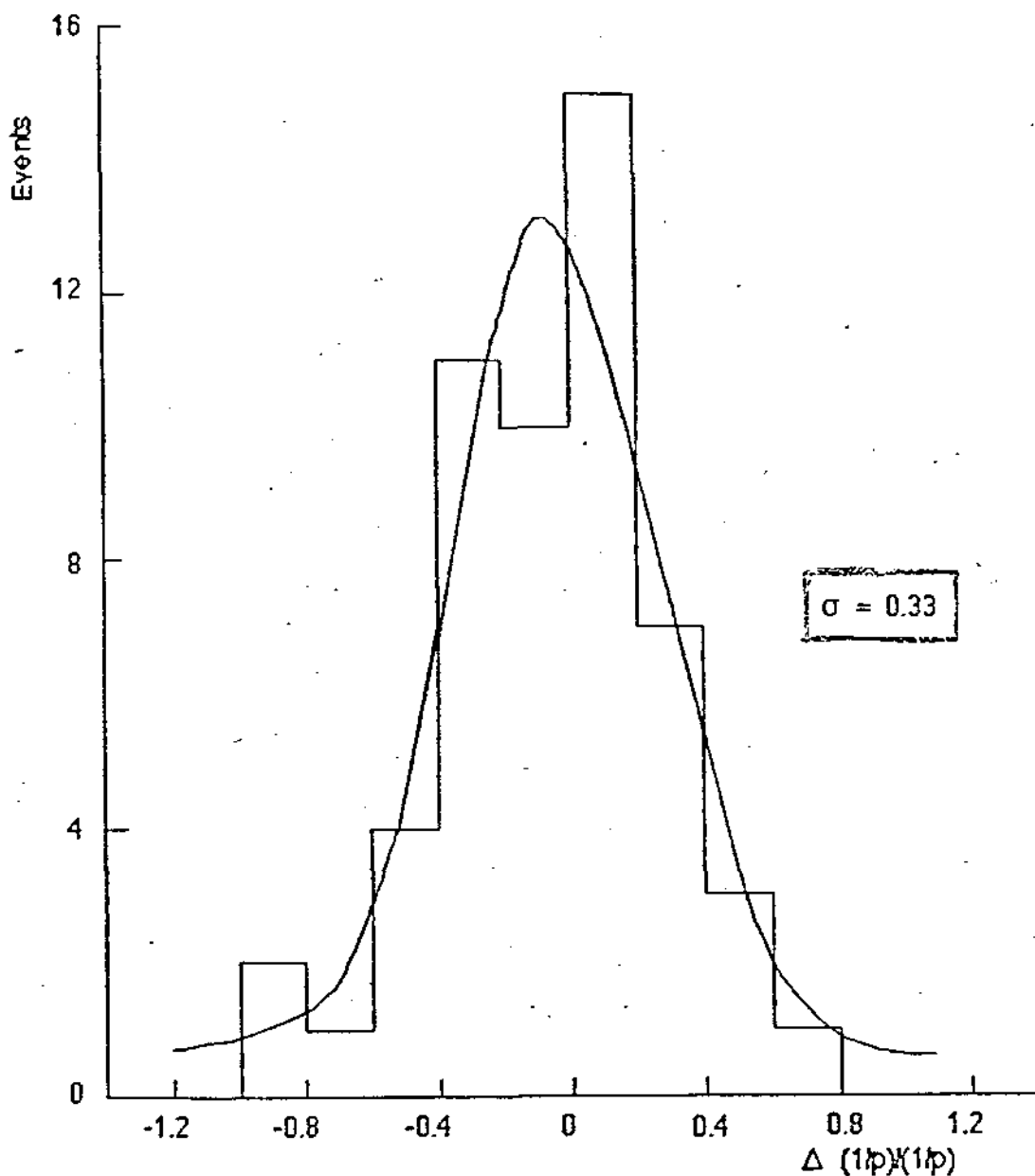


Fig. 5.13

error on P_{UA1} (3%) negligible

THE RMS VALUE OF $(1/P_{UA1} - 1/P_{LAA}) / (1/P_{UA1})$

DISTRIBUTION (33%) IS GREATER THAN

WHAT EXPECTED FROM MULTIPLE SCATTERING

IN THE ~ 10 GeV/c MOMENTUM REGION,

DUE TO:

- THE LARGE UNCERTAINTIES IN THE ENERGY LOSS CORRECTIONS (WHERE THE TRAVERSED THICKNESSES OF CALORIMETERS WERE DETERMINED BY EYE).
- THE IMPORTANT SETTING ERROR OF THE DRIFT CHAMBERS
- THE APPROXIMATION OF THE FAST RECONSTRUCTION PROGRAM USED IN LAA TEST.

WITHIN THESE ERRORS, THE MOMENTUM OF THE ROUGH LAA TEST CAN BE CONSIDERED IN GOOD AGREEMENT WITH THE MOMENTUM OF UA1.

FINANCIAL ESTIMATES

151

DETECTOR	Items	Unit price (KSF)	Quantity	Price (KSF)
TOROIDS	Fe Coils + construction	2.0/t	1376 t	2752
		2.1/t	1376 t	2890
				5642
IRON SHIELDING	Fe Construction	1.0/t	31 t	31
		1.0/t	31 t	31
				62
SCINTILLATION COUNTERS	PM Scintillator	3.3/PM ^(*)	592 PMs	1954
		0.15/Kg	7193 Kg	1079
				3033
LIMITED STREAMER TUBES (LST)	HV Electronics & cables Trigger matrices Strips Tubes & supports	0.17/(2,0) m ²	359.3 m ²	61
		9.5/sector	144 sectors	1368
		10/matrix	96 matrices	960
		0.0064/strip	24668 strips	158
		0.17/plane	12 planes	204
				2751
DRIFT CHAMBERS	HV Electronics Chambers Supports Cables (**)	0.014/cell	2968 cells	42
		0.14/wire	14840 wires	2078
		5.8/m ²	157 m ²	911
		10/plane	12 planes	120
		0.015/wire	14840 wires	223
				3374
MARK J CHAMBERS UA1 CHAMBERS	Transport & supports Supports			~ 100
				50
				150
				3524

(*) PM + HV + cable + crate + (ADC + TDC for 10% of PMs) + scalers + discriminator + input register + work

1.135

SUMMARY OF COSTS (KSF)

TOROIDS	5642
IRON	62
SCINTILLATION COUNTERS	3033
LIMITED STREAMER TUBES	2751
DRIFT CHAMBERS	3524
INSTALLATION (rough estimate)	500
	<hr/>
TOTAL	15512
+ UNPREDICTED 10%	1551
	<hr/>
TOTAL	17063

LAA - Schedule - part 1 -

shut-down
 F.T.
 ACOL

	1986												1987												1988		
SPS schedule																											
UAI Situation	IN						OUT						IN			OUT			IN								
	A	M	J	J	A	S	O	N	D	J	F	M	A	M	J	J	A	S	O	N	D	J	F	M			
Infrastructures																											
Magnet power suppl.	design + orders + installation												connection						↓ Test								
Cooling water	"												"			"			↓ "								
Gas																											
Drift chambers	preparation												"						connection								
LST	(add on UAI system)												"						"								
UAI removal																											
iron wall													↓														
μ-chambers													↓														
CALCOM													↓														
foot-bridge													↓														
floor services													↓														
Underground space																											
μ-ch. supports	new design + construction												↓														
foot-bridge													↓														
ground floor services	design + preparation												↓														
Cables																											
toroids													↓														
counters													↓														
LST													↓														
Drift ch.													↓														
Surface space																											
Assembly hall	design + construction												↓														
40 t crane	"												"			↓											
direct access	roads + gates + services												↓														
control room	order + installation												↓														
Vacuum																											
tube connection	new design + tests + construction												↓														
new rolling scenario	study + decision and test												↓														
LAA installation																											
Assembly	scenario study																										
Wiring																											
Transport																											
Survey																											
SPS support																											

ACOL - Technical

ACOL - Physics runs -

↓ dead line

LAA - Schedule - part 2 -

shut-down F.T. ACOL

	1986												1987												1988								
SPS schedule													shut-down												shut-down								
UAI Situation	IN												OUT												IN			OUT					
	A	M	J	J	A	S	O	N	D	J	F	M	A	M	J	J	A	S	O	N	D	J	F	M									
Toroids																																	
Iron	design + construction												Delivery																				
Coils	design												orders + construction												Dist.			E					
Supports	design												"												T1, T2, F1, F2			12, 16, 17					
Shielding	"												"																				
Counters	design												orders + const.																				
Scintillator	"												"												Assembly			installation			Test		
Light-guides	"												"												S3, S5			S2, S4			installation		
Supports	"												"																				
PMS + bases	orders																																
Test	long light guide																																
Oratory	1818 Building preparation																																
LSI	order material												Coating + Wiring + Tests																				
Tubes	Lab. preparation												Construction												Assembly			Test					
Strips	design + construction												orders												installation			LST5, LST4			LST2, LST1		
Supports	design + Tests																																
Front electronics																																	
Drift chambers																																	
LAA	design + tests												orders + delivery + Const.																				
Mechanics	Final Test												orders + delivery + Assembly												Installation			ACOL - Technical					
Electronics													design + construction												DC 12 to DC8								
Supports																																	
Tests																																	
Mark-J													+ Mark-J ions participation												Initial			Test					
Moving																									DC 7 to DC 4								
Supports																																	
Tests																																	
CLEAN ROOM	construction																																
Trigger																																	
Design																																	
Construction																																	
Test																																	
Assembly																																	
Data Acquisition																																	
Software	development																											Test					
Hardware	design + orders																																
Monitor																																	
Computer	order + delivery																																
Coordination	DESIGN																														INSTALLATION		

ACOL - Physics HINS -

1.138

↓ dead line

**III-2. "The lepton asymmetry analyser : LAA"
CERN SPSC 86-3, SPSC/P200 Addendum 1,
March 3, 1986.**

CERN SPSC 86-3
SPSC/P200 Addendum 1
March 3, 1986

2 - THE LEPTON ASYMMETRY ANALYZER: LAA

BCFL Collaboration

G. Bari, M. Basile, J. Berbers, G. Cara Romeo, R. Casaccia, L. Cifarelli, F. Cindolo,
A. Contin, G. D'Ali, C. Del Papa, G. Iacobucci, G. Maccarrone, T. Massam, R. Meunier,
R. Nania, F. Palmorari, G. Prisco, F. Rohrbach, P. Rotelli, G. Sartorelli, G. Susinno,
L. Yotano, M. Willutzky and A. Zichichi

Abstract

The LAA adapted to the UA1 detector is described. The results of the test run are presented.

CONTENTS

- 0 - Introduction
- 1 - Physics.
- 2 - Setup.
- 3 - Electronic logic and trigger rates.
- 4 - Data acquisition and analysis.
- 5 - Results from the LAA test run.
- 6 - Financial estimates.
- 7 - Conclusions.

- 3 -

INTRODUCTION

In connection with our LAA proposal (SPSC/P200) and after the successful test performed during the last Collider run, we propose to install in the forward and backward regions of UA1 two muon spectrometers. Each spectrometer consists of a series of iron toroids with a field of about 1.8 T, fully instrumented with LST's, scintillation counters and drift chambers. The first two equipments are for triggering purposes, in the θ range $5^\circ \leq \theta \leq 30^\circ$. The drift chambers provide an accurate momentum measurement in the very forward region from 5° to 15° , to improve the rejection against muons from π and K decays.

The assumptions made in the present proposal are that the existing CALCOM will be replaced with a new calorimeter and a new compensating magnet and that the present UA1 μ chambers can be displaced in order to make available the space needed for the installation of the spectrometers (see the minutes of the meeting held on January 13, 1986 to discuss the LAA/UA1 compatibility problems). The system of toroids represents a thicker iron shield which is going to replace the existing non-magnetized iron shield. The existing planes of UA1 LST's in the forward directions are left untouched.

1. PHYSICS

The physics of LAA has been fully discussed in the proposal (Ref. 1) and in other papers (Ref. 2). We refer the reader to these sources for all possible details. We summarize here the basic points.

The production and semileptonic decay of heavy-flavours "up-like" and/or "down-like" is assumed to follow the same trend already observed at lower energy (ISR): "leading" production for the baryon, "central" production for the associated meson (Ref. 3). As a consequence, a lepton asymmetry should show up. The sign of the asymmetry depends on the "up-like" or "down-like" nature of the new flavour(s). The amplitude of the asymmetry and its p_T dependence are functions of many parameters (see Refs. 1, 2 and 3). Three examples of our simulation programs are shown in Figs. 1.1, 1.2, and 1.3.

In addition to the problem of new flavours, our proposal will increase the hermeticity of the UA1 set-up, and will allow the possibility of studying all those phenomena where a directly produced μ , in the forward direction, can be associated with a hadronic jet.

2. SET-UP.

In Figs. 2.1a and 2.1b the top and side views of one side of the apparatus are shown. The herewith proposed set-up will not be changed in its basic structures and conceptual design, but small variations of angles, sizes and positions are expected in order to fit within details the existing area.

2.1 Toroids and shielding

T0, ... , T5 are iron toroids, magnetized at about 1.8 T. The variation of B with the radius r is always less than 20%, saturating the iron at small r. The field map for a toroid of this type is shown in fig. 2.2.

The toroids are divided in sectors for construction and installation purposes: 16 sectors of 22.5° for T0, ... , T3 and 8 of 45° for T4 and T5. Dimensions, weights and field values are given in Table 2.1.

For a cut along a horizontal plane at the beam level, the total thickness of magnetized iron as function of the polar angle θ , or pseudorapidity η , for the present design is compared in Fig. 2.3 with the present UA1 situation, where the iron is not magnetized.

Ten centimeters of iron shielding (F0 and F1) are installed behind the drift chambers in order to reject low energy particles inside the chambers.

2.2 Scintillation counters

S1,..., S8 are planes of scintillation counters. Each plane is subdivided in sectors, as detailed in Table 2.11. The disposition of the scintillation counters in a sector is illustrated in Fig. 2.4 for different planes. Scintillation counters are used in the trigger to reject halo particles, using time information, and to activate the appropriate LST trigger processor as it will be explained in §3.

2.3 Limited streamer tubes

The main logic of the trigger makes use of five planes of Limited Streamer Tubes (LST1, ... , LST5) which define the p_T acceptance of the system. Due to the radial deflection in the toroidal field, polar coordinates r and ϕ are used to tag the μ -trajectories. For this purpose radial (ϕ) and circular (r) strips are mounted on the LST planes. The ϕ -strips are shaped in such a way as to cover a $\Delta\phi=2^\circ$ each. The r-strips,

subdivided in sectors according to the number of sectors in each toroid, are designed to fulfill the needed granularity at different θ ($\Delta r \approx 1 + 2$ cm). The total number of channels for the two spectrometers will be 1800 for the ϕ -coordinate and 24688 for the r -coordinate, as illustrated in Table 2.III.

2.4 Drift chambers

Drift chamber planes DC1,...,DC12 (see Table 2.IV) are used for a second momentum measurement in the angular range $\theta=5^\circ$ to $\theta=16^\circ$. For angles bigger than 16° , the momentum measurement is done by the UA1 central detector and, for $\theta \geq 19^\circ$, by the external muon chambers.

The position and number of drift chamber planes are such as to increase the precision in the momentum measurement with decreasing polar angle θ , with the aim of a resolution dominated by multiple scattering up to a p_T of about 10 GeV/c.

Chambers made available by MARK-J group will be used in planes DC4, ..., DC7.

DC1, DC2 and DC3 are trapezoidal chambers. This is required in order to fit the inside hole of the T0 toroid. Calculations have shown that x , y determinations were necessary for obtaining good accuracy in momentum measurements. The r coordinate cannot be determined with enough precision in trapezoidal chambers. This is mainly due to the effect of the dipole field of UA1 on the μ trajectories as a function of the azimuthal angle ϕ . Each plane of the drift chambers used for the determination of the input angle of the μ 's entering the LAA detector will be made by four symmetric quadrants of special shape as shown in Fig. 2.5. Twelve identical chambers are necessary. Each of them will have 5 sense wires in x and 5 sense wires in y staggered in order to resolve left and right ambiguities and to insure good redundancy. With this design a maximum of 15 x hits and 15 y hits are consequently expected for every track.

DC4 to DC7 are constituted by 4 planes of 2 drift chambers (2540×4060 mm², 2 coordinates in x and 2 in y) presently used in the MARK J detector. Sixteen chambers are needed to cover the 2 sides of UA1.

DC8 to DC12 are constituted by 5 planes of 4 drift chambers with the same cell structure of DC1, DC2, DC3. One of these planes is shown on Fig. 2.6. This arrangement has been chosen in order to minimize the cost of the construction (40 identical chambers). The number of planes ensures a good accuracy for the determination of the exit angle of the μ 's and the redundancy needed for tracking in the high background expected at this position at the entrance of the SPS tunnel.

- 7 -

We plan to have preamplifiers on the chambers followed by amplifier discriminators in the counting room. For the measurement of the drift time, we are studying the design of a digital TDC developed at CERN (Ref. 4).

The gas proposed is a mixture of Ar and Ethane ($\approx 50\%$ each).

Prototypes of similar chambers have already been used during the test at LSS5, giving a resolution of $\approx 300 \mu\text{m}$ (see § 5).

3. ELECTRONIC LOGIC AND TRIGGER RATES.

3.1. General design.

We plan to define a first level trigger with LST and scintillation counters. Figure 3.1 shows a longitudinal section containing the beam and it illustrates the principle of our trigger. Information from the Limited Streamer Tubes read-out strips has to be used to define minimum momentum cuts which depend on the muon production angle, due account being taken of multiple scattering. Figure 3.2 shows the strips: r-strips define the muon radial trajectory; ϕ -strips establish that this trajectory is coplanar with the beam.

The r-strips are arranged so that the strip number is proportional to the angle subtended at the interaction region. A matrix coincidence to impose a p_T cut is possible and represents a basic part of our trigger, as discussed below.

For trigger purposes, each spectrometer will be divided into 8 ϕ -sectors, corresponding to the toroid octants. Each octant is treated independently and in parallel in the trigger.

An overall scheme of the foreseen trigger logic is drawn in Fig. 3.3.

A 'scintillation counters processor' (Fig. 3.4) provides a first determination of the octant hit by the traversing muon.

This processor selectively enables the 'LST r-strips processors' (Fig. 3.5a and 3.5b) which require the coincidence between one circular strip of the first LST plane with a suitable number of circular strips in the following planes, and the 'LST ϕ -strips processors' (Fig. 3.6) which require the coincidence between one radial strip in the first LST plane with two strips in the following planes.

The LST r-strips processor apply a p_T cut which can be adjusted following the wanted trigger rate. The LST ϕ -strips processor cuts out events which are not in the "right" plane, i.e. low momentum, highly scattered muons.

LST telescopes 1 and 2B will be used to trigger in the angular range $\theta > 25^\circ$ ($|\eta| < 1.5$), telescopes 1 and 3 in the range $15^\circ \leq \theta \leq 26^\circ$ ($1.5 \leq |\eta| \leq 2.0$), telescopes 2A and 4 in the range $7.5^\circ \leq \theta \leq 16^\circ$ ($2.0 \leq |\eta| \leq 2.7$), and telescopes 2A and 5 in the range $\theta < 7.5^\circ$ ($|\eta| > 2.7$).

3.2. LST r- and ϕ -strips processors.

Figure 3.5a shows the schematic design of one LST r-strips processor.

Signals from the r-strips of plane LST1 (or 2A) are detected, shaped and transmitted to the trigger electronics where a receiver circuit presents them to the memory drive latch. The 3-state register is intended to allow a test pattern to be injected. The vector of

- 9 -

hits on LST1(2A) plane causes the matrix to output a new vector which is the OR of all possible patterns on LSTn ($n=2B, 3, 4, 5$) plane compatible with the hits on LST1(2A).

The signals on plane LSTn are similarly shaped and transmitted to produce a vector of hits. Any bit-to-bit coincidence between predicted and actual vectors produces a positive response from the processor.

The allowed coincidence between the two LST planes will be sparse, so we plan to make a design with a look-up table predictor using just enough RAM circuits to cover the correlation band (see Fig. 3.5b).

Figure 3.6 shows the schematic design of one LST ϕ -strips processor.

This processor is very similar to the r-strips processor except for the matrix which will be probably replaced by some hard-wired circuitry.

We plan to build the LST r- and ϕ -strips processors using VMEbus specification in order to use available electronics for memory filling, test pattern injection, and control of the full system.

3.3. Trigger efficiency.

We have mapped the trigger efficiency of the proposed apparatus with a grid of 6000 (θ, ϕ, p_T) points.

As an example, Figs. 3.7a and b show the radial spread on the LSTn ($n=2B, 3, 4, 5$) plane(s) versus the radial coordinate in the first trigger plane LST1(2A) for two trigger configurations giving 95% efficiency at $p_T = 5$ and $p_T = 10$ GeV/c, for muons produced in the machine plane ($\phi=0^\circ, 180^\circ$). The size of the spread is comfortably higher than the size of the LST r-strips used in the trigger, leaving room for an adjustment of the effective p_T cut depending on the trigger rates.

Figure 3.8 shows the p_T efficiency curves for three trigger configurations giving 95% efficiency at $p_T = 5, p_T = 7$ and $p_T = 10$ GeV/c, for positive muons produced in the machine plane ($\phi=0^\circ, 180^\circ$) and with $\theta=8^\circ$.

Figures 3.9a and b show the 95% efficiency isolines, i.e. the apparatus limits, at $p_T = 5$ and 10 GeV/c for the corresponding settings of the p_T threshold and for positive and negative muons.

3.4. Trigger rates.

The trigger rates expected in the apparatus have been calculated using the UA1 fit (Ref. 5) to the invariant cross-section for the production of hadrons $[(h^+ + h^-)/2]$, with $|\eta| < 2.5$:

$$\frac{Ed^3\sigma}{dp^3} \propto \frac{p_0^n}{(p_0+p_T)^n}, \quad (p_0=1.49 \text{ and } n=9.87) \quad (1)$$

normalized to the total cross-section in proton-antiproton interactions at $\sqrt{s}=630$ GeV, and the η distribution of hadrons measured by UA5 (Ref. 6). We assumed a $\pi:K$ ratio of 2:1 and a decay length of 310 cm.

In Table 3.1 the first level trigger rates with different values of the threshold and for a luminosity of $4 \cdot 10^{30} \text{ cm}^{-2}\text{sec}^{-1}$ (ACOL) are indicated.

A second level trigger can be applied using the drift chambers information, in order to refine the p_T trigger.

3.5. Monte Carlo simulations.

A simulation program, using GEANT, was developed in order to study the performance of the apparatus.

To analyze the effects of the toroids on the UA1 existing trigger logic, we have generated muons at fixed p_T and equally distributed in charge, tracking them from the vertex up to the external UA1 muon chambers. In the simulation the upgraded UA1 with the new calorimeters was considered.

Calling α the angle between the line defined by the vertex and the hit on the first μ chamber and the line defined by the hits on the first and second μ chambers, we have produced the distributions of the projections of α on the two planes perpendicular to the chambers, one along the x wires (α') and the other along the y wires (α'').

The two distributions are shown in Figs. 3.10a and 3.10b for the azimuthal angle $\phi=0^\circ$, $\theta=27^\circ$ and $p_T=2.5$ GeV/c and in Figs. 3.11a and 3.11b for the same ϕ and θ , but $p_T=5$ GeV/c. At $\phi=0^\circ$ the toroidal field is vertical and affects only the projection of α on the horizontal plane (Figs. 3.10a and 3.11a). The distribution of the projection of α on a vertical plane orthogonal to the chambers (Figs. 3.10b and 3.11b) is affected only by the multiple scattering and by the central UA1 field. The effect of the magnetized iron can be deduced from a comparison between the two figures.

In Figs. 3.12 and 3.13 the distributions of the distance d between the hit on the UA1 existing LST plane and the intersection on this plane of the line defined by the vertex and the hit on the first μ chamber are given for $p_T=2.5$ GeV/c and 5 GeV/c, at $\theta=27^\circ$ and $\phi=0^\circ$. A cut on this variable may be used at the second level trigger to select high p_T tracks.

- 11 -

The hit distributions on our LST trigger planes has been carefully analyzed. As an example, the scatter plots of the radial distances from the beam line on the LST1 and LST3 planes are given in Figs. 3.14a,b,c for muons with $p_T = 5 \text{ GeV}/c$, equally distributed in charge, and at three different values of ϕ (0° , 90° and 270° , respectively).

The differences between these plots are due to the different alignment of the UA1 central field with respect to the toroidal field inside the LAA spectrometers: orthogonal at $\phi = 0^\circ$ and 180° , parallel at $\phi = 90^\circ$, and antiparallel at $\phi = 270^\circ$.

4. DATA ACQUISITION AND ANALYSIS.

We plan to make the data-acquisition system as compatible as possible with the upgraded UA1 system. Therefore, it will be based on the VMEbus "distributed intelligence" for data acquisition, reduction and monitor.

Concerning the data analysis, it is clear that the events triggered by UA1 are a scientific property of the UA1 group and for these events access to the LAA data will have to be granted. These data, fully analyzed with the appropriate software programs needed to reconstruct the muon tracks, together with timing and all other information will be made available by the LAA group to the UA1 collaboration.

Conversely, the events triggered by LAA are a scientific property of the LAA group and for these events UA1 will make available all information including event reconstruction in the central detector and in the calorimeters (*).

Combined triggers of UA1 and LAA will be a subject of collaboration and discussion between the two groups.

(*) a tentative agreement on these points has been reached in a meeting between J. Dowell, R. Klapsch, C. Rubbia and A. Zichichi, and will be submitted to the UA1 executive committee on March 5th, 1986

5. RESULTS FROM THE LAA TEST RUN

5.1 Purpose of the test run

The basic motivations for our test run were twofold.

- To prove that we are able to trigger with high efficiency on muons produced in proton-antiproton interactions, in the region near the beam pipe. This efficiency, which is p_T dependent, has been proved to follow expectations.

- To check our MonteCarlo simulation program, in order to extrapolate the trigger rates measured in the test run to the full set-up. For this to be done, the agreement we reached between predictions and measurements was essential.

5.2 Description of the test run set-up.

Two small spectrometers have been constructed and installed in the forward and backward UA1 regions.

Each spectrometer (Fig. 5.1) consists of three pieces of magnetized iron, each 51 cm thick for a total thickness of 153 cm. The cross-section of the magnet has a surface of $100 \times 60 \text{ cm}^2$ with a vertical central window of $50 \times 5 \text{ cm}^2$ to allow the installation of the coils. The current in the coils is 6000A*turns and the field is 1.7 Tesla. The field lines are shown in Fig. 5.2. The magnetic field is vertical pointing to opposite directions in the two halves of each spectrometer. Scintillation counters are inserted to veto particles crossing the magnet from one longitudinal half to the other.

The longitudinal axes of the spectrometers are pointing to the interaction vertex at 7.5° with respect to the beam line. Each spectrometer covers a pseudorapidity range $|\eta| = 2.7 \pm 0.2$ and an azimuthal angle range $\phi = 0^\circ \pm 10^\circ$.

The two spectrometers are instrumented with scintillation counters for trigger purposes and with drift chambers for momentum reconstruction. A schematic top view of the spectrometers is shown in Fig. 5.3. T1 to T4 are $28 \times 58 \text{ cm}^2$ scintillation counters defining the homogeneous region of the magnetic field all along the spectrometer. Each of the counters is viewed at both ends by two photomultipliers for a good time resolution (240 psec), as shown in Fig. 5.4. Moreover the signal time difference of the two photomultipliers gives a rough estimate of the vertical position of a track with a resolution of about 5 cm.

F1 and F2 are two planes of finger counters, each 4 cm wide and 50 cm long; 14 counters are mounted in each plane and are placed in such a way as to be aligned along the lines pointing to the interaction vertex.

D1 to D4 are $60 \times 60 \text{ cm}^2$ drift chambers. Sections of these drift chambers are

shown in Figs. 5.5a and 5.5b. Two layers of honeycomb make up a self-supporting structure with the help of fiber glass side members and lids. The gap between the two honeycomb sheets is divided into 9 cells of ± 3.5 cm, using Al partitions. Three staggered wires per cell have been used. The signal is amplified and discriminated directly on the chambers using Lecroy amplifiers (HIL 401). The chambers are filled with argon/ethane (60/40%). The general performance of the chambers has been adequate for the test: we have virtually reached the desired spatial resolution ($\approx 300 \mu\text{m}$).

5.3 Expected rates from π, K decay

Our spectrometers are installed in a region with high activity due to the halo of the beams and to the backscattering of particles from all the materials around. To know the expected flux of decay μ 's coming from primary interactions in our spectrometers, we have performed a MonteCarlo calculation using the UA1 fit (1) to the invariant cross-section and the $dn_{ch}/d\eta$ pseudorapidity distribution measured by UA5.

In our calculations we have used a decay length of 290 cm and a $\pi : k$ ratio of 2 : 1 for pions and kaons. A momentum cut, due to range, of 5 GeV/c is applied to the produced μ 's. The hardware trigger geometrical requirements are simulated in the MonteCarlo. The efficiency for the UA1 minimum bias trigger was also taken into account. A rate of $\approx (0.15 \pm 0.01)$ Hz for $L = 2 \cdot 10^{29} \text{ cm}^{-2}\text{sec}^{-1}$ on each side of our detector has been obtained when the magnet is off.

5.4 Measured rates

A trigger defined to select particles crossing all the iron and in time with the beam crossing, obtained by the coincidence of all consecutive T counters (see Fig. 5.3) plus the Collider synchronization signal, gives the following rates at $L = 2 \cdot 10^{29} \text{ cm}^{-2}\text{sec}^{-1}$ and without magnetic field :

$$\begin{aligned} \text{outgoing anti-p side} &= (0.11 \pm 0.01) \text{ Hz} \\ \text{outgoing p side} &= (0.30 \pm 0.02) \text{ Hz} \end{aligned}$$

The halo accompanying the proton beam is eliminated by timing in the outgoing anti-proton side spectrometer. This halo then traverses UA1 reaching the spectrometer in the outgoing proton side in time with particles produced in the interaction.

Adding to our trigger the UA1 minimum bias signal (which accepts 85% of the total cross-section) strongly reduces the contribution of this halo on the outgoing proton side, leaving unchanged the rate on the outgoing antiproton side. The rates in these conditions are:

- 15 -

$$\begin{aligned} \text{outgoing anti-p side} &= (0.11 \pm 0.01) \text{ Hz} \\ \text{outgoing p side} &= (0.16 \pm 0.01) \text{ Hz} \end{aligned}$$

to be compared with the expected rate, obtained with the Monte Carlo, of $(0.15 \pm 0.01) \text{ Hz}$ (see §5.3).

In Fig. 5.6 the observed rates on the finger counters before and after the spectrometer on the outgoing proton side are reported with and without UA1 minimum bias signal coincidence. To understand this figure it has to be recalled that each spectrometer is subdivided in two longitudinal halves, the finger counters being numbered from 1 to 7 in the first half of the spectrometer (starting from the nearest to the beam line) and from 8 to 14 in the second half. In the rate distribution on finger counters measured without the coincidence of UA1 minimum bias signal a contribution of tracks misaligned with respect to the spectrometer axis and parallel to the beam is clearly visible. From this figure, one can extrapolate that the halo accompanying the proton beam and traversing UA1 has a rate of 1.8 Hz/m^2 at about 1.5 m from the beam.

The residual halo contribution to the trigger, after requiring the coincidence of the UA1 minimum bias signal, can be removed by rejecting particles parallel to the beam.

The final trigger rate can easily be controlled by choosing an appropriate p_T cut. This has been achieved making use in the trigger of the finger counters, rejecting low momentum highly deflected particles.

The following configurations of finger counters have been used to this purpose

- i) Four fingers in the front plane in coincidence with the corresponding ones in the back plane. Two coincidences are defined for each half of each spectrometer with an overlap of the central finger.
- ii) One finger in the front plane in coincidence with three fingers in the back plane.
- iii) One finger in the front plane in coincidence with the corresponding one in the back plane.

Rates have been measured for the following triggers :

(a)	T counters	(B = 0)
(b)	(a) • UA1 minimum bias	(B = 0)
(c)	(b) • Fingers(i)	(B = 0)
(d)	(b) • Fingers(i)	(B = 1.7 T)
(e)	(b) • Fingers(ii)	(B = 1.7 T)
(f)	(b) • Fingers(iii)	(B = 1.7 T)

Results are given in Table 5.1 for $L = 2 \cdot 10^{29} \text{ cm}^{-2} \text{ sec}^{-1}$ and compared with estimates from the Monte Carlo calculation in which some of the above trigger selections have been simulated.

The calculated magnetic deflection for $B = 1.7 \text{ T}$ is shown in Fig. 5.7 as a function of p_T . The spread in the deflection due to multiple scattering and to vertex uncertainty is also shown as curves at constant number of standard deviations (σ).

The trigger efficiency at various p_T can be obtained from this graph for a given trigger configuration. Results for configuration (d) are shown in Fig. 5.8.

5.5 Off line analysis

Data have been collected making use of previously defined trigger (d) in order to have a reasonable rate. A summary of the data-taking is given in Table 5.11.

The distribution of the quantity $\Delta T = (T1 + T3) / 2 - T2$, where T1, T2, and T3 are the time signals from the three staggered wires of a drift chamber cell, is shown in Fig. 5.9. The two peaks correspond to left-right ambiguity resolution. Each peak has a σ -value of about 8.5 nsec, which corresponds to 425 μm in space. This gives the expected intrinsic wire resolution of 345 μm .

On the other hand, due to the short installation time made available for us it was not possible to put much care on chambers alignment, so that a setting error of the order of a millimeter has to be considered.

Figure 5.10 shows the reconstructed momentum spectrum, after the energy loss correction was applied. The ratio between the experimental and the Monte Carlo simulated p_T distributions, is compared in Fig. 5.11, with the expected efficiency for trigger configuration (d).

5.6 LAA in the UA1 trigger logic (test run data).

On the basis of the satisfactory results on rate measurement and background rejection, it was agreed to insert our trigger in the UA1 trigger logic, in order to proceed further and to study the complete events, as seen by UA1.

An integrated luminosity of 10 nb^{-1} has been collected to this purpose. A sample of events, reconstructed both in UA1 and in the LAA test spectrometer, has been selected to be scanned by eye using the event display facility of UA1 MEGATEK. This was done with a twofold purpose:

- to check the genuinity of the tracks triggered by the LAA test, i.e. their production by true proton-antiproton interactions;

- 17 -

- to check the consistency of the momenta measured by UA1 and the LAA test set-up.

The scanning consisted in a search for tracks having momenta above ≈ 5 GeV/c and whose extrapolation from UA1 central detector was pointing to the LAA test setup. By examining 116 events, we found:

- 1 double interaction event;
- 3 events with a strong unbalance of tracks between incoming p and anti-p hemispheres (probably due to beam gas interactions);
- 1 almost empty event (containing ≤ 10 reconstructed tracks);
- 2 events where the LAA trigger track was clearly identified as a halo track accompanying the p beam.

All other events ($\approx 94\%$) were indeed proton-antiproton interactions. Figure 5.12 shows a typical UA1 event containing the identified LAA trigger track.

In order to check the momentum measurement of LAA with UA1 we have taken 54 events where a track was unambiguously pointing into the LAA set-up.

The momentum reconstructed in LAA was corrected for energy losses occurred in the:

- UA1 electromagnetic and hadronic calorimeters (in the forward region);
- UA1 hadronic calorimeter (CALCOM) (in the very forward region);
- LAA iron magnet,

and then compared with the momentum measured by UA1.

Figure 5.13 shows the $\Delta(1/p)/(1/p)$ distribution, i.e. the distribution of the quantity $(1/p_{UA1} - 1/p_{LAA})/(1/p_{UA1})$. The error on p_{UA1} reconstruction ($\approx 3\%$) can be neglected. After energy loss corrections, the average momentum of the 54 tracks in exam was $\langle p_{LAA} \rangle \approx \langle p_{UA1} \rangle \approx 13$ GeV/c. The r.m.s. value of this distribution is 33%.

Such a value is essentially due to the large uncertainties in the energy loss corrections (where the traversed thicknesses of calorimeters were determined by eye) and in the drift chambers alignment, and to the approximation of our fast reconstruction program. Within these errors, the momentum measured in the rough LAA test set-up can be considered in excellent agreement with the values measured by UA1.

6. FINANCIAL ESTIMATES.

All unit costs have been estimated from existing similar detectors and on the basis of our own experience. The estimates are summarized in the table below.

Detector	Items	Unit price (kSF)	Quantity	Price (kSF)
Toroids	Fe	2.0 /t	1376 t	2752
	Coils + Construction	2.1 /t	1376 t	2890
				5642
Iron shielding	Fe	1.0/t	31 t	31
	Construction	1.0/t	31 t	31
				62
Scintillation counters	PM	3.3 /PM (*)	592 PMs	1954
	Scintillator	0.15 / kg	7193 kg	1079
				3033
Limited Streamer Tubes	H.Y.	0.17 / (r, ϕ) m ²	359.3 m ²	61
	Electronics and cables	9.5 / sector	144 sectors	1368
	Trigger matrices	10.0 / matrix	96 matrices	960
	Strips	0.0064 / strip	24668 strips	158
	Tubes and supports	0.17 / plan	12 planes	204
				2751

- 19 -

Detector	Items	unit price (kSF)	Quantity	Price (kSF)
Drift chambers	H.V.	0.014 / cell	2968 cells	42
	Electronics	0.14 / wire	14840 wires	2078
	Chambers	5.8 / m ²	157 m ²	911
	Supports	10.0 / plane	12 planes	120
	Cables (**)	0.015 / wire	14840 wires	223
				3374

MARK J chambers	Transport + supports			~ 100
UA1 chambers	Supports			50
				150
				3524

*) 3.3 kSF / PM includes : PM + H.V. + cable + crate +(ADC + TDC on 10% of the PM)+ scalers + discriminator + input register + work.

**) If halogen free cables are necessary for safety reasons the cable price must be increased to 750 kSF.

Summary of costs:

Toroids	5642
Iron	62
Scintillation counters	3033
Limited streamer tubes	2751
Drift chambers	3574
Installation (rough estimate)	500
	<hr/>
Total	15512
+ unpredicted 10%	1551
	<hr/>
Total	17063

- 21 -

7. CONCLUSIONS.

We need an urgent SPSC approval and a full support in order to immediately start the executive design and construction of the LAA set-up, thus to be ready by September 1987, which is the expected date for ACOL to operate.

REFERENCES

- 1) BCFL Coll., CERN / SPSC / 84 - 33 ; SPSC / P200
- 2) M.Basile et al., N.C. 68A, 65 (1982)
M.Basile et al., N.C. Lett., 37, 255 (1983)
M.Basile et al., Proceedings of the " 3rd Topical workshop on proton-antiproton Collider Physics", Roma 1983, CERN 83 - 04, p. 435
- 3) M.Basile et al., N.C. Lett., 30, 487 (1981)
M.Basile et al., N.C. Lett., 33, 33 (1982)
- 4) G. Delevallade and J.P. Vanuxem, "The LDT: a FASTBUS time digitizer for LEP detectors", CERN/EP Electronics Note 85-06, 22 November 1985.
- 5) UA1 Coll., Proceedings of the " 5th Topical workshop on proton-antiproton Collider Physics", St. Vincent 1985, World Scientific ed., p. 488
- 6) UA5 Coll., Proceedings of the " 3rd Topical workshop on proton-antiproton Collider Physics", Roma 1983, CERN 83 - 04, p. 75

- 23 -

Table 2.1. Toroids.

Magnetized iron:

	sectors	internal radius [mm]	external radius [mm]	length [mm]	weight [t]	B minimum [T]
T0	16	2000	5000	600	303	1.82
T1	16	357	3700	600	196	1.63
T2	16	379	2500	500	74	1.68
T3	16	379	2500	400	59	1.68
T4	8	379	1624	500	28	1.73
T5	8	379	1624	500	28	1.73

B maximum is always 2.0 T.

Total weight = 1376 t

Non-magnetized iron:

	sectors	internal radius [mm]	external radius [mm]	length [mm]	weight [t]
F0	8	1634	2600	100	9.1
F1	8	379	1732	100	6.4

Table 2.II. Scintillation counters.

	sectors	internal radius [mm]	external radius [mm]	surface [m ²]	PMs per sector	PMs total
S1	16	357	5000	64.3	6	96
S2	16	357	3700	41.6	3	48
S3	8	379	2500	17.3	5	40
S4	8	379	2500	17.3	5	40
S5	8	379	1624	7.0	2	16
S6	8	379	1624	7.0	2	16
S7	8	1634	2600	11.6	3	24
S8	8	379	1732	8.1	2	16

Each scintillator is 2 cm thick and less than 2 m in length.

Total surface (both sides) = 348.5 m²

Total weight of scintillator = 7200 Kg

Total number of PMs = 592

- 25 -

Table 2.III. Limited Streamer Tubes.

	sectors	internal radius [mm]	external radius [mm]	surface [m ²]	r-strips per sector	r-strip size [mm]
LST1	16	1550	5000	69.1	256	13.2
LST2A	8	379	2000	10.9	128	11.7
LST2B	16	3050	5000	48.1	128	14.9
LST3	16	2000	3700	29.7	128	13.0
LST4	8	1000	2500	14.9	128	10.8
LST5	8	379	1624	7.1	128	9.0

Total area (both sides) = 359.6 m²

Total number of strips (both sides) = 24688

Table 2.IV. Drift chambers.

	chambers	external sizes [mm]	shape	cells/chamber		wires/cell
				X	Y	
DC1-3	24	1848x1848	special (*)	26	26	5
DC4-7	16	2540x4060	rectangular	Mark-J XX-YY planes		
DC8-12	40	1240x1840	rectangular	26	17	5

(*) see Fig. 2.5.

- 27 -

Table 3.1. Trigger rates for different trigger configurations.

efficiency=95% at	particle sign	Trigger rate (both sides) [Hz]	
$p_T = 5 \text{ GeV}/c$	positive	6.4	11.1
	negative	4.7	
$p_T = 7 \text{ GeV}/c$	positive	4.2	7.4
	negative	3.2	
$p_T = 10 \text{ GeV}/c$	positive	2.9	5.1
	negative	2.2	

Table 5.1. Trigger rates (Hz).

Trigger	M.C. estimates / side	Outgoing anti-p side	Outgoing p side	Total
(a)	---	0.11	0.30	0.41
(b)	0.15	0.11	0.16	0.27
(c)	---	0.065	0.085	0.15
(d)	0.0093	0.015	0.020	0.035
(e)	0.0042	0.0065	0.0075	0.014
(f)	---	0.0018	0.0023	0.0041

- 29 -

Table 5.II. Test run data taking

	Date (start)	Date (stop)	Luminosity (nb ⁻¹)	Magnet current (A)	n. of triggers
LAA	29.10.1985	21.12.1985	223	+20	1.33×10^4
				-20	1.08×10^4
				0	2.45×10^4
LAA•UA1	12.12.1985	13.12.1985	10	+20	1751

Figure captions

- Fig. 1.1 : (a) Expected number of produced μ^+ (black circles) and μ^- (open circles) as a function of p_T and for an integrated luminosity of 10 pb^{-1} , with the conditions set as in Ref. 1 and for $m_t = 25 \text{ GeV}/c^2$ and $m_{sb} = 55 \text{ GeV}/c^2$. A smearing in p_T due to the estimated momentum resolution $\Delta p_T / p_T = 20\%$ is considered. The estimated background for each charge sign is indicated by the full line. The errors are purely statistic.
 (b) The expected asymmetry A^{exp} as a function of p_T .
- Fig. 1.2 : Same as Fig. 1.1 for a top mass $m_t = 25 \text{ GeV}/c^2$ and no superbeauty.
- Fig. 1.3 : Same as Fig. 1.2 for a top mass $m_t = 35 \text{ GeV}/c^2$ and no superbeauty.
- Fig. 2.1 : (a) Top view of the proposed apparatus (one side).
 T0, ..., T5 : magnetized iron with toroidal field;
 S1, ..., S8 : scintillation counters;
 DC1, ..., DC12 : drift chambers;
 LST1, ..., LST5 : Limited Streamer tubes.
 The existing (and future) UA1 detectors relevant for the forward region are indicated in white.
 (b) Side view of the proposed apparatus (one side).
- Fig. 2.2 : Magnetic field map of one quarter of T2 - T3 toroids.
- Fig. 2.3 : Iron thickness versus θ and η in the proposed apparatus and in the present (1986) UA1 configuration, at $\phi = 0^\circ$ (machine plane).
- Fig. 2.4 : Disposition of the scintillation counters in a sector for the different planes.
- Fig. 2.5 : Chamber geometry (DC1 - DC3).
- Fig. 2.6 : Chamber geometry (DC8 - DC12).
- Fig. 3.1 : Principle design of the trigger. The trigger definition region can be set in order to accept muon momenta greater than a minimum p_T for both charge signs.
- Fig. 3.2 : LST radial (r -) and azimuthal (ϕ -) strips configuration (artist's view).
- Fig. 3.3 : Overall scheme of the trigger logic.
- Fig. 3.4 : Trigger logic for scintillation counters.
- Fig. 3.5 : (a) LST r -strips processor.
 (b) Sparse RAMs defining the minimum p_T accepted by the LST r -strips processor.
- Fig. 3.6 : LST ϕ -strips processor. The coincidence between LST1 and LSTn ($n=2,3,4,5$) is hardwired, projecting one strip of the first plane into two strips on the others.

- 31 -

- Fig. 3.7 : (a) Trigger definition regions on planes LSTn (n=2,3,4,5) versus the radial coordinate on LST1, for a trigger configuration giving an efficiency of 95% at $p_T = 5$ GeV/c and in the machine plane ($\phi=0^\circ$).
 (b) Same as (a) for a trigger configuration giving an efficiency of 95% at $p_T = 10$ GeV/c.
- Fig. 3.8 : Efficiency curves as a function of p_T , for three different trigger configurations giving an efficiency of 95% at $p_T = 5, 7,$ and 10 GeV/c. The curves refer to +ve particles at $\theta = 8^\circ$.
- Fig. 3.9 : (a) Apparatus limits for tracks with $p_T = 5$ GeV/c, in the trigger configuration giving an efficiency of 95% at $p_T = 5$ GeV/c.
 (b) Same as (a) for $p_T = 10$ GeV/c.
- Fig. 3.10 : (a) Distribution of the angle α' (defined in the text), for muons generated with $\phi=0^\circ, \theta=27^\circ$ and $p_T = 2.5$ GeV/c.
 (b) Distribution of the angle α'' (defined in the text), for muons generated with $\phi=0^\circ, \theta=27^\circ$ and $p_T = 2.5$ GeV/c.
- Fig. 3.11 : (a) Same as Fig. 3.10a but for $p_T = 5$ GeV/c.
 (b) Same as Fig. 3.10b but for $p_T = 5$ GeV/c.
- Fig. 3.12 : Distribution of the distance d (as defined in the text) for muons generated with $\phi=0^\circ, \theta=27^\circ$ and $p_T = 2.5$ GeV/c.
- Fig. 3.13 : Same as Fig. 3.12 but with $p_T = 5$ GeV/c.
- Fig. 3.14 : (a) Scatter plot of r_{out} and r_{in} (as defined in the text) for positive and negative muons generated with $16^\circ \leq \theta \leq 23^\circ, \phi = 0$ and $p_T = 5$ GeV/c
 (b) Scatter plot of r_{out} and r_{in} for positive and negative muons generated with $16^\circ \leq \theta \leq 30^\circ, \phi = 90^\circ$ and $p_T = 5$ GeV/c
 (c) Scatter plot of r_{out} and r_{in} for positive and negative muons generated with $16^\circ \leq \theta \leq 30^\circ, \phi = 270^\circ$ and $p_T = 5$ GeV/c
- Fig. 5.1 : View of one of the two LAA test spectrometers.
- Fig. 5.2 : Magnetic field lines in the cross-section of one of the LAA test magnets.
- Fig. 5.3 : Top view of the LAA test spectrometer installed on the outgoing proton side:
 D = drift chamber,
 M = iron magnet,
 F = finger counter,
 T = TOF counter.
- Fig. 5.4 : Time-of-flight distribution relative to a pair of T counters. The quantity on the horizontal scale is:

$$\Delta t = t_1 - t_2, \quad \text{where } t_i = (t_i^U + t_i^D)/2 \quad \text{for } i = 1, 2$$
 (U and D stand for up and down phototubes, respectively). The Δt standard deviation is $\sigma \approx 340$ psec, which corresponds to an intrinsic time resolution of 240 psec.

- Fig. 5.5 : (a) Cross-section of the chamber showing the layers of honeycomb and the way the cells are obtained inside with Al partitions. The wires are held by injected plastic supports visible between two partitions.
 (b) Detail of the chamber end, showing wire support, wires, lid and cables bringing the signals out to the electronics.
- Fig. 5.6 : Finger counter rates observed with (light histogram) and without (dark histogram) the UA1 minimum bias signal in coincidence.
- Fig. 5.7 : Expected magnetic deflection in the LAA test apparatus as a function of p_T .
- Fig. 5.8 : Expected trigger efficiency, derived from Fig. 5.7, as a function of p_T . Side 1 is closer to the beam line.
- Fig. 5.9 : Drift time distribution in one cell. The quantity on the horizontal scale is:

$$\Delta T = (T_1 + T_2)/2 - T_3,$$
 where T_1 , T_2 and T_3 are the time signals from the 3 staggered wires. The two peaks correspond to the left and to the right sides of the cell. The ΔT standard deviation, evaluated for each peak, is ≈ 8.5 nsec, i.e. $425 \mu\text{m}$ in space, which corresponds to an intrinsic space resolution of $345 \mu\text{m}$.
- Fig. 5.10 : Reconstructed momentum distribution. The horizontal p_T scale (for $\theta = 7.5^\circ$ on the average) is also shown.
- Fig. 5.11 : Ratio of experimental and Monte Carlo simulated p_T distributions (black points). The curves of Fig. 5.8 are also shown for comparison.
- Fig. 5.12 : Showing a typical UA1 event with:
 (a) all reconstructed tracks;
 (b) tracks with $p > 4 \text{ GeV}/c$;
 (c) only the identified LAA trigger track.
- Fig. 5.13 : Comparison of UA1 and LAA reconstructed momenta in terms of:

$$\Delta(1/p) / (1/p) = (1/p_{UA1} - 1/p_{LAA}) / (1/p_{UA1}).$$
 The r.m.s. of the distribution is 33%.

top (25 GeV) AND superbeauty (5.5 GeV) PRODUCTION

$5. \leq \delta < 30.$

$\Delta p_T / p_T = 20. \%$
 (LEADING/TOTAL) = .25
 $\sigma_{\text{tot}} = .0100 \mu\text{b}, \sigma_t = .1000 \mu\text{b}$

PRODUCTION BARYONS = x-flat, MESONS = $(1-x)^2$

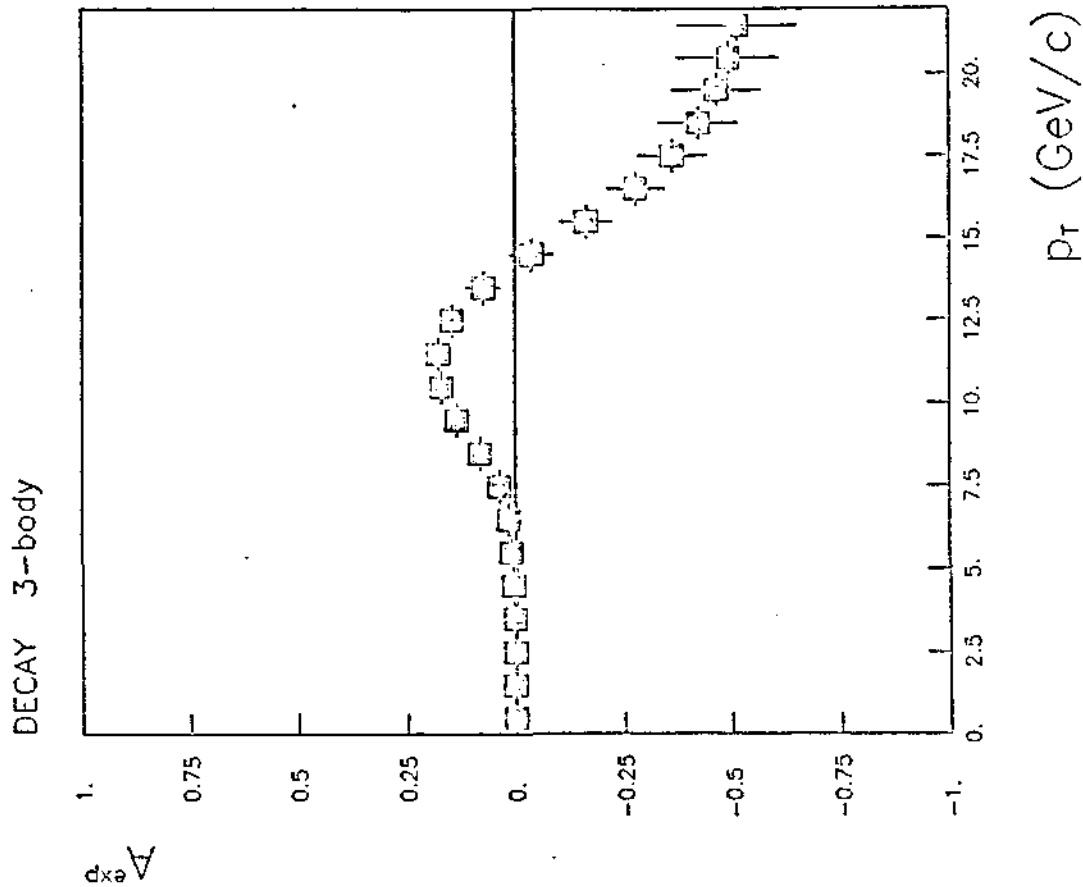
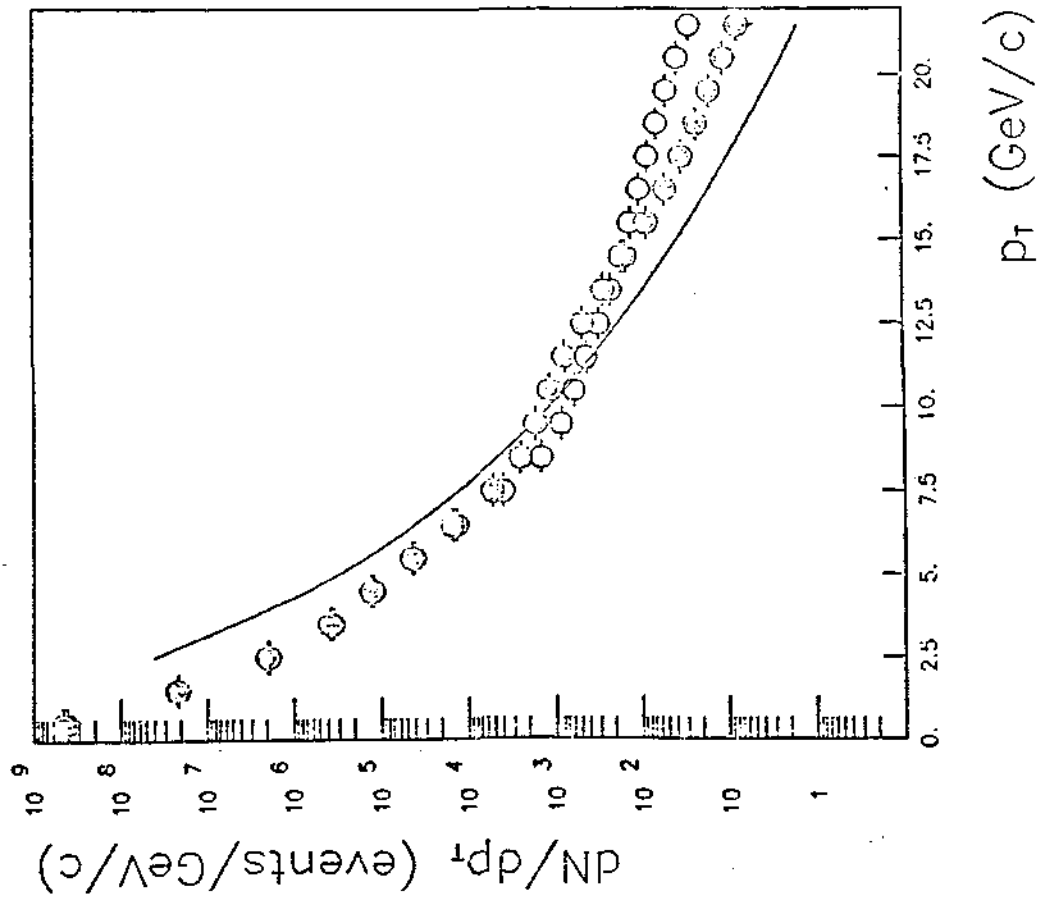


Fig. 1.1

top (25 GeV) PRODUCTION

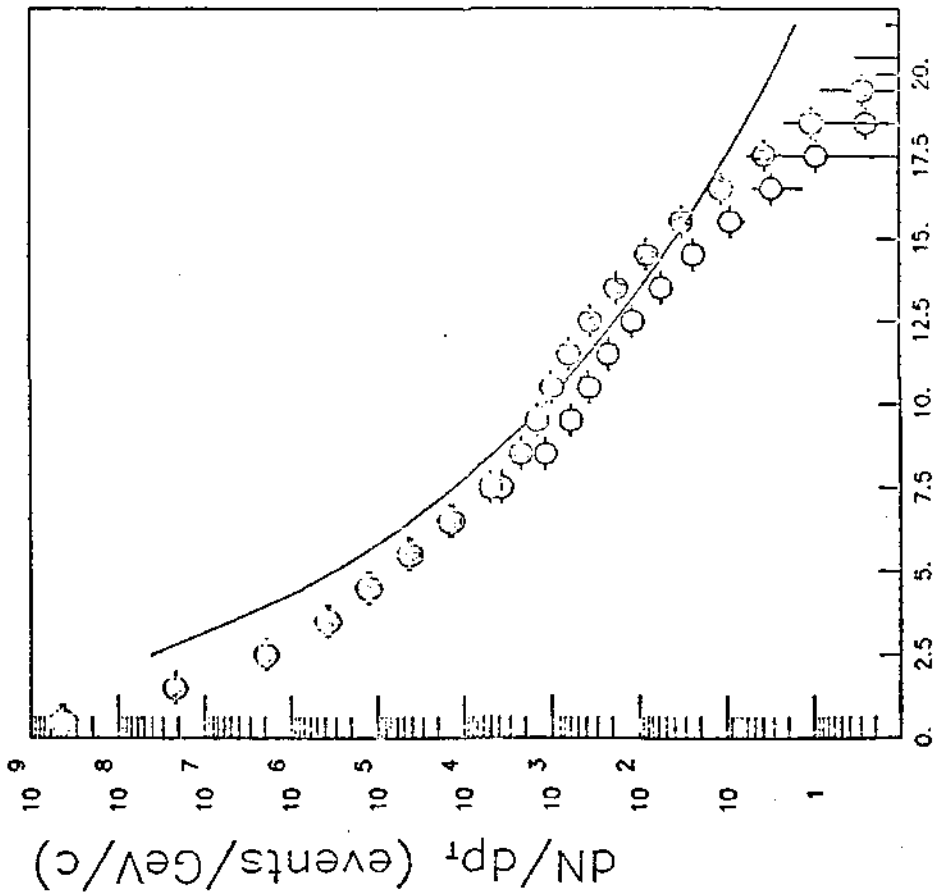
$5. \leq \theta < 30.$

$\Delta p_T / p_T = 20. \%$
(LEADING/TOTAL) = .25

$\sigma_t = .1000 \mu\text{b}$

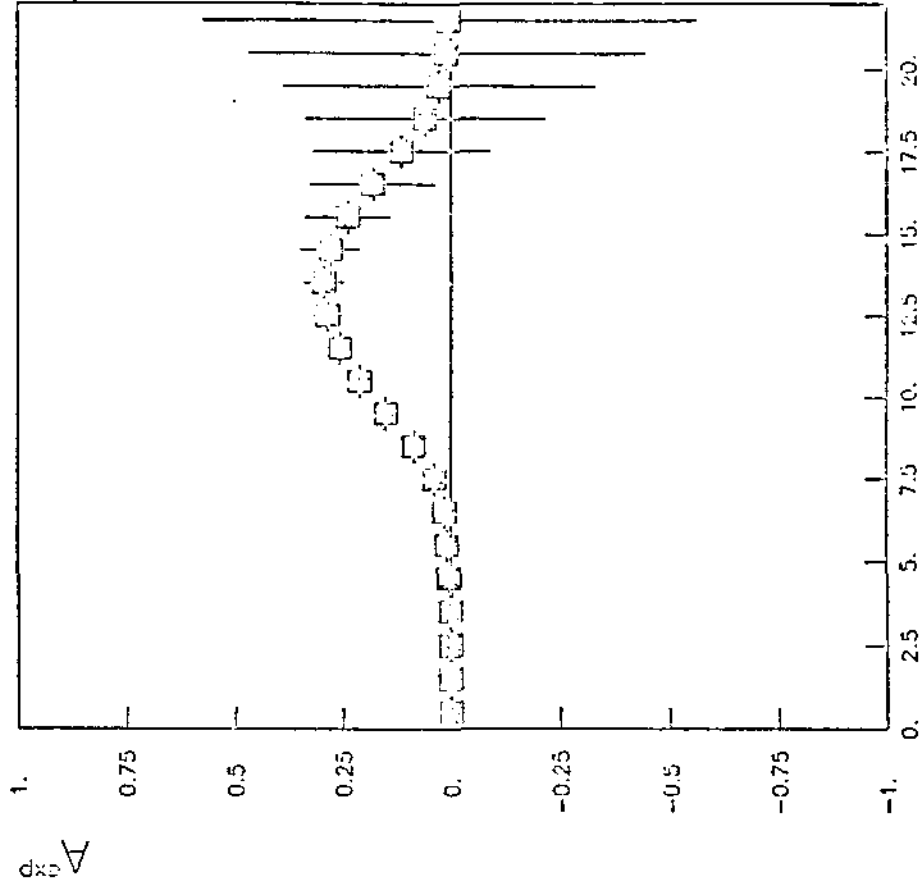
PRODUCTION BARYONS = x-flat, MESONS = $(1-x)^2$

DECAY 3-body



p_T (GeV/c)

(a)



p_T (GeV/c)

(b)

Fig. 1.2

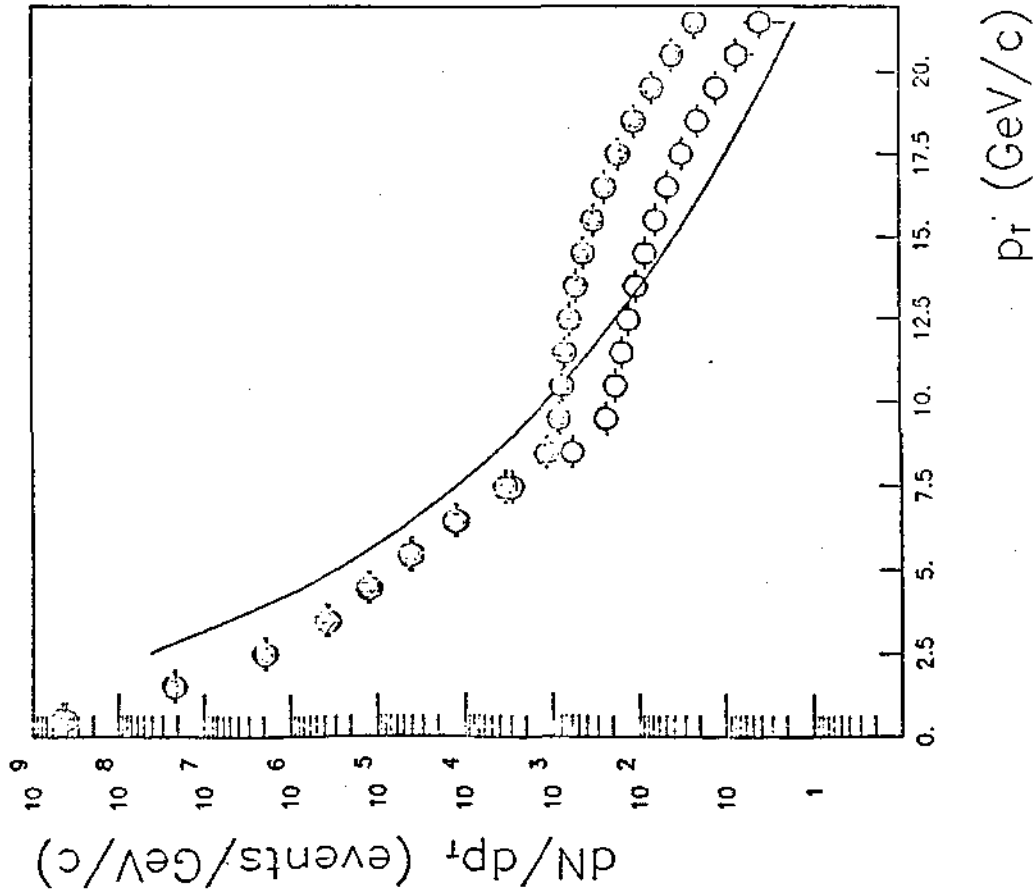
top (35 GeV) PRODUCTION

$5. \leq \theta < 30.$

$\Delta p_T / p_T = 20. \%$
(LEADING/TOTAL) = .25

$\sigma_t = .0500 \mu\text{b}$

PRODUCTION BARYONS=x-flat, MESONS=(1-x)²



DECAY 3-body

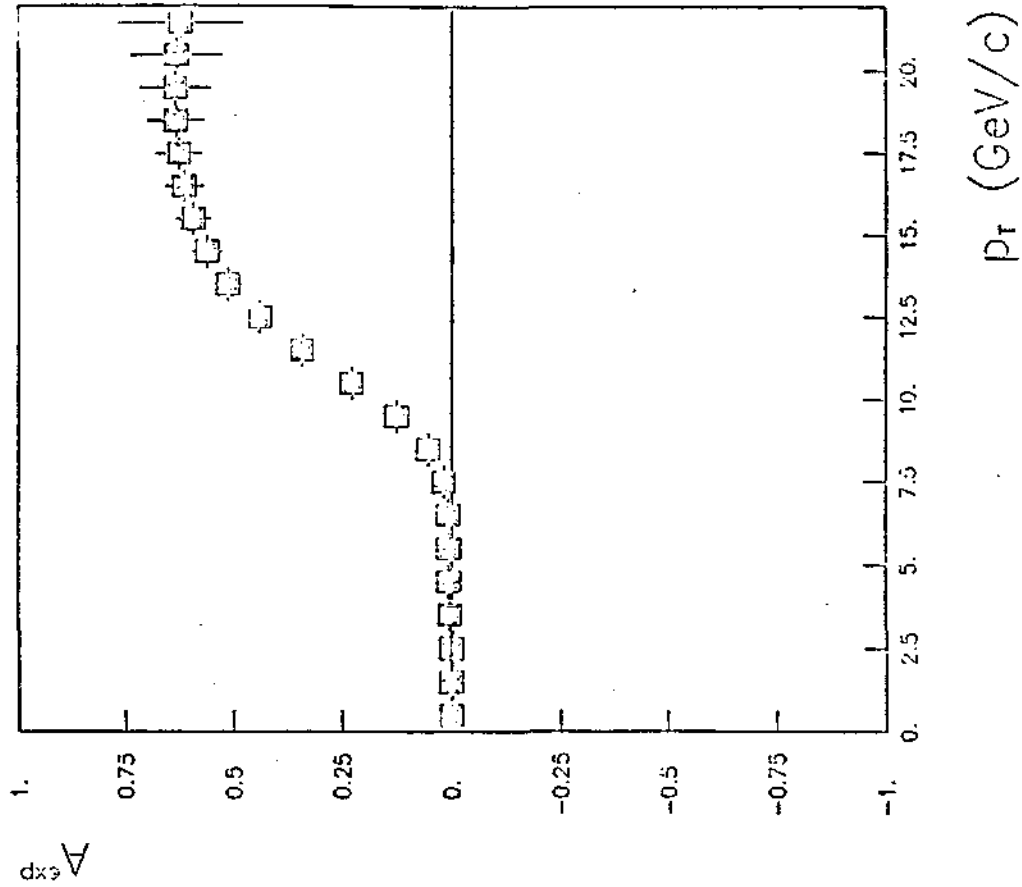


Fig. 1.3








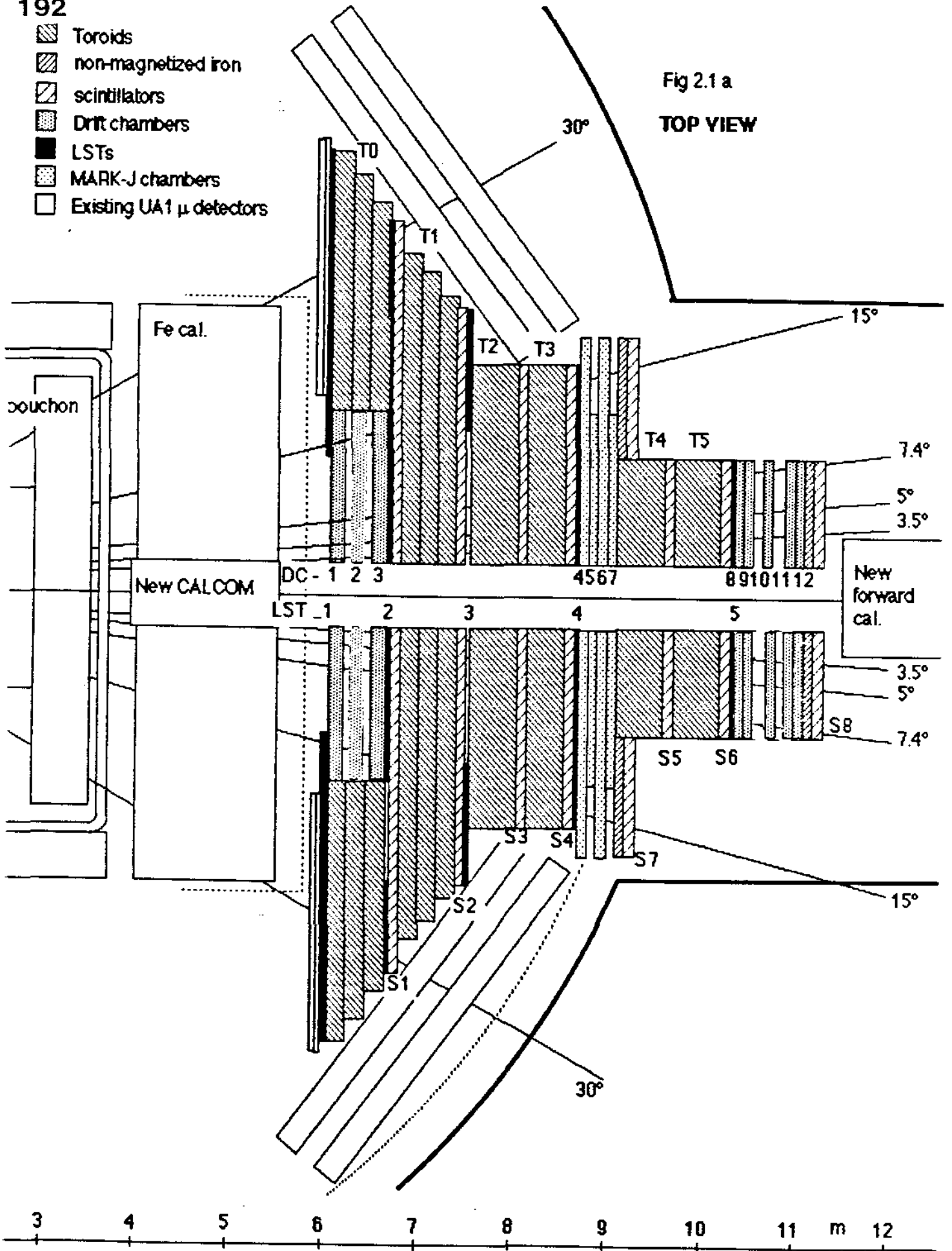
-  Toroids
-  non-magnetized iron
-  scintillators
-  Drift chambers
-  LSTs
-  MARK-J chambers
-  Existing UA1 μ detectors

Fig 2.1 a
TOP VIEW










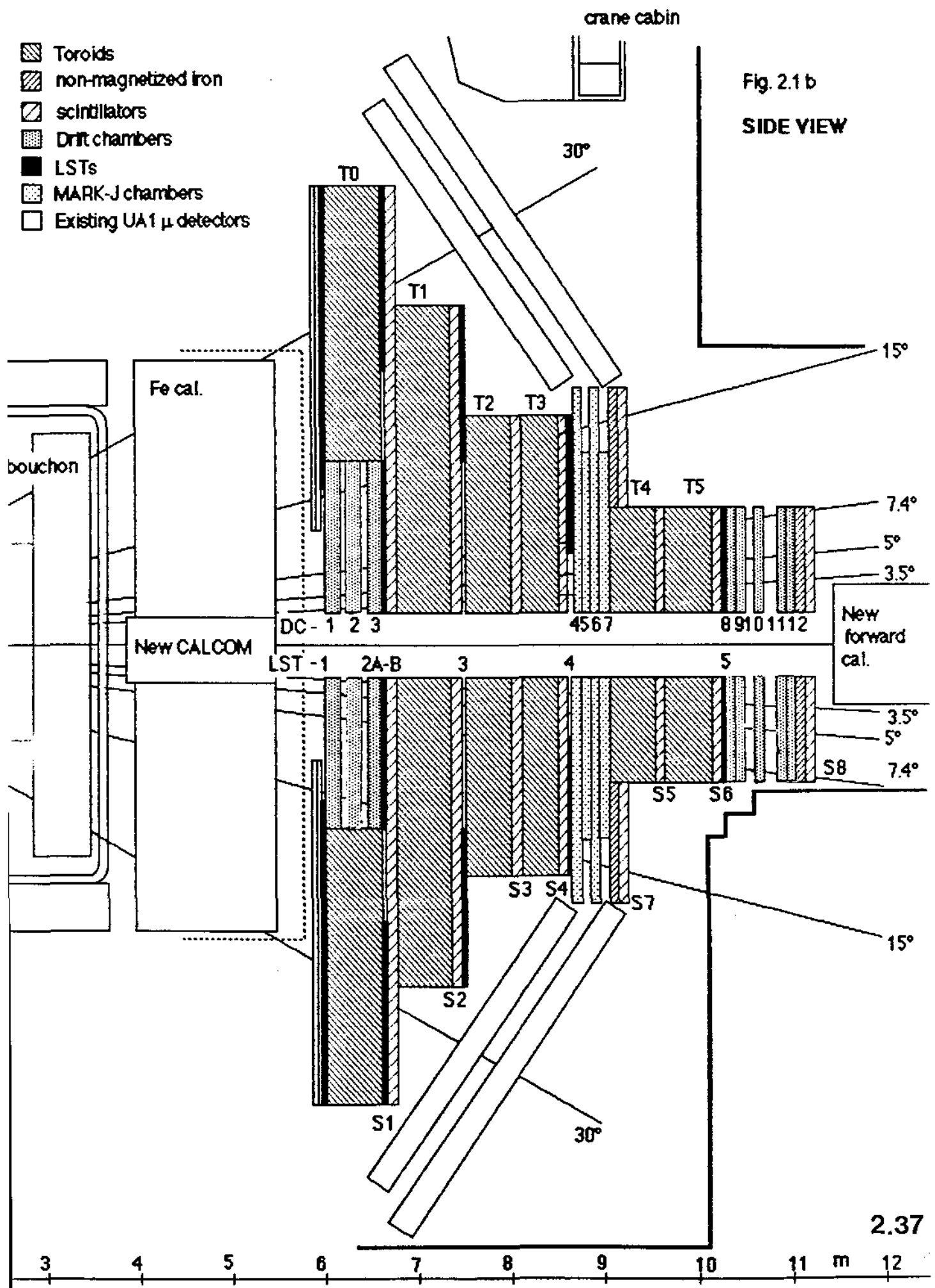
-  Toroids
-  non-magnetized iron
-  scintillators
-  Drift chambers
-  LSTs
-  MARK-J chambers
-  Existing UA1 μ detectors

Fig. 2.1 b
SIDE VIEW



2.37

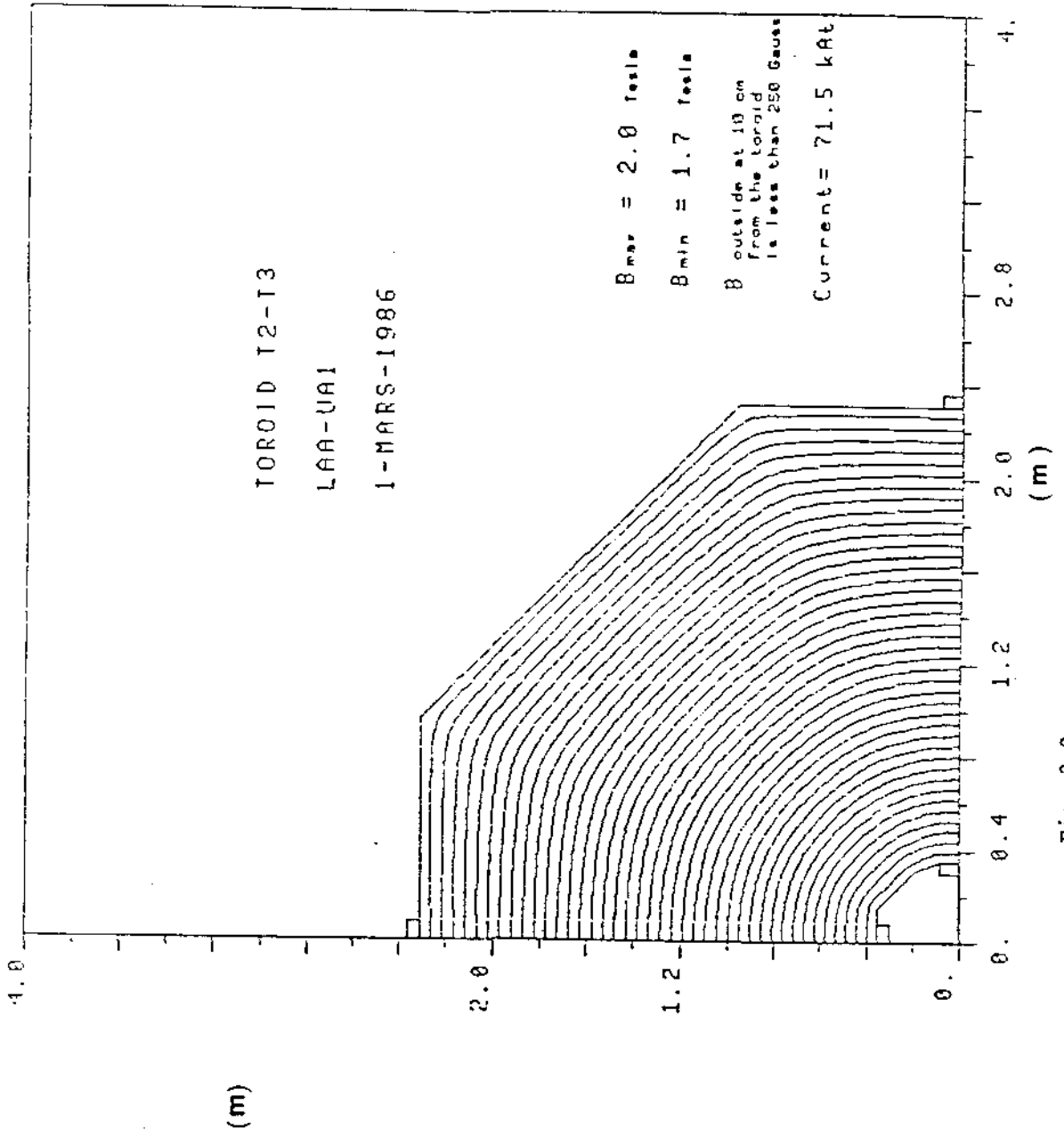


Fig. 2.2

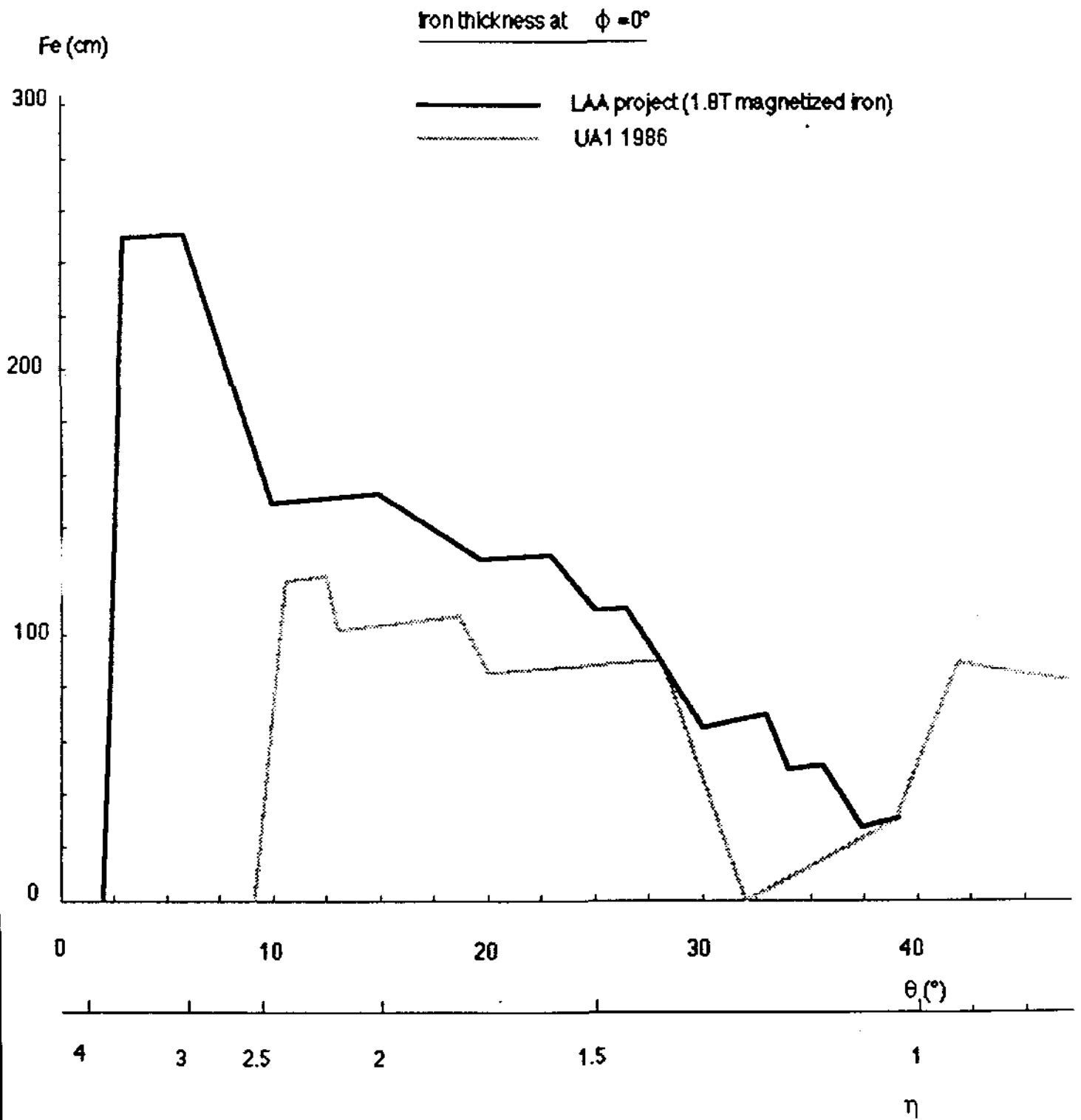


Fig. 2.3

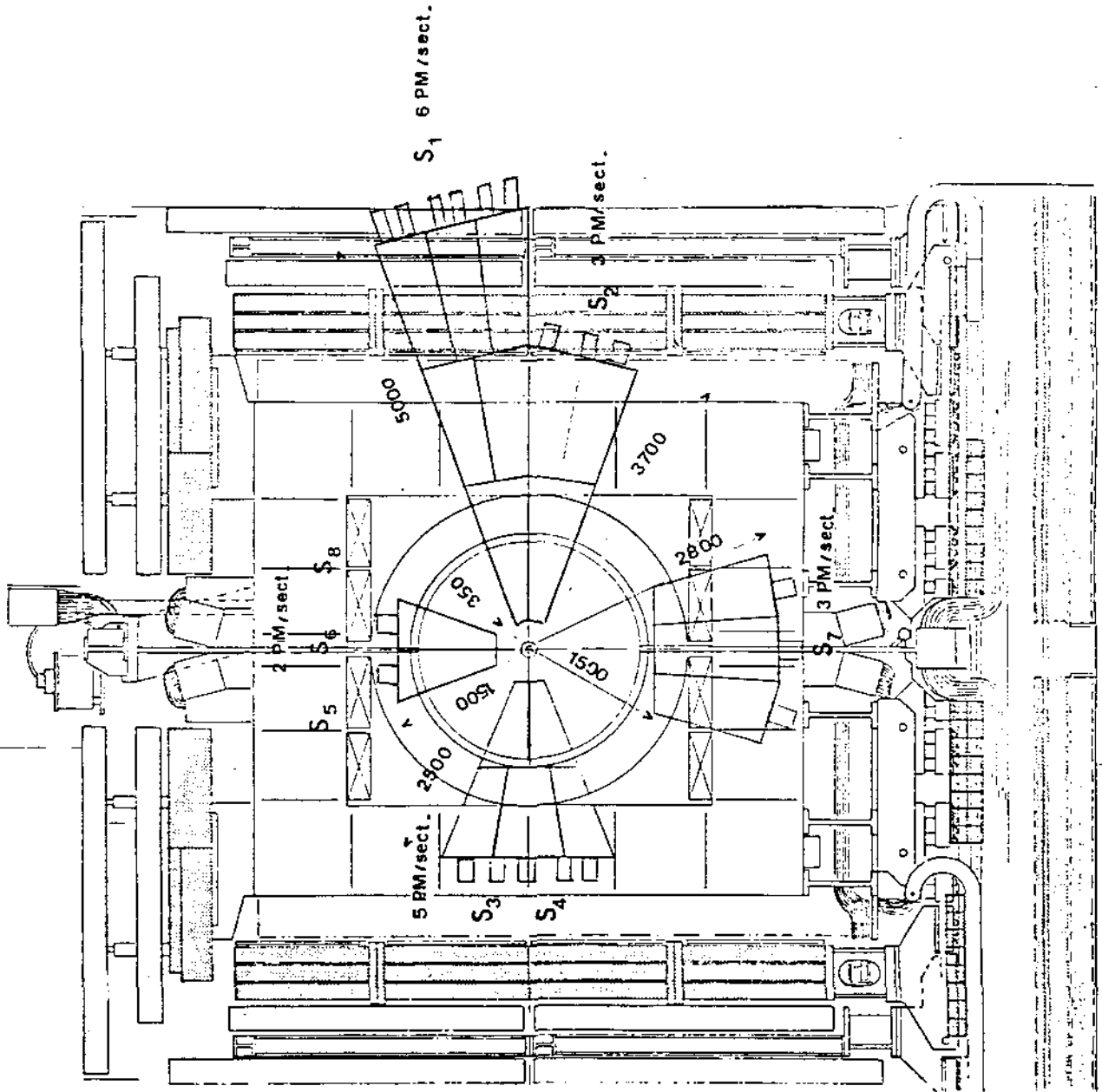


Fig. 2.4

Drift chambers DC1, DC2, DC3

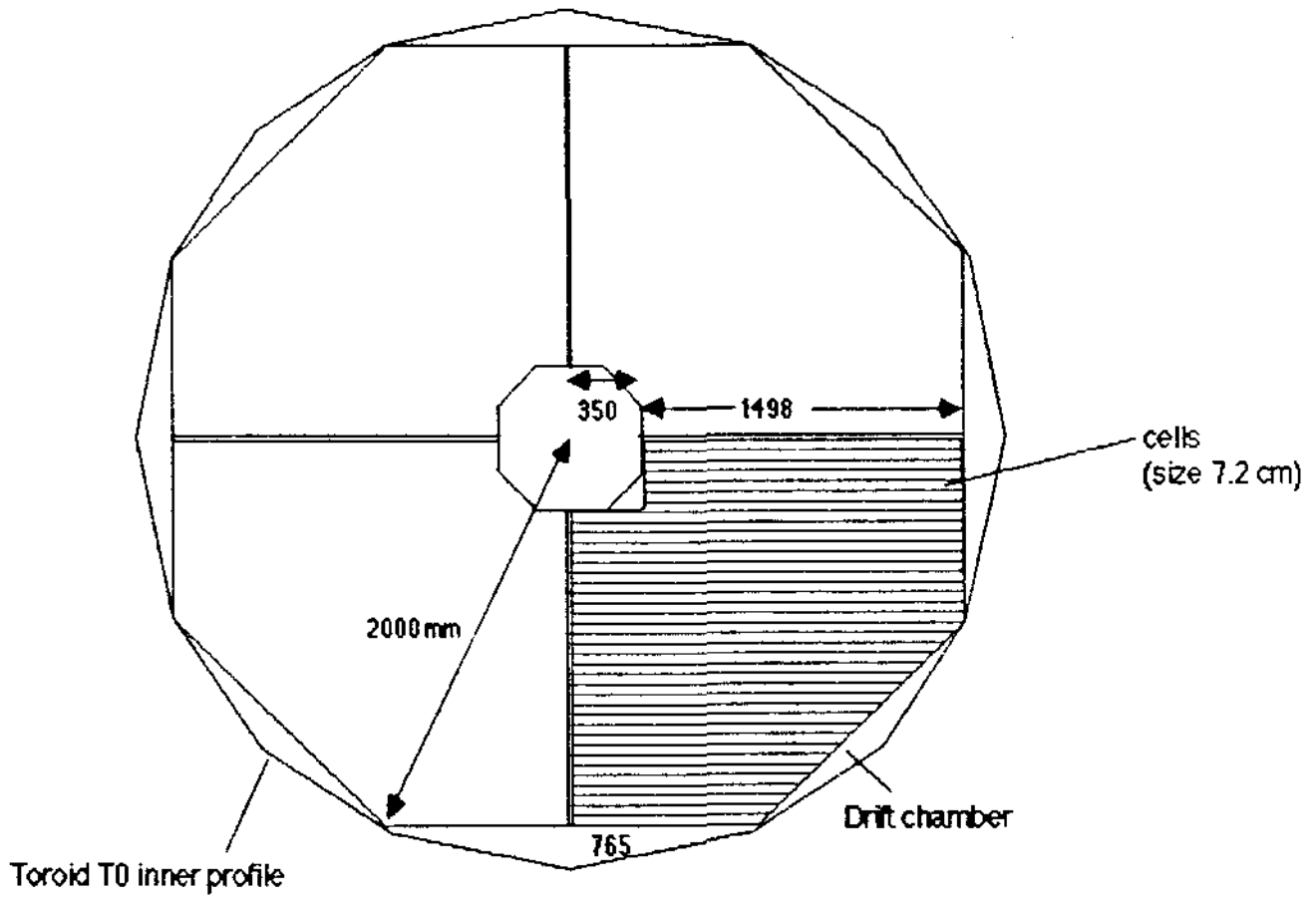


Fig. 2.5

Drift chambers DC8 to DC12

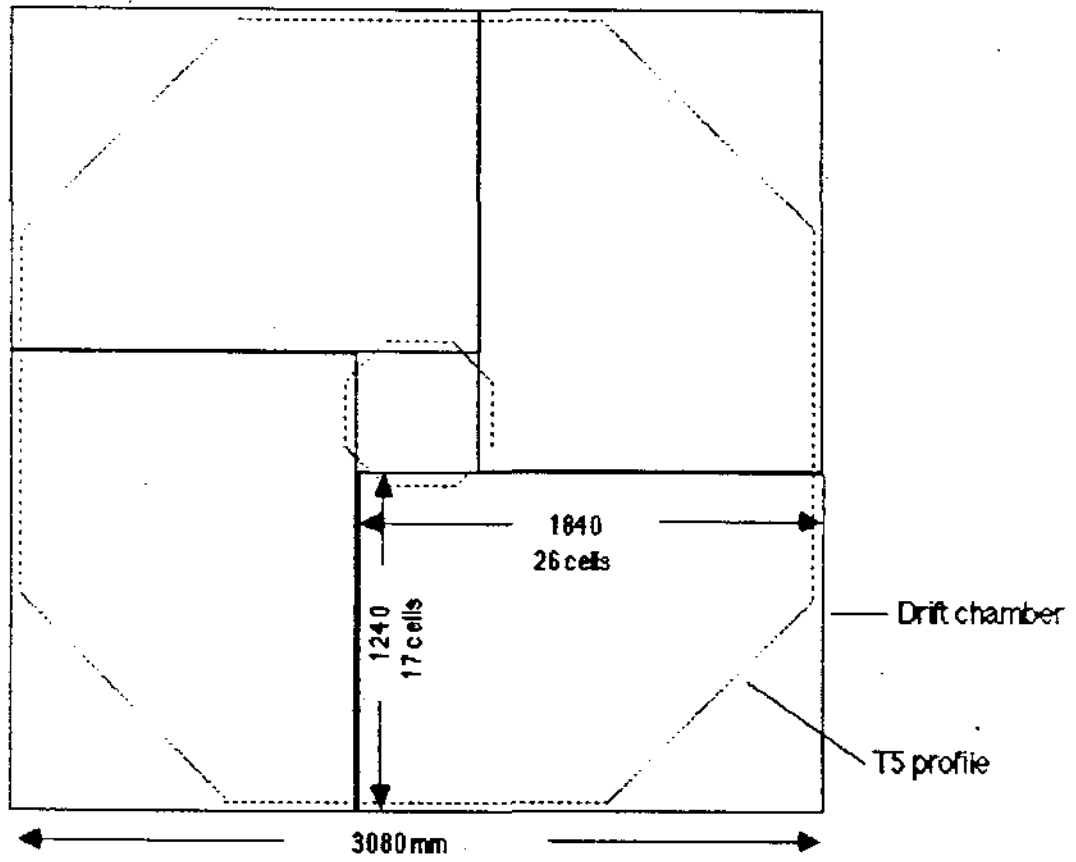


Fig. 2.6

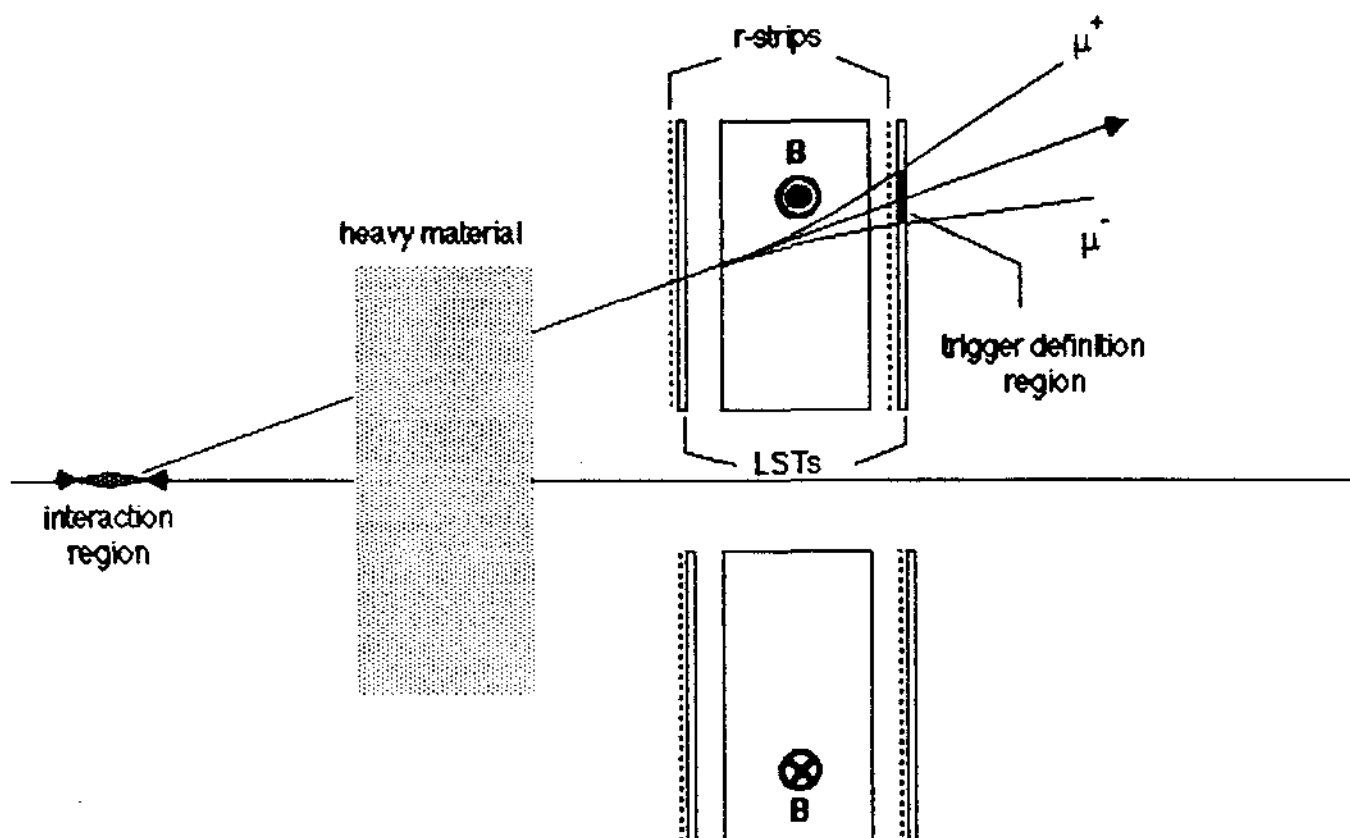


Fig. 3.1

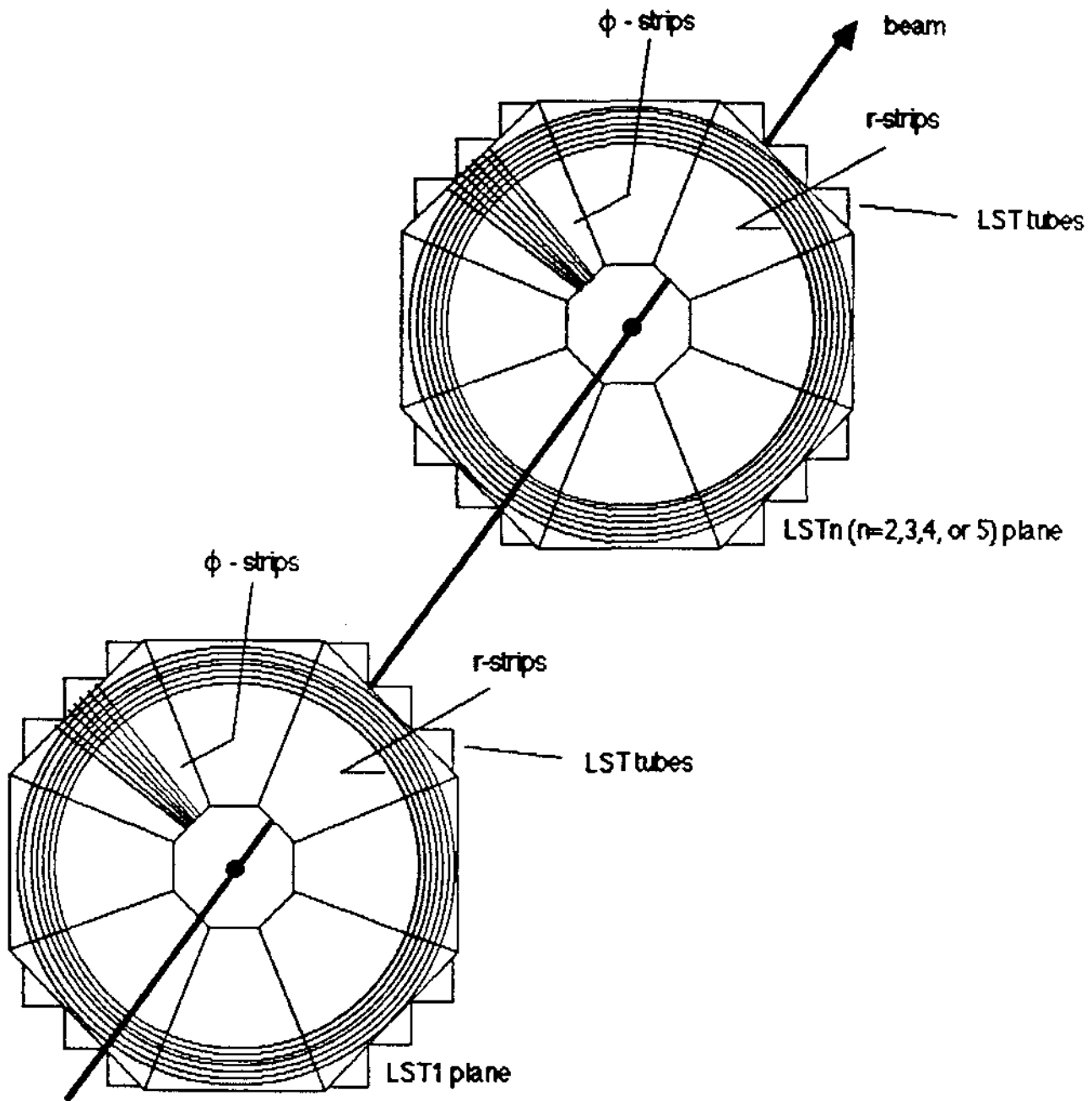


Fig. 3.2

Trigger processor

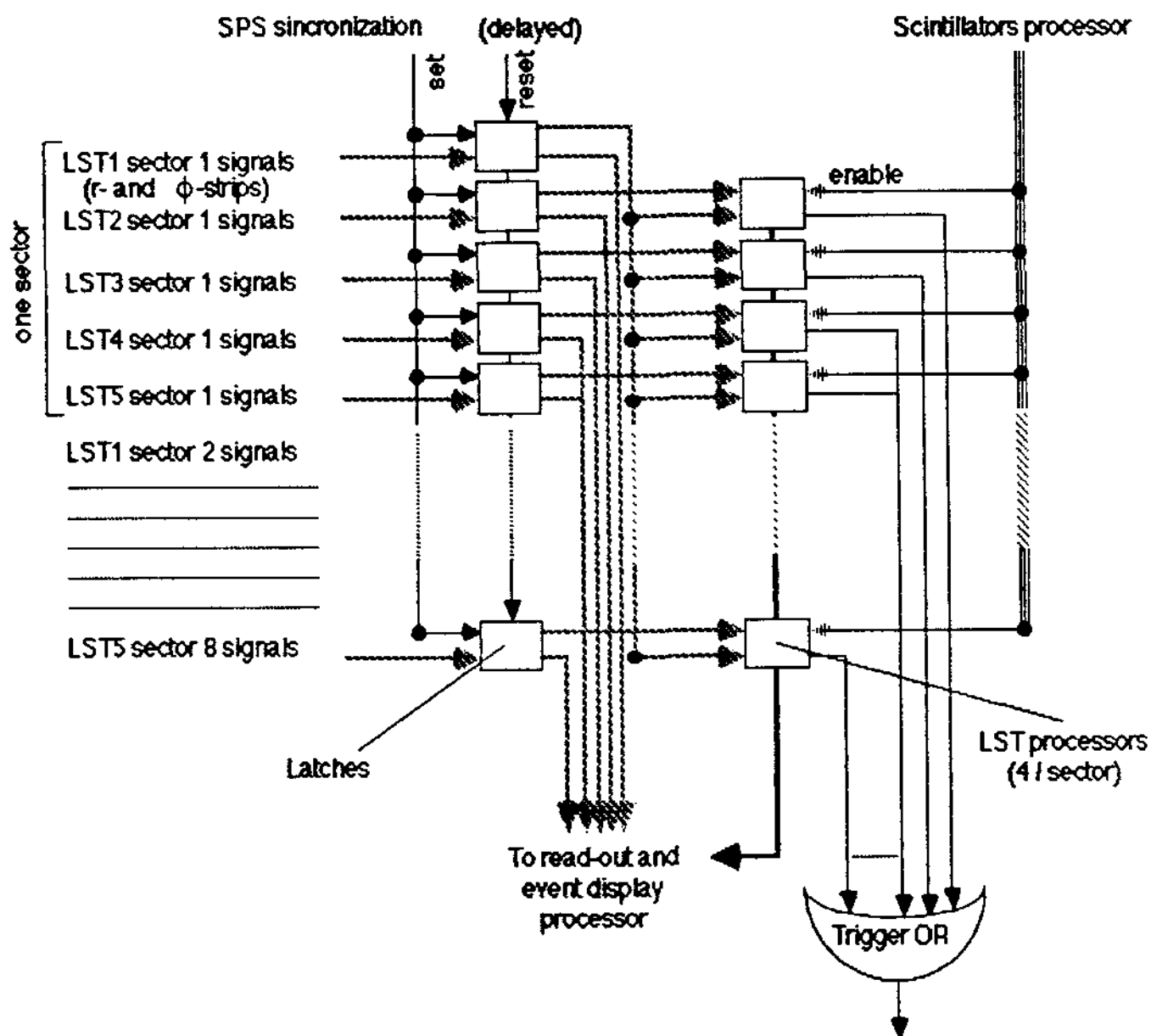
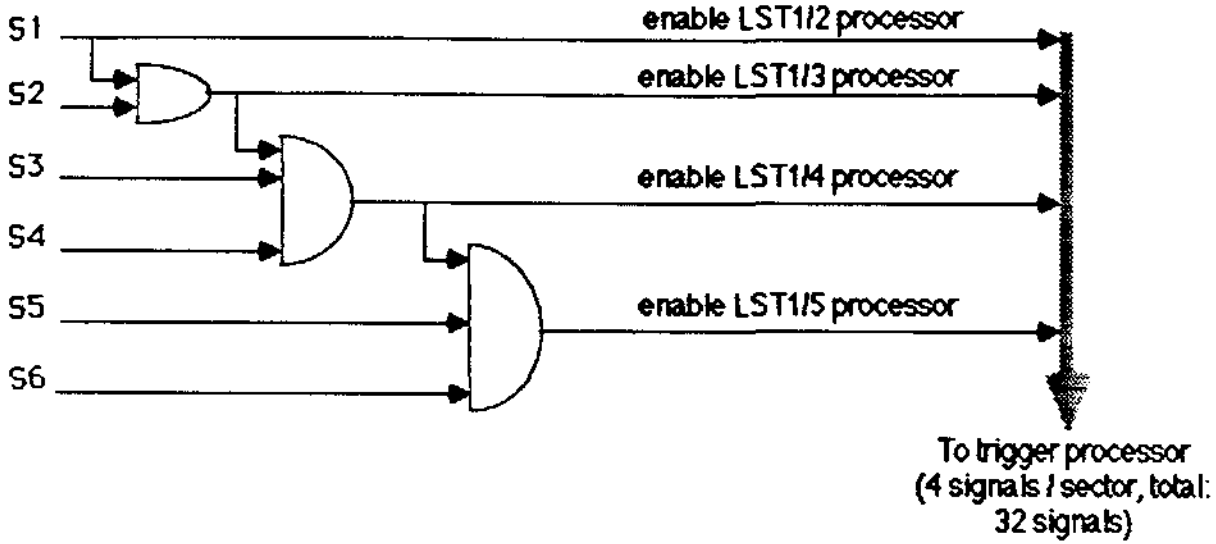


Fig. 3.3

Scintillators processor (one sector)

SPS sincronization (delayed)

Scintillator



Scintillators signals from one sector are discriminated and then ORed. A small number of ADCs and TDCs is used for monitor and calibration multiplexing to the counters signals.

Fig. 3.4

LST processor (r-strips)

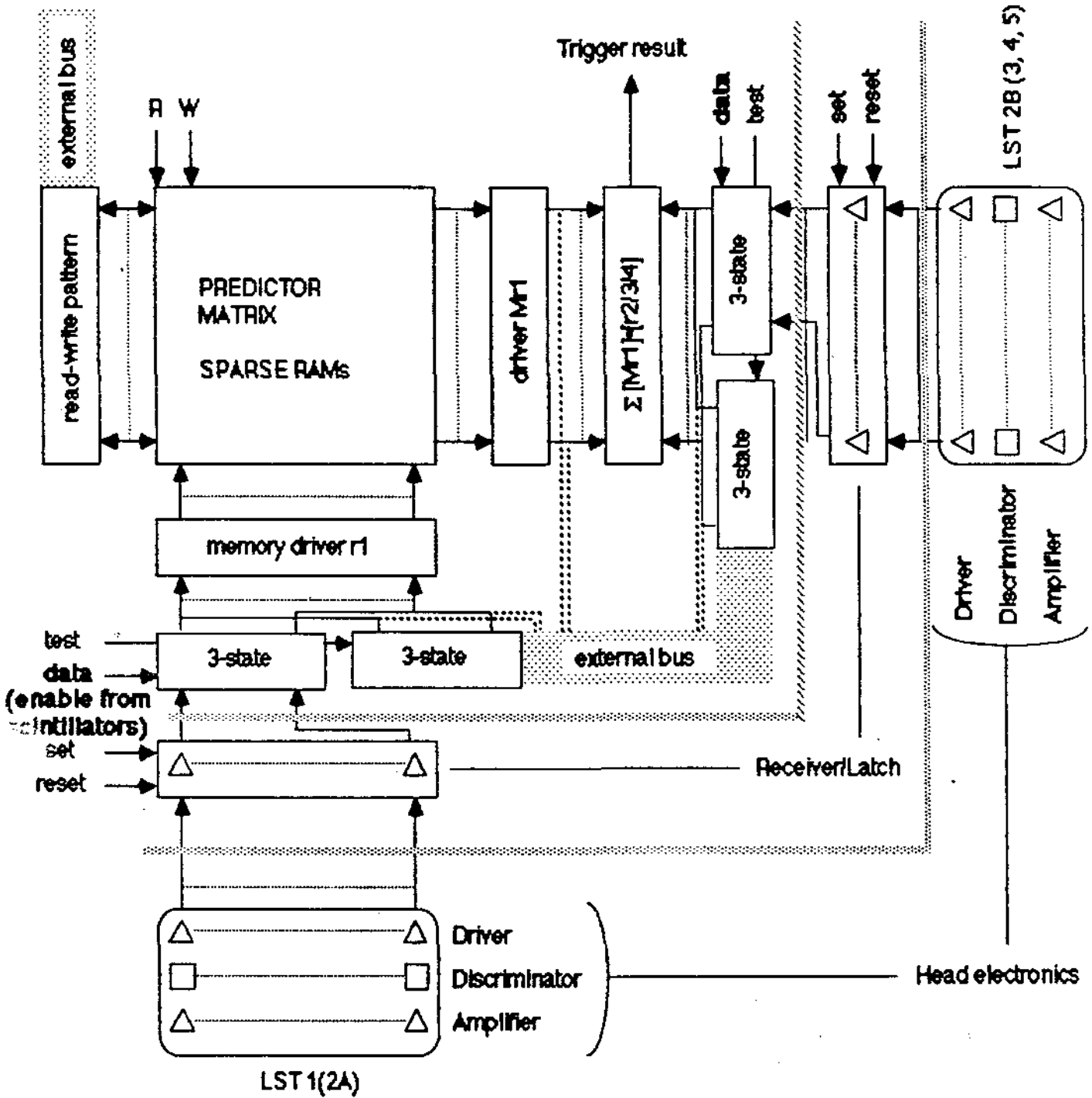


Fig. 3.5(a)

Predictor matrix

 Existing RAMs

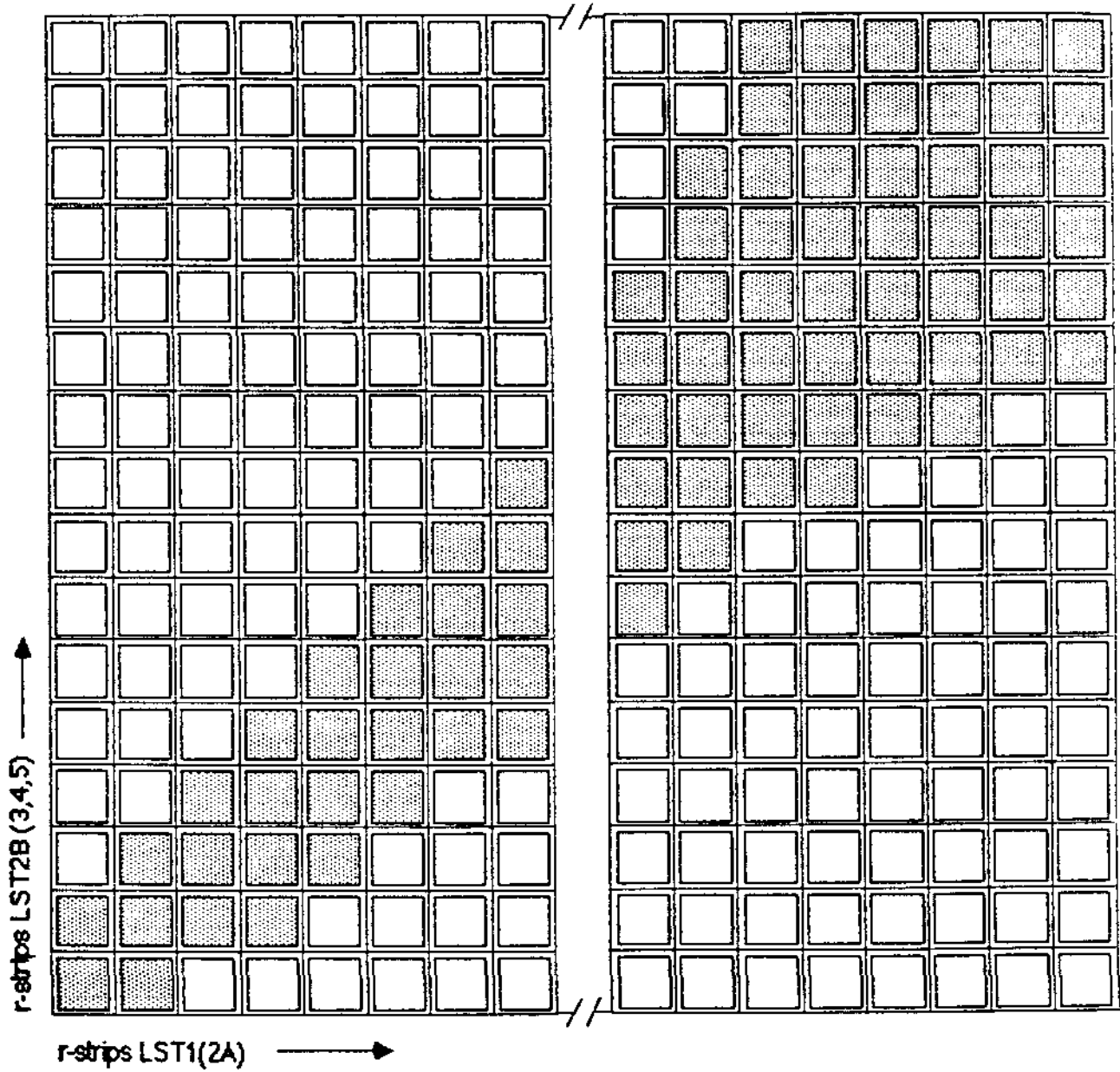


Fig. 3.5 (b)

LST processor (ϕ - strips)

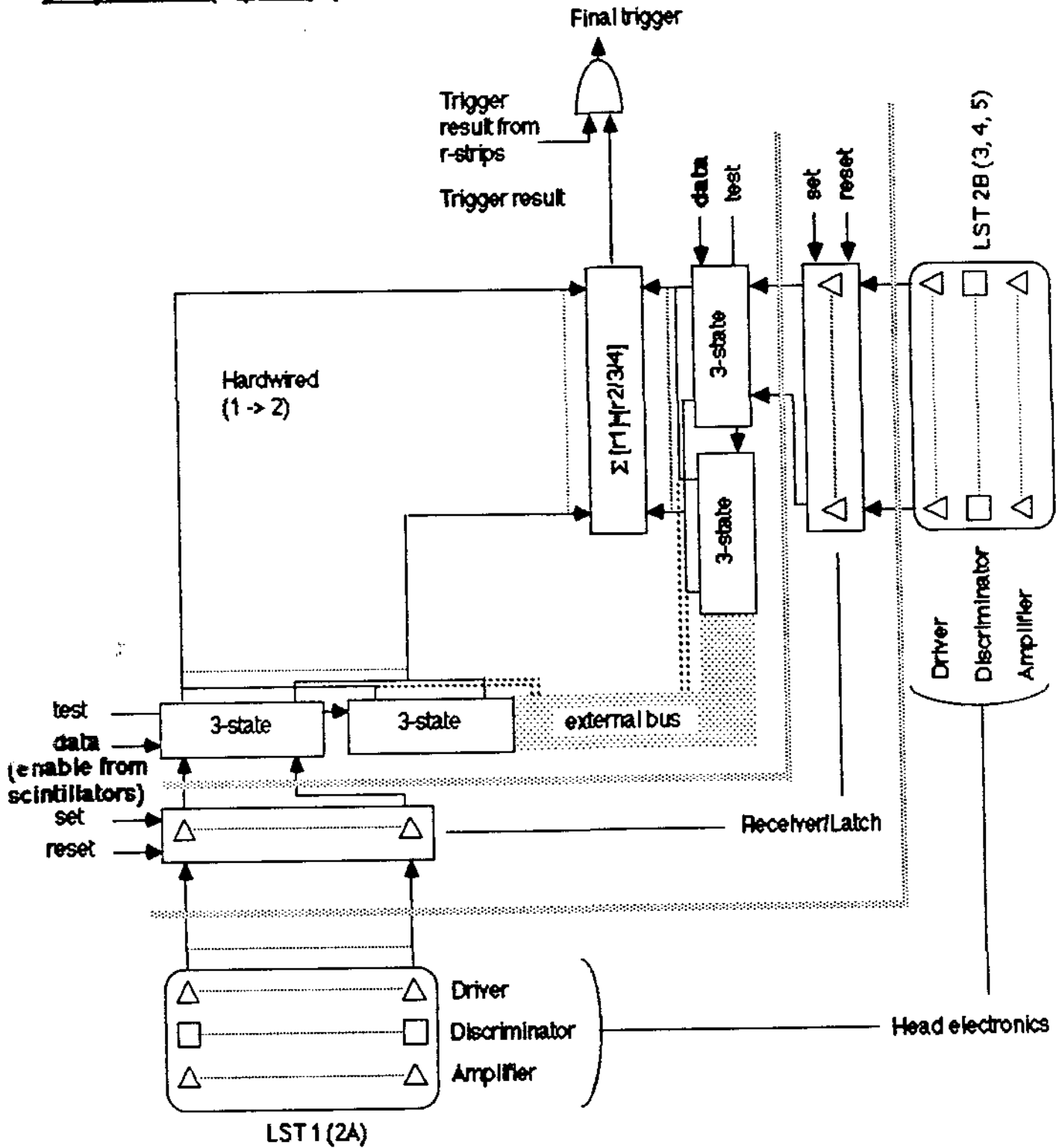


Fig. 3.6

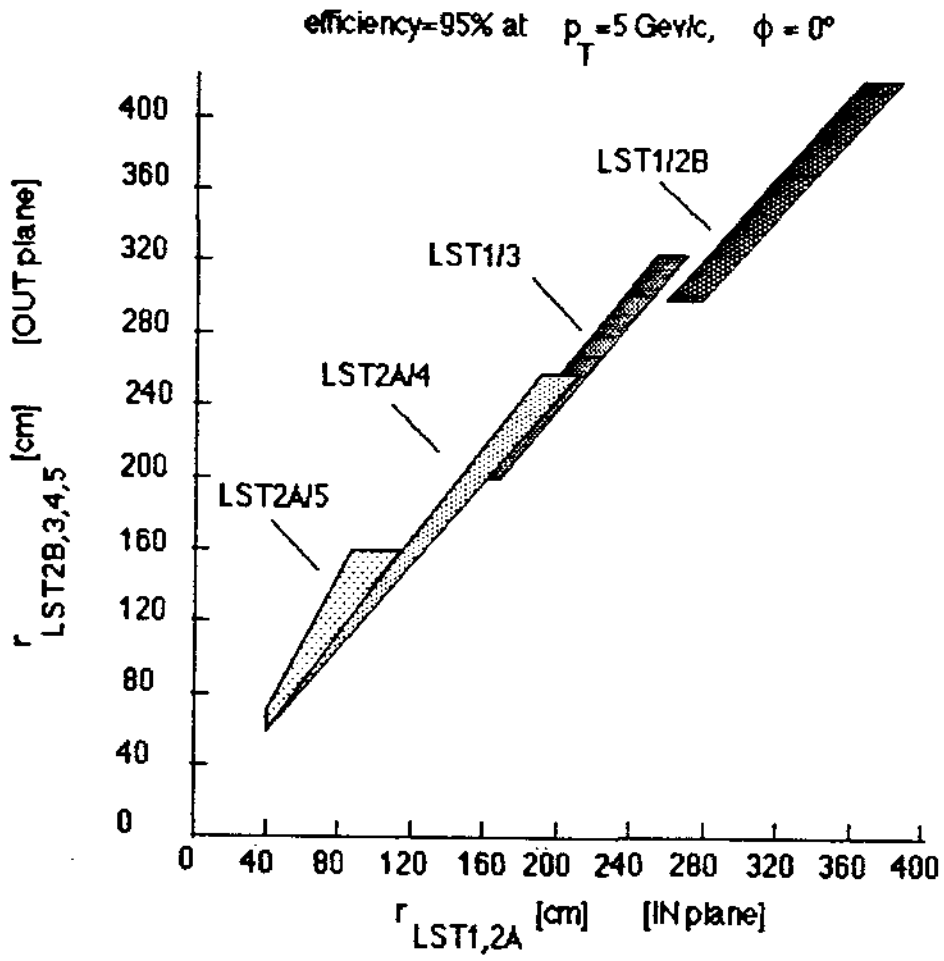


Fig. 3.7(a)

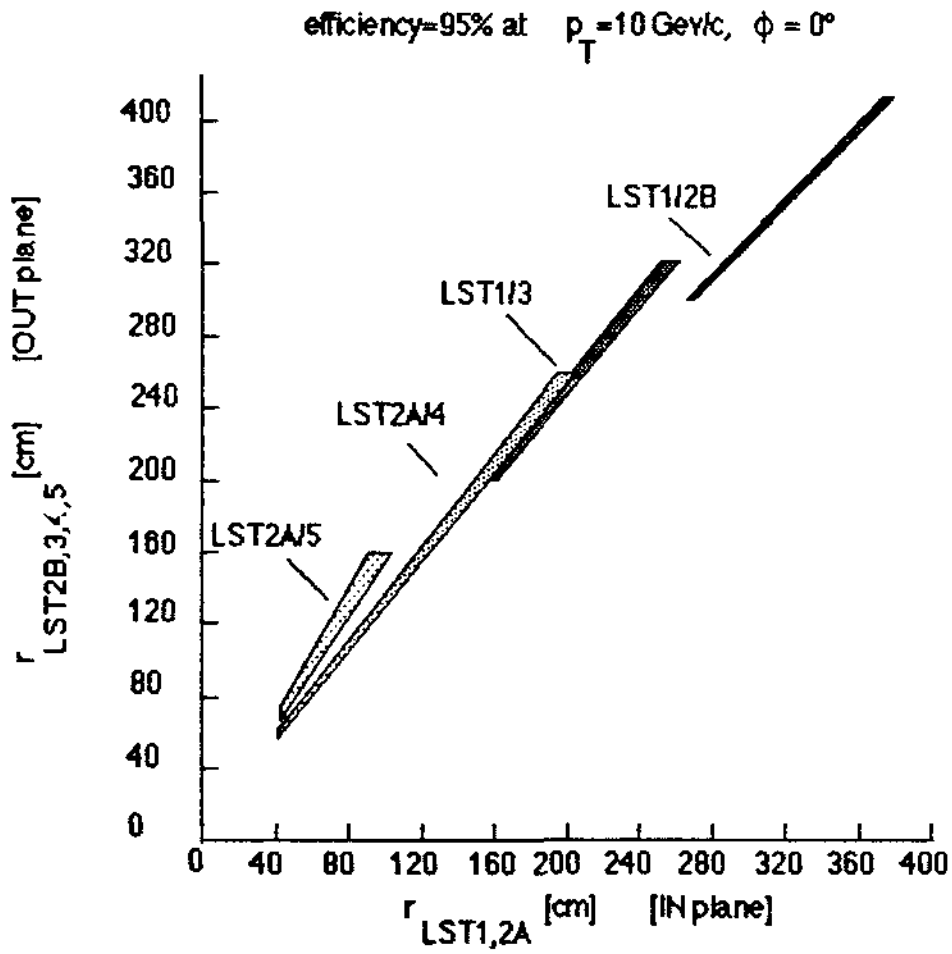


Fig. 3.7(b)

Efficiency curves for three different trigger configurations
for positive muons, at $\phi = 0^\circ$ and $\theta = 8^\circ$

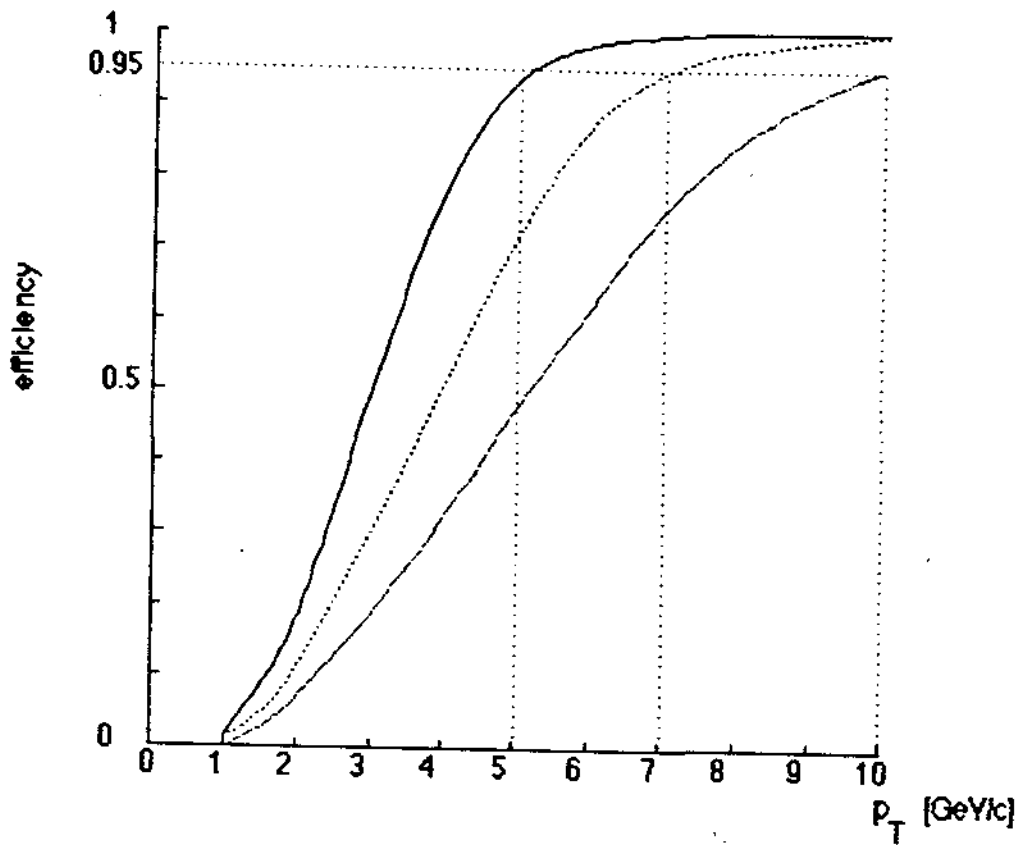


Fig. 3.8

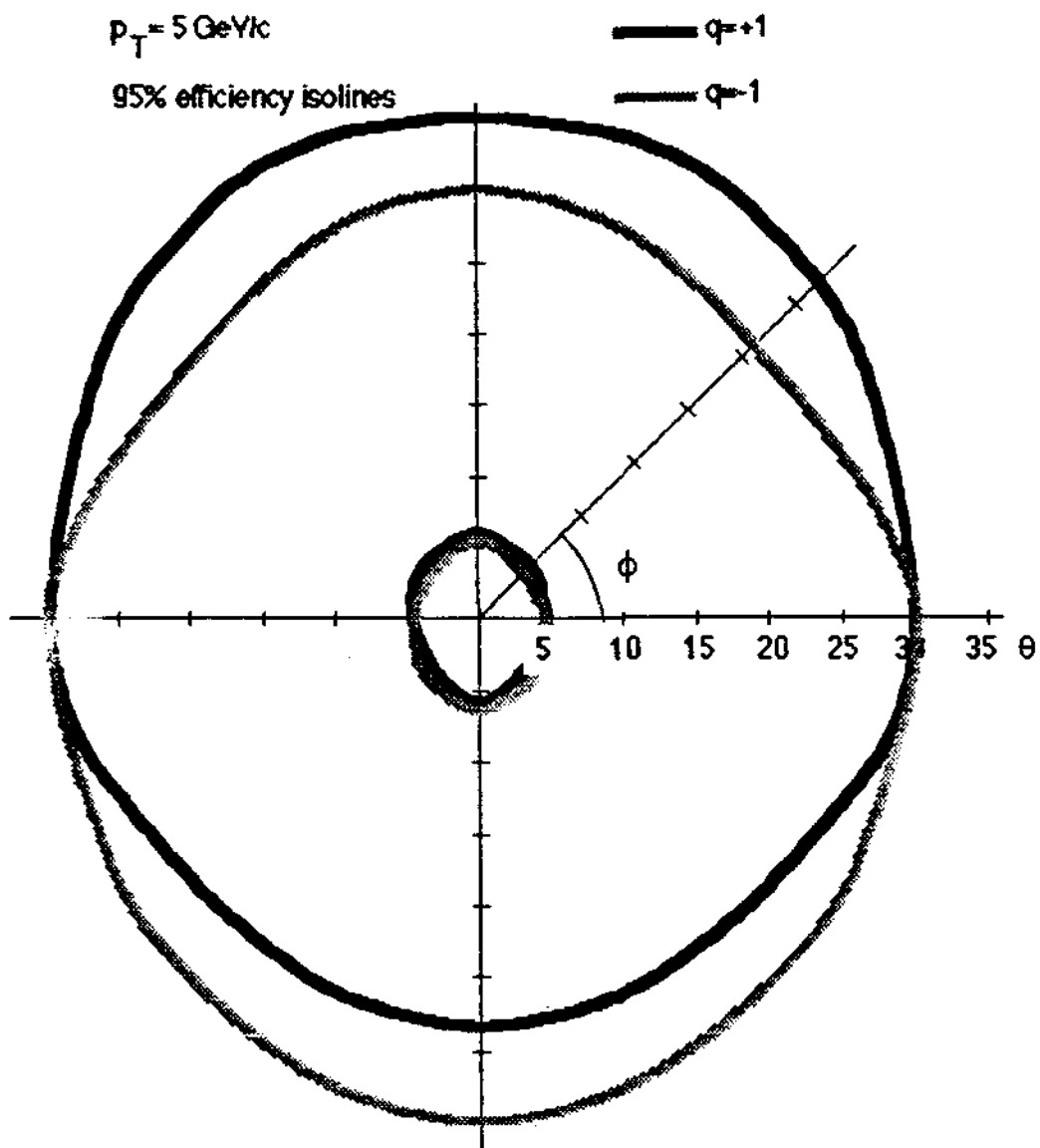


Fig 3.9(a)

$p_T = 10 \text{ GeV}/c$

95% efficiency isolines

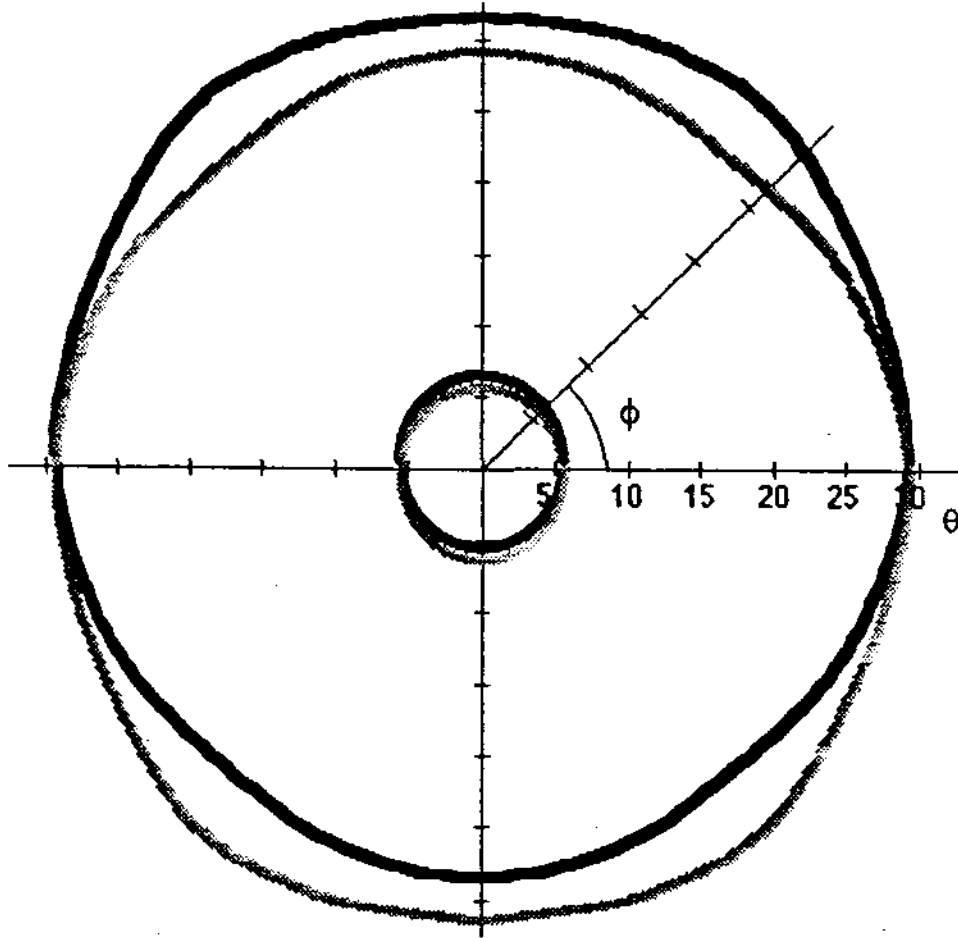
— $q=+1$ — $q=-1$ 

Fig 3.9(b)

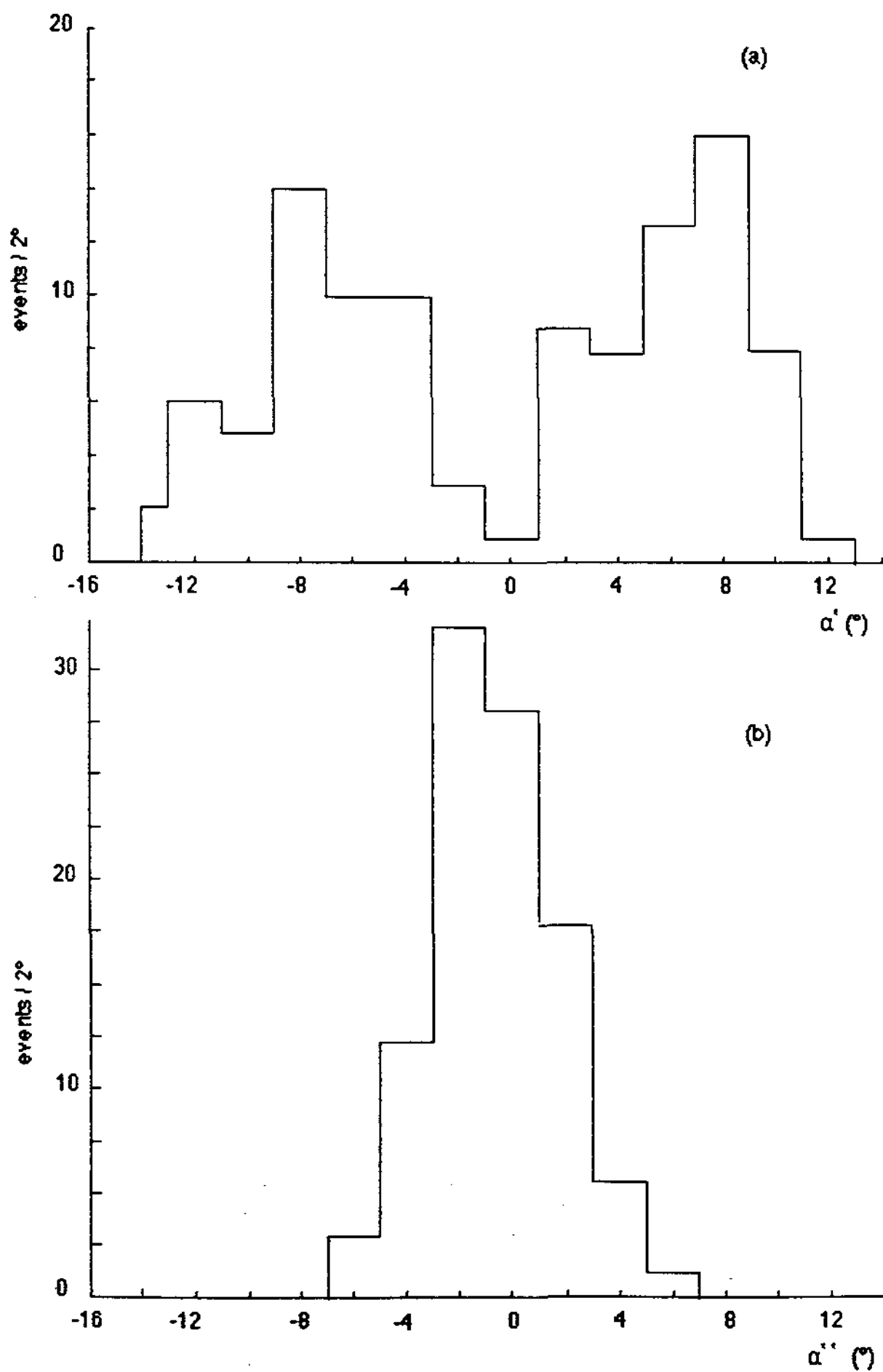


Fig. 3.10

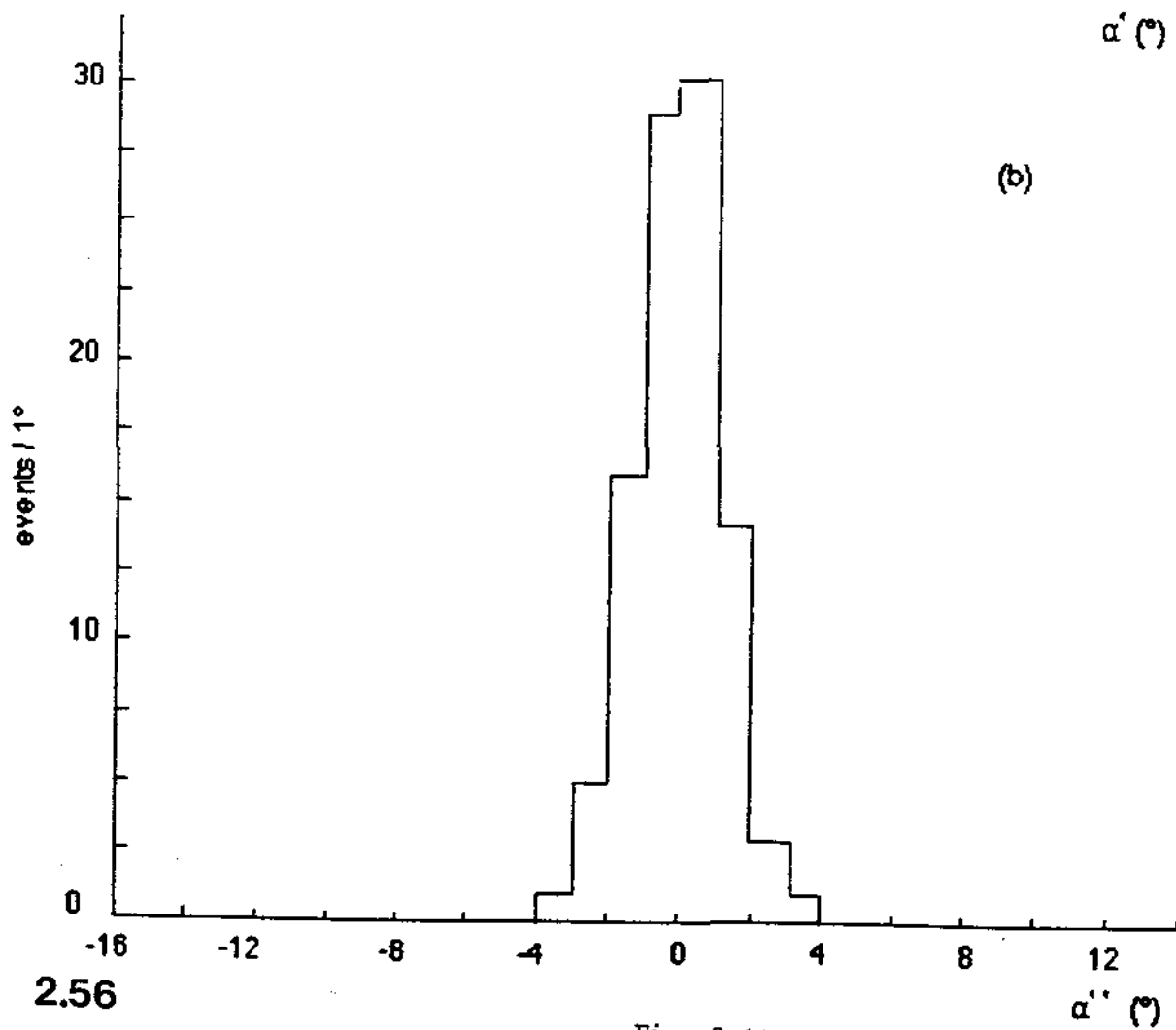
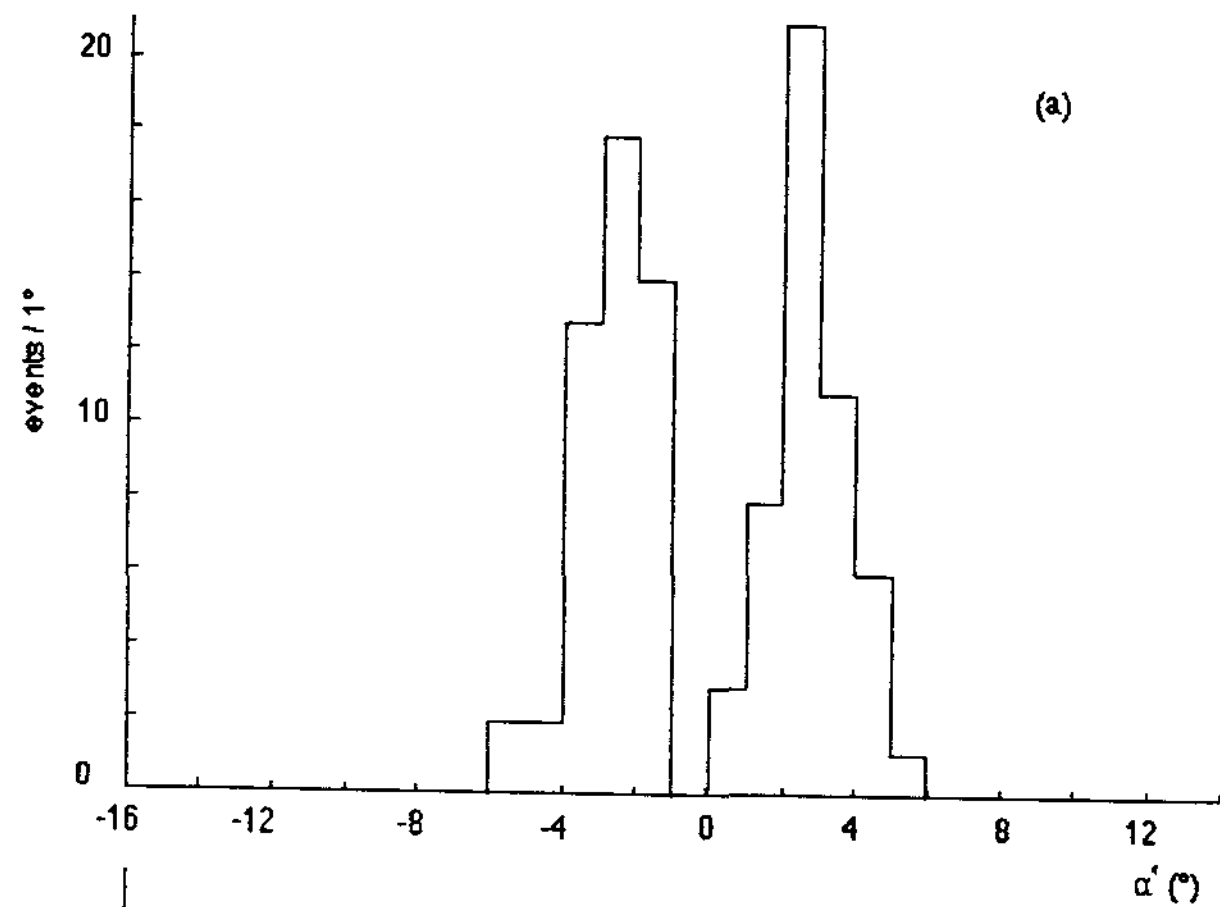


Fig. 3.11

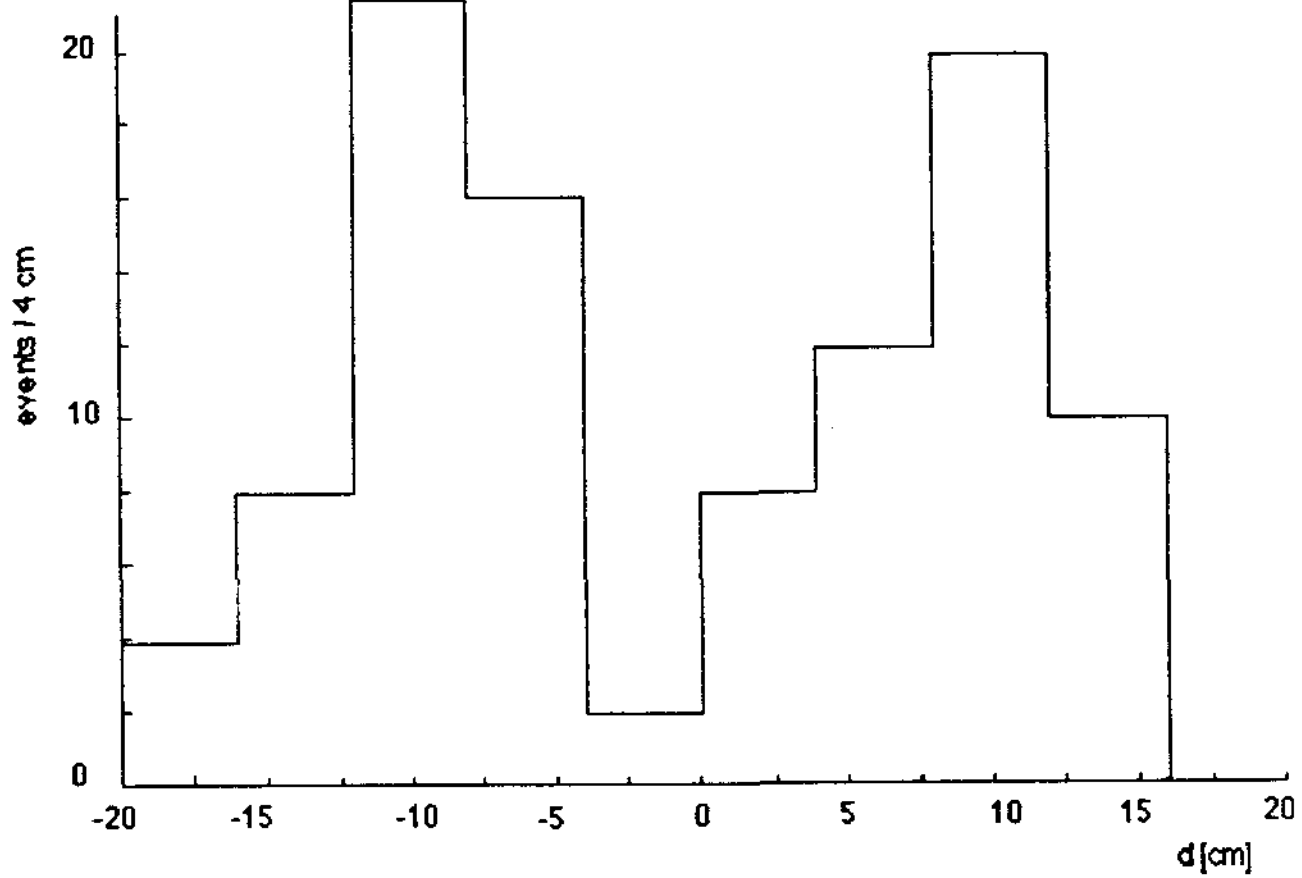


Fig. 3.12

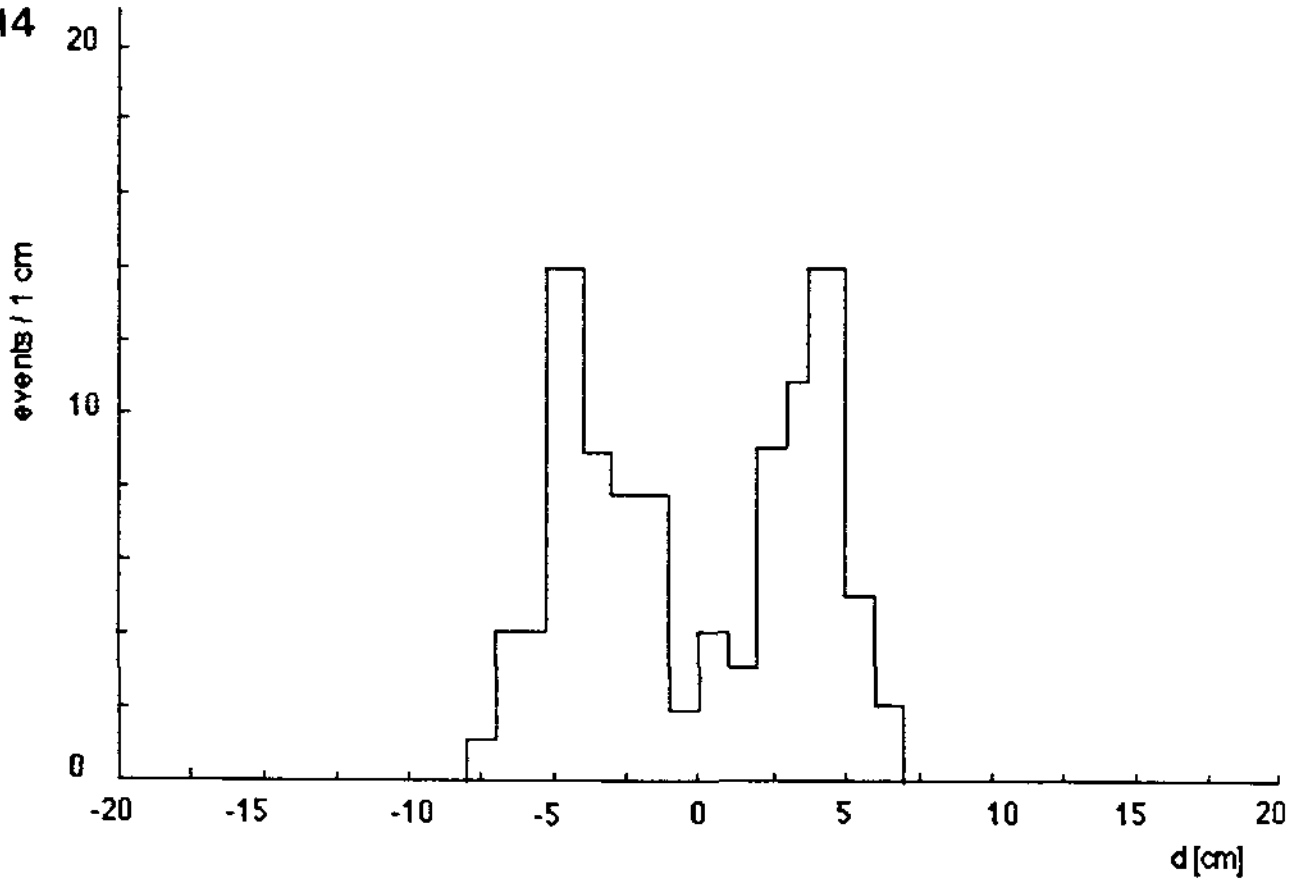


Fig. 3.13

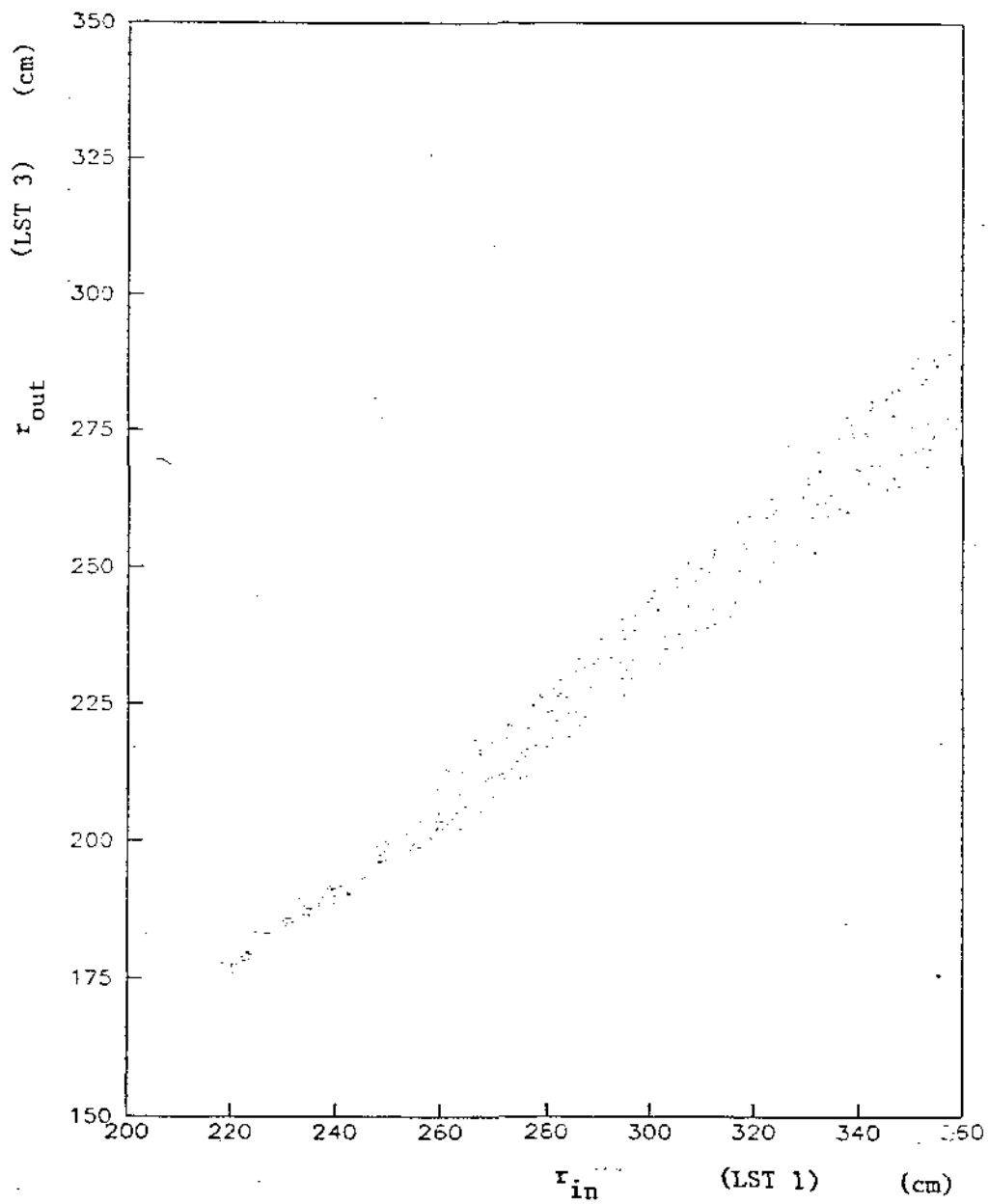


Fig. 3.14(a)

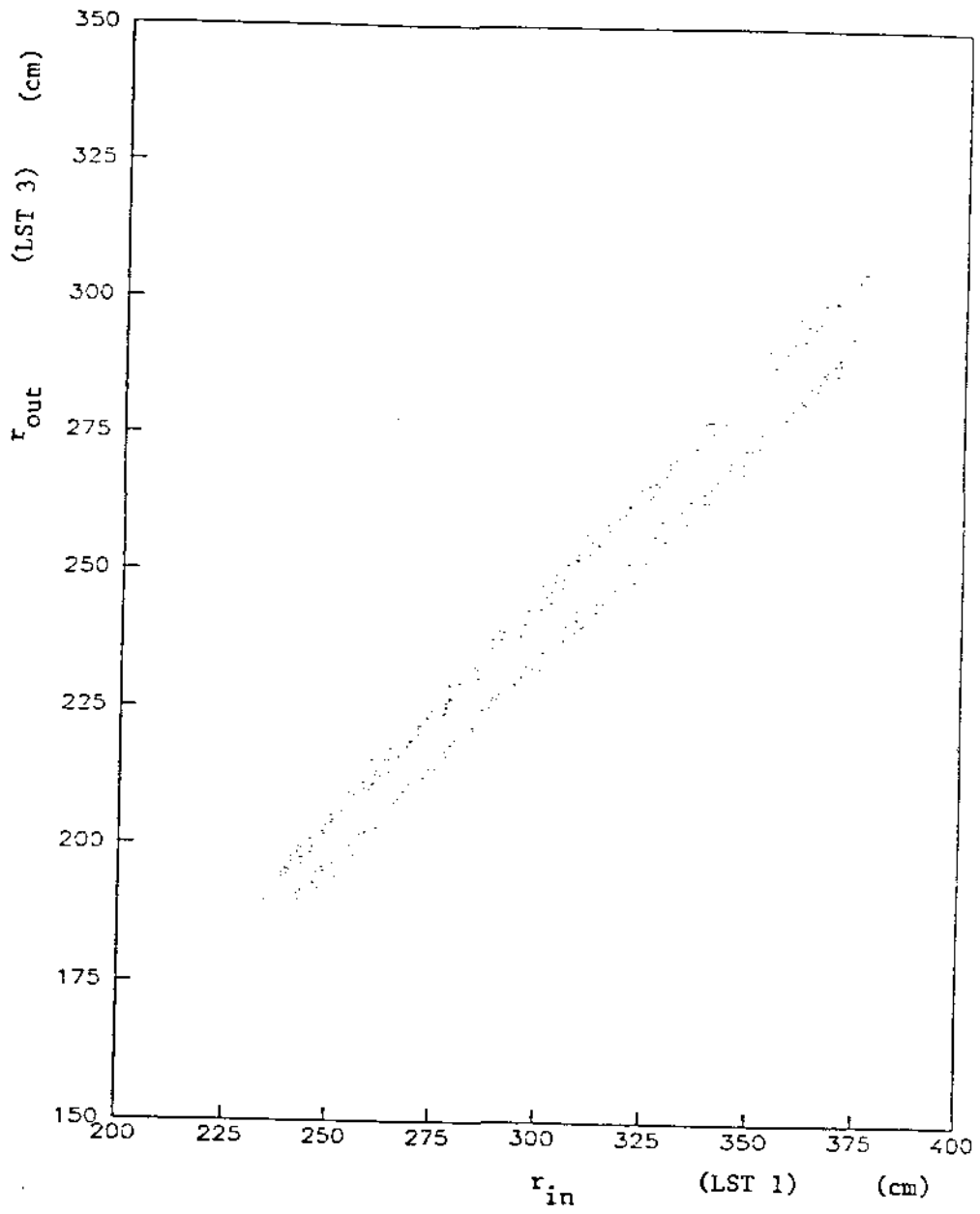


Fig. 3.14(b)

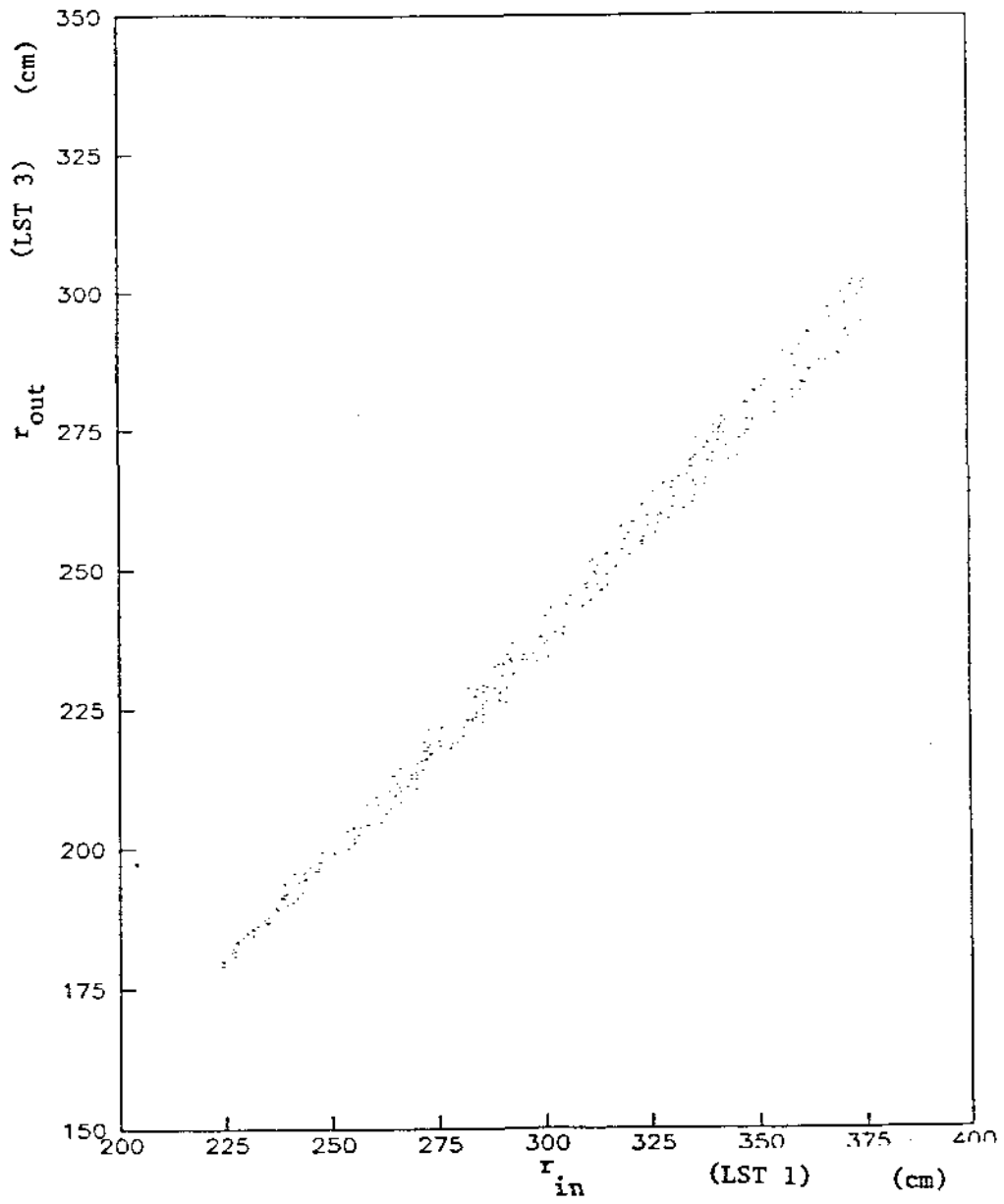


Fig. 3.14(c)

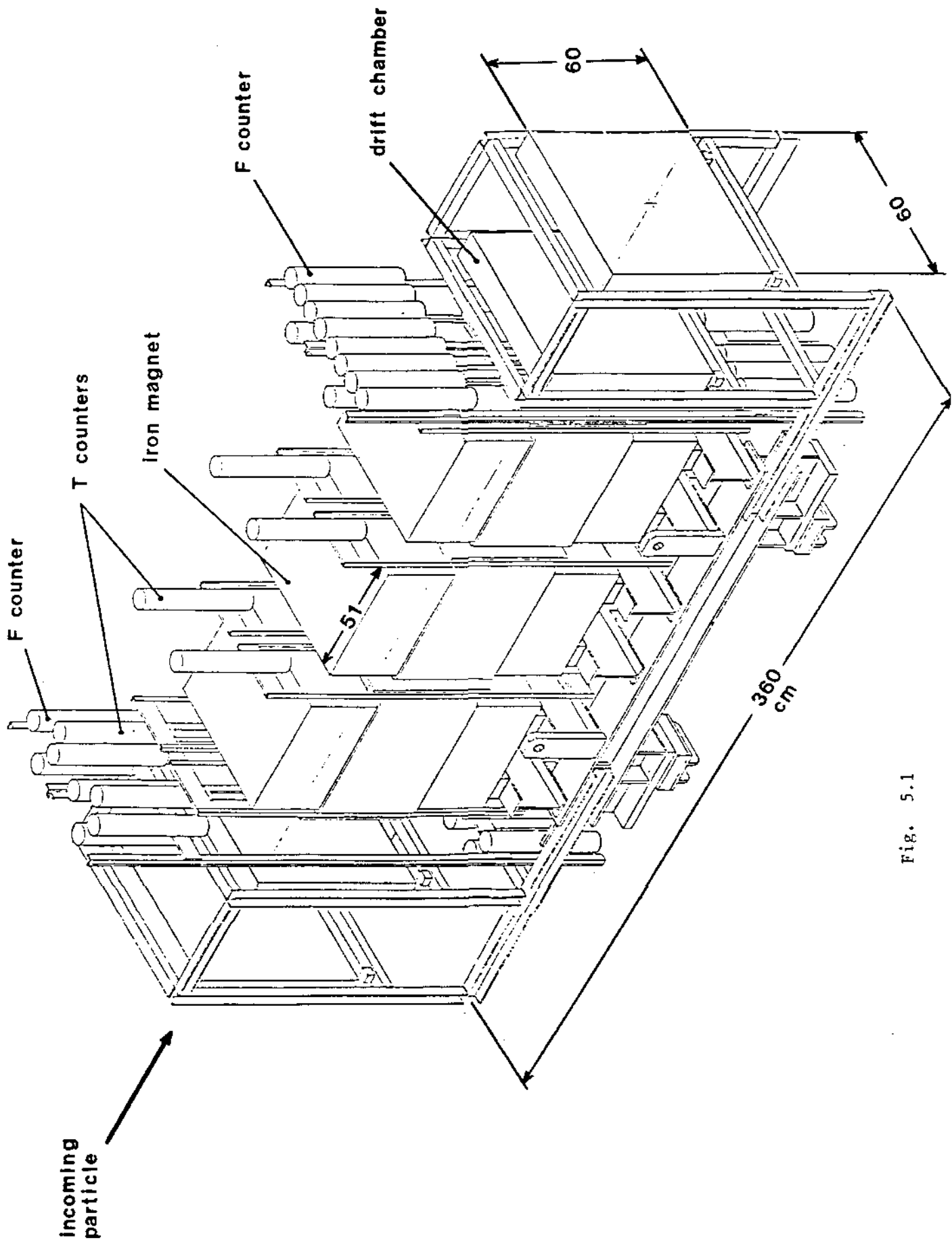


Fig. 5.1

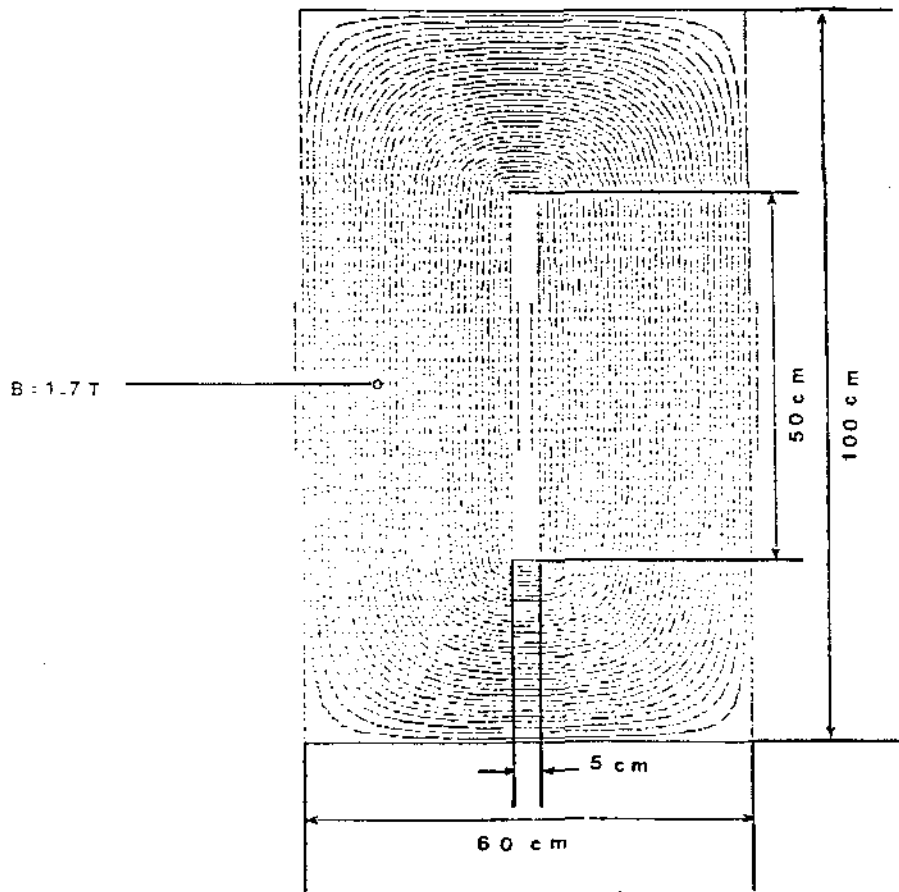


Fig. 5.2

OUTGOING
PROTON
BEAM

10 m.
from
interaction
point

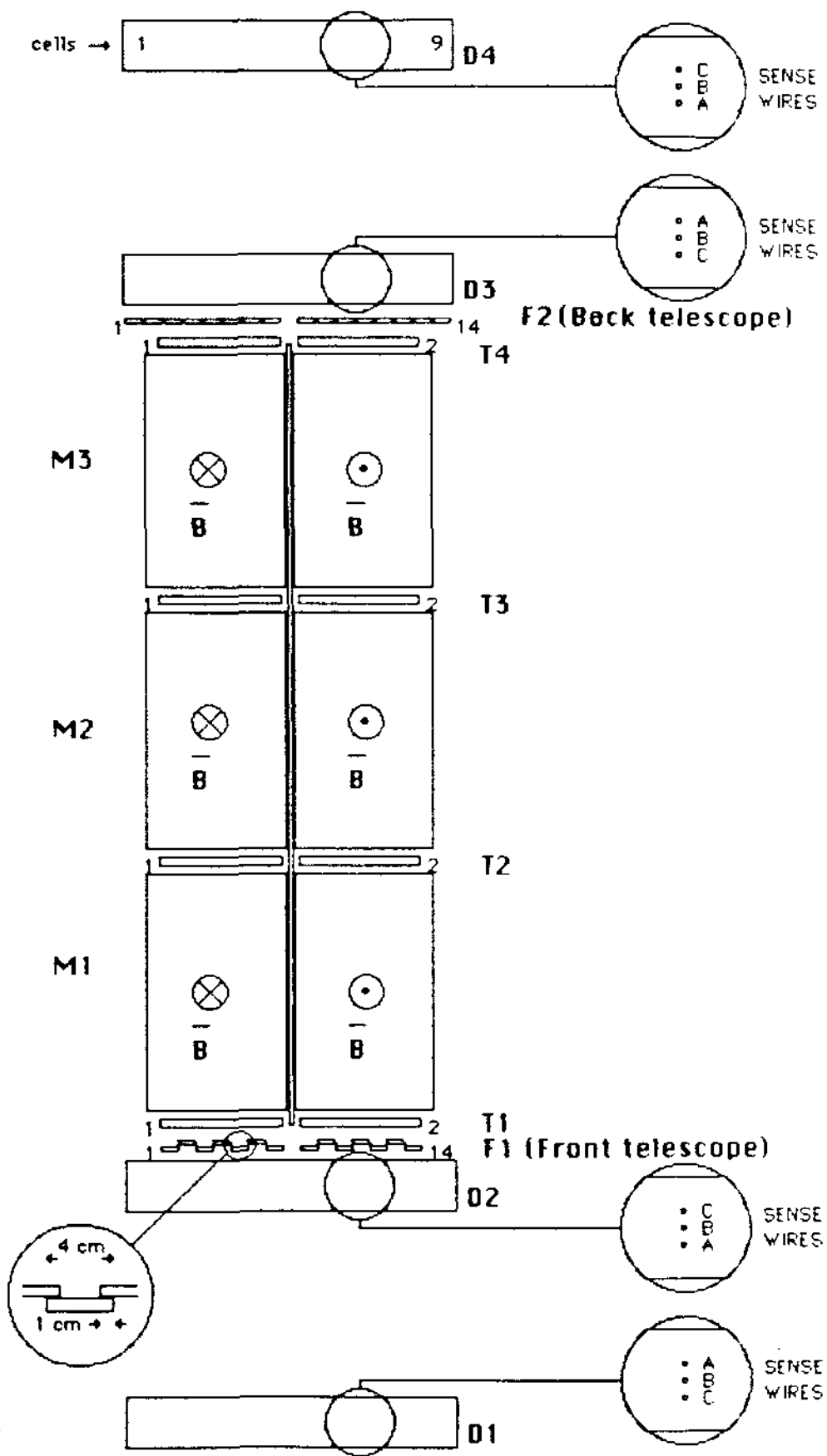


Fig. 5.3

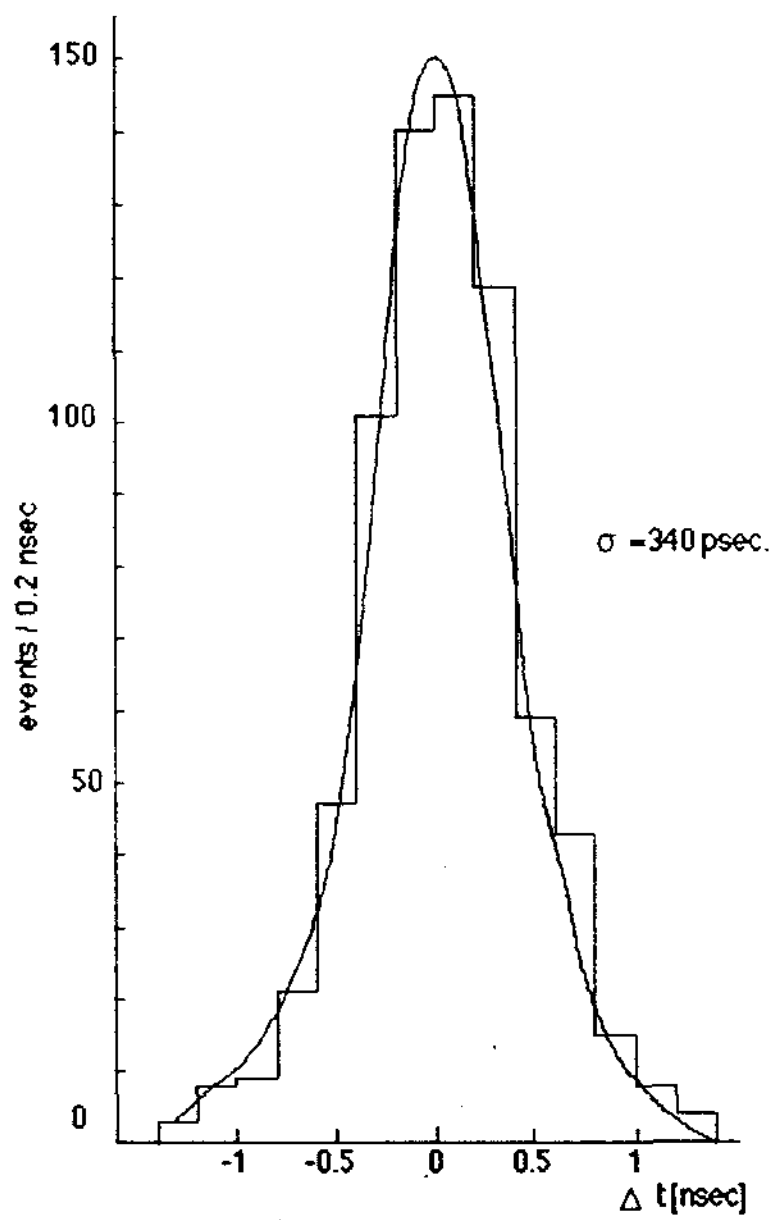


Fig. 5.4

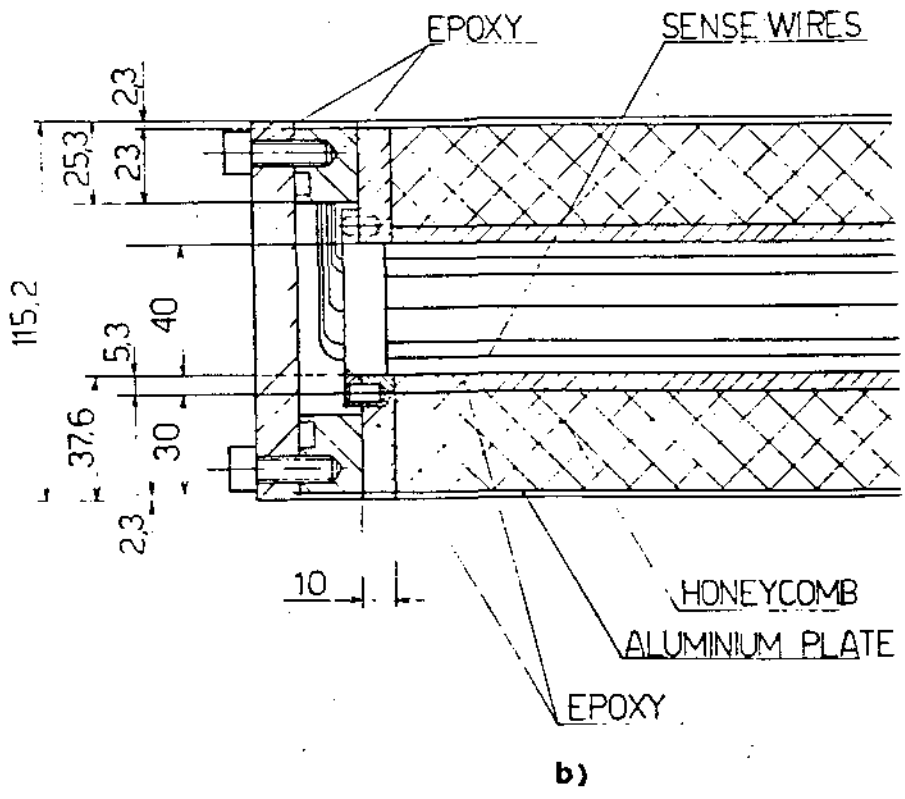
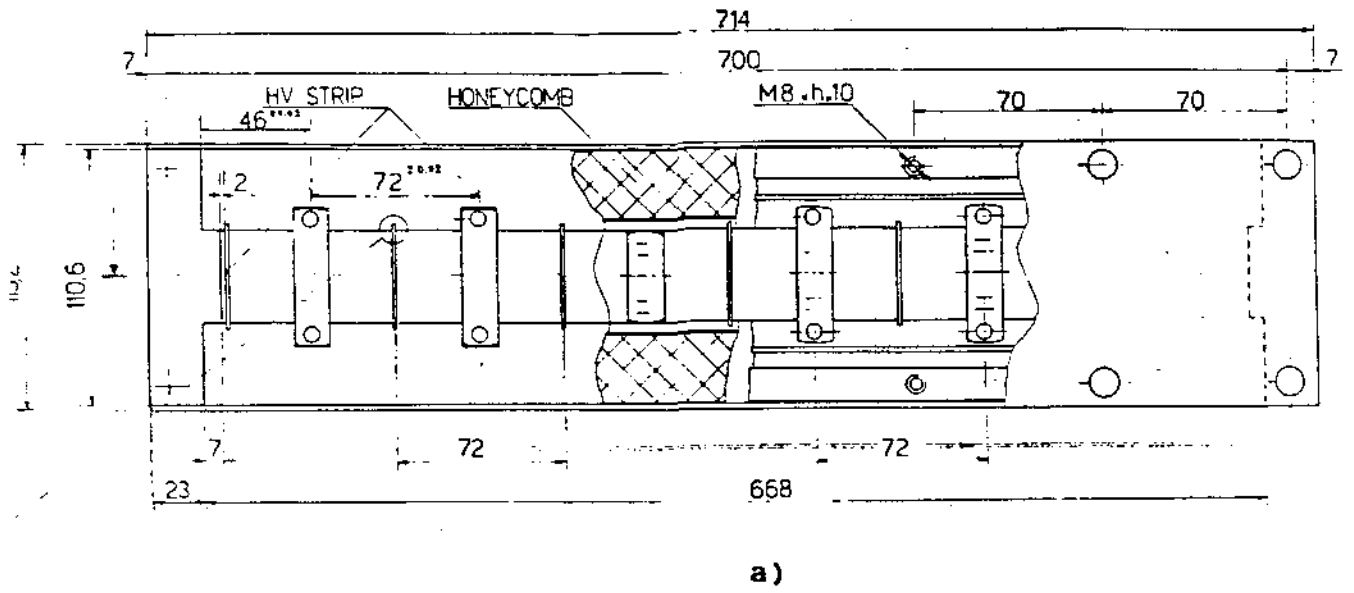


Fig. 5.5

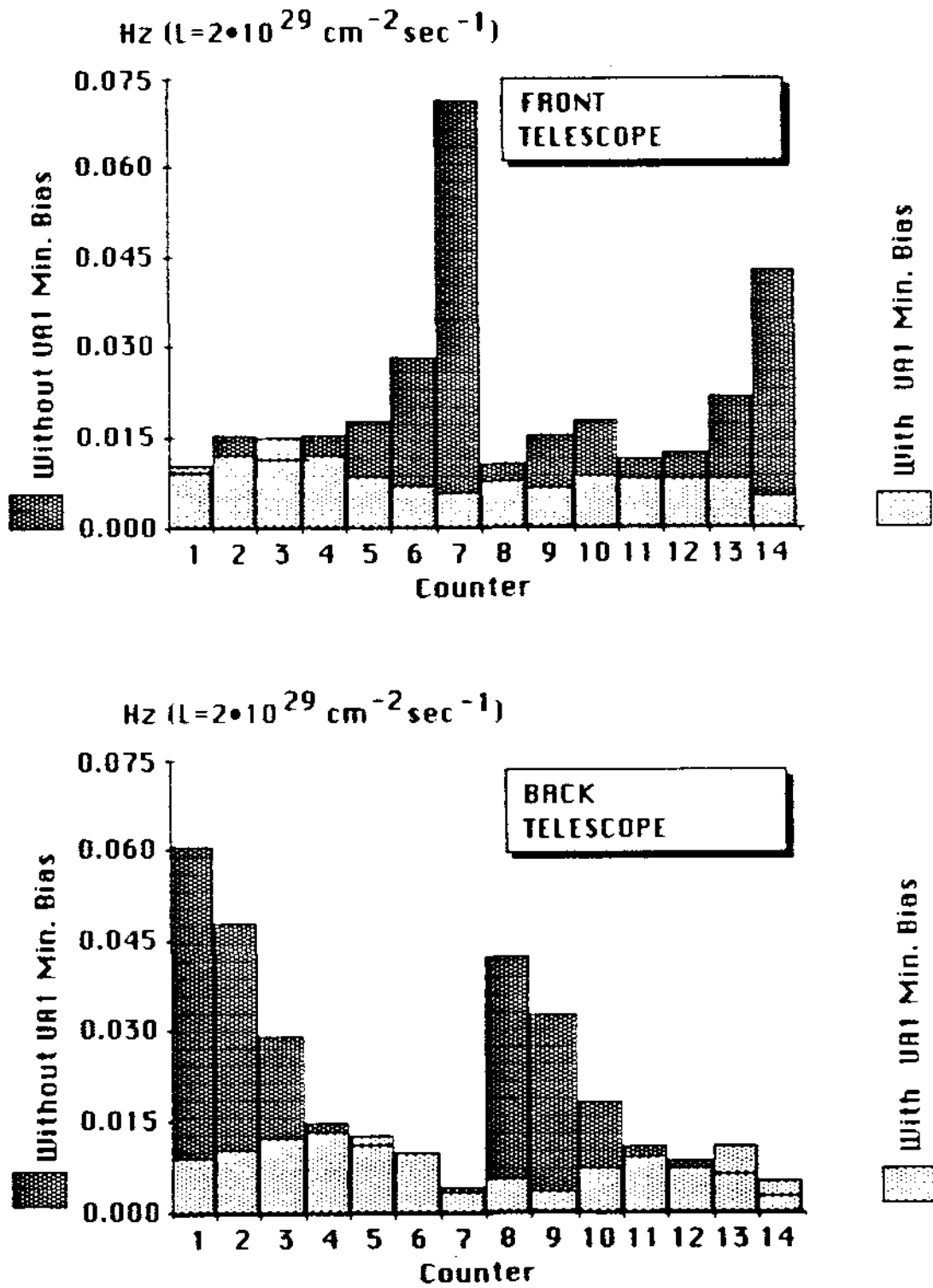


Fig. 5.6

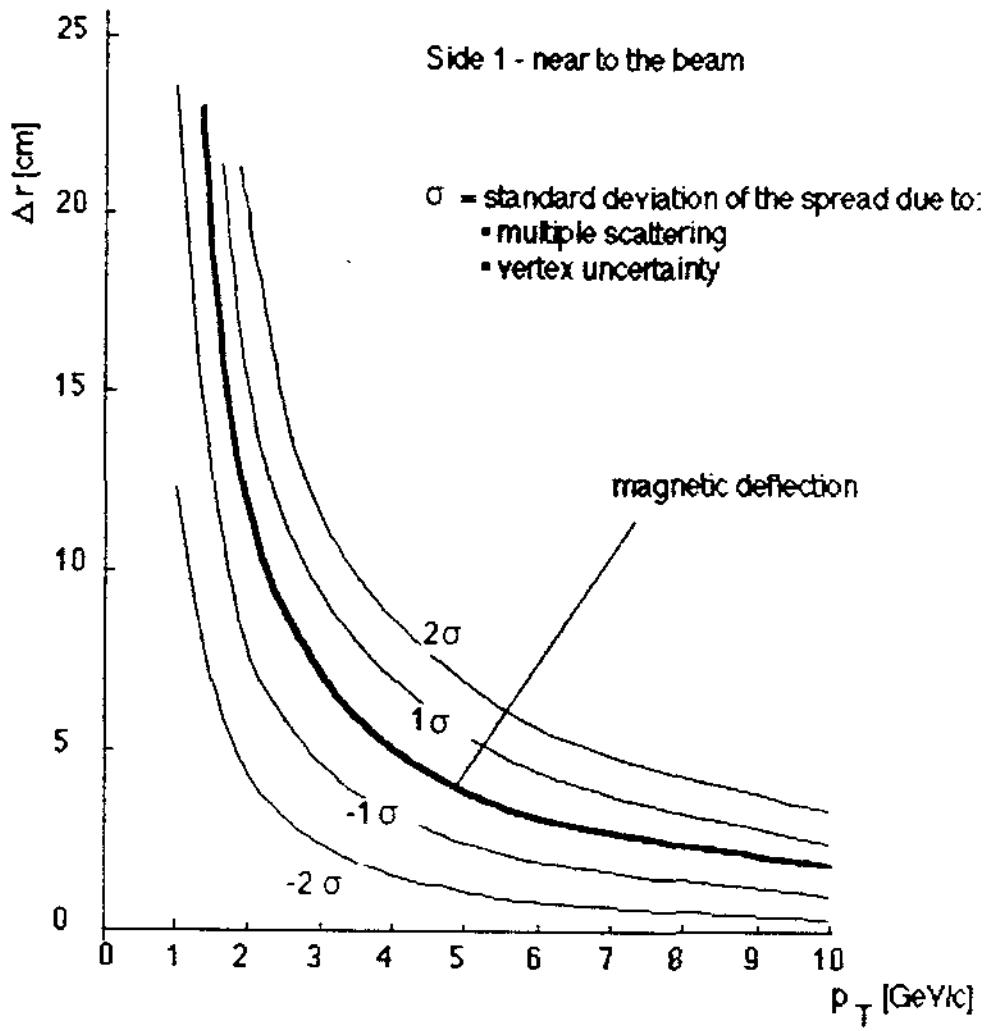


Fig. 5.7

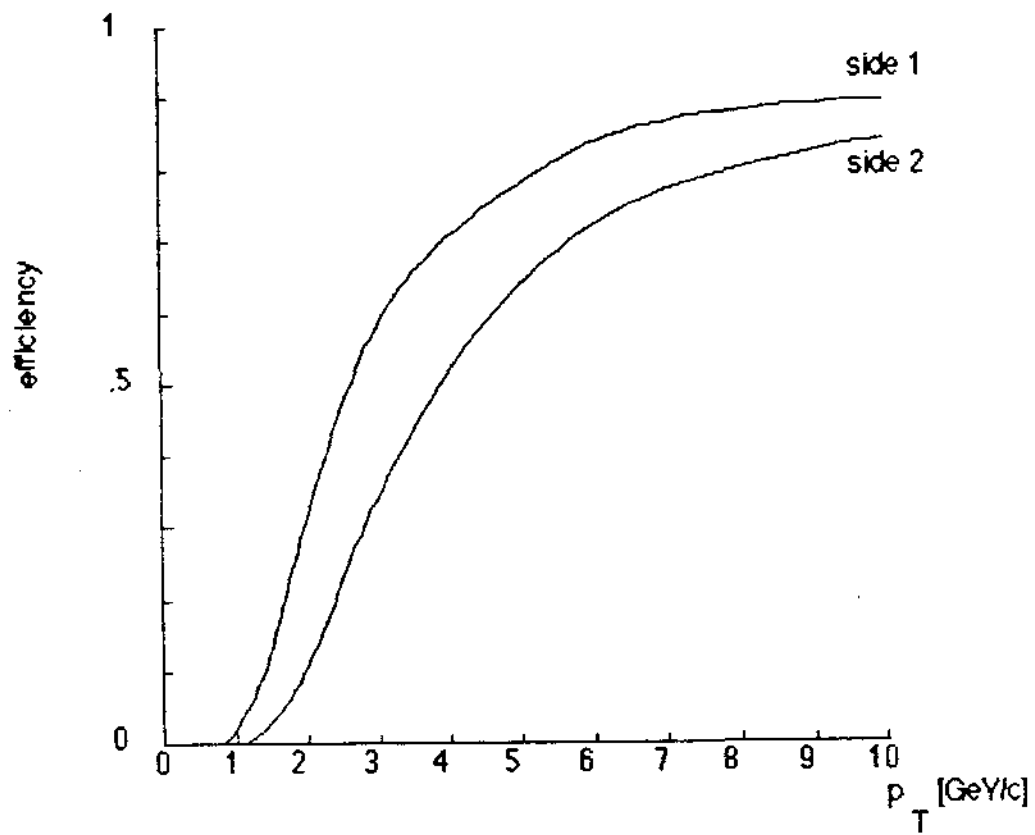


Fig. 5.8

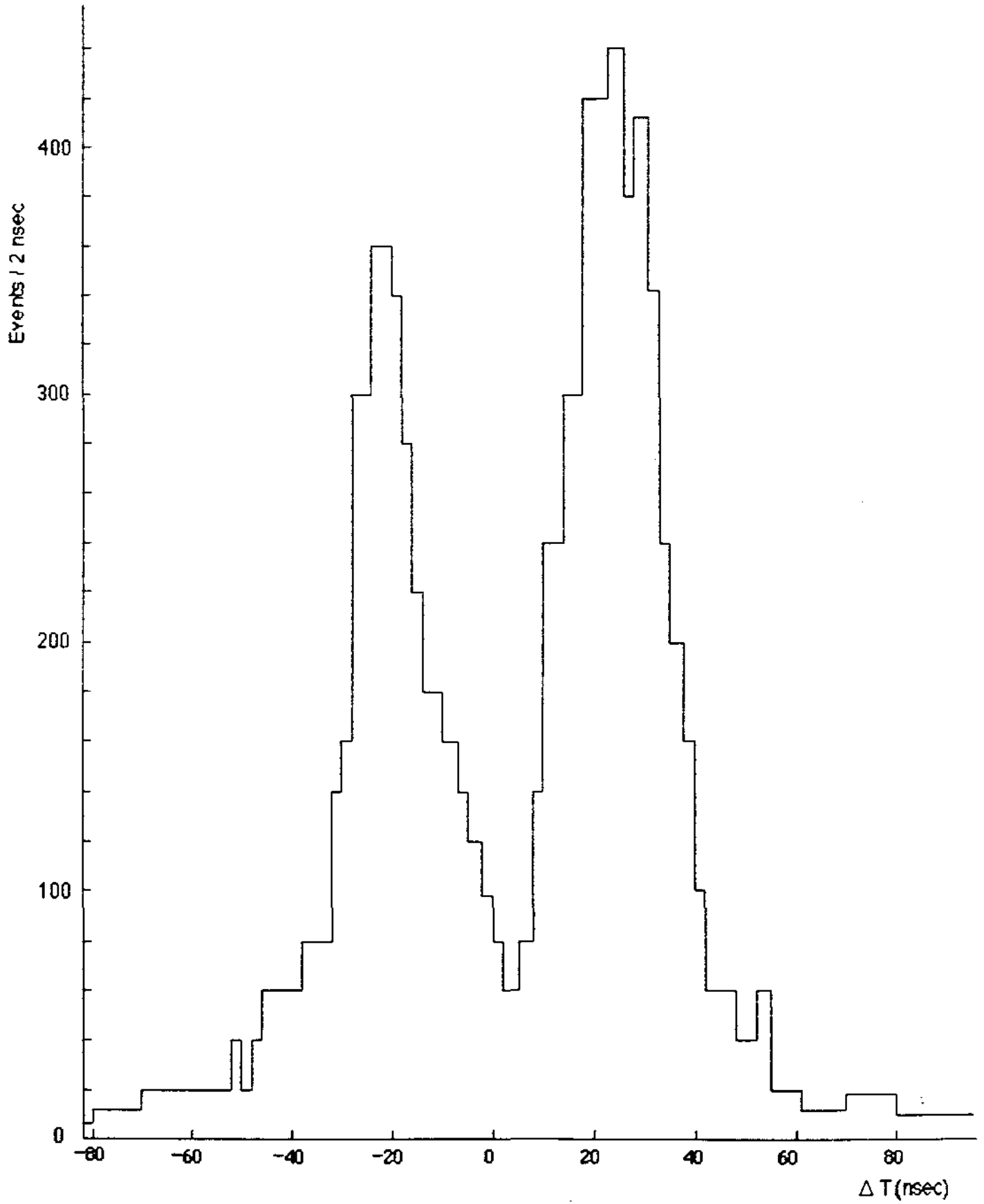


Fig. 5.9

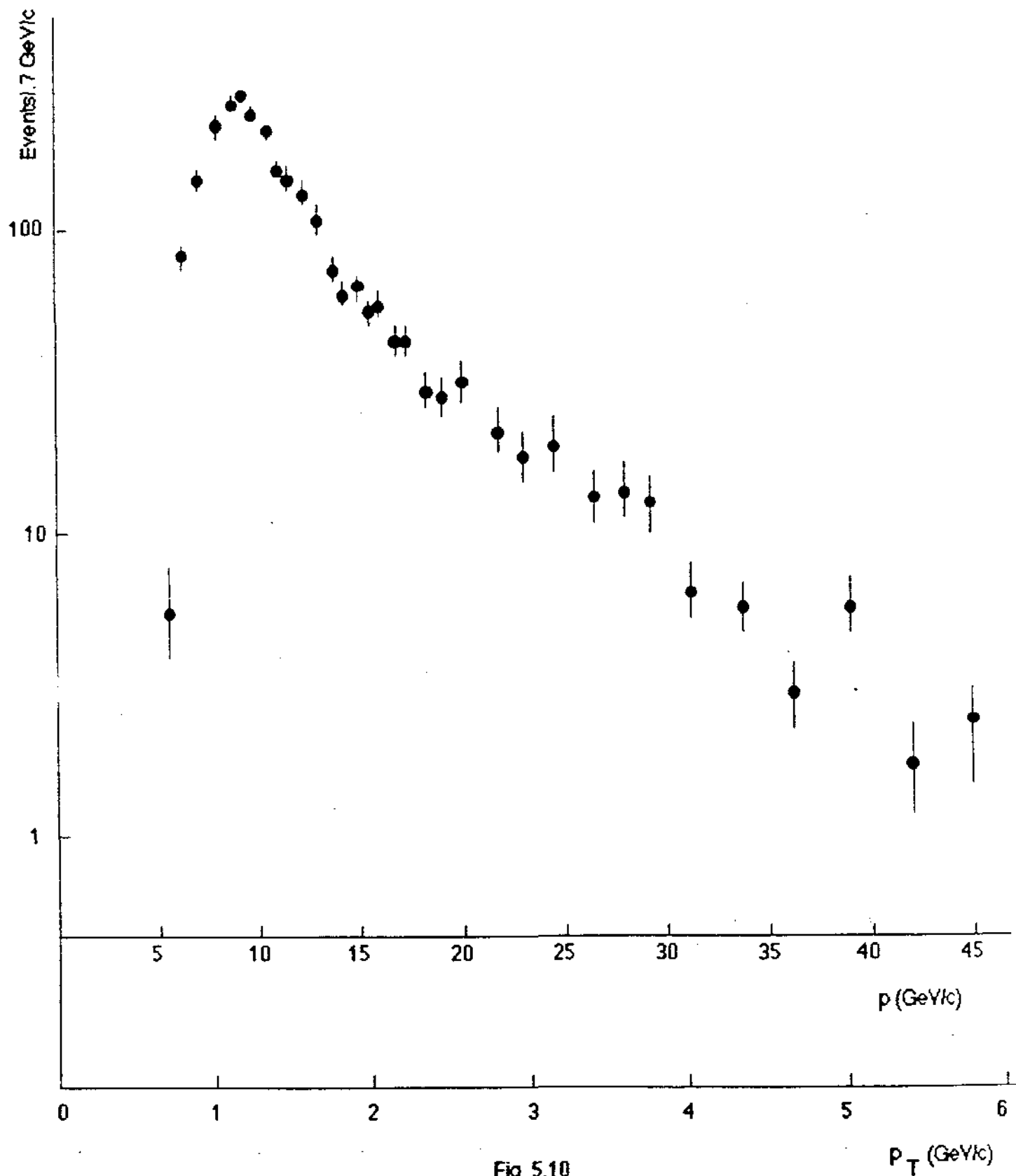


Fig. 5.10

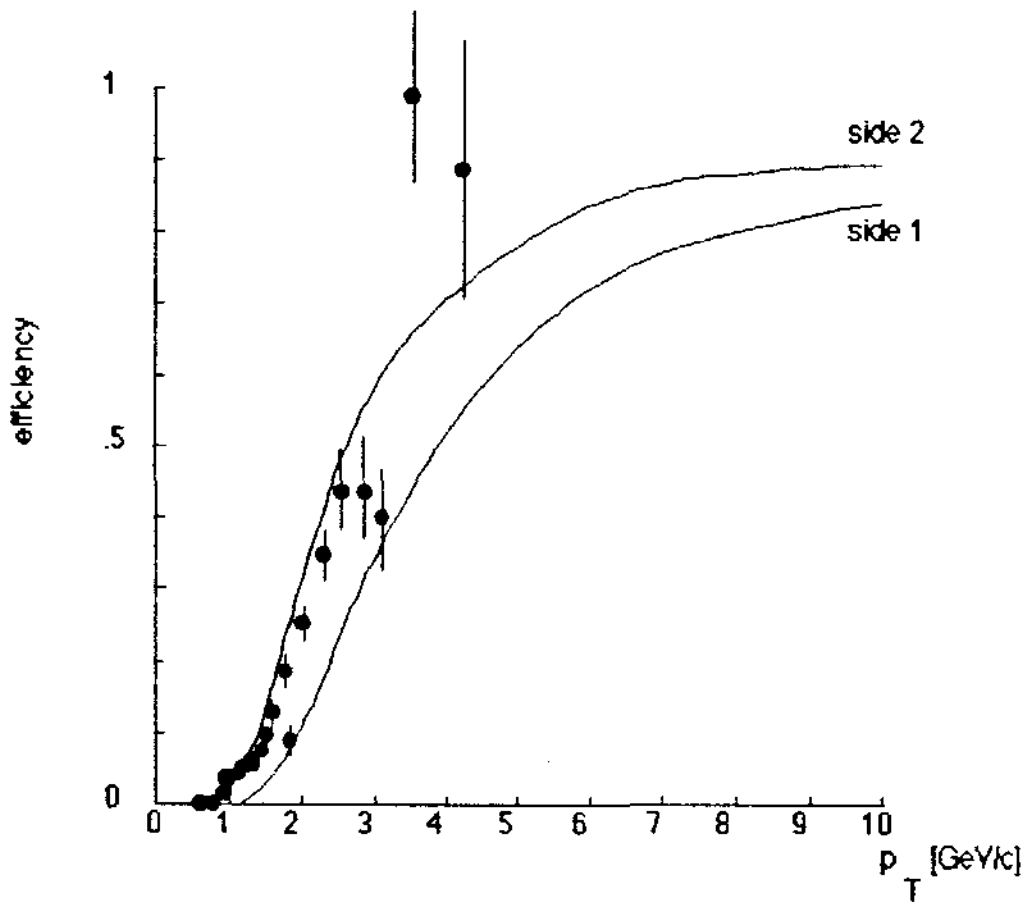


Fig. 5.11

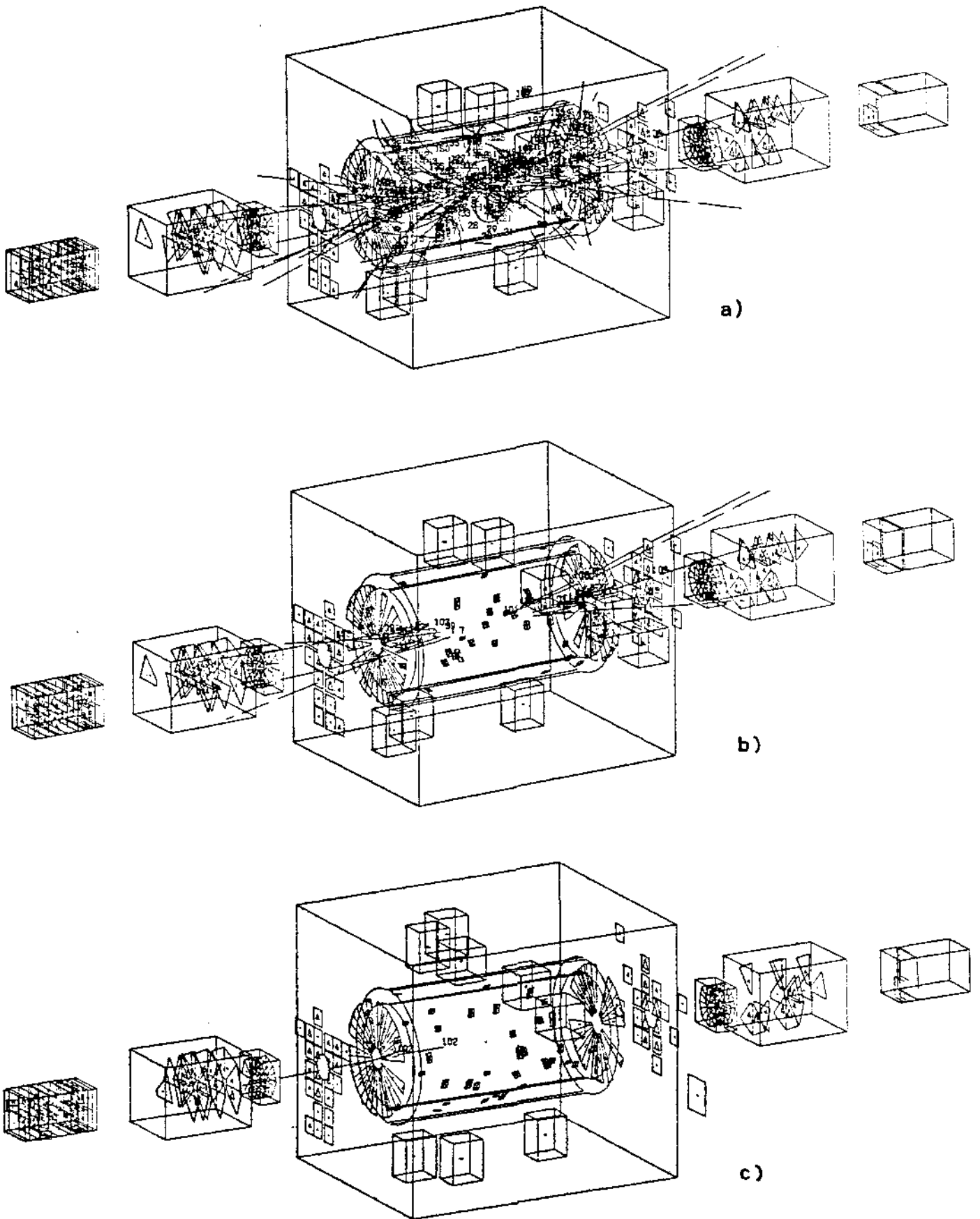


Fig. 5.12

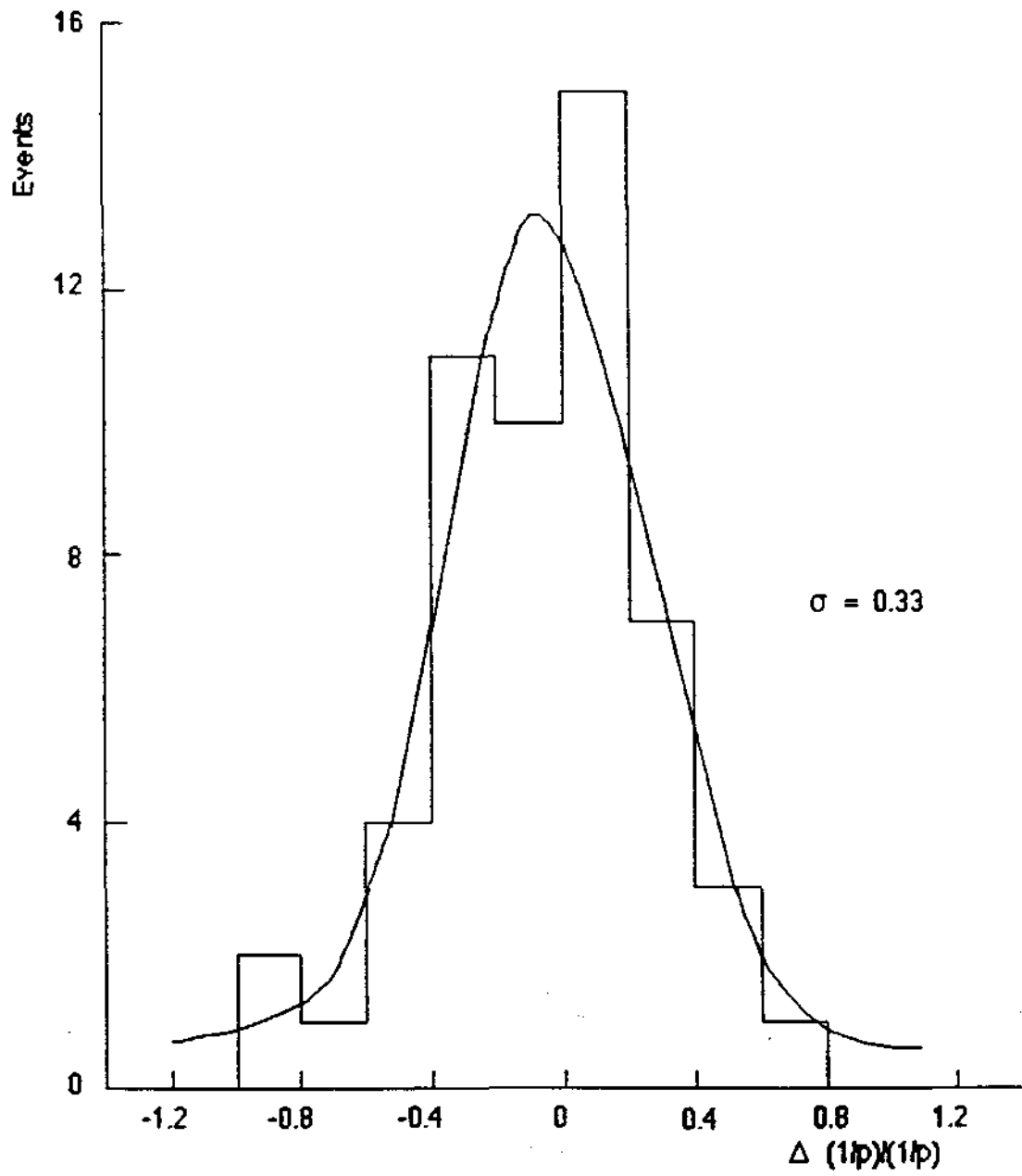


Fig. 5.13

**III-3. LAA Proposal: Memorandum to the Chairman
of the SPSC, September 4, 1984.**

September 4, 1984

3 - M E M O R A N D U M

To : L. Foa' - Chairman of the SPSC

From : A. Zichichi - BCFL Collaboration

Subject : LAA proposal (CERN/SPSC/84-33, SPSC/P200)

Copy to : R. Budde - Secretary of the SPSC

P. Bloch

M. Bourquin

P.L. Braccini

A. Donnachie

J. Drees

F. Dydak

P. Giromini

W. Hoogland

J. Iliopoulos

F. Jacquet

R. Klanner

I. Mannelli

G. Myatt

B. de Raad

A. Staude

G. Veneziano

1. ANSWER TO REFEREES' QUESTIONS

1.1 The Asymmetry with different starting hypotheses.

Following Mr. Donnachie requests, we have recomputed the lepton asymmetry starting from different hypotheses for the production and decay of heavy flavours.

Figures 1.1, 1.2 and 1.3 show the lepton asymmetry

$$A^{\text{exp}} = \frac{[N(\mu^+) + N_{\text{bg}}(\mu^+)] - [N(\mu^-) + N_{\text{bg}}(\mu^-)]}{[N(\mu^+) + N_{\text{bg}}(\mu^+)] + [N(\mu^-) + N_{\text{bg}}(\mu^-)]}$$

(where $N(\mu^+)$ and $N(\mu^-)$ are the number of positive and negative muons produced by heavy flavours, and $N_{\text{bg}}(\mu^\pm)$ is the number of background muons) for top ($m_t=25 \text{ GeV}/c^2$) and superbeauty ($m_{\text{sb}}=55 \text{ GeV}/c^2$) production, for top ($m_t=25 \text{ GeV}/c^2$) production, and for top ($m_t=35 \text{ GeV}/c^2$) production using the model outlined in the proposal which main characteristics are summarized below:

- 1a) production distributions: $d\sigma/dx = \text{const.}$ for baryons, $E(d\sigma/dx) \sim (1-x)^3$ for mesons;
- 1b) semileptonic decay: 3-body phase-space for baryons, K_{13} for mesons;
- 1c) cross-sections: $\sigma_t = 0.1 \text{ } \mu\text{b}$ ($m_t = 25 \text{ GeV}/c^2$), $\sigma_t = 0.05 \text{ } \mu\text{b}$ ($m_t = 35 \text{ GeV}/c^2$), $\sigma_{\text{sb}} = 0.01 \text{ } \mu\text{b}$ ($m_{\text{sb}} = 55 \text{ GeV}/c^2$);
- 1d) decay branching ratios: $\text{BR} = 0.1$ for all flavours;
- 1e) ratio between the baryon production cross-section and the total cross-section: $(\text{Leading}/\text{Total}) = 0.25$.

In order to take into account the effects which can produce a lower value for the asymmetry and a worse correlation between the asymmetry peaks and the mass of the heavy flavours, Mr. Donnachie asked us to recompute the asymmetry changing the following hypotheses:

- 2a) production distributions: $d\sigma/dx \sim (1-x)$ for baryons;

- 2b) semileptonic decay: mixture (50%,50%) of 3-body (as above) and 4-body phase-space for both mesons and baryons;
- 2e) ratio between baryon production cross-section and total cross-section: (Leading/Total)=0.1.

These hypotheses have been introduced one by one in the asymmetry shown in Fig. 1.1 (top and superbeauty production).

Figure 1.4 shows the effect of changing the baryon production distribution. The asymmetry at the top peak keeps unchanged because the decrease expected by the softer baryon distribution is compensated by an increase in the acceptance at low angles. The asymmetry at the superbeauty peak decreases due to the loss at high angles and to the softer baryon distribution (see, for reference, Fig. 9 of the proposal).

Figure 1.5 shows the effect of further assuming all semileptonic decays to be 4-body. The main effect is to lower the mean p_T of the μ 's in the heavy flavour decays. Nevertheless, the tails at high p_T values give rise to peaks in the asymmetry distribution whose positions are not very different from the ones obtained with the 3-body decay hypothesis. Most of the effect of assuming 4-body semi-leptonic decays for all particles is, therefore, to decrease the signal/background ratio, i.e. to decrease the μ cross-section at a fixed p_T .

Figure 1.6 shows the effect of mixing 3- and 4-body decays. The asymmetry is still very well measurable, and the correlation between peak positions and heavy flavour masses is practically unchanged.

Figure 1.7 shows the effect of lowering the (Leading/Total) ratio to 0.1. The asymmetry at the peak values decreases by about a factor 2.

The overall effect of changing the starting hypotheses from (1) to (2) on top production at $m_t=25 \text{ GeV}/c^2$ and $m_t=35 \text{ GeV}/c^2$ is shown in Figures 1.8 and 1.9.

Figures 1.10 to 1.13 shows the statistical significance of the asymmetry measurement ($A^{\text{exp}}/\Delta A^{\text{exp}}$) as function of the total cross-section and the ratio (Leading/Total). The asterisks indicate the statistical significance at the various peaks once a p_T integration in the limits specified is performed:

top and superbeauty production:

top peak : $p_T = 9-12$, $A^{\text{exp}}/\Delta A^{\text{exp}} \sim 5$

superbeauty peak : $p_T = 18-25$, $A^{\text{exp}}/\Delta A^{\text{exp}} \sim 1.5$

top ($m_t = 25 \text{ GeV}/c^2$) production:

top peak : $p_T = 11-14$, $A^{\text{exp}}/\Delta A^{\text{exp}} \sim 4.3$

top ($m_t = 35 \text{ GeV}/c^2$) production:

top peak : $p_T = 16-20$, $A^{\text{exp}}/\Delta A^{\text{exp}} \sim 5.8$

Two comments are in order.

By comparing Figs. 1.7, 1.8 and 1.9, it can be seen that the higher asymmetry peak value is associated to μ 's coming from a $35 \text{ GeV}/c^2$ top. These μ 's are in fact produced in a relatively background free p_T range ($p_T > 12 \text{ GeV}/c$). A reduction in the background also below this p_T value, achieved by requiring the presence of one or more jets and/or of a missing energy in the UA2 central detector, could improve very much the measurement of the lepton asymmetry in all the cases that have been presented here.

Even if the ratio (Leading/Total) is so small that no asymmetry can be measured, or the top and superbeauty masses are such as to produce a net zero asymmetry, the quantity of μ 's produced by heavy flavours is big enough to allow a very detailed study of their production at Collider energies. Figures 1.14a and b show the sum of positive and negative μ 's (a) and the signal/background ratio, in the case of top and superbeauty production with the most pessimistic hypotheses, as function of p_T . Figures 1.15a and b show the same quantities in the case of top ($m_t = 35 \text{ GeV}/c^2$) production.

We emphasize here the relevance of a powerful muon detector which allows the study of all physics where a lepton is produced.

1.2 Drell-Yan cross-section.

The Drell-Yan cross-section for producing a dilepton pair (e.g. $\mu^+\mu^-$) is given in the "naive" model by:

$$d\sigma/dm^2 dx = (4\pi\alpha^2/3M^4) \times F(\tau, x)$$

where

$$F(\tau, x) = [x_1 x_2 / (x^2 + 4\tau)^{1/2}] \times g(x_1, x_2)$$

with $\tau = m^2/s$, $x = x_1 + x_2$ ($m = e^+e^-$ invariant mass) and $g(x_1, x_2)$ is the quarks (flavor-matched) structure functions product:

$$g(x_1, x_2) = (1/3) \sum_{\text{flavours}} e_i^2 [q_1^i(x_1) \bar{q}_2^i(x_2) + \bar{q}_1^i(x_1) q_2^i(x_2)]$$

In order to calculate $d\sigma/dm^2 dx$ we must know the quark structure functions. We have used two parametrizations, one by Pakvasa et al. (1973) (PPT), which was also considered by Quigg (1977) and an average of the parametrizations of NA3 and CDHS (1979/80).

Most of σ^{DY} comes from small τ (small m) and, as we shall see, peaks at small θ and p_T .

In the "naive" model no k_t for the colliding quarks is assumed. When compared with data $d\sigma/dm^2$ has been found to be too small by a factor of ≈ 2 (K factor) and substantial k_t , dilepton transverse momentum, has been measured.

We have calculated $d\sigma/d\tau dx$ for (τ, x) bins (1000 X 100) and allowed the " γ " to decay into $\mu^+\mu^-$ pairs according to a transverse pol. $(1 + \cos^2\theta^*)$ dependence which should dominate, (θ^* - polar angle in " γ " rest frame). We have then Lorentz transformed each μ back to the c. m. frame (Lab. frame at collider) and binned the results in $\Delta p_T = 1$ GeV, $\Delta\theta = 1^\circ$ cells.

Imposing a cut of $5^\circ < \theta < 30^\circ$ we obtain the $d\sigma/dp_T$ curves for the muons shown in Fig. 1.16.

The σ^{DY} with cuts $5^\circ < \theta < 30^\circ$, $5 < p_T < 25$ GeV are:

$$\begin{aligned}\sigma_{cuts}^{DY}(\text{PPT}) &= 21.7 \text{ pb} \\ \sigma_{cuts}^{DY}(\text{NA3/CDHS}) &= 19.6 \text{ pb}\end{aligned}$$

In Fig. 1.17 we have added a hatched area which represents the effect of a $K=2.2$ (average of lower energy data) and applied it to the average of the PPT + NA3/CDHS. An error of 33% has been assumed (10% for K , 30% for structure functions, 10% for neglect of k_T).

Assuming $K=2.2$, we find for each hemisphere:

$$\sigma_{cuts}^{DY}(\bar{p}p \rightarrow \mu + X) = 45 \pm 15 \text{ pb}$$

With an integrated luminosity of 10 pb^{-1} this corresponds to about 450 muons per hemisphere with cuts.

In conclusion the contribution of muons coming from the Drell-Yan mechanism can be completely neglected in our background estimates.

1.3 The asymmetry in the background.

Up to now a measurement of positive to negative hadron ratios at the Collider does not exist.

To solve this problem we have asked to the UA1 Group all the available information. The UA1 Group has kindly given his collaboration in order to measure the h^+/h^- ratio, starting from their "minimum bias" data, as measured in the UA1 central detector.

The analysis is in progress and there is no doubt that in the experiment we will be able to subtract any contribution to the asymmetry coming from the background on firm experimental basis.

2. THE APPARATUS

Following our proposal, we present here the main results obtained by a detailed investigation of the basic parameters and features of the proposed set-up.

These studies have been done in collaboration with the following specialists in the various fields of interest:

- G. Petrucci (EP), who has given us all the figures for the magnets;
- G. Muratori(EP), who has kindly agreed to discuss the project and has suggested, in particular, the method of mounting the wires;
- W. Albrecht, who has promptly placed at our disposal the services of
- D. Geiss, whose hard work and enthusiasm have rendered the completion of this design in such a short time, possible;
- H. Mauch of Stasalit AG, whose advice and hospitality is gratefully acknowledged;
- H. Rigoni and K Ley, who gave us their advices on the gas distribution;
- G. Dubail (SPS), who did the drawing of the layout;
- M. Genet (SPS), with whom we discussed many details, in particular on the vacuum chamber;
- B. T'Hart and S. Bastin, who helped us on the safety aspects of the chambers.

The goal was to reduce as much as possible the cost of the apparatus with the minimum loss in the basic features of the proposed measurement:

- i) the rejection power against background;
- ii) the high efficiency for μ detection;
- iii) the momentum analysis.

The results are presented in the enclosed technical drawings, briefly illustrated in the text.

2.1 Wire chambers.

We will give here a working design of the chambers, taking into account the known boundary conditions. These are:

1. Large dimensions. It is impossible to build an 8x8 m² chamber. Evidently we will have to have various smaller chamber to cover the surface of the magnet or absorber, trying to keep the dead space at a minimum.
2. Good spatial resolution. This implies, among other things, stability of the mechanical construction. Nothing should move, sag or change shape.
3. The chambers must be thin: space in the intersection is at a premium. Since the proposed drift cell (see proposal) is 4-cm thick we should strive to make the cell thickness not much bigger than 10 cm. this point makes us exclude the possibility of using tubes a la UA1.

Point 2 (rigidity) immediately brings to mind the excellent results obtained with the hexcell used in the R422 calorimeter. If we use sheets of hexcell we will also build light chambers: so much the better for the handling, supports, etc....

Starting with two 3-cm thick honeycomb sheets parallel to each other, we have immagined an I-shaped structure, whose vertical members are Al plates (2-mm thick). In fact the obvious thing to do is to create the drift cell partition with these Al plates. The structure is now doubly solid: because of the use of hexcell and because of these vertical plates, at the same time the drift cell is defined and the electrical drift field is more uniform than it could be obtained with wires. On the negative side of course we will have a 3% dead space. To complete the chambers, we will put two external longitudinal members also in Al (insulated from the last cell-defining plate which is at high voltage). Purpose of these side member is to solidly close the chambers and provide anchorage points. We think that a groove running the whole length of the side can be used to locate and fasten the chambers to one another or to a perimetral supporting frame.

The outer surface of the hexcell will have to be clad in sheets of Al, to form a complete Faraday cage to prevent pick-up noise and atmospheric humidity from entering the chamber. Should this ground plane distort the electric field inside the cell we can redress the E-field lines with equipotentials created by printed lines on Kapton foil glued on the bottom and top of the cell.

To complete the chamber we will need: two lids, holding the electrical connections and the amplifiers, plastic pillars to hold the wires in the middle of the cells, gas connections. All the ancillary components must be placed inside the top of the chamber, since we need all the sides of the chambers free of encumbrances, to place them side by side (to form a plane of wire x or y) and back to back (to have both x and y coordinates).

2.2 Construction.

Let's now look at the enclosed drawing (no. 1). Two parallel plates of hexcell have a first skin of .3 mm thick plastic material. On the inner side a 5-mm thick layer of epoxy is laid on the plate and grooves are machined in it to lodge the vertical Al plates (glued in position). On the outer side a 2-mm thick metal sheet extends to make electrical contact with the external longitudinal members also glued in position. The chamber box is now completed.

We now have to insert the wire plane. The method is the following (See second drawing). Two injected plastic pillars will be fastened to a long Al bar using two screws. The wire holding pins are inserted in the holes, and the wires threaded through. The bar is now inserted horizontally in the cell and turned vertically. Next the two pillars are screwed on the front of the honeycomb (appropriately finished with epoxy). The Al bar can now be freed and withdrawn.

Some details are in order. The pins used are commercially available. They are fabricated by Minitubes in Grenoble. The wires once threaded through the pin can be crimped. Crimping is the only way to go since stainless steel wires

cannot be soldered. See Fig. 2.1 for details of the pins. The crimping tool is a bit more problematic since it is not commercially available. It has, however been built according to a CERN design at a cost of about 1500 SF. We foresee to glue a small printed board to the back of the rear pillar to connect all the field wires together and create a unique point of contact on the high voltage bus bar (see below). The two (front and rear) lids are of a similar construction, a flat plate of fiberglass, with a cavity on the inside for the electrical contacts. Construction will probably be made glueing a frame on a plate to create the cavity, rather than by the more expensive method of machining material out of a flat bar.

Inside the rear lid (see the drawing), two SHV connectors bring the HV's to the Al plates and to the field wires via two separate bus bars running along the upper and lower lips of the cavity. Flat springs ensure a good contact on the plates and the field wires. Evidently with this type of construction, it will suffice to screw the lid on to get all HV's contacts made without having to insert hundreds of little connectors. Furthermore, the pins, once the wire has been crimped, can be clad in shrink tube to prevent discharges between sense and field wires. The signals will be brought to the preamplifiers using wires and small feed throughs to the the printed board holding the hybrid preamplifiers (see later) and carrying the low voltage supply. The amplified signals will be carried out of the chamber by flat cables exiting through slots in the side members of the chamber. For gas tightness we hope to rely on flat gaskets rather than O-rings for reasons of cost (no grooves to machine). Mr. T'Hart, responsible for the safety, deems that this may be adequate. The prototype will be, therefore, built using a flat gasket.

To complete the chambers we only have to discuss the gas system. According to both Rigoni and K. Ley, the only way to avoid an external manifold, which would take too much space, is to feed the gas serially to the cells. A piece of fiberglass will cross the cell on one side, forcing the gas to move through each cell serially. The input and outputs will be connected on the sides where small spaces are left between adjacent chambers for cables gas, etc...

2.3 The electronics.

We believe that the most inexpensive and reliable solution will be to purchase amplifier/comparators MVL100 from Lecroy. Their ECL output can be used directly with a TDC. Preliminary tests of these devices have been done in Bologna by our technicians (Mr. Volta and Ing. Montanari).

Finally we would like to add that some of us have been in contact with A. Fucci of DD (with the blessing of DD Leader Zanella) to arrive to a digital TDC design. Although this design will have points in common with the Delphi one, original features make it worth studying in detail. We will be reporting on this point at a later time. It appears that the cost of such a TDC will be around 50 SF/channel.

2.4 Number and Dimensions of chambers.

It would have been preferable to have a unique size for all the chambers. This turns out to be impossible. However we don't think that this is a major problem. In drawings 3/4 we have designed the cross sections of magnets and absorber at the points where the chambers will be located, with the contours of the chambers on them. We have then tried to keep the length at the maximum value of 2.7 m value and played with the width to get the best overlap. We have finally come up with the following figures:

NO.	SIZE(mm ³)	VOL. (m ³)	CELLS
16	1080x1800X40	1.24	224
8	1440x1080X40	.5	152
8	1440x1440X40	.66	152
16	1440x2160X40	2.	304
16	720x2808X40	1.3	144
8	1440x2880X80	2.68	304

16	1440x2808X40	2.6	304
8	1440x2088X40	0.96	152
48	1440x2400X80	13.3	1824
--		----	----
144		25	3560

HV cables = 288;

Sense wires, Amplifiers, TDC's, signal cables = 10680.

It should be remembered that two sets of chambers at 90 degrees relative to each other are necessary to have 300 micron precision on both coordinates. To have the disposition of the horizontal chambers, it will be enough to turn the drawings by 90 degrees.

One last point. Each cell is 72 mm wide. Dividing the width of the chamber (typically 1440 mm) by 72, we get the number of cells n that would fit. However 1 cell width is used for the side supports: we then have $n-1$ cells only. The typical dead space generated is therefore 5%.

2.5 Conclusions on the chambers.

We believe we have a chamber design that, although improveable, is realistic, sturdy and not too expensive. In order to debug it, we now must build a prototype with life-size wire length. One or two cell width will probably do. We must test it in a beam and make use of the lessons learned to finalize the design. In parallel we will have to study the points of electronics mentioned above.

For the purpose of discussion we would like to reckon the overall width of the chambers. The thickness of each chamber is 11.5 cm. The total thickness of DC1,DC2,DC3 is therefore 69 cm. DC4 is double therefore it would be 46 cm,

however we can save 12 cm by making two chambers with 6 wires instead of four chambers with 3 sense wires. This way 4 layers of honeycomb are saved together with 12 cm. In conclusion the total thickness assumed in the forthcoming discussion, will be:103 cm.

One last point about the fabrication of the chambers. The chambers can be completely built industrially, with the exception of the the wire stretching. This will be done by our BCFL technicians. The industrial feasibility of the chambers has been guaranteed by Mr. Mauch (Stesalit AG). We are also in contact with another company (Aviometal, Varese, Italy) to whom we have sent our drawings for cost and feasibility estimates. With the mechanics and electronics built industrially, the task of our technicians will be reduced to an acceptable size.

2.6 Chamber support.

The chamber supports are in fact, the Al members on the sides of the structure. The shape and size of these members is only indicative. We will use any Al extruded profile that will do the job. Notice that the size of the profile is such that 2 cm of space will be left for the passage of wires and gas lines as indicated before. We plan very simply, to join the chambers with long metal bars running through the grooves on the sides of the chambers. Threaded rods, driven in the Al members will fasten the chambers to the bars and therefore to each other. The bars will then be bolted to an outer square, sturdy frame. The two frames holding vertical and horizontal chambers will be bolted to each other, in particular at the points where horizontal and vertical bars overlap (see drawing 5).

2.7 Space and general layout.

As already pointed out, we are hard pressed for space, especially along the beam axis.

The overall length available is 7.4 m. UA2 has requested 30 cm more for its calorimeter. In addition it requests to be able to slide the calorimeter by 40 cm back, to service its preshower chambers. In conclusion with the calorimeter all the way back, our apparatus will start at 4.1 m from the intersection center. This leaves us 3.3 m of space available. The chambers will take, as calculated before, 1.03 m, the Fe absorber .6 m, the magnet 1.5 m (disregarding the width of the coils estimated at 1 or 2 cm). In total 3.13 m, leaving 17 cm for the planes of Limited Streamer Tubes (LST). We propose therefore, to eliminate three of the inner planes, leaving only the two outer ones and an inner one, used for the trigger. Since each plane of tubes is 2 cm thick, including the strip, we will fit in. The disposition of chambers, LST, magnet and absorber with the UA2 calorimeter back is shown in drawing 6.

The magnet iron is laminated in slabs of weight less than 80 tons. Each slab is then cut into two halves (less than 40 tons). Three special slabs will be thinner (about two cm) and precision machined to be used as support of the strips. Briefly the operation of assembling the magnet chamber system will consist of the the following phases:

1. Assembling the strips on the special slabs of Fe.
2. Assembling the lower half slabs on their support leaving the gaps for the LST.
3. Sliding the magnet coils in.
4. Assembling the upper half slabs.
5. Sliding the tubes in, perhaps vertically.
6. Assembling the drift chambers on the faces of the magnet.

In the vertical position the tubes can be supported by small squares as in the R422 calorimeters.

One more remark. With the UA2 calorimeter all the way back, the iron of the absorber will protrude about 13 cm out of the platform (without the present wings that must be eliminated or will interfere with the magnet). We deem necessary to add two winglets to the platform for obvious safety reasons. Of course the winglets will be bolted to the existing flanges.

Finally, we should point out one problem with the vacuum chamber. Since the vacuum chamber will have to be opened to move the UA2 platform out of the intersection region, heavy valves are needed at the breaking point. They must be supported. The supports will have to be fastened to the inner hole of the magnet. However a temporary support will be needed when UA2 must move. We cannot accept a permanent support at the edge of the platform, otherwise this will be in our way if the calorimeter-absorber complex moves back. Mr Genet is looking for the best solution to this problem.

2.8 Magnets supports.

Magnets' supports including air cushions, and mechanical paraphernalia associated with their movements in and out of the intersection region, are under the direct supervision of the SPS Division. Their design will be started by the appropriate bureau as soon as the experiment will be approved. For the time being, Mr Dubail and collaborators have made a provisional study of feasibility, drawing our apparatus inside the intersection region Hall and the "Garage" (drawing 7). No major problem has arisen, but some change in the "passarelle" will be needed. The air system used for UA2 is not sufficient to lift our magnets and will have to be beefed up. A tentative budget has been given by Mr. Dubail (Fig. 2.2). It refers only to the support system for the magnets. It is very likely that, with the weight of the new calorimeters and our iron absorber, changes to the charriots and/or to the present platform will be needed. These extra expenses are not taken into account. However it is reasonable to expect that a fraction of these expenses will be supported by UA2.

2.9 General Conclusion.

If approved, We would like to proceed as follow. Continue the design of the magnet and its parts under the direction of G. Petrucci and the help of Mr. Geiss (if Mr. Albrecht agrees). This phase will probably take two months. In parallel the SPS division could design the supports of the magnets and charriots.

At the same time we would like to build a prototype of the chamber and related electronics, to finalize the design even in contact with our eventual industrial partners, whose expertise should help. Test beams will tell us if our design is sensible.

A different configuration of chambers, capable of measuring only the polar coordinate of the particle has been recently suggested. We are studying with a MonteCarlo that it is indeed possible to measure the particle momentum this way. If so, we would be able to reduce the number of planes of the chambers by a factor of two with a consequent saving in money and space (about 50 much needed cm along the beam).

2.10 Update of cost estimates.

NEW ESTIMATES OF THE COSTS

Magnet	3000	KSF
Magnet charriot	695	
Absorber and charriots	100	

Tot	3795	
Drift Chambers		
Construction	1000	
HV Power supplies	100	
Amplifiers (MVL100)	220	
TDC's	550	
Cables	100	
Mechanical supports	50	

Tot	2020	
LST's		
Construction	100	
Pads	120	
Power supplies	10	
Head electronics	340	
Trigger	250	
Cables	100	

Tot	920	
Overall total	7135	KSF

Figure captions.

Fig. 1.1 : a) Expected number of produced μ^+ (black points) and μ^- (white points), as a function of p_T and for an integrated luminosity of 10 pb^{-1} , with the conditions set in the text and for $m_t=25 \text{ GeV}/c^2$ and $m_{sb}=55 \text{ GeV}/c^2$. A smearing in p_T due to the estimated momentum resolution $\Delta p_T/p_T=20\%$ is considered. The estimated background for each charge sign is indicated by the full line. The errors are purely statistic.
b) The expected asymmetry A^{exp} as a function of p_T .

Fig. 1.2 : Same as Fig. 1.1 for a top mass $m_t=25 \text{ GeV}/c^2$ and no superbeauty.

Fig. 1.3 : Same as Fig. 1.1 for a top mass $m_t=35 \text{ GeV}/c^2$ and no superbeauty.

Fig. 1.4 : Same as Fig. 1.1 but with a baryon distribution $d\sigma/dx \sim (1-x)$.

Fig. 1.5 : Same as Fig. 1.4 but assuming all semi-leptonic decays to be 4-body phase-space.

Fig. 1.6 : Same as Fig. 1.4 but assuming a (50%,50%) mixing of 3- and 4-body for the semileptonic decays.

Fig. 1.7 : Same as Fig. 1.6 but assuming (Leading/Total)=0.1.

Fig. 1.8 : Same as Fig. 1.7 for a top mass $m_t=25 \text{ GeV}/c^2$ and no superbeauty.

Fig. 1.9 : Same as Fig. 1.7 for a top mass $m_t=35 \text{ GeV}/c^2$ and no superbeauty.

Fig. 1.10 : Statistical significance of the asymmetry measurement, $A^{\text{exp}}/\Delta A^{\text{exp}}$, as function of the total cross section and of the (Leading/Total)

ratio for the top asymmetry peak in the top ($m_t=25 \text{ GeV}/c^2$) and superbeauty ($m_{sb}=55 \text{ GeV}/c^2$) production. The limit of integration in p_T are indicated in the figure. The hypotheses are fixed as in Fig. 1.7.

Fig. 1.11 : Same as Fig. 1.10 for the superbeauty asymmetry peak.

Fig. 1.12 : Statistical significance of the asymmetry measurement, $A^{\text{exp}}/\Delta A^{\text{exp}}$, as function of the total cross section and of the (Leading/Total) ratio for the top asymmetry peak in the top ($m_t=25 \text{ GeV}/c^2$) production. The limit of integration in p_T are indicated in the figure. The hypotheses are fixed as in Fig. 1.8.

Fig. 1.13 : Same as Fig. 1.12 for a top mass $m_t=35 \text{ GeV}/c^2$. The hypotheses are fixed as in Fig. 1.9.

Fig. 1.14 : a) Expected number of produced u 's (positive plus negative - white points) as a function of p_T , for the top ($m_t=25 \text{ GeV}/c^2$) and superbeauty ($m_{sb}=55 \text{ GeV}/c^2$) production, with the conditions set in Fig. 1.7. The estimated background is indicated by the full line.
b) The expected ratio (signal= u 's from heavy flavours)/(background) as a function of p_T .

Fig. 1.15 : Same as Fig. 1.14 for a top mass $m_t=35 \text{ GeV}/c^2$ and no superbeauty.

Fig. 1.16 : Drell-Yan cross-section for two different quark parametrizations. Solid line: Pakvasa et al.; dashed line: NA3/CDHS average. This is a "naive" calculation with no k_T for quarks and no K-factor.

- Fig. 1.17 : Drell-Yan cross-section. The shaded area is the average of the two curves $\times 2.2$ (K-factor). The uncertainty has been set to 33%.
- Fig. 2.1 : CERN drawing of the proposed pins to hold the wires. These pins have already been extensively used in the UA1 central detector. They are fabricated by a French company (Minitube, Grenoble).
- Fig. 2.2 : Itemized cost of the magnet charriots as calculated by Mr. Dubail. The compressor could be rented for only a few days when needed, allowing some further savings. This estimate doesn't include the cost of the charriots supporting the iron absorbers, as specified in the text.

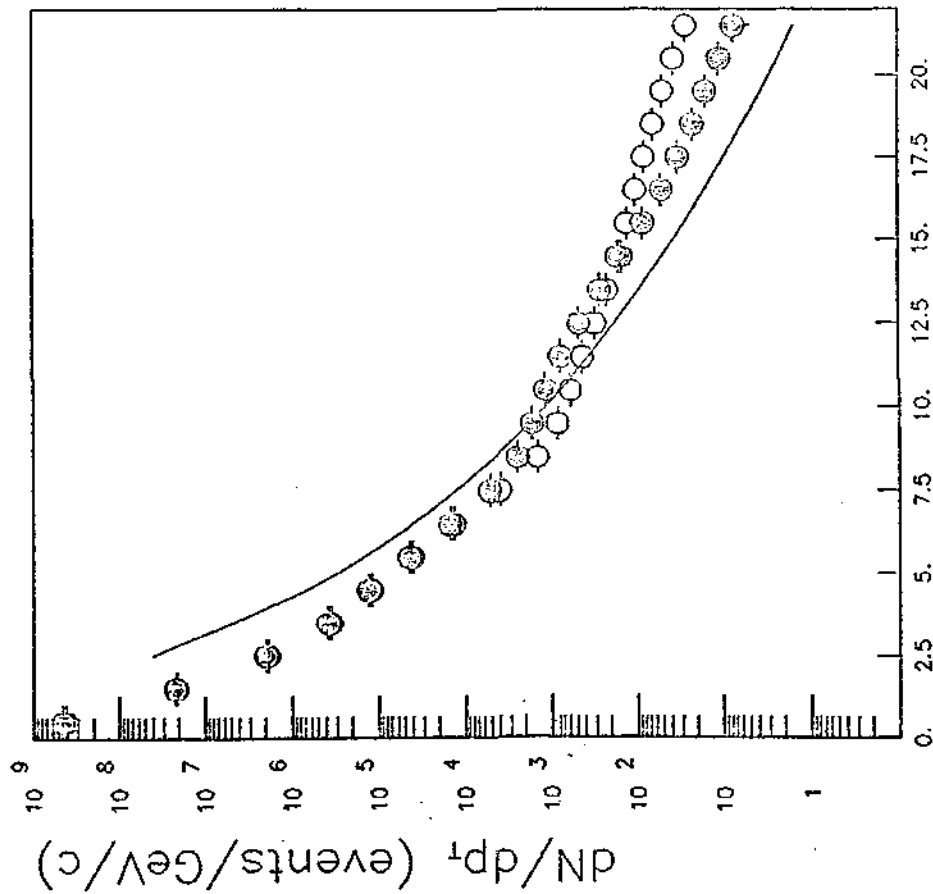
top (25 GeV) AND superbeauty (55 GeV) PRODUCTION

$5. \leq \delta < 30.$

$\Delta p_T / p_T = 20. \%$
(LEADING/TOTAL) = .25

$\sigma_{b\bar{b}} = .0100 \mu\text{b}, \sigma_t = .1000 \mu\text{b}$

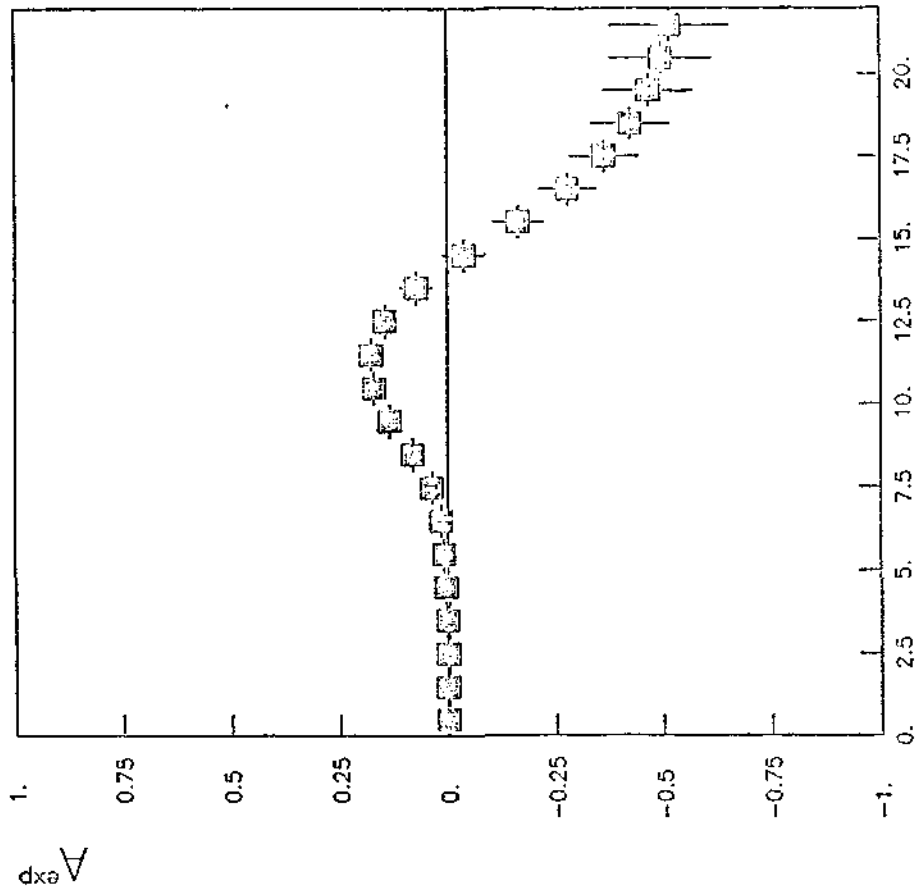
PRODUCTION BARYONS=x-flat, MESONS=(1-x)³



p_T (GeV/c)

(a)

DECAY 3-body



p_T (GeV/c)

(b)

top (25 GeV) PRODUCTION

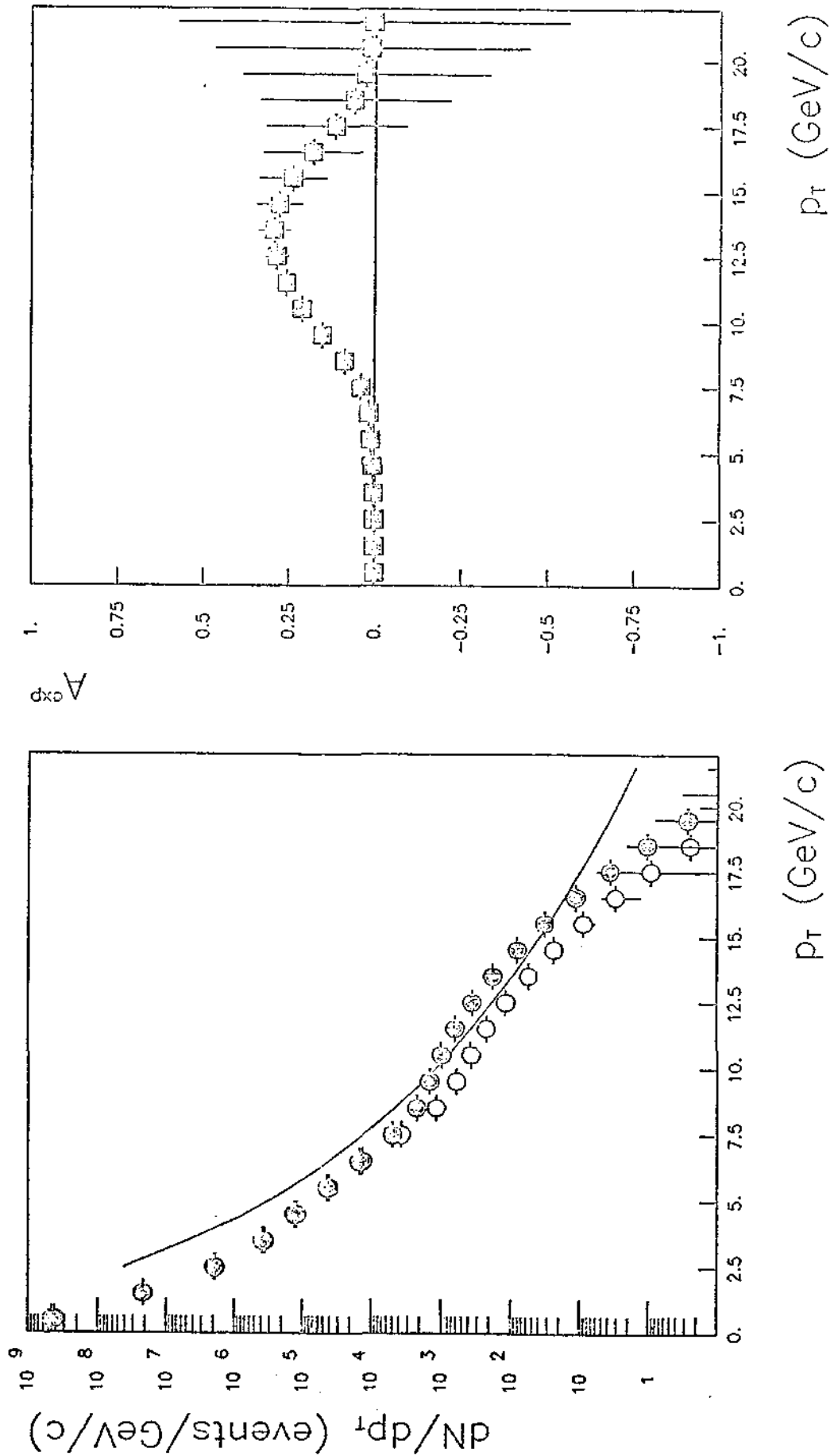
$5. \leq \theta < 30.$

$\Delta p_T / p_T = 20. \%$

(LEADING/TOTAL) = .25

$\sigma_T = .1000 \mu b$

PRODUCTION BARYONS = x-flat, MESONS = $(1-x)^2$



3.22

(a)

Fig. 1.2

(b)

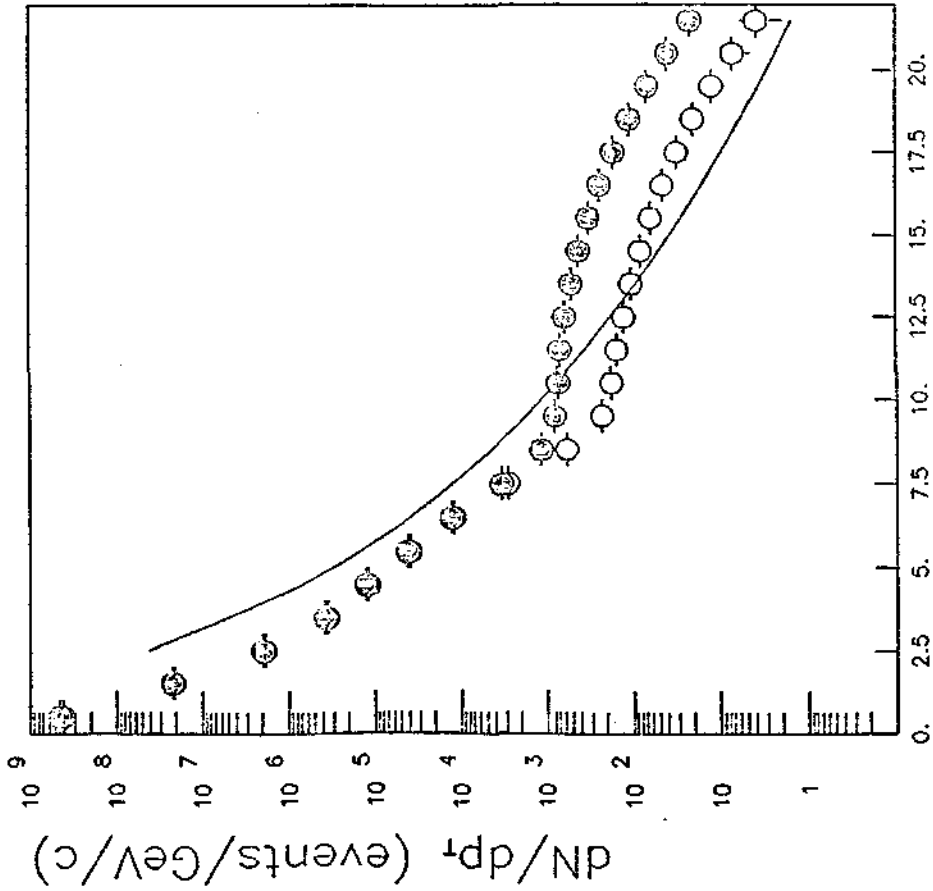
top (35 GeV) PRODUCTION

$5. \leq \phi < 30.$

$\Delta p_T / p_T = 20. \%$
 (LEADING/TOTAL) = .25

$\sigma_1 = .0500 \mu\text{b}$

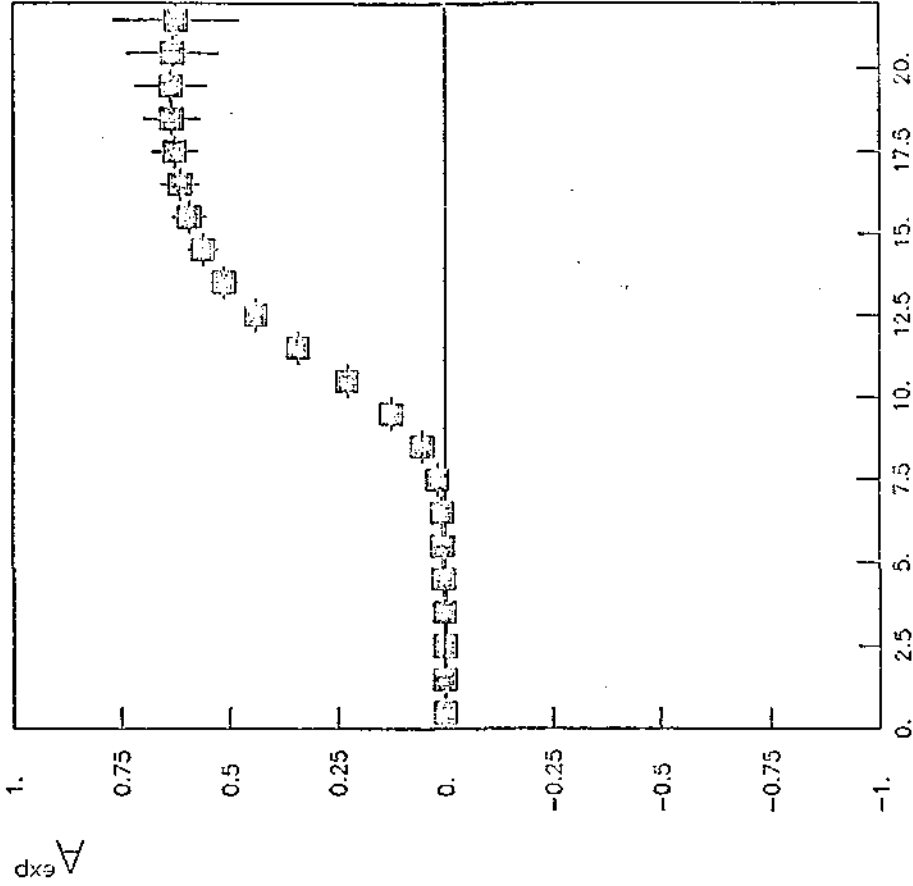
PRODUCTION BARYONS = x-flat, MESONS = $(1-x)^3$



p_T (GeV/c)

(a)

DECAY 3-body



p_T (GeV/c)

(b)

top (25 GeV) AND superbeauty (55 GeV) PRODUCTION

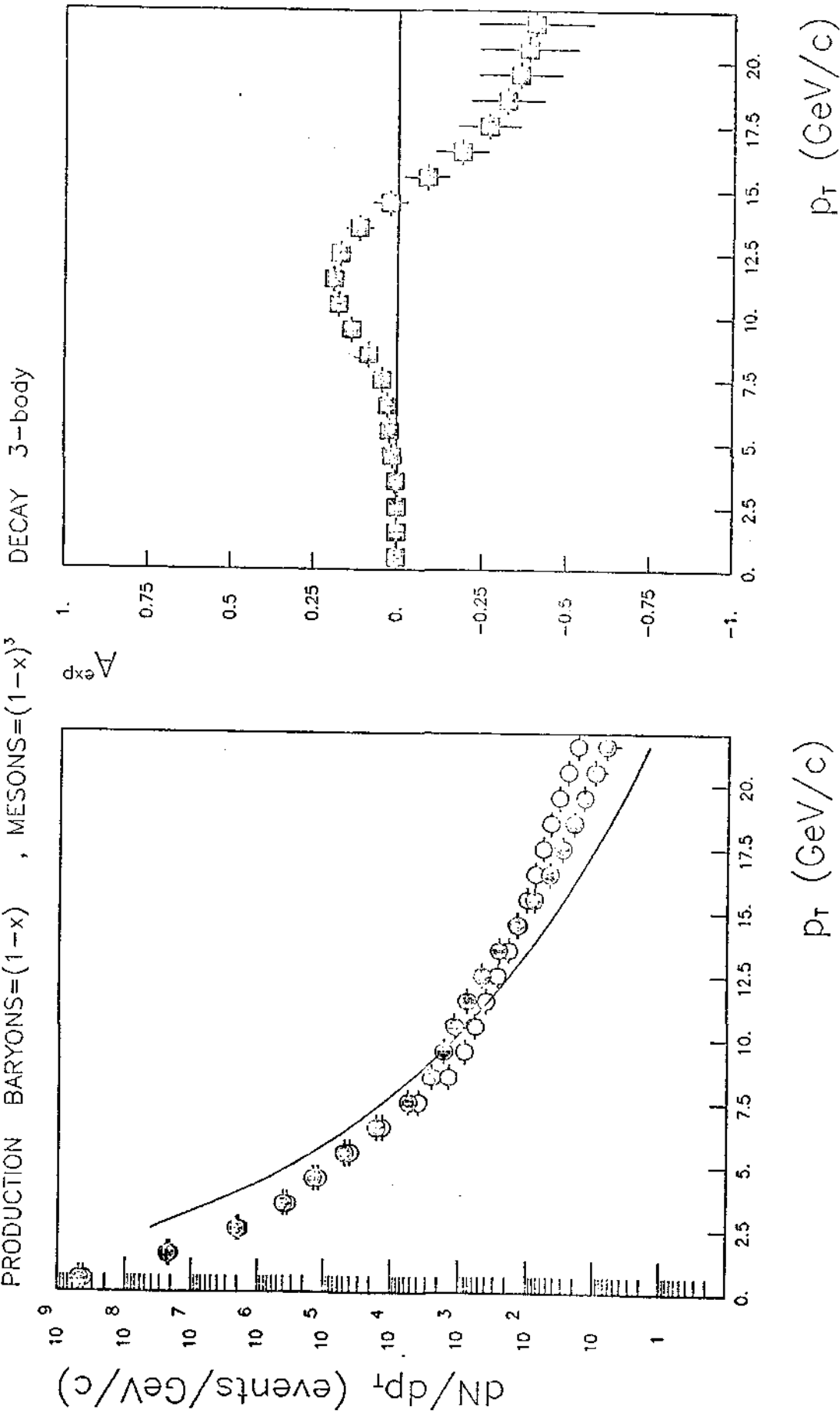
$5. \leq \delta < 30.$

$\Delta p_T / p_T = 20. \%$

(LEADING/TOTAL) = .25

$\sigma_{ab} = .0100 \mu b, \sigma_t = .1000 \mu b$

PRODUCTION BARYONS = $(1-x)$, MESONS = $(1-x)^3$



(a)

(b)

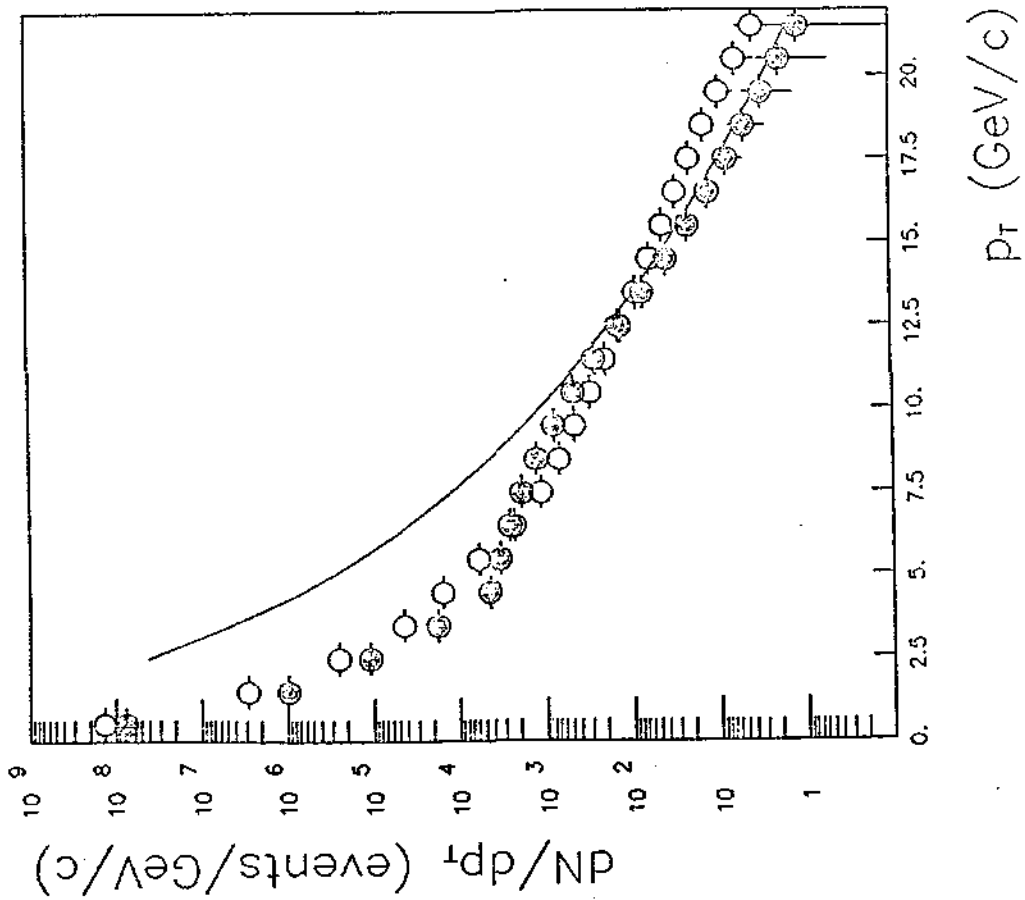
Fig. 1.4

top (25 GeV) AND superbeauty (55 GeV) PRODUCTION

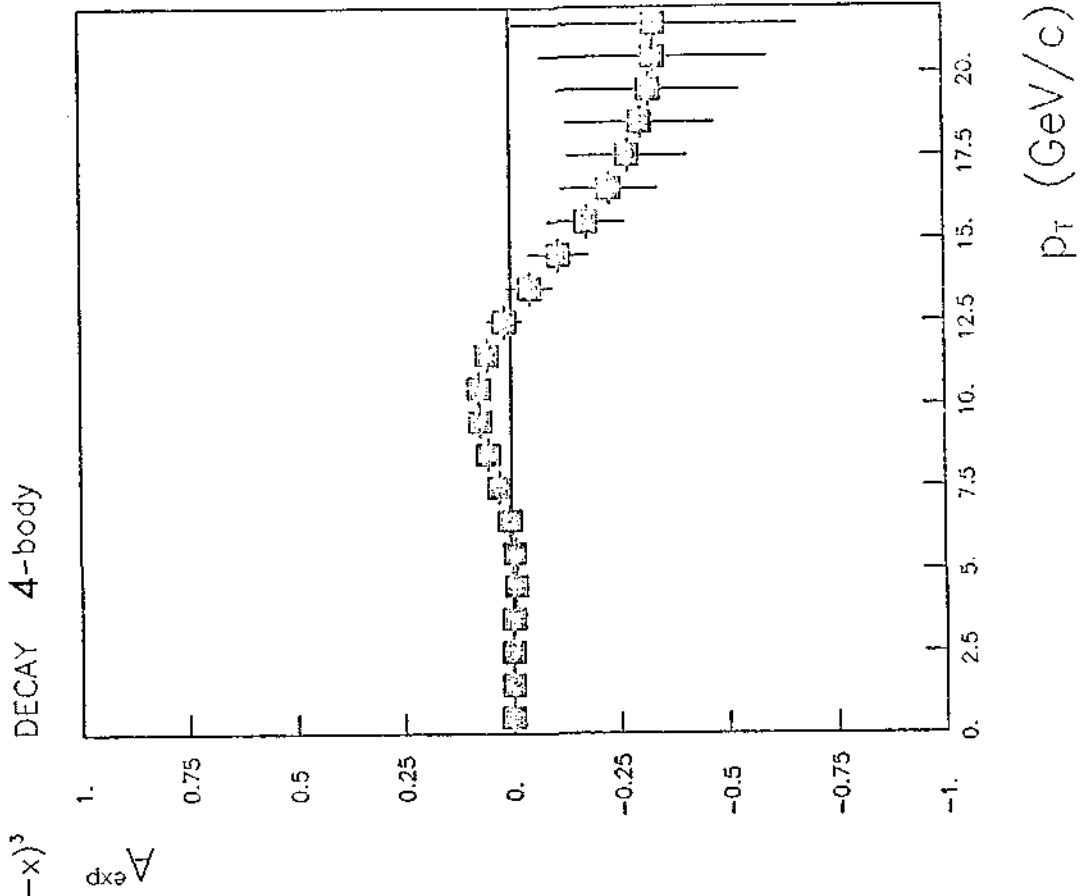
$5. \leq \phi < 30.$

$\Delta p_T / p_T = 20.7\%$
 (LEADING/TOTAL) = .25
 $\sigma_{sb} = .0100 \mu b, \sigma_t = .1000 \mu b$

PRODUCTION BARYONS = $(1-x)$, MESONS = $(1-x)^3$



(a)



(b)

Fig. 1.5

top (25 GeV) AND superbeauty (55 GeV) PRODUCTION

$5. \leq \theta < 30.$

$\Delta p_T / p_T = 20. \%$
 (LEADING/TOTAL) = .25

$\sigma_{\text{ab}} = .0100 \mu\text{b}, \sigma_t = .1000 \mu\text{b}$

PRODUCTION BARYONS = $(1-x)$, MESONS = $(1-x)^2$

DECAY .5x3-body +
 .5x4-body

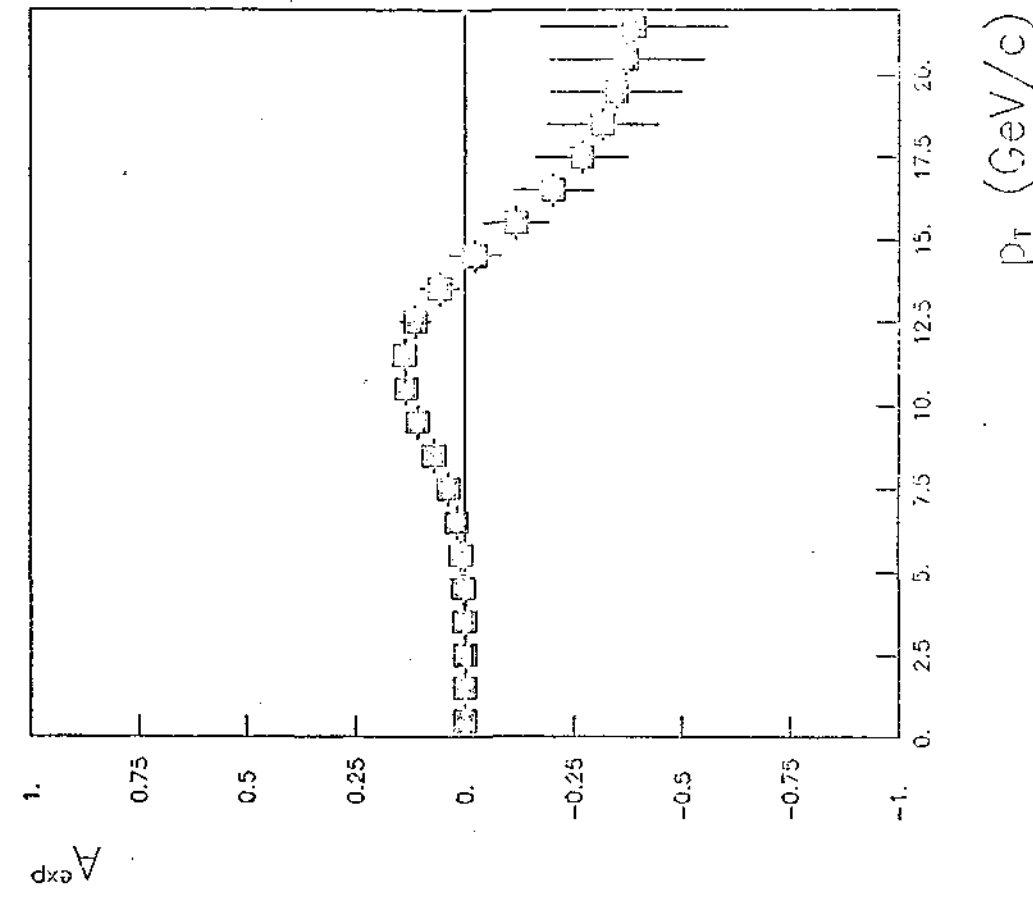
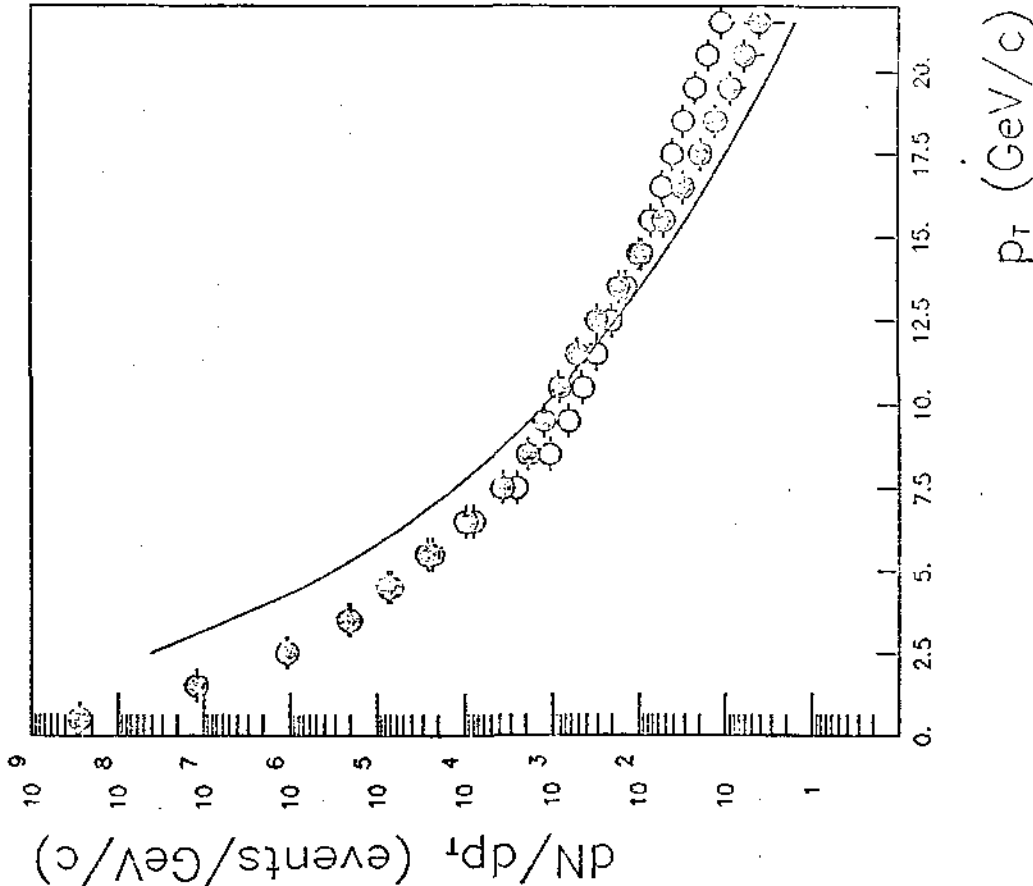


Fig. 1.6

top (25 GeV) AND superbeauty (55 GeV) PRODUCTION

$5. \le \theta < 30.$

$\Delta p_T / p_T = 20. \%$

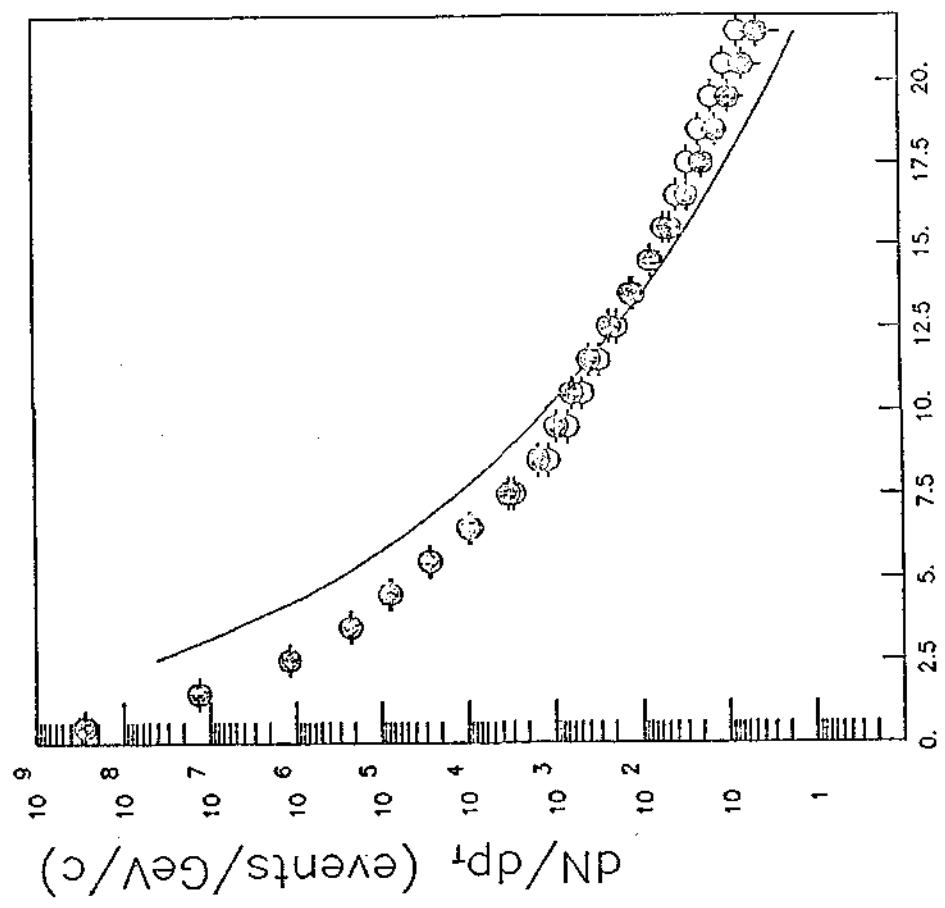
(LEADING/TOTAL) = .10

$\sigma_{\text{tot}} = .0100 \mu\text{b}, \sigma_t = .1000 \mu\text{b}$

PRODUCTION BARYONS = $(1-x)$

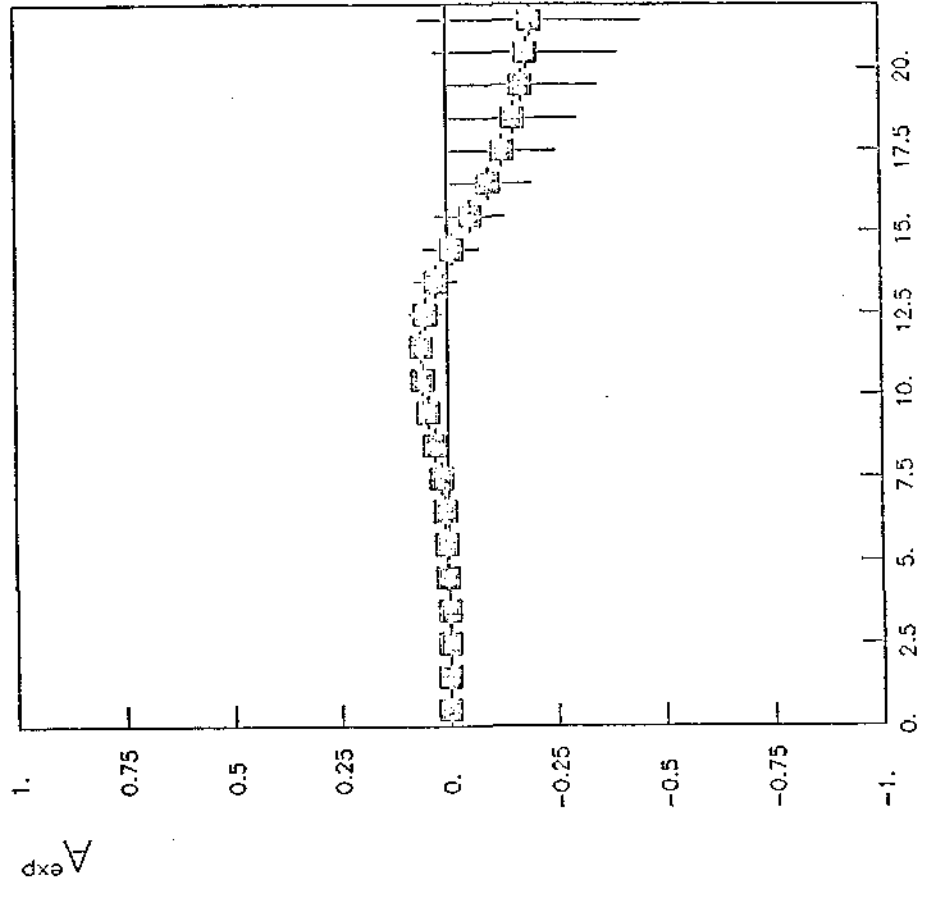
MESONS = $(1-x)^3$

DECAY .5x3-body +
.5x4-body



p_T (GeV/c)

(a)



p_T (GeV/c)

(b)

Fig. 1.7

top (25 GeV) PRODUCTION

$5. \leq \theta < 30.$

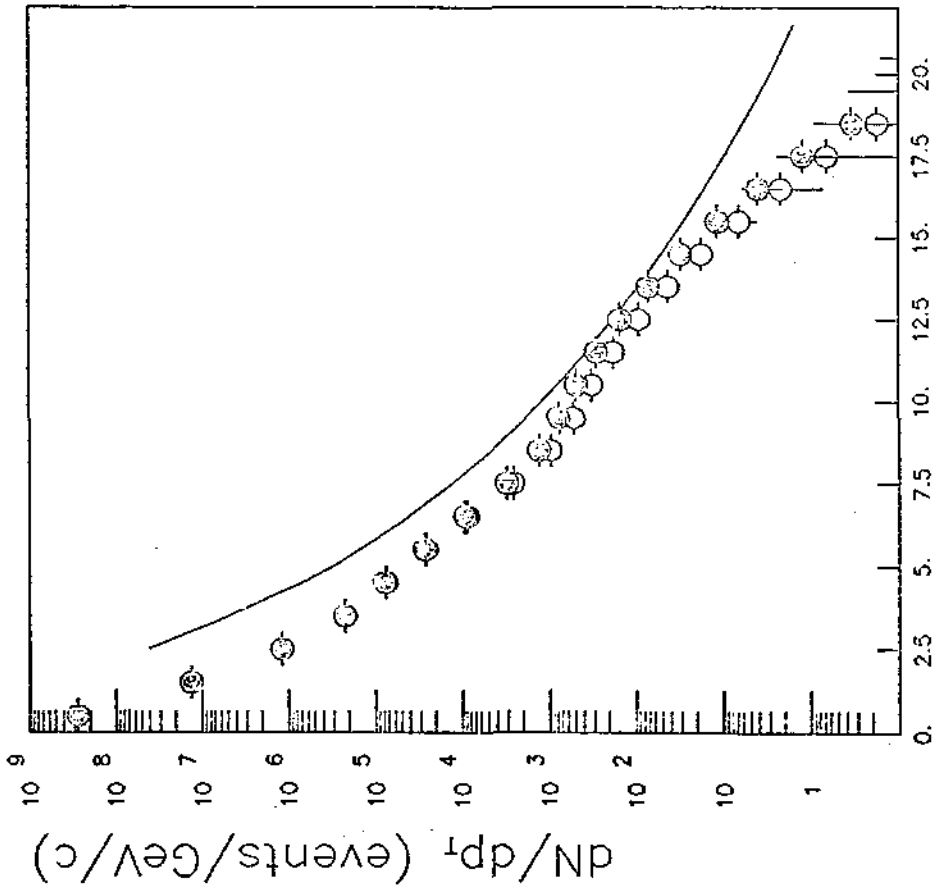
$\Delta p_T / p_T = 20. \%$

(LEADING/TOTAL) = .10

$\sigma_t = .1000 \mu b$

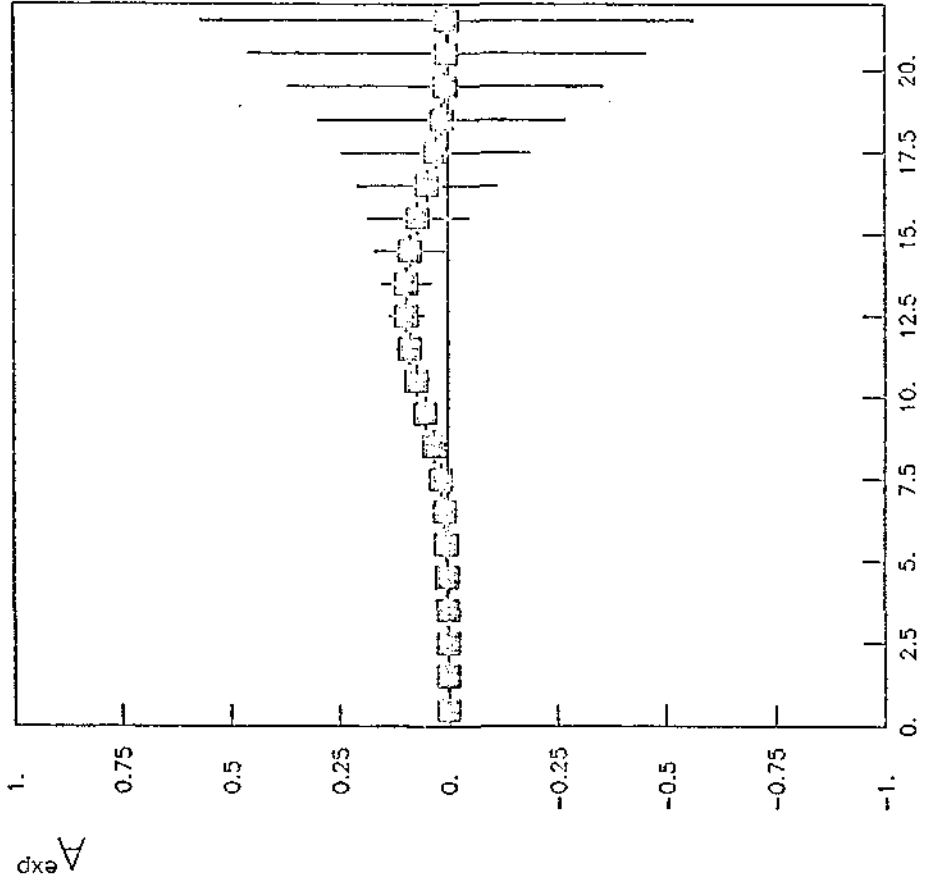
PRODUCTION BARYONS = $(1-x)$, MESONS = $(1-x)^3$

DECAY .5x3-body +
.5x4-body



p_T (GeV/c)

(a)



p_T (GeV/c)

(b)

Fig. 1.8

top (35 GeV) PRODUCTION

$5. \leq \theta < 30.$

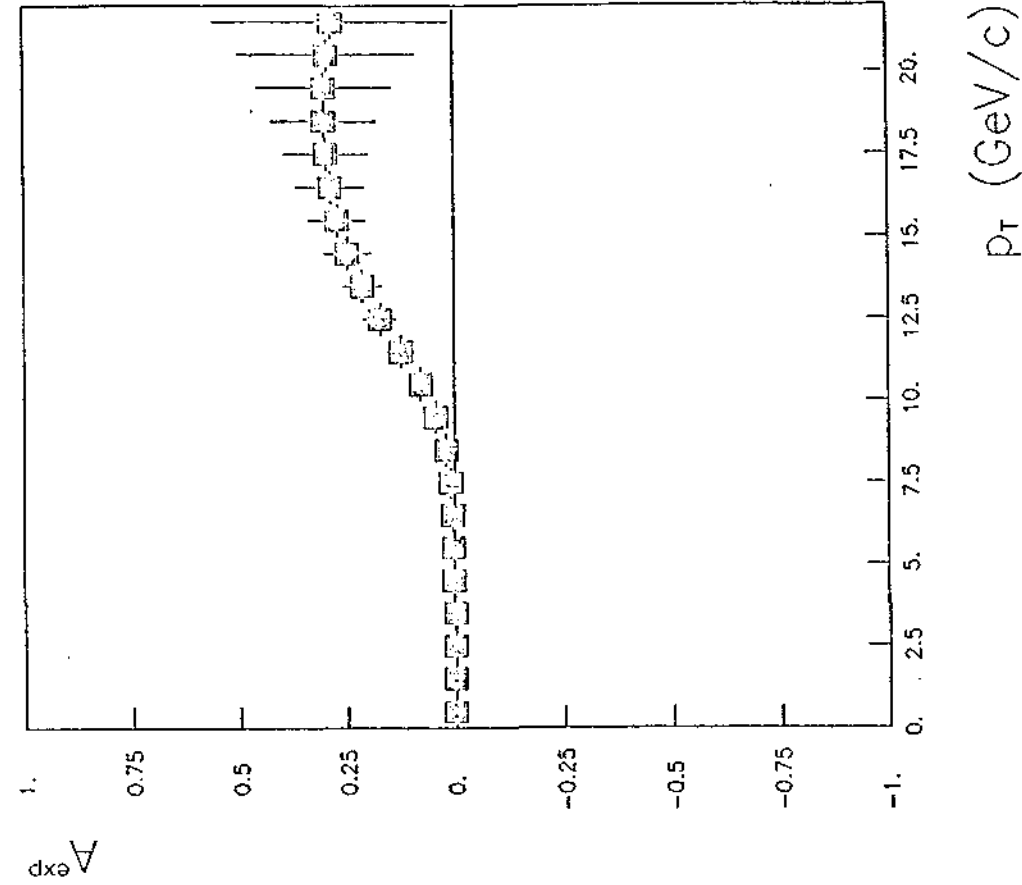
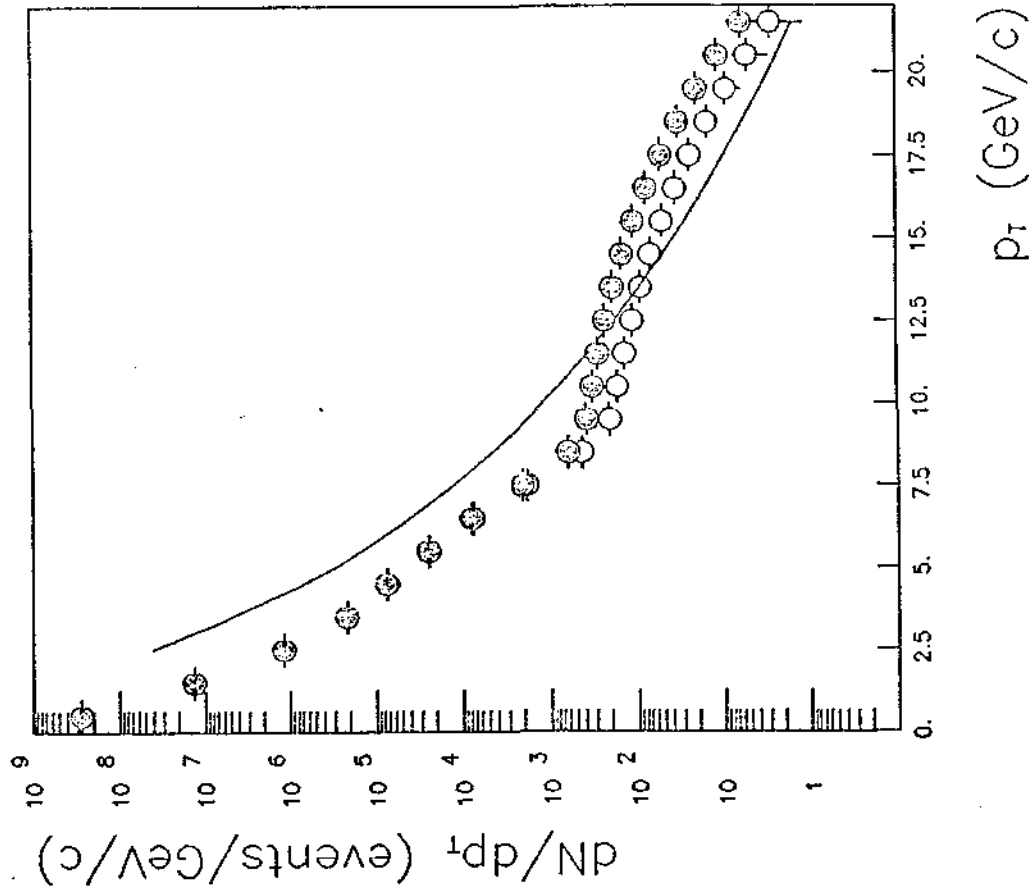
$\Delta p_T / p_T = 20. \%$

(LEADING/TOTAL) = .10

$\sigma_t = .0500 \mu\text{b}$

PRODUCTION BARYONS = $(1-x)$, MESONS = $(1-x)^3$

DECAY .5x3-body+
.5x4-body

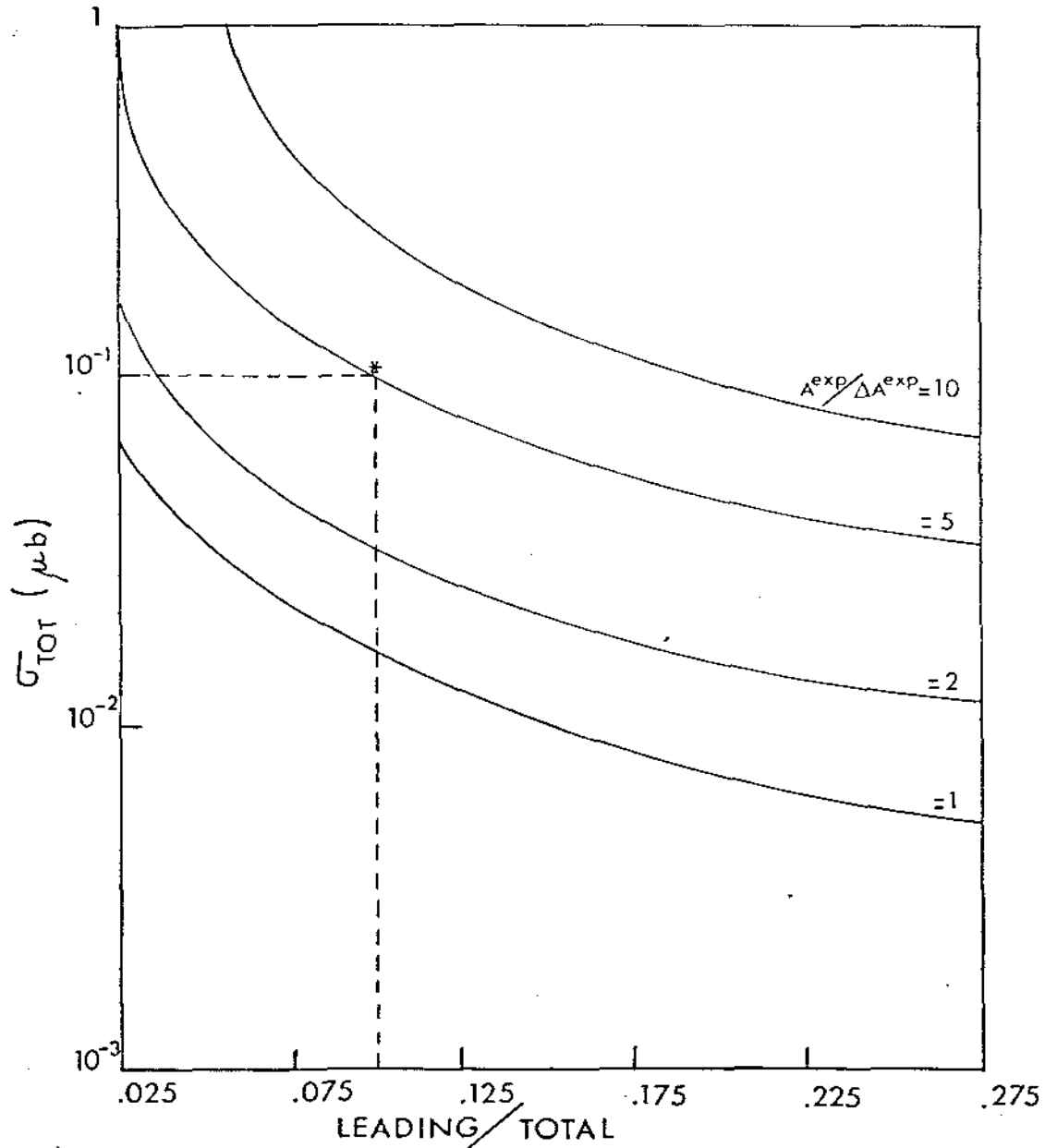


Top (25 GeV) and superbeauty (55 GeV) production

Baryons: $(1-x)$, mesons: $(1-x)^3$

Decay: $.5x3$ -body + $.5x4$ -body

TOP PEAK : $p_T = 8-13$ GeV/c



3.30

Fig. 1.10

Top (25 GeV) and superbeauty (55 GeV) production

Baryons: $(1-x)$, mesons: $(1-x)^3$

Decay: .5x3-body + .5x4-body

SUPERBEAUTY PEAK : $p_T = 18-25 \text{ GeV}/c$

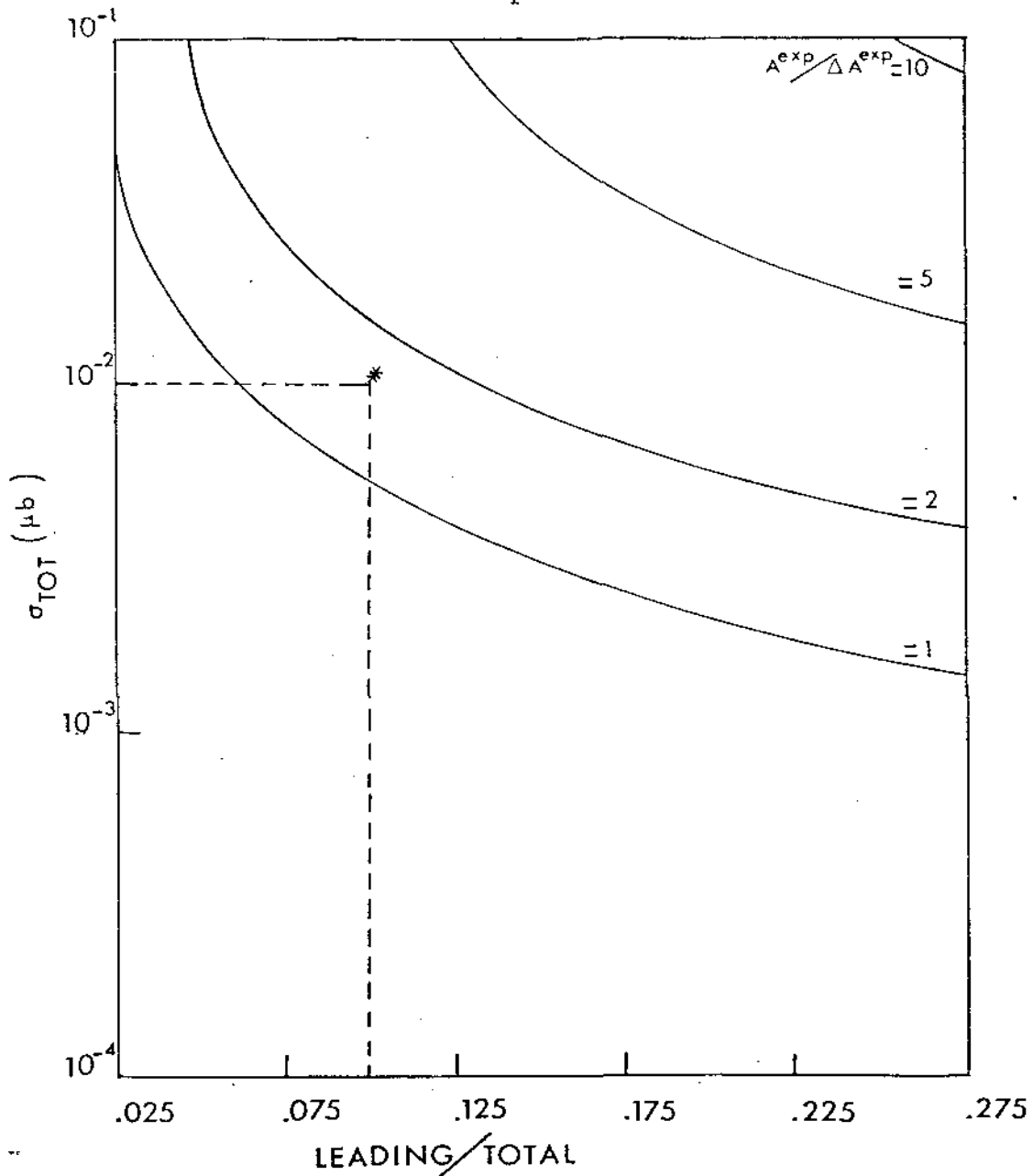


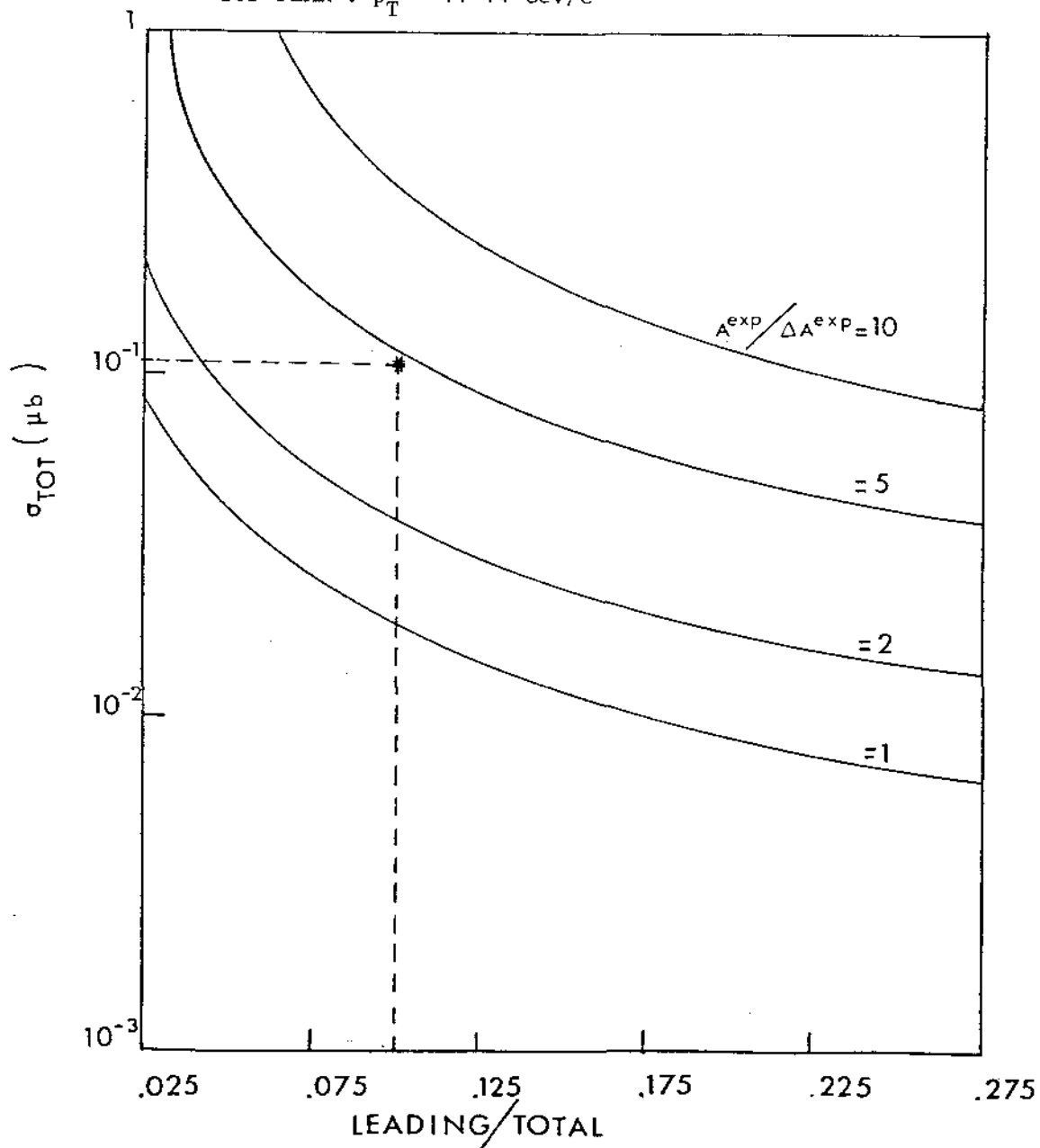
Fig. 1.11

Top (25 GeV) production

Baryons: $(1-x)$, mesons: $(1-x)^3$

Decay: $.5x3$ -body + $.5x4$ -body

TOP PEAK : $p_T = 11-14$ GeV/c



3.32

Fig. 1.12

Top (35 GeV) production

Baryons: $(1-x)$, mesons: $(1-x)^3$

Decay: $.5x3$ -body + $.5x4$ -body

TOP PEAK : $p_T = 16-20$ GeV/c

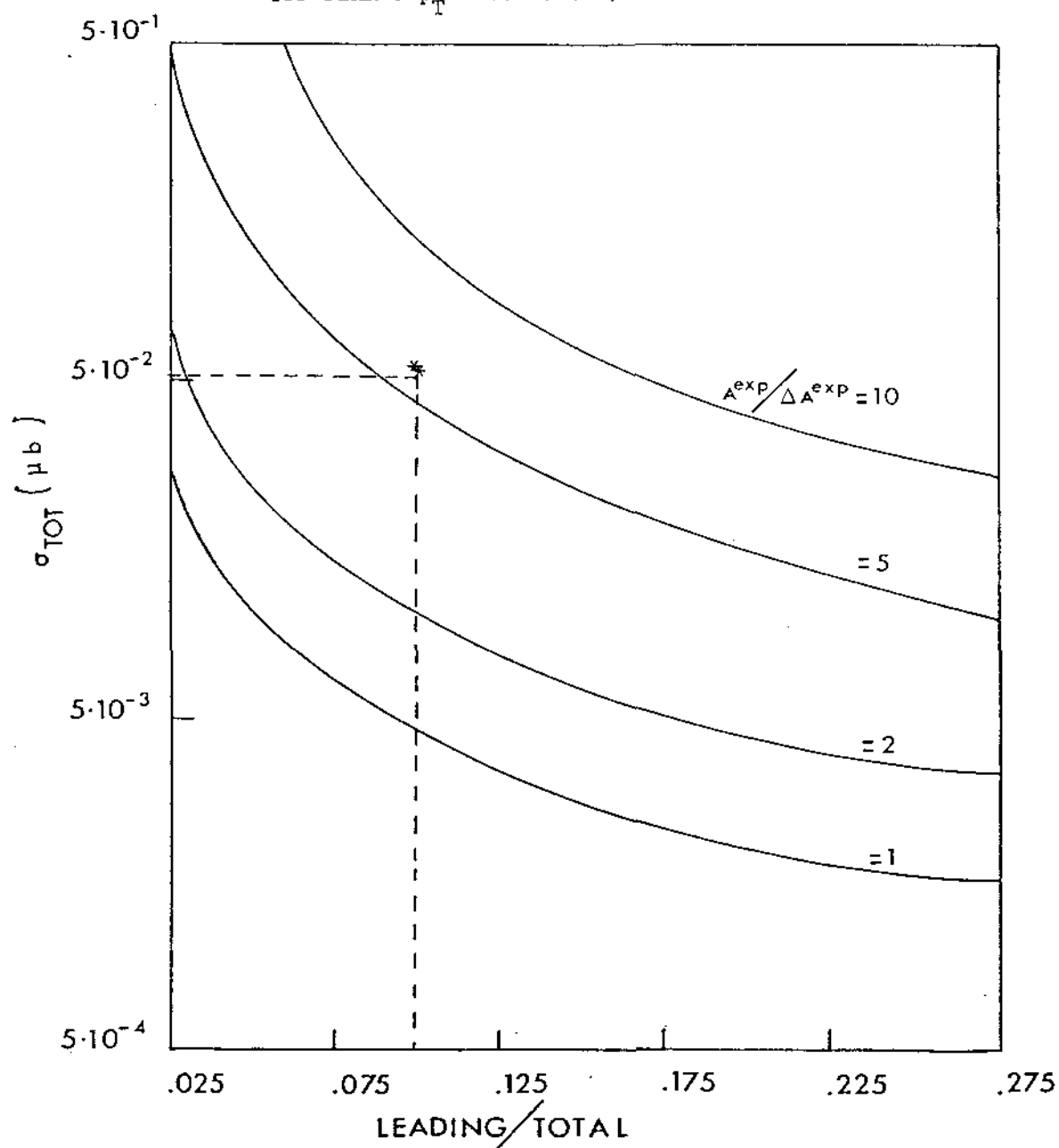
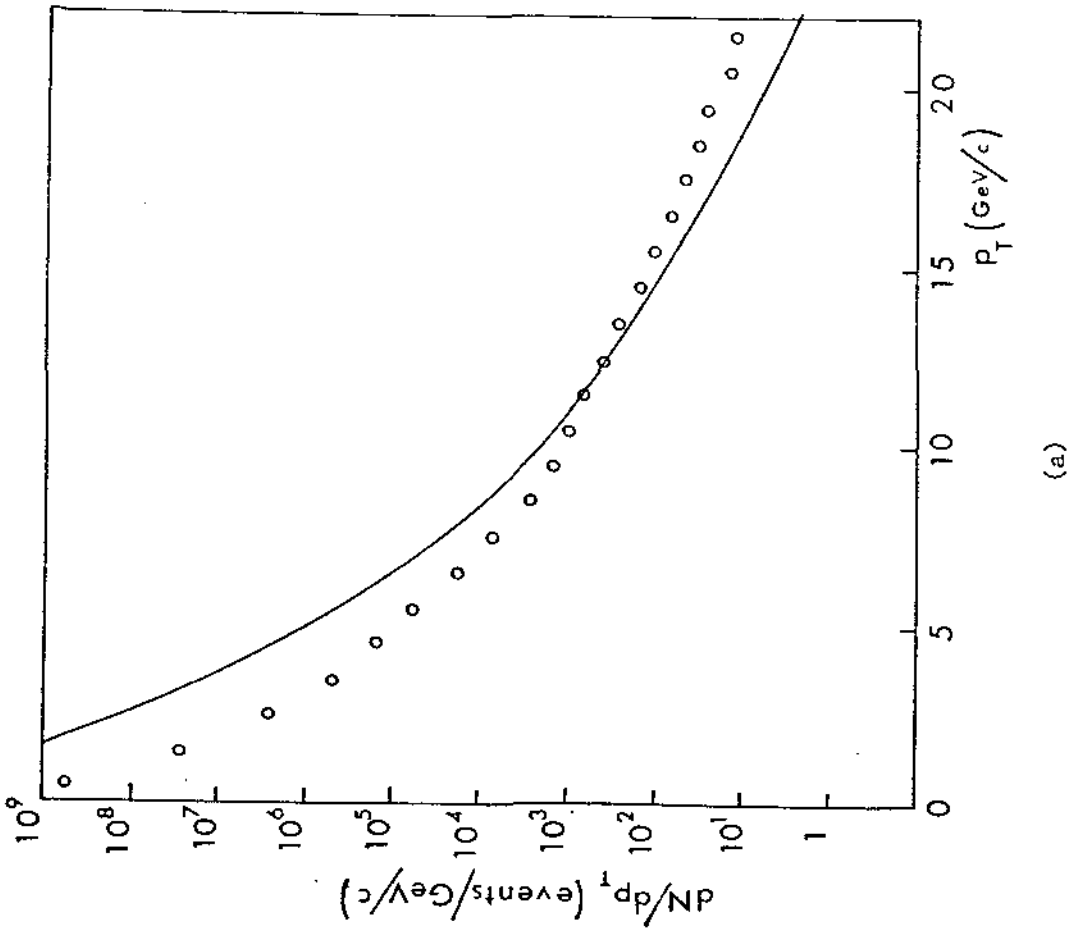
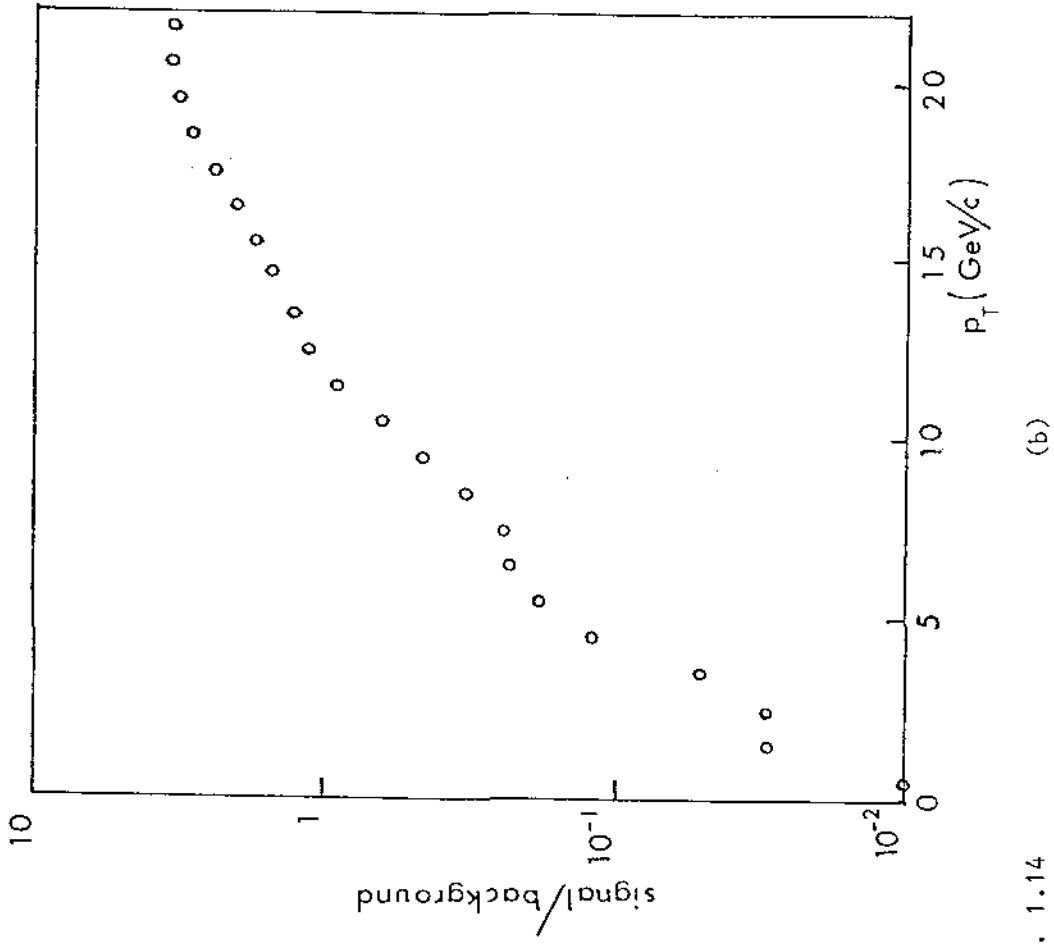


Fig. 1.13



(a)



(b)

Fig. 1.14

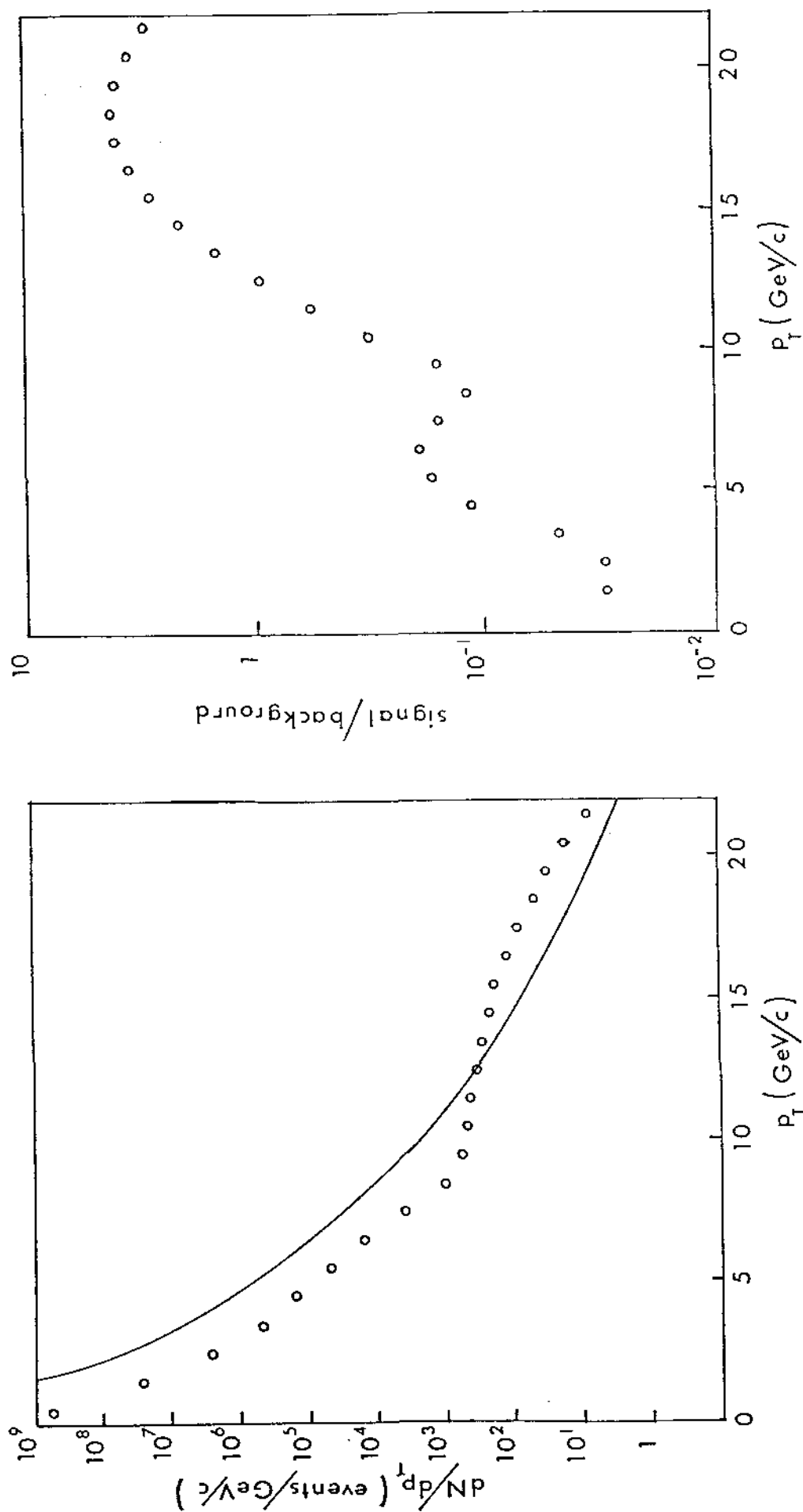


Fig. 1.15

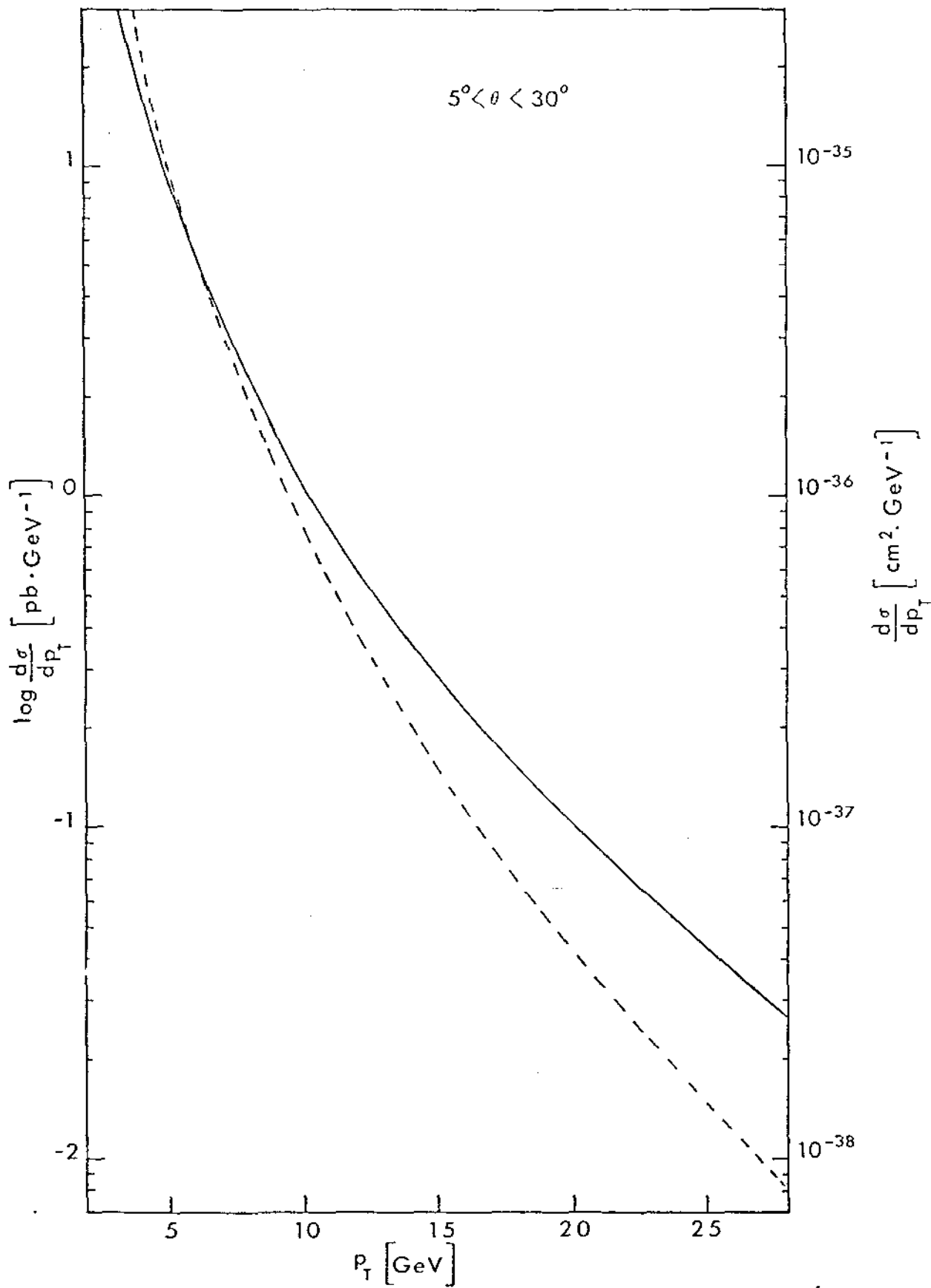


Fig. 1.16

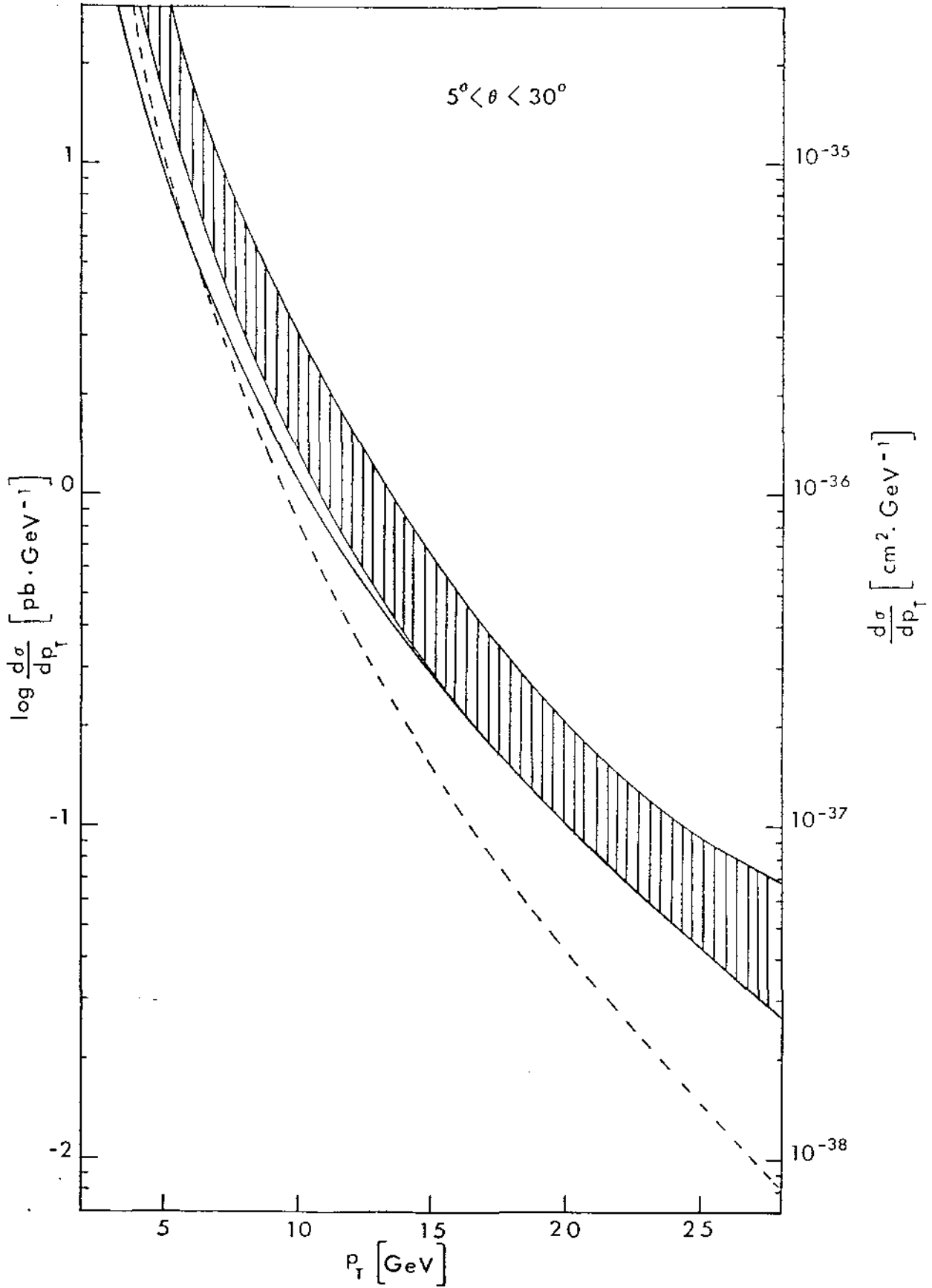
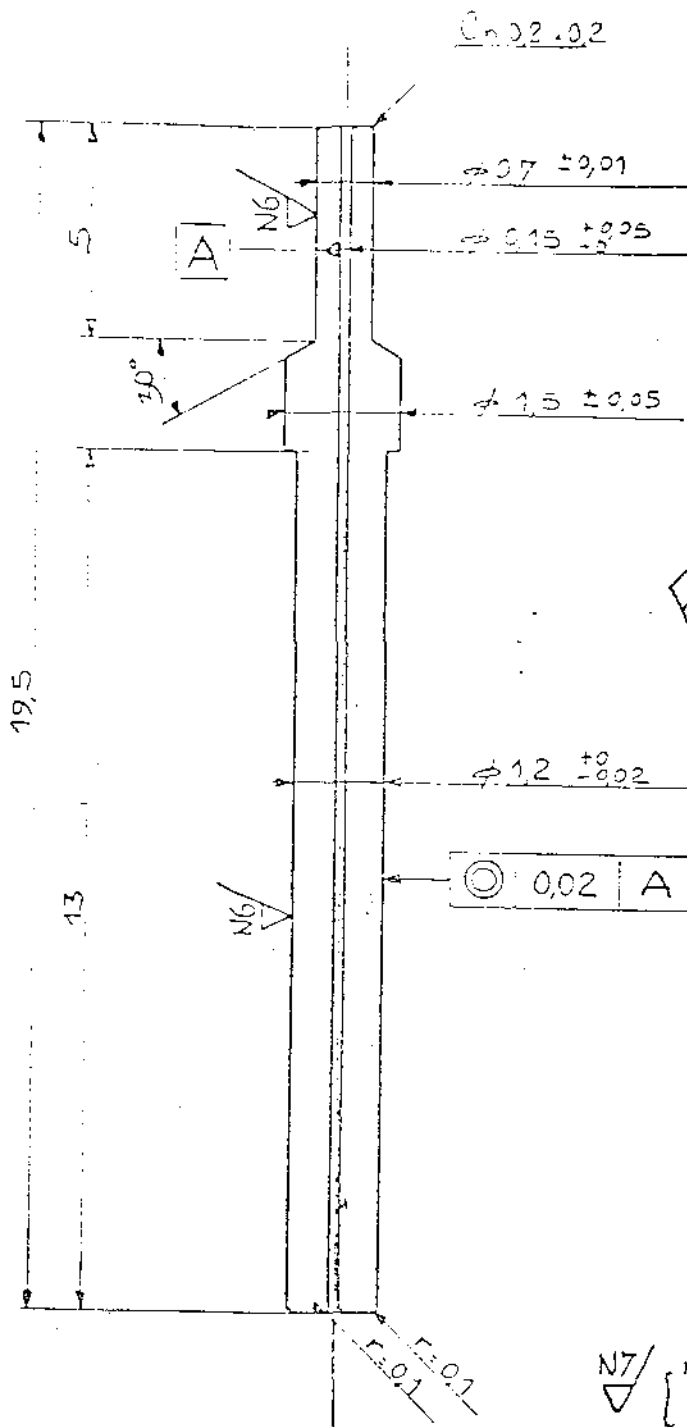


Fig. 1.17

Ech 1/1

Field Wire Pin



Field Wire Pin

N7/ [N6/] ébroué

PRODIGE PAR VITTE	DESCRIPTION	POS	Cu OFHC	Dureté 120/140 HV 0,3	FOURNISSEURS NO SCOM
	ENSEMBLE	S ENSEMBLE	MATIERE	COTES BRUTES	
UA1				NOV	DATE
Embout à sertir C. 150.11			ESCALE SCALE	DESSINE CONTRÔLE	RJ 23.7.79
			10/ 1	REMPLECE REMPLECE PAR REDUCTION	
	ORGANISATION EUROPÉENNE POUR LA RECHERCHE NUCLEAIRE EUROPEAN ORGANIZATION FOR NUCLEAR RESEARCH			NOV	
CERN-DIV: EF	TELE: 1220-836111 TELEX: GENEVE 73668			265/20.001/4	

SPS de 22.08.8

objet: implantation experience P200 dans LES4

Budget previsionnel de l'installation.

Description	Estime en k/s!
1) Feston de esble	60
2) Coussin d'air + Asservissement	200
3) Plateforme detecteurs (2 unites)	60
4) Compresseur (Achat)	75
5) " (puissance - renfort reseau)	40
6) " (location = 1 kF/jour)	
7) Tuyauterie	40
8) Motorisation	50
9) Chape epoxy.	40
10) Blocs + Demie civil	60
11) Infrastructure (modifications)	40
Total	695 ^k

Fig. 2.2

III-4. "New flavours: how they can be looked for at the ($p\bar{p}$) Collider with the Lepton Asymmetry Analyser"
Proc. of the XXII Course of the Ettore Majorana International School of Subnuclear Physics: "Quarks, Leptons and their Constituents" (Plenum Press Inc., New York-London), Erice, August 5-15, 1984.

Proceedings of the XXII Course of the
Ettore Majorana International School
of Subnuclear Physics, Erice, 1984
"Quarks, Leptons, and their
Constituents"
(Plenum Press Inc., New York-London).

5 - 15 August 1984

4 - NEW FLAVOURS: HOW THEY CAN BE LOOKED FOR AT THE (pp) COLLIDER WITH THE LEPTON ASYMMETRY ANALYSER

M. Basile, J. Berbiers, G. Cara Romeo, L. Cifarelli,
A. Contin, G. D'Ali, C. Del Papa, P. Giusti, T. Massam,
R. Nania, F. Palmonari, P. Rotelli, G. Sartorelli,
M. Spinetti, G. Susinno, L. Votano and A. Zichichi
Bologna-CERN-Frascati-Lecce Collaboration
Presented by A. Zichichi

1. INTRODUCTION

1.1 The quark families

The present status of our knowledge on quarks and leptons may be summarized as follows:

Families:	1st	2nd	3rd
Quarks:	$\begin{pmatrix} u \\ d \end{pmatrix}$	$\begin{pmatrix} c \\ s \end{pmatrix}$	$\begin{pmatrix} t \\ b \end{pmatrix}$
Leptons:	$\begin{pmatrix} \nu_e \\ e \end{pmatrix}$	$\begin{pmatrix} \nu_\mu \\ \mu \end{pmatrix}$	$\begin{pmatrix} \nu_\tau \\ \tau \end{pmatrix}$

The top quark (t) is still to be discovered.

There are good reasons to believe that our knowledge is far from being complete and thus the search for new flavours and the study of their family structure is one of the key problems in subnuclear physics.

Two theoretical arguments favour the need for new flavours:

- The Adler-Bell-Jackiw (ABJ) anomaly cancellation requires: number of leptons = number of quarks [1]. In this way a sixth quark is needed, and its natural location would be the up-like member of the 3rd family: the "top" quark.

- According to supersymmetry a very heavy quark (mass in the few $10^2 \text{ GeV}/c^2$ range) is needed in order to produce radiatively a gluino with a mass such as to avoid a conflict with existing lower limits [2]. None of the presently known quarks is heavy enough for this purpose.

Figure 1 gives the quark masses as a function of the family number. Together with the theoretical values nowadays proposed for the masses of the known quarks, we report predictions for the superbeauty and supertop masses, once you have assumed a linear log dependence of the quark masses versus family number.

On the same figure are also reported the correspondent masses for the leptons.

It is interesting to observe that the same linear fit could also apply to the latter. The slope of this line indicates the price in mass you have to pay in order to pass from one family to the next.

The maximum number of quarks allowed by supersymmetry in order to have a consistent theory (for example the unification limit not above the Planck mass) is 8, so that the total number of families would be at maximum four. The up-like quark of the 4th family should be the heavy quark needed by supersymmetry and probably the last quark ever to be discovered

These four families are shown below. The main objectives of this lecture are indicated by the dotted circles.

Families:	1st	2nd	3rd	4th
Quarks:	$\begin{pmatrix} u \\ d \end{pmatrix}$	$\begin{pmatrix} c \\ s \end{pmatrix}$	$\begin{pmatrix} t \\ b \end{pmatrix}$	$\begin{pmatrix} u_H \\ \textcircled{d_H} \end{pmatrix}$
Leptons:	$\begin{pmatrix} \nu_e \\ e \end{pmatrix}$	$\begin{pmatrix} \nu_\mu \\ \mu \end{pmatrix}$	$\begin{pmatrix} \nu_\tau \\ \tau \end{pmatrix}$	$\begin{pmatrix} \nu_H \\ L_H \end{pmatrix}$

$u_H = \text{up-like heavy} \equiv \text{supertop} = st$

$d_H = \text{down-like heavy} \equiv \text{superbeauty} = sb$

Two key questions now arise:

Are top and superbeauty accessible to (pp) Collider energies?

If yes, How can they be detected?

To answer the first point, we can look at Figure 1. If our extrapolation is right, both quarks can be observed at the Sp \bar{p} S.

The detection method is based on the leading baryon production mechanism extended to the heaviest baryon and antibaryon states [3-4].

1.2 Heavy flavours production in hadronic interactions and their decay

If you want to search for new quarks, first of all you have to look at the mechanism through which you expect to get them.

Different models have been proposed in order to explain the heavy flavour production in hadronic interaction [5].

Figure 2a shows the Feynman diagrams for three different models:

- the quark fusion,
- the gluon fusion and
- the flavour excitation.

The first two will lead essentially to a central production; the third one will account for the forward production which, as experimentally proved, represent a great part of the cross-section.

Figure 2b shows on the other hand the production of heavy flavours via a real W^{\pm} or Z^0 .

Another important feature to recall is the way in which the heavy flavours decay. Figure 3 summarize the generalized Cabibbo angles for up-like and down-like quarks.

Since all generalized Cabibbo angles measured so far are either small or compatible with being small (see Table I), we derive the following form of the matrix which connects the strong interacting states to the cabibbo generalized states:

$$\begin{pmatrix} d_c \\ s_c \\ b_c \end{pmatrix} \approx \begin{pmatrix} 1 & 0 & 0 \\ 0 & 1 & 0 \\ 0 & 0 & 1 \end{pmatrix} \begin{pmatrix} d \\ s \\ b \end{pmatrix} \quad \text{Matrix 1}$$

We will suppose that the same form of the matrix is valid when we extrapolate to the fourth family

$$\begin{pmatrix} d_c \\ s_c \\ b_c \\ sb_c \end{pmatrix} \approx \begin{pmatrix} 1 & 0 & 0 & 0 \\ 0 & 1 & 0 & 0 \\ 0 & 0 & 1 & 0 \\ 0 & 0 & 0 & 1 \end{pmatrix} \begin{pmatrix} d \\ s \\ b \\ sb \end{pmatrix} \quad \text{Matrix 2}$$

TABLE I

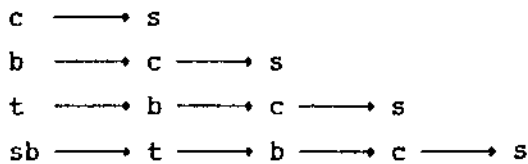
	d	s	b
u	0.9737 ± 0.0075	0.231 ± 0.003	< 0.005
c	0.231 ± 0.003	0.972 ± 0.002	0.044 ± 0.005
t	< 0.015	0.043 ± 0.001	> 0.999

It is worth to stress that in the normal generalized Cabibbo scheme, you would pay a factor of $\sin\theta$ passing from one family to the other, $\sin^2\theta$ if you jump two families, and $\sin^3\theta$ when you jump three families (Fig. 4a).

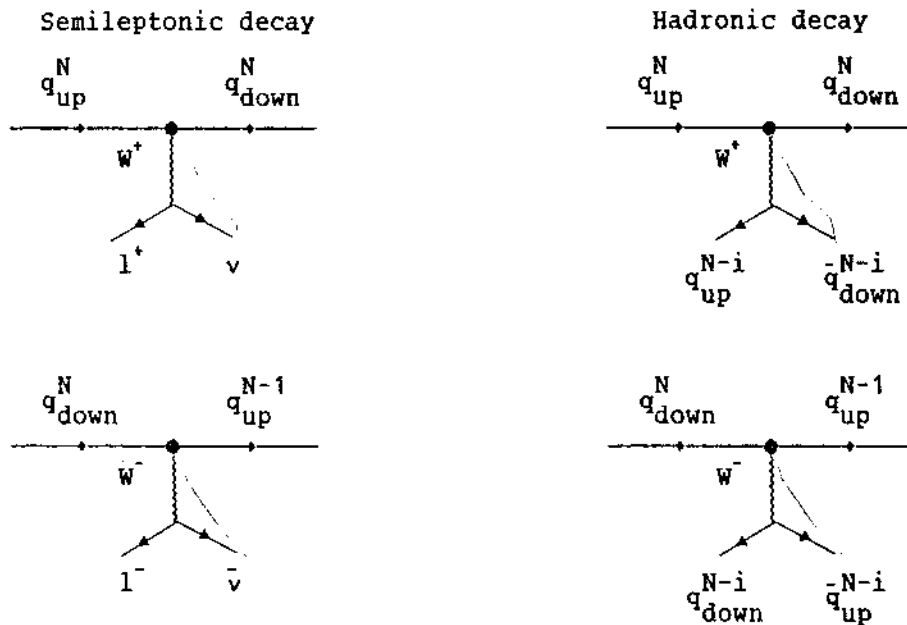
However recent evidence based on beauty lifetime results suggests that probably the coupling between neighbouring families is governed by different angles (let us call them α, β, γ with $\alpha > \beta > \gamma$). This is shown in Figure 4b, where we have set some equivalences between the angles α, β, γ and θ for sake of convenience.

It is clear that, if this new scheme is valid, it will be more difficult to make a jump of more than one family.

We will however forget this new interesting but still uncertain development, and follow the traditional path given by matrix 2, i.e. we will consider the decay chains to be the following



The above decays proceed via the emission of a virtual W^\pm which appears as a (lepton-antilepton) or (quark-antiquark) pair according to the diagrams



Where N is the family and $1 < i < N$.

1.3 Some methods of detection

Various methods have been proposed to detect heavy flavours at the ($p\bar{p}$) Collider.

1. Detection of a hidden state via invariant mass of lepton pairs.
2. Detection of an open state via the identification of a hadronic decay channel.
3. Study of multilepton events.
4. Study of the inclusive p_T spectrum of directly produced leptons.

5. Study of the directly produced p_T spectrum in events with an associated hadronic jets (dilepton and jet masses).

All of these methods have problems. We have summarized them in Table II.

TABLE II

METHODS \ PROBLEMS	1	2	3	4	5
Small production Cross sections	•				
Low global branching ratios		•	•		
High background level		•		•	
Poor experimental resolution of the quantities to be measured					•

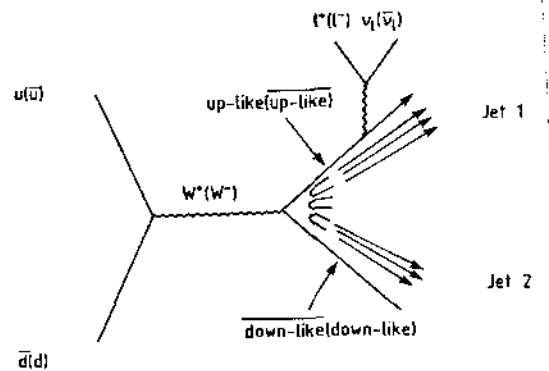
Moreover, unless the flavoured or anti-flavoured nature of the decaying state can be determined, none of these methods allow to identify the up-like or down-like nature of the new heavy flavour.

Only the mass, or the mass difference, of the two quarks involved in the decay can be determined.

Let us now describe in some details the new experimental results coming from the UA1 collaboration at the Sp \bar{p} S [6]. They have looked in their data for interactions with the following topology:

$$p\bar{p} \longrightarrow l + \text{jet} + \text{jet} + (\text{missing energy})$$

and they have interpreted the six events found as coming from the $W^{+(-)}$ decaying into $\bar{t} b$ ($t\bar{b}$). See diagram below.



Looking at the invariant mass, they found a global invariant mass ($lv \text{ jet}_1 \text{ jet}_2$) peaked around 80 GeV and the invariant mass ($lv \text{ jet}_2$) peaked in the 40 GeV region (Figure 5). Their conclusion is that these six events are evidence for the existence of the top quark with mass around 40 GeV.

Waiting for a confirmation of this signal, we would like to make few general remarks:

- The lepton charge sign does not give any information on the uplike or downlike nature of the decaying quark, unless one of the two flavours is independently identified (see below).

$$W^+ \longrightarrow (\text{up-like}, \overline{\text{down-like}})$$

$$\downarrow \qquad \qquad \downarrow$$

$$l^+ \qquad \qquad l^+$$

$$W^- \longrightarrow \overline{\text{up-like}}, \text{down-like}$$

$$\downarrow \qquad \qquad \downarrow$$

$$l^- \qquad \qquad l^-$$

- The p_T spectrum depends only on the mass difference of the parent-daughter quarks, which is unknown.
- This method cannot be applied to search for superbeauty production.

In fact:

$$1) \quad W^+ \longrightarrow (st, \overline{sb})$$

$$W^- \longrightarrow (\overline{st}, sb)$$

are not possible because no energy is available.

2) The following processes

$$\begin{array}{ll}
 W^+ \longrightarrow (t \bar{s}b) & W^- \longrightarrow (\bar{t} sb) \\
 & (\bar{c} sb) \\
 & (\bar{u} sb) \\
 & (c \bar{s}b) \\
 & (u \bar{s}b)
 \end{array}$$

are strongly suppressed because of the smallness of all generalized Cabibbo angles involved.

1.4 Conclusions

To investigate heavy flavour production at ($p\bar{p}$) Collider, and especially the existence of a 4th family, a different approach is needed.

In the following a new method to tackle this difficult experimental task is presented.

This method is based on the extrapolation to ($p\bar{p}$) energies of the leading effect in heavy flavour production observed at the CERN ISR.

2. HEAVY FLAVOUR PRODUCTION AT THE ISR AND EXTRAPOLATION TO Sp \bar{p} S

Our starting point is the study of the experimental data available on heavy flavour production at the ISR. Figures 6a-e show the measurements on the fractional energy and p_T distribution measured by our collaboration for the Λ_c^+ and D^0 produced at $\sqrt{s} = 62$ GeV [7-12]. These results demonstrate that the baryons with heavy flavour are indeed produced in a leading way, while the mesons are centrally produced. It is important to notice that this leading effect seems to increase with the particle mass (Fig. 6-b) [13].

But is the leading effect present even at Sp \bar{p} S energies?

To assess this fact, we have extrapolated the ISR results to the Collider energies with a Monte Carlo Simulation: the goal was to explain some UA1 and UA5 results as the consequence of a leading behaviour of the proton.

The details of this work have already been reported in the other lecture I gave at this school. Here it's enough to mention the main results.

- 1) The $\langle n_{ch} \rangle$ measured at the Collider is consistent only with the hypothesis of a flat $d\sigma/dx_F$ of the proton (Fig. 7-a);
- 2) We predict the forward-backward correlation (Fig. 7-b)[14];
- 3) We predict the charged multiplicity distribution (Fig.7-c)[15].

We conclude that, even at Sp \bar{p} S, the baryons should be produced in a leading way.

3. A NEW METHOD TO SEARCH FOR HEAVY FLAVOUR PRODUCTION AT (p \bar{p}) COLLIDERS

3.1 The principle of the method

Our new method is based on fact that due to the leading baryon production mechanism, extended to the heaviest baryon and anti-baryon states, a charge asymmetry of the leptons originating from the decay can be observed in a selected region of phase-space. In fact, in the outgoing proton hemisphere, as a consequence of the leading effect, you should expect in the forward region more baryons than mesons or anti-mesons or anti-baryons, that means more leptons coming from the heavy quark decay than from the anti-heavy quark. This will create in the forward region an asymmetry in the lepton charge (see Fig.8 for a qualitative behaviour).

The sign of this asymmetry will determine the up-like or down-like nature of the parent flavours; moreover it will show an energy (p_T) dependence characteristic of the masses of the decaying states.

Let us now define in a more quantitative way the lepton asymmetry. We introduce the quantity:

$$A^0 = \frac{N(l^+) - N(l^-)}{N(l^+) + N(l^-)}$$

where

$$N(l^\pm) = N(l^\pm; p_T, \theta_{cut}^{0max}) \equiv$$

\equiv number of positive or negative leptons produced with transverse momentum p_T in the angular range $0^\circ < \theta < \theta^{max}$.

The number of positive or negative leptons $N(l^\pm)$ is expressed by:

$$N(l^\pm) = L [n_{sb}(l^\pm) + n_t(l^\pm) + n_b(l^\pm) + n_c(l^\pm)]$$

where

$n_f(l^\pm)$ (with $f = sb, t, b, c$) \equiv is the contribution from the direct production of sb, t, b, c states, and L is the luminosity.

The leptons originating from the decay of the various flavours are summarized below:

sb \rightarrow

$$\left. \begin{array}{l} t \rightarrow b + l^+ \\ t \rightarrow b \rightarrow c + s + l^+ \end{array} \right\} l^+$$

$$\left. \begin{array}{l} t + l^- \\ t \rightarrow b \rightarrow c + l^- \end{array} \right\} l^-$$

t \rightarrow

$$\left. \begin{array}{l} b + l^+ \\ b \rightarrow c + s + l^+ \end{array} \right\} l^+$$

$$b \rightarrow c + l^- \quad \left. \right\} l^-$$

b \rightarrow

$$c + s + l^+ \quad \left. \right\} l^+$$

$$c + l^- \quad \left. \right\} l^-$$

c \rightarrow

$$s + l^+ \quad \left. \right\} l^+$$

For the corresponding anti-flavours the charge sign of the lepton is reversed.

$n_f(l^+)$ and $n_f(l^-)$ can then be expressed in terms of the following quantities:

- σ_f^T \equiv total cross section for the production of open (f, \bar{f}) pairs;
- $e_{Mf}, e_{\bar{M}f}, e_{Bf}, e_{\bar{B}f}$ \equiv ratio between the inclusive cross-section for producing meson (M), antimeson (\bar{M}), baryon (B), antibaryon (\bar{B}) states and the total cross-section σ_f^T ;
- $BR_{Mf}, BR_{\bar{M}f}, BR_{Bf}, BR_{\bar{B}f}$ \equiv semileptonic branching ratio of the various states with flavour f ($f = c, b, t, sb$);
- $\epsilon_{Mf}(l^\pm), \epsilon_{\bar{M}f}(l^\pm), \epsilon_{Bf}(l^\pm), \epsilon_{\bar{B}f}(l^\pm)$ \equiv acceptance for l^\pm from leptonic decay^f of the flavour f' produced in^f the decay chain of the state with flavour f .

This acceptance is a function of the lepton p_T and of the cut $\theta < \theta_{cut}^0$ applied to the lepton polar angle.

Accordingly, for the case of the superbeauty, we have:

$$n_{sb}(l^+) = \sigma_{sb}^T \left\{ e_{Msb} \left[BR_{Mt} \epsilon_{Msb}(l_t^+) + BR_{Mc} \epsilon_{Msb}(l_c^+) \right] \right. \\ + e_{\bar{M}sb} \left[BR_{\bar{M}sb} \epsilon_{\bar{M}sb}(l_{sb}^+) + BR_{\bar{M}b} \epsilon_{\bar{M}sb}(l_b^+) \right] \\ + e_{Bsb} \left[BR_{Bt} \epsilon_{Bsb}(l_t^+) + BR_{Bc} \epsilon_{Bsb}(l_c^+) \right] \\ \left. + e_{\bar{B}sb} \left[BR_{\bar{B}sb} \epsilon_{\bar{B}sb}(l_{sb}^+) + BR_{\bar{B}b} \epsilon_{\bar{B}sb}(l_b^+) \right] \right\}$$

$$n_{sb}(l^-) = \sigma_{sb}^T \left\{ e_{Msb} \left[BR_{Mt} \epsilon_{Msb}(l_t^-) + BR_{Mc} \epsilon_{Msb}(l_c^-) \right] \right. \\ + e_{\bar{M}sb} \left[BR_{\bar{M}sb} \epsilon_{\bar{M}sb}(l_{sb}^-) + BR_{\bar{M}b} \epsilon_{\bar{M}sb}(l_b^-) \right] \\ + e_{Bsb} \left[BR_{Bt} \epsilon_{Bsb}(l_t^-) + BR_{Bc} \epsilon_{Bsb}(l_c^-) \right] \\ \left. + e_{\bar{B}sb} \left[BR_{\bar{B}sb} \epsilon_{\bar{B}sb}(l_{sb}^-) + BR_{\bar{B}b} \epsilon_{\bar{B}sb}(l_b^-) \right] \right\}$$

The analogous expressions for $n_t(l^\pm)$, $n_b(l^\pm)$, $n_c(l^\pm)$ can be easily derived and are not reported here.

From the above formulas it can be seen that in order to evaluate the lepton asymmetry A^0 one needs to know:

1. The total cross section $\rightarrow \sigma^T$
2. The decay branching ratios $\rightarrow BR$
3. The production distributions of the baryon and meson states, and the lepton distributions in the decay $\rightarrow \epsilon$
4. The relative fraction of baryons and mesons $\rightarrow \rho$.

3.2 Cross-sections estimates

We will try to estimate the production cross-section at $S_{pp\bar{S}}$ energies for very high flavour masses using the QCD flavour excitation predictions [16] (Fig. 9), i.e.:

$$\sigma_c \sim 2000 \mu\text{b}$$

$$\sigma_b \sim 10 \mu\text{b}$$

$$\sigma_t \sim 1 \mu\text{b} \quad \text{with} \quad m_{\text{top}} = 25 \text{ GeV}/c^2.$$

For the extrapolation to heavier quarks we make use of dimensionality and scaling to write the expression

$$\sigma(m) \sim \frac{1}{m^2} f\left(\frac{s}{m^2}\right).$$

To check its validity we have used

- strangeness data to predict charm
- strangeness and charm data to predict beauty [17, 18].

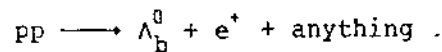
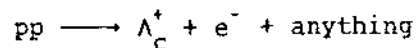
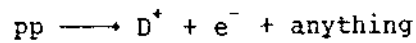
The results of this prediction are shown in Figs. 10a-b, together with the experimental cross-sections and their agreement is satisfactory. Consequently, from the above formula we can deduce the following cross-sections:

$$\sigma_t \sim 0.05 \mu\text{b} \quad \text{for} \quad m_t = 35 \text{ GeV}/c^2$$

$$\sigma_{sb} \sim 0.01 \mu\text{b} \quad \text{for} \quad m_{sb} = 55 \text{ GeV}/c^2 .$$

3.3 Production distributions

For what concerns the production distributions of baryon and meson states, we have used the ISR results on the reactions:



These measurements [8,9,11,12] indicate for the longitudinal momentum distribution:

$$\frac{d\sigma}{dx} \sim \begin{cases} \text{const} \\ (1 - |x|)^1 \end{cases}$$

for heavy flavoured baryons (i.e. a rather flat x-distribution);

$$E \frac{d\sigma}{d|x|} \sim (1 - |x|)^3$$

for heavy flavoured mesons (i.e. a softer x-distribution),
and, for the transverse momentum distribution of both baryons and mesons

$$\frac{d\sigma}{dp_T} \sim p_T e^{-2.5p_T}$$

3.4 The relative yield of baryons and mesons

In (pp) collisions the following reactions dominate (L = leading, C = central production):

$$(L) p_1 p_2 \longrightarrow \bar{M}_{\text{central}} + (B_{\text{leading}})_1 + \text{any} \equiv \left[\bar{M}_C; B_{L_1} \right]$$

$$(L) p_1 p_2 \longrightarrow \bar{M}_{\text{central}} + (B_{\text{leading}})_2 + \text{any} \equiv \left[\bar{M}_C; B_{L_2} \right]$$

$$(C) p_1 p_2 \longrightarrow \bar{M}_{\text{central}} + M_{\text{central}} + \text{any} \equiv \left[\bar{M}_C; M_C \right]$$

In $(p\bar{p})$ collisions, due to the presence of an anti-flavoured anti-baryonic state, other leading reactions can occur:

$$(L) p_1 \bar{p}_2 \longrightarrow \bar{M}_{\text{central}} + (B_{\text{leading}})_1 + \text{any} \equiv \left[\bar{M}_C; B_{L_1} \right]$$

$$(L) p_1 \bar{p}_2 \longrightarrow M_{\text{central}} + (\bar{B}_{\text{leading}})_2 + \text{any} \equiv \left[M_C; \bar{B}_{L_2} \right]$$

$$(L) p_1 \bar{p}_2 \longrightarrow (B_{\text{leading}})_1 + (\bar{B}_{\text{leading}})_2 + \text{any} \equiv \left[B_{L_1}; \bar{B}_{L_2} \right]$$

$$(C) p_1 \bar{p}_2 \longrightarrow M_{\text{central}} + \bar{M}_{\text{central}} + \text{any} \equiv \left[M_C; \bar{M}_C \right]$$

The indices (1,2) are redundant in the $(p\bar{p})$ case and will be omitted from now on.

The relative yields for the production of central mesons/antimesons and of leading baryons/antibaryons, are therefore:

$$\left. \begin{aligned} e_M &= \left[\sigma \left[M_C; \bar{B}_L \right] + \sigma \left[M_C; \bar{M}_C \right] \right] / \sigma^T \\ e_{\bar{M}} &= \left[\sigma \left[\bar{M}_C; B_L \right] + \sigma \left[\bar{M}_C; M_C \right] \right] / \sigma^T \end{aligned} \right\} \equiv 1 - \frac{\text{leading}}{\text{total}}$$

$$\left. \begin{aligned} e_B &= \left[\sigma \left\{ \bar{M}_C; B_L \right\} + \sigma \left\{ B_L; \bar{B}_L \right\} \right] / \sigma^T \\ e_{\bar{B}} &= \left[\sigma \left\{ M_C; \bar{B}_L \right\} + \sigma \left\{ B_L; \bar{B}_L \right\} \right] / \sigma^T \end{aligned} \right\} = \frac{\text{leading}}{\text{total}}$$

with

$$\begin{aligned} \sigma^T &= \text{total cross-section} = \\ &= \sigma \left\{ \bar{M}_C; B_L \right\} + \sigma \left\{ M_C; \bar{B}_L \right\} + \sigma \left\{ \bar{M}_C; M_C \right\} + \sigma \left\{ B_L; \bar{B}_L \right\} . \end{aligned}$$

At the ISR, the ratio leading/total is:

$$\sim 1/16 \quad \text{for} \quad \text{strangeness}$$

$$\sim 1/8 \quad \text{for} \quad \text{charm}$$

Possible extrapolations for the leading/total ratio are given in Fig. 11. However, in our discussion we will study the behaviour of the lepton asymmetry A^0 as a function of the ratio leading/total.

3.5 The decay branching ratios

In our Monte Carlo we have used the known semileptonic branching ratios for charm

$$\frac{(D \rightarrow l^\pm)}{(D \rightarrow \text{all})} \simeq 0.085$$

$$\frac{(\Lambda_C^+ \rightarrow l^\pm)}{(\Lambda_C^+ \rightarrow \text{all})} \simeq 0.045 .$$

For all other heavier particles we assumed the value

$$\text{BR}(l^\pm) = 0.1 .$$

It is worth to note that this is a pessimistic figure if we compare it with the recent data from the CLEO collaboration which has measured [19b] the following beauty quark decay

$$\frac{(M_b \rightarrow l^{\pm})}{(M_b \rightarrow \text{all})} \simeq 0.13 .$$

Note however, that the choosen value of 10% is in agreement with what we should expect from the quarks colours and lepton counting rule, i.e.:

$$\text{BR (leptonic)} = \frac{\sum_{i=1}^N \text{lepton families}}{\sum_{i=1}^N \text{lepton families} + 3 \sum_{i=1}^N \text{quarks families}} = 25\%$$

where N is the total number of families taken into consideration.

3.6 The decay distributions and multiplicities

Again the CLEO collaboration [19b] has studied the reaction $M_b \rightarrow Xev$, discovering that:

- i) the mass recoiling with respect to the leptons is very near to the D mass;
- ii) the mean charged multiplicity of the decay is 4.1, of which 2.5 are, on average, contributed by the D decay.

These results suggest that even at the high mass value of M_b , the semi-leptonic decay proceeds via a 3-body decay, with a mass difference very near to the value.

$$\Delta m = \text{mass}_{\text{beauty}} - \text{mass}_{\text{charm}} .$$

On the other hand, data on the hadronic decay of beauty mesons show that the mean multiplicity is 6.3:

At this point let us focus our attention on the momentum spectrum of the observable l_R^+ and l_L^- . We will have two cases:

1) Up-like $\rightarrow l_R^+ \nu_L d_L$

The l_R^+ with maximum energy = $m/2$ is forbidden, since the spins do not couple in the right way. The spectrum will be as in Fig. 12a.

2) Down-like $\rightarrow l_L^- \bar{\nu}_R u_L$

The l_L^- with maximum energy = $m/2$ is allowed. The spectrum will be as in Fig. 12b.

Figure 13 summarize the p_T distributions of the leptons coming from a decay of the type t ($35 \text{ GeV}/c^2$) $\rightarrow b$ ($5.5 \text{ GeV}/c^2$) + x : various assumptions are reported.

It is clear from the curves shown that in principle it should be possible to determine the nature of the quark only from the p_T distribution.

4. THE LEPTON ASYMMETRY IN AN IDEAL EXPERIMENT, A⁰

4.1 Kinematic analysis of muons from the primary decay of baryons and mesons

A Monte Carlo simulation has been performed with the above mentioned assumptions and we have evaluated the lepton asymmetry for

a) $m_t = 25 \text{ GeV}/c^2$ and $m_{sb} = 55 \text{ GeV}/c^2$

b) $m_t = 35 \text{ GeV}/c^2$,

as measured by an ideal experiment capable of detecting muons in the azimuthal and polar intervals

$$0^\circ < \theta < 30^\circ$$

$$0 < \varphi < 360^\circ$$

In the following figures are shown the results from this Monte Carlo simulation.

Figure 14 show the angular distribution of muons from primary decays of baryons and mesons; we have chosen for the leading/total ratio a value of 0.25 to normalize the spectra of baryons and mesons. Figure 15a shows again the angular distribution of muons

from the decay $t \rightarrow b\mu\nu$ ($m_t = 35 \text{ GeV}/c^2$); here we have added baryons and mesons contribution to the same sign muon. In the same figure we have reported also the muon yield obtained with a different leading baryon distribution $[(1-x)^1]$. Figure 15b shows the same distribution, but in this case for the decay $sb \rightarrow t\mu\nu$.

From these figures we deduce that the asymmetry should be more pronounced in the low θ region and that there is no particular difference between various baryons longitudinal distributions.

Another important feature of these muons can be derived from Figs. 16a-c. Here we report the iso-rate curves in the plane p_T - θ for baryons and mesons. Also reported are the lines of the constant x_F . It is clear that a cut in the x_F variable will improve the rejection for uninteresting muons coming from mesons decay.

Figure 17 shows the expected ideal lepton asymmetry A^0 as computed with our Monte Carlo simulation.

4.2 A^0 versus Δm and leading/total

We want to stress that the peak positions expected in the asymmetry distributions depends only on the mass difference between parent and daughter particles.

In fact, as shown in Fig. 18, if you use the variable $p_T/\Delta m$, all distributions coincide independently of the decay processes considered.

This is more evident in Fig. 19 where we have reported the mass difference ΔM in function of the p_T : a linear dependence is conceivable.

I have already stressed the importance of studying with our Monte Carlo the dependence of the asymmetry on the ratio leading/total. We have evaluated this dependence and the results are shown in Figs. 20a-b.

We can conclude that, within reasonable variation of this ratio, the value of the ideal asymmetry A^0 does not change very much.

5. THE EXPERIMENTAL LEPTON ASYMMETRY A^{exp}

5.1 The Lepton Asymmetry Analyser (LAA)

In order to evaluate the lepton asymmetry in a real experiment, two factors have to be taken into account:

- 1) The detector acceptance
- 2) The background level as determined by physics and by the apparatus rejection power.

In Fig. 21 we show a schematic view of the Lepton Asymmetry Analyser (LAA) [20], an apparatus for muon detection which could be installed behind the upgraded UA2 detector. The angular region defined by the apparatus will be $5^\circ < \theta < 30^\circ$, and this cut affect the lepton asymmetry as shown in Fig. 22.

We can observe that the effect of the lower cut in the angular coverage of the apparatus is to make disappear the asymmetry due to charm and beauty. The lepton asymmetry remains for heavier flavours.

5.2 The background evaluation and the μ/π rejection

In our Monte Carlo simulation, two types of background have been studied.

- 1) Background due to muons produced by π and K decay.

We have here extrapolated, above $p_T = 10$ GeV/c, the UA1 data which best fit is

$$E \frac{d^3\sigma}{d^3p} = A p_0^n / (p_0 + p_T)^n \quad \left[\text{for } \frac{h^+ + h^-}{2} \right]$$

($A = 0.37 \text{ mb c}^2 \text{ GeV}^{-2}$; $p_0 = 1.3 \text{ GeV/c}$; $n = 8.99$) [21].

Integrating this distribution in the rapidity interval

$$1.3 < y < 3.1$$

and using a K/ π ratio of $\sim 0.17/0.83$, the extrapolated hadron rates have then been multiplied by the rejection power of the apparatus. To calculate this rejection, a decay and hadron shower Monte Carlo have been used.

As a result of this simulation, two groups of μ show up

- i) μ from decay in flight (full primary energy)
- ii) μ from decay during the hadron shower development (scaled by 30% in energy on average).

Approximately an equal number of μ from the two groups were sufficiently energetic to penetrate to the end of the toroid. The final rejection power computed is reported in Fig. 23.

- 2) Background from prompt muon sources other than heavy flavours, i.e. W^\pm, Z^0 .

The relevance of this background is shown in Fig. 24, where the expected muon rates coming from different processes are reported [22].

From these data, we conclude that this background is relevant above $p_T \gtrsim 15$ GeV/c.

5.3 The experimental asymmetry parameter

Having introduced the background in our Monte Carlo, we can now see how our asymmetry will be affected.

Figure 25 shows an example of the various contributions to the muon spectrum as computed by our simulation. We can use these data to evaluate the experimental asymmetry A^{exp} defined as

$$A^{\text{exp}}(p_T, \theta) = \frac{[N(\mu^+) + N_{\text{bg}}(\mu^+)] - [N(\mu^-) + N_{\text{bg}}(\mu^-)]}{[N(\mu^+) + N_{\text{bg}}(\mu^+)] + [N(\mu^-) + N_{\text{bg}}(\mu^-)]}$$

where $N_{\text{bg}}(\mu^+) = N_{\text{bg}}(\mu^-) = N_{\text{bg}}(\mu) \equiv$ number of background μ^\pm .

The obtained A^{exp} distribution is shown in Fig. 26. It is interesting to see how the W contribution affects this distribution: Fig. 27 is answering this question.

5.4 The effect of momentum resolution

Since we want to put ourselves in real experimental conditions, we must evaluate how A^{exp} will be affected by the momentum resolution of the apparatus.

Figures 28a and b show how the asymmetry value at the peak varies in function of $\Delta p/p$ of the apparatus. The figures refer to the cases of top ($25 \text{ GeV}/c^2$) and superbeauty ($55 \text{ GeV}/c^2$). Notice that the expected momentum resolution of the LAA is about 20%.

5.5 A^{exp} for the cases

- a) $m_t = 25 \text{ GeV}/c^2$
- b) $m_t = 35 \text{ GeV}/c^2$
- c) $m_t = 25 \text{ GeV}/c^2$ and $m_{sb} = 55 \text{ GeV}/c^2$.

At this point we can systematically study the behaviour of the lepton asymmetry for various assignments of the top and superbeauty masses.

For each case the p_T distribution of the muons and the asymmetry versus p_T behaviour is reported (Figs. 29-31).

We underline that in our calculations, we have used an integrated the luminosity of 10 pb^{-1} .

5.6 A^{exp} and its statistical significance

Once we have established in a quantitative way the asymmetry behaviour for different heavy quark masses, we have to go back and analyse the variations of the results with the most critical inputs of our Monte Carlo, i.e.:

- 1) the leading/total ratio,
- 2) the cross-section estimates,
- 3) the baryons longitudinal distributions.

For what concerns the first item, we report in Figs. 32a-c, the asymmetry peak and the statistical significance of the asymmetry versus the leading/total ratio.

Figures 33 to 36 show again the asymmetry peak values and the statistical significance in function of the cross-sections (the arrow indicates the value chosen till now).

It is evident from the data that cross-sections lower even of a factor 5 or 10 will allow a valuable measurement of the lepton asymmetry.

Finally, in Figs. 37-38 we report the p_T distribution of the muon and the dependence of the experimental asymmetry versus p_T for two different assumptions in the longitudinal momentum distribution.

The variations obtained in the asymmetry distribution are small.

6. CONCLUSIONS

Let me summarize the logic we have followed in this lecture.

Starting from the leading effect found at the ISR, and deeply studied by the BCF collaboration, we have deduced the existence of a similar effect at the Sp \bar{p} S.

We have consequently developed a new method to search for heavy flavours baryons and antibaryons produced in a leading way and decaying semileptonically.

Our procedure is based on the measurement of the μ^\pm asymmetry:

- from its sign we can deduce the up-like or down-like nature of the new flavour carried by the baryon;
- from its amplitude we can measure the cross-section for producing leading baryons (anti-baryons);
- from its p_T dependence we can derive the mass difference between the new flavour and its nearest state.

Since the collider energy opens a region of masses well above the 3rd family, we will be allowed to search for the lightest state (down-like) of the 4th family: the superbeauty.

Notice that mass difference between "superbeauty" and "top" will be crucial for the μ^\pm asymmetry produced by top.

We have proposed a new detector to measure this asymmetry: the Lepton Asymmetry Analyser (LAA), whose main features are:

- is positioned behind the forward/backward UA2 calorimeters;
- consists of iron filters, tracking chambers, limited streamer tubes for triggering, 2.0 T in iron toroids;
- covers the angular regions

$$0^\circ \leq \phi \leq 360^\circ \quad \text{and} \quad \begin{cases} 5^\circ \leq \theta \leq 30^\circ \\ 150^\circ \leq \theta \leq 175^\circ ; \end{cases}$$

- provides a momentum accuracy $\Delta p/p \lesssim 20\%$ up to $p = 150 \text{ GeV}/c$;
- separates muons from hadrons with a rejection power of 10^{-3} at $p_T = 3 \text{ GeV}/c$, up to 10^{-4} at $p_T = 20 \text{ GeV}/c$.

Simulating in details the experimental condition, we have then studied three cases:

- i) "Top" with mass = $25 \text{ GeV}/c^2$.
- ii) "Top" with mass = $35 \text{ GeV}/c^2$.
- iii) "Top" with mass = $25 \text{ GeV}/c^2$ and "superbeauty" with mass = $55 \text{ GeV}/c^2$.

The influence of the uncertainties in the Monte Carlo inputs has been evaluated.

As a result of this detailed work, the expected asymmetries are shown in Figs. 39-40.

At this point I would like to underline the main items followed in my lecture:

- i) demonstrate to you the importance of the search for new heavy quarks;
- ii) prove that the simple measurement of a mass is not enough to understand the properties of a new state;
- iii) propose an apparatus (the LAA) which will be able to determine the up-like or down-like nature of a new quark, its mass and its cross-section;
- iv) try to give to all of you (especially the theorists) the feeling of how complicate is to build a new instrument capable of measuring the flavour of a new quark.

REFERENCES

- [1] C. Bouchiat et al., Physics Letters 38B, 1972.
- [2] S. Ferrara, private communication.
- [3] M. Basile et al., Nuovo Cimento 68A, 65 (1982).
- [4] M. Basile et al., Nuovo Cimento Letters 37, 255 (1983).
- [5] F. Halzen, Proc. XXIst Int. Conf. on High Energy Physics, Paris, 1982 [J. Phys. (France) C3, 1983], p.381.
- [6] UA1 Collaboration, data presented at the International Conference on High Energy Physics, Leipzig, July 1984.
- [7] M. Basile et al., Nuovo Cimento 63A, 230 (1981).
- [8] M. Basile et al., Nuovo Cimento Letters 30, 481 (1981).
- [9] M. Basile et al., Nuovo Cimento Letters 30, 487 (1981).
- [10] M. Basile et al., Nuovo Cimento 65A, 457 (1981).
- [11] M. Basile et al., Nuovo Cimento Letters 33, 33 (1982).
- [12] M. Basile et al., Nuovo Cimento Letters 33, 17 (1982).
- [13] For a general review of the BCF Collaboration results on heavy flavour production at the ISR, see M. Basile et al., Proc. XIXth Course of the "Ettore Majorana" Int. School of Physics, Erice, Italy, August 1981, "The unity of the fundamental interactions", (Plenum Press, New York, 1984), p. 409.
- [14] M. Basile et al., Nuovo Cimento Letters 38, 359 (1983).
- [15] M. Basile et al., preprint CERN-EP/84-95 (1984).
- [16] R. Odorico, Physics Letters 107B, 231, 1981.
- [17] M. Basile et al., Nuovo Cimento Letters 31, 97 (1981).
- [18] M. Basile et al., Nuovo Cimento 65A, 391 (1981).
- [19] a) K. Chadwick et al., Phys. Rev. 270, 475 (1983).
b) L. Olsen, Proc. Moriond Workshop on New Flavours, Les Arcs, 1982 (Ed. Frontières, Gif-sur-Yvette, 1983), p. 367.
- [20] C. Alberini et al., "The Lepton Asymmetry Analyser: a proposal", CERN/SPSC/84-33 and SPSC/P200.
- [21] G. Arnison et al., Phys. Lett. 118B, 167 (1982).
- [22] G. Arnison et al., Physics Letters 134B, 469 (1984).

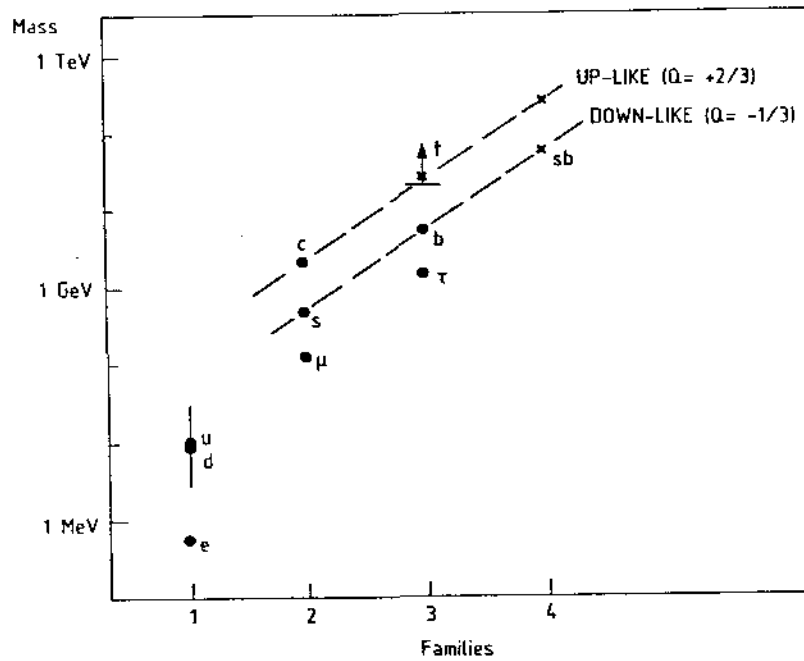


Fig. 1 Quark masses as a function of the family number.

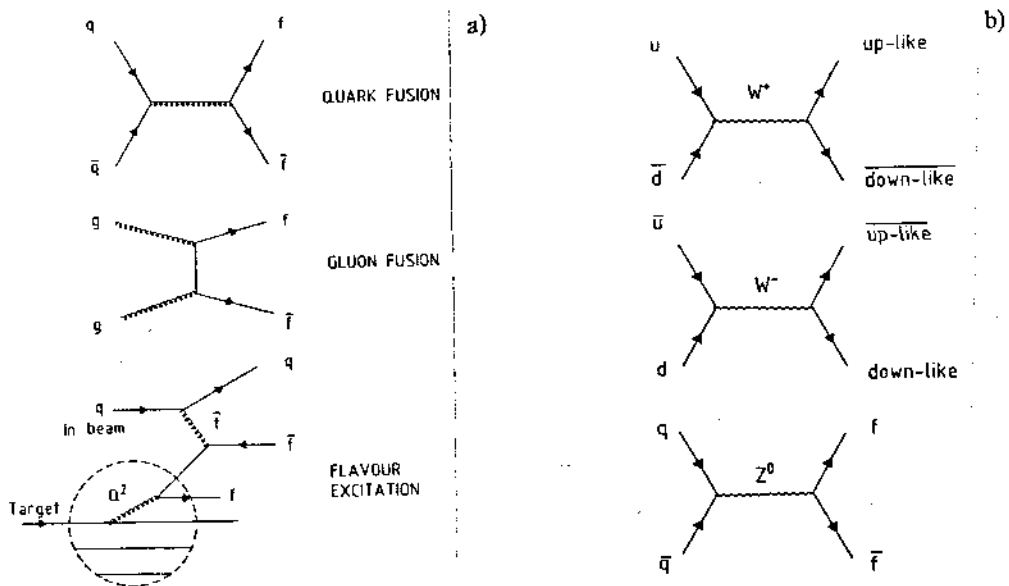


Fig. 2 a) heavy quarks production mechanisms. b) W^{\pm} and Z^0 production mechanisms.

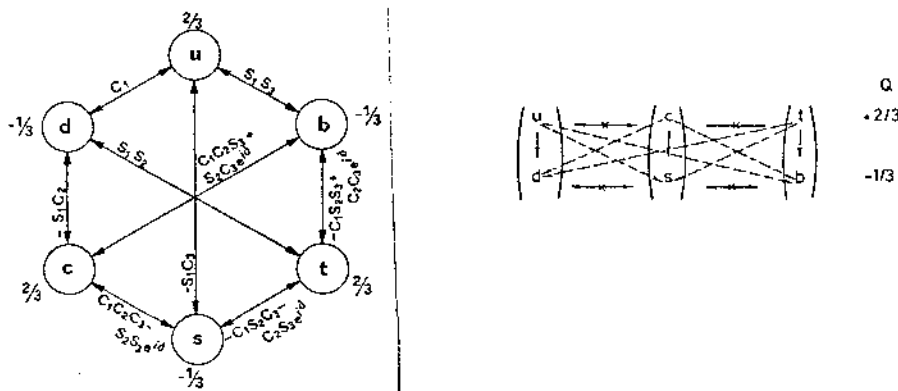


Fig. 3 Generalized Cabibbo angles.

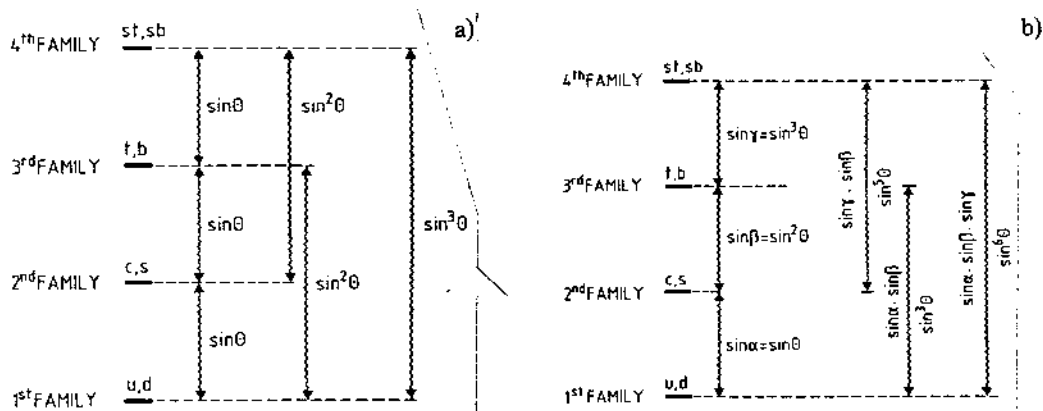


Fig. 4 Schematic diagram illustrating for a quark the probability to jump between two families: a) standard theory, b) as suggested by the beauty life time.

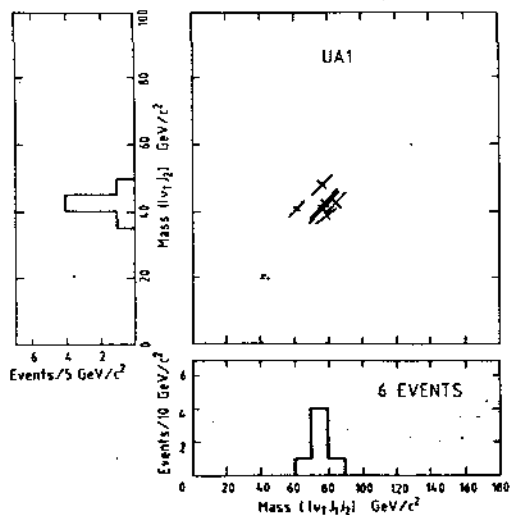


Fig. 5 UA1 results: invariant masses combinations for 6 events of the type $pp\bar{p} \rightarrow l + \text{jet} + \text{jet} + (\text{missing energy})$.

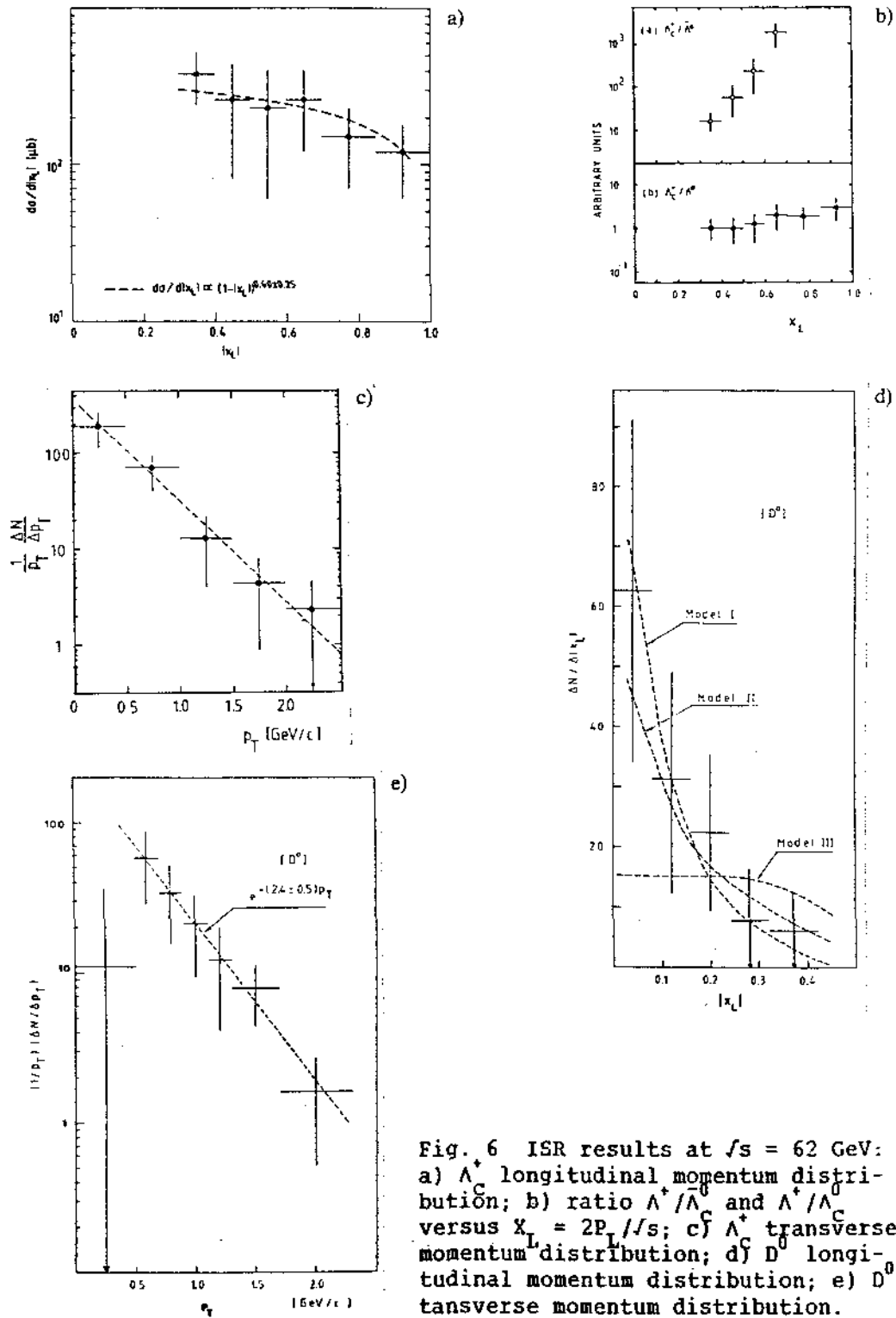


Fig. 6 ISR results at $\sqrt{s} = 62$ GeV: a) Λ^+ longitudinal momentum distribution; b) ratio Λ^+/Λ^0 and Λ^+/Λ_C^+ versus $x_L = 2P_L/\sqrt{s}$; c) Λ^+ transverse momentum distribution; d) D^0 longitudinal momentum distribution; e) D^0 transverse momentum distribution.

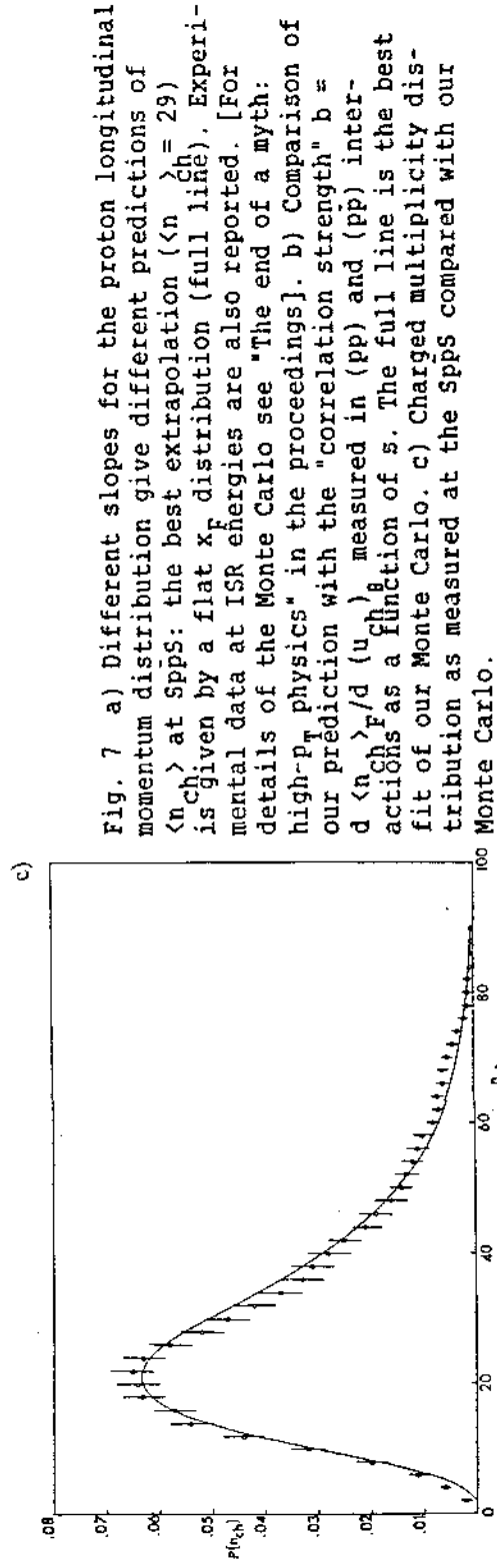
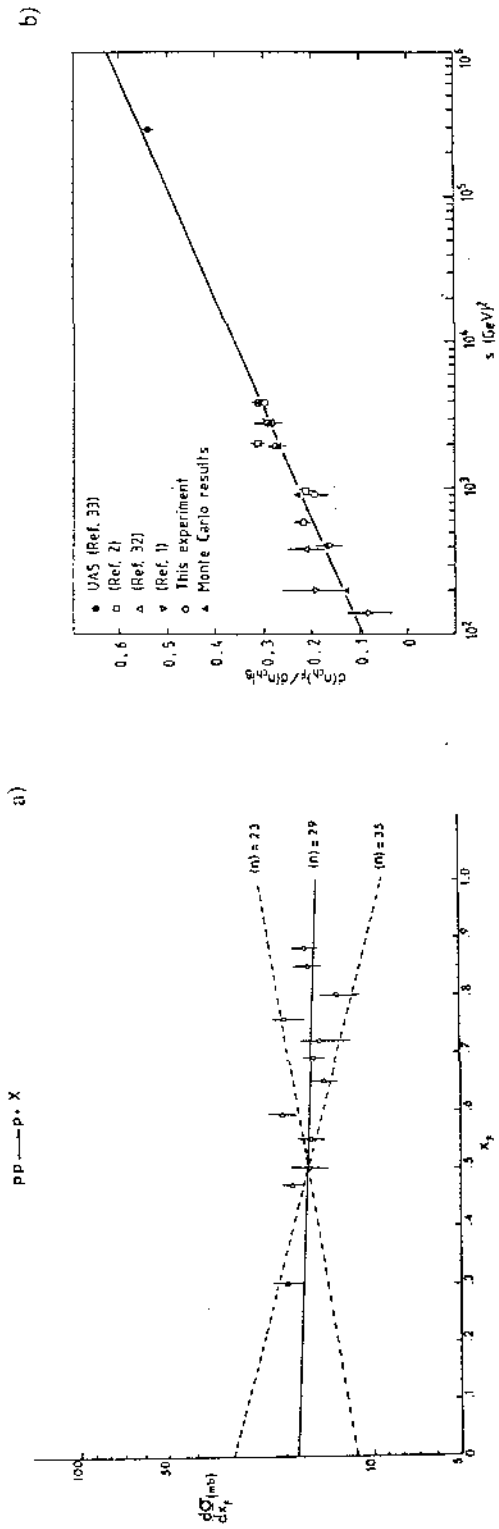


Fig. 7 a) Different slopes for the proton longitudinal momentum distribution give different predictions of $\langle n_{ch} \rangle$ at Spps: the best extrapolation ($\langle n_{ch} \rangle = 29$) is given by a flat x_F distribution (full line). Experimental data at ISR energies are also reported. [For details of the Monte Carlo see "The end of a myth: high- p_T physics" in the proceedings]. b) Comparison of our prediction with the "correlation strength" $b = d \langle n_{ch} \rangle / d \ln s$ measured in (pp) and (pp) interactions as a function of s . The full line is the best fit of our Monte Carlo. c) Charged multiplicity distribution as measured at the Spps compared with our Monte Carlo.

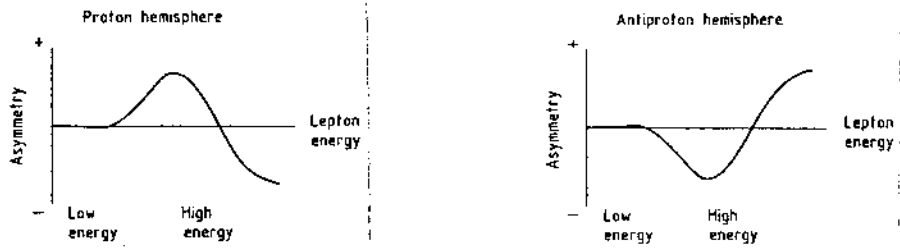


Fig. 8 Qualitative behaviour of the lepton charge asymmetry.

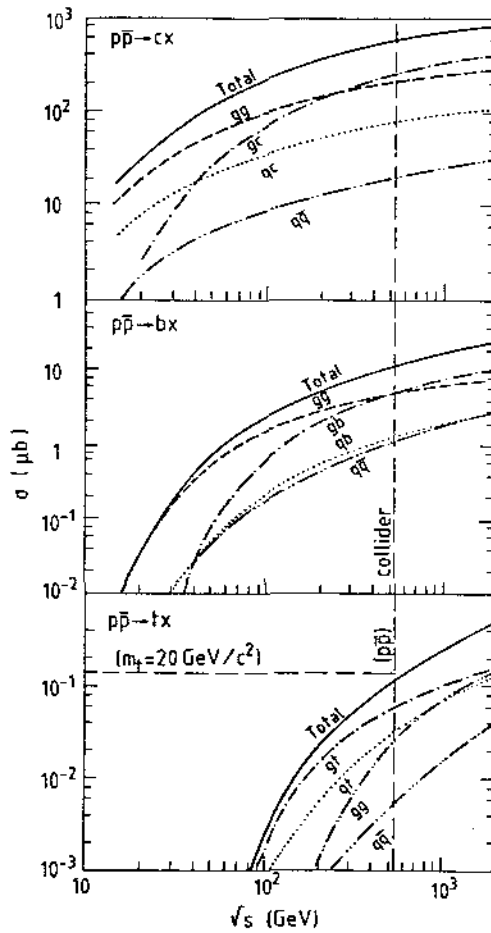


Fig. 9 Total cross-sections for top, beauty and charm in function of \sqrt{s} as predicted by QCD flavour excitation.

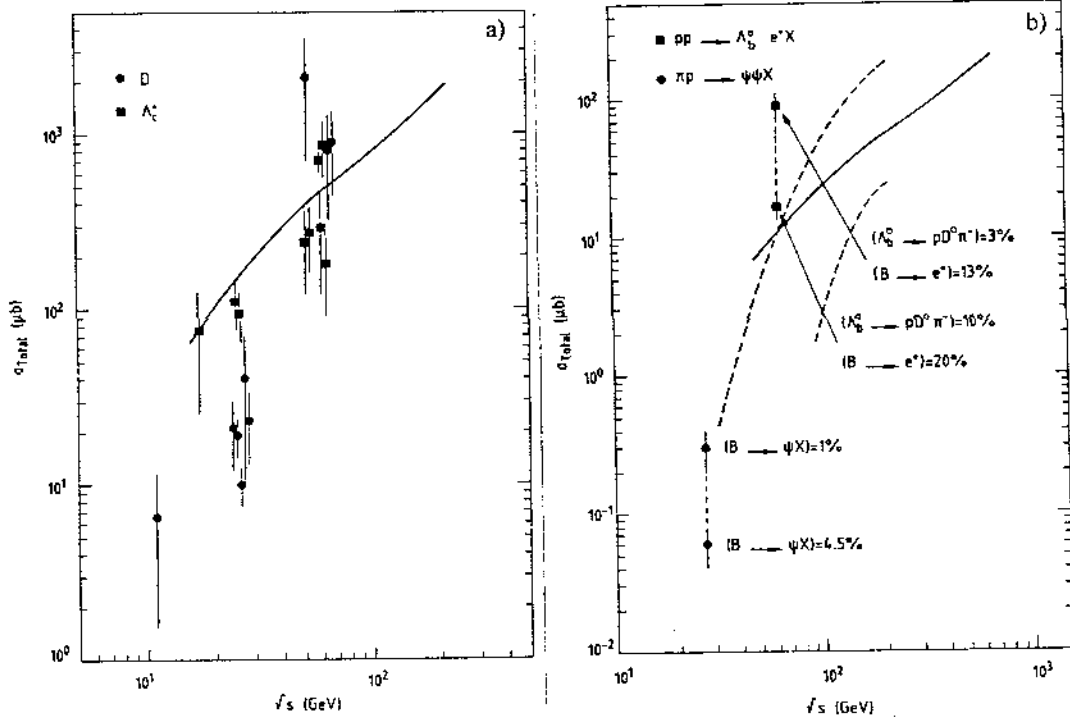


Fig. 10 a) The full line is charm cross section as extrapolated from the strange quark production; b) Beauty cross-section as extrapolated from charm (dashed lines) and strange (full line). The available experimental data are also reported.

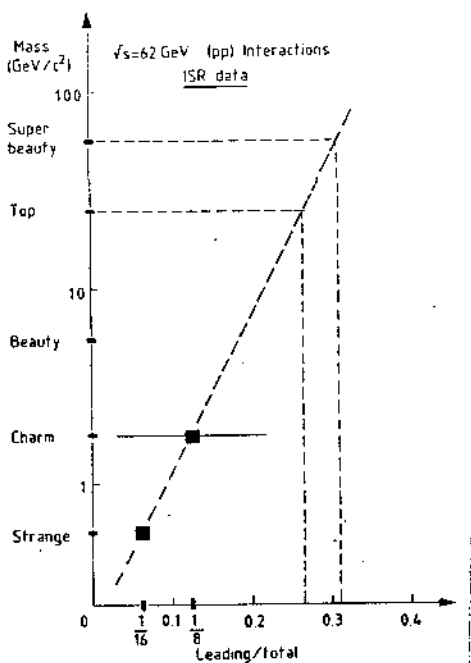


Fig. 11. Linear extrapolation of the ratio Leading/Total in function of the quark mass.

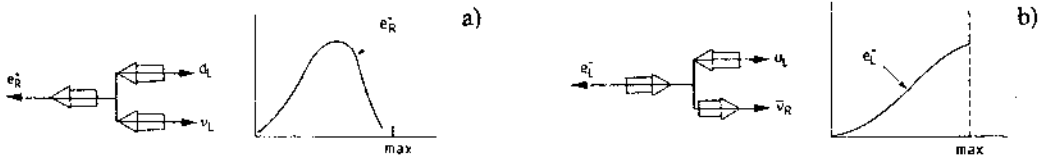


Fig. 12 Lepton energy spectrum for the semileptonic decay of a quark: a) up-like, b) down-like.

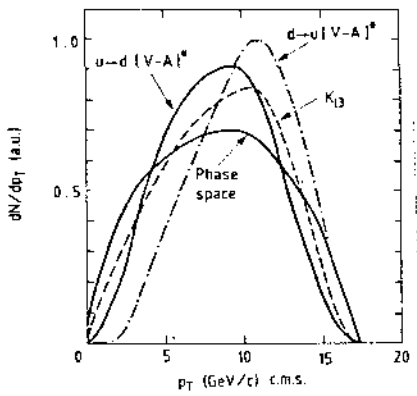


Fig. 13 Lepton transverse momentum spectrum for the semileptonic decay of a quark under various hypothesis.

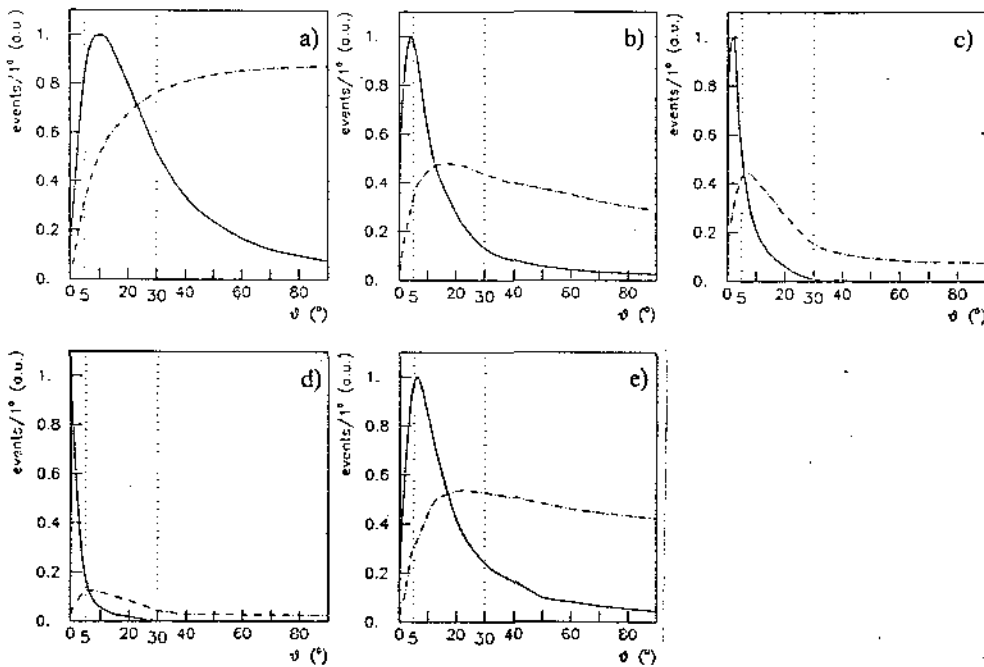


Fig. 14 Angular distributions of muons from primary decays of baryons (full line) and mesons (dashed and dotted lines): a) $sb (55 \text{ GeV}/c^2) \rightarrow t (25 \text{ GeV}/c^2) \mu\nu$; b) $t (25 \text{ GeV}/c^2) \rightarrow b\mu\nu$; c) $b \rightarrow c\mu\nu$; d) $c \rightarrow s\mu\nu$; e) $t (35 \text{ GeV}/c^2) \rightarrow b\mu\nu$.

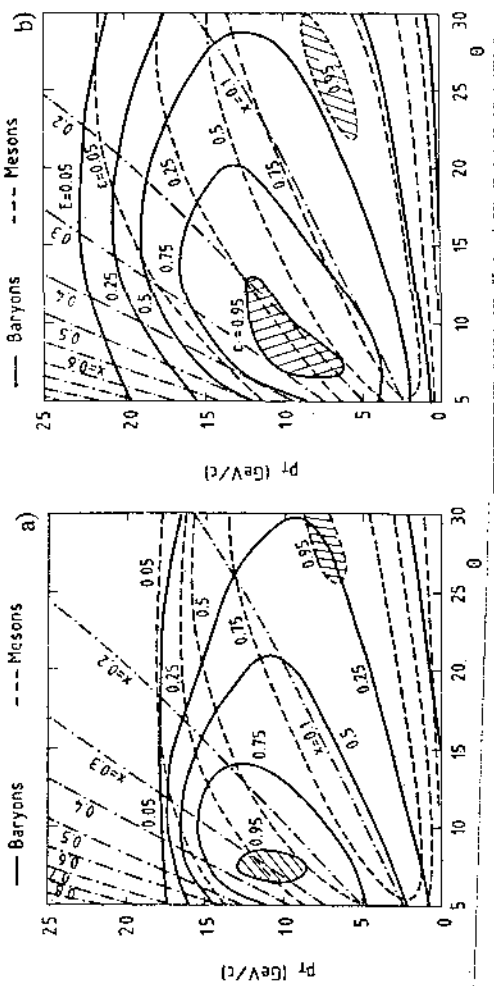


Fig. 16 Iso-rate curves in the p_T - θ plane, for
 a) t ($35 \text{ GeV}/c^2$) $\rightarrow b\mu\nu$,
 b) sb ($55 \text{ GeV}/c^2$) $\rightarrow t$
 ($25 \text{ GeV}/c^2$) $\mu\nu^2$
 c) t ($25 \text{ GeV}/c^2$) $\rightarrow b\mu\nu$.

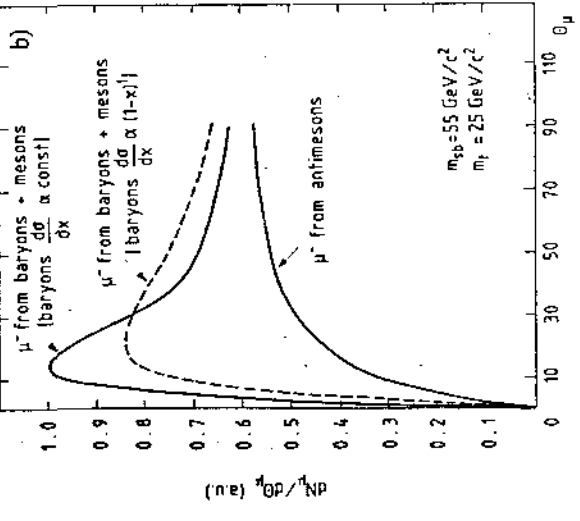
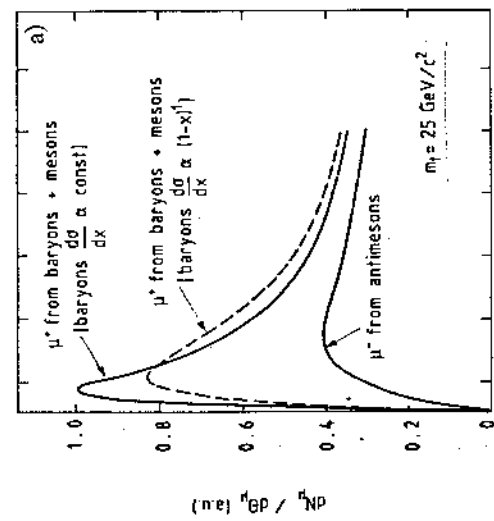


Fig. 15 Muon angular distribution in the decay of a) $t \rightarrow b\mu\nu$ and b) $sb \rightarrow t\mu\nu$.

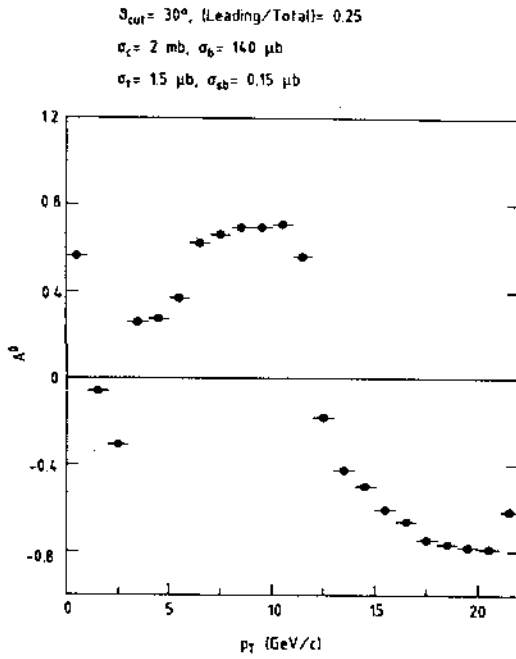


Fig. 17 Expected ideal asymmetry A_0 as computed via Monte Carlo.

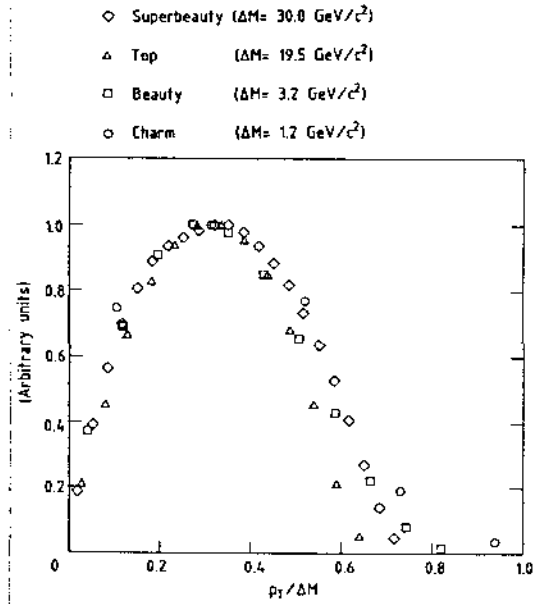


Fig. 18 Distributions of muons coming from the primary decay of heavy quarks plotted in the variable $p_T/\Delta m$.

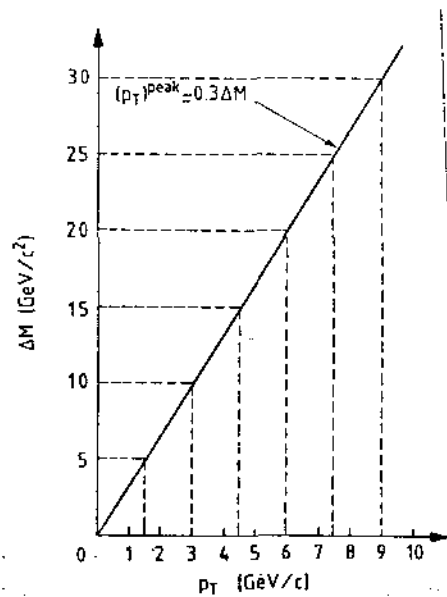


Fig. 19 Transverse muon momentum versus the difference in mass between parent and daughter particles in a heavy quark decay.

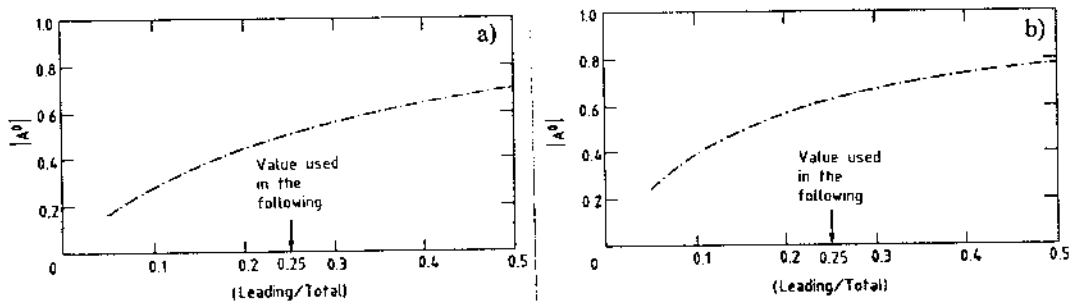


Fig. 20 Ideal Assymetry, A^0 in function of the ratio (Leading/Total) for top = 25 GeV/c² (a) and Superbeauty = 55 GeV/c² (b).

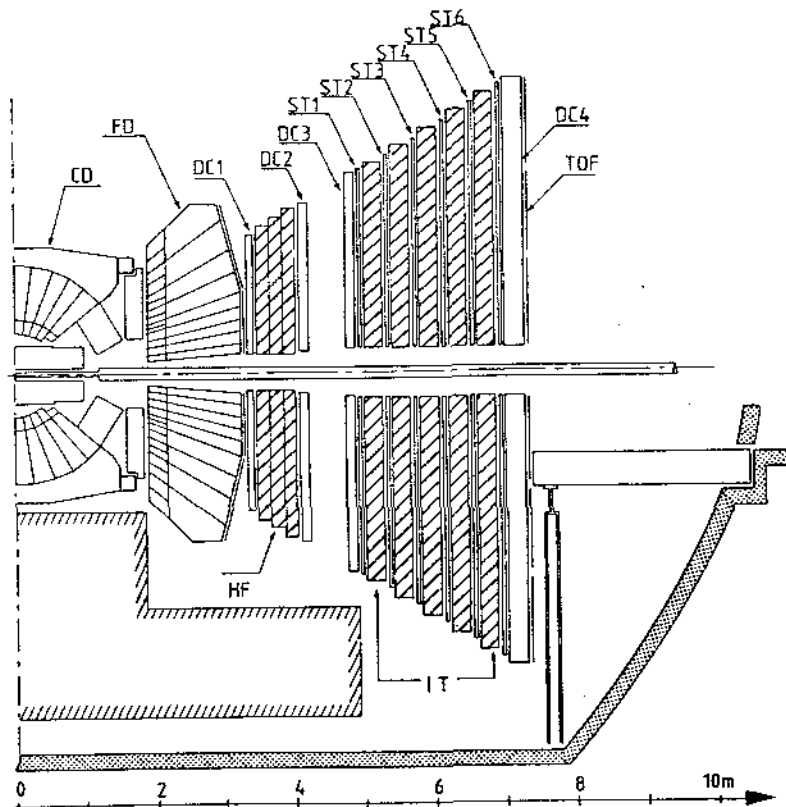


Fig. 21 Schematic view of the Lepton Asymmetry Analyser (LAA). CD = UA2 Central Detector, FD = UA2 Forward Detector, DC = Drift Chambers, ST = Limited Streamer Tubes, HF = Iron Absorber, IT = Iron Toroids.

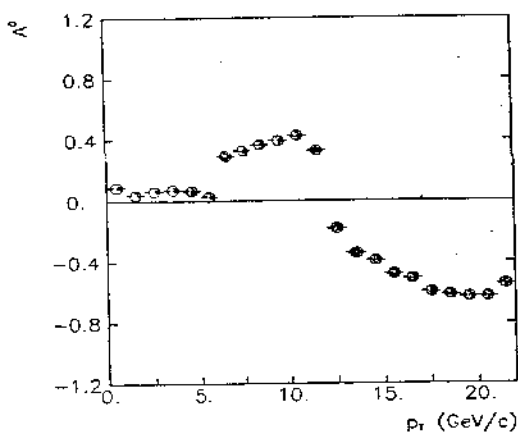


Fig. 22 Ideal Asymmetry A^0 as seen by the LAA apparatus.

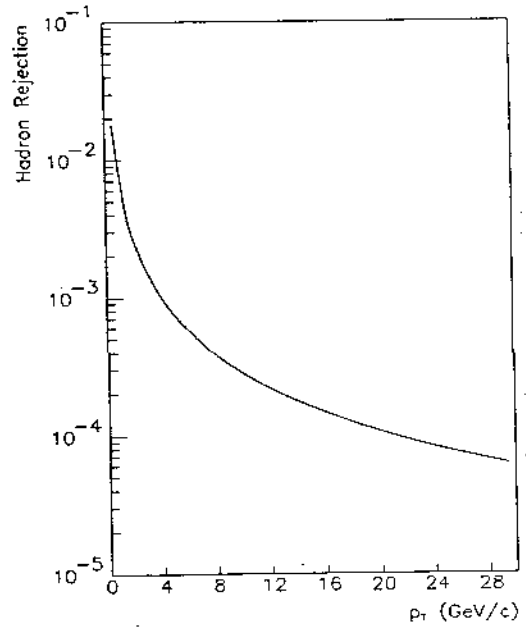


Fig. 23 Hadron rejection versus transverse momentum for LAA.

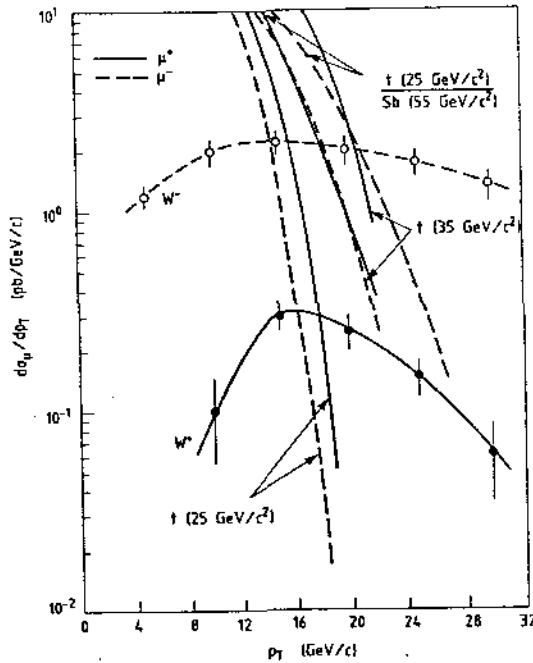


Fig. 24 Muon background from W^+ and Z^0 decay compared with those coming from heavy flavours.

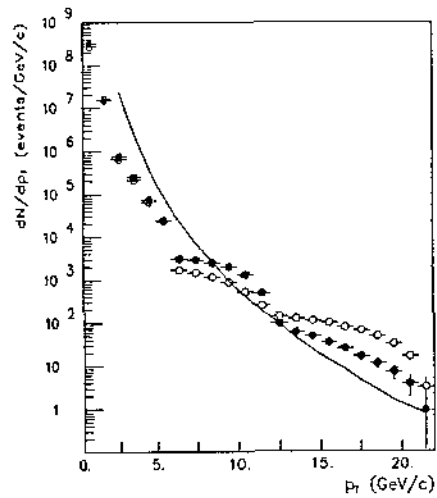


Fig. 25 Inclusive transverse momentum distribution for sb (55 GeV/c²) and top (25 GeV/c²) production [$\sigma_{sb} = 0.01 \mu\text{b}$; $\sigma_t = 0.1 \mu\text{b}$; $\sigma_b = 10 \mu\text{b}$; $\sigma_c = 2 \text{mb}$]. Integrated luminosity $\approx 10 \text{pb}^{-1}$. Full dots = μ^+ , empty dots = μ^- , full line = hadrons x rejection.

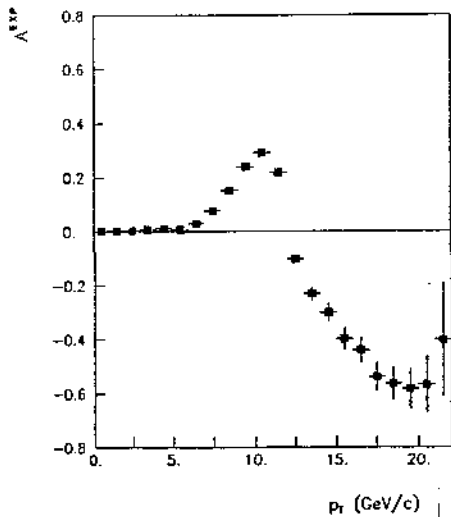


Fig. 26 The experimental Asymmetry A^{exp} versus the transverse momentum of the muon. The Monte Carlo parameters are those used in fig. 25.

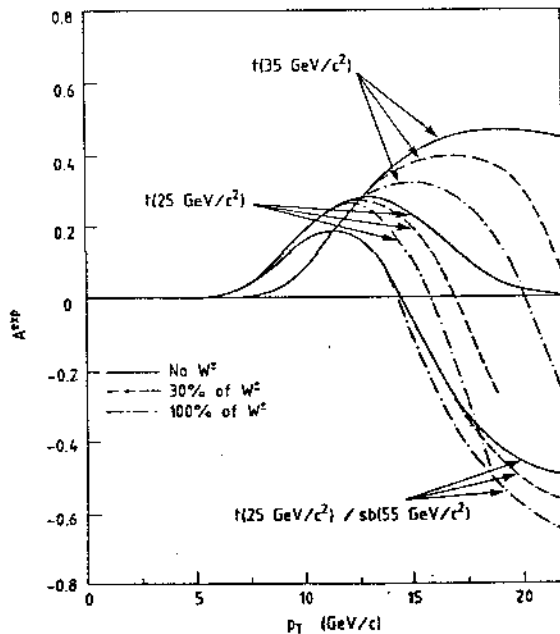


Fig. 27 Effect of the decay $W^+ \rightarrow \nu \mu$ on A^{exp} .

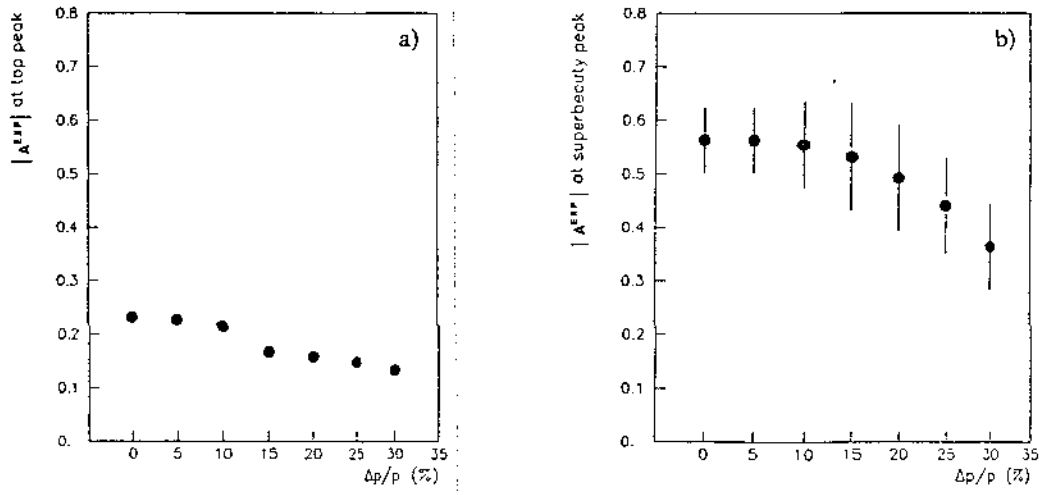


Fig. 28 Variation of A^{exp} , at its peak, in function of the momentum resolution of the LAA for a) top ($25 \text{ GeV}/c^2$); b) sb ($55 \text{ GeV}/c^2$).

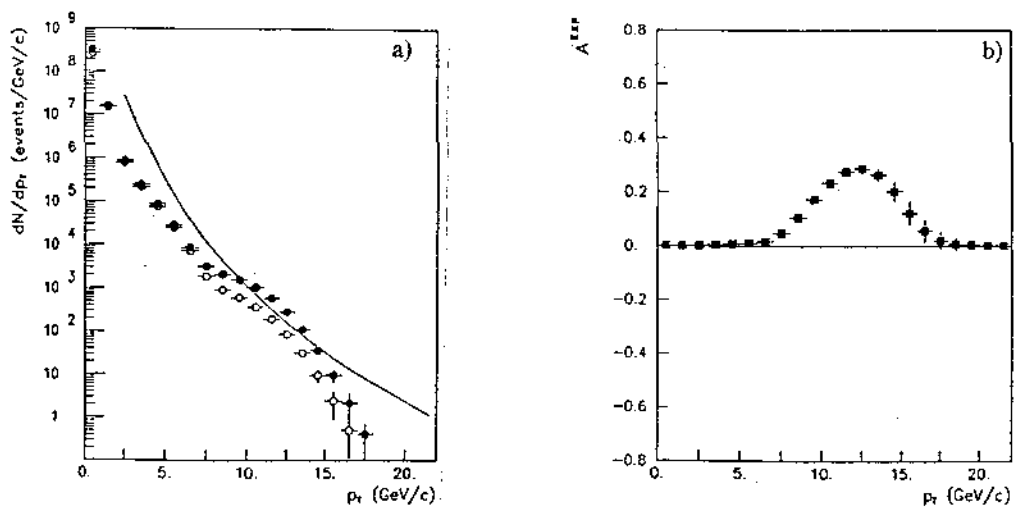


Fig. 29 Top ($25 \text{ GeV}/c^2$) production. a) muons and hadrons p_T distributions (same symbols as fig. 25). b) A^{exp} versus p_T .

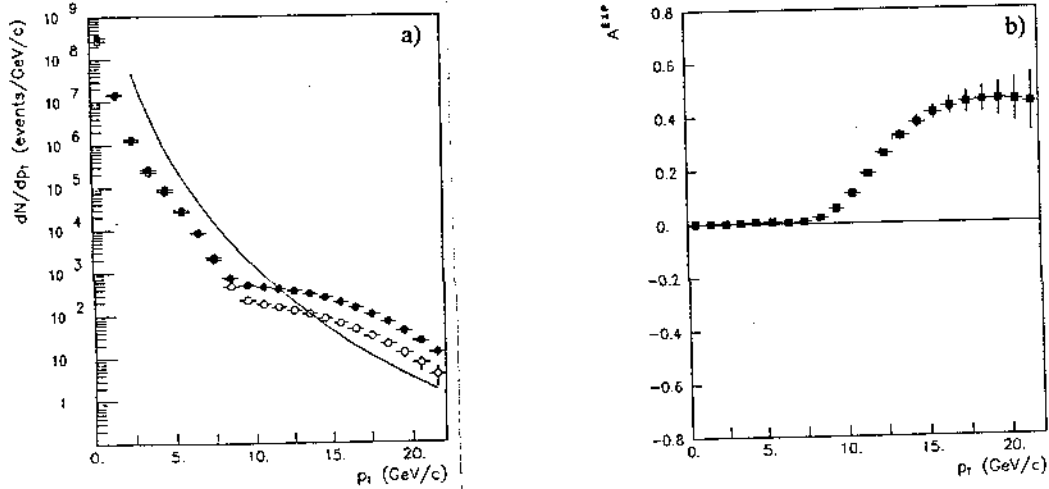


Fig. 30 As fig. 29 but for top ($35 \text{ GeV}/c^2$) production.

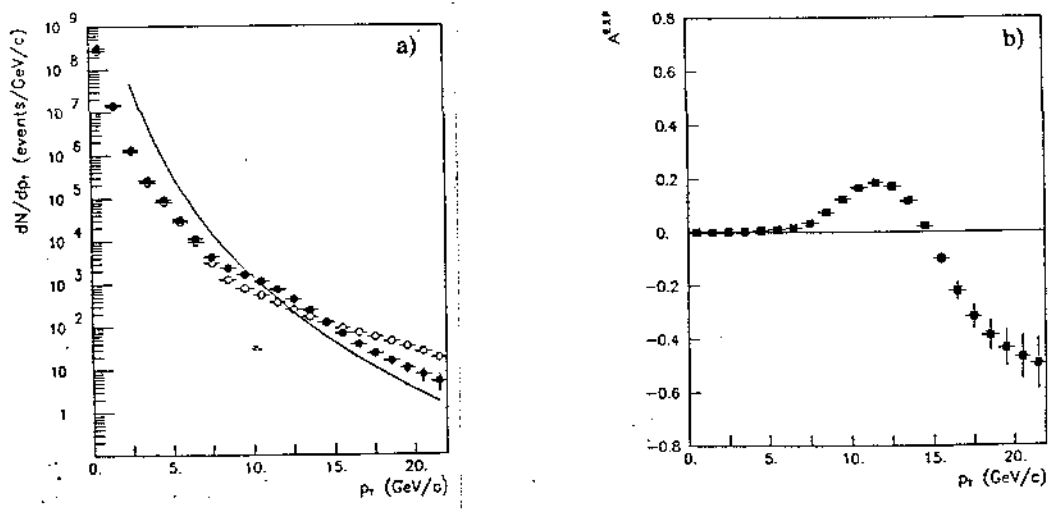


Fig. 31 As fig. 29 but for Superbeauty ($55 \text{ GeV}/c^2$) and Top ($25 \text{ GeV}/c^2$) production.

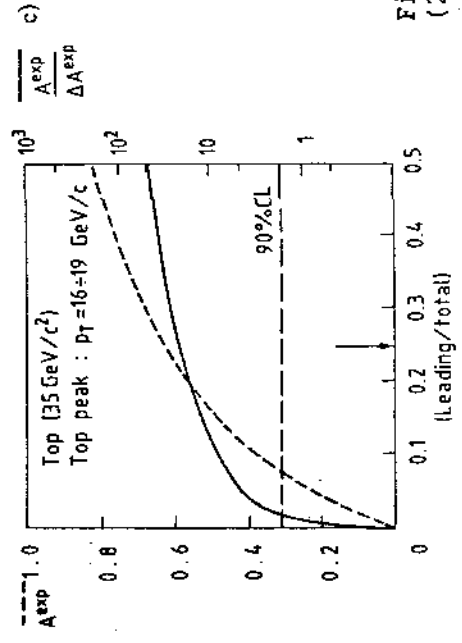
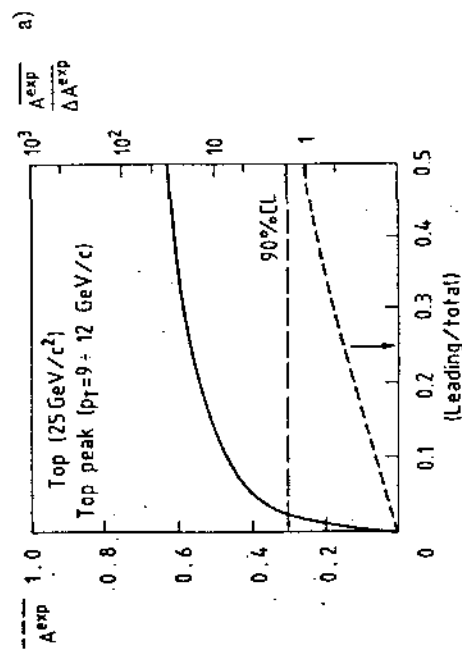
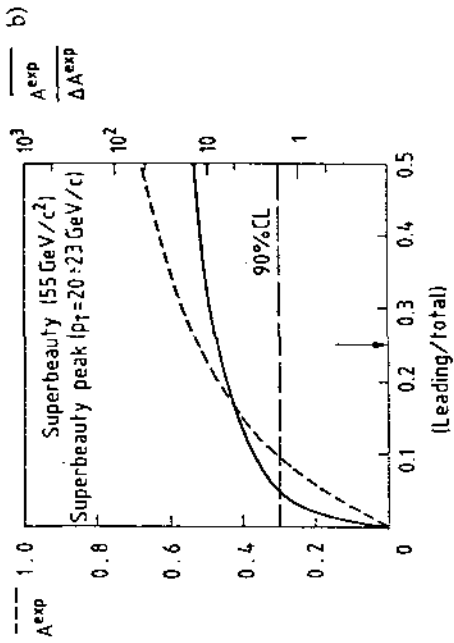


Fig. 31 As fig. 29 but for Superbeauty (55 GeV/c²) and Top (25 GeV/c²) production.

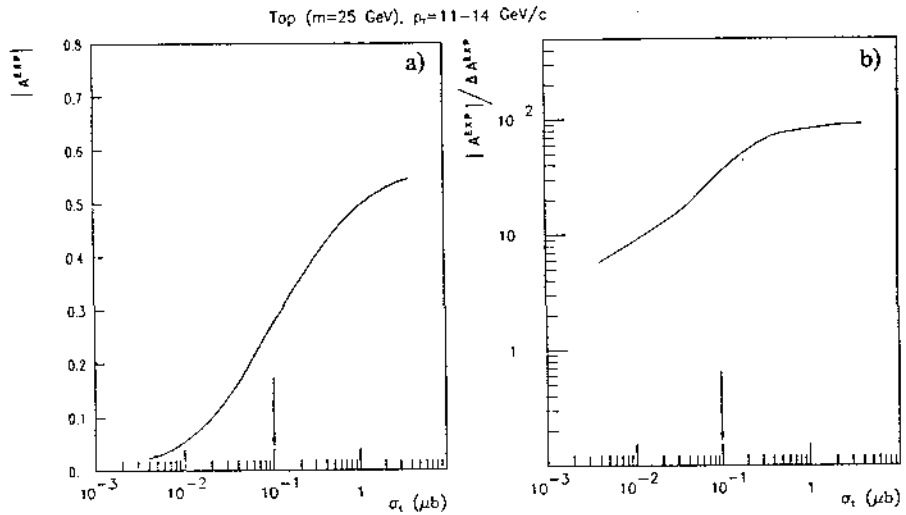


Fig. 33 The asymmetry parameter A^{exp} (a) and its statistical significance (b) versus the production cross-sections for top ($25 \text{ GeV}/c^2$) production.

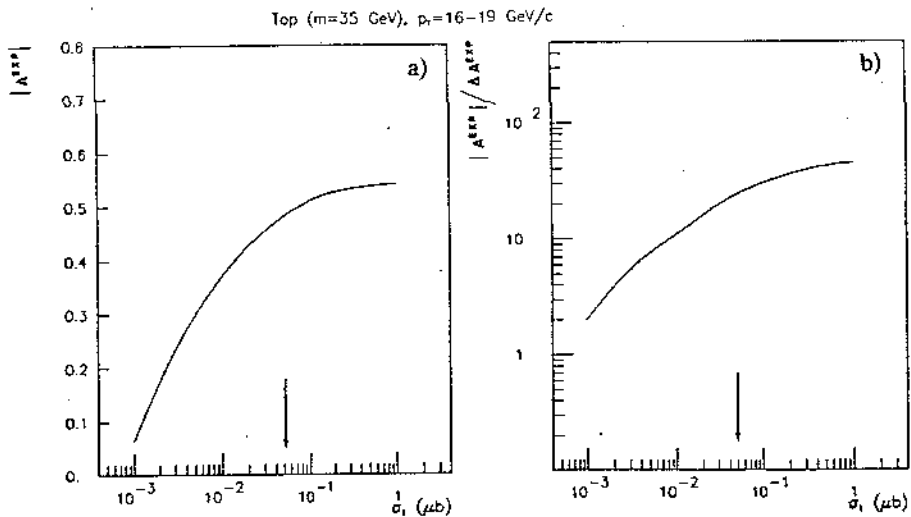


Fig. 34 As fig. 33 but for top ($35 \text{ GeV}/c^2$) production.

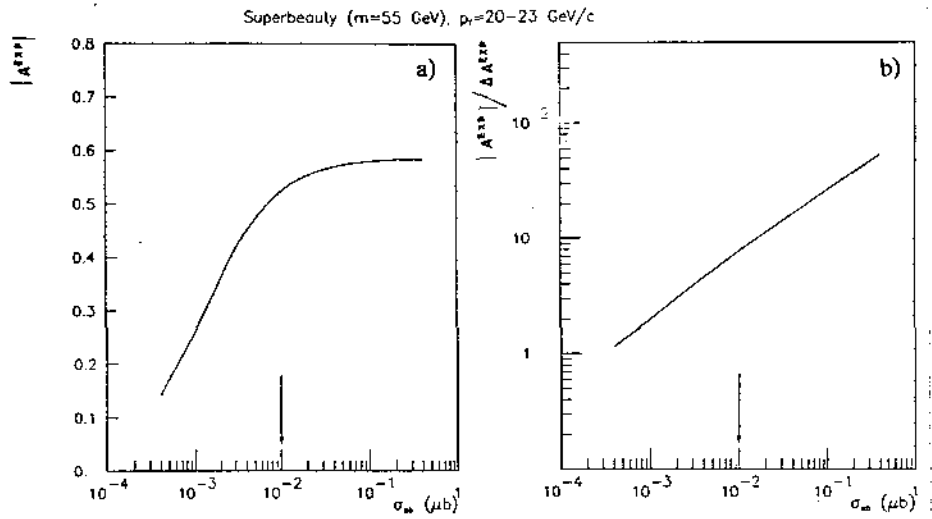


Fig. 35 As fig. 33 but for Superbeauty ($55 \text{ GeV}/c^2$) production.

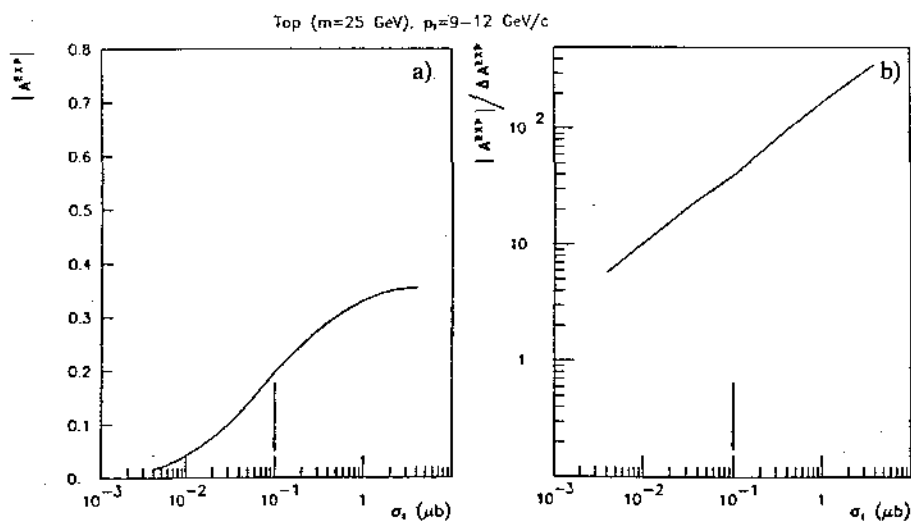


Fig. 36 As fig. 33 but here we consider the top ($25 \text{ GeV}/c^2$) decay when the top comes from Superbeauty.

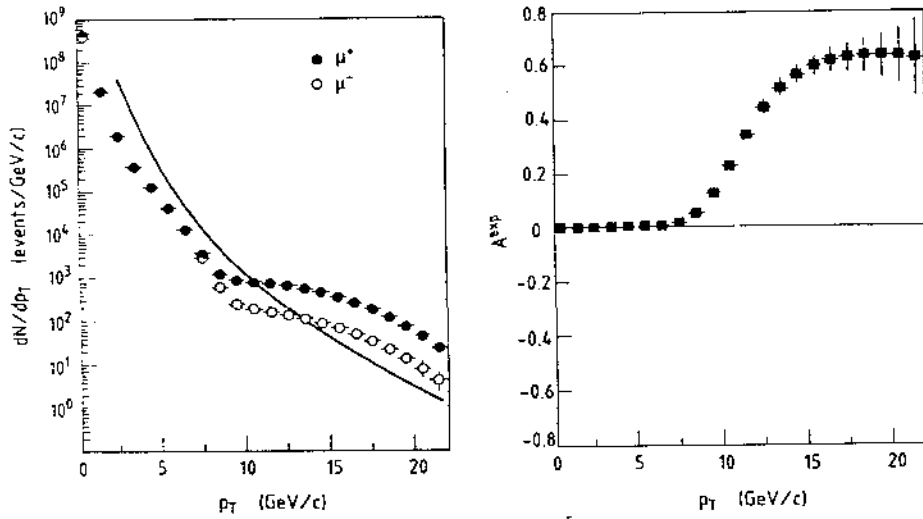


Fig. 37 As fig. 29 but for top ($35 \text{ GeV}/c^2$) production and $(d\sigma/dx)(\text{baryons}) \propto \text{const.}$

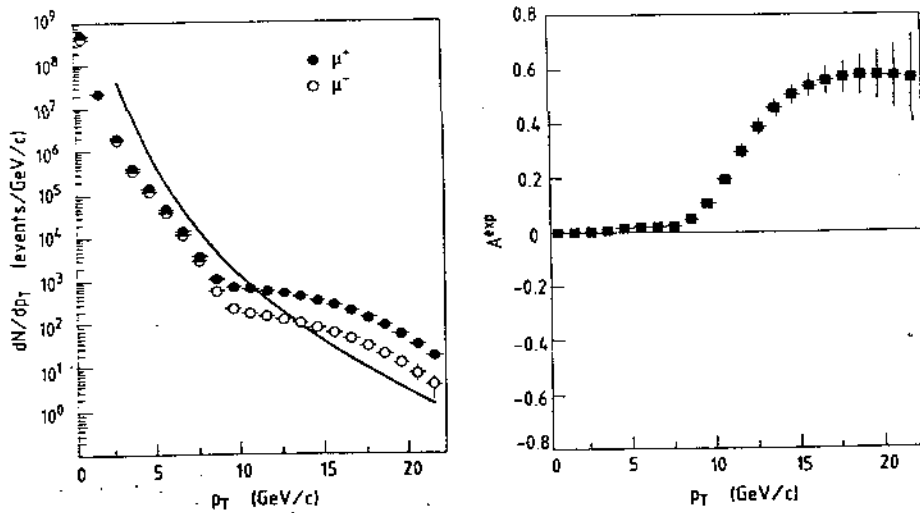


Fig. 38 As fig. 37 but with $(d\sigma/dx)(\text{baryons}) \propto (1 - x)$.

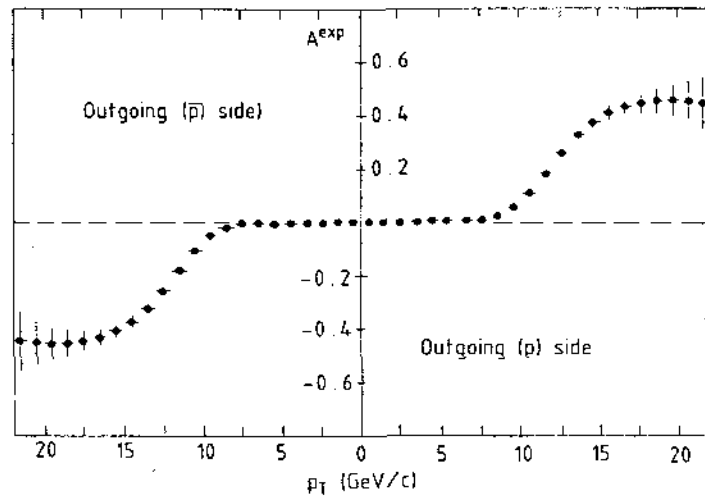


Fig. 39 A^{exp} versus p_T , as seen in LAA with $\delta p/p = 20\%$. The Monte Carlo simulation is with the following inputs: $\sigma_t = 0.05 \mu\text{b}$ (top = $35 \text{ GeV}/c^2$), $\sigma_{b\bar{b}} = 10 \mu\text{b}$, $\sigma_c = 2 \text{ mb}$ and integrated luminosity of 10 pb^{-1} .

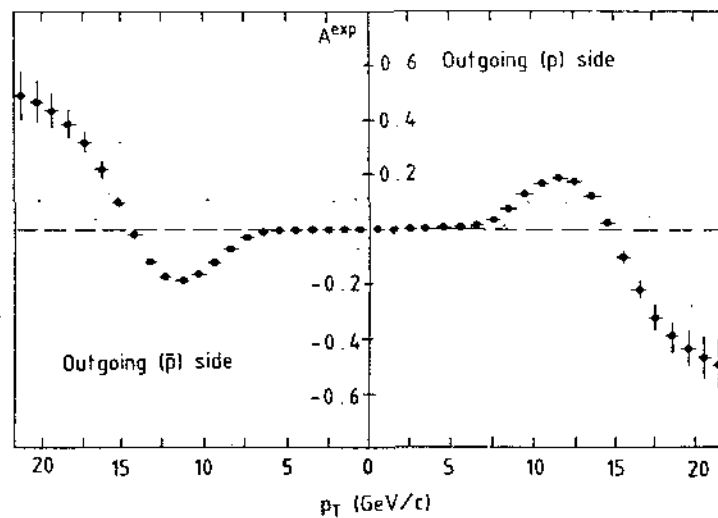


Fig. 40 As fig. 39 but with the following inputs in the Monte Carlo: $\sigma_{b\bar{b}} = 0.01 \mu\text{b}$, $\sigma_t = 0.1 \mu\text{b}$, $\sigma_b = 10 \mu\text{b}$, $\sigma_c = 2 \text{ mb}$ and integrated luminosity of 10 pb^{-1} .

**III-5. LAA Proposal: Memorandum to the Chairman
of the SPSC, August 2, 1984.**

August 2, 1984

5 - MEMORANDUM

To : L. Foa' - Chairman of the SPSC

From : A. Zichichi - BCFL Collaboration

Subject : Proposal for future activity at the $p\bar{p}$ Collider and LAA

Copy to : R. Budde - Secretary of the SPSC

P. Bloch

M. Bourquin

P.L. Braccini

A. Donnachie

J. Drees

F. Dydak

P. Giromini

W. Hoogland'

J. Iliopoulos

F. Jacquet

R. Klanner

I. Mannelli

G. Myatt

B. de Raad

A. Staude

G. Veneziano

Following our proposal to build a Lepton Asymmetry Analiser (LAA) to be used in conjunction with the UA2 set-up, we would like to clarify some points.

1 - The LAA proposal was not intended to be an instrument without future. We consider the LAA the first step of a super-detector to be constructed for the second generation experiments at the CERN Collider. We have already dedicated some of our time to study a detector much more powerful than existing ones. The CERN Collider will start its improved performance period in 1987. An improved Collider needs improved detectors.

We understand that a fully new detector would have been difficult to be ready by 1987: this is why we thought of proposing the first part of a new detector.

The LAA has the structure to be considered the completion of the new detector. "Inside" LAA there will be the UA2 detector in the first stage and the second generation detector in the final stage.

2 - In our proposal to the SPSC we discussed LAA only in its function as a detector to establish the "up"-like or "down"-like nature of new heavy flavours produced at the Collider. It should be emphasized that the measurement of a mass has nothing to do with the type of "flavour" (up-like or down-like) associated with the mass. So the problem is: how much are we prepared to pay in order to know the mass of a new state, and how much money is worth spending in order to know the "flavour" of a new state.

3 - Notice that the direct production of new heavy flavours can provide a great deal of information on QCD processes. Last example: the "discovery" of new production mechanisms for charm in the ISR energy range.

4 - The present UA1 data on a new heavy mass object does not exclude for the top mass a value consistent with the naive expectations shown in Fig. 1 of our proposal [CERN/SPSC/84-33 - SPSC/P200]: i.e. $m_t \approx 25 \text{ GeV}/c^2$. If this is corroborated by further evidence, it could be that the "down-like" member of the 4th family, the superbeauty, would really be at a mass expected from the above quoted "naive" extrapolation, i.e. $m_{sb} \approx 55 \text{ GeV}/c^2$. In this case the W-method is out of question to detect, even as a mass state, the "superbeauty". In fact the down-like member of the 4th family is Cabibbo favoured to be produced, in the W-decay, together with the "up-like" member of the same family: i.e. the supertop. As its mass is expected to be in the 200 GeV range, the W-decay into the flavours of the 4th family, is forbidden by energy conservation. The decay into the up-like flavour of the 3rd family and the down-like flavour of the 4th family is Cabibbo forbidden.

5 - The proposed set of reasonable values for heavy-flavour

- i) production cross-sections,
- ii) (leading/total) ratio,
- iii) 3-body dominant decay,
- iv) semileptonic branching ratios,

is the starting point to justify the LAA. In fact the limits of sensitivity to an asymmetry are such that it would appear unreasonable to make more pessimistic hypotheses. Nevertheless, following the SPSC request, we have considered also a set of combined pessimistic assumptions and the asymmetry appears to be visible in a wide range of possibilities. We will present in a forthcoming memorandum the data regarding the main further points raised by the SPSC Referees on our LAA proposal.

6 - Let us nevertheless suppose that for a series of unreasonable coincidences (for example $m_t = m_{sb}$) the lepton asymmetry is zero. We have not emphasized

in our proposal that, in this case, the μ -spectrum -not the subtraction (μ^+ - μ^-) but the sum ($\mu^+ + \mu^-$)- would show a deviation (the graph will be included in our next memorandum to the SPSC). This deviation would be the starting point to analyse, in conjunction with the UA2 detector, the detailed structure of the events associated with it. Notice that we have as an important tool the sign of the muon, to be studied in association with the event in the UA2 detector. It could be that the patterns associated with opposite muon charges would be different.

- 7 - Let us emphasize that the $p\bar{p}$ Collider should be exploited at the maximum level of machine and technical performances open to all physics possibilities.

Apart from the expected "new" heavy flavours, the following new phenomena can be investigated with the LAA coupled to the UA2 detector:

- i) (μ -jet) events,
- ii) (μ -e) events,
- iii) (μ -e) events with jets,
- iv) (μ -e) with missing energy plus jets,
- v) (multijets) events with μ and missing energy.

The above list is just an example of events associated with well identified muons in LAA. Genuine muon events can be studied if LAA is available. It should not be forgotten that, in addition to the expected events (top, superbeauty, supertop, Higgs, supersymmetric particle states, new leptons), the search for new states should be based on the capabilities of the experimental set-up. The μ phenomenology associated with the event structure observed in a powerful central detector should be the tool available for the exploitation of the ACOL Collider age.

- 8 - Let us clarify our views on UA1 and D0.

i) UA1 can never reach our muon selection power. Our detector has the further advantage of being the first part of a new super-detector. It should be remarked that the laboratory policy has been to encourage competitive set-ups. At LEP this number is greater than two.

ii) D0 can do what we can do. In fact they are planning a LAA with $(3^\circ \pm 30^\circ)$ aperture in θ . The fact that a LAA-like detector is installed at Fermilab should, by analogy with the above point i), bring to the conclusion that at least one LAA at CERN should be built. To appreciate this, it is enough to imagine if we would like to have it here, now.

9 - We have not emphasized our interest to extend at the Collider our ISR hadronic analysis. So far we have shown that (n_F/n_B) multiplicity correlations, the charged particle multiplicity distribution and the total multiplicity observed at the Collider are perfectly consistent with being the leading effect present and as important as it is at the ISR. The detailed study of hadronic physics at the Collider, as we have done at the ISR, is one of our physics programs for the super-detector.

Enclosed : recent publications of the BCFL Collaboration.

SCALING IN THE CHARGED PARTICLE MULTIPLICITY DISTRIBUTIONS AT THE ISR
AND COMPARISON WITH (e^+e^-) DATA.

M. Basile, G. Cara Romeo, L. Cifarelli, A. Contin, G. D'Ali,
C. Del Papa, B. Esposito, P. Giusti, T. Massam, R. Nania,
F. Palmonari, G. Sartorelli, M. Spinetti, G. Susinno, L. Votano
and A. Zichichi

Dipartimento di Fisica dell'Universita', Bologna, Italy

Istituto Nazionale di Fisica Nucleare, Bologna, Italy

CERN, Geneva, Switzerland

Istituto Nazionale di Fisica Nucleare, LNF, Frascati, Italy

ABSTRACT

The distributions of the charged particle multiplicities at the ISR are studied in terms of the effective energy available for particle production in (pp) interactions.

These distributions are found to scale once the effective energy, obtained via the leading subtraction method, is used.

A comparison with the charged particle distributions measured in (e^+e^-) annihilation shows a clear difference.

This could be interpreted in terms of, gluon induced and quark induced jets; where the gluon induced jets are characterized by a wider multiplicity distribution with respect to quark induced jets.

(Submitted to Nuovo Cimento Letters)

FIGURE CAPTIONS

Fig. 1 : The average charged multiplicity measured in (pp)⁶⁾ and (e⁺e⁻)^{10,12)}. Notice that the (pp) interactions are studied following our method of subtracting the leading proton effect. The quantity $\sqrt{(q_{\text{tot}}^{\text{had}})^2}$ is the effective energy available in a (pp) interaction once the leading effects are correctly taken into account (see text for its exact definition). The quantity $(\sqrt{s})_{e^+e^-}$ is the energy available in an (e⁺e⁻) annihilation.

Fig. 2 : The $n_{\text{ch}}/\langle n_{\text{ch}} \rangle$ distributions measured in our experiment in (pp) interactions, for two different intervals of $\sqrt{(q_{\text{tot}}^{\text{had}})^2}$ [open circles: $10 \leq \sqrt{(q_{\text{tot}}^{\text{had}})^2} \leq 15$ GeV; solid circles: $25 \leq \sqrt{(q_{\text{tot}}^{\text{had}})^2} \leq 30$ GeV]. The solid curve is the best fit to the (pp) data (this experiment). The nominal (pp) c.m. energy was $(\sqrt{s})_{\text{pp}} = 62$ GeV. The dashed line is the best fit to the (e⁺e⁻) data⁸⁻¹¹⁾

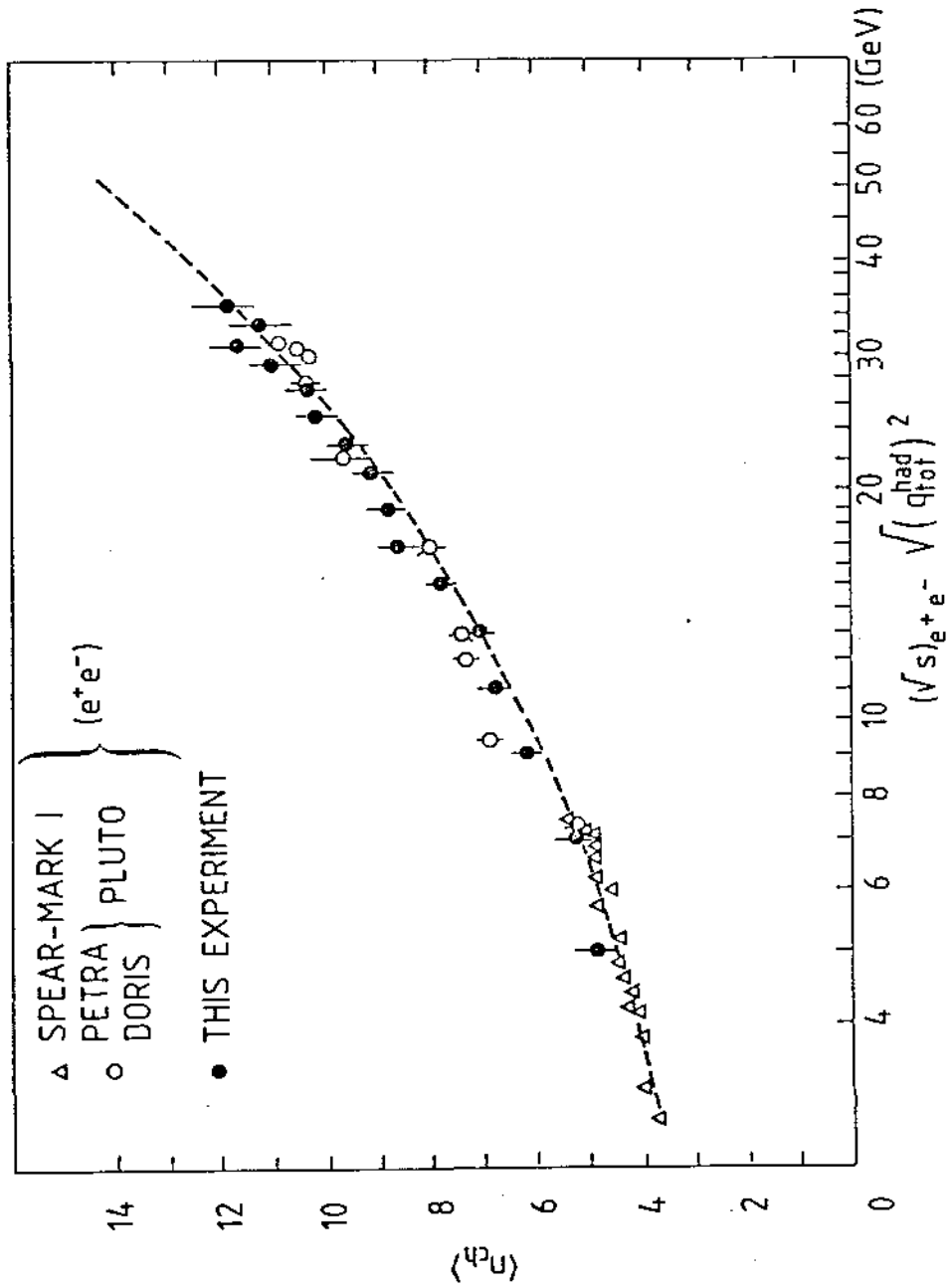


Fig. 1

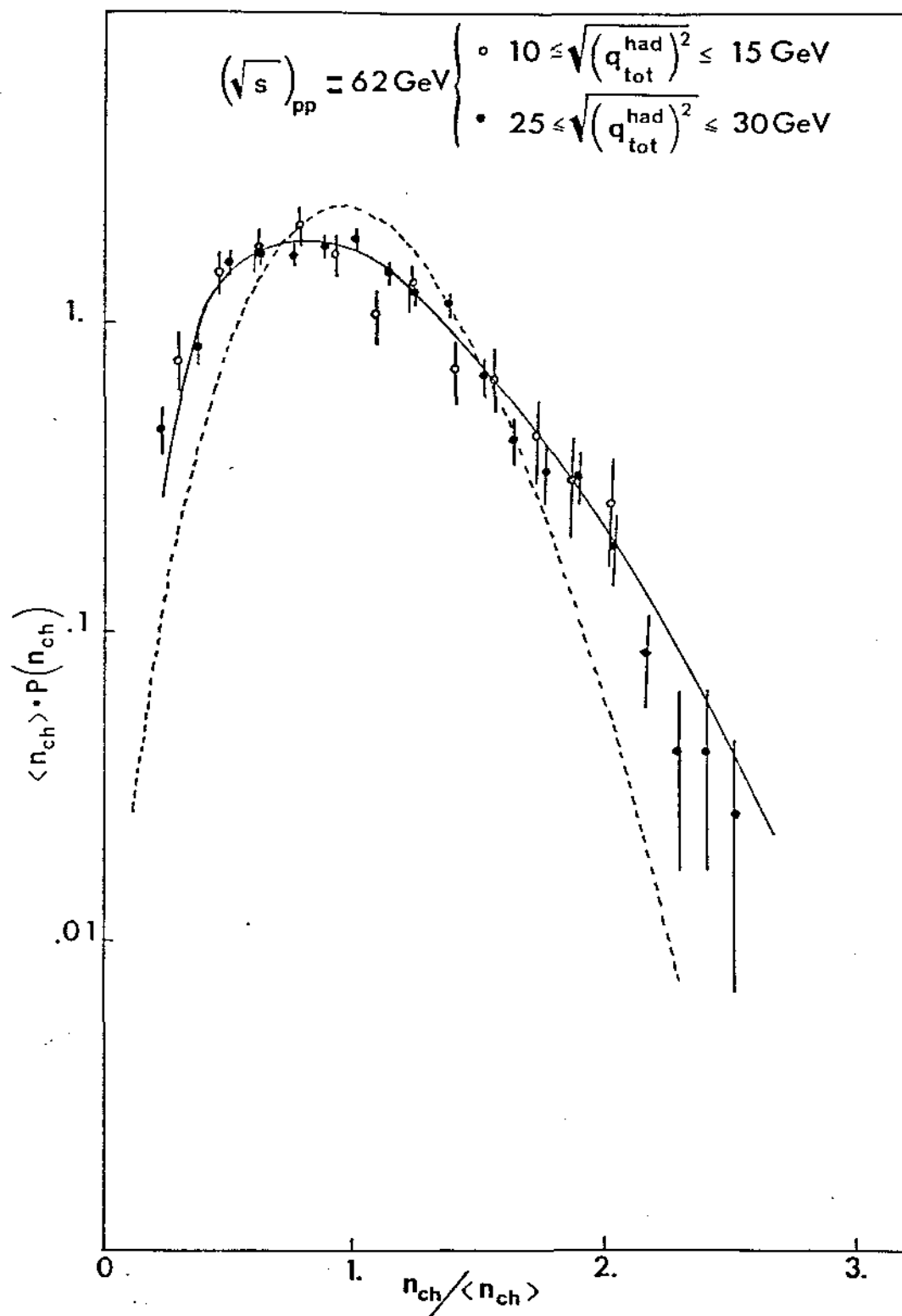


Fig. 2

THE LEADING EFFECT EXPLAINS THE CHARGED PARTICLE MULTIPLICITY
DISTRIBUTION OBSERVED AT THE CERN $p\bar{p}$ COLLIDER.

M. Basile, G. Cara Romeo, L. Cifarelli, A. Contin, G. D'Ali,
C. Del Papa, , P. Giusti, T. Massam, R. Nania, F. Palmonari,
G. Sartorelli, M. Spinetti, G. Susinno, L. Votano
and A. Zichichi

Dipartimento di Fisica dell'Universita', Bologna, Italy

Istituto Nazionale di Fisica Nucleare, Bologna, Italy

CERN, Geneva, Switzerland

Istituto Nazionale di Fisica Nucleare, LNF, Frascati, Italy

ABSTRACT

The assumption that the leading effect, and the charged-particle multiplicity distributions, measured at the ISR, scale with energy, and that the mean charged multiplicity, measured at the ISR, can be extrapolated up to Collider energy using the leading subtraction method, allows a prediction of the charged multiplicity distribution at the CERN $p\bar{p}$ Collider.

This prediction is found to be in excellent agreement with the experimental data obtained at the Collider by the UA5 group.

(Submitted to Nuovo Cimento Letters)

FIGURE CAPTIONS

- Fig.1 : The charged particle multiplicity distribution measured by the UA5 collaboration¹⁾ at $(\sqrt{s})_{p\bar{p}} = 540$ GeV. The dashed curve is the KNO³⁾ scaling prediction based on the fit by P. Slattery¹⁵⁾. The solid curve is the UA5 fit¹⁾.
- Fig.2 : The $n_{ch}/\langle n_{ch} \rangle$ distributions measured in our ISR experiment²⁾ in (pp) interactions, for two different intervals of $\sqrt{(q_{tot}^{had})^2}$ [open circles: $10 \leq \sqrt{(q_{tot}^{had})^2} \leq 15$ GeV; solid circles: $25 \leq \sqrt{(q_{tot}^{had})^2} \leq 30$ GeV]. The curve is the best fit to the data.
- Fig.3 : Inclusive differential cross-section $d\sigma/dx_F$ as a function of x_F ($x_F = 2p_L/\sqrt{s}$) measured^{8,9)} in the reaction $pp \rightarrow p + X$, at ISR energies. Open circles are Ref.8; solid circles are Ref.9.
- Fig.4 : The average charged multiplicities measured⁶⁾ in (pp) interactions at the ISR versus $\sqrt{(q_{tot}^{had})^2}$, i.e. using the leading subtraction method⁶⁾ (open circles). The average charged multiplicities measured^{13,14)} in (pp) interactions versus $(\sqrt{s})_{pp}$, i.e. using the standard method (solid circles). The open triangle is the average charged multiplicity measured by UA5 collaboration¹⁾ at the CERN $p\bar{p}$ Collider, again using the standard method. The dashed curve corresponds to formula (2) and the solid curve to formula (3) in the text.
- Fig.5 : The charged particle multiplicity distribution measured by UA5 collaboration¹⁾ at $(\sqrt{s})_{p\bar{p}} = 540$ GeV. The curve is our own prediction based on formula (4).

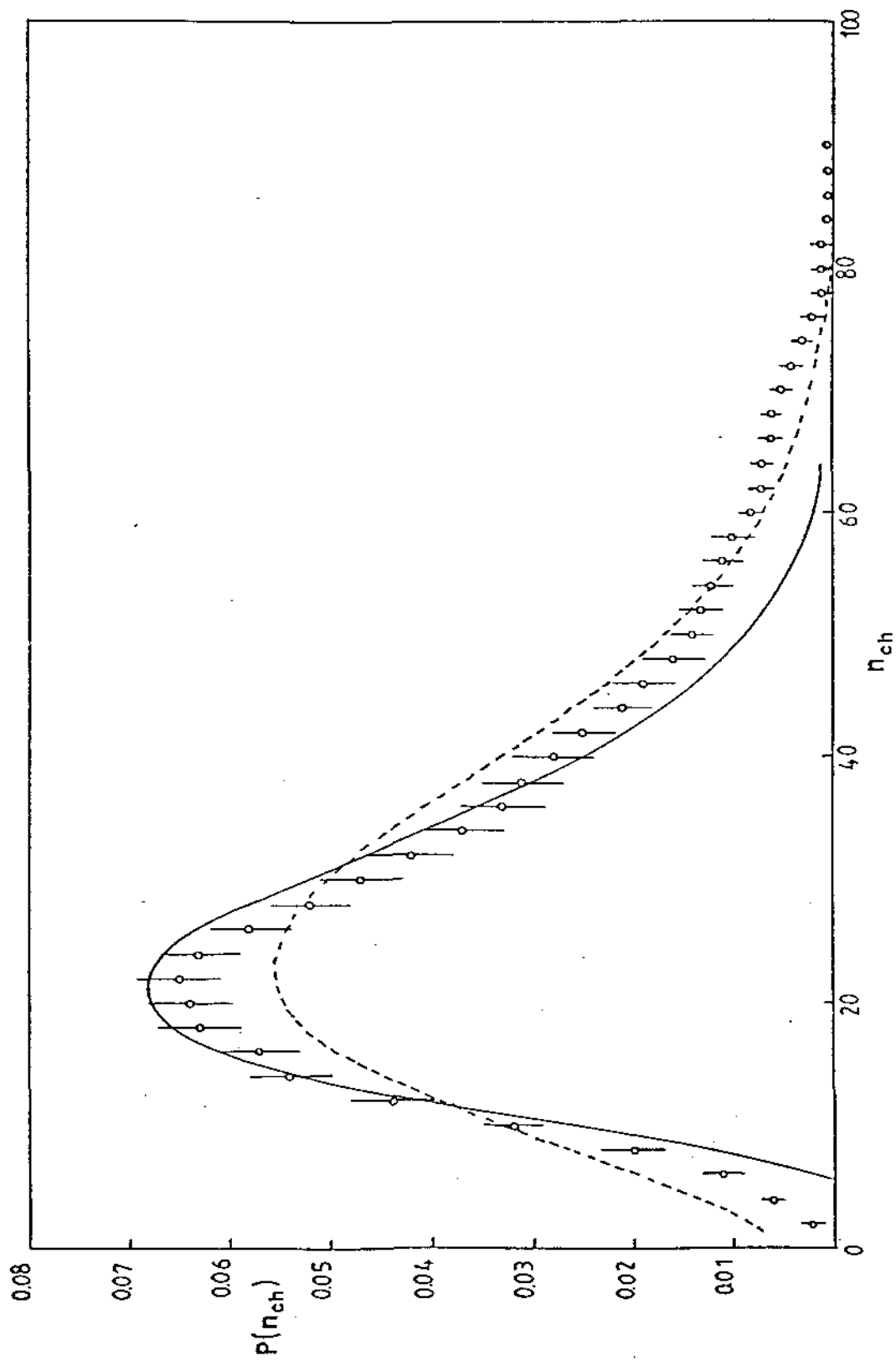


Fig. 1

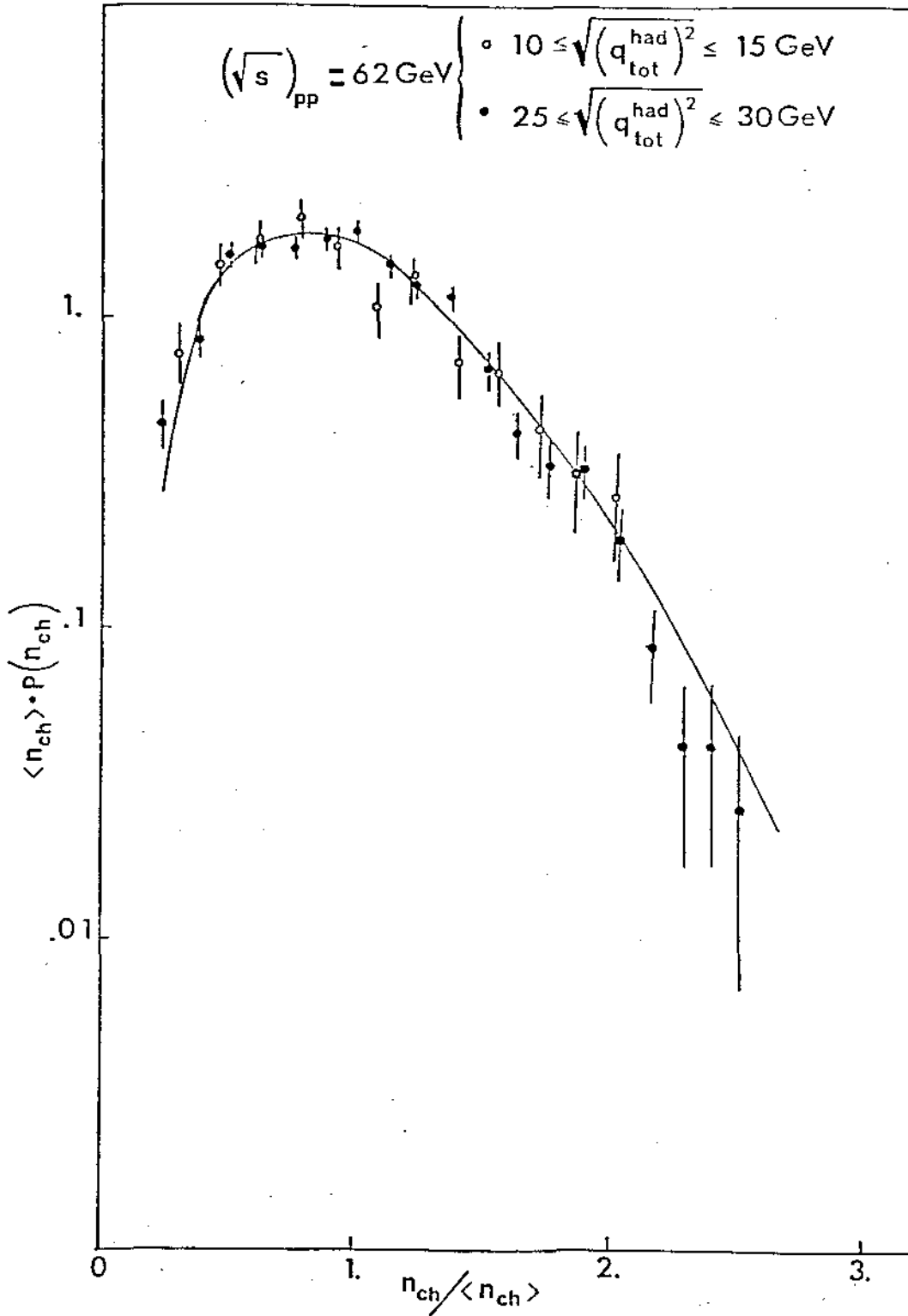


Fig. 2

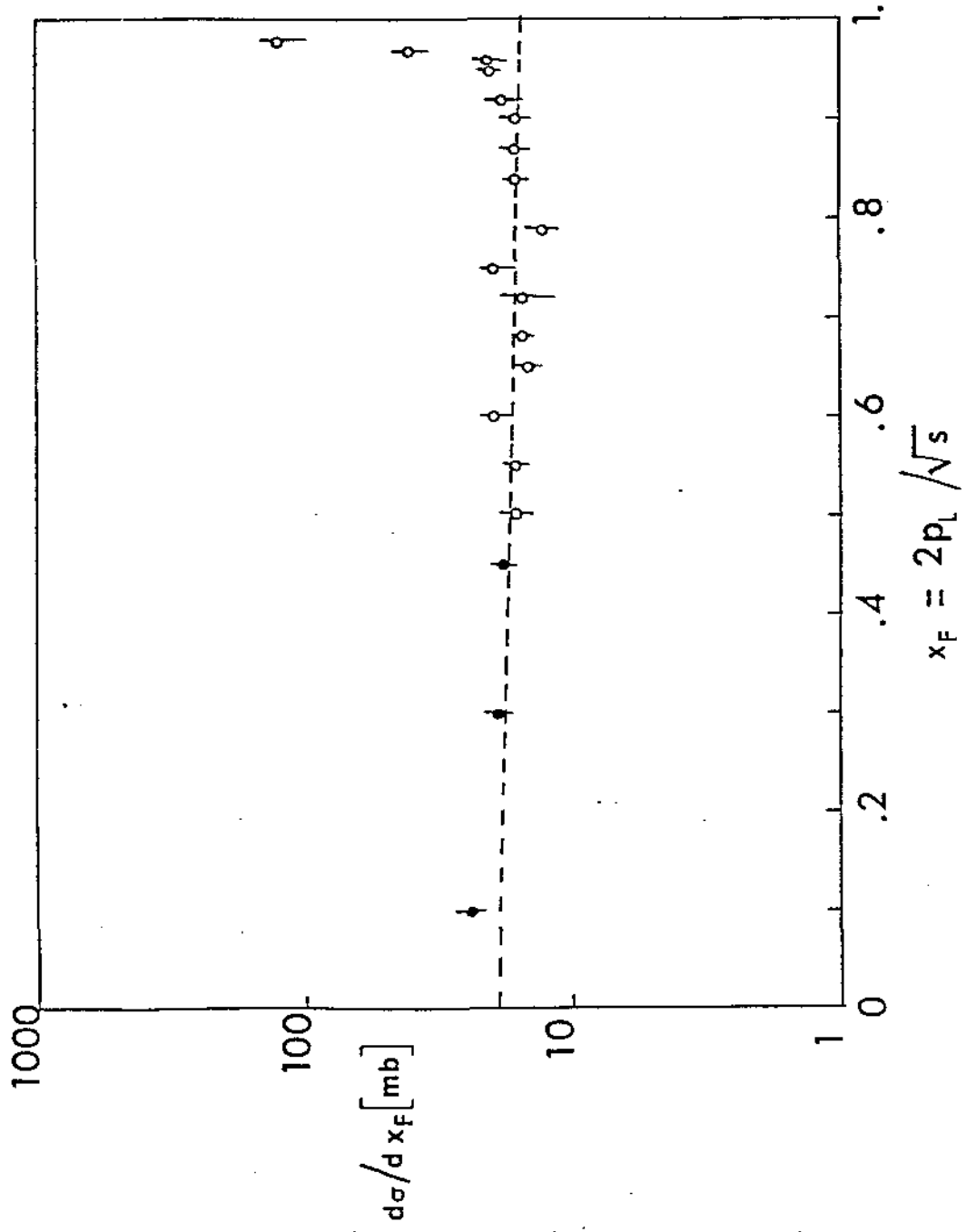


Fig. 3

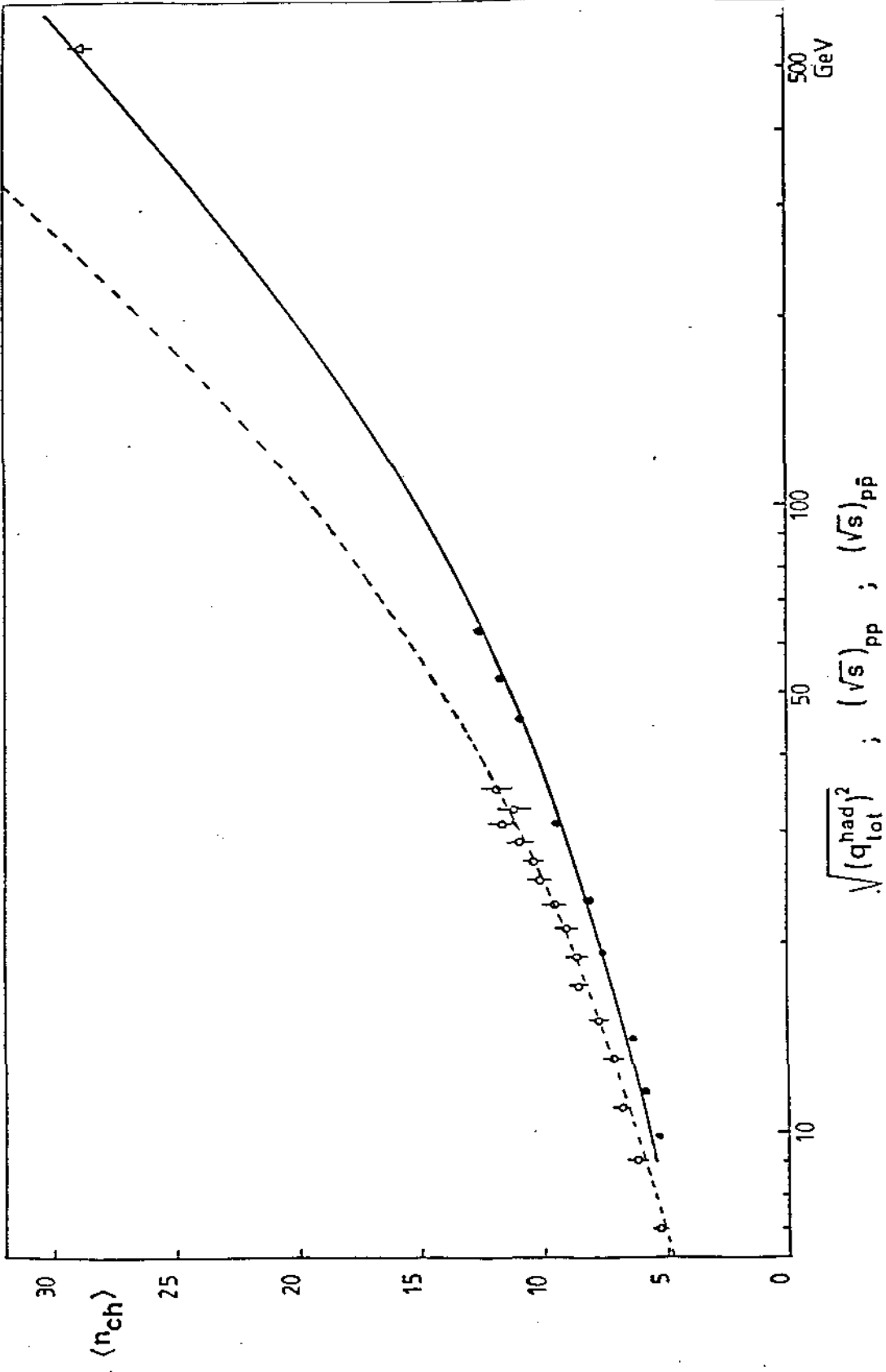


Fig. 4

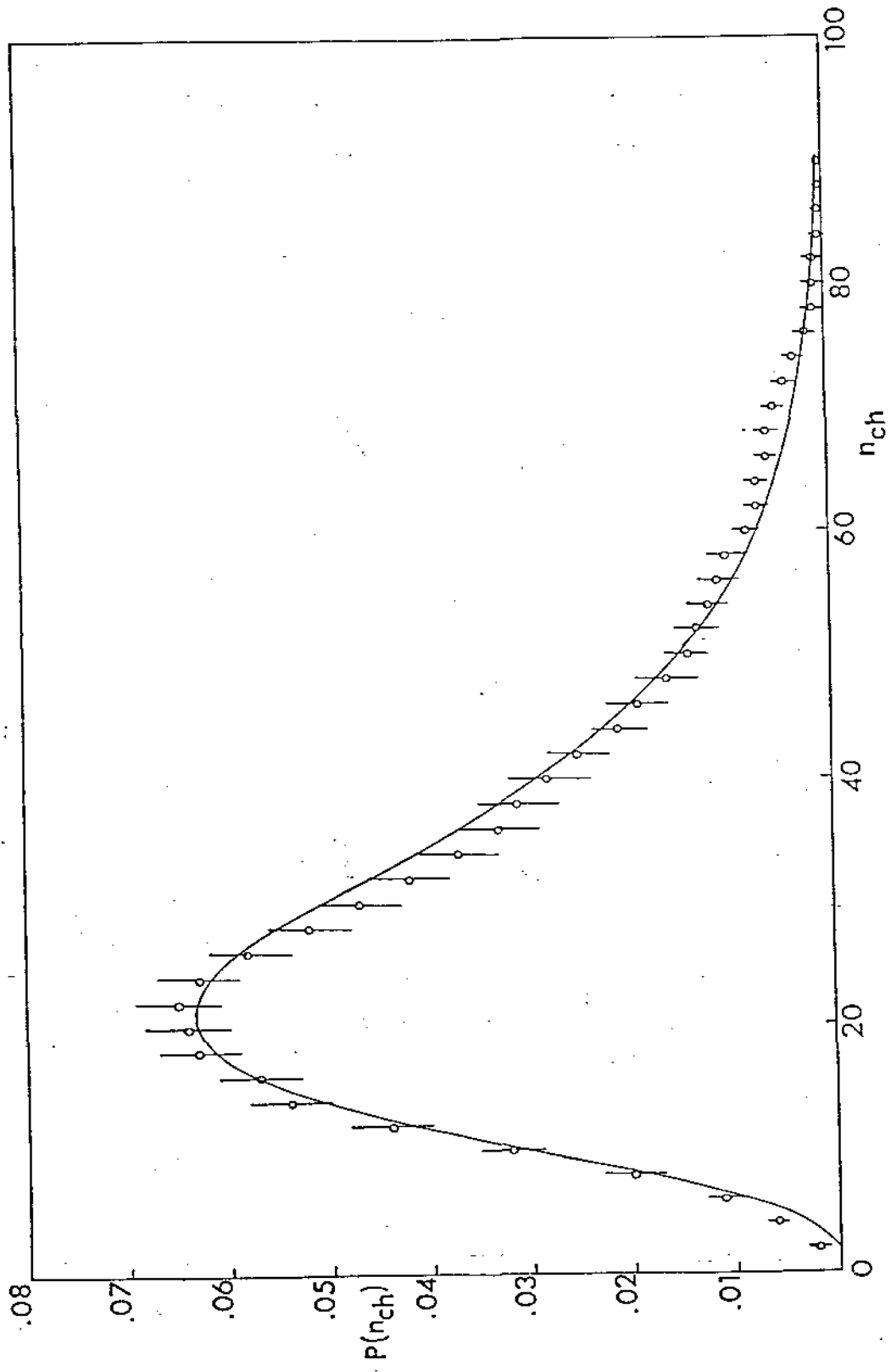


Fig. 5

EUROPEAN ORGANIZATION FOR NUCLEAR RESEARCH

July 28, 1984

TRANSVERSE AND LONGITUDINAL PHYSICS FROM ISR
TO COLLIDER ENERGIES

M. Basile, G. Cara Romeo, L. Cifarelli, A. Contin, G. D'Ali,
C. Del Papa, , P. Giusti, T. Massam, R. Nania, F. Palmonari,
G. Sartorelli, M. Spinetti, G. Susinno, L. Votano
and A. Zichichi

Dipartimento di Fisica dell'Universita', Bologna, Italy

Istituto Nazionale di Fisica Nucleare, Bologna, Italy

CERN, Geneva, Switzerland

Istituto Nazionale di Fisica Nucleare, INF, Frascati, Italy

ABSTRACT

The inclusive fractional energy distributions measured in the low p_T (longitudinal) and in the high p_T (transverse) range at the CERN ISR and at the CERN $p\bar{p}$ Collider, show an impressive analogy, once the "leading" effect is taken into account.

(Submitted to Nuovo Cimento Letters)

FIGURE CAPTIONS

Figure 1: Comparison of fractional energy distributions obtained in (pp) interactions [ISR, this experiment] at low p_T , in (e^+e^-) annihilation [PETRA, TASSO collaboration], and in ($p\bar{p}$) interactions [CERN $p\bar{p}$ Collider, UA1 Collaboration] at high p_T . The "leading subtraction" method is adopted.

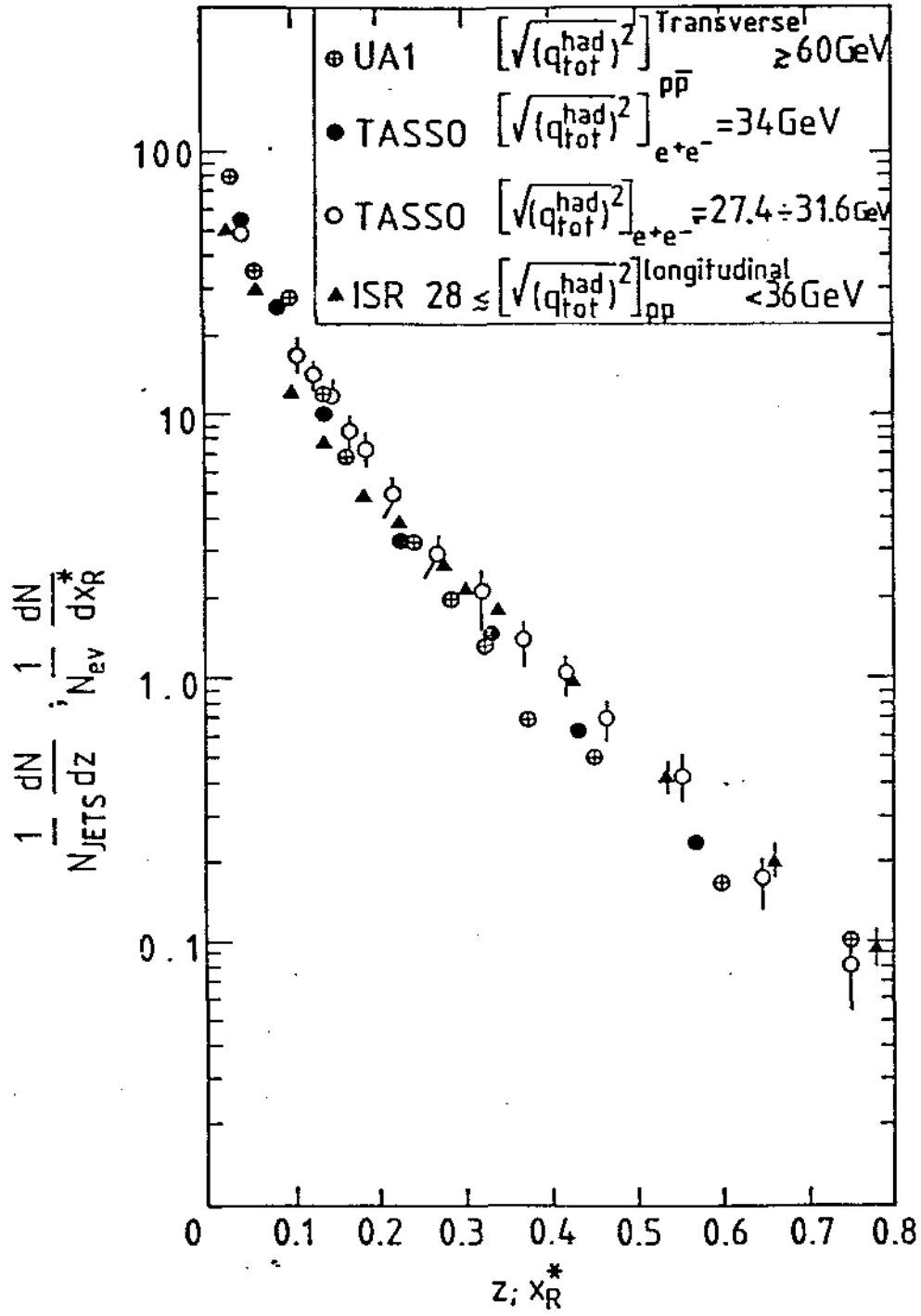


Fig. 1

July 30, 1984

THE LEADING EFFECT IN (e^+e^-) ANNIHILATION COMPARED WITH
(pp) INTERACTIONS.

M. Basile, G. Cara Romeo, L. Cifarelli, A. Contin, G. D'Ali,
C. Del Papa, , P. Giusti, T. Massam, R. Nania, F. Palmonari,
G. Sartorelli, M. Spinetti, G. Susinno, L. Votano
and A. Zichichi

Dipartimento di Fisica dell'Universita', Bologna, Italy

Istituto Nazionale di Fisica Nucleare, Bologna, Italy

CERN, Geneva, Switzerland

Istituto Nazionale di Fisica Nucleare, LNF, Frascati, Italy

ABSTRACT

Recently the leading effect has been observed in the multihadronic states produced in (e^+e^-) annihilation at PETRA.

The inclusive fractional energy and the transverse momentum distributions, are shown to be in excellent agreement with (pp) data, once the effective and not nominal energies, both in (pp) and in (e^+e^-) , are used as the basis for a comparison between the two processes.

(Submitted to Nuovo Cimento Letters)

FIGURE CAPTIONS

- Figure 1: Two schematic (e^+e^-) events, one of the standard jet-jet type, the other with a leading particle.
- Figure 2: Fractional energy distribution without "leading subtraction", in (e^+e^-) annihilation. The histogram refers to standard jets (without a leading particle) at $(\sqrt{s})_{e^+e^-} = 34.4$ GeV. The solid circles superimposed are relative to jets accompanying a D^* (leading particle), at the same energy.
- Figure 3: Same as Figure 2 after the "leading subtraction" method was applied. The dashed-line curve shows the standard jet distribution obtained at an energy, $(\sqrt{s})_{e^+e^-} = 14$ GeV, which is reduced with respect to the nominal 34.4 GeV value to account for the "leading subtraction". The (pp) interaction data corresponding to a similar effective energy, $\sqrt{(q_{tot}^{had})^2} = (10 \div 16)$ GeV, are superimposed.
- Figure 4: Showing the agreement of (e^+e^-) and (pp) data in terms of $d\sigma/p_t^2$, where p_t is the transverse momentum with respect to the jet axis, once the "leading subtraction" method is applied. The TASSO data correspond to events with jets plus a D^* (leading particle). The (pp) data are relative to an effective energy range, $\sqrt{(q_{tot}^{had})^2} = (13 \div 17)$ GeV, which is lower than the nominal $(\sqrt{s})_{e^+e^-} = 34.4$ GeV and corresponds to a "residual" energy of 14 GeV, once the D^* leading effect is considered.

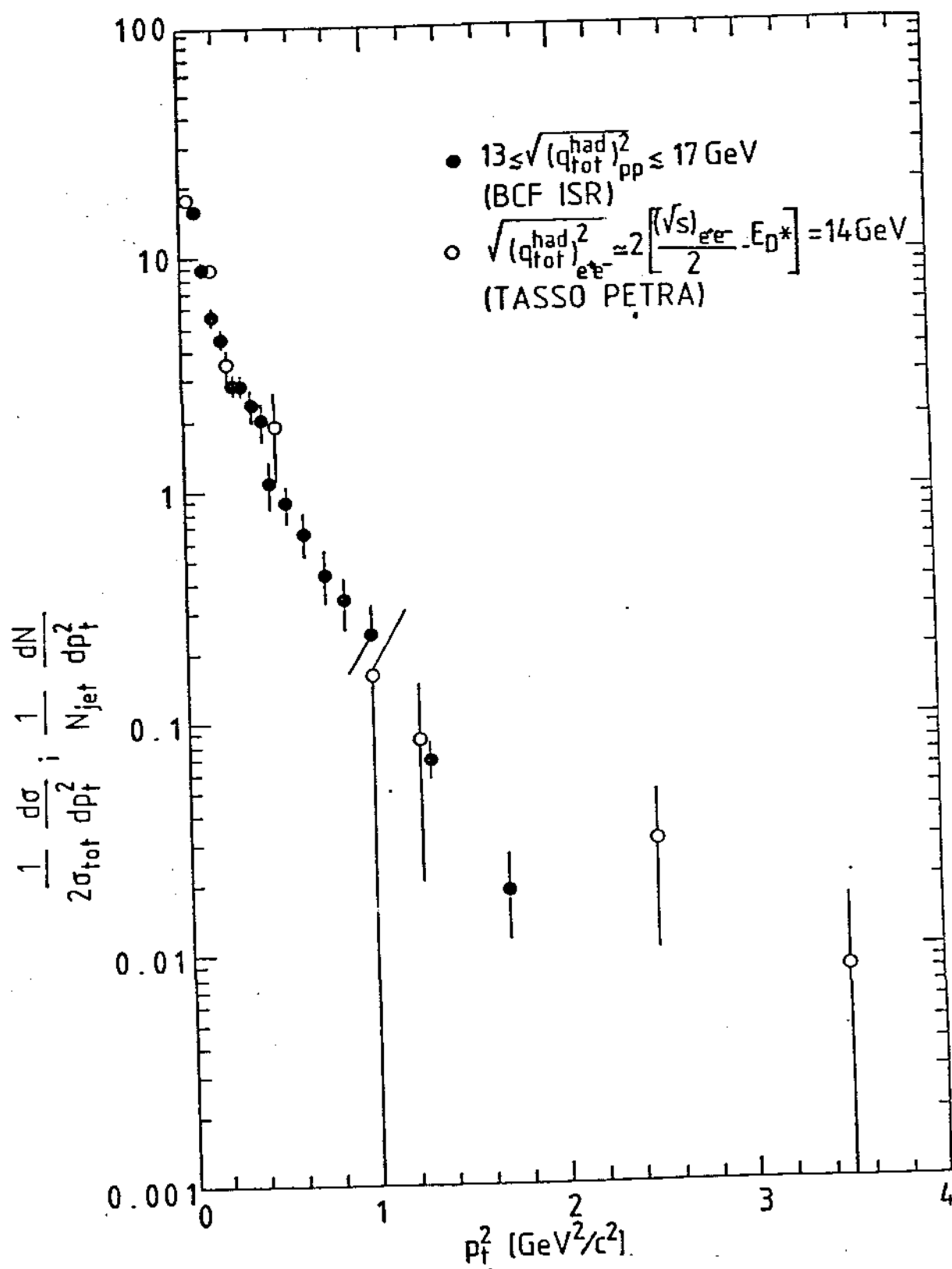


Fig. 4

**III-6. LAA Proposal: Memorandum to the SPSC referees
(Prof. A. Donnachie and Prof. R. Klanner),
June 28, 1984.**

Date: June 28, 1984

6 - M E M O R A N D U M

To : Prof. A. Donnachie
Prof. R. Klanner

From : BCFL Collaboration

Ref. : THE LEPTON ASYMMETRY ANALYSER: A PROPOSAL
CERN/SPSC/84-33 - SPSC/P200

Subject: Answers to the Referees' questions

Copy to: Prof. L. Foa' (Chairman of SPSC)
Prof. R. Budde (Secretary of SPSC)

QUESTION 1 - What is the effect on the asymmetry due to $d\sigma/dx_F \rightarrow 0$ as $x_F \rightarrow 1$, for leading baryons.

ANSWER 1 - We have studied the case $d\sigma/dx_F \propto (1-|x_F|)^\alpha$ with $\alpha=1$ (See Fig.1, where the other distributions are also shown). Fig.2 shows the angular distributions of μ s from baryons produced with

$$d\sigma/dx_F = \text{const.}$$

and

$$d\sigma/dx_F \propto (1-|x_F|)^\alpha, \quad \alpha = 1$$

For completeness the contribution from mesons is also shown. The corresponding asymmetry versus p_T is reported in Fig.3. The case considered is "top" with $m_t=35 \text{ GeV}/c^2$ and the standard ratio (leading/total)=0.25. The change in asymmetry is very small with respect to the case of baryons produced with $d\sigma/dx_F = \text{const.}$ as can be seen from a comparison with Fig.28 of the proposal (reported here for convenience of the reader). Fig.4 shows the case for the production of an "up-like" and a "down-like" heavy flavoured baryon, $m_t=25 \text{ GeV}/c^2$ and $m_{sb}=55 \text{ GeV}/c^2$. The Montecarlo for (superbeauty/top) case with $\alpha=1$, takes too long to be done. On the basis of the previous case ($m_t=35 \text{ GeV}/c^2$) we believe that the change in asymmetry is negligible.

QUESTION 2 - What is the effect on the asymmetry of a reduced (baryon/total) ratio for heavy flavour production.

ANSWER 2 - We have considered heavy flavour production of top ($25 \text{ GeV}/c^2$) and superbeauty ($55 \text{ GeV}/c^2$) and of top ($35 \text{ GeV}/c^2$). The results are shown in Fig.5,6,7, in terms of A^{exp} and of $A^{\text{exp}}/\Delta A^{\text{exp}}$. If we choose the 90% confidence level, the ratio (leading/total) can be, 5.0 (superbeauty), 10.0 (top, $35 \text{ GeV}/c^2$) and 10.0 (top, $25 \text{ GeV}/c^2$) times smaller than the value chosen in the proposal. It should be noticed that our analysis on the data obtained at the Collider shows that the leading effect should be the same as observed at the ISR. Concerning heavy flavour production, the data available so far seem to

indicate that the leading effect increases with increasing quark mass (see Fig.12 and 13 for a comparison of propagation of (s), (u) and (d)). Moreover Λ_c/Λ_s leading effect favours Λ_c (see Fig.4 of our proposal).

QUESTION 3 - What is the effect on the asymmetry (through smearing of the lepton p_T distribution) and on the determination of the quark mass difference, due to the semileptonic decay being 4-body (or even 5-body).

ANSWER 3 - We have assumed the basic decay to be of the type

$$q_1 \rightarrow q_2 + \mu\nu \quad (1)$$

This doesn't imply that the final state (1) will consist of 3 bodies. The number of final state particles in (1) will be given by the "hadronization" of q_2 . If q_2 hadronizes into 10 π 's, the final state (1) will consist of 12 particles. However the "hadronization" of q_2 should produce a small "smearing". Let us consider another possibility: the decay goes via an "excited" quark state $(q_2)^*$, i.e. a quark whose mass is greater than the constituent quark mass,

$$q_1 \rightarrow (q_2)^* + \mu\nu$$



$q_2 + n\pi$. In this case the peak in the μp_T distribution

will change according to the scaling law

$$p_T/\Delta M$$

as shown in Fig.8. The changes are not very large for reasonable q^* excitations. However we believe that reaction (1) with subsequent "hadronization" of q_2 is a reasonable model to describe heavy quarks decays. On the other hand we would not know how to simulate multibody semileptonic decays where the "multibody" is at the $(q_1 \rightarrow q_2)$ level. There is a hint which supports our model (1) based on the "hadronization" of q_2 . Data from CLEO on the semileptonic decay of beauty mesons, $M_B \rightarrow X e \nu$, show that the mass recoiling with respect to the leptons is very near to the c-quark mass. The mean charged particles multiplicity of the decay was reported by the CLEO group to be 3.5 [S.L. Olsen in Proceedings of the Second Moriond Workshop on New Flavours, Jan. 1982, p.147] and later 4.1

[M.S. Alam et al., P.R.L., 49, 357 (1982)]. As, on the average, the mean charged multiplicity attributable to the D-decay is 2.5, we have $(4.1-2.5) = 1.6$ of which 1 is the leptonic component. Therefore the c-quark shows, on the average, an additional "hadronization" of 0.6 charged, i.e. 1, particle, per event, with undetectable smearing on the c-quark mass entering in the b-quark decay. The problem of quarks with very large masses is open, however it is not inconsistent with our hypothesis (1), i.e. dominant 3 body decay with a q_2 "hadronization" with a small additional mass.

QUESTION 4 - In connection with question 1 and 2, how practical is to impose a minimum x_F cut on the leptons, in order to restore the asymmetry?

ANSWER 4 - A clean way to answer this question is to plot the isorate acceptance curves for muons coming from baryons and mesons. This is shown in a plot of p_T versus θ , for constant x_F -values (Fig.9,10,11). The $(p_T - \theta)$ range, with $0.2 \leq x_F \leq 0.4$ is where the μ from baryon decays are more abundant. The μ from mesons are with $x_F < 0.1$. The x_F cut is a choice to be made once the background is directly measured in the experimental conditions. It could be very helpful.

QUESTION 5 - One expects an asymmetry between π^+ and π^- even at high p_T , due to the charge-quark content of p and \bar{p} . How big is it? How can it be measured and how does it influence the measured asymmetry?

ANSWER 5 - The π^+/π^- asymmetry (due to the quark content of p and \bar{p}) is x_F and p_T dependent. To the best of our knowledge its effect on the lepton asymmetry due to baryons carrying heavy flavours should be negligible. In fact the π^+/π^- asymmetry decreases with decreasing x_F and with increasing p_T . The x_F range of the lepton asymmetry is $0.1 \leq x_F \leq 0.4$. The transverse momentum range is $p_T \geq 5$ GeV/c. In these x_F and p_T ranges the π^+/π^- asymmetry is expected to be negligible. The review of what is known in this field follows.

In our paper "The Leading Particle Effect in Hadron Physics" [Nuovo Cimento, 66A,129(1981)] we have studied the leading effect when only one quark propagates, from the initial to the final state. This has been done using the $(p\bar{p})$ data at $P_{\text{Lab}}=100$ GeV/c (Fig.12) and the ISR data at $(\sqrt{s})=25-62$ GeV (Fig.13). The value of the quantity L scales in the ISR energy range and it is in good agreement with the lower energy data. This means that even at Collider energies the L value is expected to be ~ 0.5 .

Let us consider the case of 3 quarks propagation, at the ISR, and compare the results with 1 quark propagation. This means that we will take the ratio of proton to π in the final state of (pp) interaction at the ISR. The result is shown in Fig.14 where we see that at $x_F=0.7$ $p/\pi=25$ while at $x_F=0.25$ $p/\pi=1$. As mentioned above, the 1 quark propagation has $L=0.5$, while the 3 quarks propagation has $L=3$. If $p/\pi=1$ at $x_F=0.25$, there is no question that π^+/π^- cannot be worse: i.e. $\pi^+/\pi^-\cong 1$ at $x_F=0.25$. Notice that these are low p_T data, i.e. $p_T < 1.5$ GeV/c.

We now discuss why we expect that at high p_T the π^+/π^- ratio should be 1. Let us first emphasize that the p_T dependence of the "leading" effect has never been measured (we wanted to do it at the ISR). It should decrease with increasing p_T . Using the scarce ISR data [P.Capiluppi et al. Nucl. Phys. B79,189(1974)] we can conclude that the ratio π^+/π^- in (pp) interactions, in the energy range $(\sqrt{s})=20-60$ GeV, doesn't change with \sqrt{s} . The ratio π^+/π^- at the ISR is compatible with a p_T dependence such that at $p_T \cong \text{few GeV/c}$, $\pi^+/\pi^-=1$ (see Fig.15 a), 15 b)). These results are affected by large errors, however they do not contradict our hypothesis. Up to now there are no data on this topic in $(p\bar{p})$ interactions at $(\sqrt{s})=540$ GeV (UA1: Della Negra, private communication).

Let us try to infer an answer from other well established results. From data on high p_T jets at Fermilab and at the ISR, the leading effect should be depressed by two orders of magnitude, when $p_T \geq 3$ GeV/c [C.Bromberg et al. Int.

Conf. on High-Energy Physics, Geneva(1979)p.488 and T.Akesson et al. Phys. Lett. 118B,185(1982)]. From Collider data, by 3 orders of magnitude when $p_T > 10$ GeV/c [UA1 collab. Phys. Lett. 123B,115(1983) and UA2 collab. CERN-EP/83-94].

Let us consider the ratio

$$R = \sigma(\pi)_{E_T} / \sigma(\text{jet})_{E_T}$$

where $\sigma(\text{jet})_{E_T}$ is the inclusive cross-section for the production of a jet with transverse energy E_T , and $\sigma(\pi)_{E_T}$ is the cross section for the production of a single particle with the same transverse energy E_T . The values of R measured at the ISR and at the CERN (p \bar{p}) Collider are, as mentioned above

$$R(\text{pp})_{\text{ISR}} = 10^{-2} \quad , \quad R(\text{p}\bar{\text{p}})_{\text{Collider}} = 10^{-3}$$

in the transverse energy range, above 5 GeV/c at the ISR and above 10 GeV/c at the Collider. We interpret the above ratios as the amount of leading effect which remains at high transverse energies. This would mean that the ratio (π^+/π^-) should be 1, in the p_T range of interest to our experiment. Let us emphasize the self consistency of the data quoted and of their interpretation in terms of the x_F and p_T dependence of the leading effect.

Notwithstanding the above considerations, in order to see the effect of anomalous (π^+/π^-) ratios in (p \bar{p}) collisions we have studied the experimental asymmetry for two values of the ratio (π^+/π^-)=2 and 4, in the proton hemisphere. We have coupled these anomalous (π^+/π^-) ratios with the cross-section values which are two, ten, twenty, times smaller than our extrapolated values. The results are presented in Fig.16-33. The conclusion is that the proposed experiment can cope with a large safety margin. In fact the signal becomes difficult to be seen either when the ratio (π^+/π^-)=2 and the cross-section 20 times lower than expected, or (π^+/π^-)=4 and the cross-section 10 times lower. Both cases are anomalous and unrealistic.

QUESTION 6 - Which are the uncertainties of the estimates on the μ /hadron rejection, given in the proposal? How can it be measured experimentally?

ANSWER 6 - Only a carefully calibration of the apparatus in a test beam can answer this question. We have done all we could, using known facts.

QUESTION 7 - What determines the maximum acceptance angle? Would the experiment be possible in the range 5° - 20° ?

ANSWER 7 - The maximum angle is determined by:

a) the fiducial volume in which we have equal acceptances for positive and negative particles. The angular range of this fiducial volume is $5^\circ \leq \theta \leq 25^\circ$ for an apparatus extending from 5° to 30° .

b) the statistical significance we can obtain. This is linked to the total number of events we can collect, i.e. to the apparatus angular acceptance. Fig.34-37 show the quantities A^{exp} and $A^{\text{exp}}/\Delta A^{\text{exp}}$ versus θ^{max} for various cases.

A maximum in $A^{\text{exp}}/\Delta A^{\text{exp}}$, i.e. the statistical significance of the measurement, shows up in a range of θ^{max} between 20° and 30° (Fig.34) for the case of top at $25 \text{ GeV}/c^2$. In the case of superbeauty production, where lower cross-section values are expected, an angular acceptance up to 30° is needed (Fig. 35). Fig.36 shows the case of top at $35 \text{ GeV}/c^2$ mass. Again here $\theta^{\text{max}} \approx 20^\circ$ would be acceptable. However, if we take, for the production distribution $d\sigma/dx_F \propto (1-|x_F|)$, the θ^{max} at 30° is clearly safer (Fig. 37).

The choice of $\theta^{\text{max}} \approx 30^\circ$ is in order not to be blind to "low" cross-sections and to "less" leading production mechanisms.

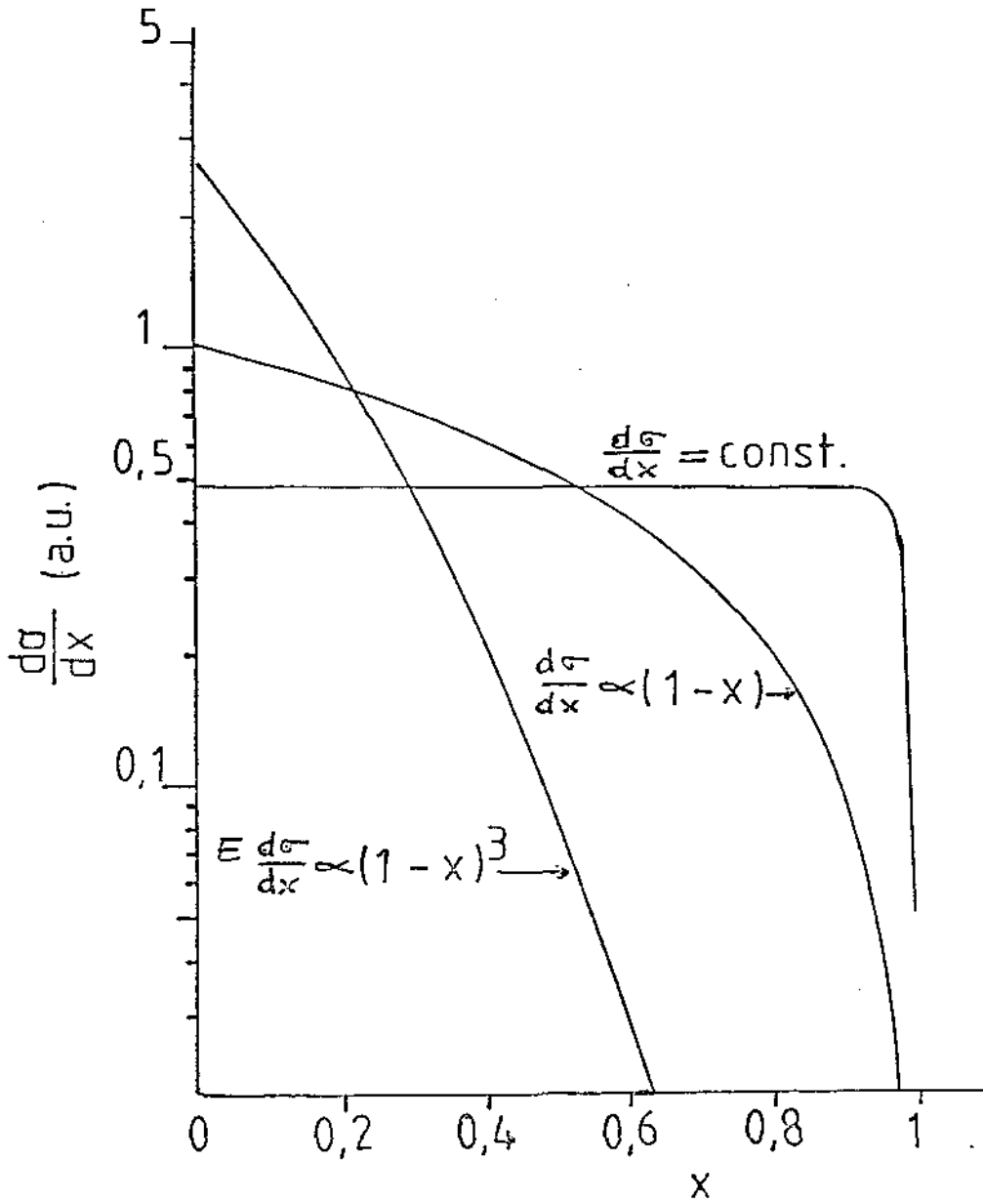


Fig.1

Shape of the differential production cross section as function of x for three different assumption. (Curves are normalized to the total area)

Baryons normalized to the total n° of events.

Mesons/Baryons normalized to (Leading/total) = 0.25

$$t \rightarrow b \mu \nu$$

$$M_T = 35 \text{ GeV}/c^2$$

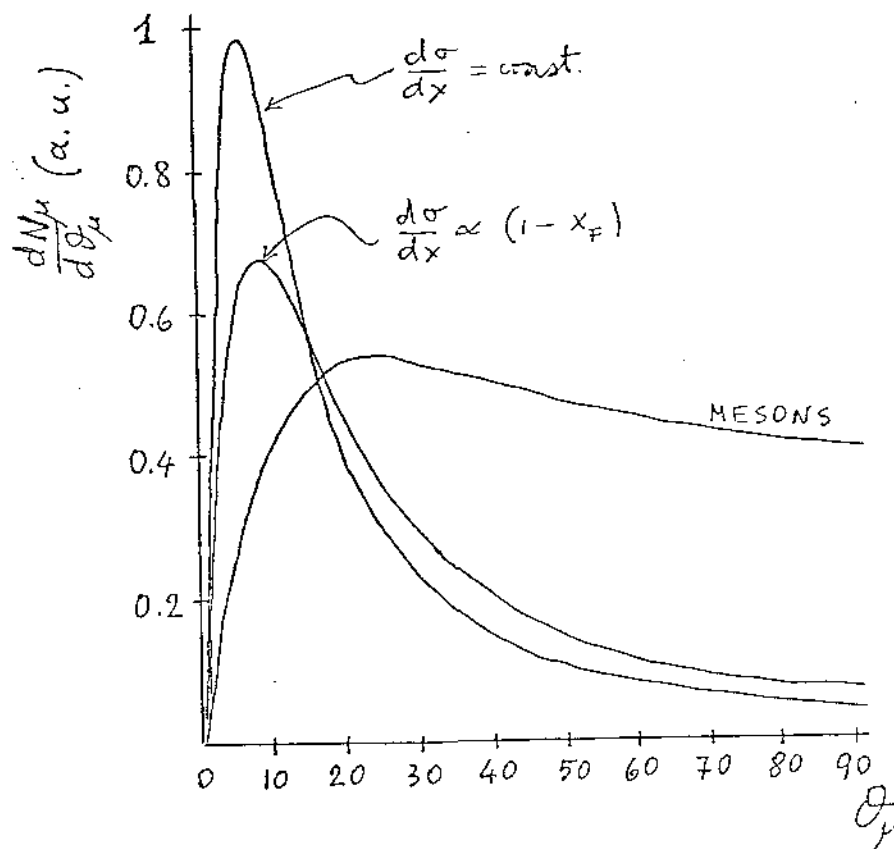


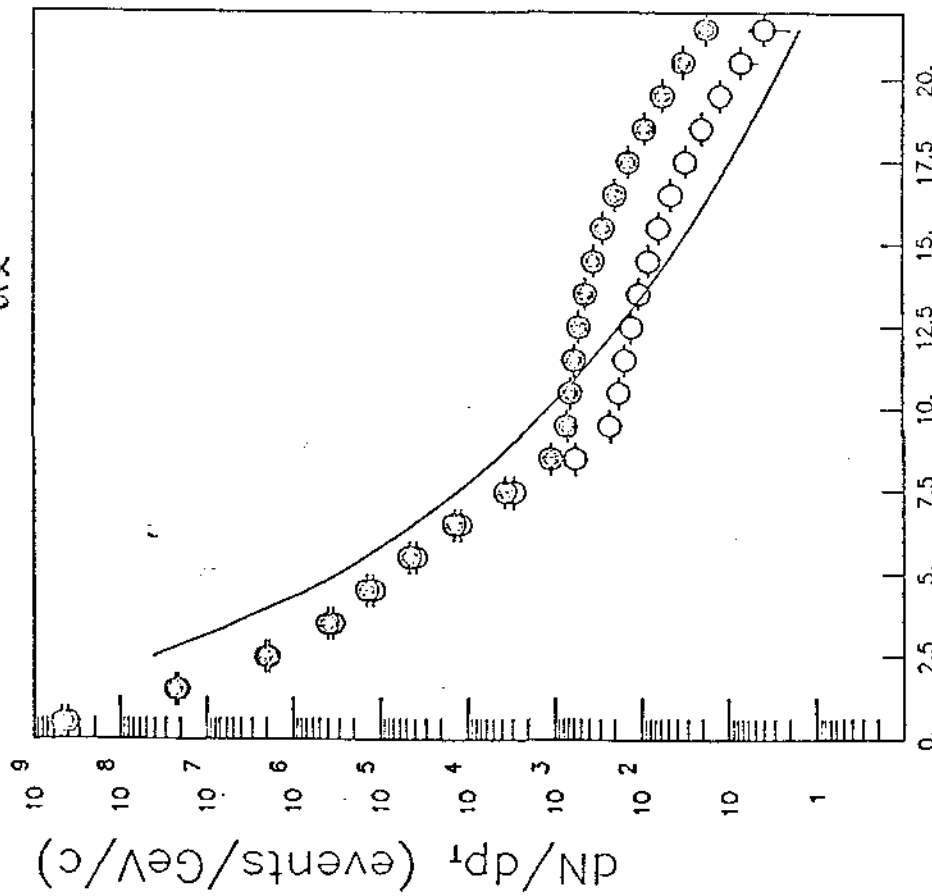
Fig. 2

top (35 GeV) PRODUCTION

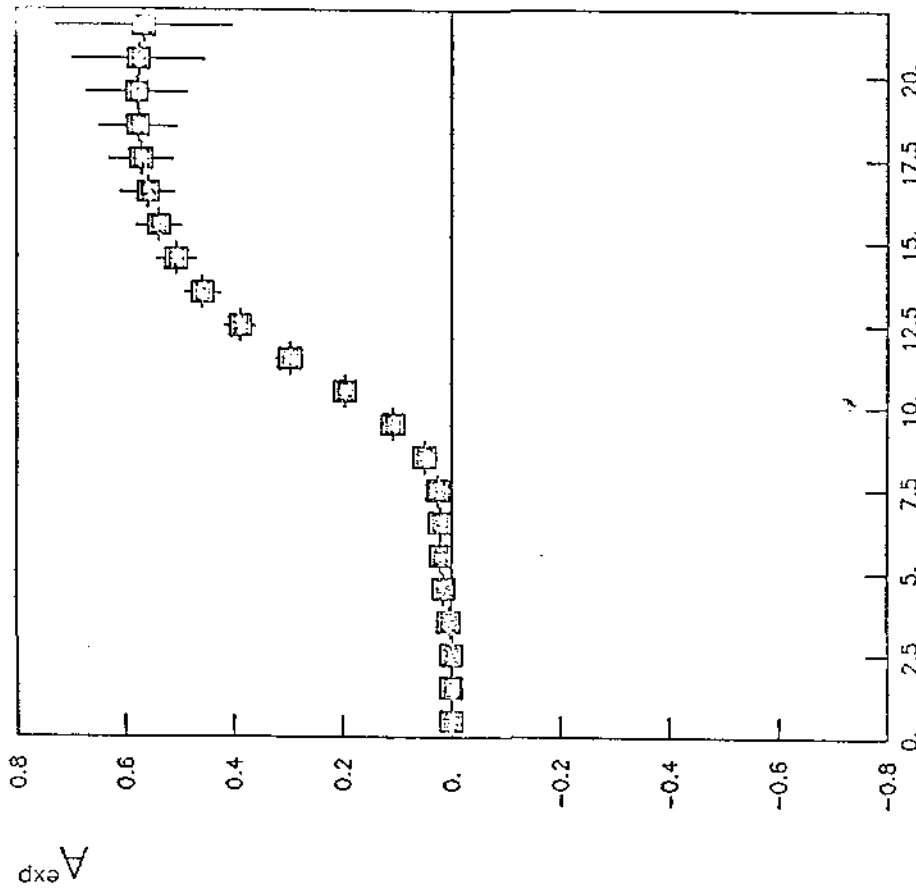
$5. \leq \delta < 30.$

BARYONS GENERATED WITH $\frac{dN}{dx} \propto (1-x)^1$

$\Delta p_T / p_T = 20. \%$



(a)



(b)

Fig. 3

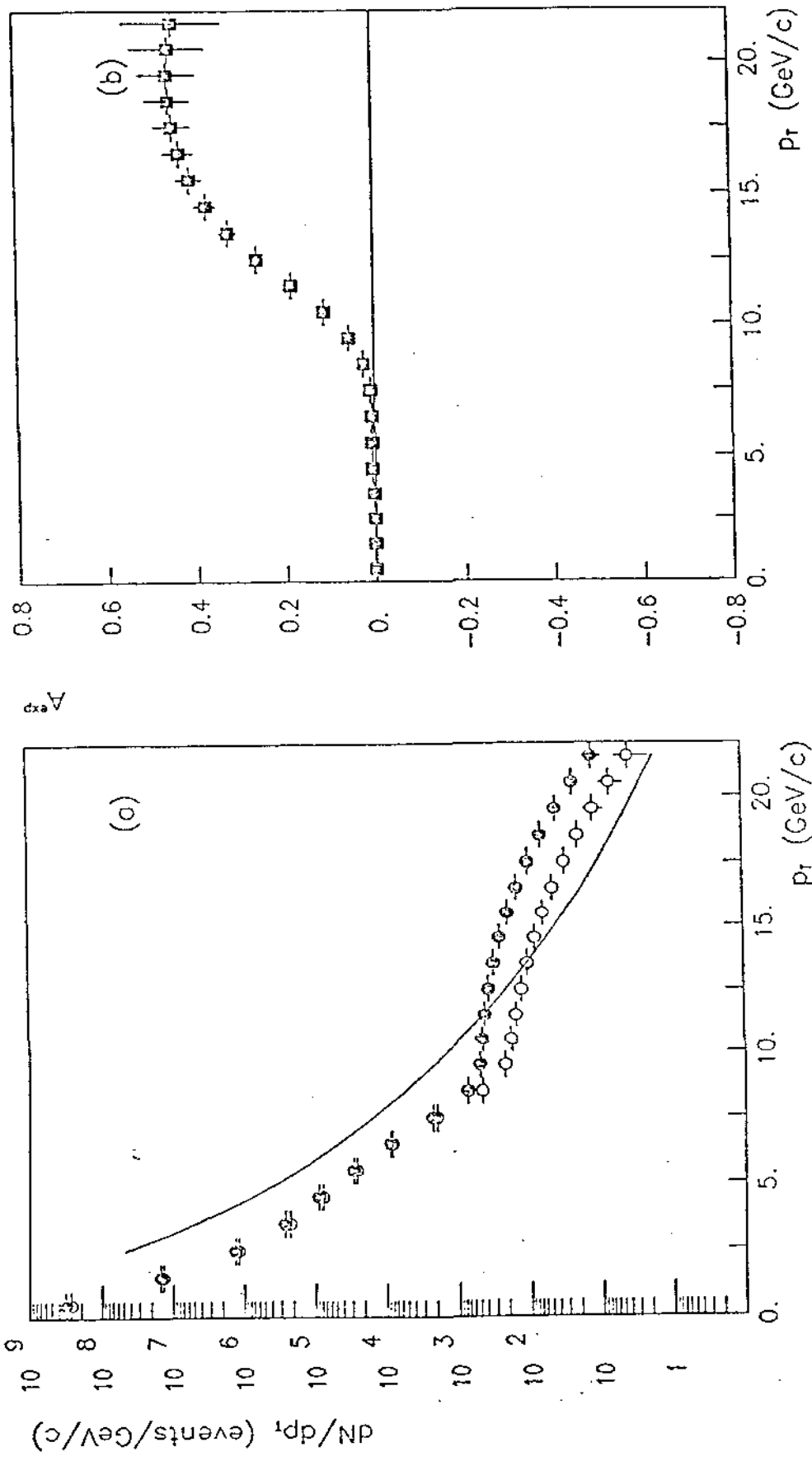
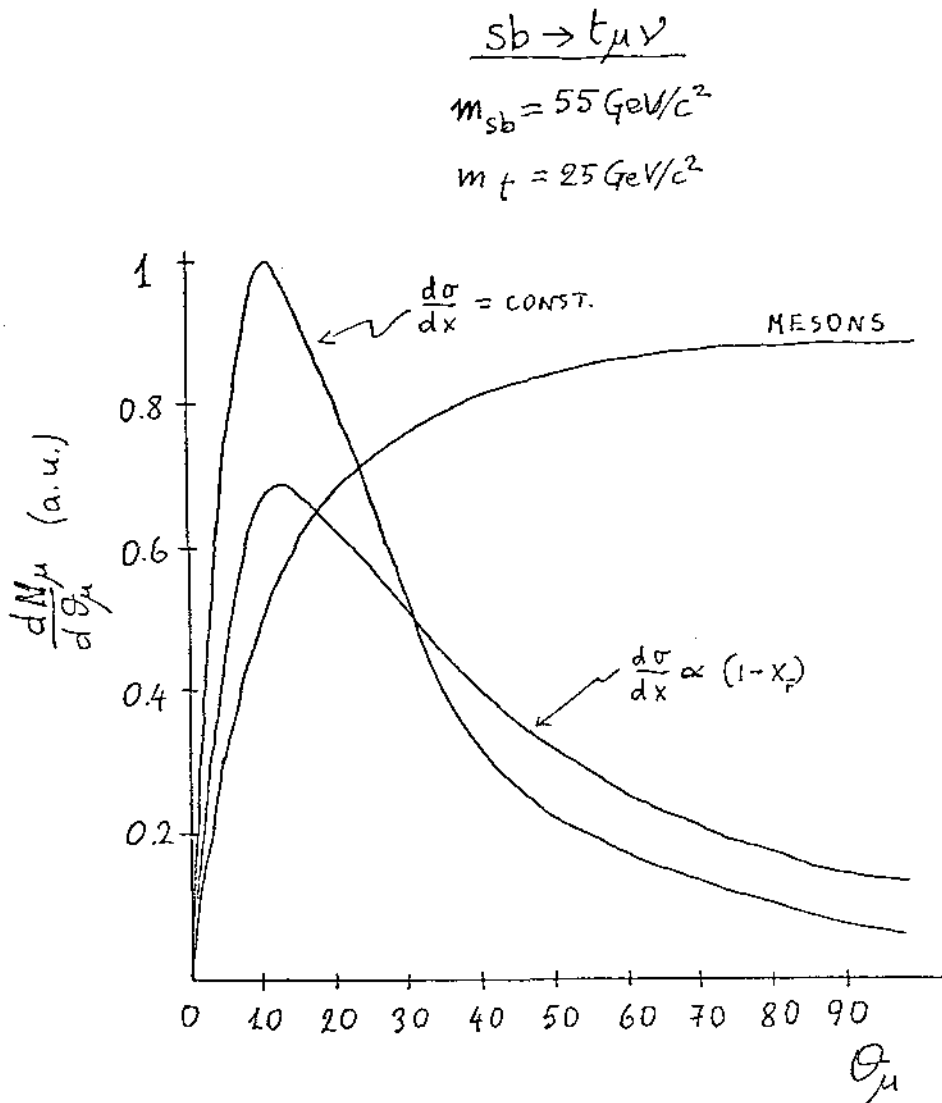


FIG. 28 from the Proposal



TOP ($25 \text{ GeV}/c^2$) AND SUPERBEAUTY ($55 \text{ GeV}/c^2$) PRODUCTION

$$[\Delta p_T / p_T = 20\%]$$

$$[\int L dt = 10 \text{ pb}^{-1}]$$

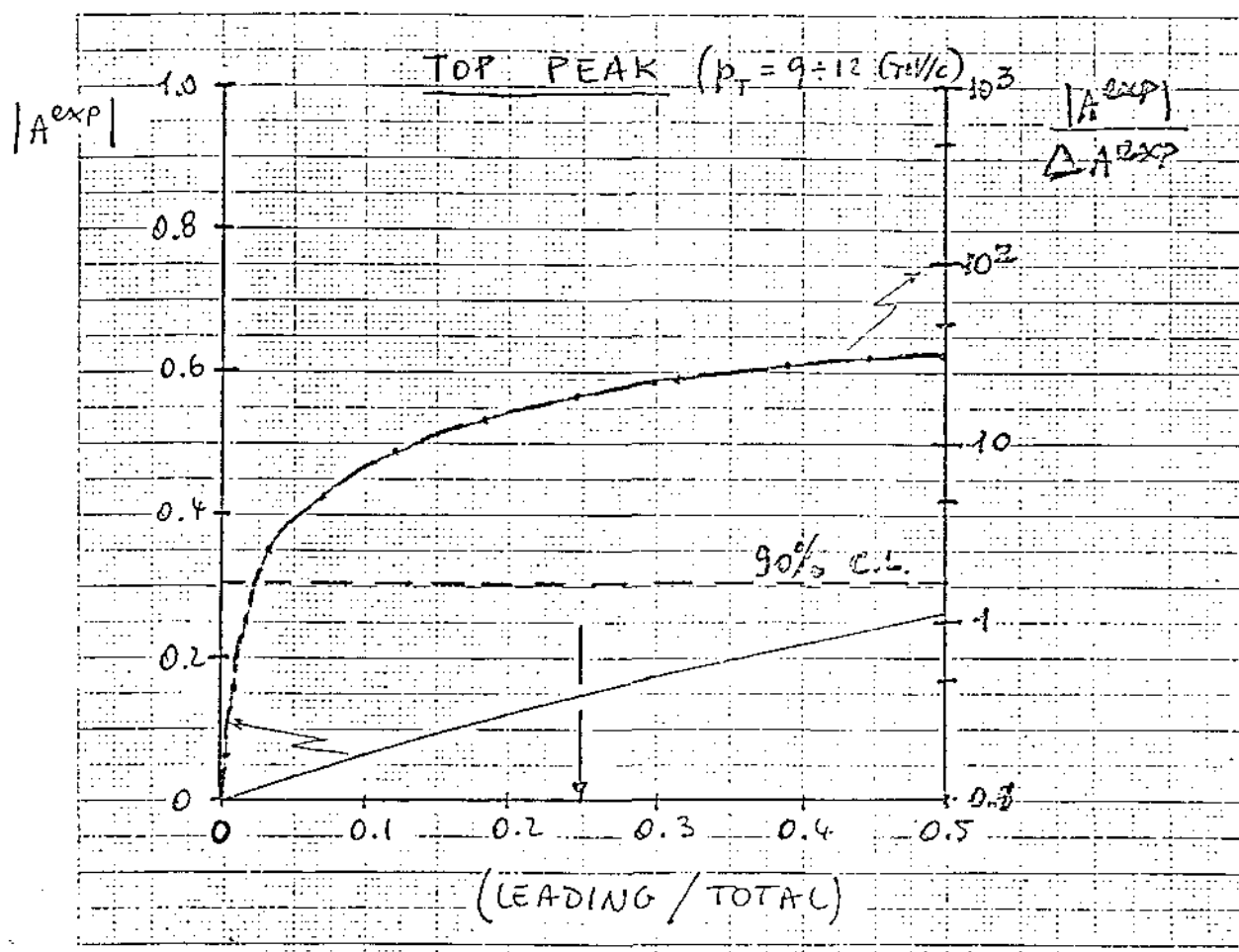


Fig. 5

TOP ($25 \text{ GeV}/c^2$) AND SUPERBEAUTY ($55 \text{ GeV}/c^2$) PRODUCTION

$$[\Delta p_T / p_T = 20\%]$$

$$[\int L dt = 10 \text{ pb}^{-1}]$$

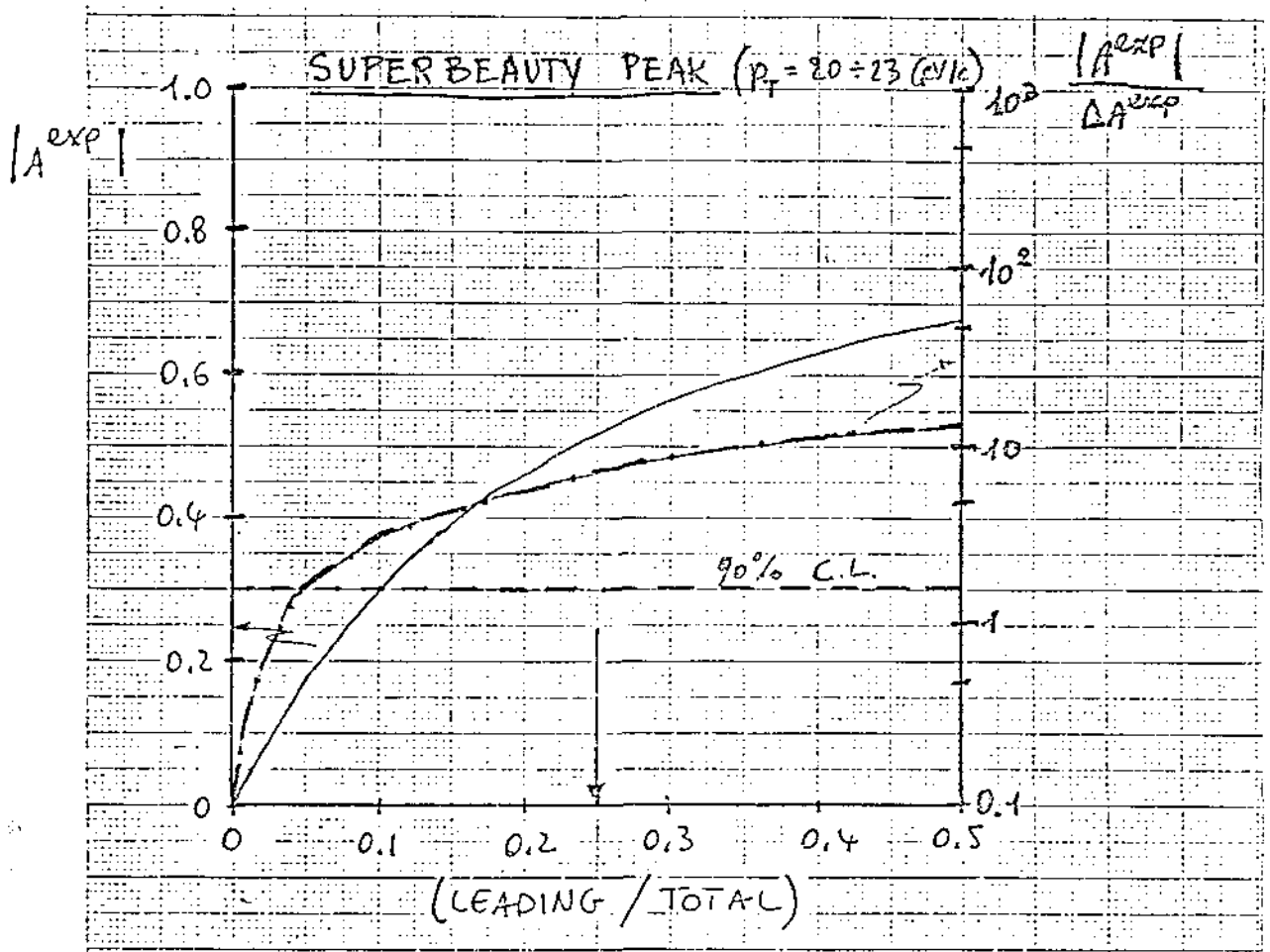


Fig. 6

TOP ($35 \text{ GeV}/c^2$) PRODUCTION

$$[\Delta p_T/p_T = 20\%]$$

$$[\int L dt = 10 \text{ pb}^{-1}]$$

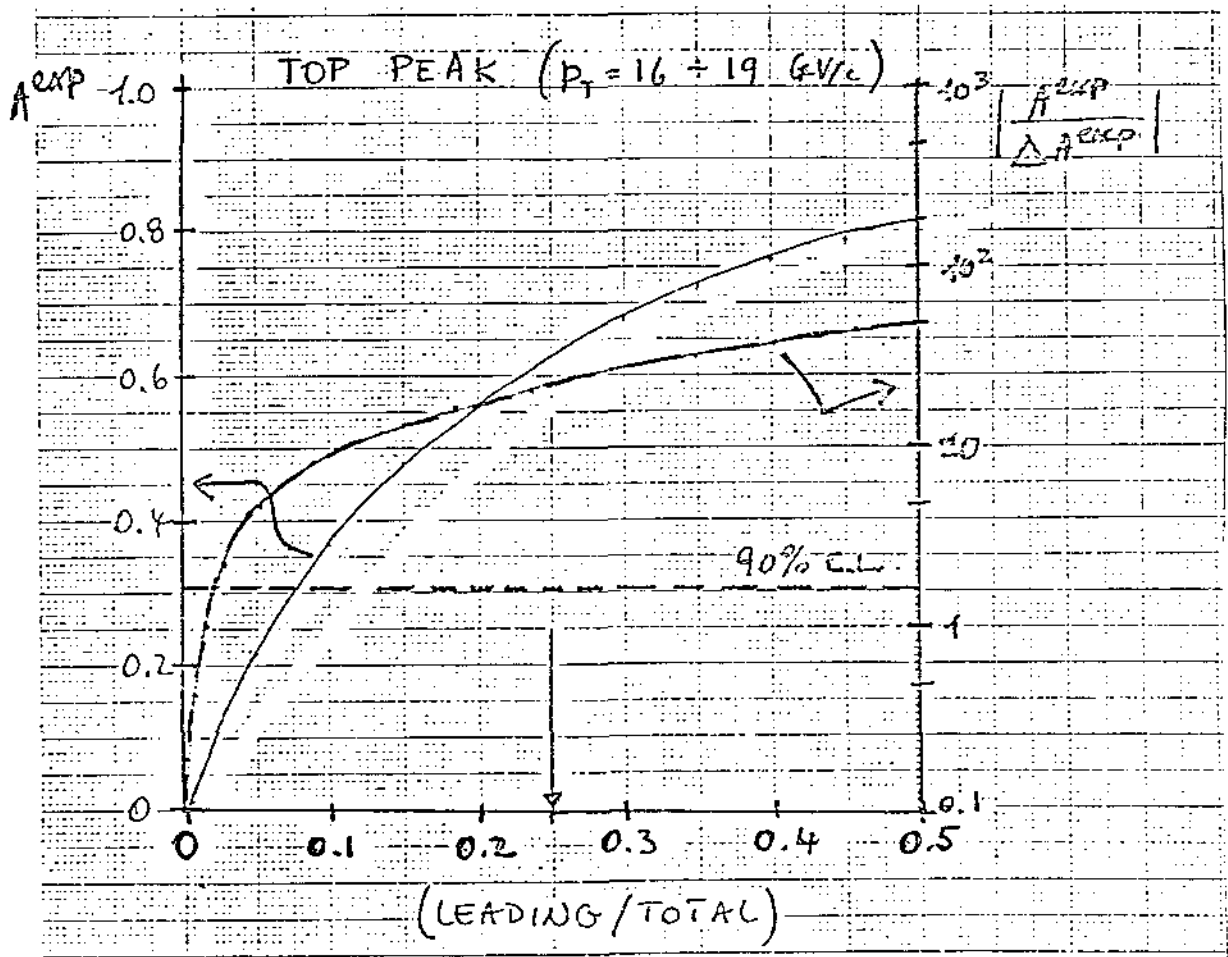


Fig. 7

P_T peak as function of $\Delta\pi$ in the decay

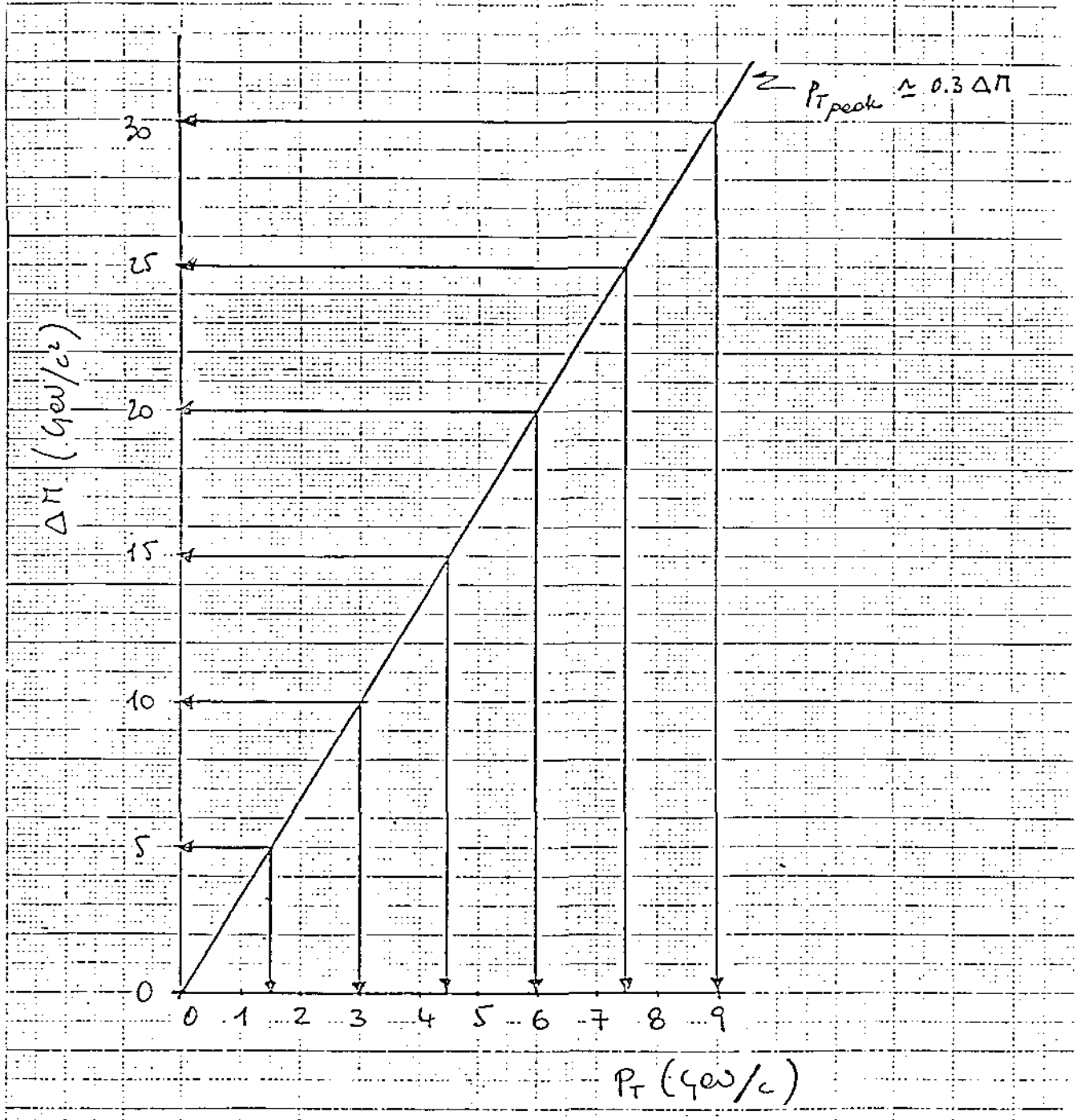
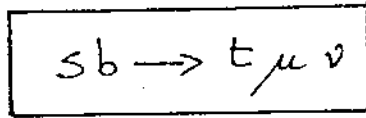


Fig. 8

Isorate levels $\mathcal{E} = d^2N/dp_T d\theta$ for μ from the decay:



$$m_{sb} = 55 \text{ GeV}/c^2$$

$$m_t = 25 \text{ GeV}/c^2$$

———— Baryons
 - - - - Mesons

\mathcal{E} is given in arbitrary unit ($\mathcal{E}=1$ at the peak)
 Also shown are the curves of constant x

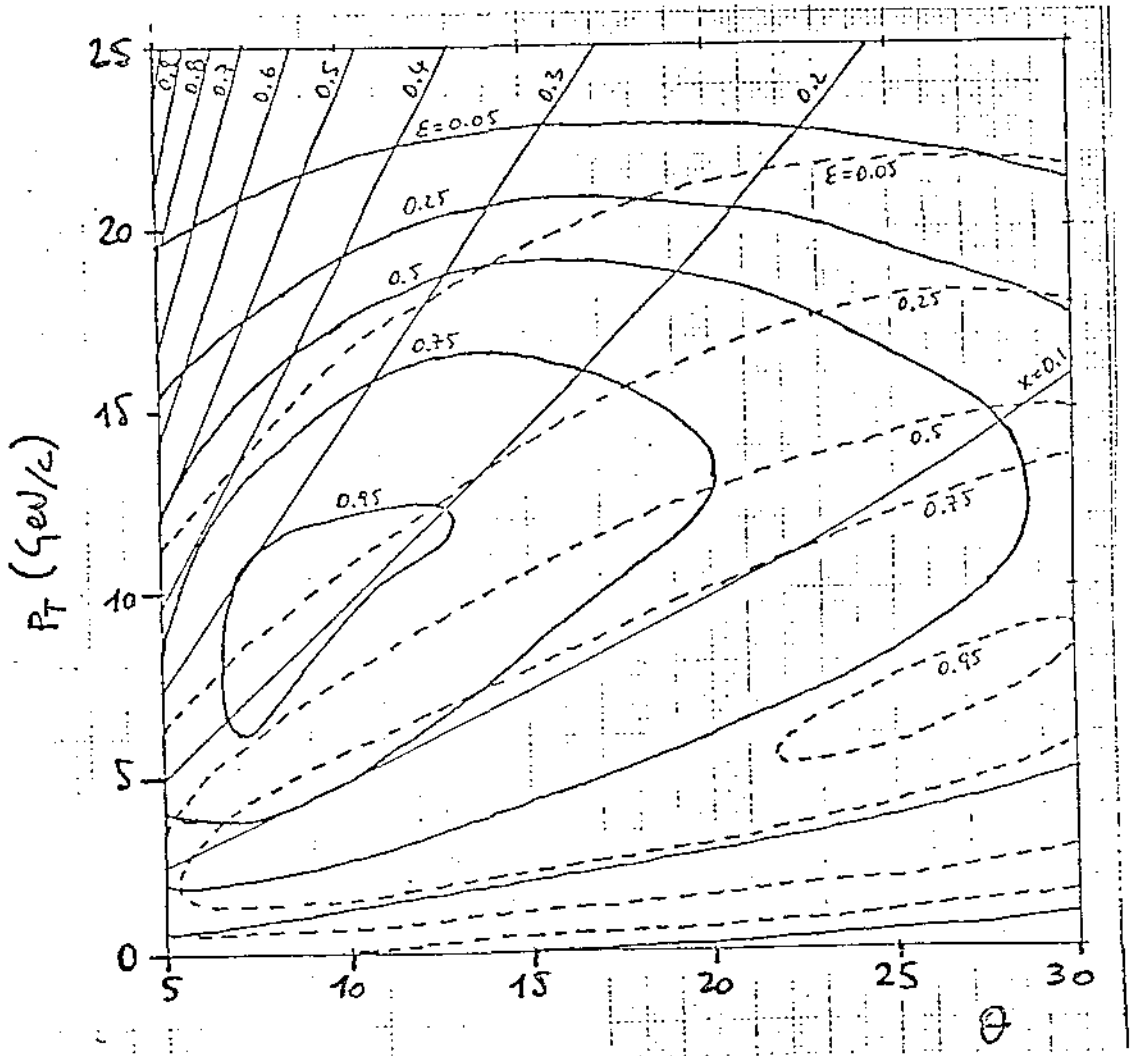
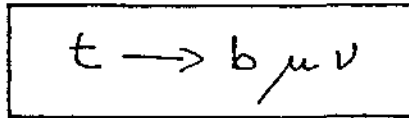


Fig. 9

Isorate levels $\mathcal{E} = d^2N/dp_T d\theta$ for μ from the decay:



$$m_t = 25 \text{ GeV}/c^2$$

\mathcal{E} is given in arbitrary unit ($\mathcal{E}=1$ at the peak)

Also shown are the curves of constant x

————— Baryons
 - - - - - Mesons

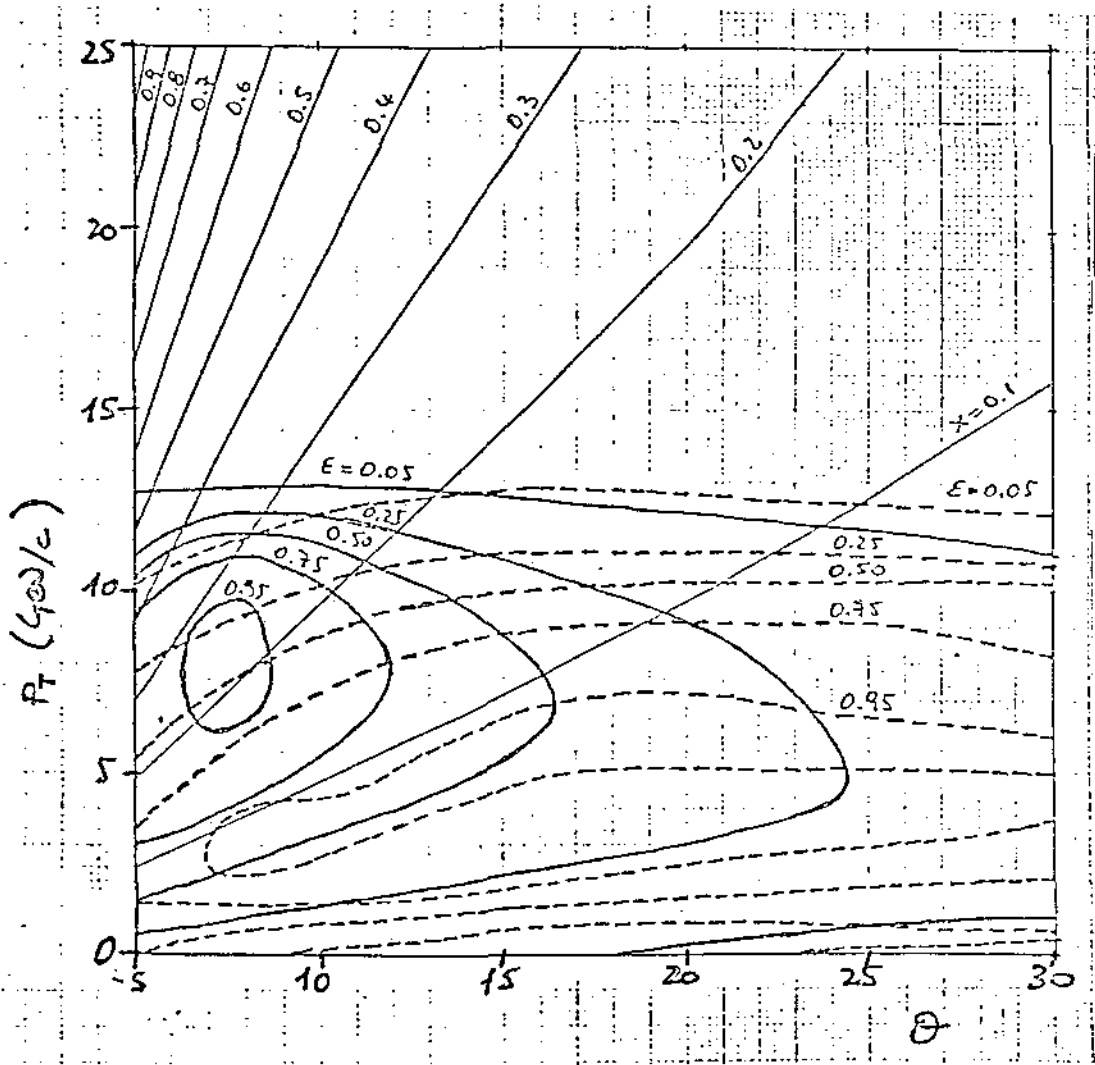
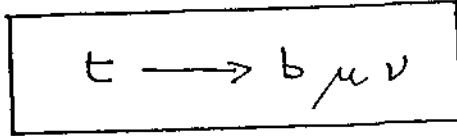


Fig. 10

Isorate levels $\mathcal{E} = d^2N/dp_T d\theta$ for μ from the decay:



$$m_t = 35 \text{ GeV}/c^2$$

———— Baryons
 - - - - Mesons

\mathcal{E} is given in arbitrary unit ($\mathcal{E}=1$ at the peak)
 Also shown are the curves of constant x

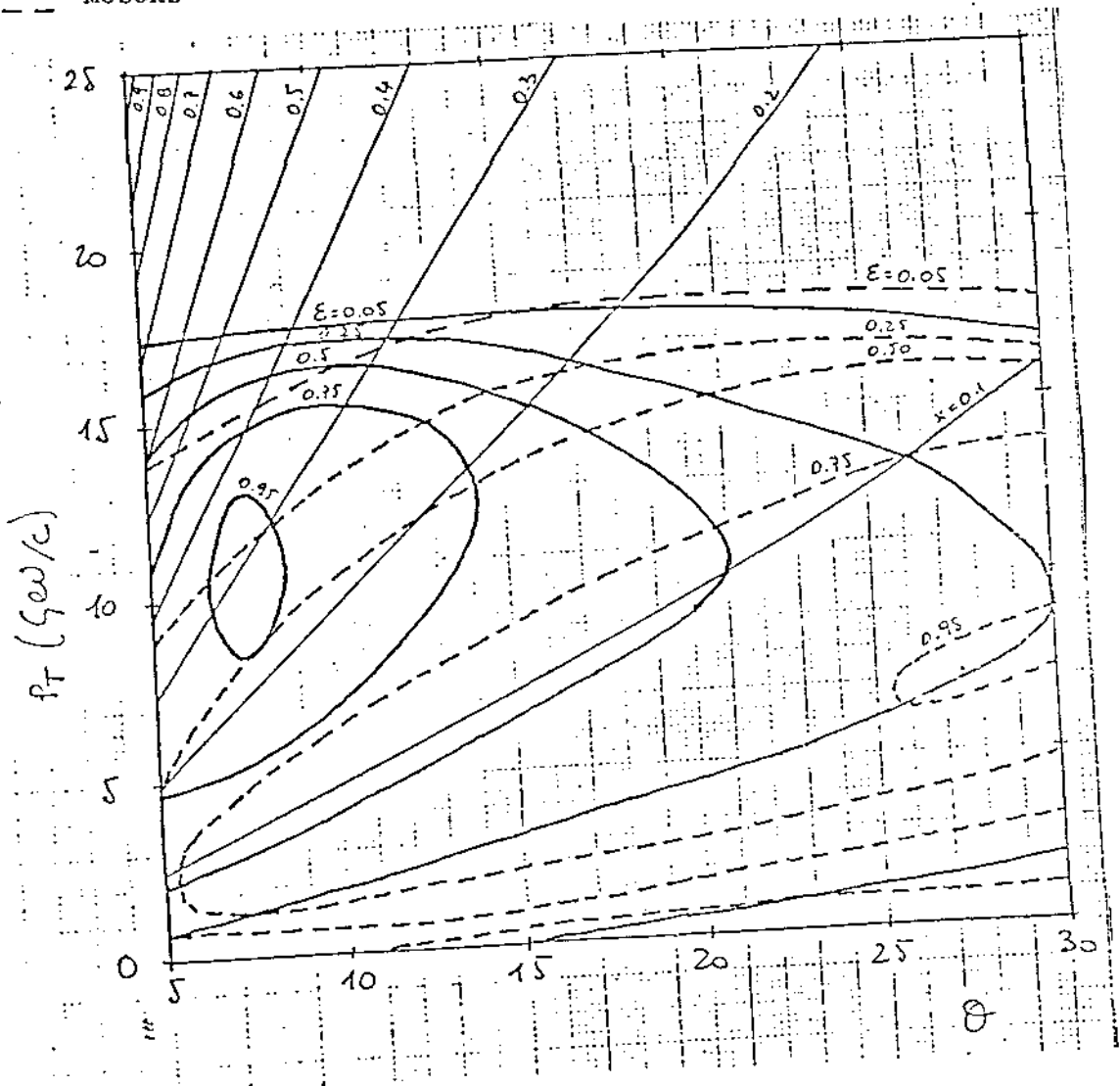
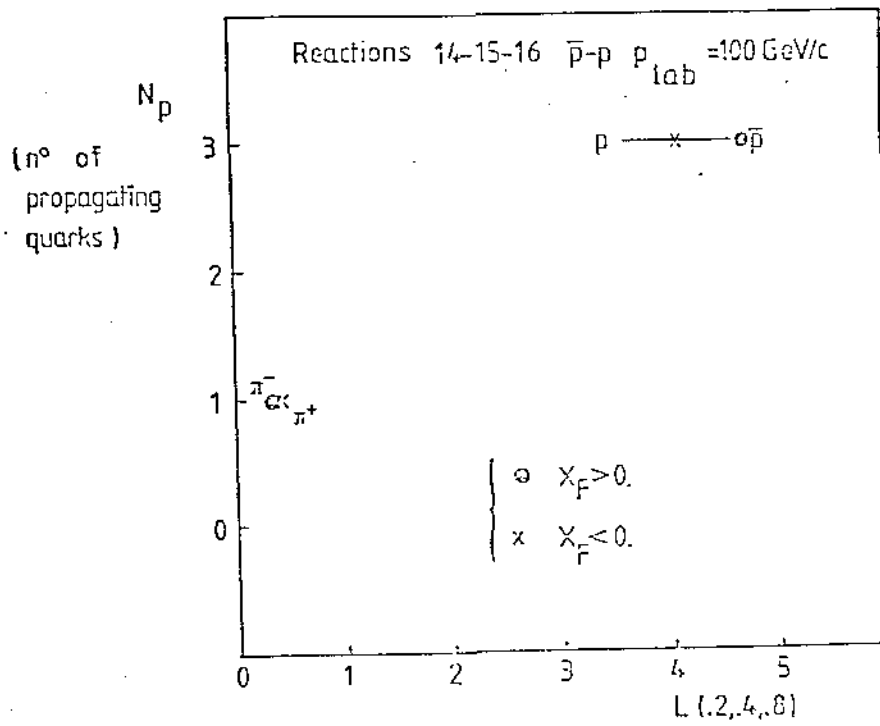


Fig. 11



$\pm L(0.2, 0.4, 0.8)$ for final-state hadrons produced in \bar{p} -p collisions at $P_{lab} = 100 \text{ GeV}/c$.

Fig. 12

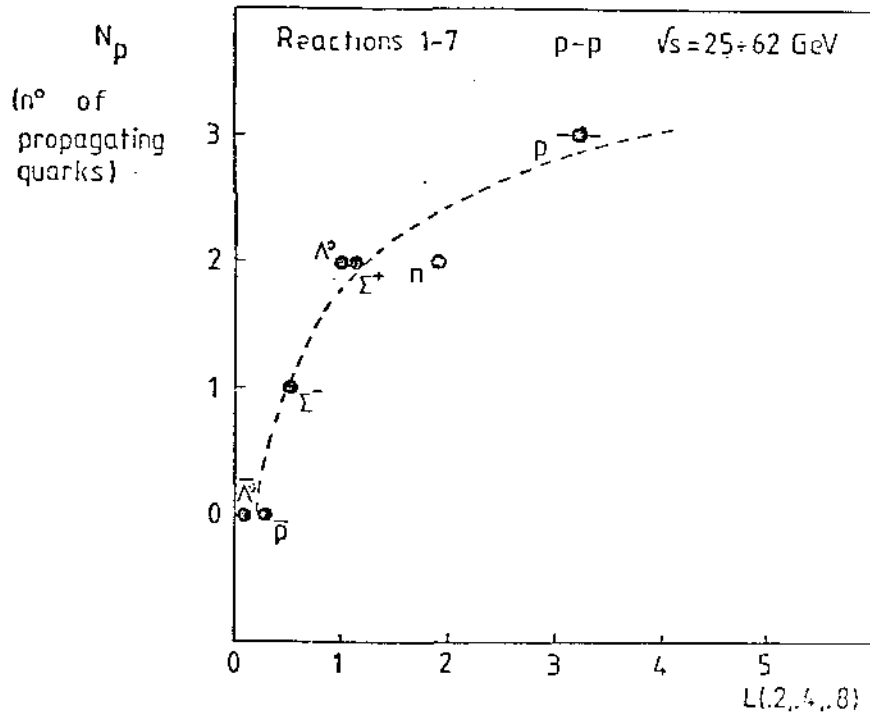


Fig. 13 - The leading quantity $L(0.2, 0.4, 0.8)$ for various final-state hadrons in pp collisions at ISR energies ($25+62 \text{ GeV}$) is plotted vs. the number of propagating quarks from the incoming into the final-state hadrons. The dashed line is obtained by using a parametrization of the single-particle inclusive cross-section, as described in the text.

Fig. 13

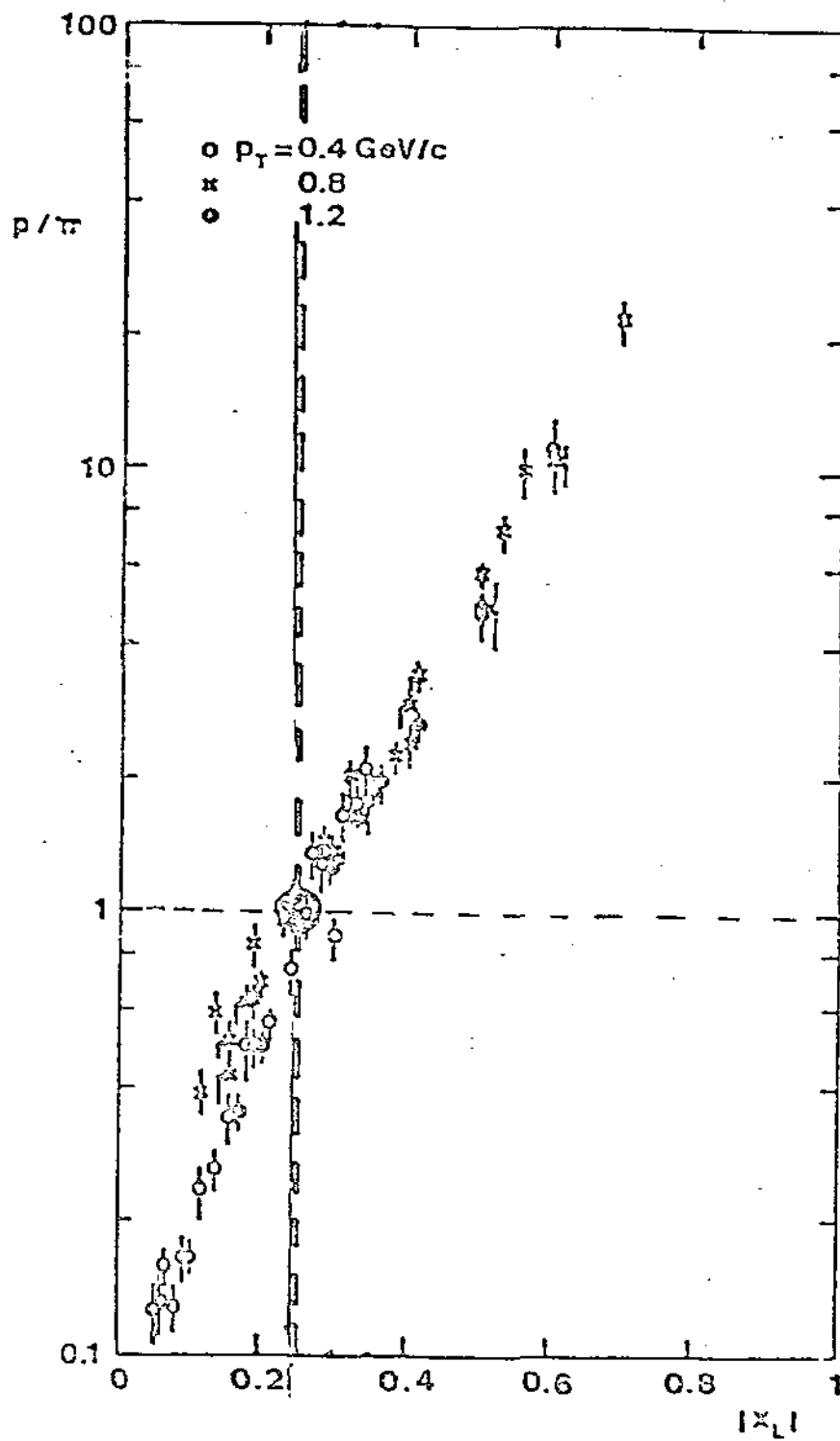


Fig. 14

Proton over pion production ratio in (pp) interactions
as function of x , for various p_T .

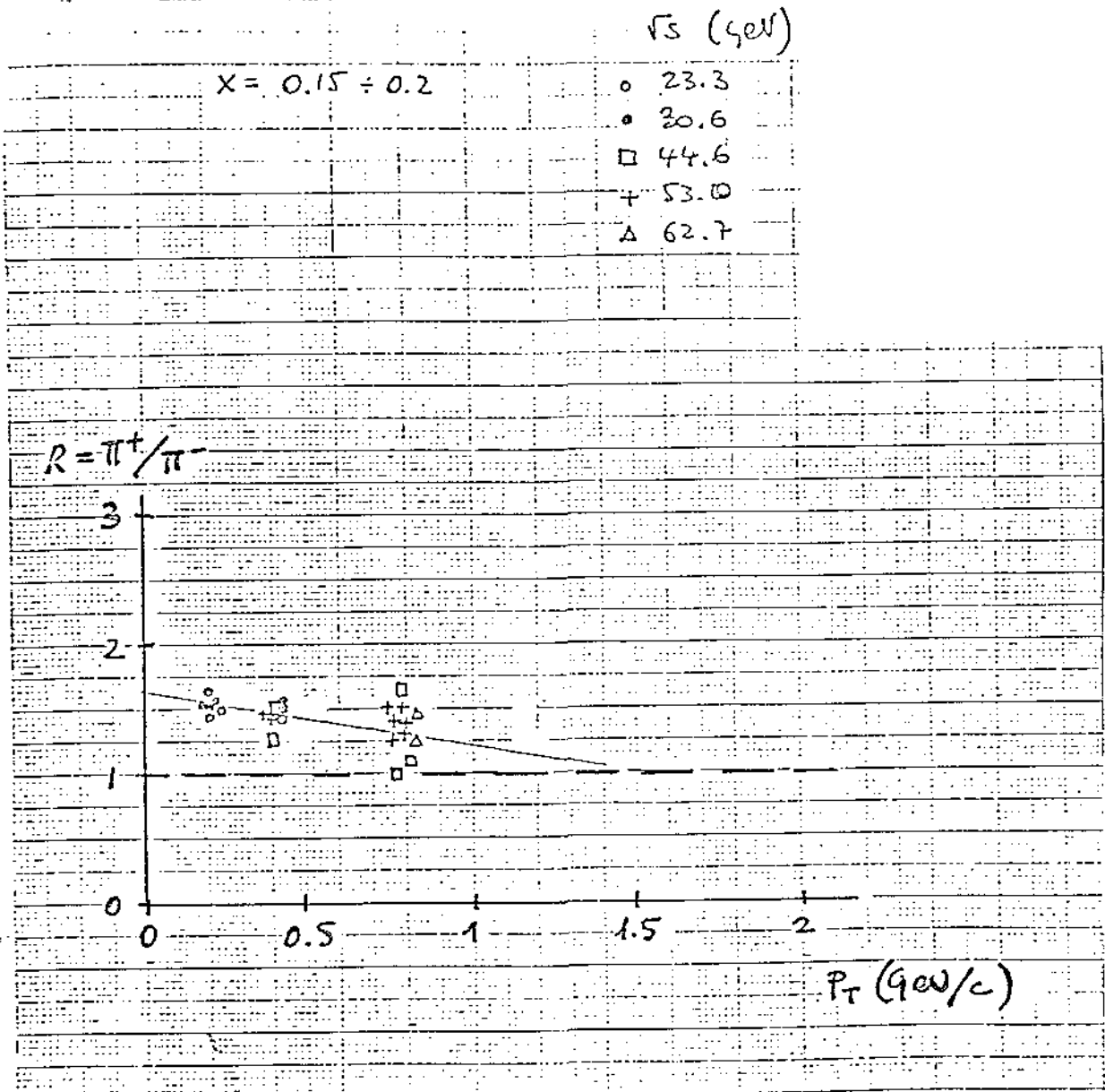


Fig. 15a

$x = 0.3 \div 0.35$	V_S (GeV)
○	23.3
●	30.6
□	44.6
+	53.0
△	62.7

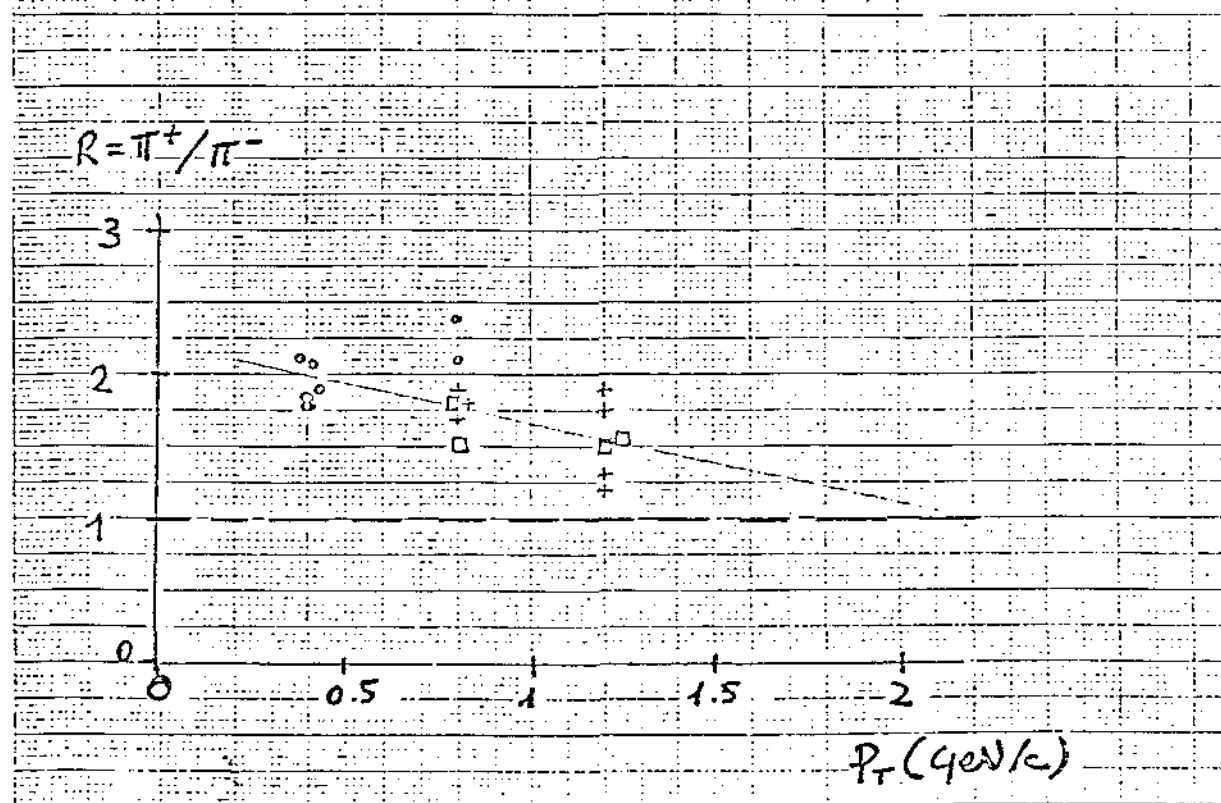


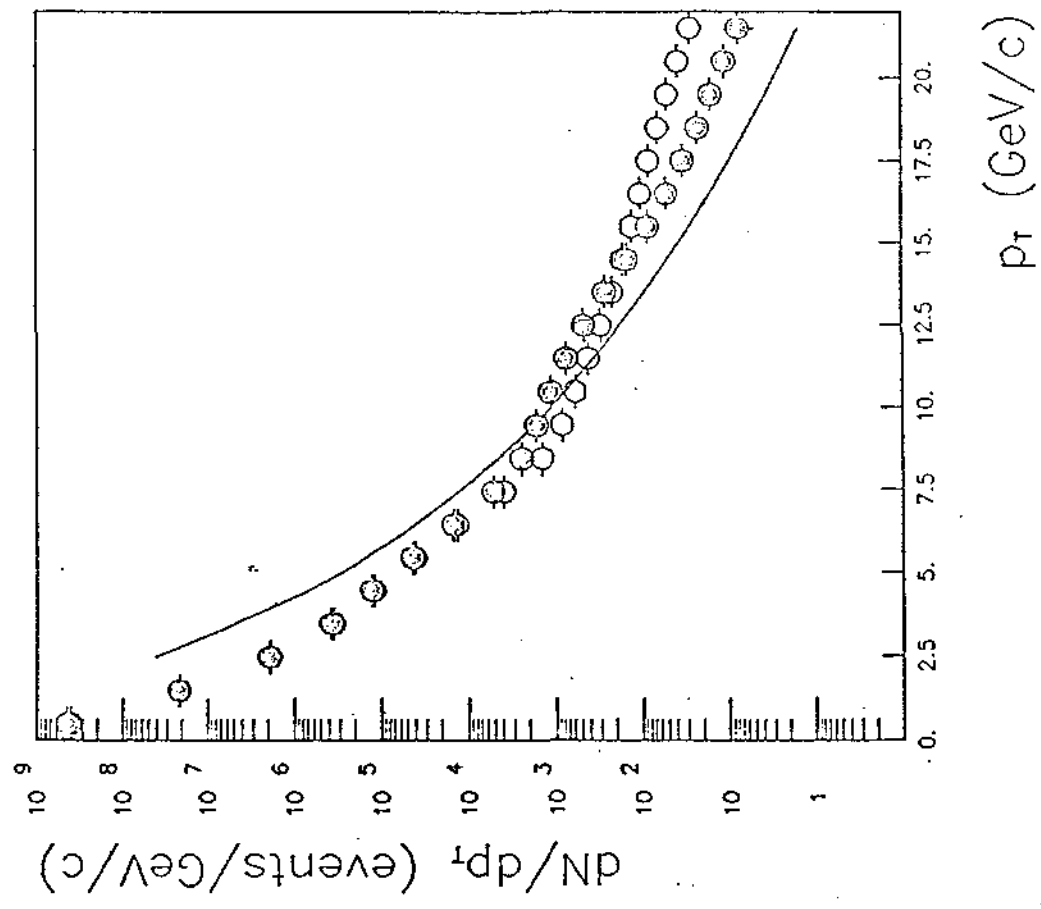
Fig. 15b

top (25 GeV) AND superbeauty (55 GeV) PRODUCTION

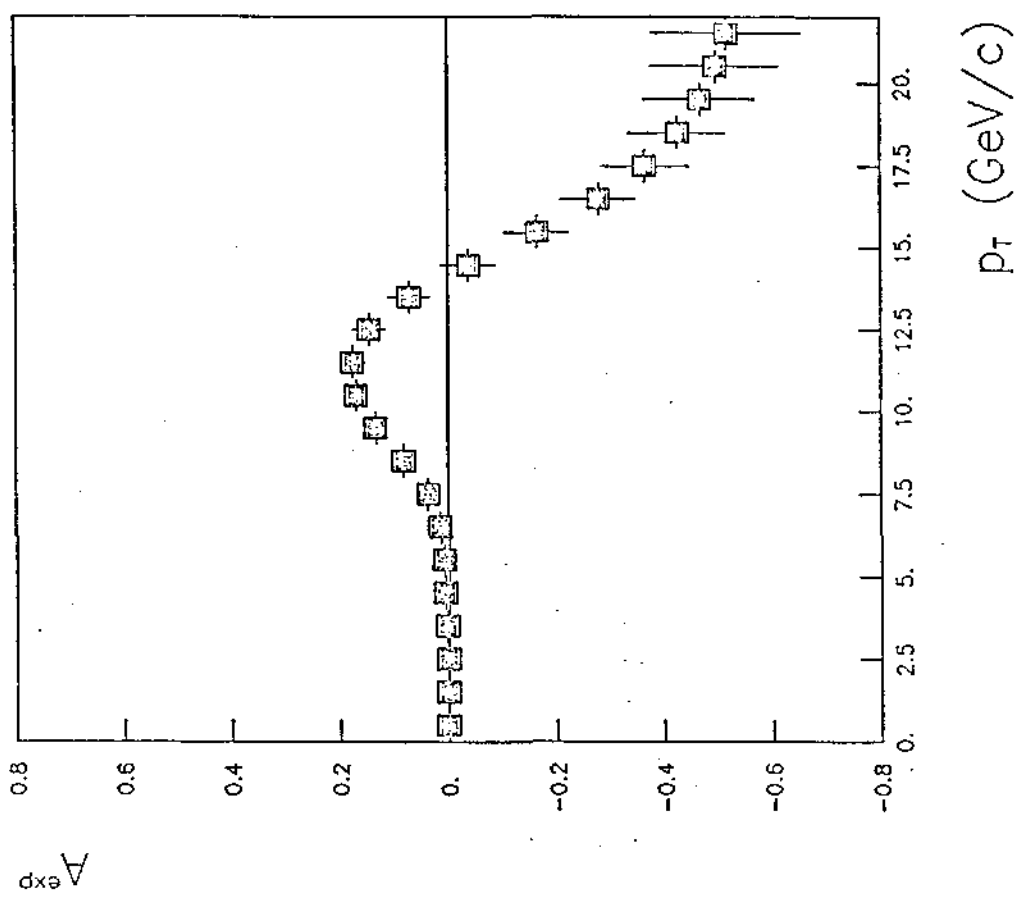
$5. \leq \eta < 30.$

$\Delta p_T / p_T = 20. \%$

$\frac{\pi^+}{\pi^-} = 1$ $\left. \begin{array}{l} \sigma_T = 0.1 \mu\text{b} \\ \sigma_{cb} = 0.01 \mu\text{b} \end{array} \right\} \text{assumed values}$



(a)



(b)

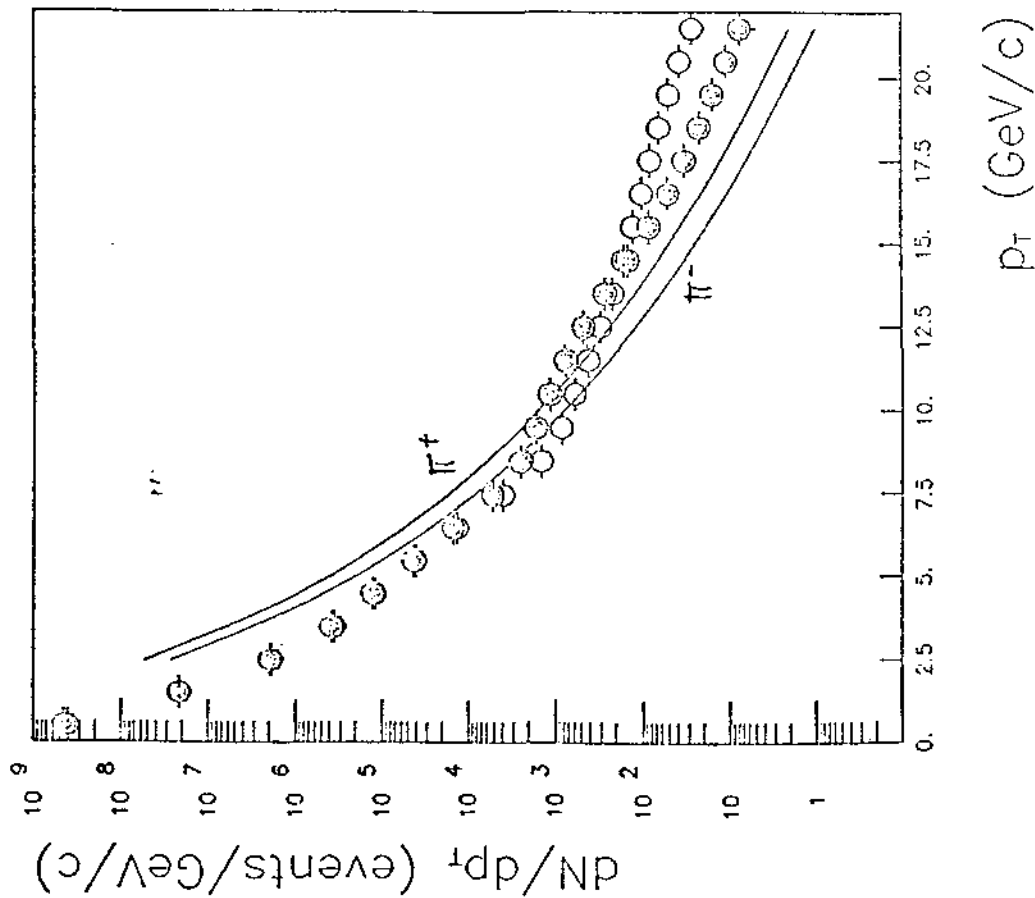
Fig. 15

top (25 GeV) AND superbeauty (55 GeV) PRODUCTION

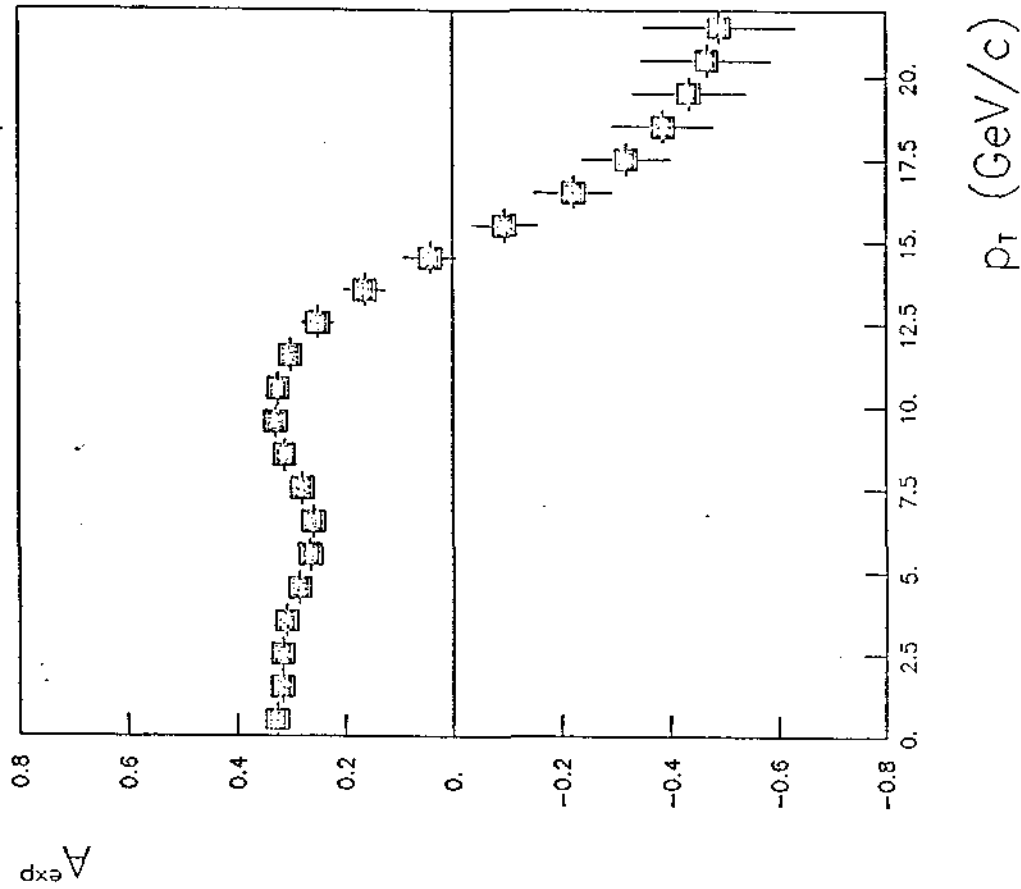
$5. \leq \theta < 30.$

$\Delta p_T / p_T = 20. \%$

$$\frac{\pi^+}{\pi^-} = 2, \quad \begin{cases} \sigma_t = 0.1 \mu b \\ \sigma_{sb} = 0.01 \mu b \end{cases} \left| \begin{array}{l} \text{assumed} \\ \text{values} \end{array} \right.$$



(a)



(b)

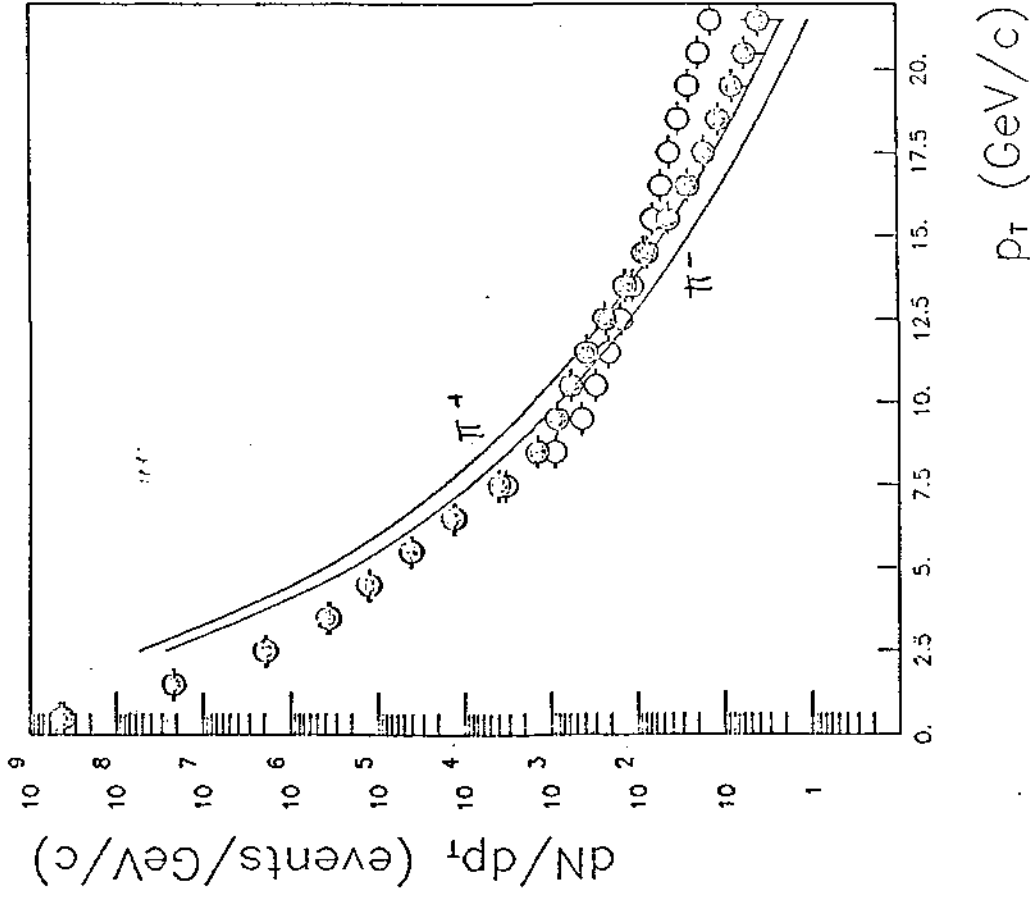
Fig. 17

top (25 GeV) AND superbeauty (55 GeV) PRODUCTION

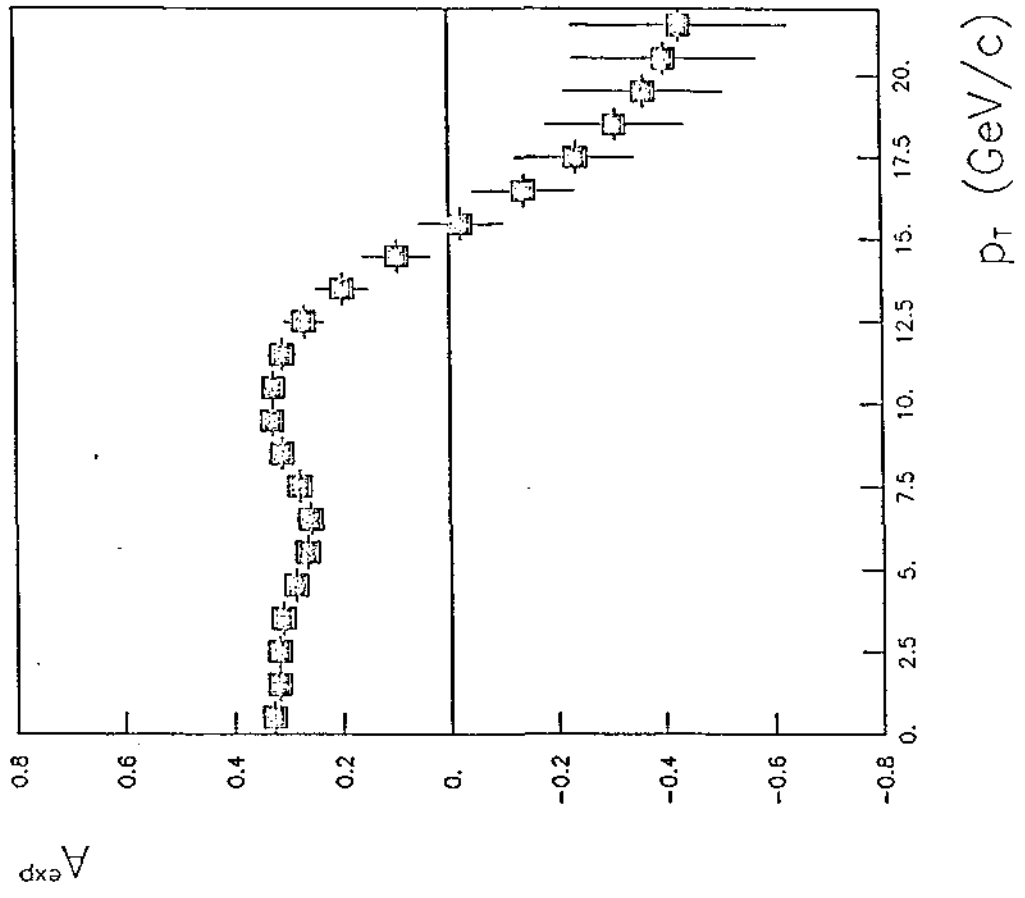
$5. \leq \theta < 30.$

$\Delta p_T / p_T = 20. \%$

$\frac{\pi^+}{\pi^-} = 2$
 $\sigma_T = 5 \times 10^{-2} \mu\text{b}$ } factor 2
 $\sigma_{SB} = 5 \times 10^{-3} \mu\text{b}$ } lower



(a)



(b)

Fig. 18

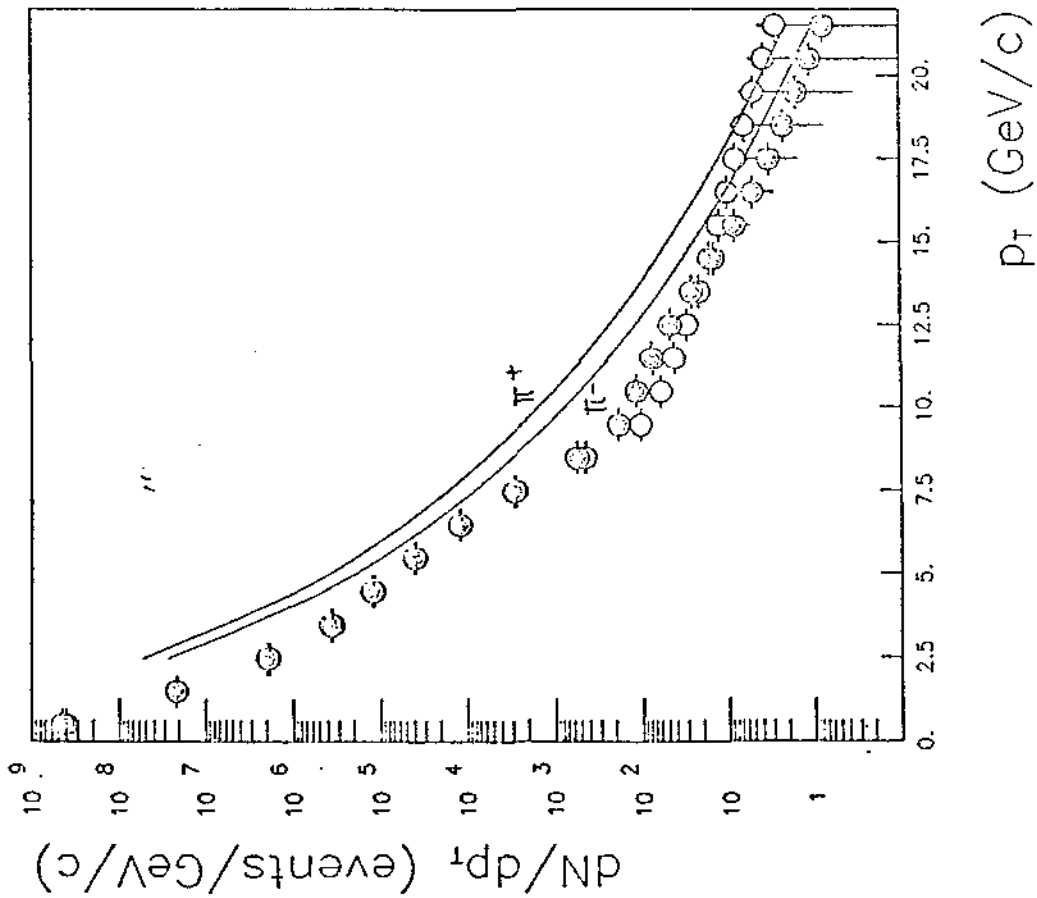
top (25 GeV) AND superbeauty (55 GeV) PRODUCTION

$5. \leq \theta < 30.$

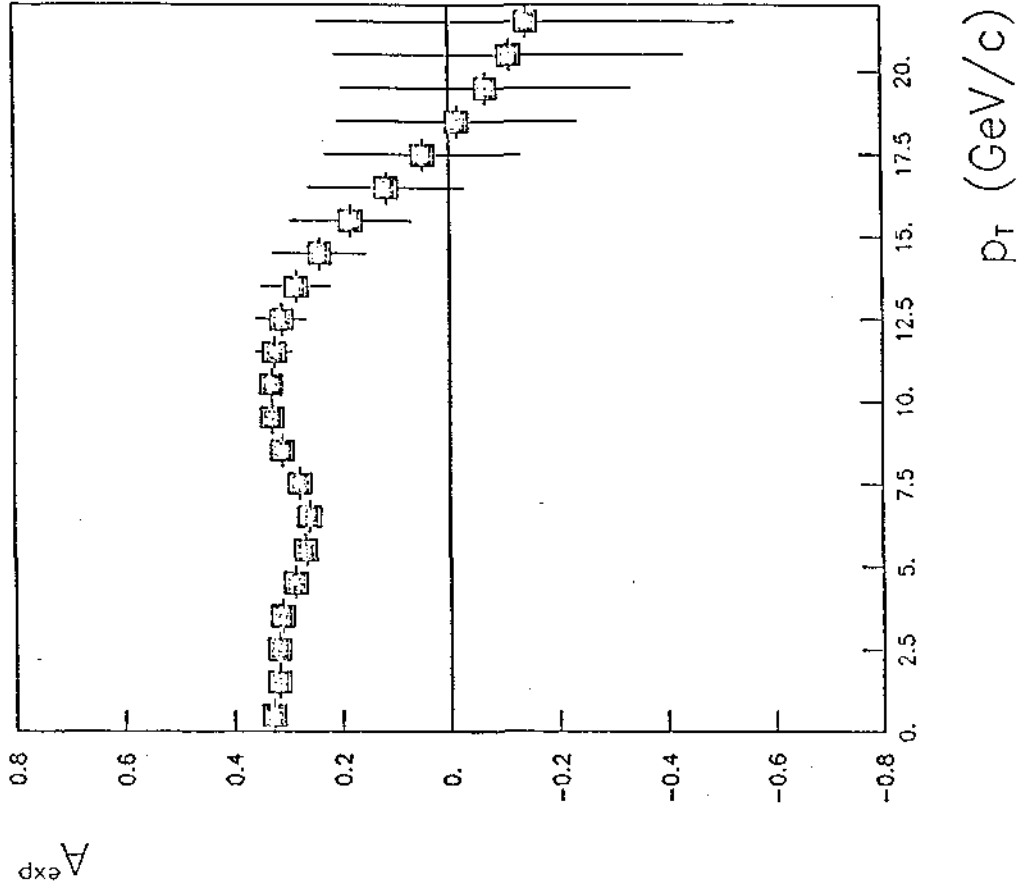
$\Delta p_T / p_T = 20. \%$

$\frac{\pi^+}{\pi^-} = 2$

$\sigma_t = 10^{-2} \mu b$
 $\sigma_{sb} = 10^{-3} \mu b$ } factor 10 lower



(a)



(b)

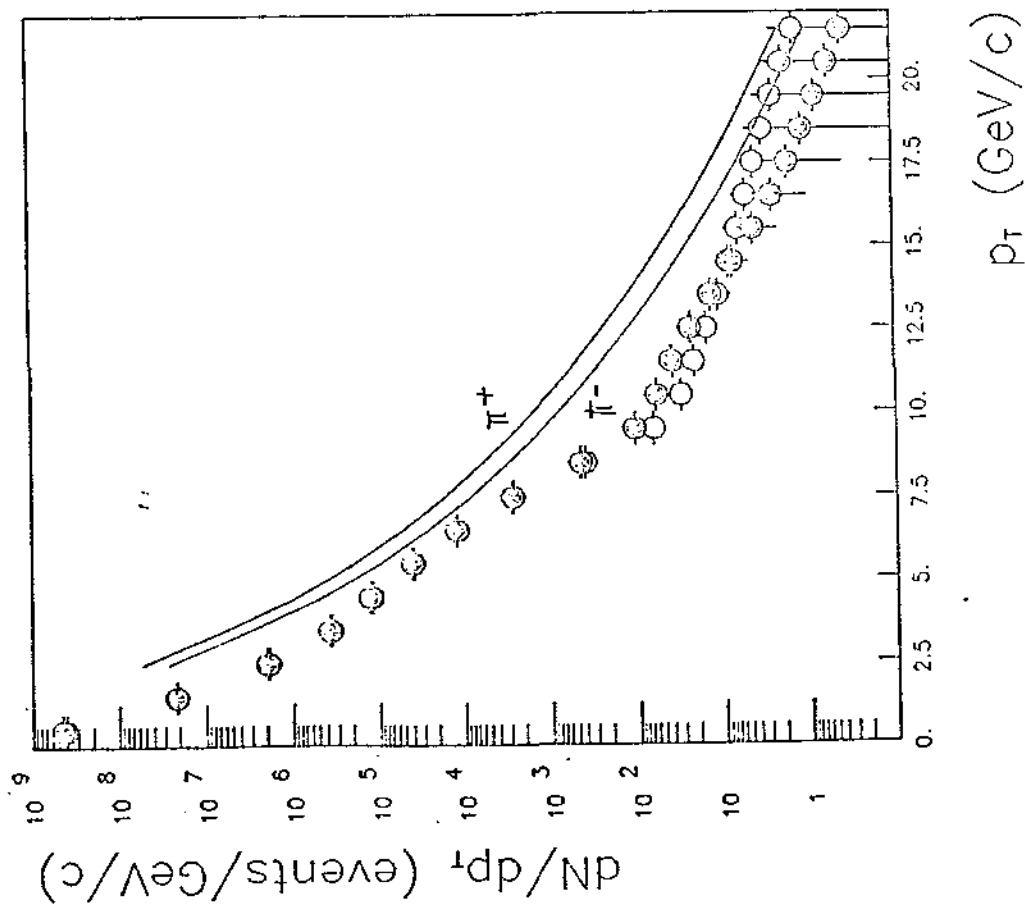
Fig. 19

top (25 GeV) AND superbeauty (55 GeV) PRODUCTION

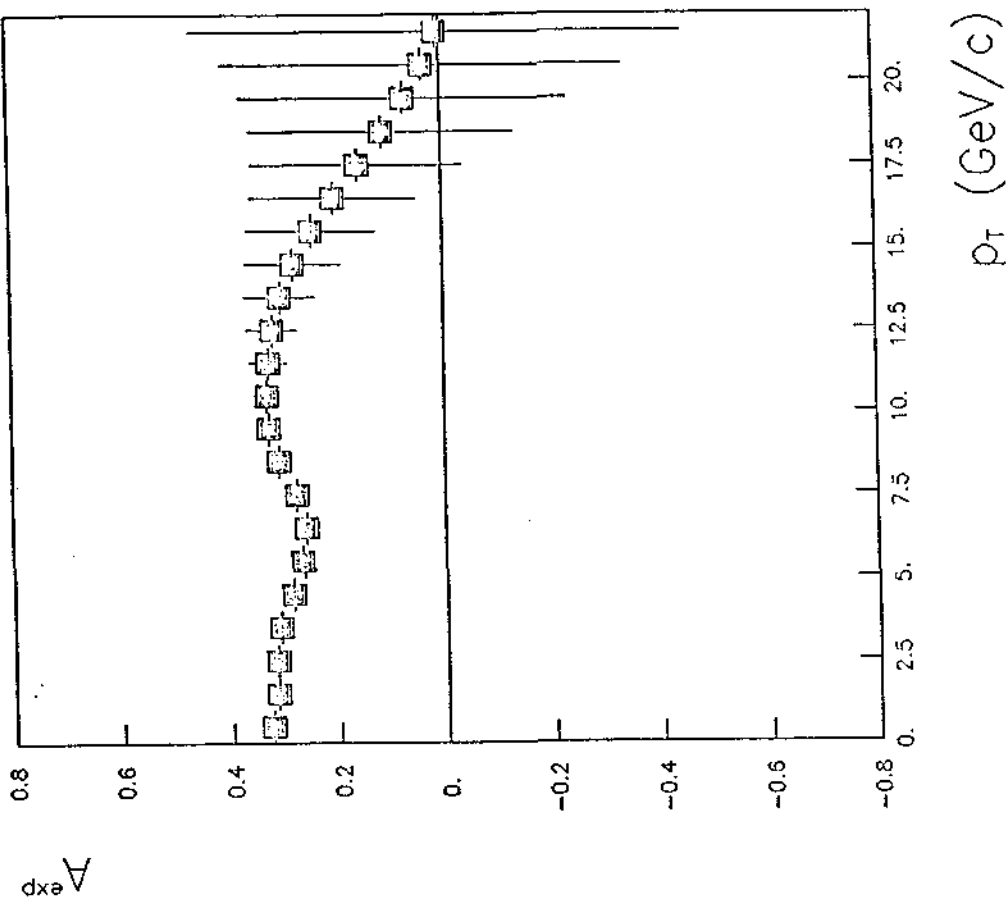
$5. \leq \eta < 30.$

$\Delta p_T / p_T = 20\%$

$\frac{\pi^+}{\pi^-} = 2$ } factor 20
 $\sigma_t = 5 \times 10^{-2} \mu b$ }
 $\sigma_{sb} = 5 \times 10^{-4} \mu b$ } lower



(a)



(b)

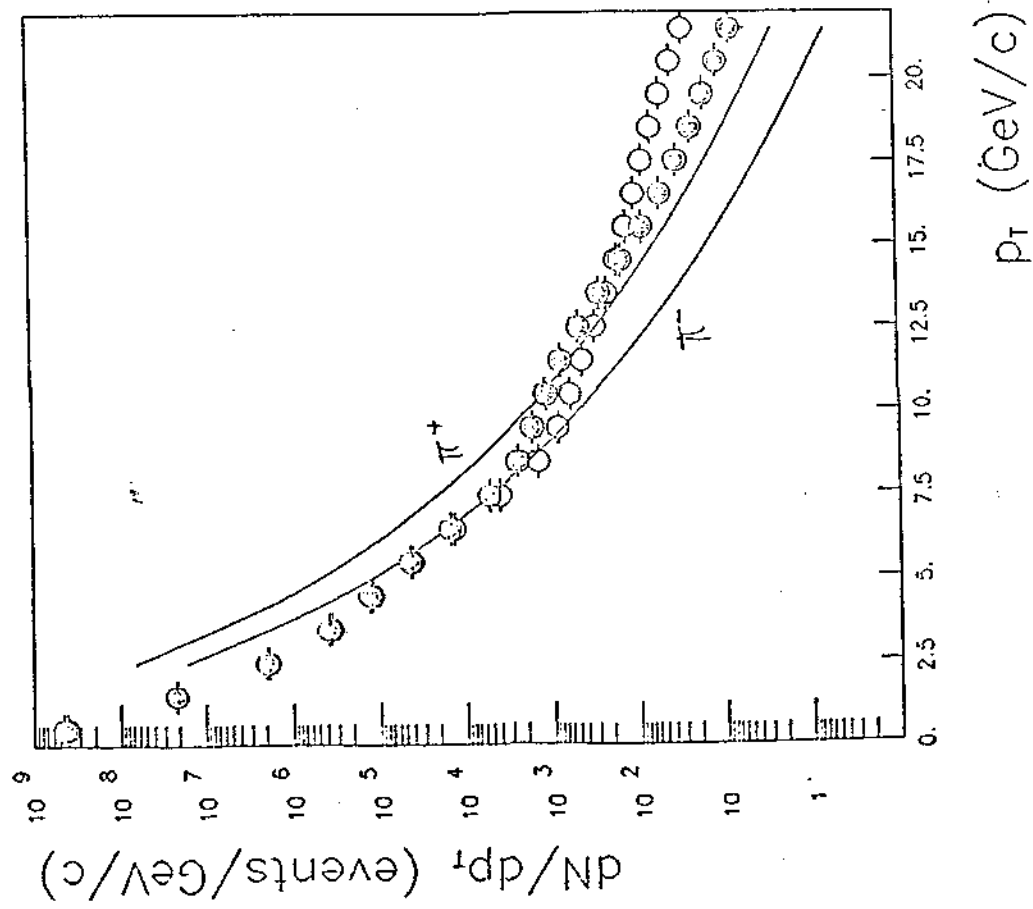
top (25 GeV) AND superbeauty (55 GeV) PRODUCTION

6.30

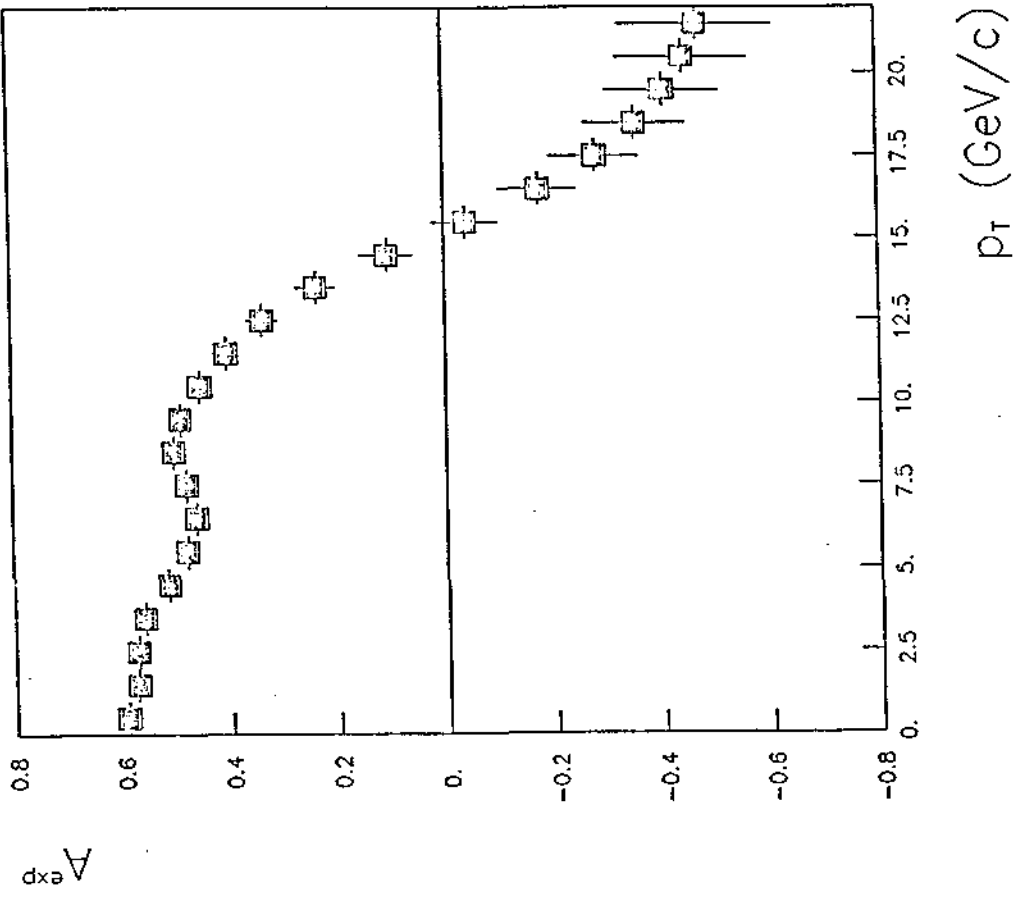
$5. \leq \theta < 30.$

$\Delta p_T / p_T = 20. \%$

$\frac{\pi^+}{\pi^-} = 4$ } assumed values
 $\sigma_t = 0.1 \mu\text{b}$
 $\sigma_{sb} = 0.01 \mu\text{b}$



(a)



(b)

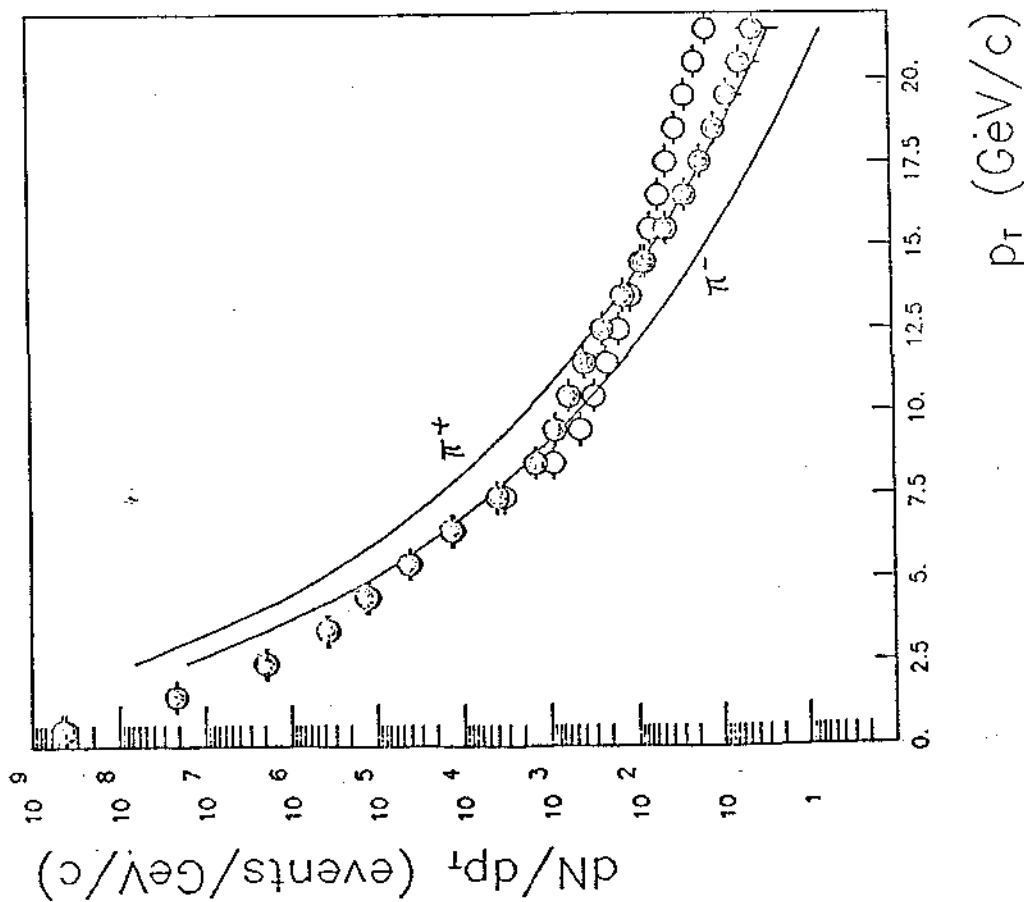
FIG. 21

top (25 GeV) AND superbeauty (55 GeV) PRODUCTION

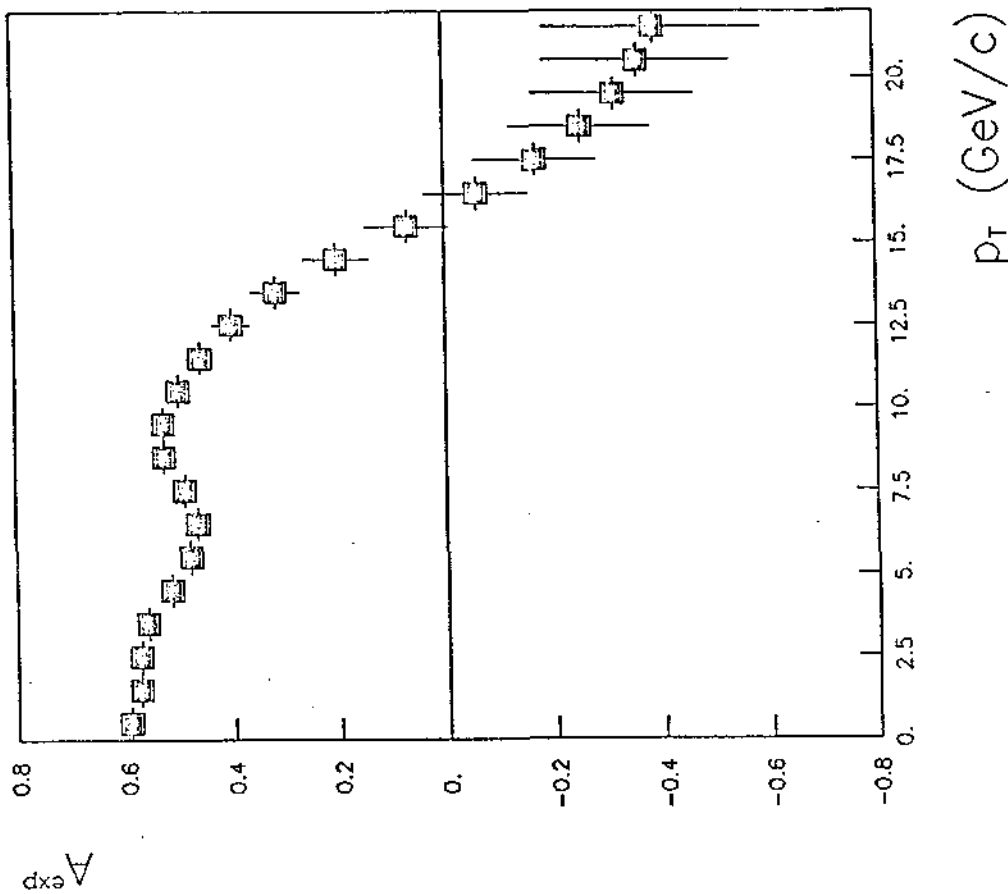
$5. \le \delta < 30.$

$\Delta p_T / p_T = 20. \%$

$\frac{\pi^+}{\pi^-} = 4$
 $\sigma_t = 65 \times 10^{-2} \mu b$
 $\sigma_{sb} = 5 \times 10^{-3} \mu b$ } factor 2 Error



(a)



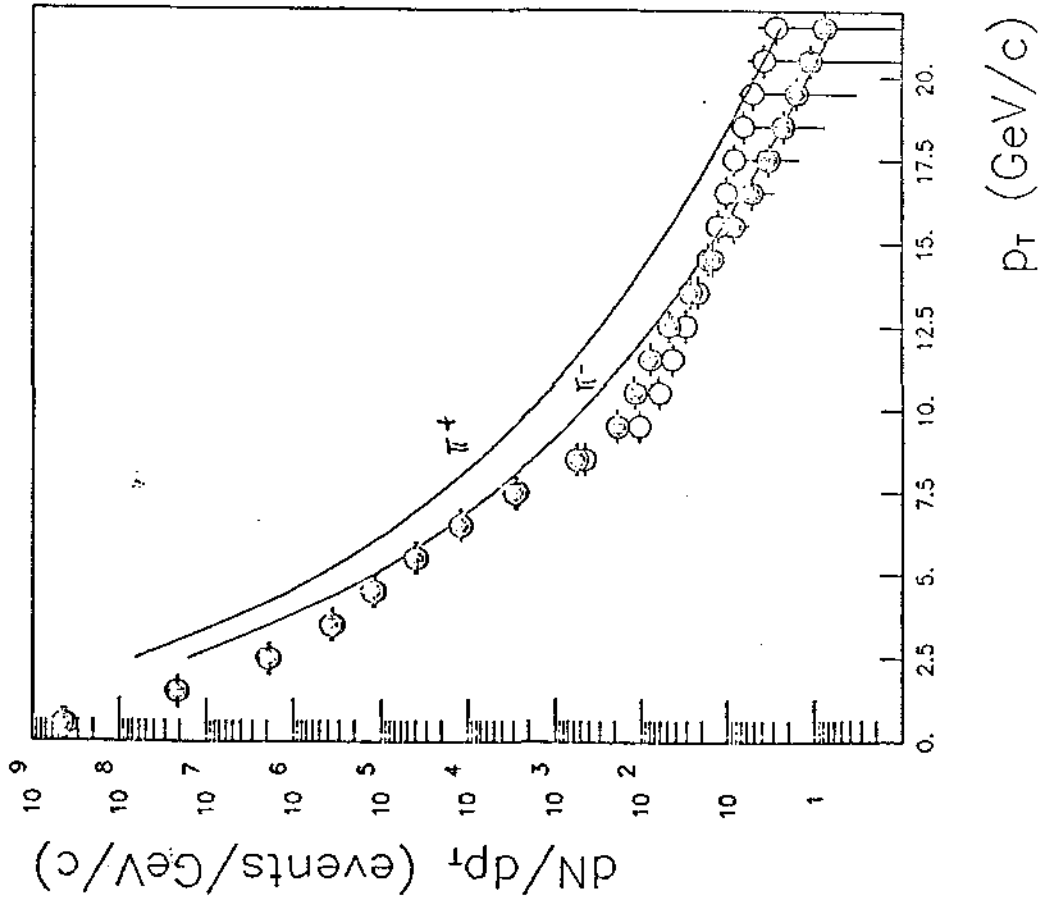
(b)

top (25 GeV) AND superbeauty (55 GeV) PRODUCTION

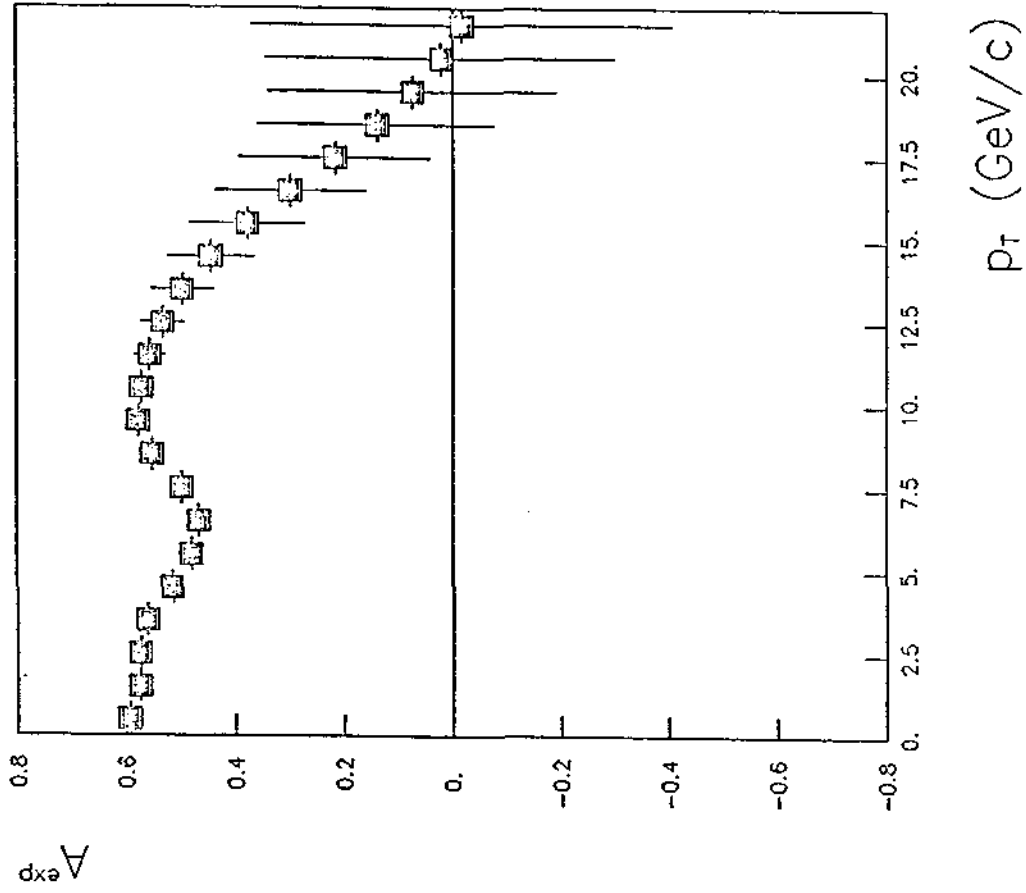
$5. \leq \theta < 30.$

$\Delta p_T / p_T = 20. \%$

$\frac{\pi^+}{\pi^-} = 4$ } factor 40
 $\frac{\sigma_{\pi^+}}{\sigma_{\pi^-}} = 10^{-2} \mu b$ } lower
 $\frac{\sigma_{\pi^+}}{\sigma_{\pi^-}} = 10^{-3} \mu b$ }



(a)



(b)

FIG. 23

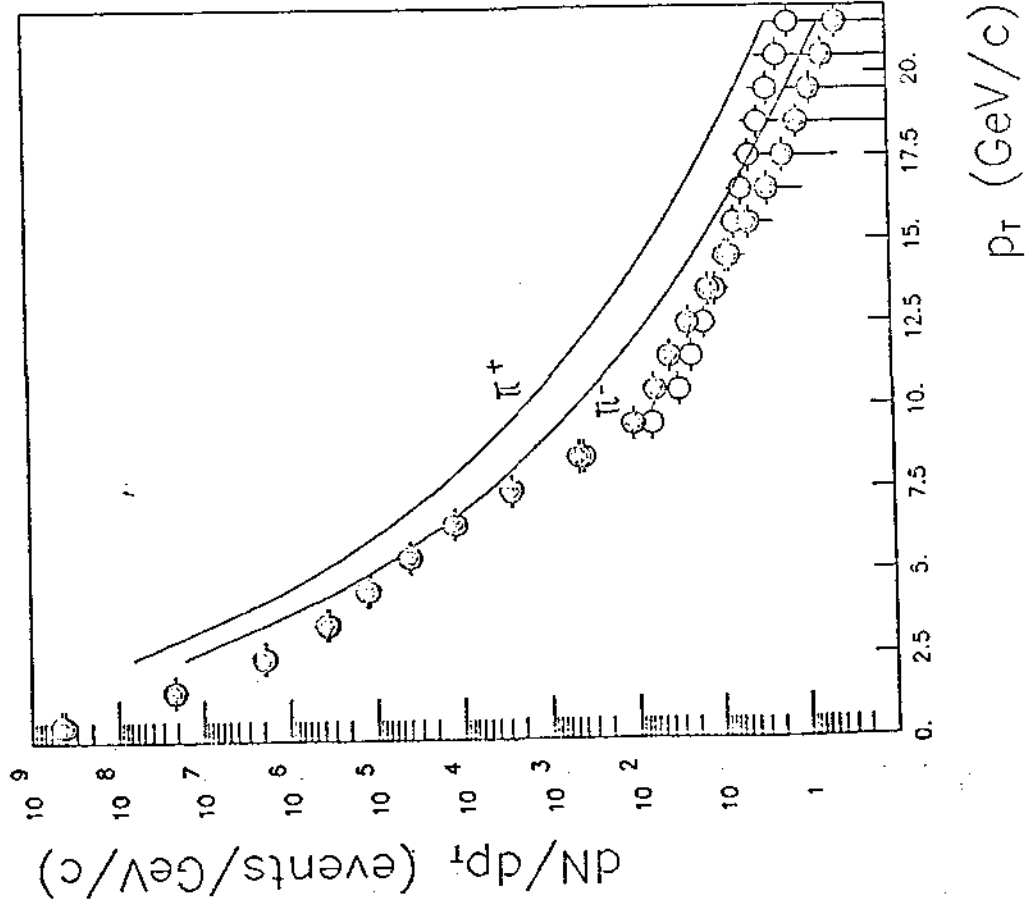
top (25 GeV) AND superbeauty (55 GeV) PRODUCTION

$5. \leq \theta < 30.$

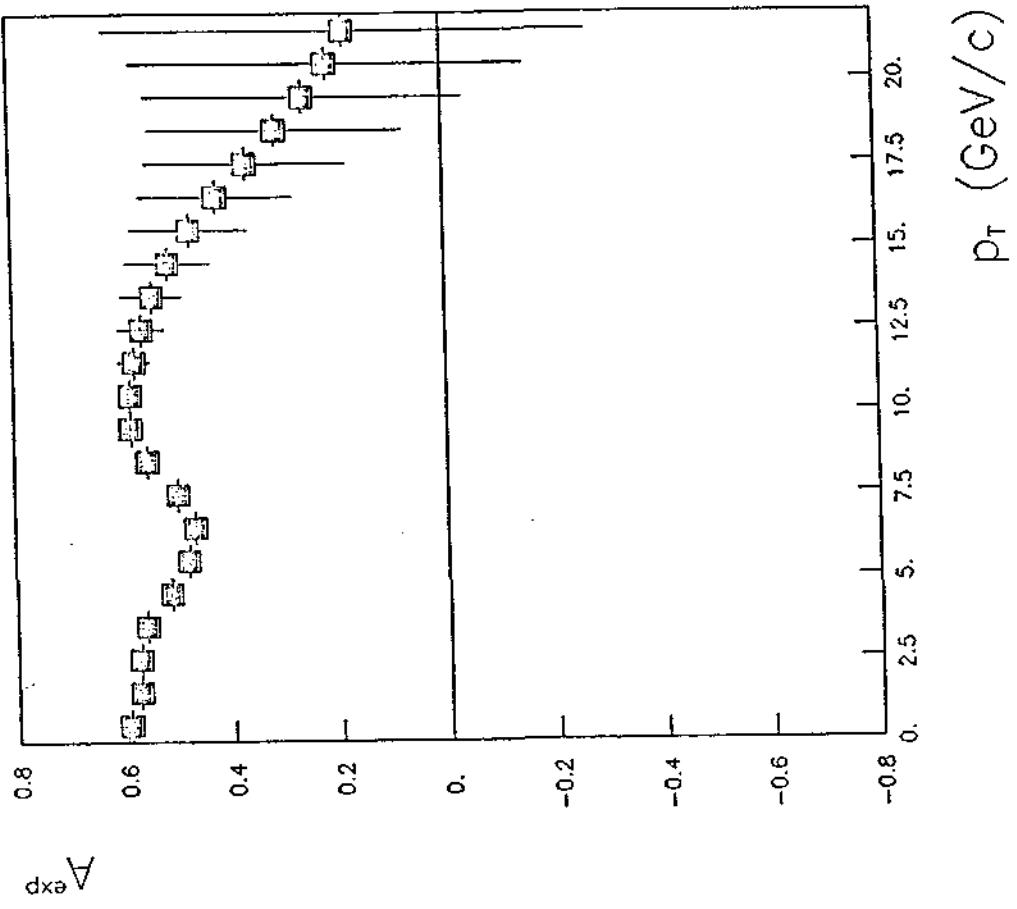
$\Delta p_T / p_T = 20. \%$

$\sigma_E = 5 \times 10^{-3} \mu b$
 $\sigma_{55} = 5 \times 10^{-4} \mu b$ } factor 20 lower

$\frac{\pi^+}{\pi^-} = 4$



(a)



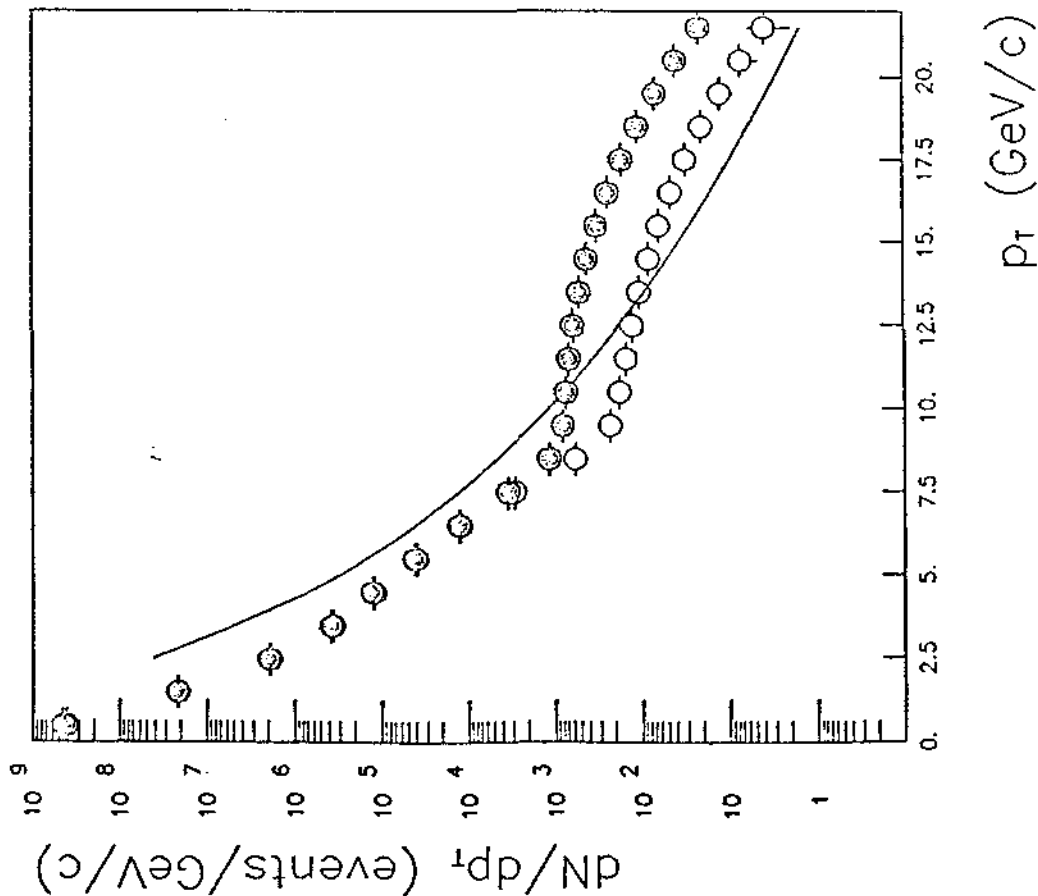
(b)

top (35 GeV) PRODUCTION

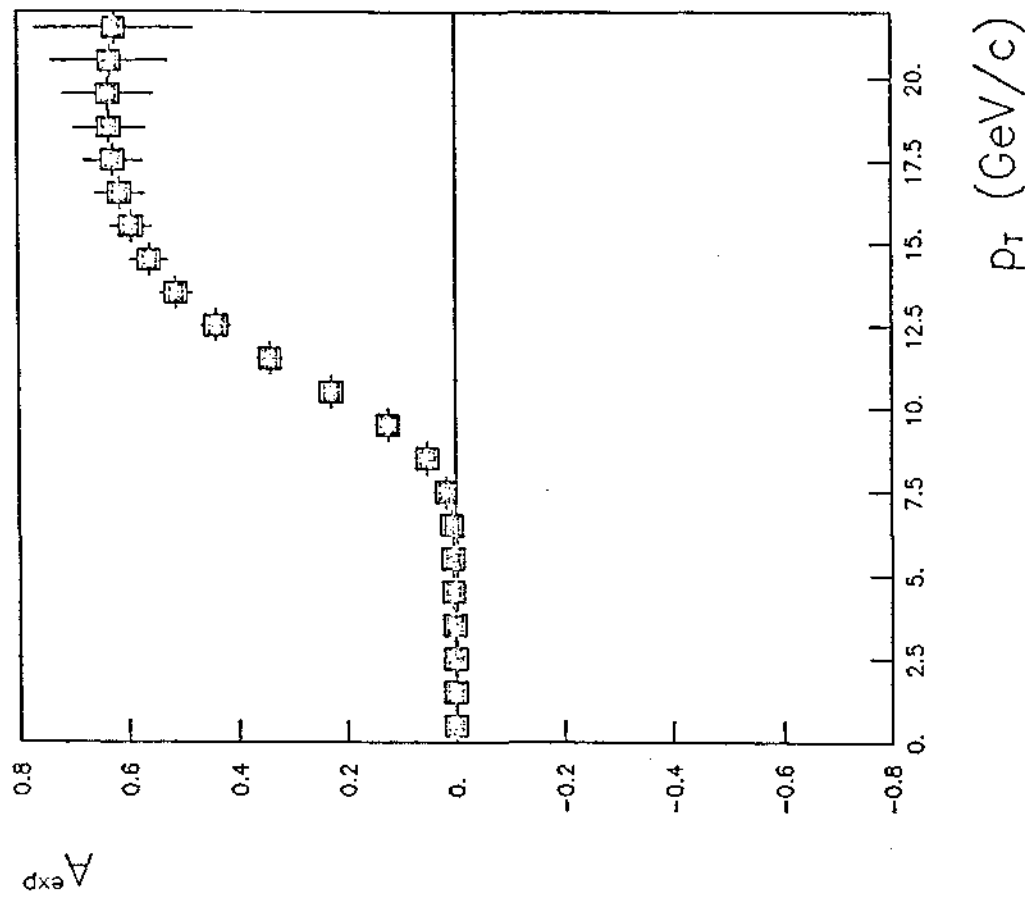
$5. \le \theta < 30.$

$\Delta p_T / p_T = 20. \%$

$\frac{\pi^+}{\pi^-} = -1$
 $\sigma_t = 0.05 \mu b$ assumed value



(a)



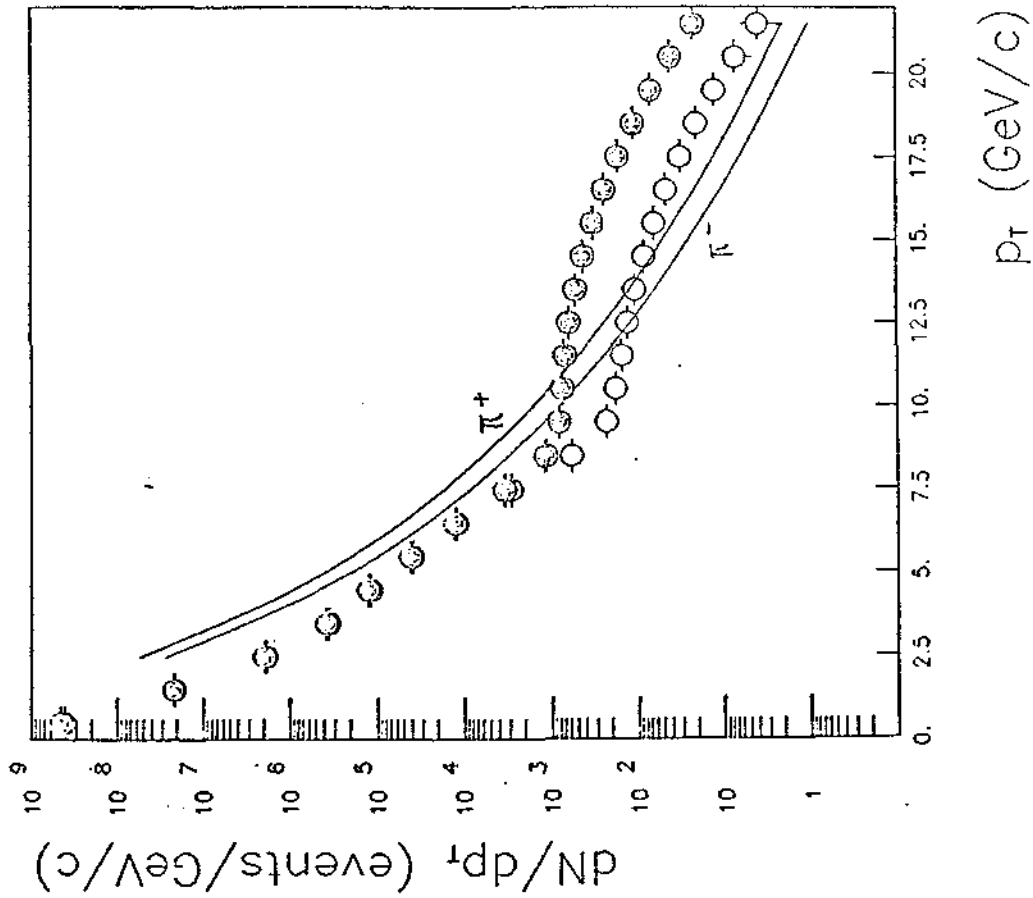
(b)

FIG. 25

top (35 GeV) PRODUCTION

$5. \leq \theta < 30.$

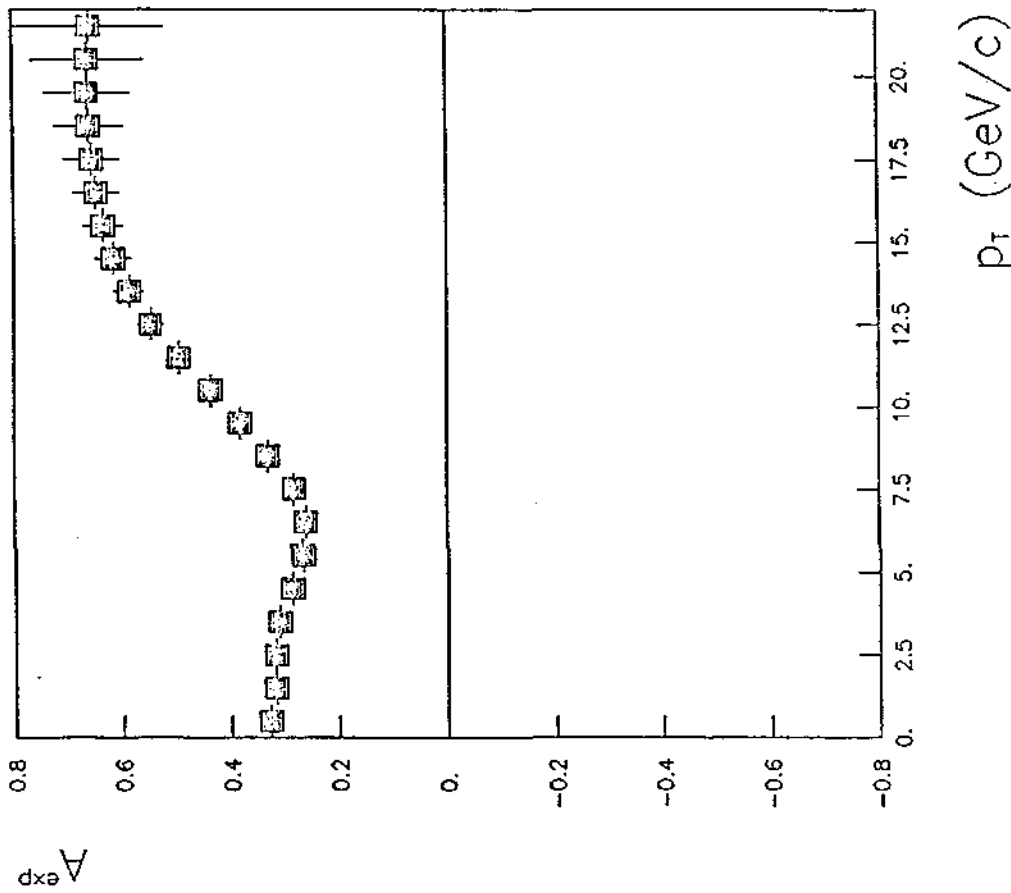
$\Delta p_T / p_T = 20. \%$



(a)

6.35

$\frac{\pi^+}{\pi^-} = 2$ $\sigma_t = 0.05 \mu b$ assumed value



(b)

FIG. 26

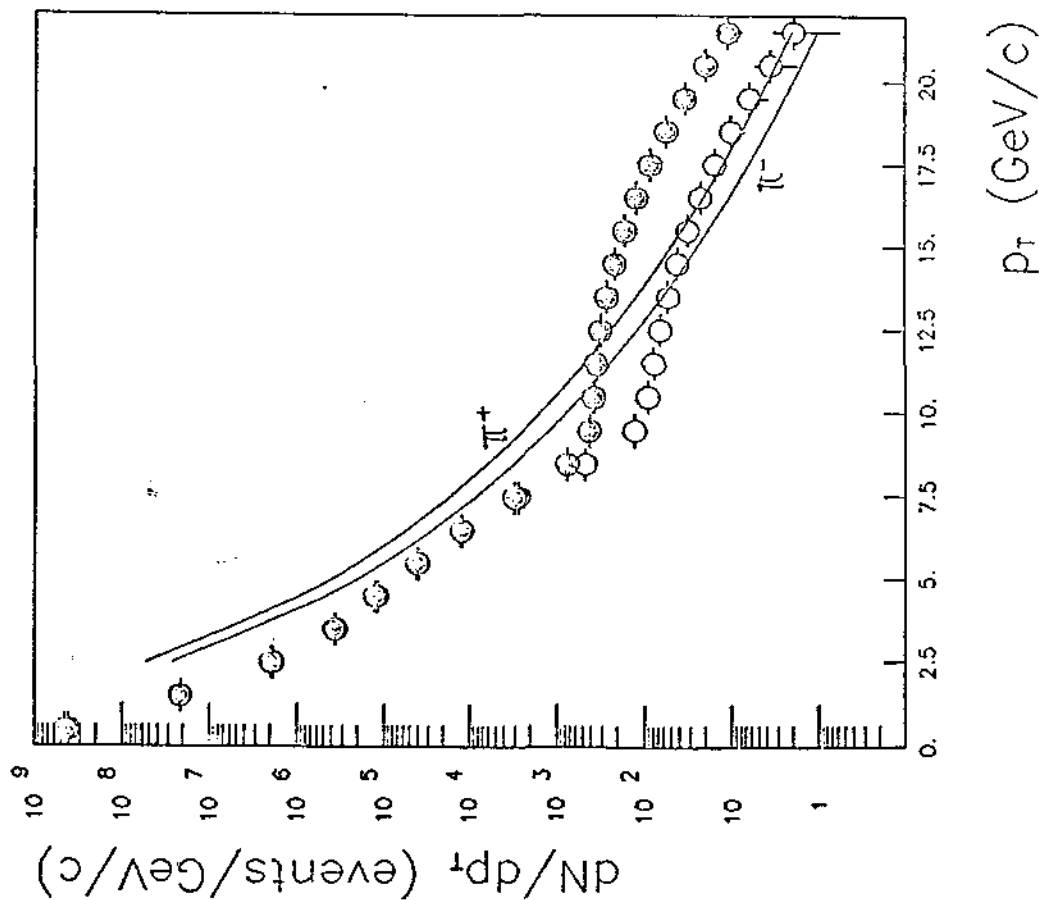
top (35 GeV) PRODUCTION

$5. \le \theta < 30.$

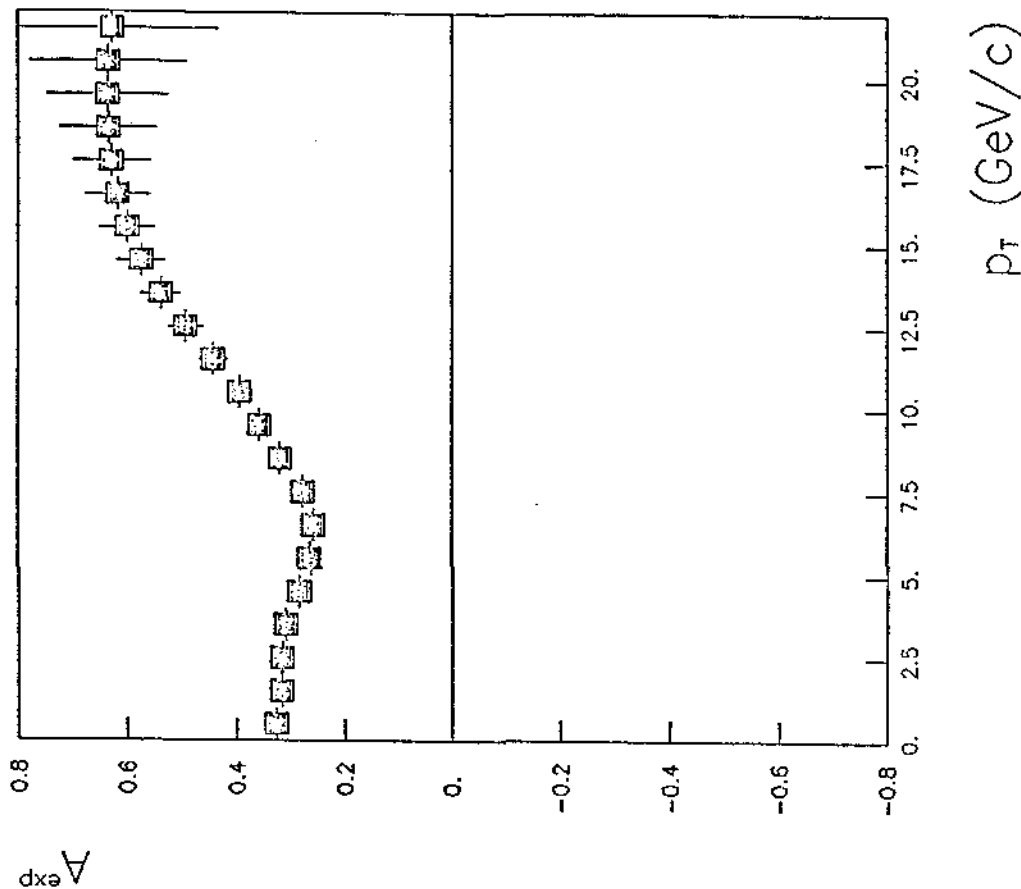
$\Delta p_T / p_T = 20. \%$

$$\frac{\pi^+}{\pi^-} = 2$$

$\sigma_T = 2.5 \times 10^{-2} \mu b$ factor 2 lower



(a)



(b)

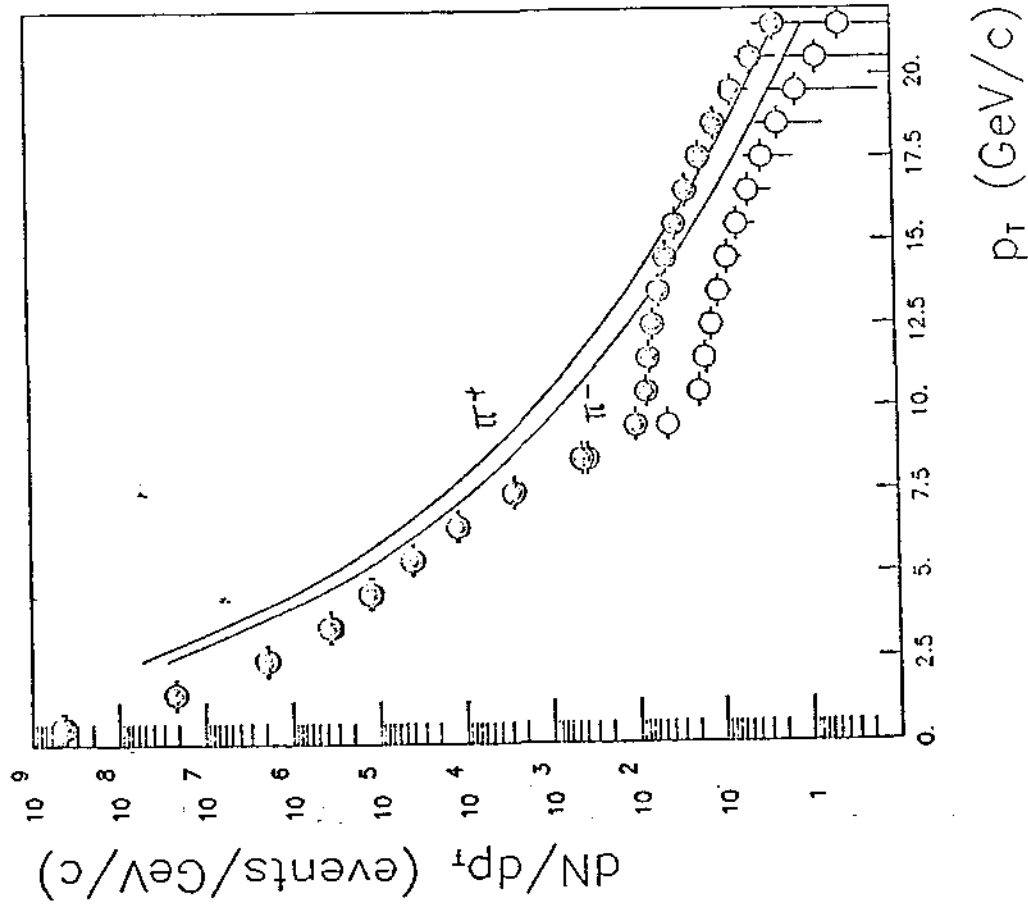
Fig. 27

top (35 GeV) PRODUCTION

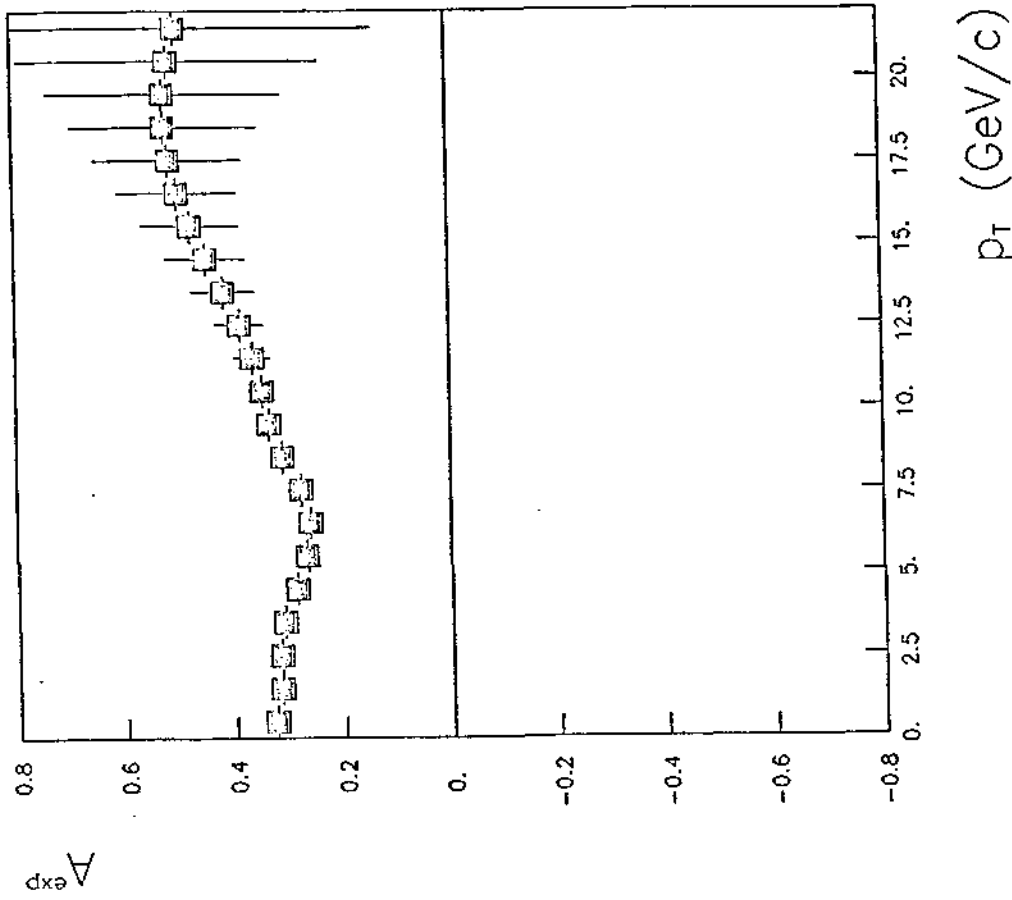
$5. \leq \theta < 30.$

$\Delta p_T / p_T = 20. \%$

$\frac{\pi^+}{\pi^-} = 2$ factor 10 lower
 $\sigma_e = 5 \times 10^{-3} \mu b$



(a)



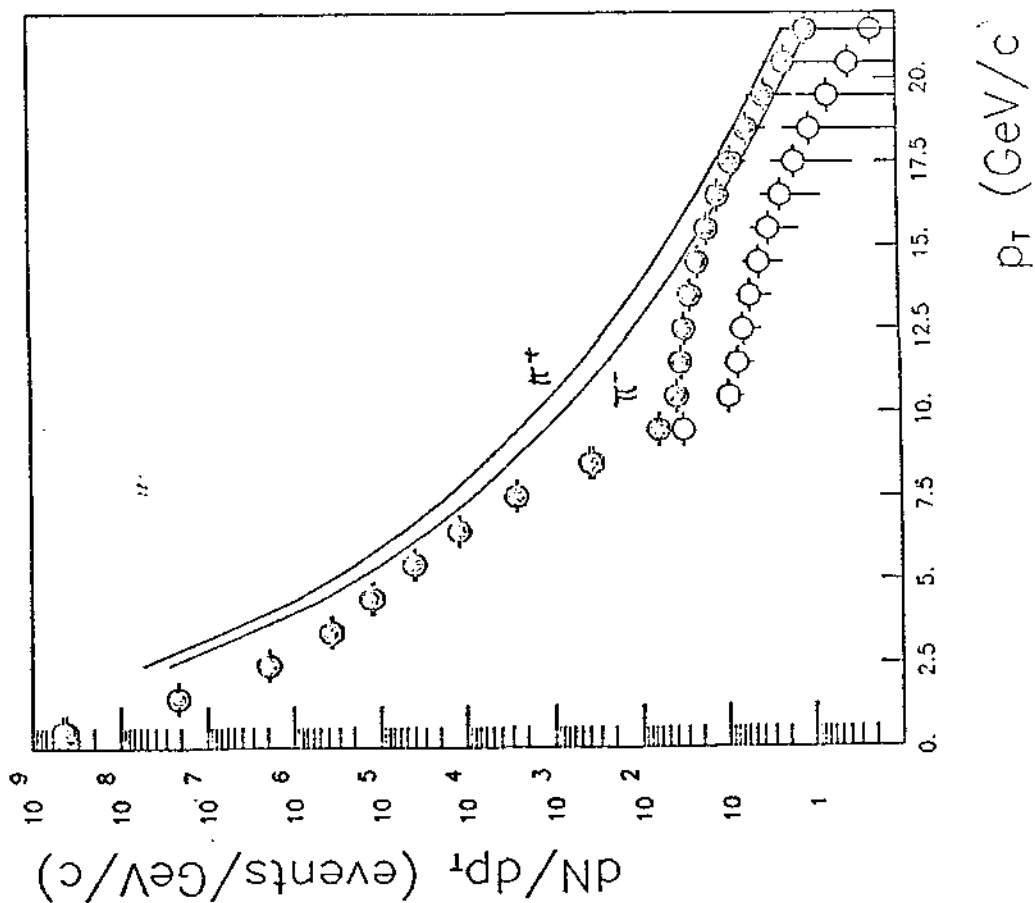
(b)

top (35 GeV) PRODUCTION

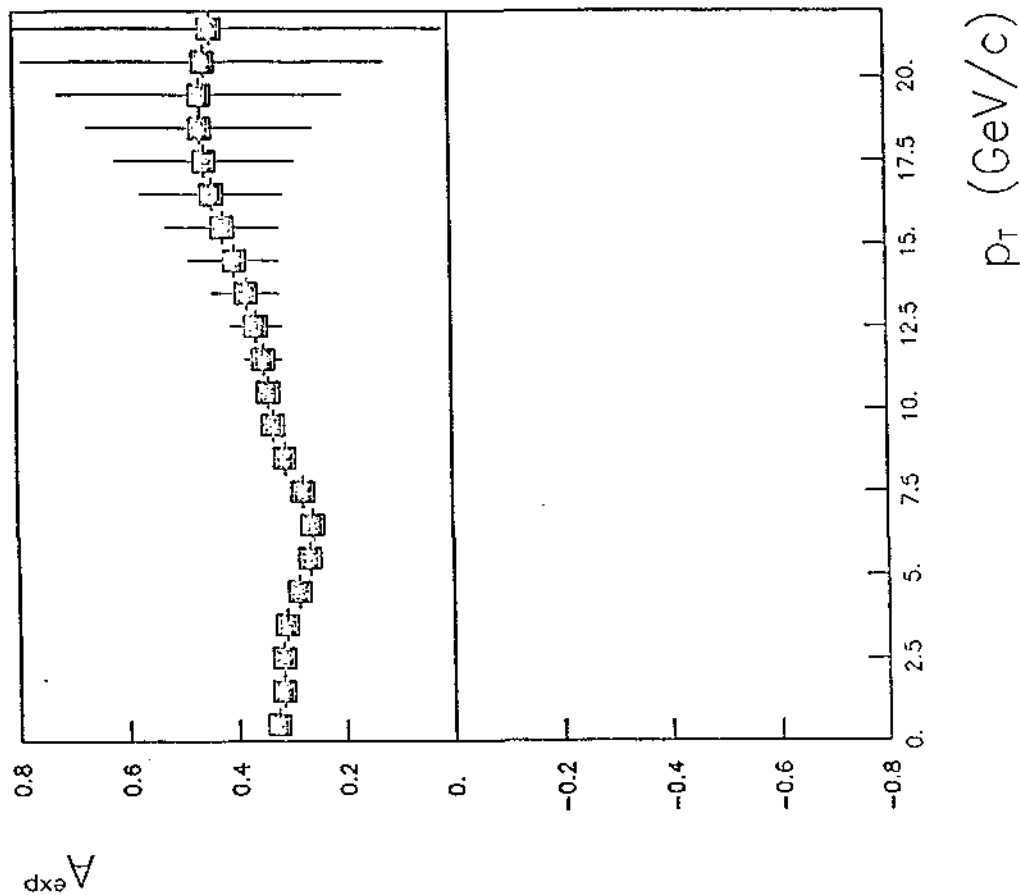
$5. \leq \theta < 30.$

$\Delta p_T / p_T = 20. \%$

$\frac{\pi^+}{\pi^-} = 2$ $\sigma_e = 2.5 \times 10^{-3} \mu b$ factor 20 lower



(a)



(b)

FIG. 29

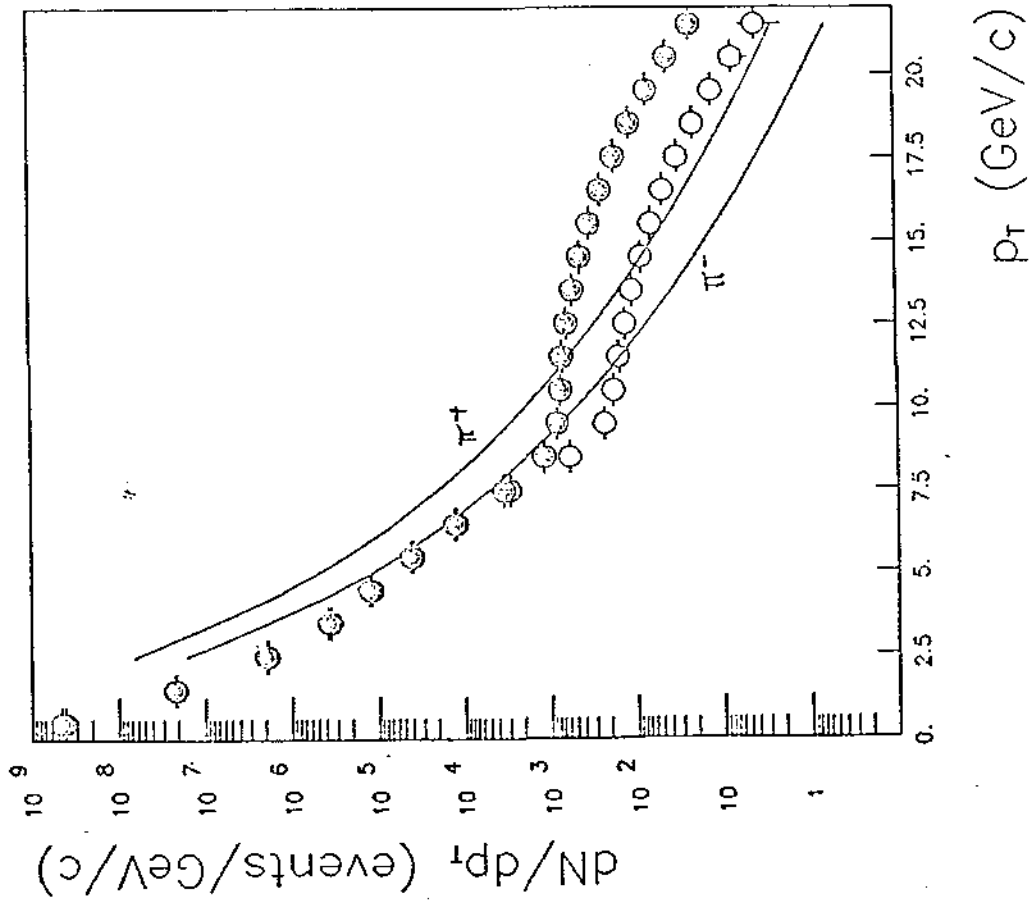
top (35 GeV) PRODUCTION

$5. \le \delta < 30.$

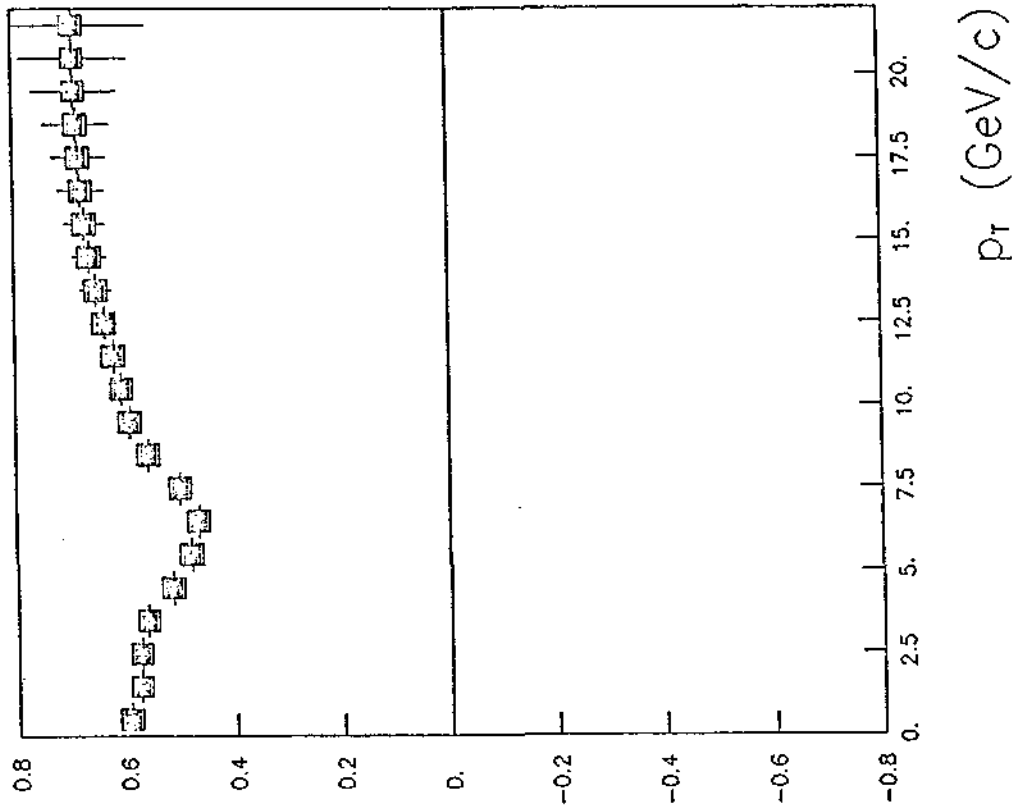
$\Delta p_T / p_T = 20. \%$

$$\frac{\pi^+}{\pi^-} = 4$$

$\sigma_T = 0.05 \mu b$ assumed value



(a)



(b)

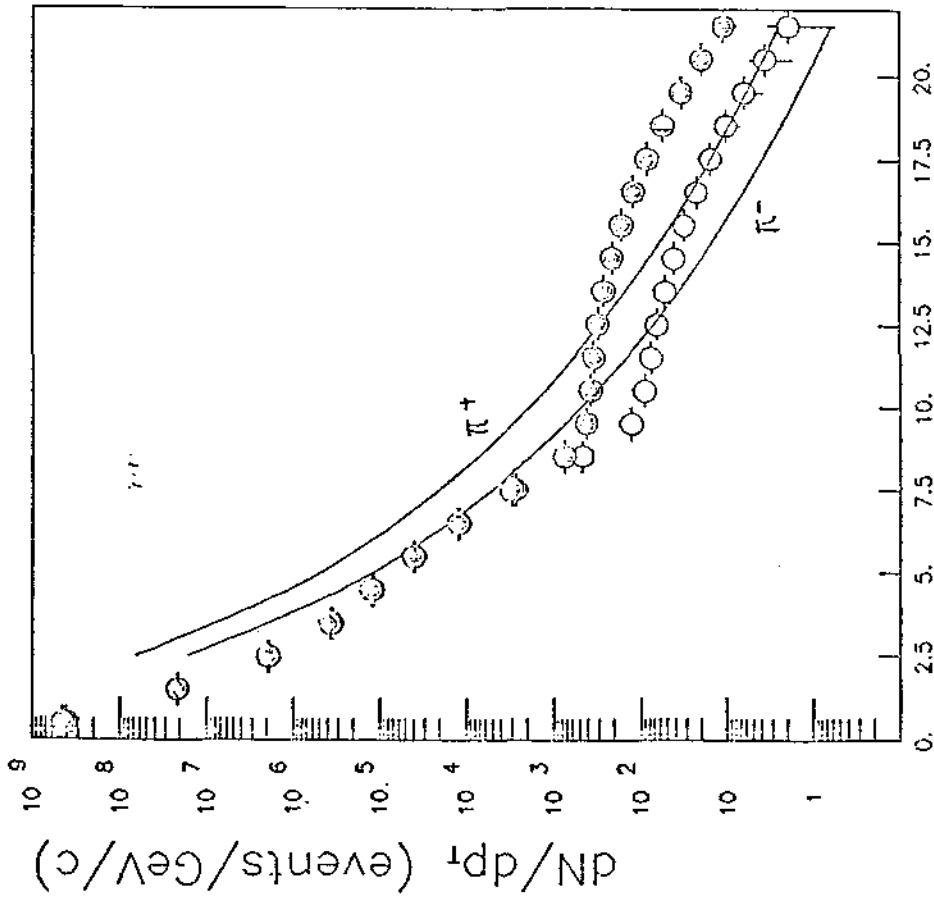
top (35 GeV) PRODUCTION

$5. \leq \theta < 30.$

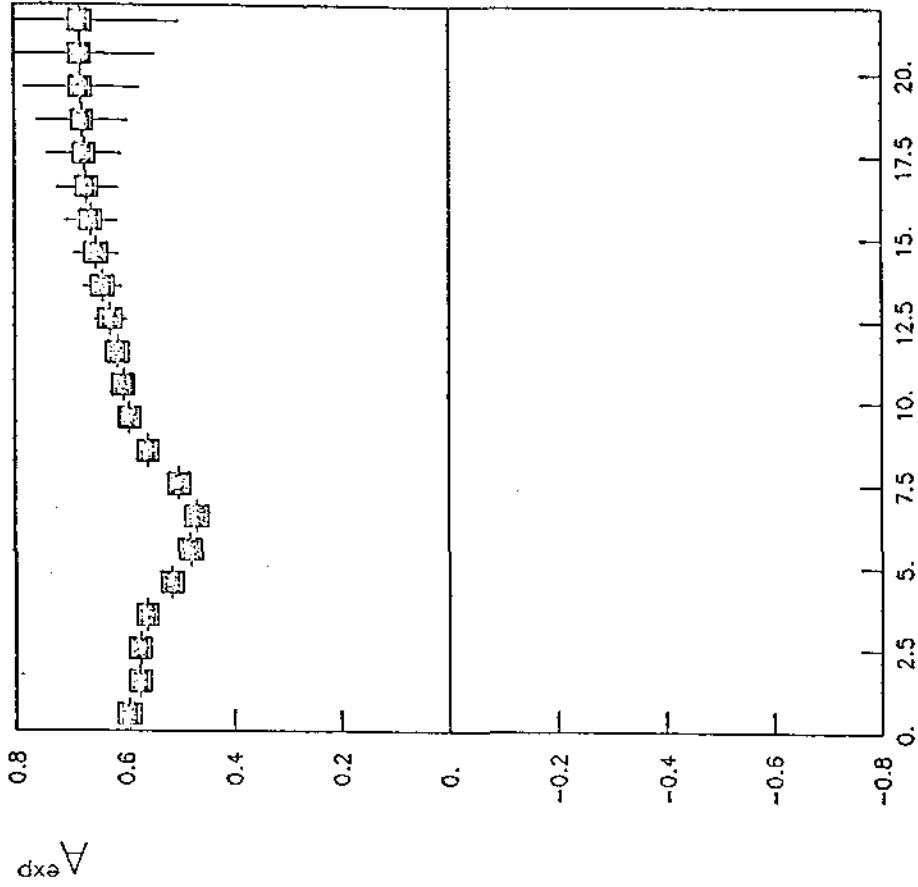
$\Delta p_T / p_T = 20. \%$

$\frac{\pi^+}{\pi^-} = 4$

$\sigma_T = 2.5 \times 10^{-2} \mu b$ factor 2 lower



(a)



(b)

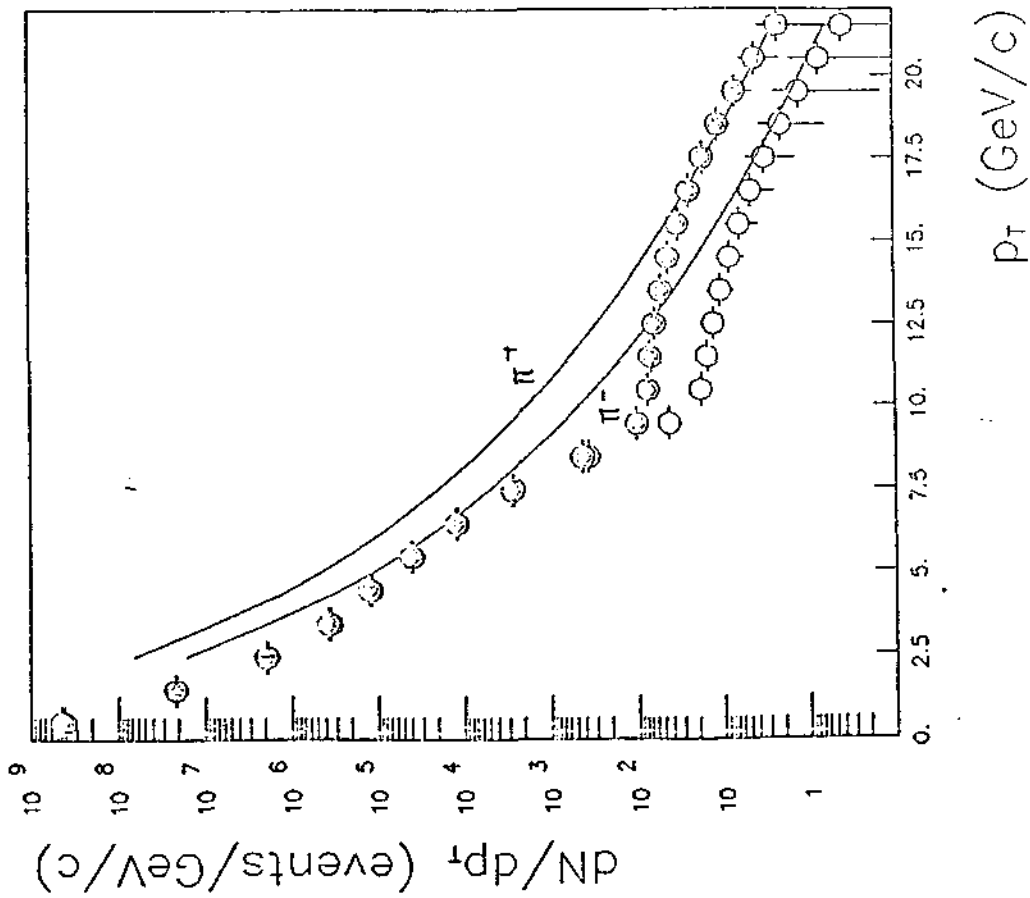
Fig. 31

top (35 GeV) PRODUCTION

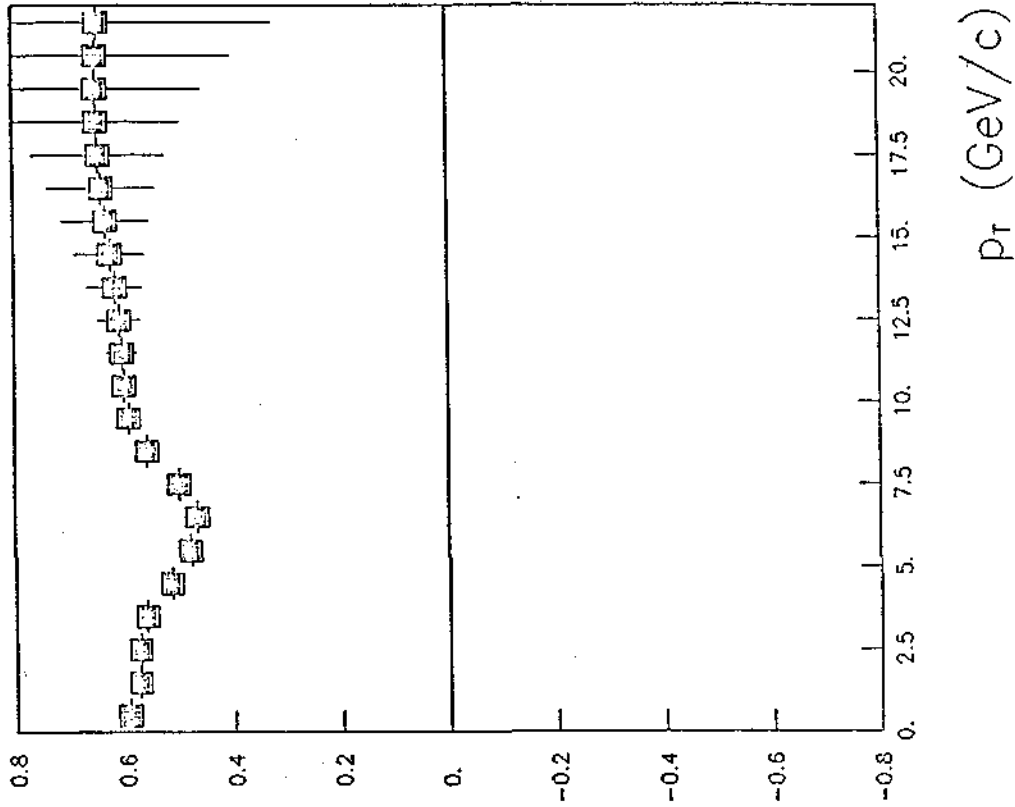
$5. \leq \theta < 30.$

$\Delta p_T / p_T = 20. \%$

$\frac{\pi^+}{\pi^-} = 4$ $\sigma_t = 5 \times 10^{-3} \mu b$ factor 10 lower.



(a)



(b)

FIG. 32

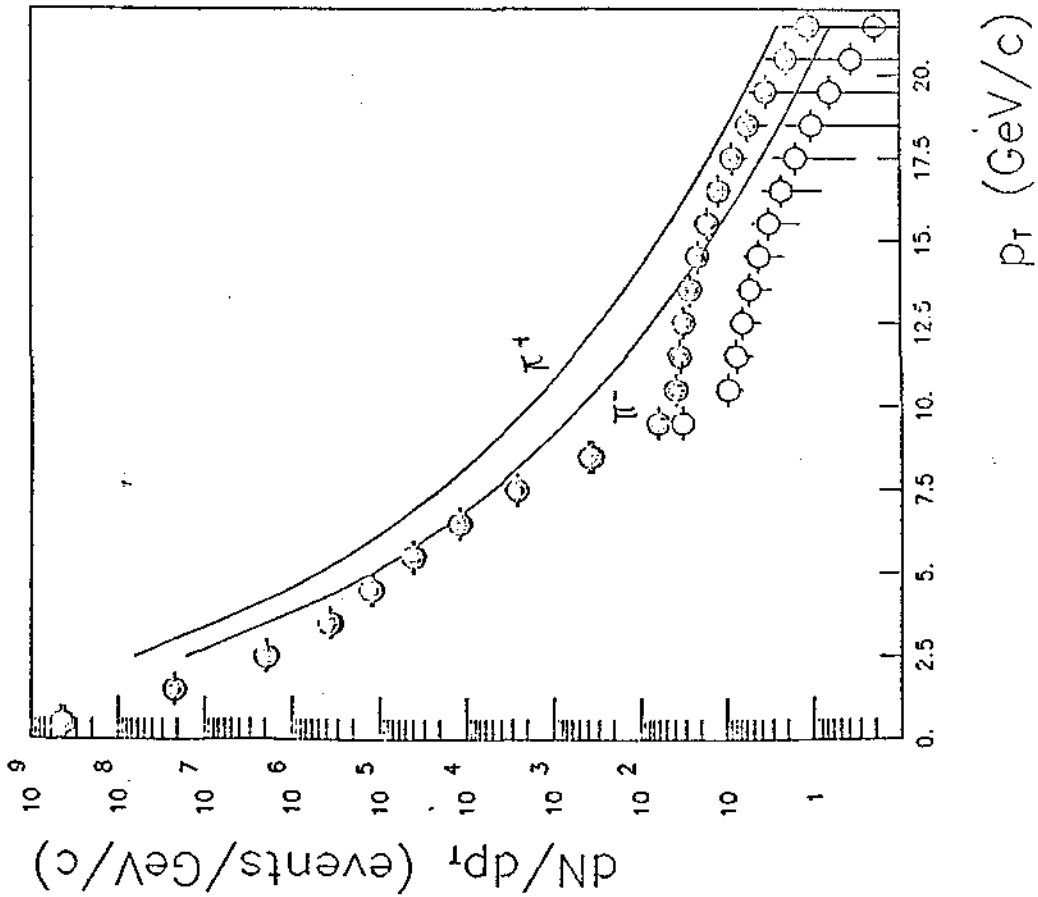
top (35 GeV) PRODUCTION

$5. \leq \theta < 30.$

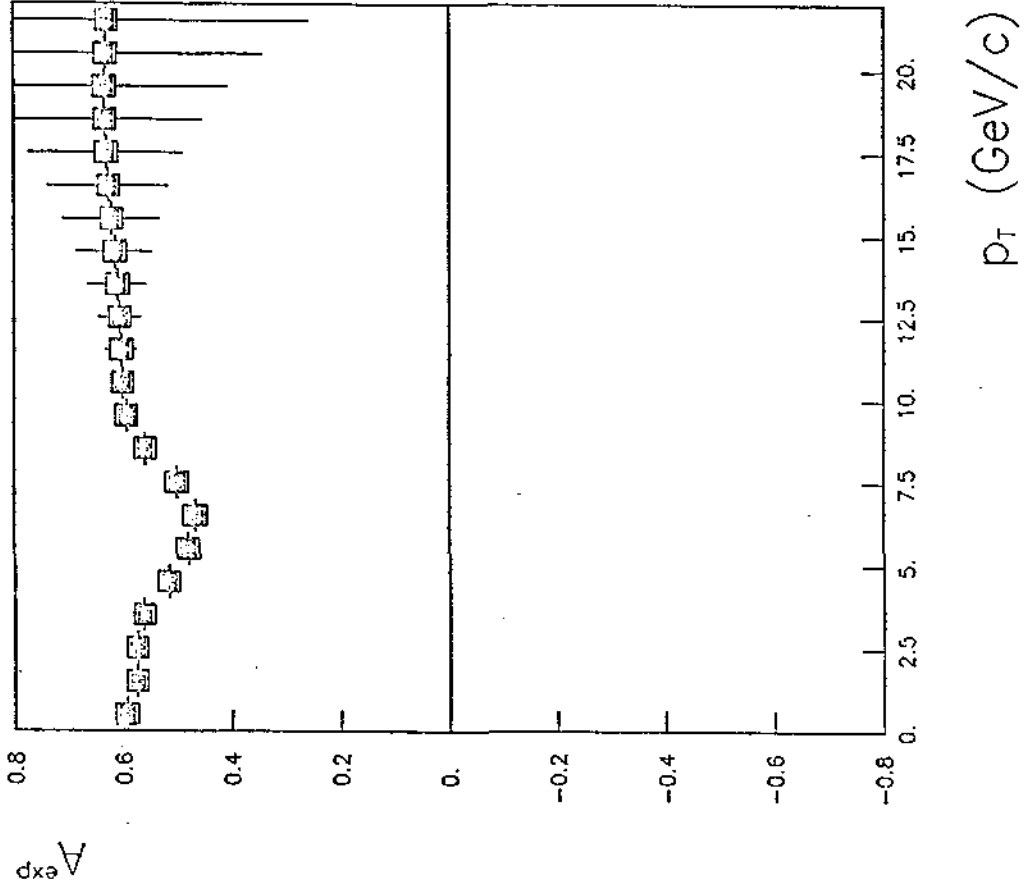
$\Delta p_T / p_T = 20. \%$

$$\frac{\pi^+}{\pi^-} = 4$$

$$\sigma_T = 2.5 \times 10^{-3} \mu\text{b} \quad \text{factor 20 lower}$$



(a)



(b)

Fig. 33

TOP ($25 \text{ GeV}/c^2$) AND SUPERBEAUTY ($55 \text{ GeV}/c^2$) PRODUCTION

$[\Delta p_T/p_T = 20\%]$

$[\int L dt = 10 \text{ pb}^{-1}]$

TOP PEAK ($p_T = 9 \div 12 \text{ GeV}/c$)

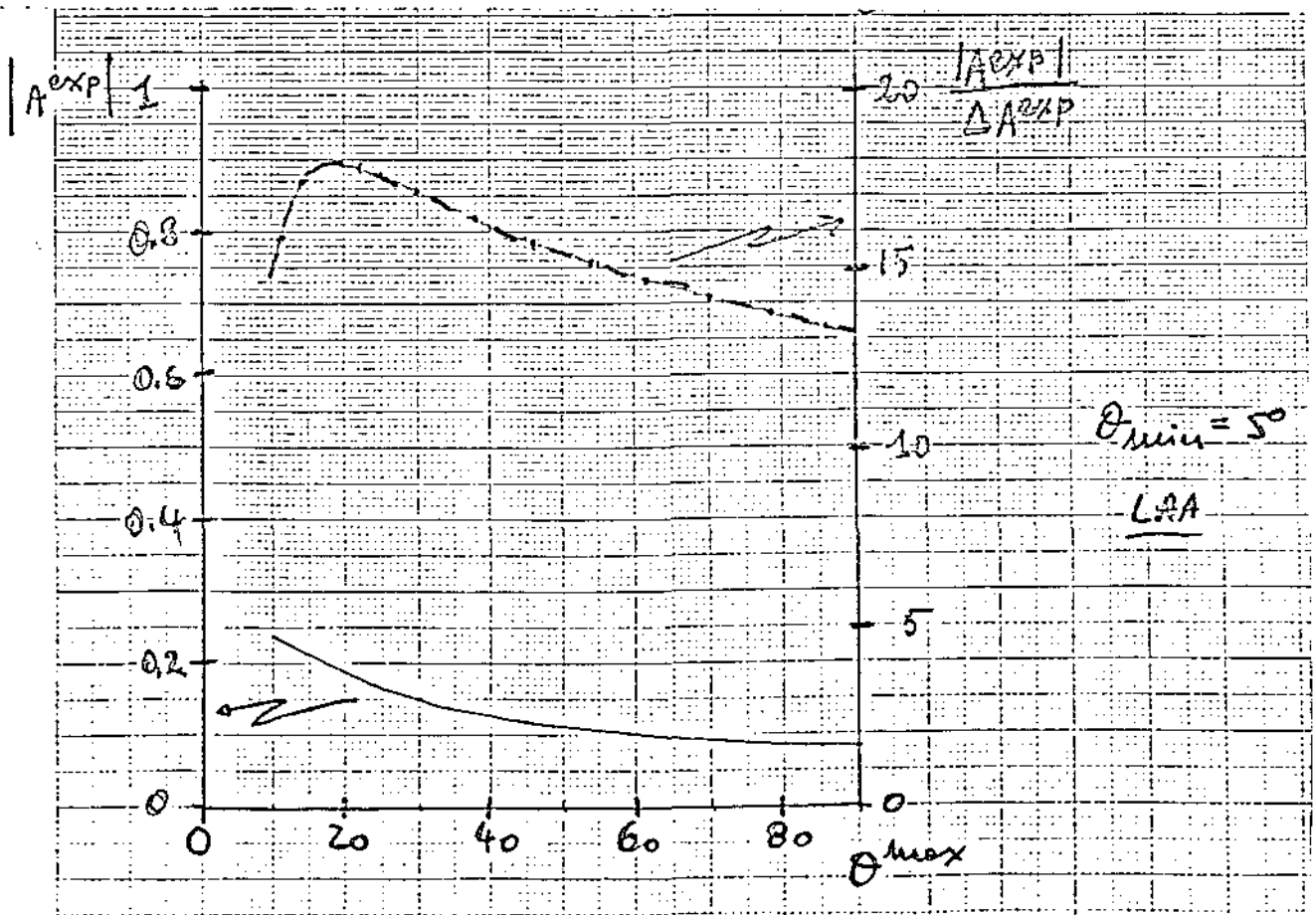


Fig. 34

TOP ($25 \text{ GeV}/c^2$) AND SUPERBEAUTY ($55 \text{ GeV}/c^2$) PRODUCTION

$$[\Delta p_T/p_T = 20\%]$$

$$[\int L dt = 10 \text{ pb}^{-1}]$$

SUPERBEAUTY PEAK ($p_T = 20 \div 23 \text{ GeV}/c$)

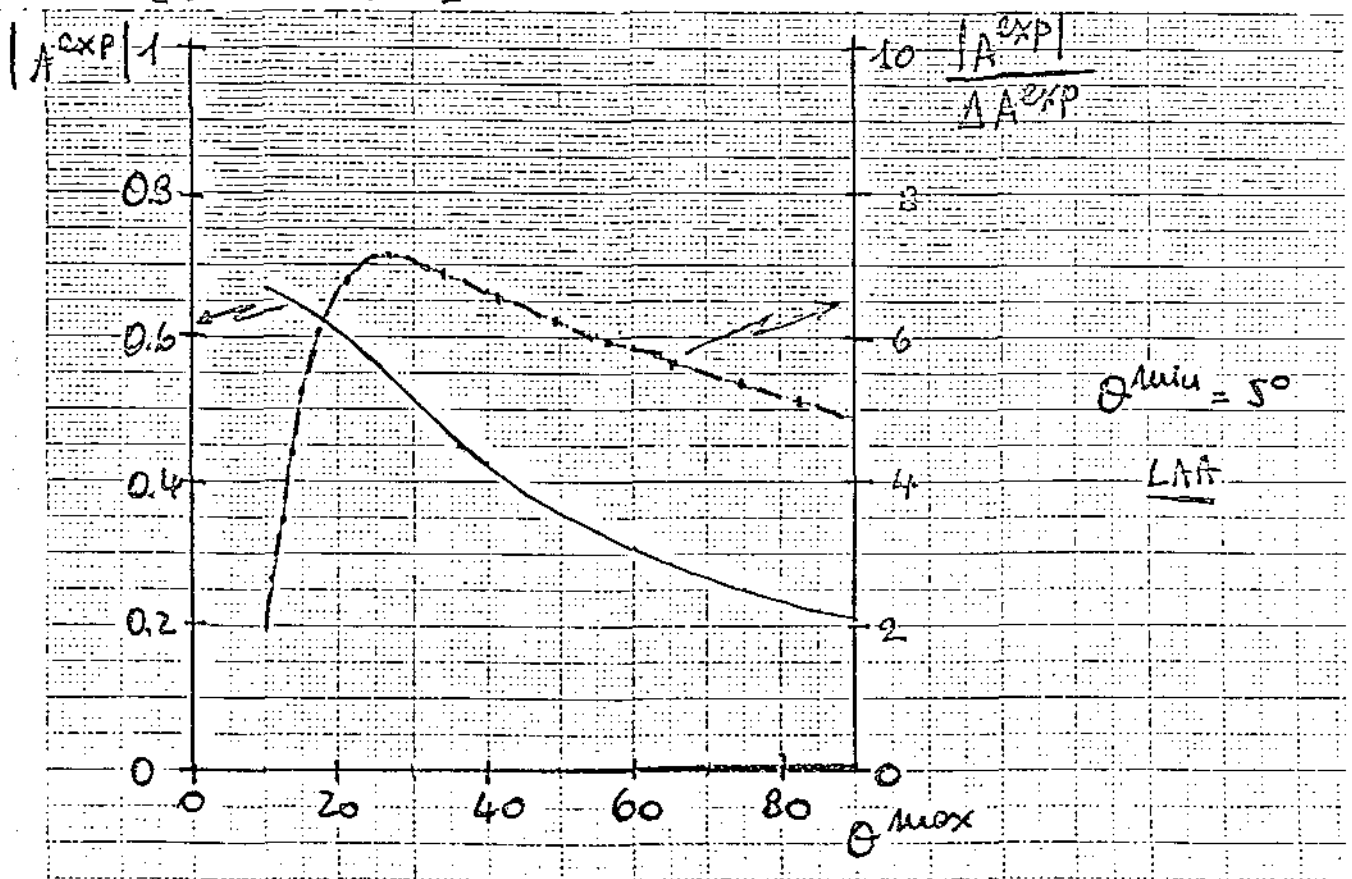


Fig. 35

TOP ($35 \text{ GeV}/c^2$) PRODUCTION

$[\Delta p_T/p_T = 20\%]$

$[\int L dt = 10 \text{ pb}^{-1}]$

TOP PEAK ($p_T = 16 \div 19 \text{ GeV}/c$)

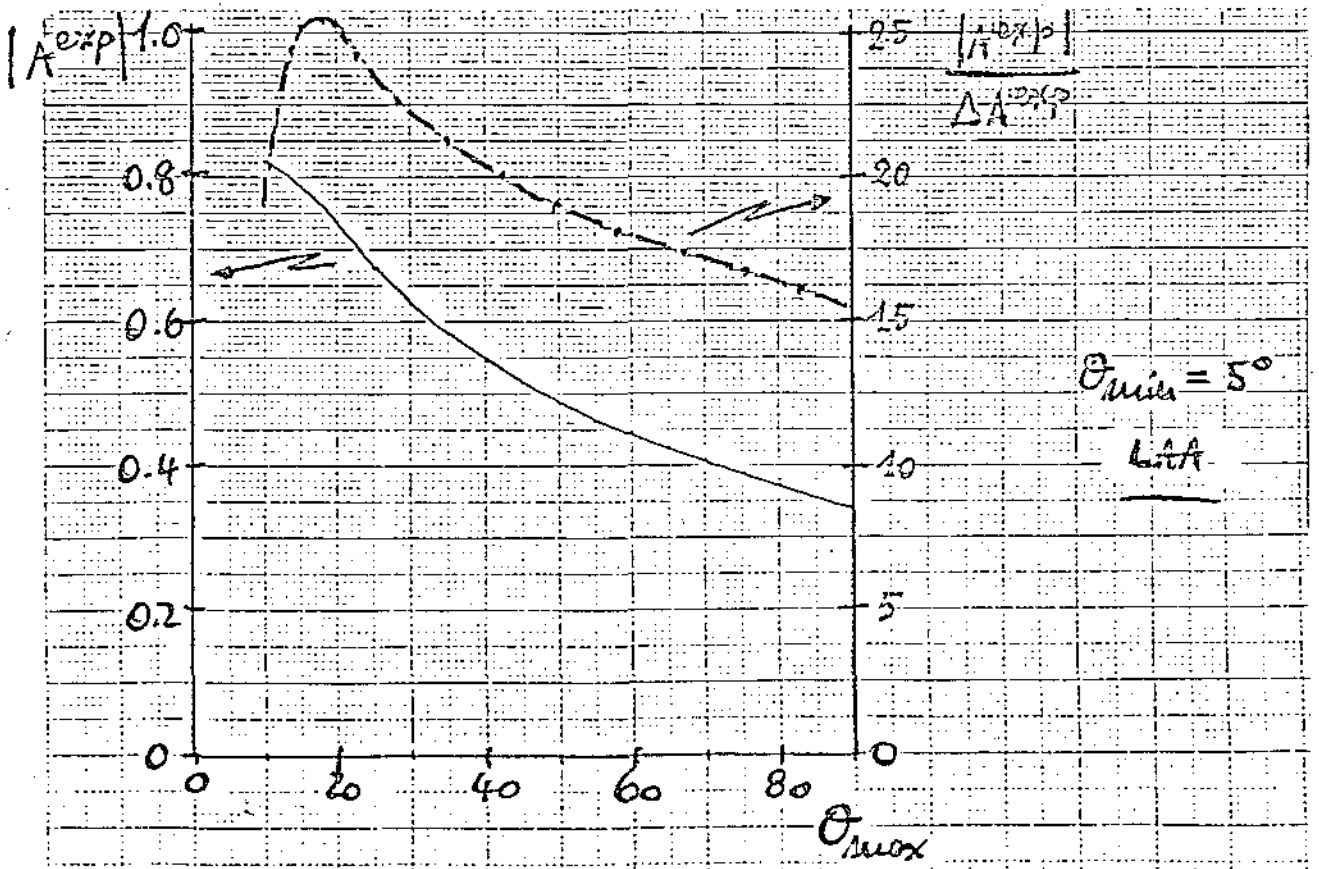


Fig. 36

TOP ($35 \text{ GeV}/c^2$) PRODUCTION

$$[\Delta p_T/p_T = 20\%]$$

$$[\int L dt = 10 \text{ pb}^{-1}]$$

$$\frac{d\sigma}{dx} \propto (1-x_F)$$

TOP PEAK ($p_T = 16 \div 19 \text{ GeV}/c$)

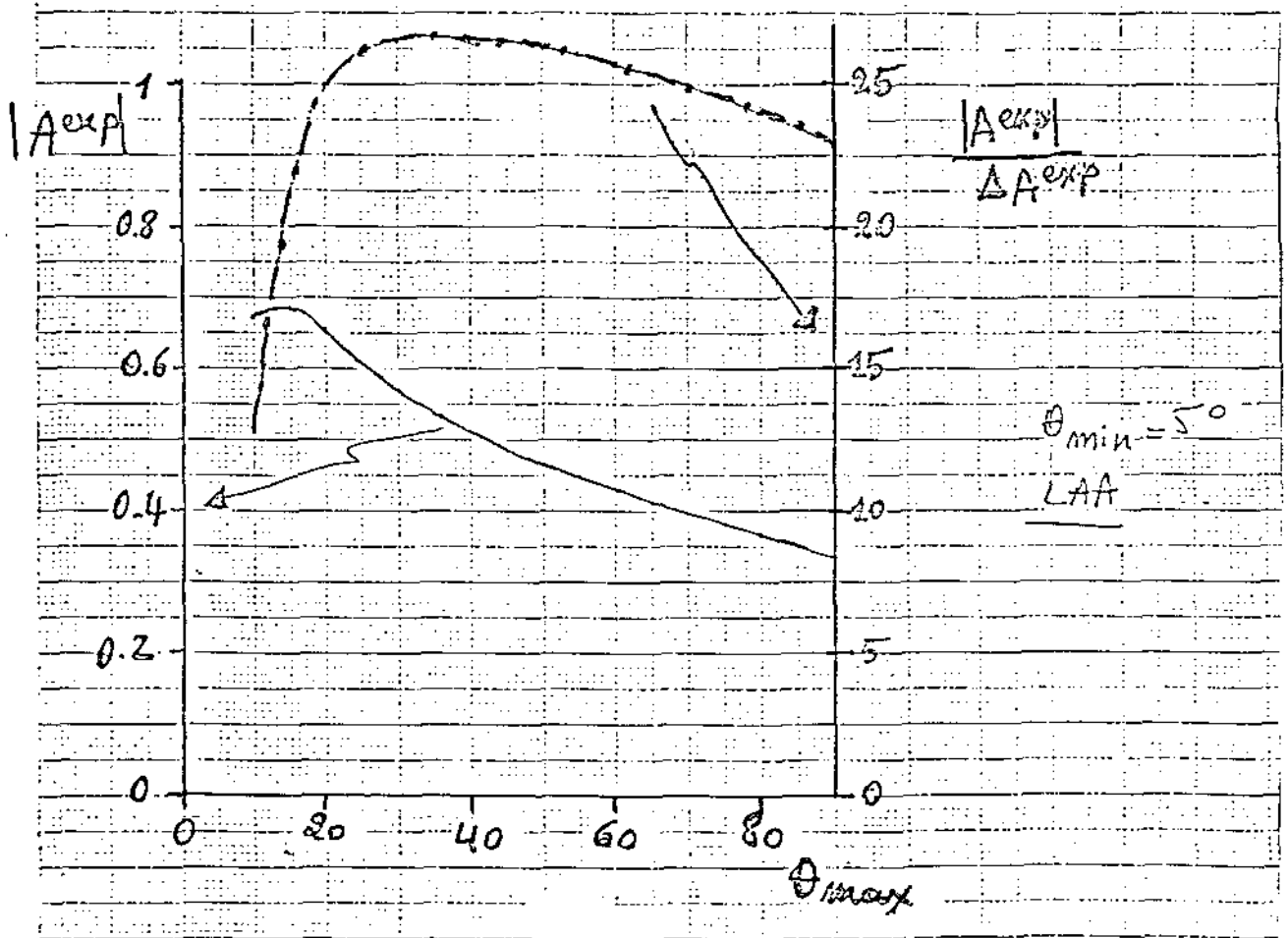


Fig. 37

III-7. "The lepton asymmetry analyser : a proposal"
CERN SPSC 84-33, SPSC/P200, May 16, 1984.

CERN/SPSC/84-33

SPSC/P200

May 16, 1984

7 - THE LEPTON ASYMMETRY ANALYSER: A PROPOSAL

C. Alberini, M. Basile, J. Berbiers, G. Cara Romeo, L. Cifarelli,
A. Contin, G. D'Ali, C. Del Papa, M.I. Ferrero, D. Galli,
G. Iacubucci, P. Giusti, T. Massam, R. Meunier (*), R. Nania,
F. Palmonari, G. Rinaldi, F. Rohrbach, P. Rotelli,
G. Sartorelli, M. Spinetti, G. Susinno, L. Votano and A. Zichichi

Dipartimento di Fisica dell'Universita', Bologna, Italy

Istituto Nazionale di Fisica Nucleare, Bologna, Italy

CERN, Geneva, Switzerland

Istituto Nazionale di Fisica Nucleare, LNF, Frascati, Italy

Dipartimento di Fisica dell'Universita', Lecce, Italy

(*) Visitor C.E.N.S. - D.Ph.P.E.

ABSTRACT

A proposal to search for new heavy flavours produced in hadronic interactions at the CERN ($p\bar{p}$) Collider is presented.

The proposal is based on the measurement of the μ^+ asymmetry in the proton and antiproton hemispheres. The sign of this leptonic asymmetry depends on the "up-like" or "down-like" nature of the new flavour. For a given heavy flavour, the sign of the asymmetry changes from the proton to the antiproton outgoing telescopes, thus allowing an important cross-check on the effect looked for.

Cases of simultaneous production of "up-like" and "down-like" new heavy flavours are considered, in addition to the simpler case of only one flavour, either "up-like" or "down-like".

The detailed description of the lepton asymmetry analyser is presented. It is shown that, if new heavy flavours are produced with masses above the present limit of $22 \text{ GeV}/c^2$, the lepton asymmetry should be clearly observable, with the expected integrated luminosity of 10 pb^{-1} , even for cross-section values ten times lower than the QCD extrapolations.

SUMMARY

1. INTRODUCTION.

2. PHYSICS MOTIVATIONS.

2.1. THE "LEADING" EFFECT.

2.2. NOTE ON THE SEMILEPTONIC DECAY MODES: GENERALIZED CABIBBO DOMINANCE.

2.3. CROSS-SECTIONS ESTIMATES .

2.4. THE STUDY OF THE LEPTON CHARGE ASYMMETRY AND OF ITS ENERGY
DEPENDENCE AS A WAY TO DETECT NEW HEAVY FLAVOURED STATES
(BARYONIC AND ANTIBARYONIC) AT THE ($p\bar{p}$) COLLIDER.

2.4.1. The total cross-sections.

2.4.2. The decay branching ratios.

2.4.3. The production distributions of baryon and meson states.

2.4.4. The lepton decay distributions.

2.4.5. The relative yield of mesons and baryons.

2.4.6. Estimates of the Asymmetry A^0 .

3. THE APPARATUS.

3.1. THE UA2 CALORIMETER.

3.2. THE HADRON ABSORBER.

3.3. THE IRON TOROID MAGNETS.

3.4. THE TRACKING CHAMBERS.

3.4.1. Drift chambers.

3.4.2. Limited Streamer Tubes.

4. μ IDENTIFICATION.

4.1. μ/π REJECTION.

4.2. MOMENTUM RESOLUTION.

5. ESTIMATE OF THE ASYMMETRY PARAMETER IN EXPERIMENTAL CONDITIONS

- 5.1. THE EFFECT OF THE ANGULAR CUT.
 - 5.2. THE BACKGROUND.
 - 5.3. THE MOMENTUM RESOLUTION.
 - 5.4. OTHER HYPOTHESES ON THE NEW HEAVY FLAVOUR MASSES AND ON THE PRODUCTION CROSS-SECTIONS.
 - 5.5. EFFECTS FROM $W^{\pm} \rightarrow \mu^{\pm} \nu$ AND $W^{\pm} \rightarrow tb \rightarrow \ell \nu X$.
-
6. TRIGGER LOGIC AND TRIGGER RATES.
 - 6.1. TRIGGER RATE WITH PERFECT SELECTION.
 - 6.2. DESIGN OF TRIGGER CONDITIONS.
-
7. TIME SCALE AND COSTS.

1. INTRODUCTION

Our ISR studies have shown the importance of the "Leading" effect in hadronic interactions. These studies allow to conclude that the "Leading" effect has to be present, at least with the same strength, at the Collider energies. Using this as a starting point, we propose a new method to search for new heavy flavours carried by baryonic and antibaryonic states, produced in the "Leading" way and decaying semileptonically. For example, if a baryon is produced with "top" flavour, its semileptonic decay will produce an excess of μ^+ on the outgoing proton side.

This new method is thus based on the measurement of the μ^\pm asymmetry in the proton and antiproton hemispheres. The sign of the asymmetry depends on the "up-like" or "down-like" nature of the new heavy flavour carried by the barionic state. An important feature of the asymmetry is that in the two hemispheres it has opposite sign.

Several possibilities have been studied in detail: for example, we have assumed, for the "top" mass, two values : $25 \text{ GeV}/c^2$ and $35 \text{ GeV}/c^2$. The asymmetry varies with p_T , according to the mass difference between the new heavy flavour and its nearest decay state. For the "top" case, the nearest state is "beauty".

On the other hand, the Collider energy opens a region of masses which could belong to heavy flavours above the third family. According to the present trend, the lightest state of the fourth family is expected to be "down-like". How far is away this new heavy flavour from the "top" mass is crucial for the μ^\pm asymmetry produced by the "top" and for its p_T dependence. Thus, we have studied the case where "top" and the "down-like" member of the fourth family ("superbeauty") are both produced. A specific case has been considered with "superbeauty" mass at $55 \text{ GeV}/c^2$ and "top" at $25 \text{ GeV}/c^2$.

The main parameters of the new method are the cross-section values for the production of the "Leading" baryons (antibaryons) and the background level. Both points have been studied to the best of present knowledge.

It turns out that the μ^\pm asymmetry looks a very powerful tool to investigate the existence of new heavy flavours and to establish their "up-like" or "down-like" nature.

The muon detector, positioned behind the forward/backward UA2 calorimeter consists of an iron hadron filter, tracking chambers, a system of limited Streamer Tubes for triggering, and a 3.0 Tm iron toroid. The detector covers the full azimuthal angle in the polar angle intervals $5^\circ \leq \theta \leq 30^\circ$ and $150^\circ \leq \theta \leq 170^\circ$.

Muons are separated from hadrons with a rejection power of 10^{-3} at a transverse momentum $p_T=3$ GeV/c, increasing up to 10^{-4} at $p_T=20$ GeV/c. The momentum accuracy $\Delta p/p$ provided by the iron toroids is better than 20% up to $p=150$ GeV/c.

The detector is compatible, both for the mechanical and the trigger rate points of view, with the UA2 detector, even in its proposed upgraded version.

Apart from its main task, relative to the new heavy flavours detection, the proposed set-up allows the study of $(\mu^\pm \mu^\mp)$ pairs produced in $(p\bar{p})$ interactions, and other processes where a well identified muon can be coupled to the event detected in the UA2 apparatus.

2. PHYSICS MOTIVATIONS.

The present status of our knowledge on quarks and leptons may be summarized as follows:

Families:	1 st	2 nd	3 rd
Quarks:	$\begin{pmatrix} u \\ d \end{pmatrix}$	$\begin{pmatrix} c \\ s \end{pmatrix}$	$\begin{pmatrix} ? \\ b \end{pmatrix}$
Leptons:	$\begin{pmatrix} \nu_e \\ e \end{pmatrix}$	$\begin{pmatrix} \nu_\mu \\ \mu \end{pmatrix}$	$\begin{pmatrix} \nu_\tau \\ \tau \end{pmatrix}$

There are very good reasons to believe that our knowledge is far from being complete and thus the search for new heavy flavours and the study of their family structure is one of the key problems in Subnuclear Physics.

Two "theoretical" arguments favour the need for new quarks. The Adler-Bell-Jackiw (ABJ) anomaly cancellation requires the number of leptons to be equal to the number of quarks. This means that a sixth quark is needed. Its natural location would be the "up-like" member of the 3rd family, i.e. the "top" quark.

According to SuperSymmetry, a very heavy quark with a mass in the few 10^2 GeV/c² range is needed in order to produce radiatively (see Fig. 1) a gluino with a mass such as to avoid a conflict with existing lower limits [1]. None of the presently known quarks (s, c and b) is heavy enough for this purpose.

Apart from these theoretical arguments we should not underevaluate that Nature has often provided physicists with more regularities than needed (for example the equality between the proton and the electron charges, which took more than three decades to be understood).

We propose to consider the ratio between the masses of the known heavy quarks as a limit for the regularity in their masses. There are good reasons [2] to consider the strange quark heavy enough to be used in our argument.

At present we know that:

- i) $(m_c / m_s) \cong (1.8 / .5) \cong 3.5 \sim 4$;
- ii) $(m_b / m_s) \cong (5.5 / .5) \cong 11 \sim 10$.

Suppose that (i) and (ii) are of general validity, i.e. :

$$(m_c / m_s) = [m(\text{uplike quark}) / m(\text{downlike quark})] = 4 , \quad (1)$$

and:

$$(m_b / m_s) = [m(\text{family N+1}) / m(\text{family N})] = 10 . \quad (2)$$

We ignore the 1st family (u,d) because of its very light mass. On the other hand, the ratios (1) and (2) would not be inconsistent with the various models used to derive from bound states the quark masses [2].

The validity of (1) and (2) would allow to conclude that the "top" mass is in the 20 GeV/c² range. This is too light for SuperSymmetric models to avoid a gluino mass in conflict with experimental data. On the other hand, SuperSymmetry tells us that the maximum number of flavours, n_f , allowed in order to have a consistent theory (for example: the unification limit not above the Planck mass) is $n_f=8$. This means that the maximum number of families is 4. In the theories that ignore SuperSymmetry, the asymptotic freedom is lost if $n_f > 16$.

What is not forbidden, in Nature, does take place. Thus, the message from SuperSymmetry is twofold:

- i) four families of quarks are allowed;
- ii) quarks heavier than (d,u,s,c,b and t) are needed.

Formulas (1) and (2) tell us that the 4th family would have the "up-like" mass wanted by SuperSymmetry. In fact, using (2), the heavy "down-like" quark (called, in the following, "superbeauty" or sb) would have a mass in the 50 GeV/c² range:

$$m(\text{down-4}^{\text{th}}\text{family}) = m(\text{"superbeauty"}) = 10 \times 5.5 = 55 \text{ GeV}/c^2 ,$$

but, using (1), the heavy "up-like" quark would have a mass in the 200 GeV/c^2 range:

$$m(\text{up-4}^{\text{th}}\text{family}) = m(\text{"supertruth"}) = 55 \times 4 = 220 \text{ GeV}/c^2 .$$

If SuperSymmetry and asymptotic freedom were Bible-like truths, this flavour should be the last ever to be discovered.

The four families are shown in Table I, where the main objectives of the present proposal are indicated by the dotted circles.

It should however be emphasized that the measurement of the lepton asymmetry is a tool open to the detection of any "up-like" or "down-like" new state in the mass range above the present limits: i.e. $m(\text{heavy-flavour}) \geq 220 \text{ GeV}/c^2$.

Let us come to a key question: if "top" and "superbeauty" are accessible to $(p\bar{p})$ Collider energies, how can they be detected?

Many methods are in principle possible. For example:

- i) detection of a hidden state with the study of the invariant mass of the lepton pairs;
- ii) detection of an open state with the identification of hadronic decay channels;
- iii) study of multilepton events;
- iv) study of the inclusive transverse momentum spectrum of the leptons from semileptonic decays;
- v) study of the transverse dilepton (ℓ, ν) and jets masses.

All of these methods present, in various degrees, experimental problems related to small production cross-sections, low global branching ratios, high background levels, poor experimental resolution of the quantities needed to be measured. Moreover, none of them, but (ii), is able to identify the "up-like"

or "down-like" nature of the new flavours. However, method (ii) seems out of present experimental reach.

We propose here a new method to observe the production of heavy mass states, either "up-like" ("top") or "down-like" ("superbeauty") which is based on the "Leading" production mechanism, extended to the the heaviest baryon and antibaryon states. In fact, due to this production mechanism, a charge asymmetry of the leptons (ℓ^+, ℓ^-), originating from these heavy flavours can be observed in a selected region of phase-space. Moreover, this asymmetry will show a p_T dependence characteristic of the masses of the decaying states.

More precisely, the "top" baryonic state will decay semileptonically into ℓ^+ and produce a positive asymmetry in the outgoing proton hemisphere

$$A_p = (\ell^+ - \ell^-) / (\ell^+ + \ell^-) = \text{positive} .$$

The "anti-top" antibaryonic state will produce a negative asymmetry in the outgoing antiproton hemisphere

$$A_{\bar{p}} = (\ell^+ - \ell^-) / (\ell^+ + \ell^-) = \text{negative} .$$

The signs of these asymmetries will be reversed for the "superbeauty" case. Fig. 2 shows the main trend of the measurement we propose.

The p_T range where to measure the ℓ^\pm asymmetry, and the separation between the maxima and minima, depend on the parent-daughter mass difference in the decay of the two new flavours. Extending the validity of the Generalized Cabibbo Dominance (GCD) to the 4th family, the mass differences in the "superbeauty" and "top" decays would be:

$$\Delta m = m(\text{top}) - m(\text{beauty}) \approx 20 \text{ GeV}/c^2 ,$$

$$\Delta m = m(\text{superbeauty}) - m(\text{top}) \approx 30 \text{ GeV}/c^2 .$$

The Asymmetry will change sign with increasing lepton p_T . Notice that this GCD condition, if not valid, would not spoil our method. It would shift the lepton p_T spectrum to higher values, thus making the measurement cleaner.

To check the validity of our new method, we have considered, not only the case with only one new flavour produced, but also the production of two new heavy flavours, one "up-like" and one "down-like". For this last case we have followed the mass extrapolations (1) and (2), i.e.:

$$\begin{aligned} m(\text{"top"}) &= 25 \text{ GeV}/c^2 \\ m(\text{"superbeauty"}) &= 55 \text{ GeV}/c^2. \end{aligned}$$

The single "up-like" case has been evaluated at

$$\begin{aligned} m(\text{"top"}) &= 25 \text{ GeV}/c^2, \text{ and} \\ m(\text{"top"}) &= 35 \text{ GeV}/c^2. \end{aligned}$$

Note that present (e^+e^-) data impose a lower limit $m_t \geq 22 \text{ GeV}/c^2$.

Let us emphasize a detail concerning the sequence of new heavy flavour masses. This sequence could be opposite to present expectations. If, for example:

$$\begin{aligned} m(\text{"down-like"}) &= 25 \text{ or } 35 \text{ GeV}/c^2, \text{ and} \\ m(\text{"up-like"}) &= 55 \text{ GeV}/c^2, \end{aligned}$$

the asymmetry would still be there, with opposite sign and minor effects on the lepton p_T spectrum.

As we will see in section 2.4 and chapter 5, the amplitude of the effect depends on:

- i) the "Leading" effect;
- ii) the decay angular and momentum distributions;
- iii) the branching ratios into semileptonic channels;

iv) the acceptance and rejection power of the experimental set-up designed to observe the leptons produced by these "new" flavours decay.

2.1 THE "LEADING" EFFECT.

A result which was theoretically unpredicted is the "Leading" effect which shows up in the production of heavy flavours.

A detailed study of (pp) interactions at the ISR showed that the Λ_c^+ is produced in a "Leading" way [3].

After this experimental result was obtained, a series of theoretical proposals were presented, to account for the "Leading" Λ_c^+ production. The longitudinal momentum distribution for Λ_c^+ was in fact found at the ISR [3] to be:

$$E(d\sigma/d|x|) \sim (1-|x|)^\alpha \text{ with } \alpha \sim 0.$$

The results are shown in Fig. 3. The charmed meson production [4] was on the other hand measured to be "non-Leading", i.e.

$$E(d\sigma/d|x|) \sim (1-|x|)^\alpha \text{ with } \alpha \approx 3.$$

This can "a posteriori" be qualitatively understood in terms of the Λ_c^+ obtained by a recombination of the spectator c-quark with a valence (ud) pair in the proton; while the D production is given by the recombination of the spectator c-quark with at most one valence quark [5,7].

Figure 4a shows how the "Leading" Λ_c^+ and Λ_s^0 productions compare. This indicates that the "Leading" effect does not decrease with increasing flavour mass. Figure 4b shows the qualitative behaviour, as a function of the flavour mass, of the quantity (Leading/Total). This quantity will be defined in section

2.4.5 as the ratio between the inclusive cross-section for producing leading baryons with flavour "f" and the total cross-section for producing the same flavour "f". This figure shows that, at ISR energies, the (Leading/Total) production does not decrease with increasing flavour mass.

A more complete summary of "charm" production in purely hadronic interactions is reported in Table II [8]. There is no model which can fit all measured quantities [8].

The conclusion of this short review on the "charm" flavour production in (pp) interactions is therefore:

- i) the cross-section values found are at least an order of magnitude above the "theoretical" predictions of perturbative QCD;
- ii) the x-distribution for Λ_c^+ , i.e. the "Leading" effect, was theoretically unpredicted;
- iii) with "new" models (essentially flavour excitation [5,6] and non-perturbative QCD [7]) both cross-sections values and x-distributions can be "theoretically" derived.

All this should be quite a warning for QCD prediction on New Heavy Flavours production at extreme energies such as those of the (pp) CERN Collider.

2.2 NOTE ON THE SEMI-LEPTONIC DECAY MODES: GENERALIZED CABIBBO DOMINANCE.

A fact of Nature is that the matrix which relates the "down-like" "weak" flavours "Cabibbo mixed"

$$\begin{pmatrix} d_c \\ s_c \\ b_c \end{pmatrix}$$

to the "strong" flavours

$$\begin{pmatrix} d \\ s \\ b \end{pmatrix}$$

is approximately a unit matrix

$$\begin{pmatrix} d_c \\ s_c \\ b_c \end{pmatrix} \approx \begin{pmatrix} 1 & 0 & 0 \\ 0 & 1 & 0 \\ 0 & 0 & 1 \end{pmatrix} \begin{pmatrix} d \\ s \\ b \end{pmatrix}$$

as shown in Figs. 5a and 5b.

In order to extend the generalized Cabibbo dominance to the 4th Family, we make the following extrapolations:

- i) all the generalized Cabibbo angles, even those coming from the existence of the 4th family, are small;
- ii) the flavour-changing neutral currents are forbidden to any order of family;
- iii) the amplitude for the transition from family N to family N±α has a coefficient

$$\prod_{i=1, \alpha} (\sin \theta_i) .$$

As a consequence, the Cabibbo-favoured decay chains of flavours c, b, t and sb are:

$$\begin{aligned} c &\rightarrow s \\ b &\rightarrow c \rightarrow s \\ t &\rightarrow b \rightarrow c \rightarrow s \\ sb &\rightarrow t \rightarrow b \rightarrow c \rightarrow s. \end{aligned}$$

A sequence $t \rightarrow b \rightarrow c \rightarrow s$ will be accompanied by the semileptonic series giving rise to $\ell^+ \rightarrow \ell^- \rightarrow \ell^+$. For the antiquark sequence $\bar{t} \rightarrow \bar{b} \rightarrow \bar{c} \rightarrow \bar{s}$, the charges will be reversed ($\ell^- \rightarrow \ell^+ \rightarrow \ell^-$).

2.3 CROSS-SECTION ESTIMATES.

We will try to estimate the production cross-section for very high flavour masses using the QCD predictions from Halzen [9] for $m_{\text{top}} = 25 \text{ GeV}/c^2$ at Collider energies ($\sigma_{\text{top}} \sim 0.1 \text{ } \mu\text{b}$). For this extrapolation we make use of dimensionality and scaling:

$$\sigma(m) \sim (1/m^2) \times f(s/m^2) \quad (3)$$

In order to check dimensionality and scaling, we have used:

- i) the strangeness data to predict c and b;
- ii) the "charm" data to predict b.

The results are shown in Figs. 6-7. There is no violent disagreement between extrapolated results and experimental findings.

2.4 THE STUDY OF THE LEPTON CHARGE ASYMMETRY AND ITS ENERGY DEPENDENCE AS A WAY TO DETECT NEW HEAVY FLAVOURED STATES (BARYONIC AND ANTIBARYONIC) AT THE (p \bar{p}) COLLIDER.

The leptonic decay chains, following the generalized Cabibbo dominance, for the various flavours c,b,t,sb, are shown in Fig. 8.

Once a particle-antiparticle pair has been produced, on the average the number of positive and negative leptons from its decay is equal. However we will

discuss under which conditions an asymmetry in the number of positive and negative leptons can be observed, due to the different longitudinal momentum production distribution for baryons and mesons, and to the dependence of the lepton p_T spectra from the product particle mass.

Let us define the Asymmetry parameter as

$$A^0(p_T, \theta_{cut}) = \frac{N(\ell^+) - N(\ell^-)}{N(\ell^+) + N(\ell^-)}$$

where $N(\ell^+) \equiv N(\ell^+; p_T, \theta_{cut})$ and $N(\ell^-) \equiv N(\ell^-; p_T, \theta_{cut})$ are the number of positive and negative leptons produced in the angular range $0^\circ < \theta < \theta_{cut}$ and with transverse momentum p_T .

The number of positive leptons ℓ^+ is expressed by

$$N(\ell^+) = L[n_{sb}(\ell^+) + n_t(\ell^+) + n_b(\ell^+) + n_c(\ell^+)]$$

where L is the total integrated luminosity and $n_f(\ell^+)$ (with $f = sb, t, b, c$) is the contribution from the direct production of sb, t, b, c states.

Analogously the number of negative leptons is given by

$$N(\ell^-) = L[n_{sb}(\ell^-) + n_t(\ell^-) + n_b(\ell^-) + n_c(\ell^-)]$$

The leptons originated by the decay of the various flavours and ant flavours are summarized in Tables III and IV.

In order to write down explicitly $n_f(\ell^+)$ let us define:

- i) $\sigma_f^T \equiv$ total cross-section for the production of open (f, \bar{f}) pairs;
- ii) $\rho_{Mf}, \rho_{\bar{M}\bar{f}}, \rho_{Bf}, \rho_{\bar{B}\bar{f}} \equiv$ ratio between, the inclusive cross-section for producing [$M =$ meson, $\bar{M} =$ antimeson, $B =$ baryon, $\bar{B} =$ antibaryon] states with flavour "f", and the total cross section σ_f^T ;

- iii) $BR_{Mf'}, BR_{\bar{M}\bar{f}'}, BR_{Bf'}, BR_{\bar{B}\bar{f}'}$ \equiv semileptonic branching ratio of the various states with flavour f' ($f' = c, b, t, sb$) ;
- iv) $\epsilon_{Mf}(\ell_{f'}^{\pm}), \epsilon_{\bar{M}\bar{f}}(\ell_{\bar{f}'}^{\pm}), \epsilon_{Bf}(\ell_{f'}^{\pm}), \epsilon_{\bar{B}\bar{f}}(\ell_{\bar{f}'}^{\pm})$ \equiv acceptance for ℓ^{\pm} from the leptonic decay of the flavour f' produced in the decay chain of the state with flavour f . This acceptance is a function of the lepton p_T and of the cut $\theta < \theta_{cut}$ applied to the lepton polar angle.

Accordingly we have, for the case of "superbeauty":

$$n_{sb}(\ell^+) = \sigma_{sb}^T \{ \rho_{Msb} [BR_{Mt} \epsilon_{Msb}(\ell_t^+) + BR_{Mc} \epsilon_{Msb}(\ell_c^+)] \\ + \rho_{\bar{M}\bar{sb}} [BR_{\bar{M}\bar{sb}} \epsilon_{\bar{M}\bar{sb}}(\ell_{\bar{sb}}^+) + BR_{\bar{M}\bar{b}} \epsilon_{\bar{M}\bar{sb}}(\ell_{\bar{b}}^+)] \\ + \rho_{Bsb} [BR_{Bt} \epsilon_{Bsb}(\ell_t^+) + BR_{Bc} \epsilon_{Bsb}(\ell_c^+)] \\ + \rho_{\bar{B}\bar{sb}} [BR_{\bar{B}\bar{sb}} \epsilon_{\bar{B}\bar{sb}}(\ell_{\bar{sb}}^+) + BR_{\bar{B}\bar{b}} \epsilon_{\bar{B}\bar{sb}}(\ell_{\bar{b}}^+)] \}$$

and

$$n_{sb}(\ell^-) = \sigma_{sb}^T \{ \rho_{\bar{M}\bar{sb}} [BR_{\bar{M}\bar{t}} \epsilon_{\bar{M}\bar{sb}}(\ell_{\bar{t}}^-) + BR_{\bar{M}\bar{c}} \epsilon_{\bar{M}\bar{sb}}(\ell_{\bar{c}}^-)] \\ + \rho_{Msb} [BR_{Msb} \epsilon_{Msb}(\ell_{sb}^-) + BR_{Mb} \epsilon_{Msb}(\ell_b^-)] \\ + \rho_{\bar{B}\bar{sb}} [BR_{\bar{B}\bar{t}} \epsilon_{\bar{B}\bar{sb}}(\ell_{\bar{t}}^-) + BR_{\bar{B}\bar{c}} \epsilon_{\bar{B}\bar{sb}}(\ell_{\bar{c}}^-)] \\ + \rho_{Bsb} [BR_{Bsb} \epsilon_{Bsb}(\ell_{sb}^-) + BR_{Bb} \epsilon_{Bsb}(\ell_b^-)] \}$$

The analogous expressions for $n_t(\ell^{\pm}), n_b(\ell^{\pm}), n_c(\ell^{\pm})$ can be easily derived and are not reported here.

From the above formulae it can be seen that in order to evaluate the Asymmetry parameter A^0 one needs to know:

- i) the total cross-sections : σ^T ;
- ii) the decay branching ratios : BR ;
- iii) the production distributions of the baryons or mesons states and the lepton distributions in the decays : ϵ ;
- iv) the relative fraction of baryons and mesons : ρ ;

We will now discuss in some detail the assumptions made for these quantities.

2.4.1 The total cross-sections.

The total cross-sections for the heavy flavours at the ($p\bar{p}$) Collider ($\sqrt{s}=540$ GeV) are taken from perturbative QCD calculations [5,9]:

$$\begin{aligned}\sigma_c &\sim 2000 \quad \mu\text{b} , \\ \sigma_b &\sim 10 \quad \mu\text{b} , \\ \sigma_t &\sim 0.1 \quad \mu\text{b} .\end{aligned}$$

where the "top" mass is taken to be $m_t = 25 \text{ GeV}/c^2$.

To get consistent values for higher masses, for example $m_{sb} = 55 \text{ GeV}/c^2$, we use dimensionality and scaling, as outlined in section 2.3. The result for $m_{sb} = 55 \text{ GeV}/c^2$ is

$$\sigma_{sb} \sim 0.01 \mu\text{b} .$$

We will see that cross-section values even ten times lower than these QCD extrapolations give rise to a measurable Asymmetry.

2.4.2 The decay branching ratios.

Recent data from CLEO [16] give for the semileptonic branching ratio of the "beauty" mesons:

$$(N_b \rightarrow \ell^\pm) / (N_b \rightarrow \text{all}) \approx 0.13 .$$

In our Monte Carlo we assume the known semileptonic branching ratios for "charm":

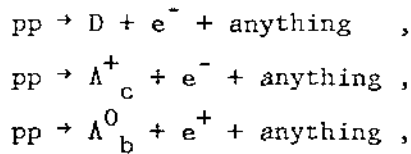
$$(D \rightarrow \ell^{\pm}) / (D \rightarrow \text{all}) \approx 0.085 ,$$

$$(\Lambda_c^+ \rightarrow \ell^{\pm}) / (\Lambda_c^+ \rightarrow \text{all}) \approx 0.045 ,$$

and the conservative value of 0.1 for all other heavier particles.

2.4.3 The production distributions of baryon and meson states.

The study of the reactions:



at the ISR, indicate that in baryon-baryon collisions the heavy flavoured baryons are produced according to a rather flat x-distribution:

$$(d\sigma/dx) \sim \text{const.} ,$$

while the heavy flavoured mesons are produced with softer x-distribution of the type:

$$E(d\sigma/d|x|) \sim (1-|x|)^3 .$$

These distributions will be assumed all along the following discussion, together with the p_T dependence:

$$(d\sigma/dp_T) \sim p_T \exp(-2.5p_T)$$

observed at the ISR in the production of heavy flavours [17, 18].

2.4.4 The lepton decay distributions.

The data from CLEO [19] show that in the semileptonic decay of "beauty" mesons, M_b , the magnitude of the mass recoiling with respect to the leptons is very near to the D mass:

$$M_b \rightarrow X_{\text{ev}} , \text{ with } M_X \sim M_D \approx 2.0 \text{ GeV}/c^2$$

Moreover, the mean charged multiplicity of the decay is 3.5, where the D contributes with 2.5 charged particles on the average. We can conclude that, even at values of the mass as high as the mass of the M_b , the semileptonic decay proceeds via a 3-body decay. On the contrary, the mean charged multiplicity in the hadronic decays of the M_b mesons is 6.3, i.e. the hadronic decay of the M_b produces, on the average, one D plus four charged particles plus two neutral particles:

$$M_b \rightarrow D + 6\text{-bodies} .$$

In the following we will assume that the total multiplicity of all semileptonic decays is 3 and the decay is K_{23} -like for mesons and phase-space for baryons, while the total multiplicity of all the hadronic decays have the known values for "charm" and "beauty" (~ 3 for "charm", $\sim \text{charm} + 6$ for "beauty"), and, for "top" and "superbeauty", the same multiplicity as "beauty". It should be noted that this is already a conservative hypothesis, since the hadronic decays of "top" and "superbeauty" can be expected to produce more particles than "beauty". Higher values of multiplicity would dump the leptonic spectra of unwanted processes. The genuine asymmetry will thus remain unaffected.

2.4.5 The relative yield of meson and baryons.

From the data on strangeness production at the ISR, it can be assumed that, in (pp) collisions the following reactions dominate (L and C indicate "Leading" and "Central" production) :

- (L) $p_1 p_2 \rightarrow \bar{N}_{\text{Central}} + (B_{\text{Leading}})_1 + \text{anything} \equiv \{\bar{N}_C; B_{L1}\}$,
- (L) $p_1 p_2 \rightarrow \bar{N}_{\text{Central}} + (B_{\text{Leading}})_2 + \text{anything} \equiv \{\bar{N}_C; B_{L2}\}$,
- (C) $p_1 p_2 \rightarrow \bar{N}_{\text{Central}} + N_{\text{Central}} + \text{anything} \equiv \{\bar{N}_C; M_C\}$.

In (p \bar{p}) collisions, due to the the presence of an anti-flavoured antibaryonic state, another leading reaction can occur :

- (L) $p_1 \bar{p}_2 \rightarrow \bar{N}_{\text{Central}} + (B_{\text{Leading}})_1 + \text{anything} \equiv \{\bar{M}_C; B_{L1}\}$,
- (L) $p_1 \bar{p}_2 \rightarrow \bar{N}_{\text{Central}} + (\bar{B}_{\text{Leading}})_2 + \text{anything} \equiv \{M_C; \bar{B}_{L2}\}$,
- (L) $p_1 \bar{p}_2 \rightarrow (B_{\text{Leading}})_1 + (\bar{B}_{\text{Leading}})_2 + \text{anything} \equiv \{B_{L1}; \bar{B}_{L2}\}$.
- (C) $p_1 \bar{p}_2 \rightarrow N_{\text{Central}} + \bar{N}_{\text{Central}} + \text{anything} \equiv \{M_C; \bar{M}_C\}$.

The indices (1,2) are redundant in the (p \bar{p}) case and will be omitted from now on.

The ratio between the inclusive cross-sections for producing the four classes of particles M_C , \bar{M}_C , B_L and \bar{B}_L and the total cross-sections are:

$$\begin{aligned} \rho_M &= \{\sigma\{M_C; \bar{B}_L\} + \sigma\{\bar{M}_C; M_C\}\} / \sigma^T , \\ \rho_{\bar{M}} &= \{\sigma\{\bar{M}_C; B_L\} + \sigma\{M_C; \bar{M}_C\}\} / \sigma^T , \\ \rho_B &= \{\sigma\{\bar{M}_C; B_L\} + \sigma\{B_L; \bar{B}_L\}\} / \sigma^T , \\ \rho_{\bar{B}} &= \{\sigma\{M_C; \bar{B}_L\} + \sigma\{B_L; \bar{B}_L\}\} / \sigma^T ; \end{aligned}$$

with:

$$\sigma^T = \sigma\{\bar{M}_C; B_L\} + \sigma\{M_C; \bar{B}_L\} + \sigma\{\bar{M}_C; M_C\} + \sigma\{B_L; \bar{B}_L\} .$$

Notice that the ratio (Leading/Total) = $p_B = p_{\bar{B}}$.

At ISR, in each hemisphere, the ratio (Leading/Total) is $\sim 1/16$ for strangeness and $\sim 1/8$ for "charm". In our discussion we will study the behaviour of A^0 as a function of (Leading/Total).

2.4.6 Estimates of the Asymmetry A^0 .

In order to estimate the lepton Asymmetry parameter A^0 , we have considered the case: lepton \equiv muon.

The angular and momentum distributions of the muons have been evaluated by means of a Monte Carlo simulation, with the conditions set in the previous sections. Figures 9a to 9d shows the angular distribution of the muons from the primary decay of "superbeauty", "top", "beauty" and "charm" [baryon and meson states]. For further reference, also the distribution of muons from the decay $t \rightarrow b \mu \nu$ with $m_t = 35 \text{ GeV}/c^2$ is shown in Fig. 9e.

For the "superbeauty" case, a choice of $\theta_{\text{cut}} = 30^\circ$ gives a good acceptance for the detection of muons from baryons, which contribute to the asymmetry, while keeping low the acceptance for muons from mesons, which destroy it.

Figures 10a to 10c show the (θ vs p_μ) plots for muons coming from the "superbeauty" ($m_{sb} = 55 \text{ GeV}/c^2$), "top" ($m_t = 25 \text{ GeV}/c^2$) and "top" ($m_t = 35 \text{ GeV}/c^2$); all being baryon decays.

The detection acceptances ϵ have been computed for 5 values of θ_{cut} ($\theta_{\text{cut}} = 10^\circ, 20^\circ, 30^\circ, 40^\circ$ and 90°) as will be seen in Figs. 14 and 15.

Figures 11a to 11t show the μ^\pm acceptances for $\theta_{\text{cut}} = 30^\circ$ for baryons, mesons and antimsons. The acceptances for μ^\pm originated by the decay of antibaryons are, of course, negligible, because of the central nature of the production mechanism.

Fig. 12 shows the behaviour of $A^0(p_T, 30^\circ)$, for (Leading/Total) = 0.25. There are two main peaks, one positive around $p_T = 10 \text{ GeV}/c$, due to the "top" baryon decay into μ^+ , and one negative around $p_T = 19 \text{ GeV}/c$, due to "superbeauty" baryon decay into μ^- .

It is interesting to note that the separation between the two peaks depends only on the mass differences in the semileptonic decays of "superbeauty" and "top" states. In fact, in the 3-body semileptonic decay, the transverse momentum spectrum of the muons scales with $p_T/\Delta m$, where Δm is the difference between the parent mass and the mass of the hadronic particle produced in the decay. This is shown in Fig. 13 where the normalized $p_T/\Delta m$ spectra of the muons produced in the decays :

- i) $\Lambda_{sb}^0 \rightarrow \Lambda_t^+ \mu^- \nu$;
- ii) $\Lambda_t^+ \rightarrow \Lambda_b^0 \mu^+ \nu$;
- iii) $\Lambda_b^0 \rightarrow \Lambda_c^+ \mu^+ \nu$;
- iv) $\Lambda_c^+ \rightarrow \Lambda_s^0 \mu^+ \nu$;

are reported.

The mass differences Δm have the following values:

- i) $\Delta m = m(\Lambda_{sb}^0) - m(\Lambda_t^+) \approx 30 \text{ GeV}/c^2$ for the "sb" baryon decay ;
- ii) $\Delta m = m(\Lambda_t^+) - m(\Lambda_b^0) \approx 19.5 \text{ GeV}/c^2$ for the "t" baryon decay ;
- iii) $\Delta m = m(\Lambda_b^0) - m(\Lambda_c^+) \approx 3.2 \text{ GeV}/c^2$ for the "b" baryon decay ;
- vi) $\Delta m = m(\Lambda_c^+) - m(\Lambda_s^0) \approx 1.2 \text{ GeV}/c^2$ for the "c" baryon decay ;

The amplitude of the two peaks, for "top" and "superbeauty", as a function of θ_{cut} and (Leading/Total), is shown in Figs. 14 ("top") and 15 ("superbeauty"). The strong difference in the longitudinal momentum production distributions between baryons and mesons does produce a charge asymmetry which remains high, even with low values of the ratio (Leading/Total). We will assume a value of (Leading/Total)=0.25 in most of the graphs, showing the expected asymmetry versus different parameters. However the way in which the asymmetry changes with the quantity (Leading/Total) is easily derivable from Figs. 14 and 15.

3. THE APPARATUS.

A layout of the proposed apparatus is shown in Fig. 16.

The apparatus has been designed with the limitations imposed by planned UA2 extensions and by the experimental hall. This leads to some compromises being necessary on the background level in the experiment, in the efficiency of the trigger, and in the momentum resolution, but it does not affect the general feasibility of the experiment. However, the following points had to be borne in mind in the planning:

- The effect on the precision of the incident track and the smearing of the incident track direction by multiple scattering.
- Energy losses, leading to a reduction in momentum at the magnet.
- Background from decay of π and K.

3.1 THE UA2 CALORIMETER.

In this section we will give some relevant parameters of the UA2 layout before describing the lepton asymmetry analyser.

In the forward/backward direction they consist of a pre-shower converter which has a negligible effect on muons, an electromagnetic detector of 20 radiation lengths and a hadron calorimeter of 57 radiation lengths. The space available for our apparatus starts at 330 cm. from the interaction.

3.2 THE HADRON ABSORBER.

Since there is still an appreciable rate of pion punch-through from the UA2 apparatus and to avoid putting a magnetic field immediately by existing photomultiplier bases, we place 60 cm of non-magnetized iron close behind the hadron calorimeter. Two drift chambers are incorporated for defining the incident muon direction and for recognizing interactions. The absorber is followed by an air gap and a third drift chamber to obtain a good lever arm for the track direction entering the magnet. It will be possible to displace this part of the apparatus, mass approximately 85 tons, along the beam line by the length of the air gap so as to give access to the UA2 calorimeter electronics.

3.3 THE IRON TOROID MAGNETS.

Momentum analysis around each outgoing beam direction is made with two toroidal magnet assemblies. Each of these is made of five circular iron plates, 30 cm thick and with radii varying from 3.0 to 4.0 metres. The plates are separated by 10 cm spaces in which we insert planes of Limited Streamer Tubes. The design parameters of each magnet assembly are:

Field	20 K gauss
Weight	450 tons
Power	500 KW.
Windings	Two Cu windings, water cooled, common to the five plates.
Resolution	~14% $\Delta p/p$ (limited by multiple scattering).

3.4 THE TRACKING CHAMBERS.

Two types of chamber are used: Limited Streamer Tubes, LST, for selecting transverse momentum in a fast decision logic and for coarse tracking in the magnet to avoid ambiguous momentum measurements; Drift Chambers, DC, for final reconstruction to provide more accurate measurements of the incident and emergent track positions and directions.

3.4.1 Drift Chambers.

Each of the first three chamber planes provides three measurements in the directions x and y. The fourth chamber, following the magnet, is double this so as to give the exit point of the track and a sufficient information on the emergent track direction. Space limitations prevent increasing the lever arm.

The characteristics of each drift cell (Fig. 17) are:

Track length sampled	3 cm
Cell width	6 cm
Cathode Voltage	-6000 V
Field wire voltage	-1000 V
Field wire diameter	100 μm
Sense wire diameter	20 μm
Sense wire field	330 KV/cm ^(*)
Typical drift field	~ 1.5 KV/cm ^(*)
Average drift velocity	47 $\mu\text{m}/\text{nsec}$ ^(*) (Ar/CO2 90/10)
Spatial resolution	300 μm ^(*)
Read-out channels	5800

The quantities marked with an asterisk have been calculated with a Monte Carlo program written by J. Va'Vra at SLAC [20]. In particular the spatial

resolution obtained was 100 μm . We estimate however that systematic errors will worsen it to the quoted value.

Elimination of ghost points will be achieved by charge division or by delay line read-out, but, if possible, by extrapolation of the LST information. This point is being studied.

3.4.2 Limited Streamer Tubes.

The construction will be of 1 cm square PVC tubes with high resistance cathodes. The read-out system will take full advantage of the properties of this type of tube which allow read-out by external pick-up electrodes whose shapes are independent of the wire configuration.

Before the magnet, there is a pair of chamber planes with orthogonal wires, and their pick-up electrodes are concentric circles centred on the beam line so that the electrode number directly measures the muon production angle. Corresponding electrodes on the two planes are connected in OR configuration for the fast trigger to remove most of the 14% inefficiency which is caused by the side walls of the tubes.

Following the magnet is a similar pair of chambers so that the difference in radial electrode position between the first and last chambers gives the magnetic deflection.

Tube planes within the magnet will be fitted with rectangular or sector-shaped read-out pads with analog read-out to detect interactions in the magnet and to reduce ambiguities.

On each plane of the first and fourth chambers, there will be 116 annular electrodes, each divided into 12 azimuthal segments, giving a total of approximately 11000 data channels for this type of chambers. The pick-up pads will require a similar number of electronic channels.

4. μ IDENTIFICATION.

4.1 μ/π REJECTION.

A basic level of decay muons and punch through pions emerges from the UA2 apparatus. As described previously, 60cm of iron is placed immediately after the UA2 calorimeter to remove residual hadrons before they decay.

Background muon rates from pions and K have been calculated in two steps. In the first step, a decay and hadron shower Monte Carlo [21] has been used to find the background from π and K of fixed energy. Two groups of muons show up in the simulation: muons of the full energy range from decay in flight; muons from decay during the hadron shower development. The latter group has an energy spectrum scaled down by 30% relative to the decay spectrum. Approximately equal numbers of muons in the two groups were sufficiently energetic to penetrate to the end of the toroid.

In the second step of the calculation, the single particle distributions from the UA1 results [22] were used with the results of the first step (scaled proportional to energy) to obtain the muon flux in our apparatus as function of p_T . Figure 18 shows the ratio of background muon flux to parent hadron flux as a function of p_T after integration over the apparatus.

The total rate of muons penetrating to the end of the magnet, without any cut in p_T is 1 muon/300 interactions. The effect of this background on the asymmetry parameter is given in section 5.2.

4.2 MOMENTUM RESOLUTION.

The influence of chamber resolution and multiple scattering on the muon momentum measurement has been simulated with a Monte Carlo program, for the configuration of the magnetic spectrometer shown in Fig. 16. The main detector parameters relevant for this study were:

- calorimeter thickness in radiation lengths : $74 X_0$
- iron absorber thickness in radiation lengths: $34 X_0$
- magnetized iron (toroid) thickness in rad. lengths : $85 X_0$
- magnetic field inside iron : 20 KG
- single wire overall positional accuracy for drift chambers in front of and behind the toroid : 300 μm
- distance between the two chambers in front of the toroid: 80 cm.

The range of muon momenta under study was determined by the angular acceptance of the spectrometer ($5^\circ \leq \theta \leq 30^\circ$) and the transverse momentum (p_T) interval where the maximum asymmetry effect was expected for muons from "top" decay. Assuming a "top" flavour mass of $35 \text{ GeV}/c^2$ and the production plus decay distributions discussed in section 2.4, the relevant p_T range is $4 \div 15 \text{ GeV}/c$ ($p = 8 \div 172 \text{ GeV}/c$), as shown in Fig. 10c. Muons were generated in the Monte Carlo with $p_T = 4, 9.5$ and $15 \text{ GeV}/c$ and $\theta = 5, 10, 20, 30^\circ$.

The contributions from ionization, bremsstrahlung, pair production and nuclear interactions to the mean total energy loss of the muon (see Figs. 19a,b) inside the calorimeter, the first iron absorber and the toroid were taken into account [23]. Fluctuations around the mean value were then allowed according to a Landau distribution. For multiple scattering, the gaussian approximation was used [24].

The momentum determination was based on the measurement of the ingoing muon angle θ , provided by all the drift chambers placed before the toroid, and of the exit point of the muon track, obtained by extrapolating back to the toroid end face the outgoing track fitted in the planes of the last drift chamber. The information from the LST planes inside the toroid was not used for track fitting.

The results of our simulation are expressed in terms of the muon p_T accuracy, which is relevant for the charge asymmetry measurement. The $\Delta p_T/p_T$ resolution values given here are the r.m.s. relative to the distributions of the quantity

$$[p_{\text{generated}} - (p_{\text{measured}} + \text{energy loss correction})] / p_{\text{generated}}$$

obtained in the Monte Carlo. The energy loss correction refers to the total momentum degradation of the particle before and inside the toroid. Since these distributions are not gaussian, if the FWHM/2.36 is used instead of the r.m.s., the improvement of the quoted resolution is $\sim 2\%$. The behaviour of the transverse momentum resolution as a function of the total momentum is shown in Figs. 20a to 20c for fixed p_T values of 4.0, 9.5 and 15.0 GeV/c, respectively. For each value of p_T , the effect of the drift chamber intrinsic resolution σ_{DC} was studied. The curves shown in Figs. 20a to 20c correspond to $\sigma_{DC}=300$ and 600 μm , respectively. The expected value of the proposed drift chamber system is ~ 300 μm . In this case the p_T resolution obtained in the whole momentum range relevant to the asymmetry measurement is better than $\sim 20\%$. When $\sigma_{DC}=600$ μm , the resolution exceeds 20% only at $p_T=15$ GeV/c for $p>75$ GeV/c.

The uncertainty on the vertex determination when tracing back the muon track to the origin was also studied. Examples of Δx , Δy , Δz distributions, corresponding to $p_T=9.5$ GeV/c, $\theta=10^\circ$ and $\sigma_{DC}=300$ μm , are shown in Figs. 21a to 21c. The error on the vertex coordinate along the colliding beams direction (y) is ~ 11 cm (the jitter of the interaction point in the Monte Carlo generation was ± 10 cm), while the errors on the transverse coordinates are ~ 1.5 cm. The boundary values of the errors at the vertex in the p_T and θ region considered in our exercise, are $10.5 \div 17$ cm along y and $1 \div 6$ cm along x or z .

5. ESTIMATE OF THE ASYMMETRY PARAMETER IN EXPERIMENTAL CONDITIONS.

5.1 THE EFFECT OF THE ANGULAR CUT.

We have already shown in Figs. 9a to 9e the angular distributions of the muons originating from the semileptonic decays of the heavy-flavour particles, as they are computed by our Monte Carlo.

When taking into account the lower cut in the angular coverage of the apparatus described in chapter 3, $\theta \geq 5^\circ$, the acceptance for muons from baryon decay decreases very much for low quark masses. This is due both to phase-space limits - the maximum x_F of the baryon decreases with increasing quark mass - and to the transverse momentum of the muon in the decay - it decreases with decreasing quark mass. Figure 22 shows the Asymmetry A^0 computed with the angular cut $5^\circ \leq \theta \leq 30^\circ$.

By comparing Figs. 12 and 22 it can be seen that the $\theta \geq 5^\circ$ cut makes disappear the asymmetry at low p_T due to charm and beauty, and decreases by a small amount the asymmetry at higher p_T due to "top" and "superbeauty".

5.2 THE BACKGROUND.

In what has been described so far, the background contamination in the sample of prompt muons has not been considered. As discussed in chapter 4, the background is mainly due to muons produced by π and K decay. This contribution can be computed from the inclusive pion cross-section as measured by the UA1 experiment [22], using the fit to their data:

$$E(d^3\sigma/dp^3) = A \times p_0^n / (p_0 + p_T)^n \quad (4)$$

with $A = 0.37 \pm 0.06 \text{ mb c}^2 \text{ GeV}^{-2}$, $p_0 = 1.3 \pm 0.18 \text{ GeV c}^{-1}$ and $n = 8.99 \pm 0.15$.

Formula (4) is relative to charged hadrons (averaged over the two charges) and is given in unit of rapidity. The rapidity interval over which we integrated the background is given by the angular acceptance of the apparatus:

$$5^\circ \leq \theta \leq 90^\circ \rightarrow \Delta y \approx 1.8.$$

The extrapolated background rate should be multiplied by the rejection in the experimental apparatus, given in Fig. 18.

Another source of background, which will be discussed later, is the prompt muons sources other than open heavy flavoured states i.e. W^\pm , Z^0 . It will be shown that this kind of background is relevant only above very high values of p_T ($p_T > 20$ GeV/c).

Due to the background source previously described, the experimental Asymmetry parameter is given by:

$$A^{\text{exp}}(p_T, \theta_{\text{cut}}) = \frac{[N(e^+) + N_{\text{bg}}(e^+)] - [N(e^-) + N_{\text{bg}}(e^-)]}{[N(e^+) + N_{\text{bg}}(e^+)] + [N(e^-) + N_{\text{bg}}(e^-)]}$$

where $N_{\text{bg}}(e^\pm)$ is the number of background muons.

In order to have an estimate for the experimental errors on A^{exp} , we assume a total integrated luminosity $L=10$ pb $^{-1}$, i.e. 3000 hours of running with a luminosity $L=10^{30}$ cm $^{-2}$ sec $^{-1}$.

Figure 23a shows, for the case of simultaneous production of "top" (25 GeV/c 2) and "superbeauty" (55 GeV/c 2), the expected number of produced muons as a function of p_T . Superimposed is the computed background.

Figure 23b shows the plot of A^{exp} as a function of p_T . The errors are purely statistical.

5.3 THE MOMENTUM RESOLUTION.

We have studied the amplitude and the position of the peaks in the experimental asymmetry A^{exp} as a function of the finite momentum resolution of the proposed apparatus.

The results are shown in Figs. 24a and 24b for the "top" peak, and in Figs. 25a and 25b for the "superbeauty" peak. The smearing effect of the momentum resolution decreases the absolute amplitude of A^{exp} and shifts the peaks upward by a relatively small amount.

Figures 26a and 26b show the number of events and the experimental asymmetry as a function of p_T , for a momentum resolution $\Delta p/p=20\%$, as expected in the proposed apparatus (see section 4.2).

5.4 OTHER HYPOTHESES ON THE NEW HEAVY FLAVOUR MASSES AND ON THE PRODUCTION CROSS-SECTIONS.

With our Monte Carlo program, we have tested the capability of the proposed apparatus to cope with different heavy flavour masses and with lower cross sections for heavy flavour production.

We have repeated our analysis turning off the "superbeauty" signal and using two assumptions for the "top" mass:

- i) $m_t=25 \text{ GeV}/c^2$, as in the previous analysis;
- ii) $m_t=35 \text{ GeV}/c^2$.

The cross-section for a "top" mass of $35 \text{ GeV}/c^2$, $\sigma_t \sim 0.05 \mu\text{b}$, is the result of extrapolation using the same method as the one outlined in sections 2.3 and 2.4.1.

Figures 27a and 27b, 28a and 28b show the number of expected events and the experimental asymmetry A^{exp} for case (i) and, respectively, (ii).

The effect of different cross-section values has been studied for the three hypotheses:

- i) $m_t=25 \text{ GeV}/c^2$, $m_{sb}=55 \text{ GeV}/c^2$ (simultaneous production of two flavours);
- ii) $m_t=25 \text{ GeV}/c^2$, no "superbeauty" (only one flavour);
- iii) $m_t=35 \text{ GeV}/c^2$, no "superbeauty" (only one flavour).

The values of the experimental Asymmetry peaks and the statistical significance of the measurements for the three hypotheses indicated above, are reported in Figs. 29 to 32: the experimental asymmetry remains measurable for values of the heavy flavour production cross-sections even a factor ten lower than those expected from QCD extrapolations.

5.5 EFFECTS FROM $W^{\pm} \rightarrow \mu^{\pm} \nu$ AND $W^{\pm} \rightarrow tb \rightarrow \ell \nu X$.

As it is well known, the direct leptons from W^{\pm} have a pronounced asymmetry which is opposite to the one we are looking for in the case of "up-like" baryonic and antibaryonic states. A detailed calculation shows that the maximum effect expected from the $W^{\pm} \rightarrow \mu^{\pm} \nu$ decay does not exceed the 10% level with 50% efficiency for W^{\pm} identification in the UA2 central detector.

As nothing is known on the process $W^{\pm} \rightarrow tb \rightarrow \ell \nu X$, we assume that all the leptons it produces behave similarly to the direct leptons from W^{\pm} . We can evaluate an upper limit to this effect if we know its total cross-section. Various estimates exist in the literature: for example, with a "top" mass $m_t=40 \text{ GeV}/c^2$ and for leptons with $p_T > 10 \text{ GeV}/c$:

$$B(W \rightarrow tb \rightarrow \ell \nu X) \times \sigma_W = 36 \text{ pb (ref. [26]);}$$

$$B(W \rightarrow tb \rightarrow \ell \nu X) \times \sigma_W = 29 \text{ pb (ref. [27]).}$$

From the above figures we can conclude that the background from this source is at most one half of the background from the muons directly produced by W^{\pm} .

6. TRIGGER LOGIC AND TRIGGER RATES.

The maximum trigger rate which is acceptable to the UA2 data acquisition system is 1 Hz and the decision of whether to accept or reject an individual event must be reached within a time delay of 1 μ sec. This can be done by applying a cut in p_T around 2 GeV and this cut must be made with little loss in efficiency above $p_T=5$ GeV/c where the interesting events lie. Clearly any system which requires a wire-by-wire read out is excluded. What is needed is a fast parallel logic .

As indicated in the LST description, a suitable method is to make coincidences between one circular strip of the first chamber with a suitable group of circular strips in the last chamber.

6.1 TRIGGER RATE WITH PERFECT SELECTION.

To evaluate the trigger rates, the ISAJET Monte Carlo [28] was used to simulate event production at the $p\bar{p}$ Collider at 540 GeV. Each track produced in the angular intervals $5^\circ \leq \theta \leq 30^\circ$ and $150^\circ \leq \theta \leq 175^\circ$ was then followed through all the apparatus using a Monte Carlo [21] in which particles are allowed to produce showers and to decay; energy loss and multiple scattering are taken into account. The average number of particles reaching the toroids was evaluated to be .08 per event on each side. All particles traversing the toroids were found to be muons mostly produced by the decay in flight of primary particles in the central detector and partially by the decay of particles produced in the hadronic showers inside the calorimeters. Trigger rates were estimated for a luminosity of $10^{30} \text{ cm}^{-2} \text{ sec}^{-1}$ for different p_T cuts on particles traversing the toroids. In Table V the 90% C.L. upper limits for the trigger rates are given. Trigger conditions are defined for each side of the detector and the rate is given by the OR of the two sides.

6.2 DESIGN OF TRIGGER CONDITIONS.

The Monte Carlo results were used to find out the strip correlations between the first and the last chamber planes. Particles produced at a fixed angle and fixed transverse momentum were tracked through one strip of the first plane and through the last plane. The radial spread on the back plane to be accepted for 100% efficiency at that p_T and angle was thus determined and is shown in Fig. 33. We use the curve for $p_T \geq 5$ GeV/c in our design.

In the next step, these strip coincidence configurations are assumed fixed and the acceptance for lower values of p_T was determined using the same program. Figure 34 shows the results. For example, at $\theta = 5^\circ$, $p_T = 2$ GeV/c, the efficiency is 30%. The important point is that full efficiency is reached for $p_T \geq 5$ GeV/c. A more detailed simulation is to be made when the design is made final.

The best way to realize the hardware coincidence conditions is being studied. Each strip-sector of the first plane has to be put in coincidence with between 3 and 20 sectors of the last plane, and the OR of all coincidences must be taken.

7. COSTS AND TIME SCALE .

An estimate of costs is shown in the table below:

		KSFr.	KSFr.
Magnet		3000	
Magnet chariots		1000	4400
Preabsorber and chariots		400	
Drift chambers	Construction		3050
	Supplies	1300	
	Head Electronics		
	Cables		
	Mechanical supports	250	
	TDC system	1500	
IST	Construction	600	2800
	Pads	200	
	Mechanical support	200	
	Head electronics (pads)	680	
	Head electronics (x,y,strips)	200	
	Trigger and read-out	620	
	Cables	300	
General fast electronics	250		
Crates and Controllers	300	550	
TOTAL			10800

The foreseen time table for the experiment is as follows:

- 1984 : Full design of the various parts of the apparatus and in particular of the iron absorber and the toroid; tendering and contracts.
- 1984-1985 : Prototypes construction and tests for DC and LST.
- 1985 : Complete design and construction for DC and LST; material delivery.
- 1985-1986 : Calibrations.
- 1986-1987 : Final assembling.

REFERENCES

- [1] S. Ferrara, private communication.
- [2] A. Martin, The masses of the Heavy Flavoured Hadrons, CERN Preprint TH-3314, 28 May 1982.
- [3] M. Basile et al., Nuovo Cimento Lett. 30 (1981) 487.
- [4] M. Basile et al., Nuovo Cimento Lett. 33 (1982) 33.
- [5] R. Odorico, Phys. Lett. 107B (1981) 231.
- [6] V. Barger, F. Halzen and W.Y. Keung, Phys. Rev. D24 (1981) 1428.
- [7] F. Halzen, W.Y. Keung and D.M. Scott, Madison Rep. MAD/PH/63 (1982).
- [8] M. Basile et al., Proceedings of the Third Topical Workshop on Proton-Antiproton Collider Physics, Rome, Jan-1983, p.435.
- [9] F. Halzen, Rapp. Talk, XXI Int. Conf. on High Energy Physics, Paris.
- [10] M. Basile et al., Nuovo Cimento 63A (1981) 230.
- [11] M. Basile et al., Nuovo Cimento 65A (1981) 457.
- [12] M. Basile et al., Nuovo Cimento 67A (1982) 40.
- [13] D. Drijard et al., Phys. Lett. 85B (1979) 452;
K. Giboni et al., Phys. Lett. 85B (1979) 437;
W. Lockman et al., Phys. Lett. 85B (1979) 443;
J. Eickmeyer et al., XX ICHEP (Madison, 1981);
D. Drijard et al., Phys. Lett. 81B (1979) 250;
P. F. Jacques et al., Phys. Rev. D21 (1980) 1206;
P. Coteus et al., Phys. Rev. Lett. 42 (1979) 1438;
A. Soukas et al., Phys. Rev. Lett. 44 (1980) 564;
A.E. Asratyan et al., Phys. Lett. 74B (1978) 497;
P. Alibrand et al., Phys. Lett. 74B (1978) 134;
T. Hansl et al., Phys. Lett. 74B (1978) 139;
A. Bosetti et al., Phys. Lett. 74B (1978) 143;
M. Fritze et al., Phys. Lett. 96B (1980) 427;
D. Jonker et al., Phys. Lett. 96B (1980) 435;
H. Abramowicz et al., Cern Preprint CERN-EP/82-17;
M. Aguilar-Benitez et al., CERN Preprint CERN-EP/81-131;

- T. Aziz et al., Nucl. Phys. B199 (1982) 424;
J. Sandweiss et al., Phys. Rev. Lett. 44 (1980) 1104.
- [14] M. Basile et al., Nuovo Cimento 65A (1981) 391.
[15] J. Badier et al., XXI Int. Conf. on High Energy Physics, Paris 1982.
[16] K. Chadwick et al., preprint CLNS/82/546.
[17] M. Basile et al., Nuovo Cimento Lett. 30 (1981) 481.
[18] M. Basile et al., Nuovo Cimento Lett. 33 (1982) 17.
[19] L. Olsen, Moriond workshop on New Flavours, Les Arcs 1982.
[20] J. Va'Vra, Proceedings of the Vienna Wire Chamber Conference (1983).
[21] A. Baroncelli, Nucl. Instr. Meth. 188 (1974) 445.
[22] G. Arnison et al., UA1 Collaboration, Preprint CERN-EP/82-171.
[23] C. Richard-Serre, CERN report 71-18.
[24] B. Rossi, High Energy Particles (Prentice-Hall), p.63-77.
[25] T. Hansl and Kozaneka, Preprint CERN-EP/83-193.
[26] R. Odorico, Preprint CERN TH-3678/83.
[27] R. Kinnunen, Preprint CERN-EP/84-19.
[28] F.E. Paige and S.D. Protopopescu, BNL 31987, September 1982.

TABLE I.

The four families of quarks and leptons.

The dashed circles indicate the main objectives of this proposal.

Families:	1 st	2 nd	3 rd	4 th
Quarks:	$\begin{pmatrix} u \\ d \end{pmatrix}$	$\begin{pmatrix} c \\ s \end{pmatrix}$	$\begin{pmatrix} \textcircled{t} \\ b \end{pmatrix}$	$\begin{pmatrix} u_H \\ d_H \end{pmatrix}$
Leptons:	$\begin{pmatrix} \nu_e \\ e \end{pmatrix}$	$\begin{pmatrix} \nu_\mu \\ \mu \end{pmatrix}$	$\begin{pmatrix} \nu_\tau \\ \tau \end{pmatrix}$	$\begin{pmatrix} \nu_H \\ L_H \end{pmatrix}$

TABLE II.
Experimental findings versus theoretical predictions for
"charm" production.

	experiment	models		
		diffractive	flavour excitation	fusion
Leading effect	yes	yes	yes	no
threshold behaviour	steeper than $\ln^2 s$	$\ln s$	steeper than $\ln^2 s$	\gg steeper than $\ln^2 s$
mass dependence	?	$1/m^2$	stronger than $1/m^2$	\gg stronger than $1/m^2$
cross section	large	large	large	small
A^α dependence	$\alpha < 2/3$ (*)	$\alpha = 2/3$	$\alpha = 1$	$\alpha = \dots$

(*) The p_T dependence is derived from data on strangeness.

TABLE III.

The heavy-flavour decay chains producing ℓ^+ and ℓ^- .

Flavour	Decays producing ℓ^+	Decays producing ℓ^-
sb	$sb \rightarrow t \rightarrow b + \ell^+$ $sb \rightarrow t \rightarrow b \rightarrow c + s + \ell^+$	$sb \rightarrow t + \ell^-$ $sb \rightarrow t \rightarrow b + c + \ell^-$
t	$t \rightarrow b + \ell^+$ $t \rightarrow b \rightarrow c + s + \ell^+$	$t \rightarrow b \rightarrow c + \ell^-$
b	$b \rightarrow c + s + \ell^+$	$b \rightarrow c + \ell^-$
c	$c + s + \ell^+$	

TABLE IV.

The heavy-antiflavour decay chains producing ℓ^+ and ℓ^- .

Antiflavour	Decays producing ℓ^+	Decays producing ℓ^-
\overline{sb}	$\overline{sb} \rightarrow \bar{t} + \ell^+$ $\overline{sb} \rightarrow \bar{t} + \bar{b} + \bar{c} + \ell^+$	$\overline{sb} \rightarrow \bar{t} + \bar{b} + \ell^-$ $\overline{sb} \rightarrow \bar{t} + \bar{b} + \bar{c} + \bar{s} + \ell^-$
\bar{t}	$\bar{t} \rightarrow \bar{b} + \bar{c} + \ell^+$	$\bar{t} \rightarrow \bar{b} + \ell^-$ $\bar{t} \rightarrow \bar{b} + \bar{c} + \bar{s} + \ell^-$
\bar{b}	$\bar{b} \rightarrow \bar{c} + \ell^+$	$\bar{b} \rightarrow \bar{c} + \bar{s} + \ell^-$
\bar{c}		$\bar{c} \rightarrow \bar{s} + \ell^-$

TABLE V.

90% C.L. upper limits for trigger rates.

Trigger	Rate (Hz)
no p_T cut	240.
$p_T \geq 2$ Gev/c	4.4
$p_T \geq 3$ Gev/c	.5

Figure captions.

Fig. 1 : The diagram illustrates how a gluino can acquire a mass from radiative processes, where a spin 1/2 quark and a spin 0 antiquark are virtually produced. The quark mass must be in the 10^2 GeV/c² range, in order to allow a gluino mass of the order of a few GeV/c².

Fig. 2 : Main trend of the muon charge Asymmetry in the proton hemisphere (a) and in the antiproton hemisphere (b).

Fig. 3 : Experimental longitudinal momentum distribution of Λ_c^+ .

Fig. 4 : a) Λ_c^+ and Λ_s^0 leading effects compared.
b) Qualitative behaviour of the quantity (Leading/Total) as a function of the heavy flavour mass, at $\sqrt{s}=62$ GeV.

Fig. 5 : a) The six quark mixing with CP violation. $S_i = \sin\theta_i$, $C_i = \cos\theta_i$.
b) Transitions among the various states. The Cabibbo dominance opens the dashed channels. The horizontal transitions are forbidden for any value of the mixing angle. Allowed neutral currents are: $u\bar{u}$, $c\bar{c}$, $t\bar{t}$, $d\bar{d}$, $s\bar{s}$ and $b\bar{b}$.

Fig. 6 : Charm cross-section derived from strange cross-section following formula (3). The data are taken from refs. 10, 11, 12 and 13.

Fig. 7 : "Beauty" cross-section derived from strange (full line) and "charm" (dashed lines - notice the width due to the experimental uncertainties) cross-sections following formula (3). The data are taken from refs. 14 and 15.

Fig. 8 : Diagram illustrating all possible electric charge signs of the muons originating from the semileptonic decay of the flavours c, b, t and sb, and the corresponding anti-flavour states..

Fig. 9 : Angular distribution of the muons from the semileptonic decays:

- a) $sb \rightarrow t\mu\nu$;
- b) $t \rightarrow b\mu\nu$;
- c) $b \rightarrow c\mu\nu$;
- d) $c \rightarrow s\mu\nu$;
- e) $t \rightarrow b\mu\nu$ ($m_t = 35 \text{ GeV}/c^2$).

The full lines refer to baryon states, the dashed/dotted lines to meson states.

The dotted vertical lines indicate the angular acceptance of the proposed apparatus (see chapter 3).

The spectra from baryons and mesons are normalized to a ratio (Leading/Total)=0.25.

Fig. 10 : θ vs. p_μ plots from the decays:

- a) $\Lambda_{sb}^0 \rightarrow \Lambda_t^+ \mu^- \nu$; ($m_{sb} = 55 \text{ GeV}/c^2$);
- b) $\Lambda_t^+ \rightarrow \Lambda_b^0 \mu^+ \nu$; ($m_t = 25 \text{ GeV}/c^2$);
- c) $\Lambda_t^+ \rightarrow \Lambda_b^0 \mu^+ \nu$; ($m_t = 35 \text{ GeV}/c^2$).

Fig. 11 : (a) to (t): Acceptances ϵ for the various states and decay chains.

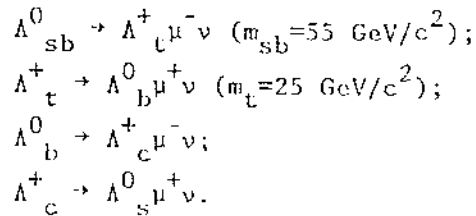
Fig. 12 : Plot of $A^0(p_T, \theta_{\text{cut}})$ as a function of p_T . The value assumed for the angular cut and for the ratio (Leading/Total) are:

$$\theta_{\text{cut}} = 30^\circ;$$

$$(\text{Leading/Total}) = 0.25.$$

The heavy flavour masses are taken to be: $m_t = 25 \text{ GeV}/c^2$ and $m_{sb} = 55 \text{ GeV}/c^2$

Fig. 13 : Normalized ($p_T/\Delta m$) spectra of the muons from the decays:



The Δm values relative to the four decays are indicated.

Fig. 14 : Plot of $\Lambda^0(p_T=10 \text{ GeV}/c, \theta_{cut})$ ("top" peak, $m_t=25 \text{ GeV}/c^2$) as a function of (Leading/Total) for different values of θ_{cut} .

Fig. 15 : Plot of $\Lambda^0(p_T=19 \text{ GeV}/c, \theta_{cut})$ ("superbeauty" peak, $m_{sb}=55 \text{ GeV}/c^2$) as a function of (Leading/Total) for different values of θ_{cut} .

Fig. 16 : Showing a schematic side view of the experimental apparatus.
 CD and FD are the central and forward detectors of UA2 ;
 DC are the drift chambers for momentum measurement;
 ST are the Limited Streamer Tubes with pad read out for triggering;
 HF is the iron hadron filter;
 IT is the iron toroidal magnet.
 Also shown is the mobile UA2 platform.

Fig. 17 : a) The equipotentials map of a drift cell is shown. Two sets of seven guard wires define the cell. The middle plane contains seven wires: four field and three sense wires alternated. The three sense wires are staggered by $\pm 500 \mu\text{m}$ relative to the field wire plane to resolve left-right ambiguity.
 b) The drift of electrons generated by a track and reaching wires: 2(sense), 3(field), 4(sense).

Fig. 18 : The ratio of background muons to parent hadrons as function of p_T , and integrated over the angular acceptance of the apparatus.

- Fig. 19 : The mean energy loss of muons in iron (I=ionization, B=bremsstrahlung, P=pair creation, N=nuclear interaction). The horizontal scale refers to the muon kinetic energy. [(a):different contributions to the mean energy loss, (b):total mean energy loss].
- Fig. 20 : The muon transverse momentum resolution as a function of the total momentum, for $p_T=4, 9.5$ and 15 GeV/c, $5^\circ < \theta < 30^\circ$ and two values of drift chamber resolution.
- Fig. 21 : Distributions of the reconstructed vertex coordinates transverse to the beams direction [(a):DX and (b):DZ] and along the beams direction [(c):DY]. The vertex jitter along y was ≈ 10 cm in the Monte Carlo generation.
- Fig. 22 : Plot of A^0 as a function of p_T in the angular acceptance defined by the apparatus ($5^\circ \leq \theta \leq 30^\circ$).
- Fig. 23 : a) Expected number of produced μ^+ (black points) and μ^- (white points), as a function of p_T and for an integrated luminosity of 10 pb^{-1} , with the conditions set in the text and for $m_t=25 \text{ GeV}/c^2$ and $m_{sb}=55 \text{ GeV}/c^2$. The estimated background for each charge sign is indicated by the full line. The errors are purely statistic.
b) The expected asymmetry A^{exp} as a function of p_T
- Fig. 24 : a) Position in p_T of the peak of the experimental Asymmetry coming from "top" ($m_t=25 \text{ GeV}/c^2$) decay as a function of the momentum measurement error $\Delta p/p$.
b) Absolute value of the A^{exp} peak position given in (a) as a function of $\Delta p/p$.
- Fig. 25 : Same as Fig. 24 for "superbeauty" peaks ($m_{sb}=55 \text{ GeV}/c^2$).

- Fig. 26 : Same as Fig. 23, with the smearing in p_T due to the expected momentum resolution $\Delta p/p=20\%$.
- Fig. 27 : Same as Fig. 23 for a "top" mass $m_t=25 \text{ GeV}/c^2$ and no "superbeauty".
- Fig. 28 : Same as Fig. 23 for a "top" mass $m_t=35 \text{ GeV}/c^2$ and no "superbeauty".
- Fig. 29 : a) "Top" peak experimental Asymmetry amplitude;
b) statistical significance of the measurement.
Both quantities are plotted versus the production cross-section for the hypothesis (i) defined in the text (simultaneous production of "up-like" and "down-like" flavours). The curves correspond to a p_T integration in the interval specified in the figure. The arrows indicate the cross-section value used so far (see section 2.4.1).
- Fig. 30 : Same as Fig. 29 but for "superbeauty" peak (simultaneous production of "up-like" and "down-like" flavours).
- Fig. 31 : Same as Fig. 29 but for hypothesis (ii) in the text (only one flavour produced).
- Fig. 32 : Same as Fig. 29 but for hypothesis (iii) in the text (only one flavour produced).
- Fig. 33 : Number of circular pads in the last LST plane projected by one pad in the first LST plane as function of θ and p_T of the muons. This number corresponds to full efficiency for μ of both charge signs.
- Fig. 34 : Trigger efficiency vs. θ for different values of p_T , for a trigger configuration 100% efficient at $p_T \geq 5 \text{ GeV}/c$.

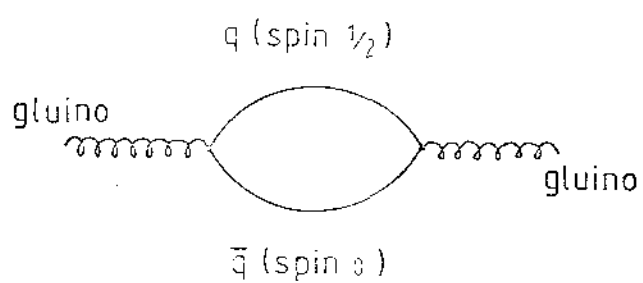


FIG. 1

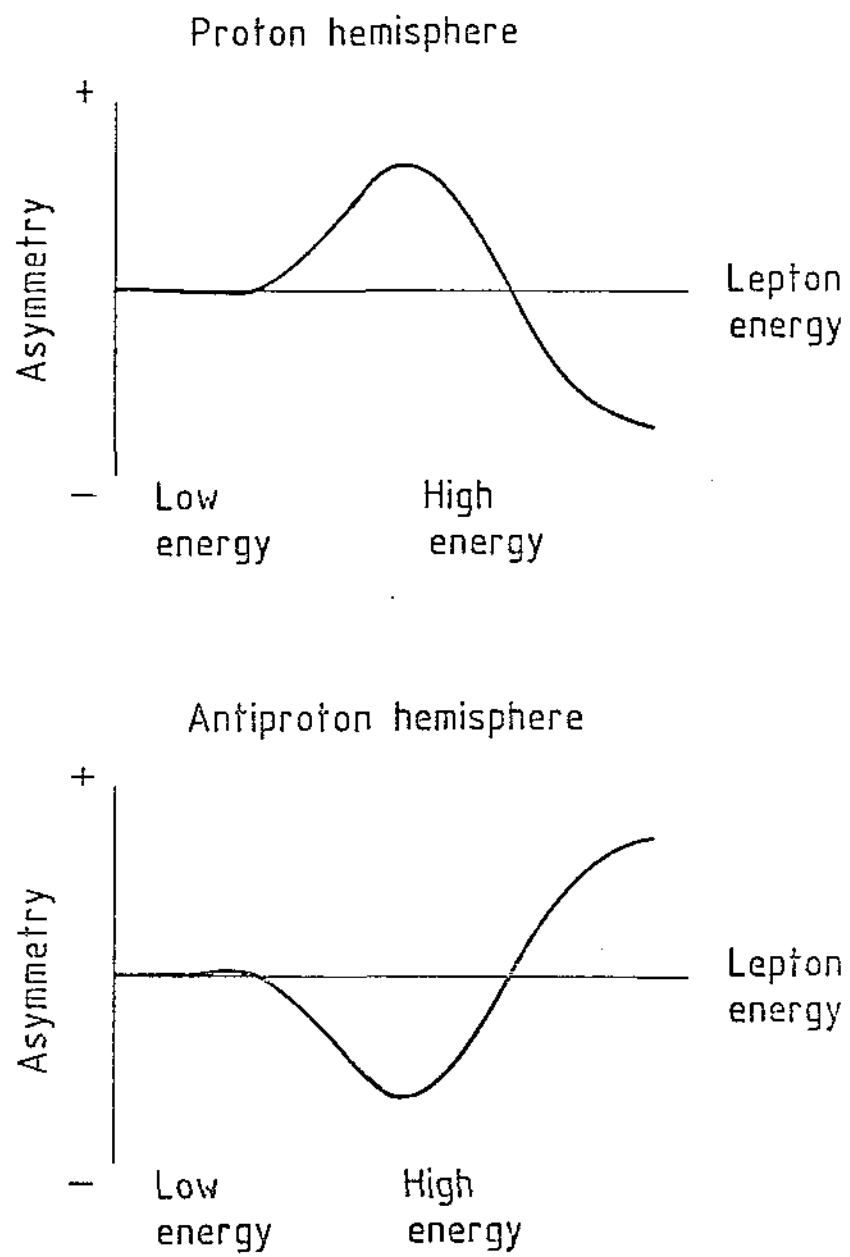


FIG. 2

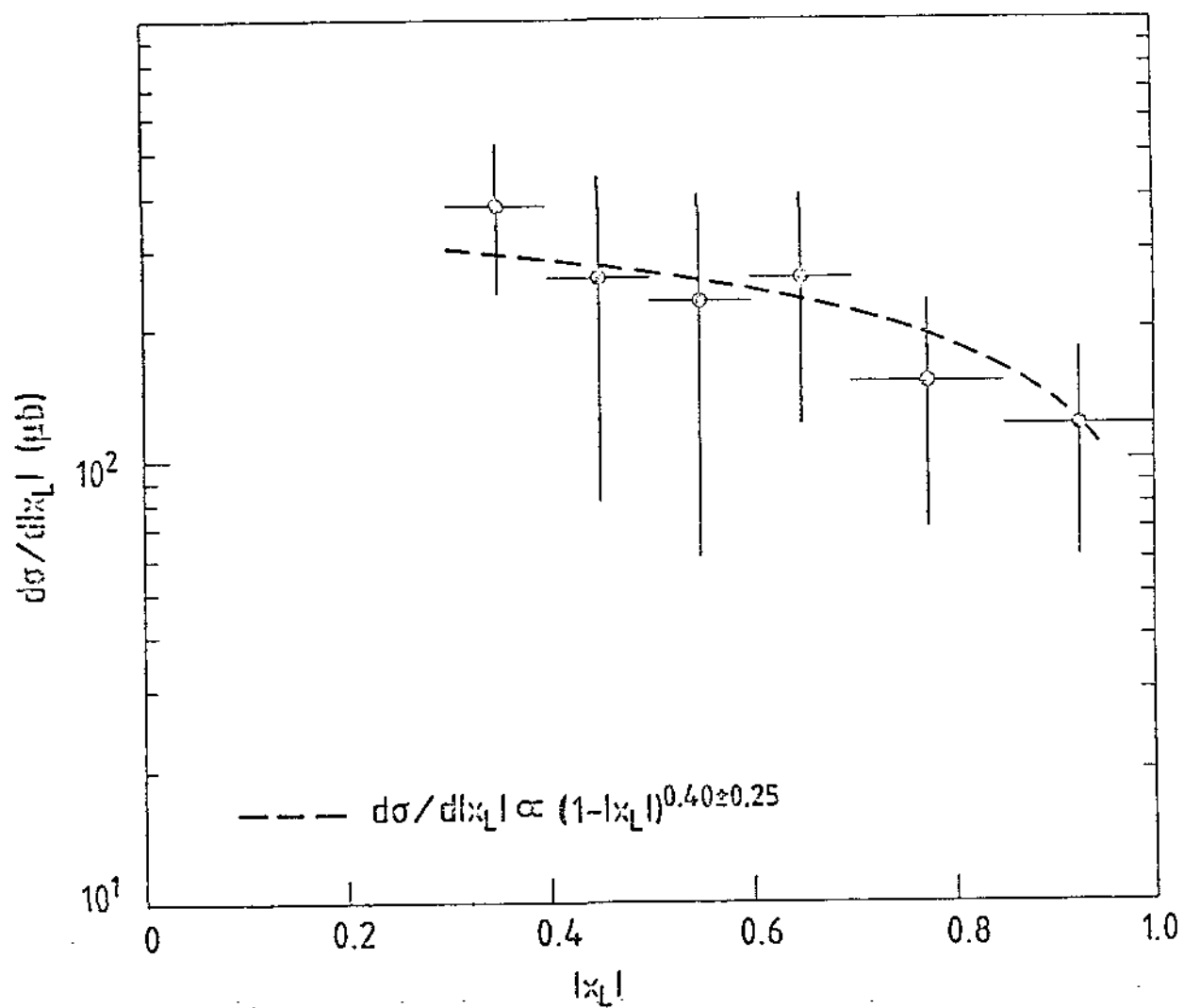


FIG. 3

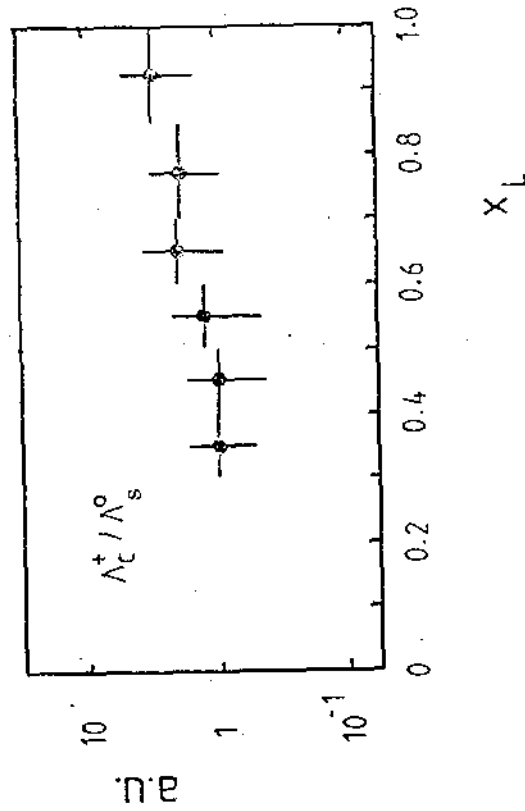
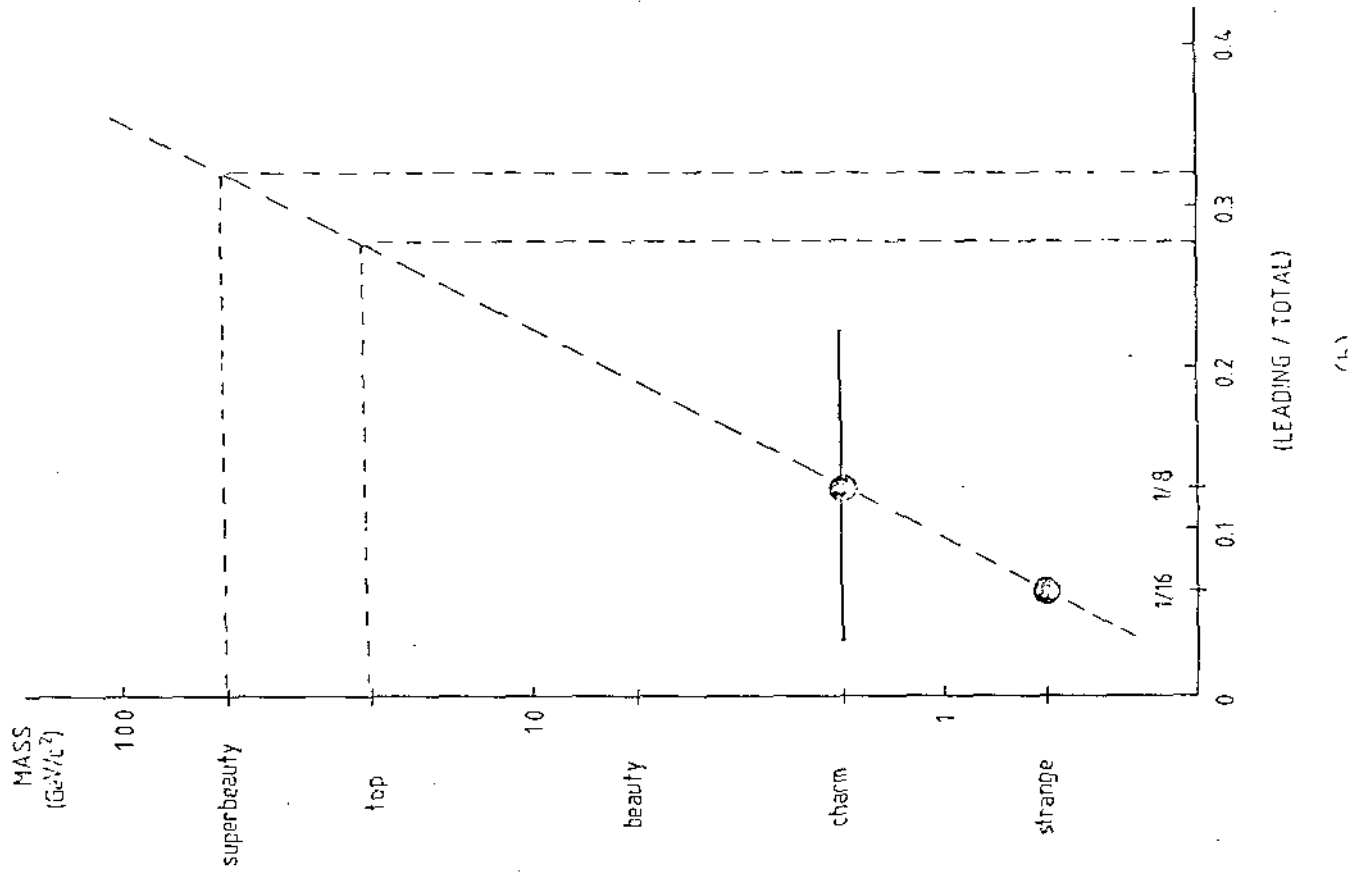
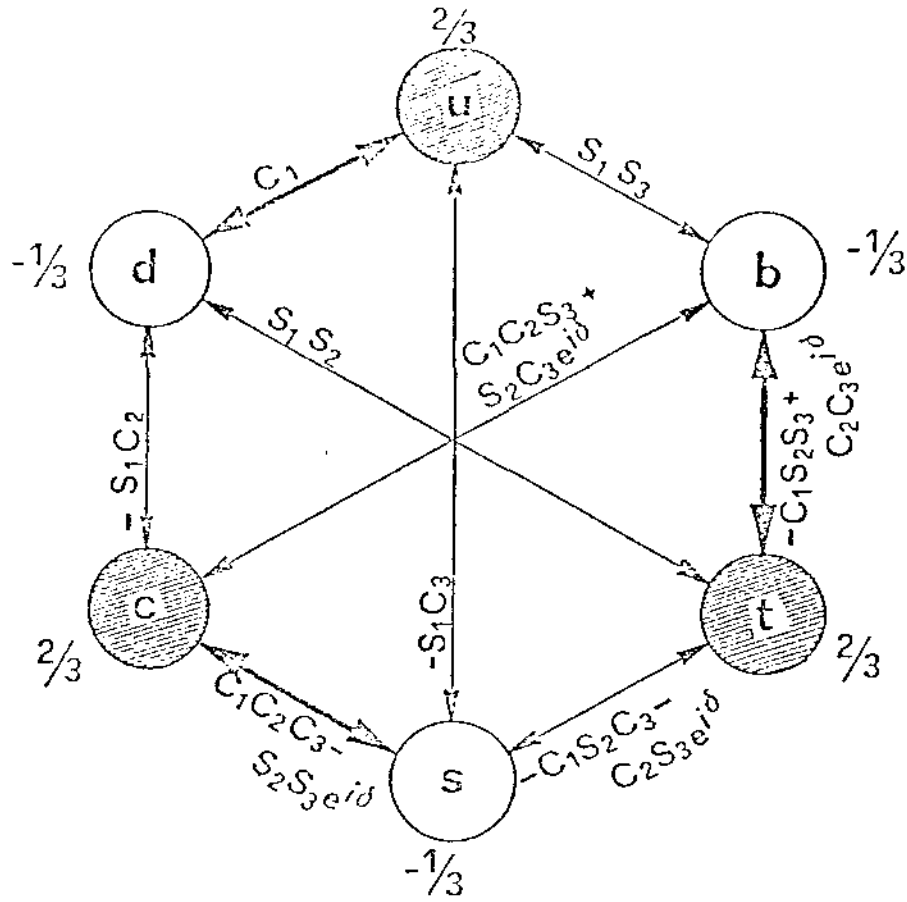
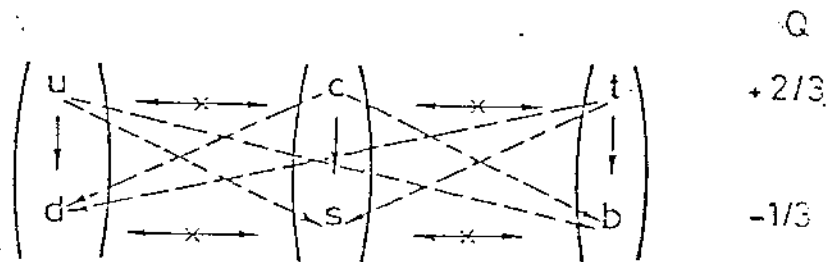


FIG. 4



(a)



(b)

FIG. 5

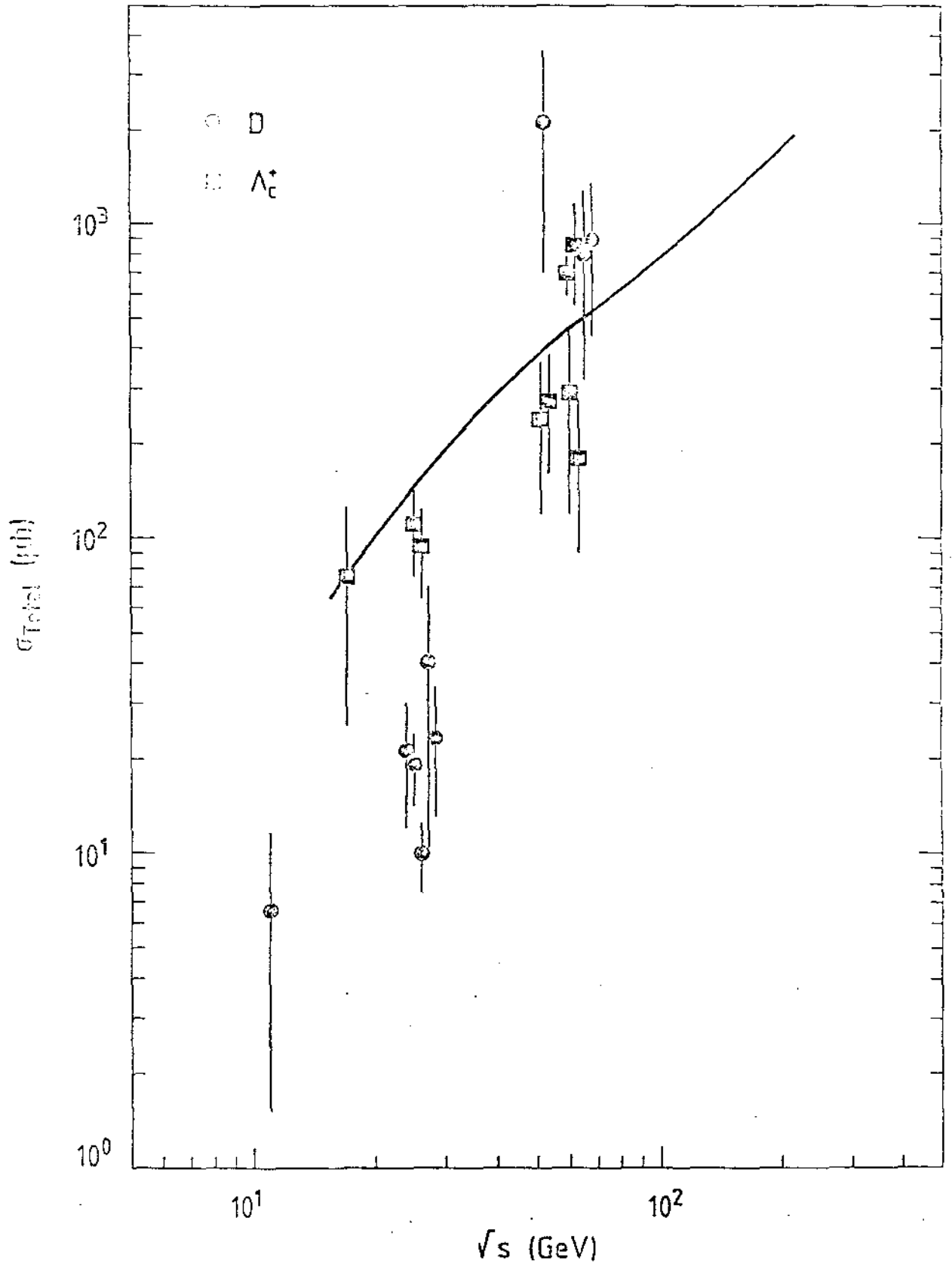


FIG. 6

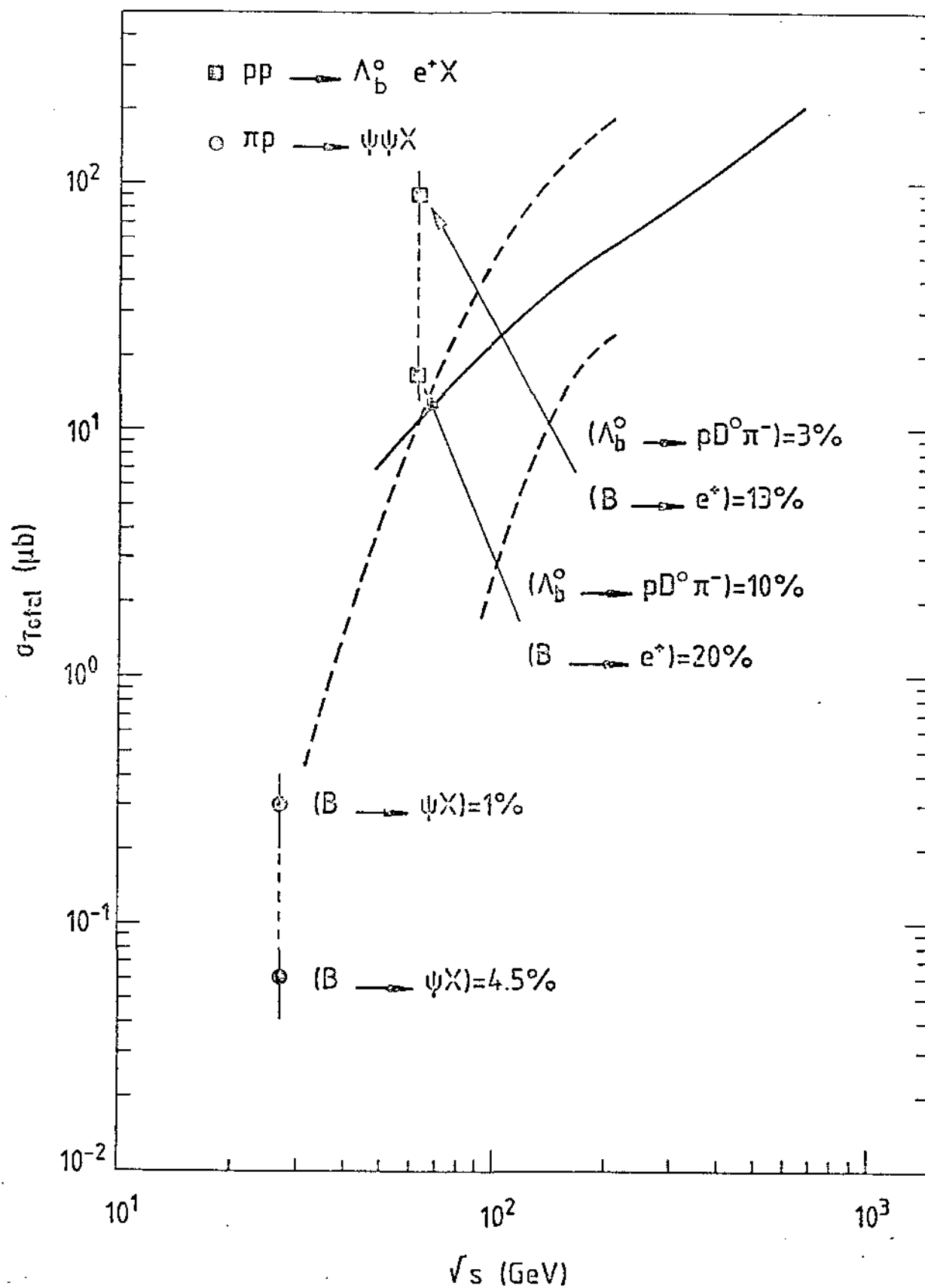


FIG. 7

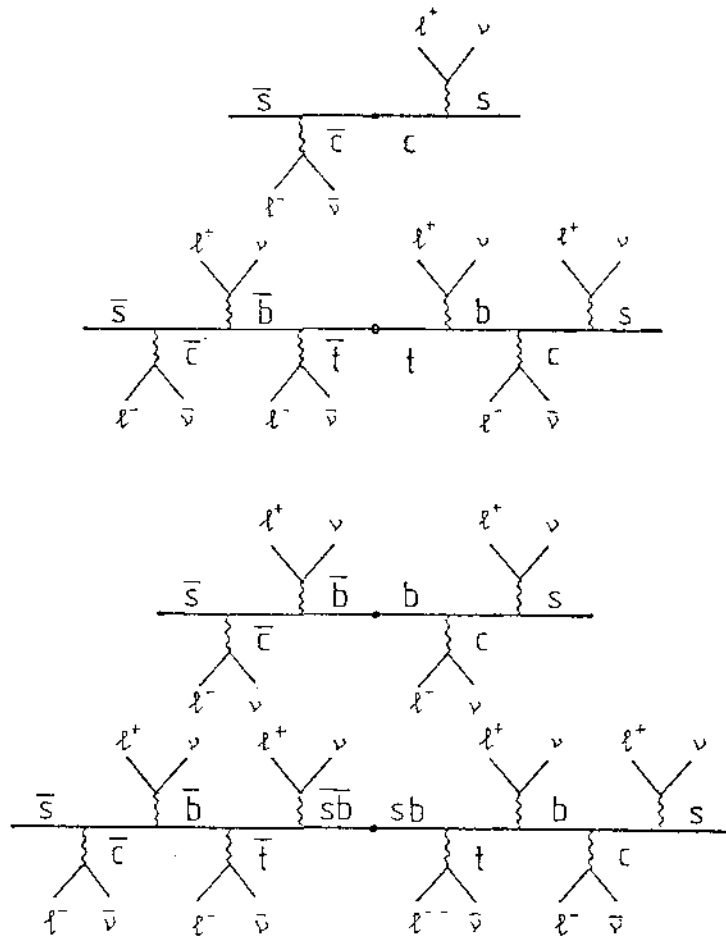


FIG. 8

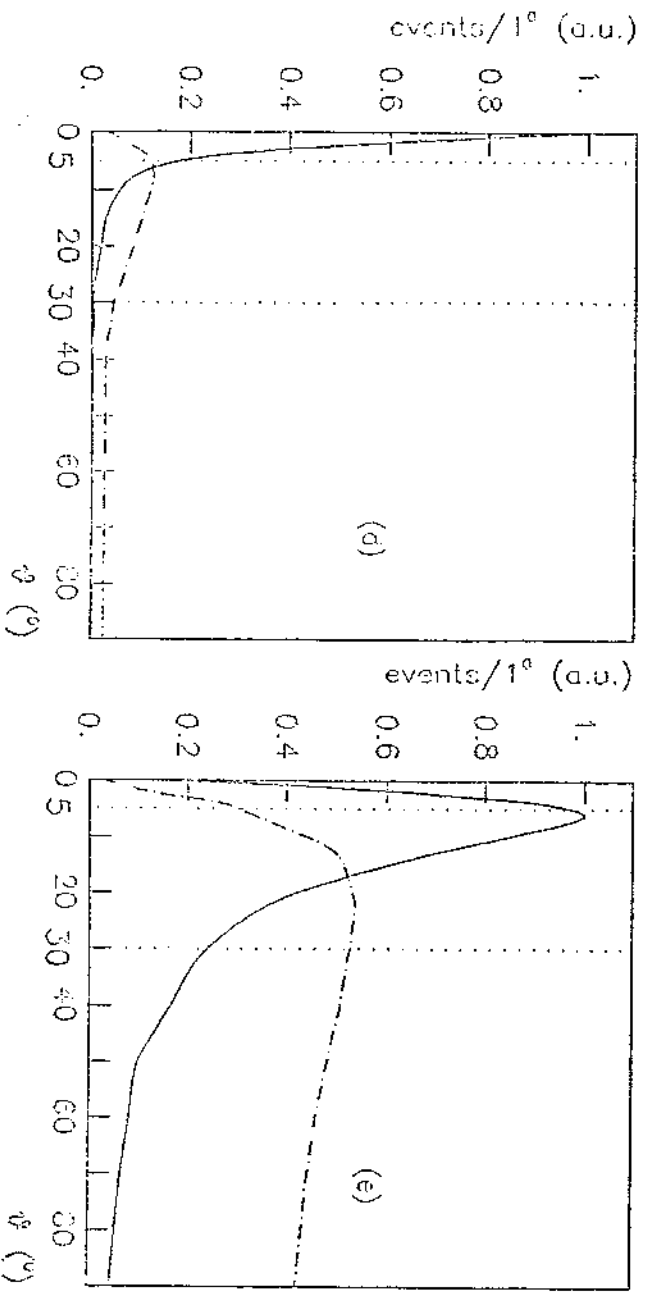
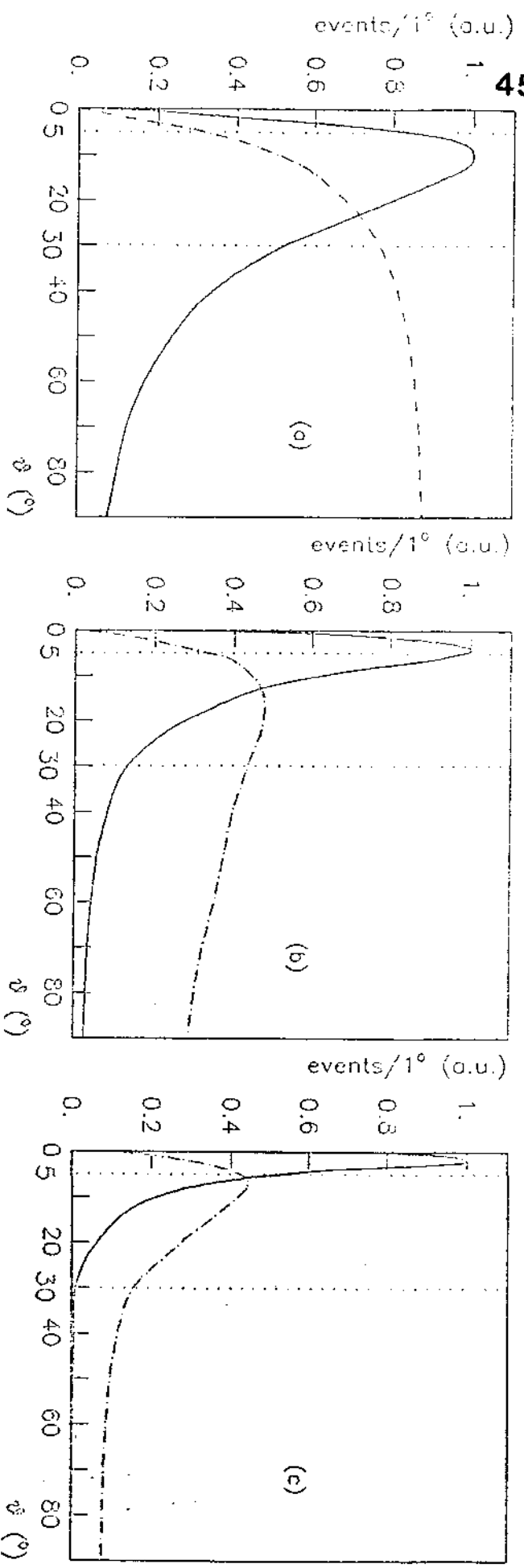


FIG. 9

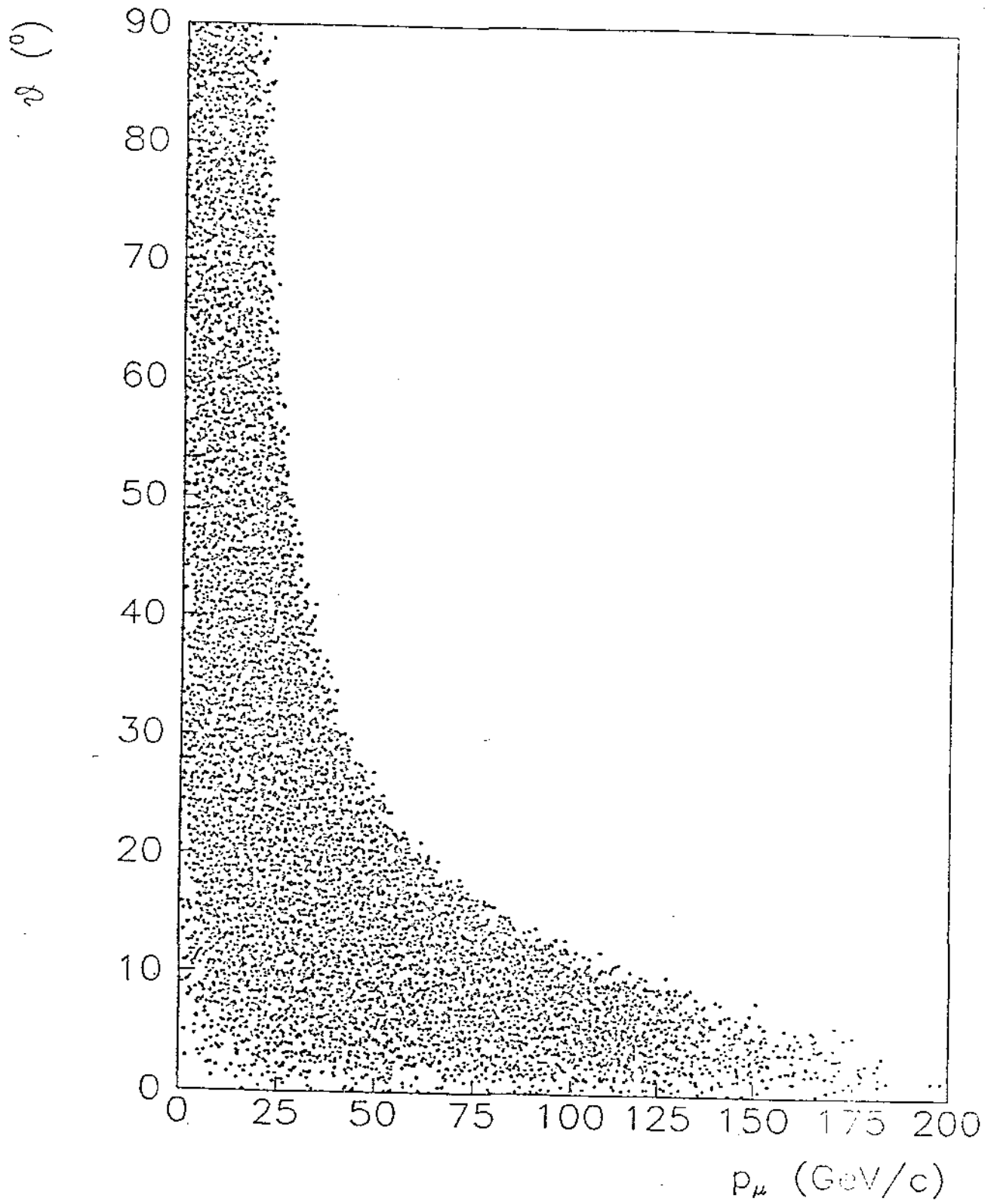


FIG. 10 a)

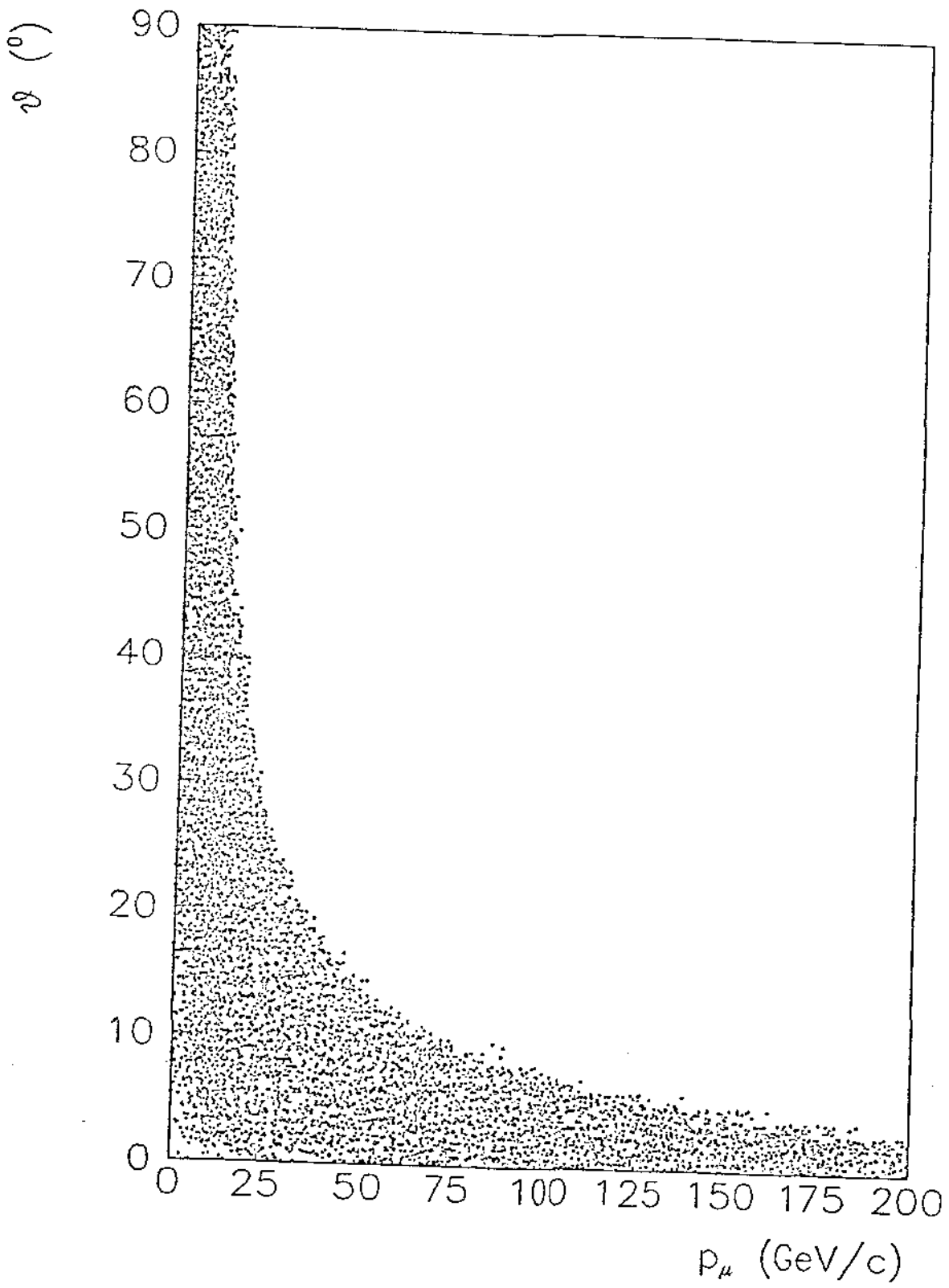


FIG. 10 b)

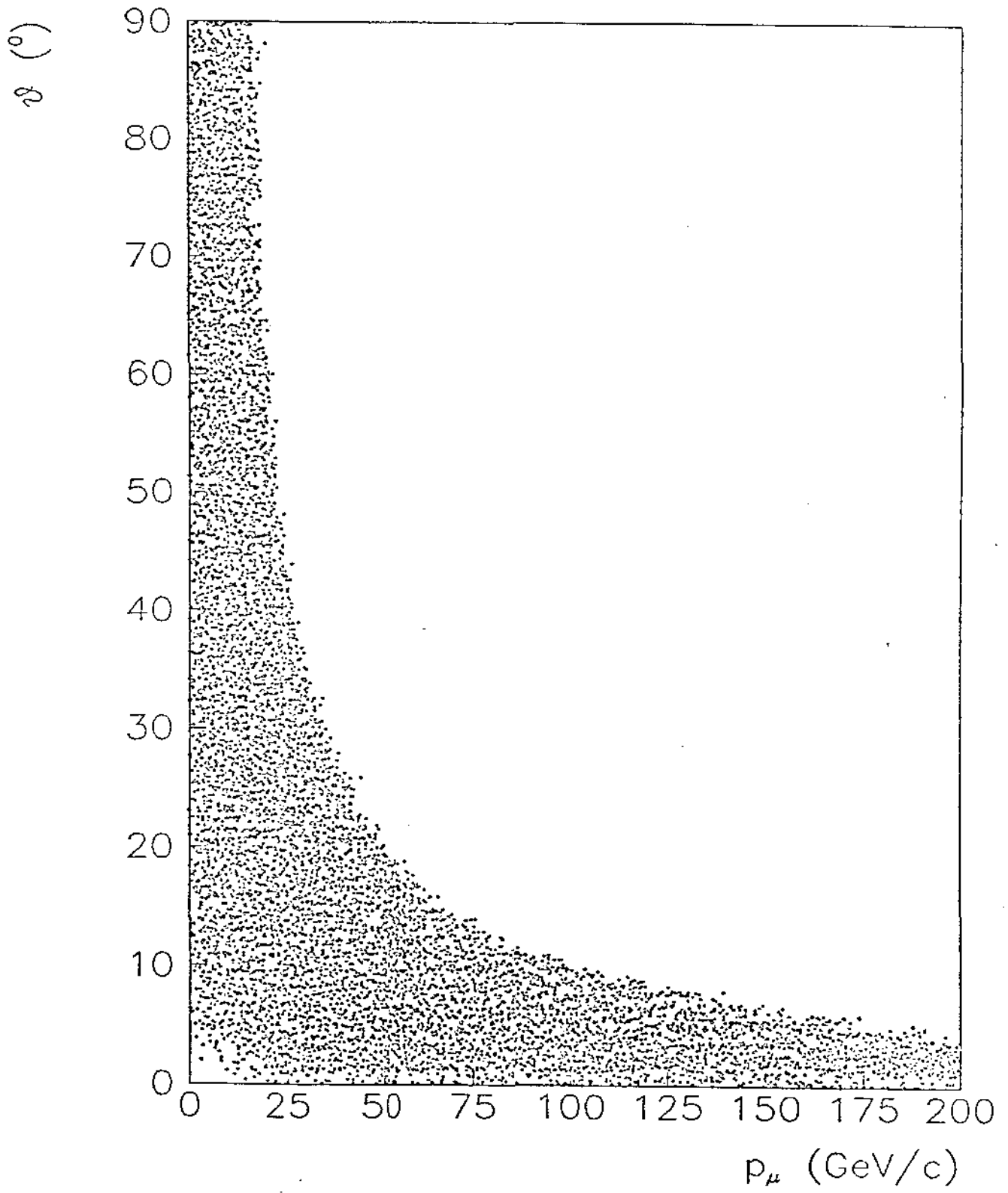


FIG. 10 c)

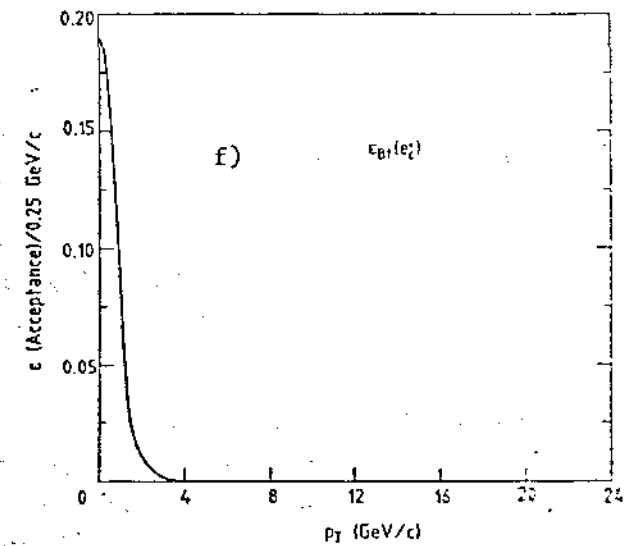
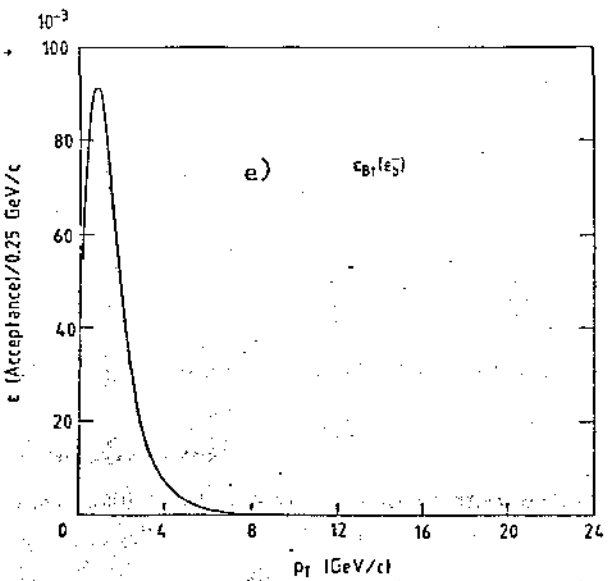
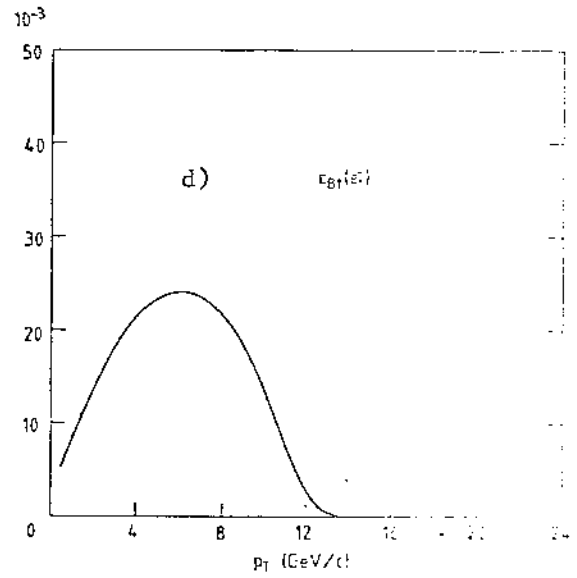
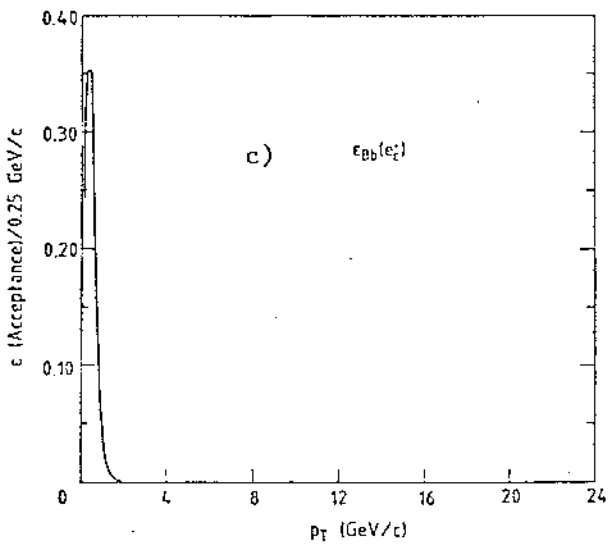
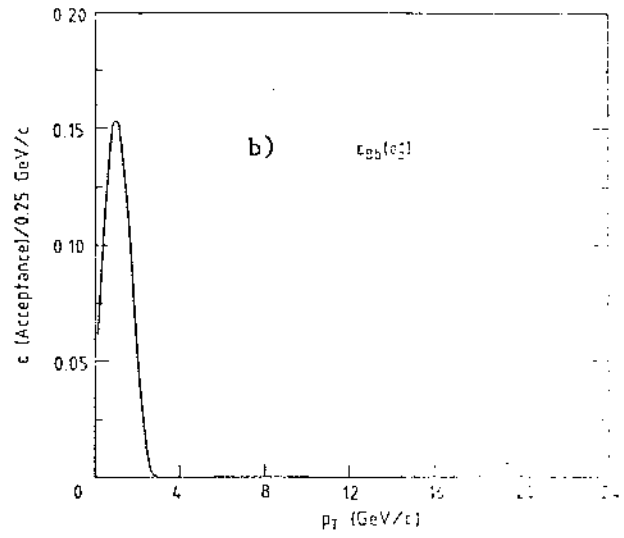
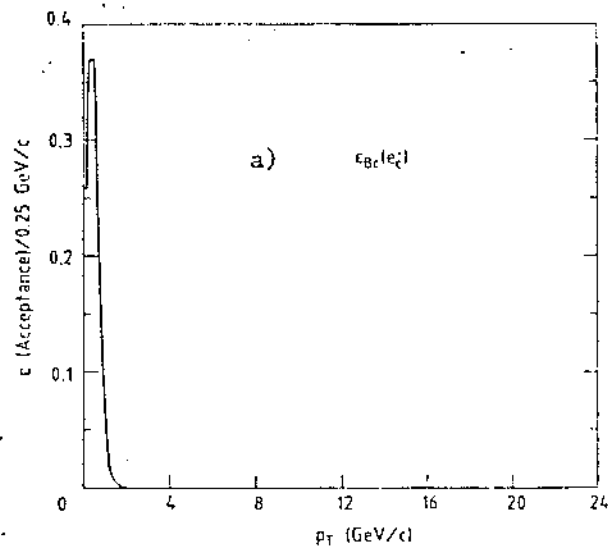


FIG. 11 a) to f)

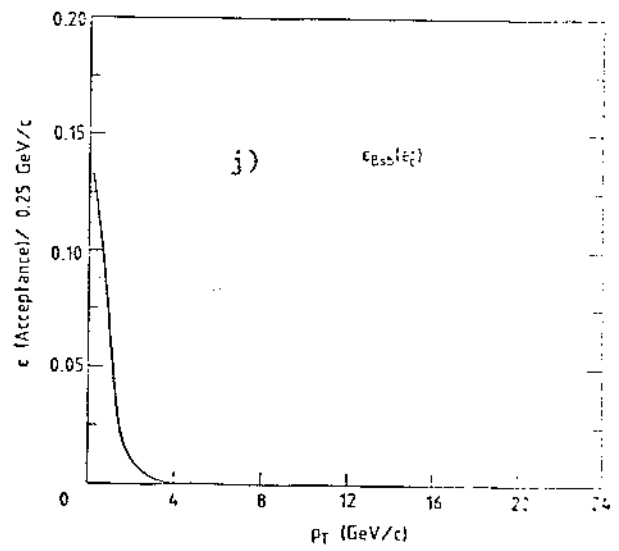
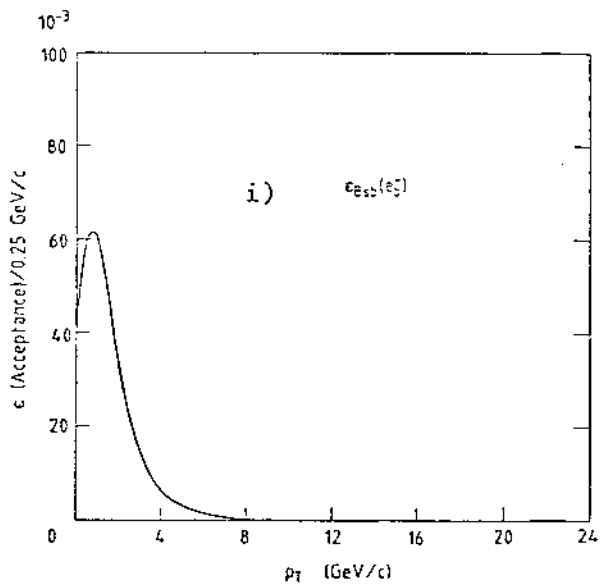
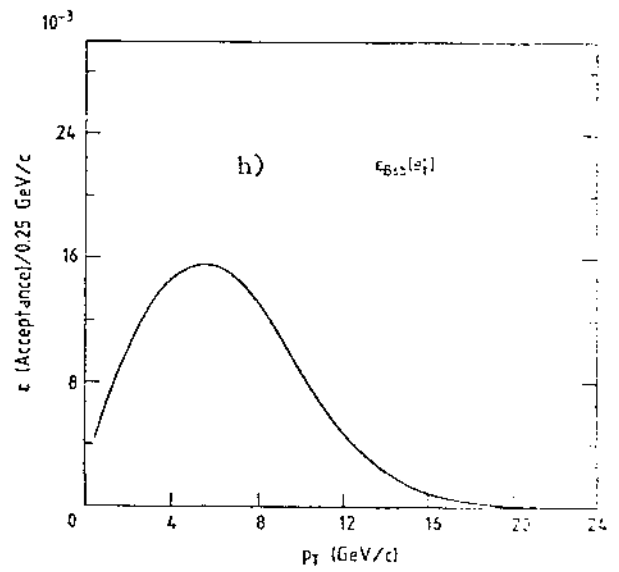
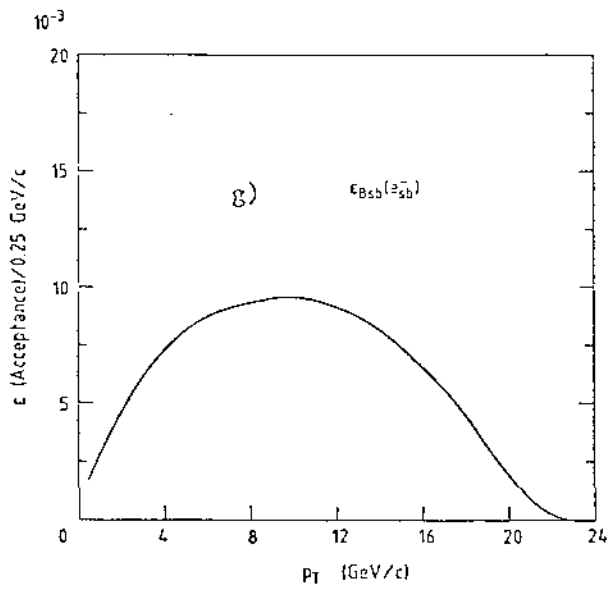


FIG. 11 g) to j)

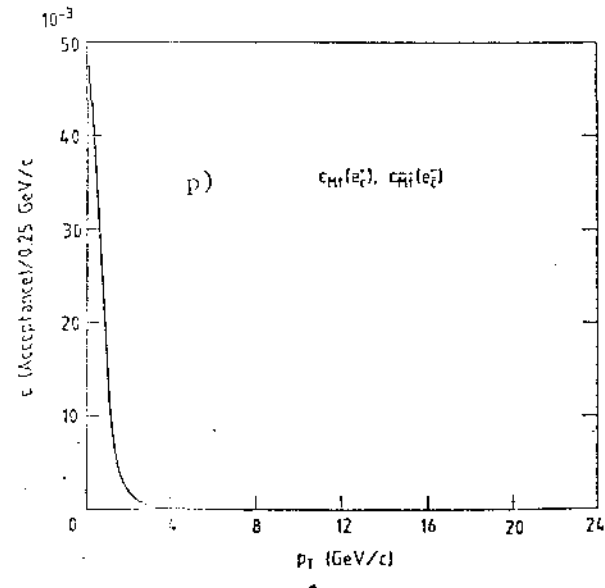
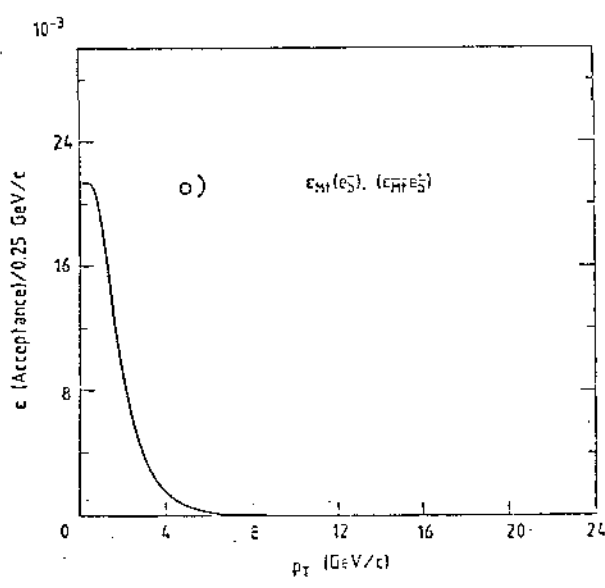
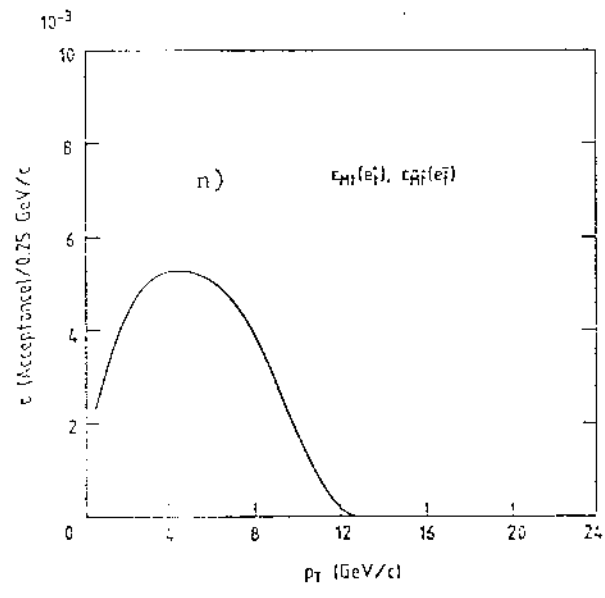
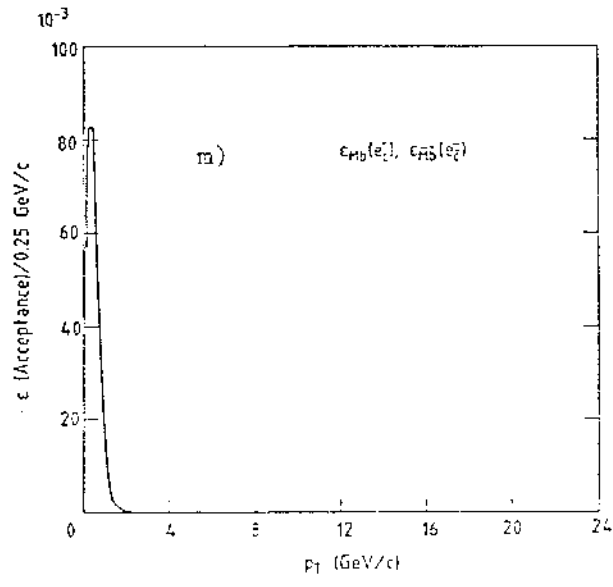
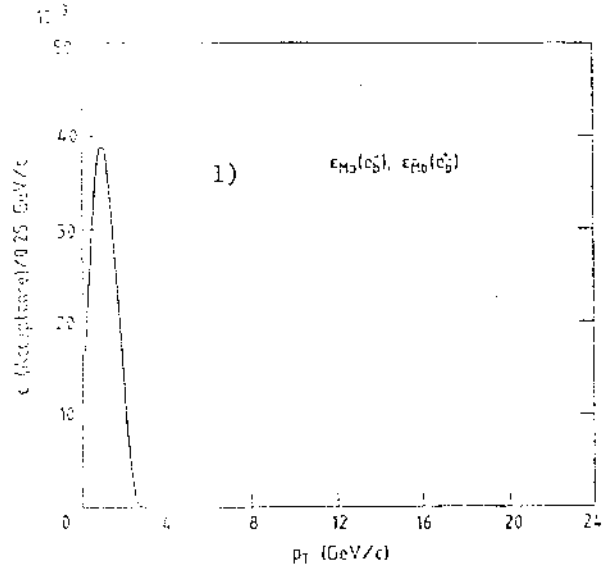
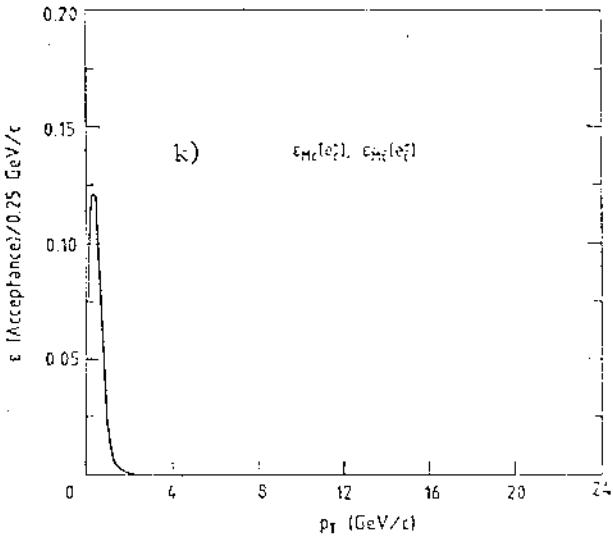


FIG. 11 k) to p)

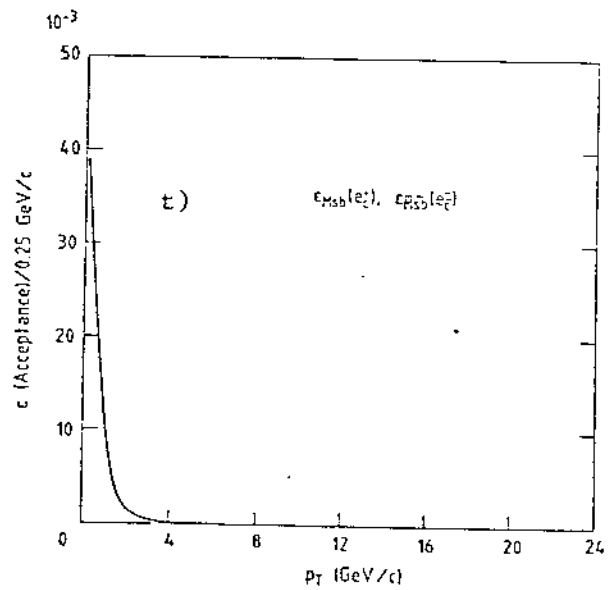
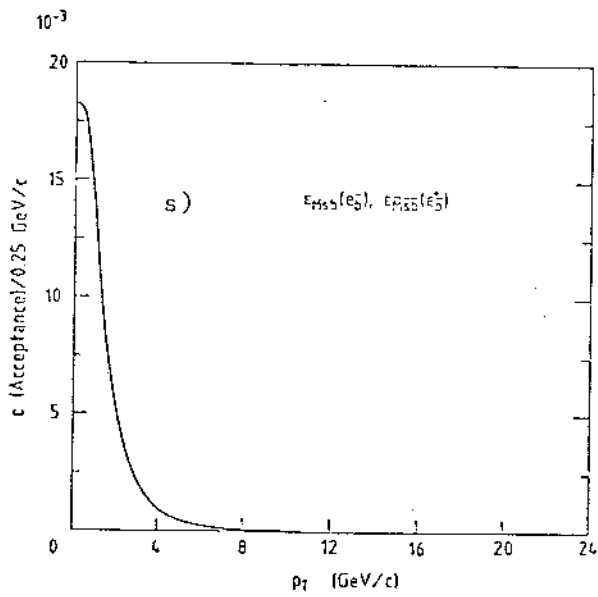
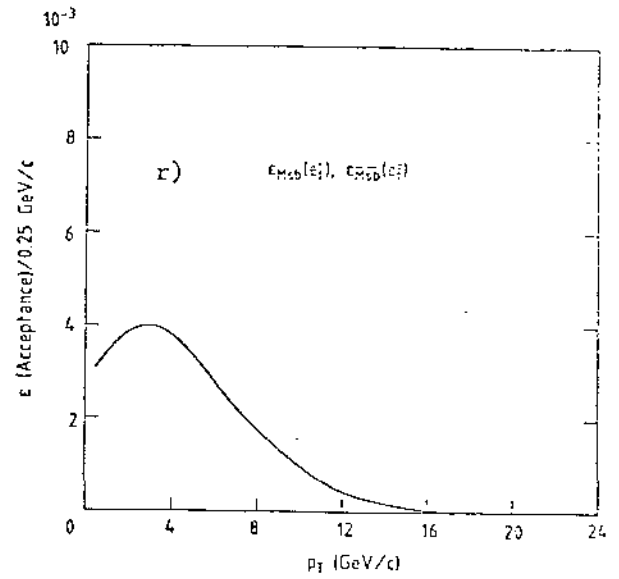
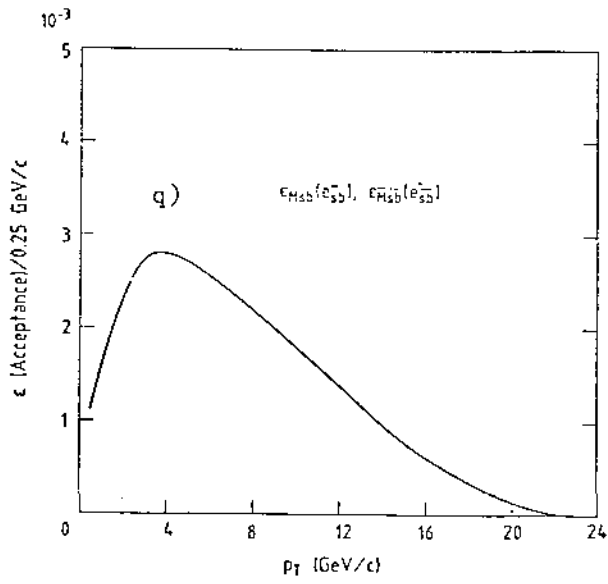


FIG. 11 q) to t)

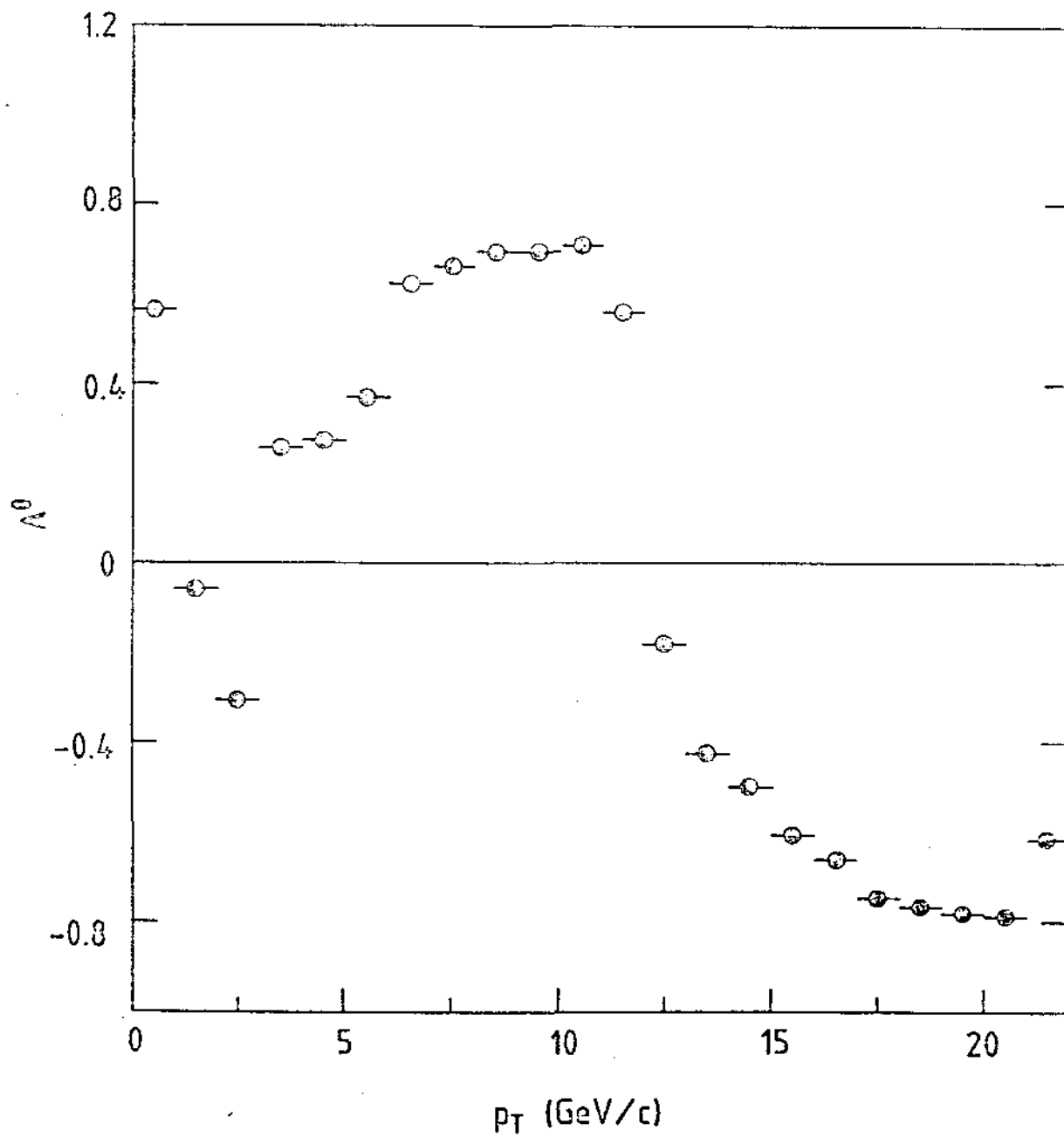
$\vartheta_{\text{cut}} = 30^\circ, (\text{Leading/Total}) = 0.25$ 

FIG. 12

- ◇ Superbeauty ($\Delta M = 30.0 \text{ GeV}/c^2$)
- △ Top ($\Delta M = 19.5 \text{ GeV}/c^2$)
- Beauty ($\Delta M = 3.2 \text{ GeV}/c^2$)
- Charm ($\Delta M = 1.2 \text{ GeV}/c^2$)

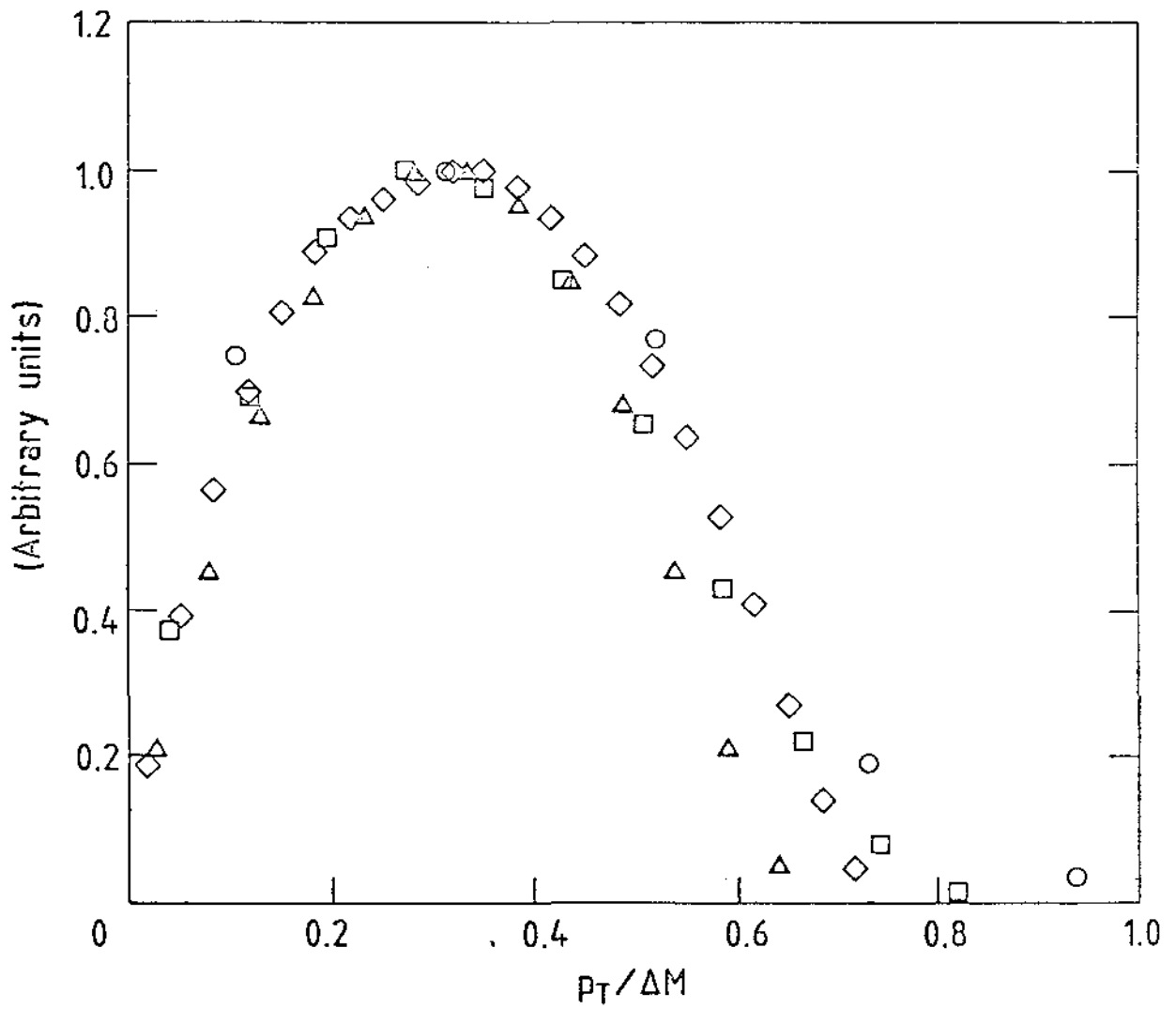


FIG. 13

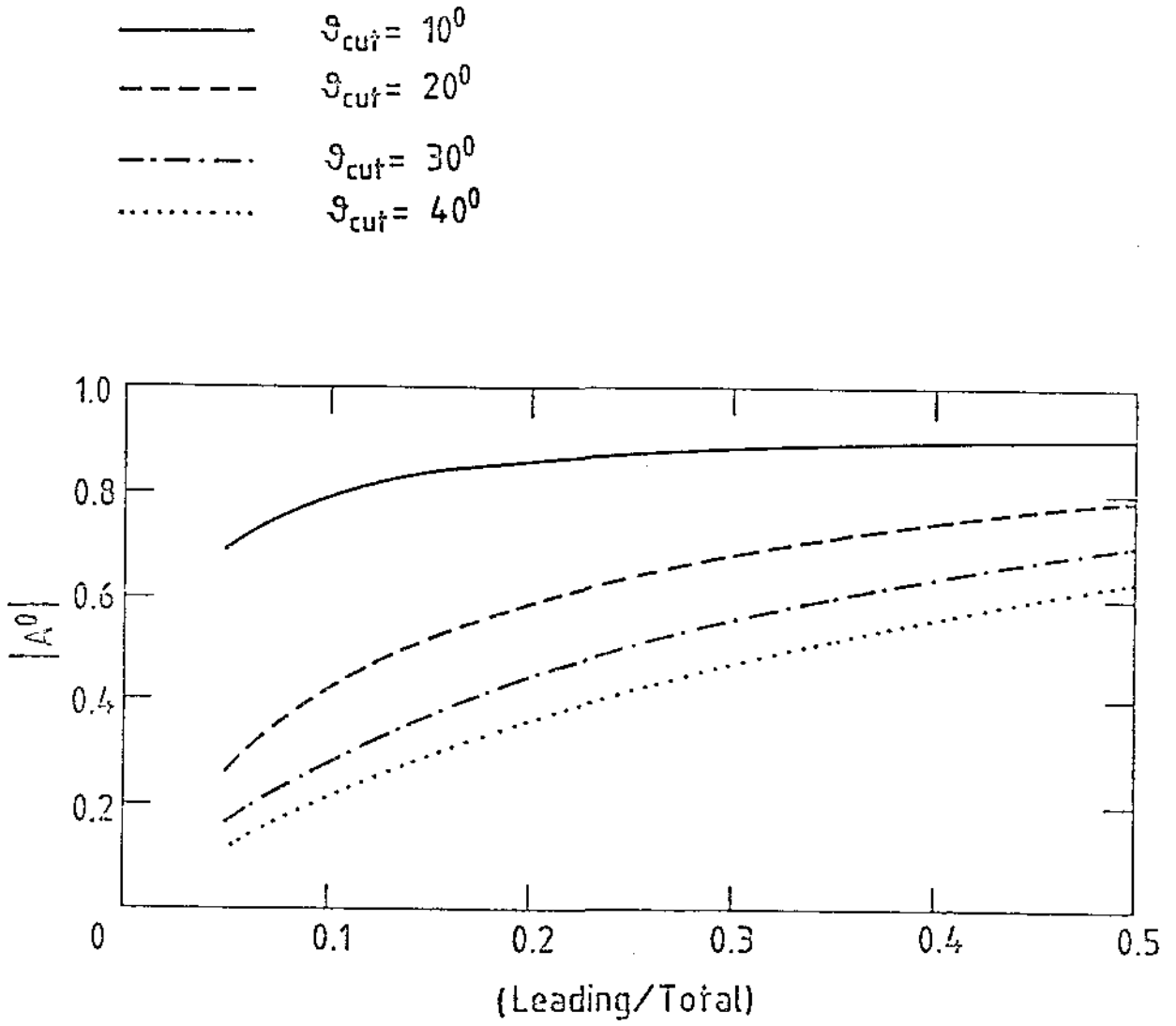


FIG. 14

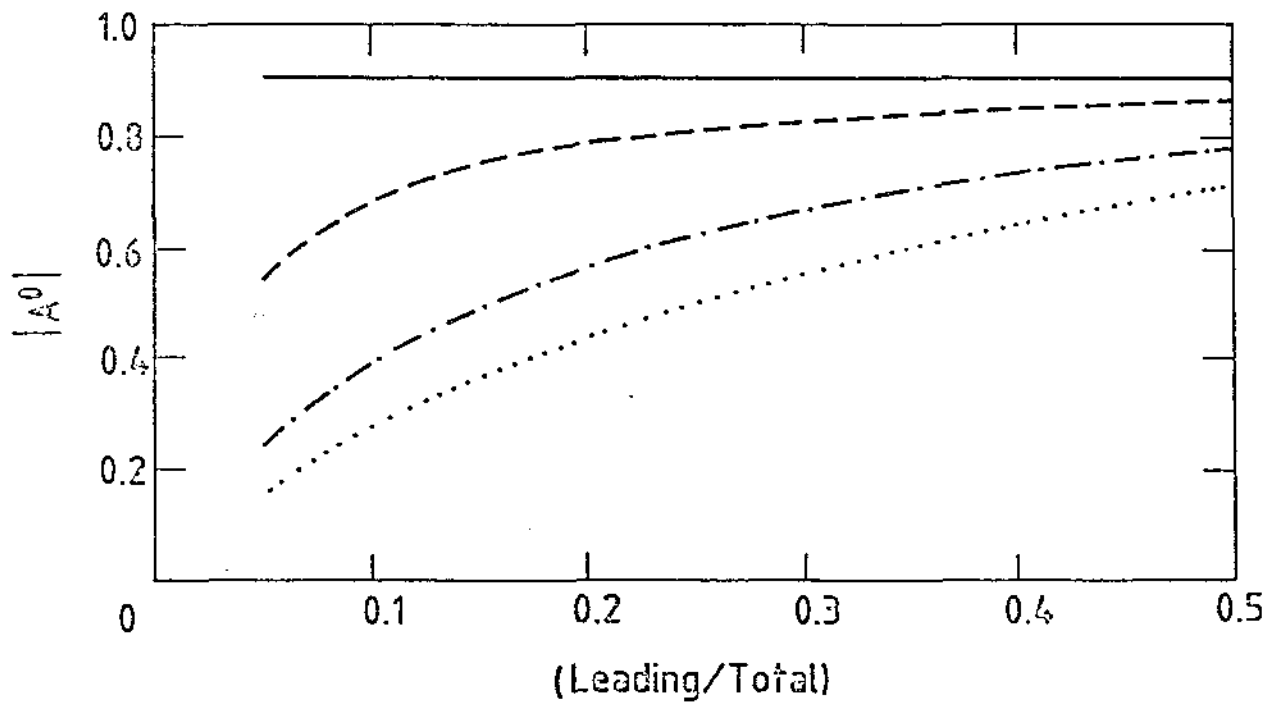
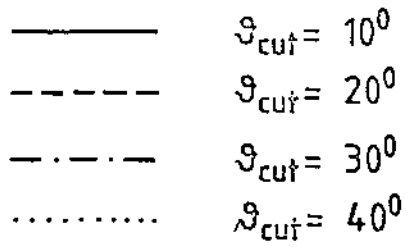


FIG. 15

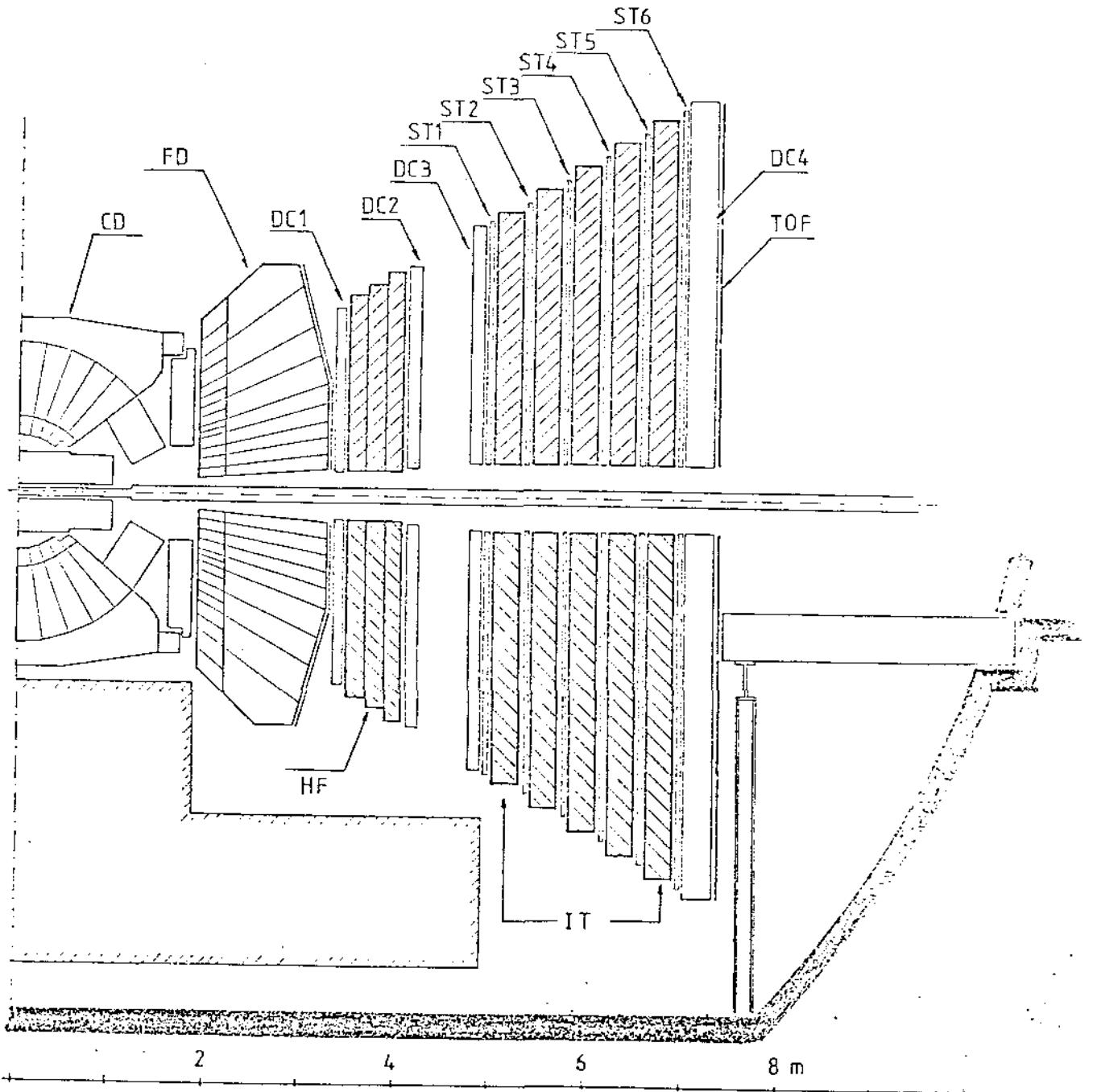


FIG. 16

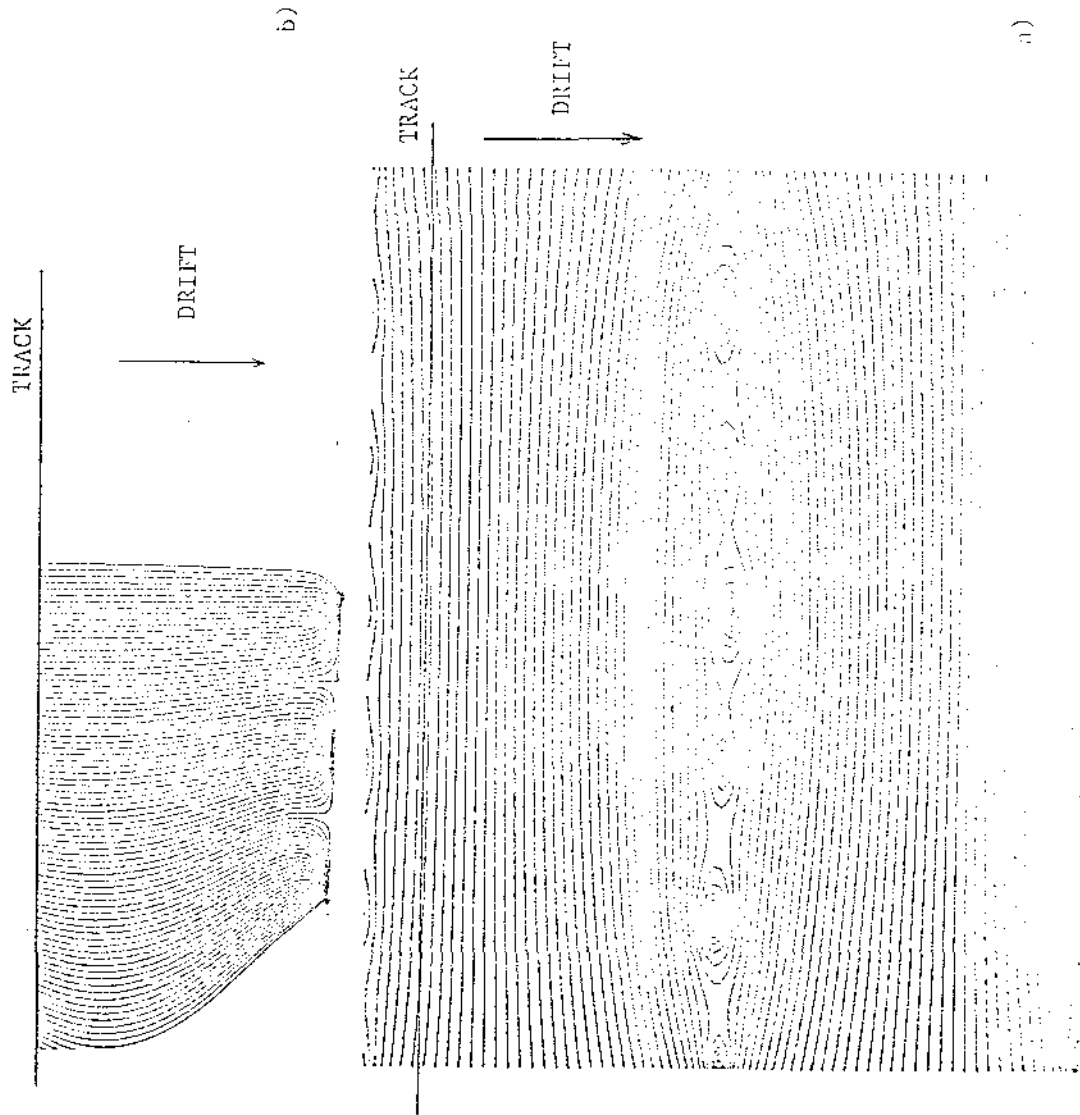


FIG. 17

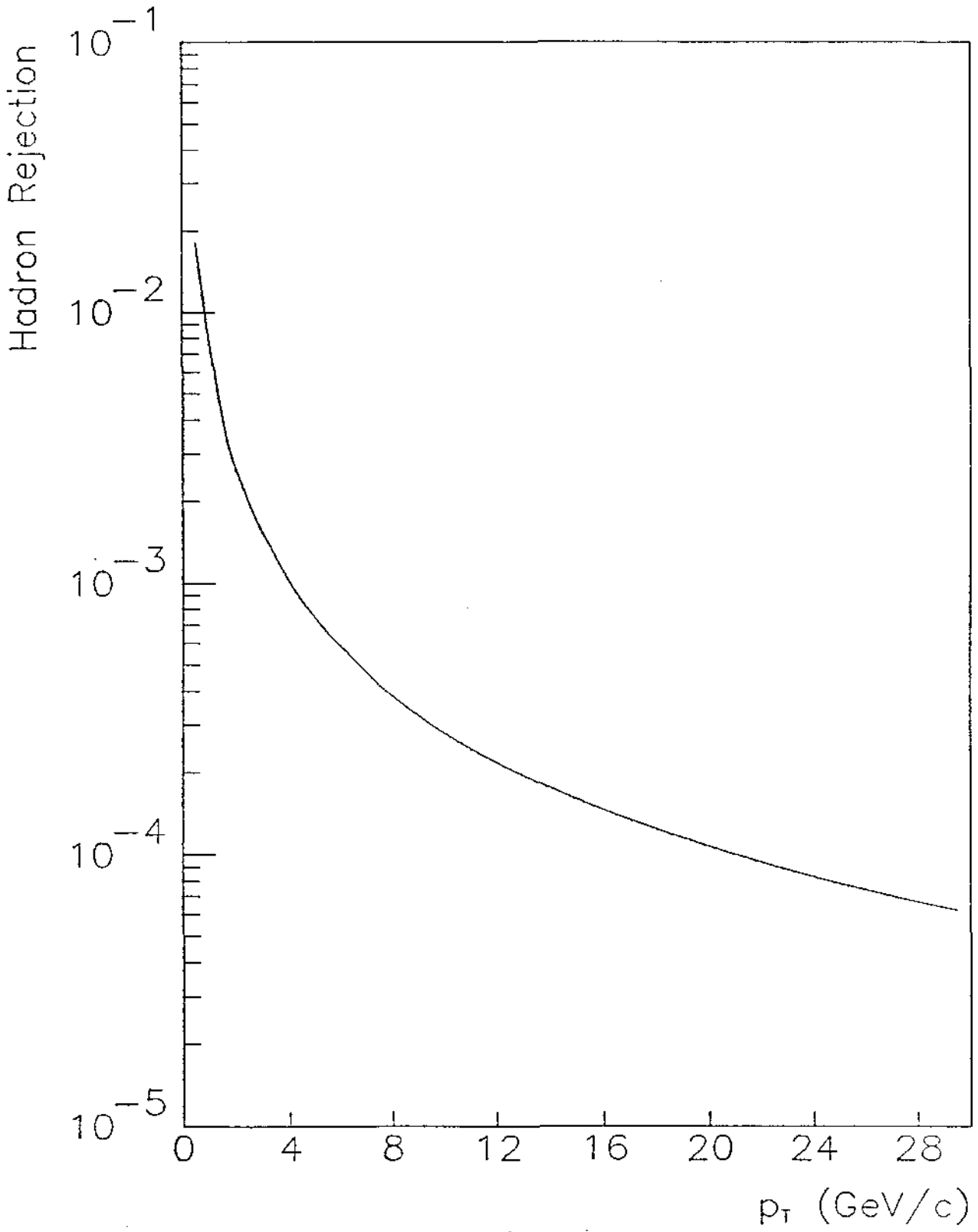


FIG. 18

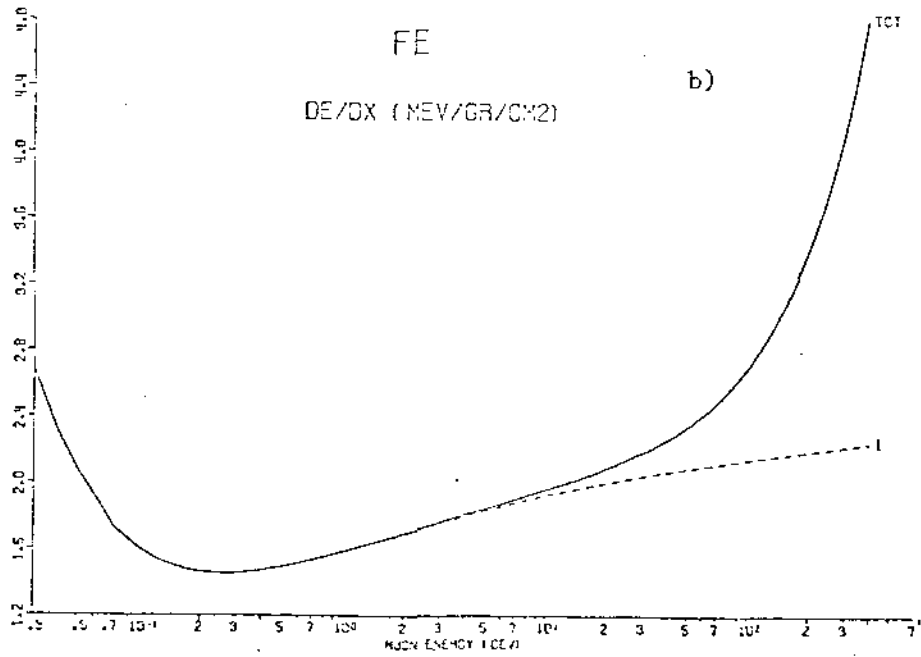
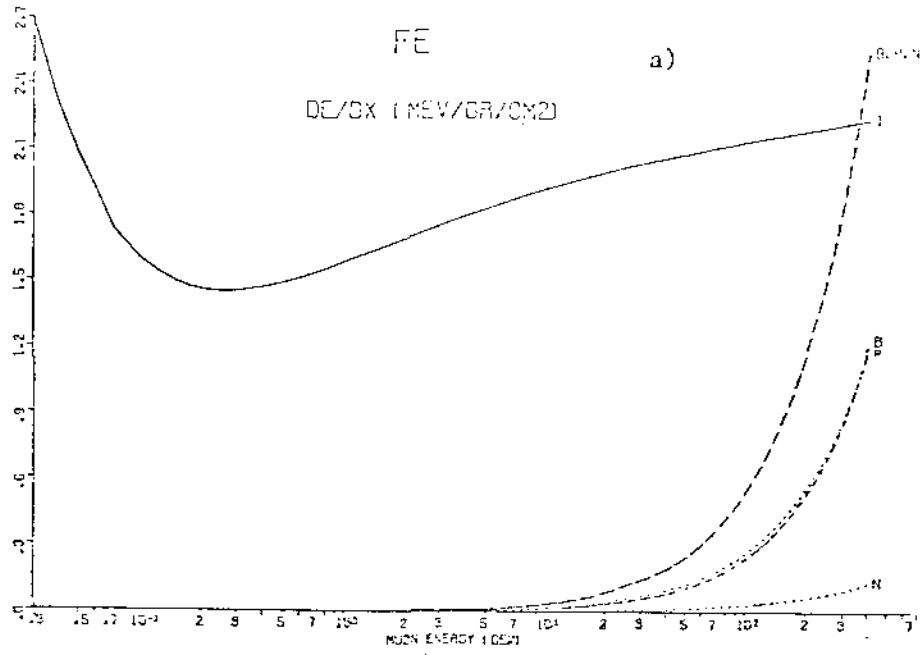


FIG. 19

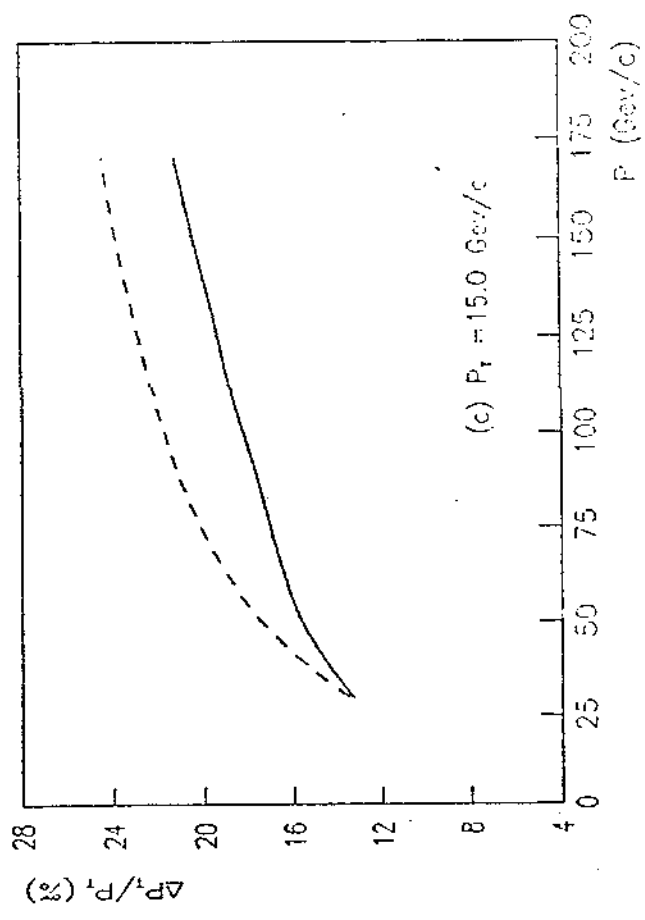
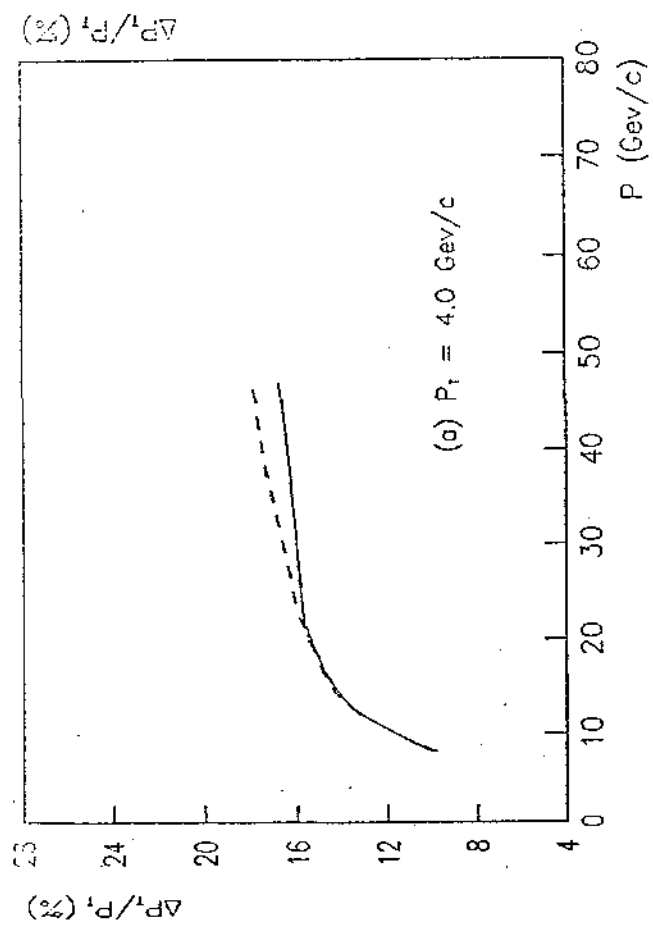
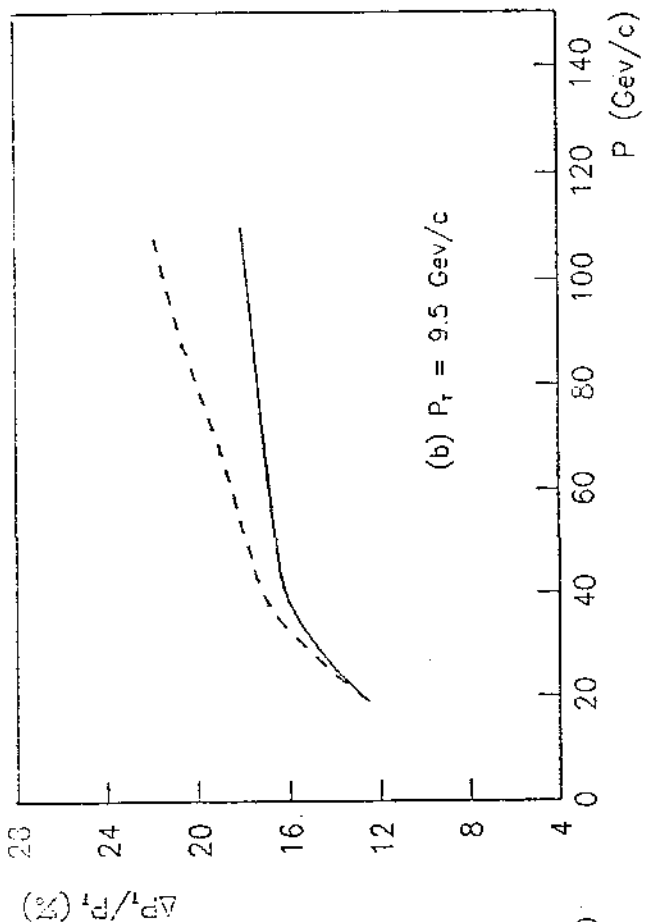


FIG. 30

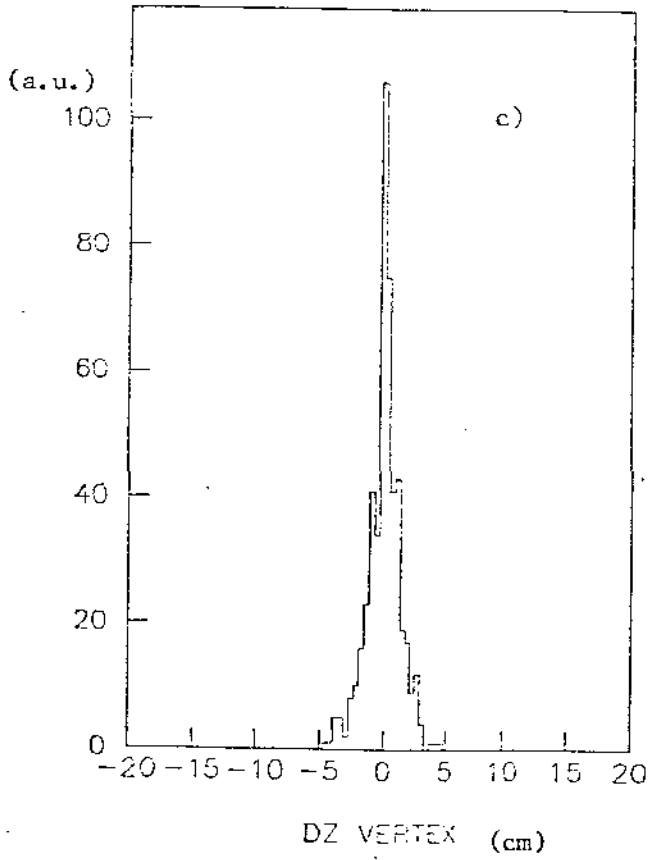
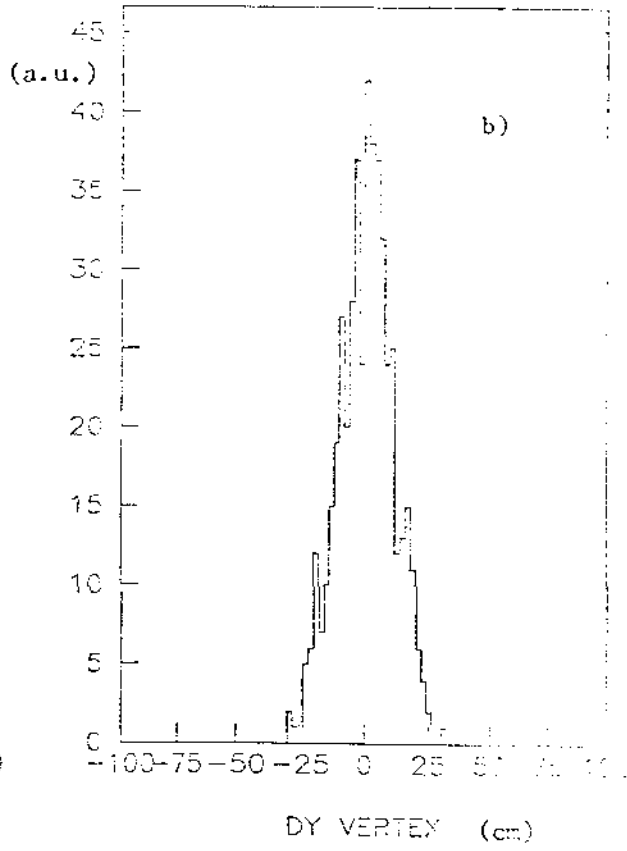
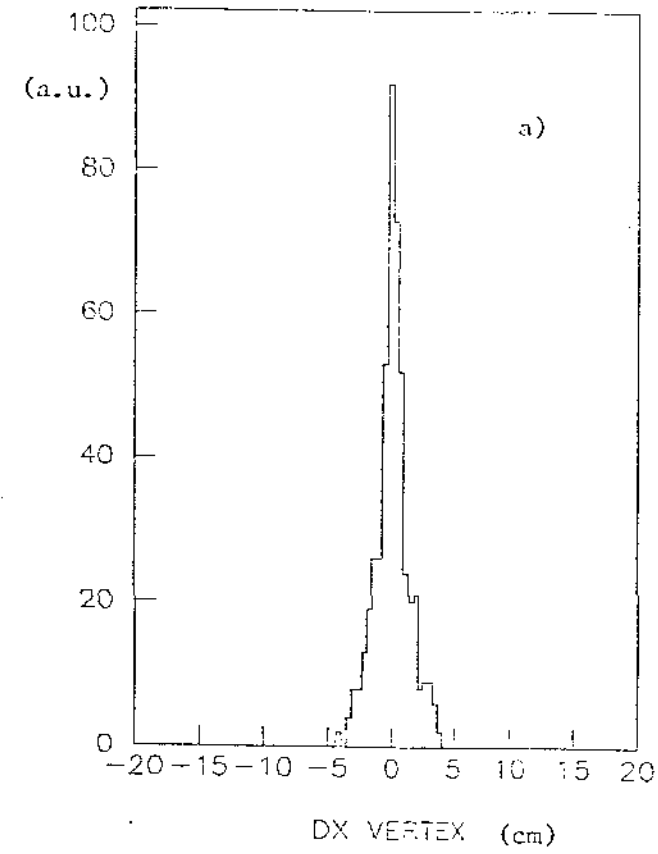


FIG. 21

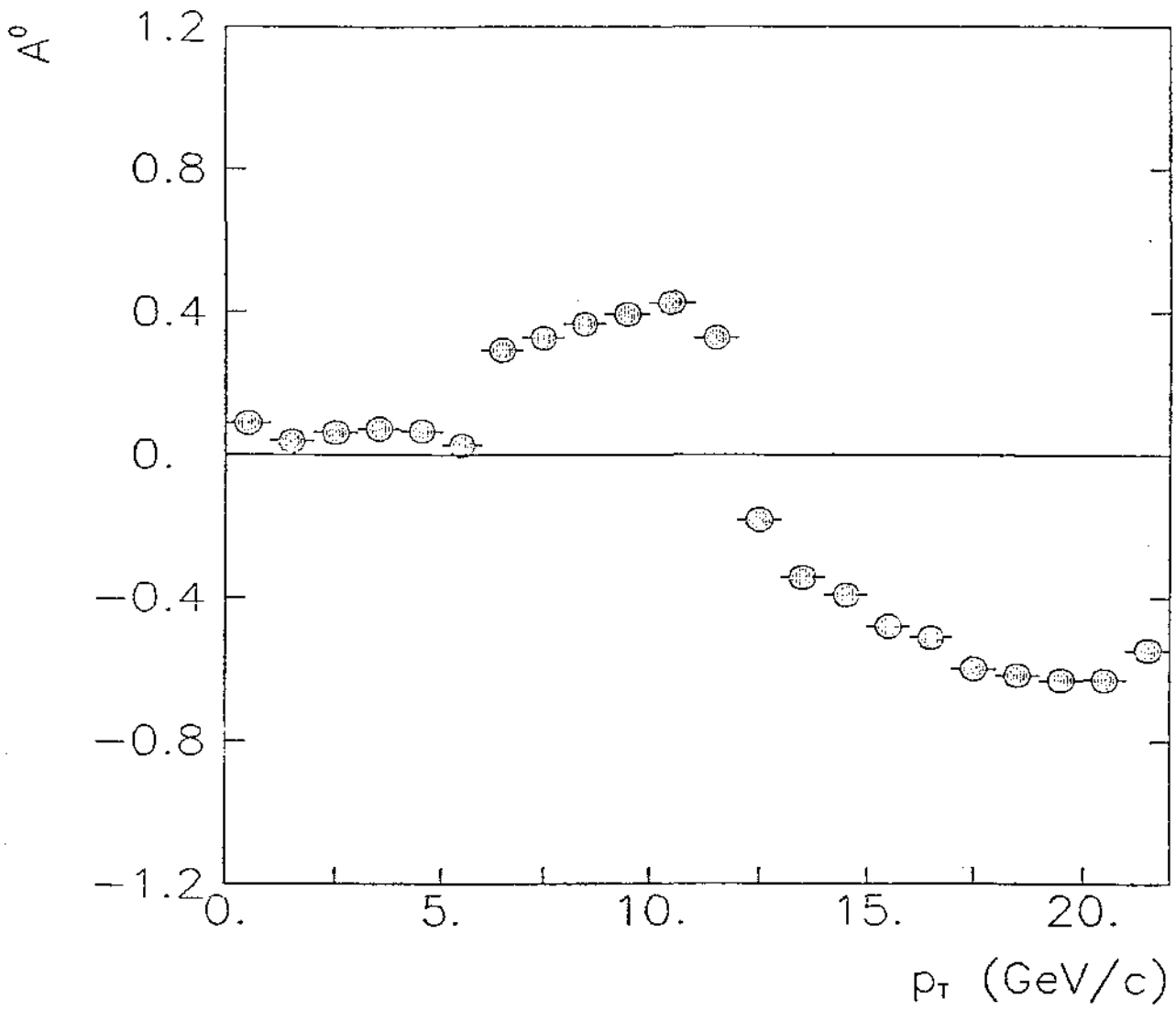


FIG. 22

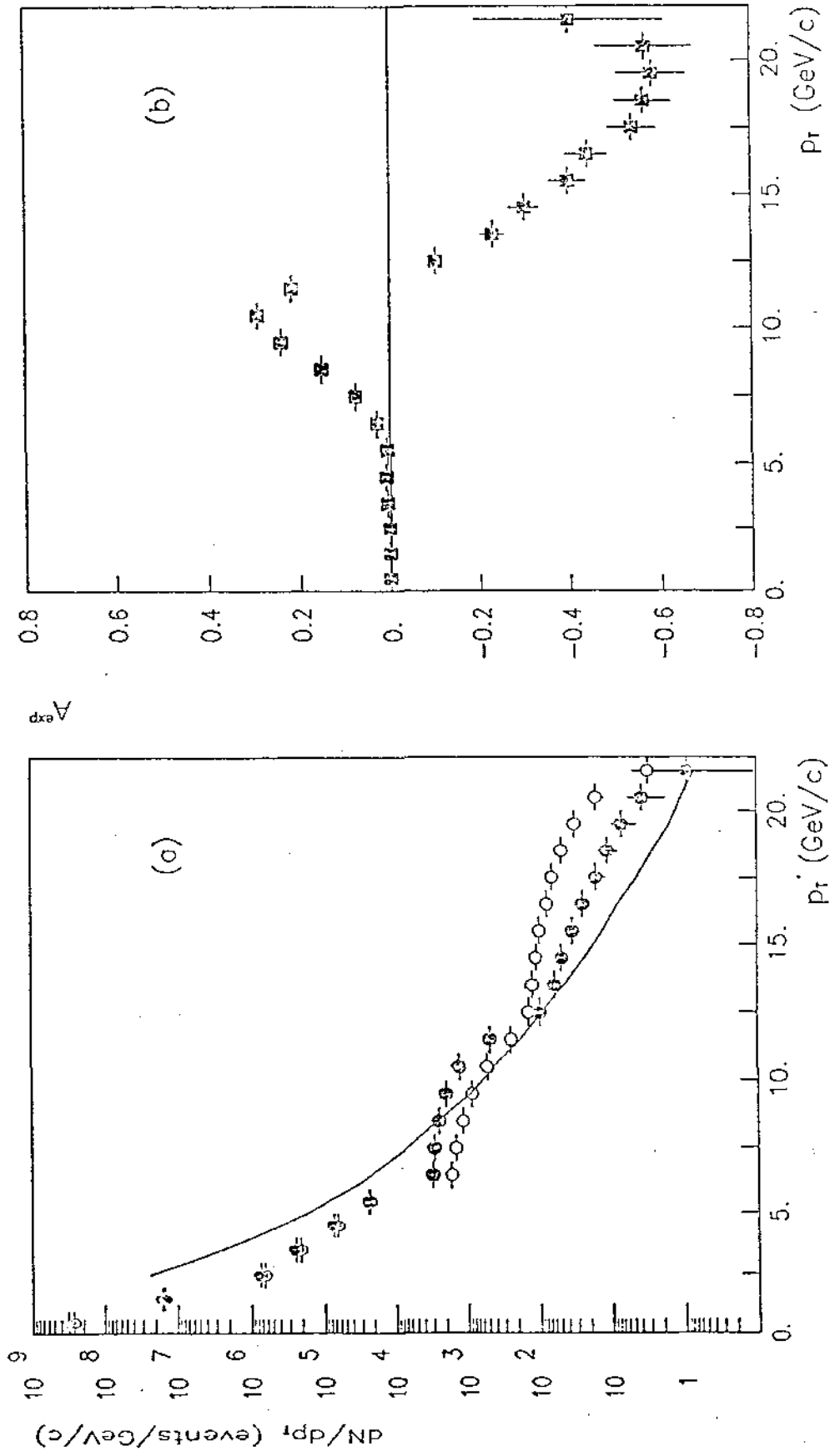


FIG. 23

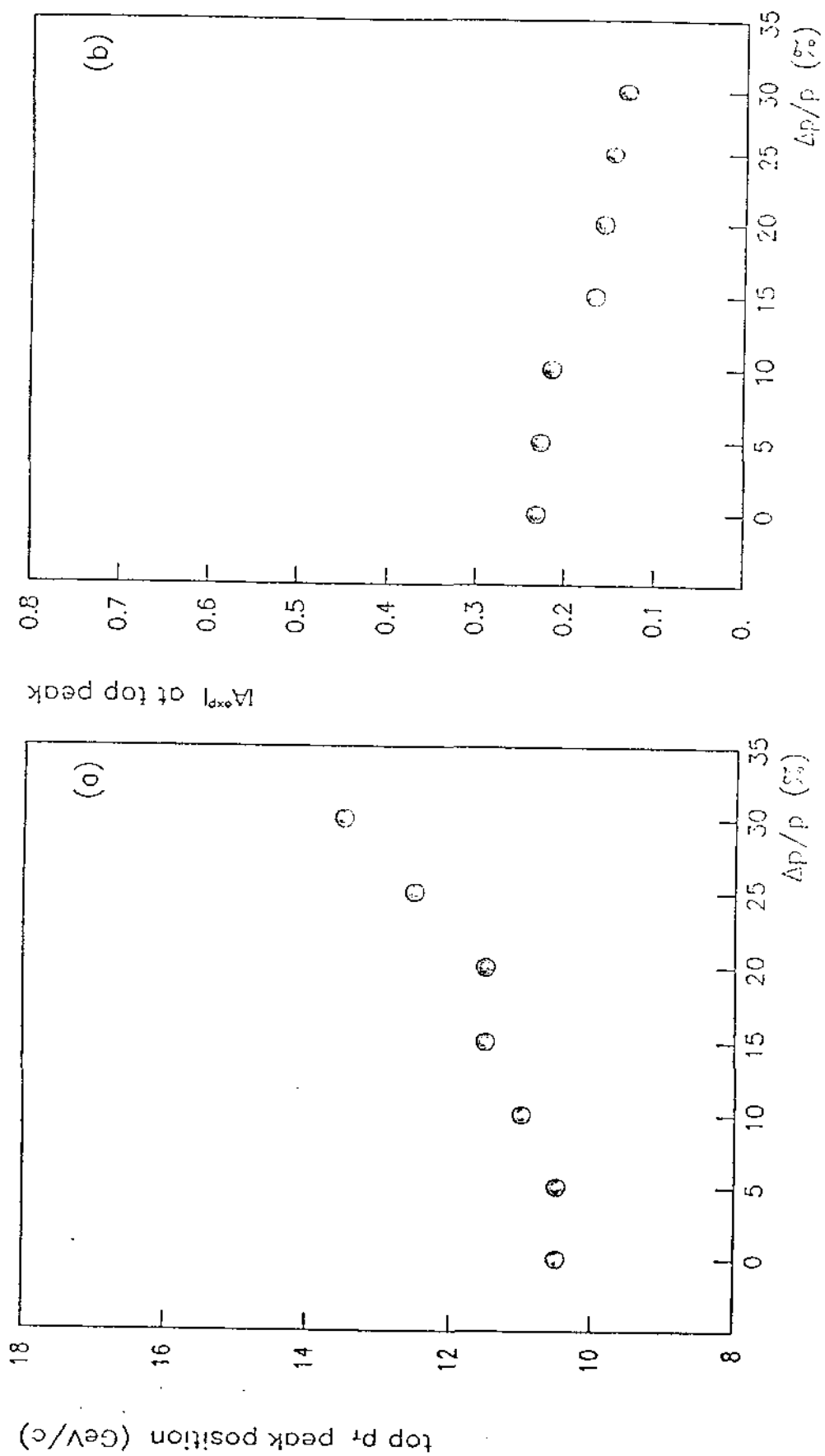


FIG. 34

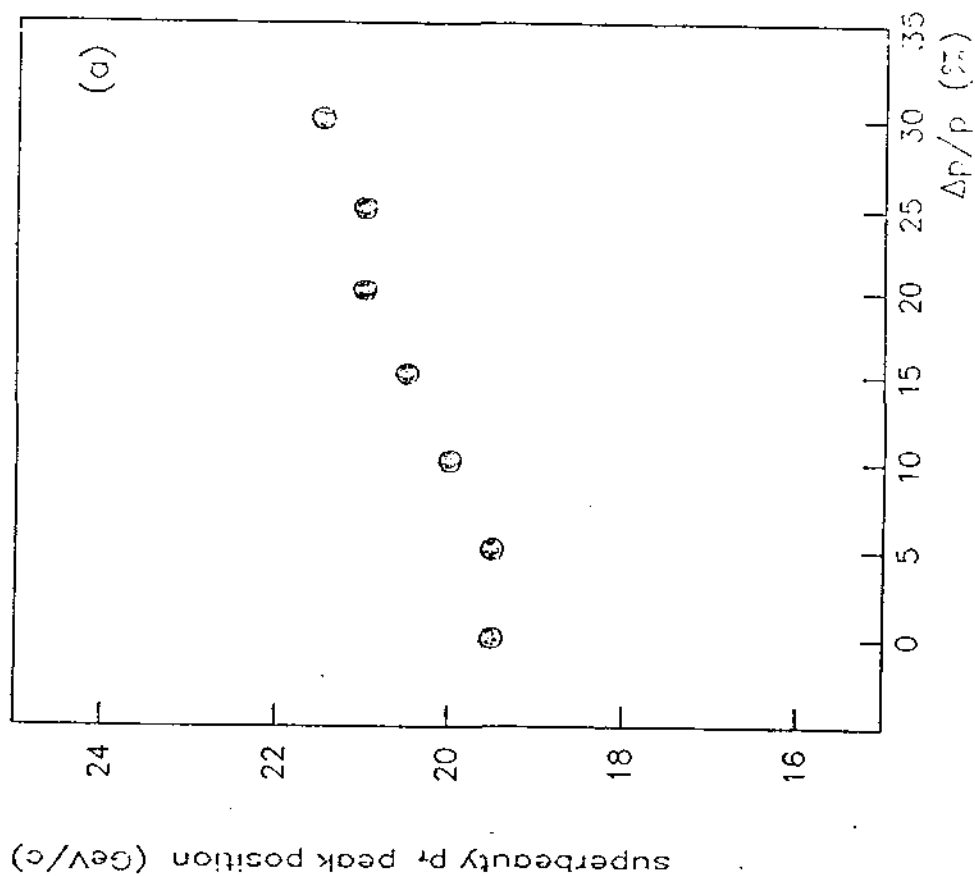
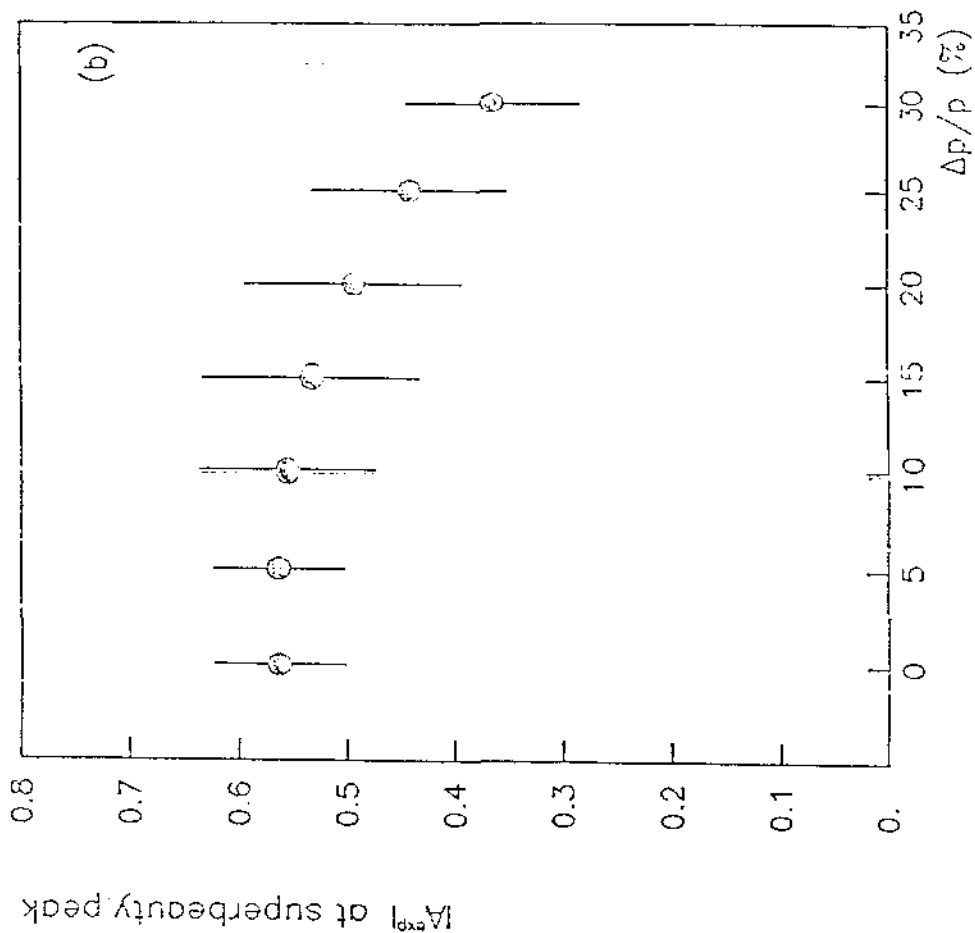


FIG. 25

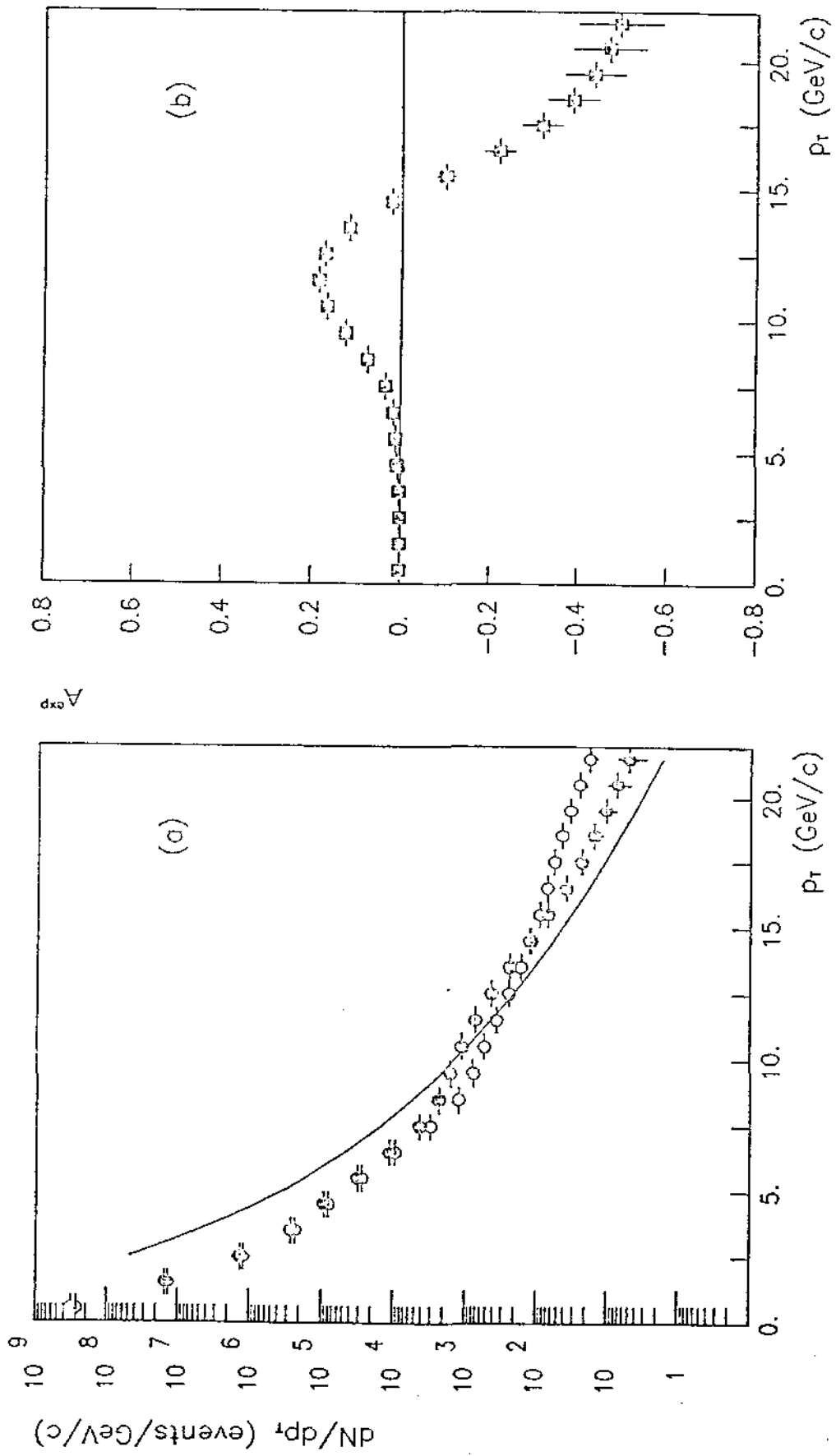


FIG. 26

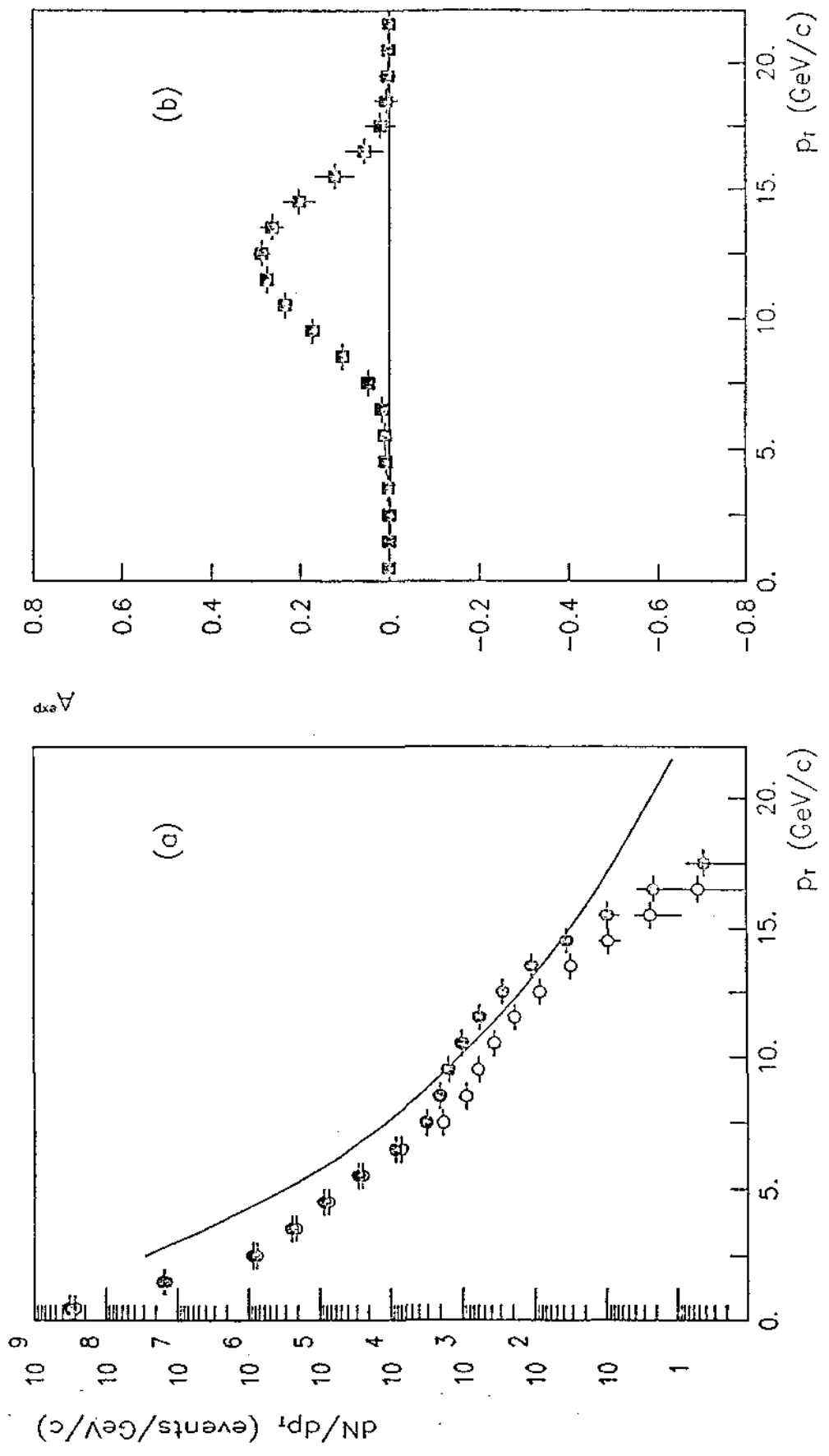


FIG. 27

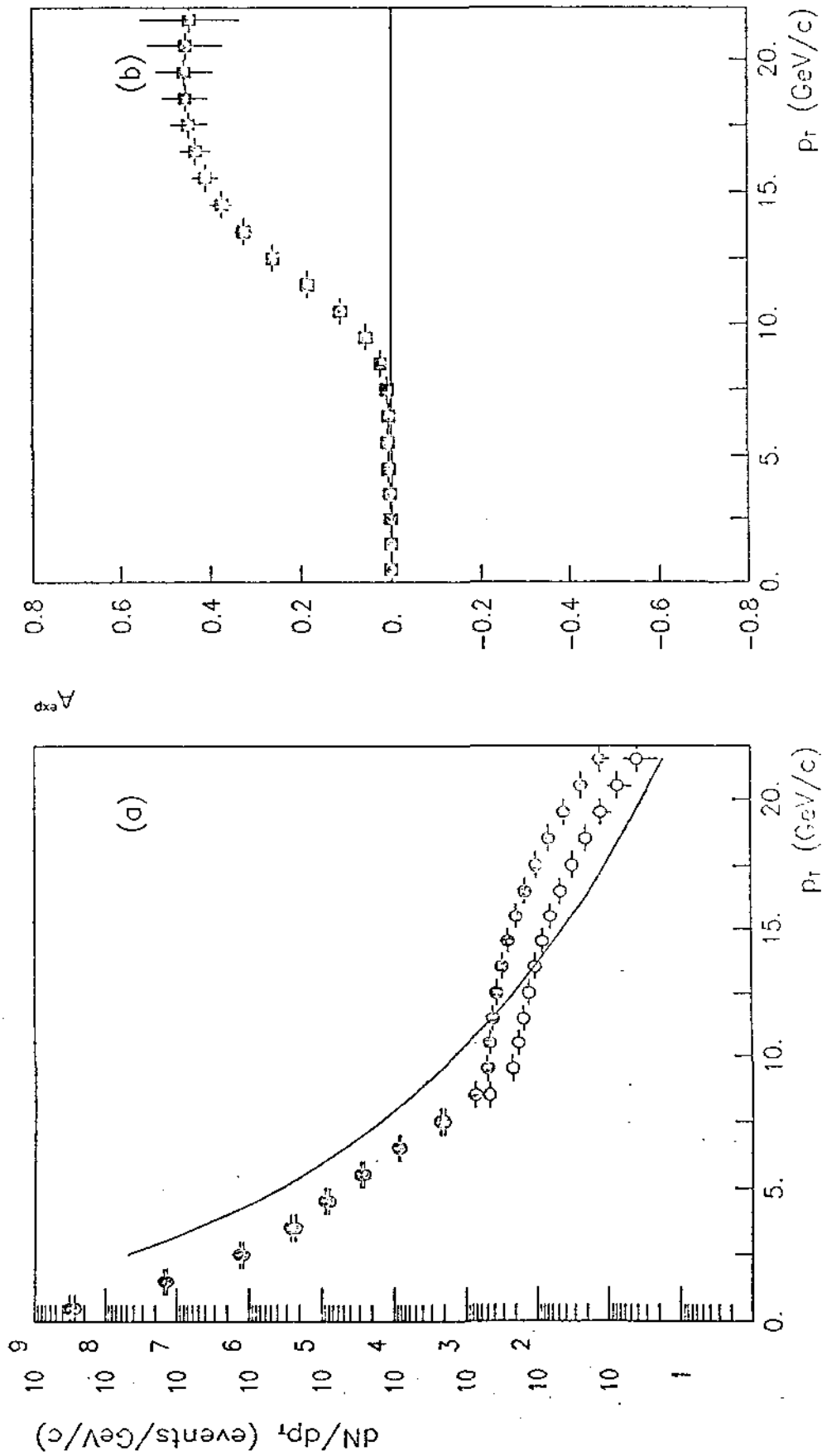


FIG. 28

Top ($m=25$ GeV), $p_T=9-12$ GeV/c

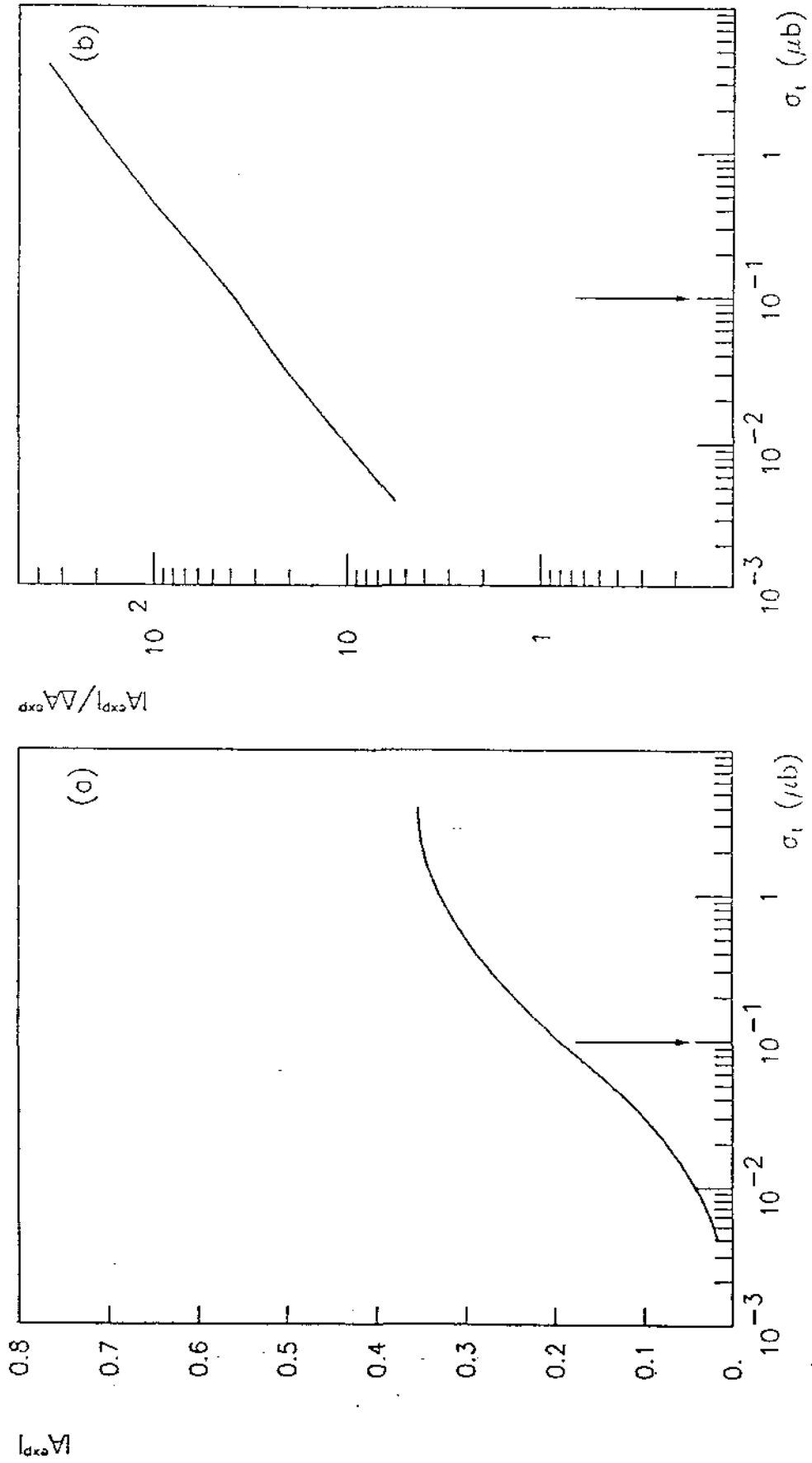


FIG. 29

Superbeauty ($m=55$ GeV), $p_T=20-23$ GeV/c

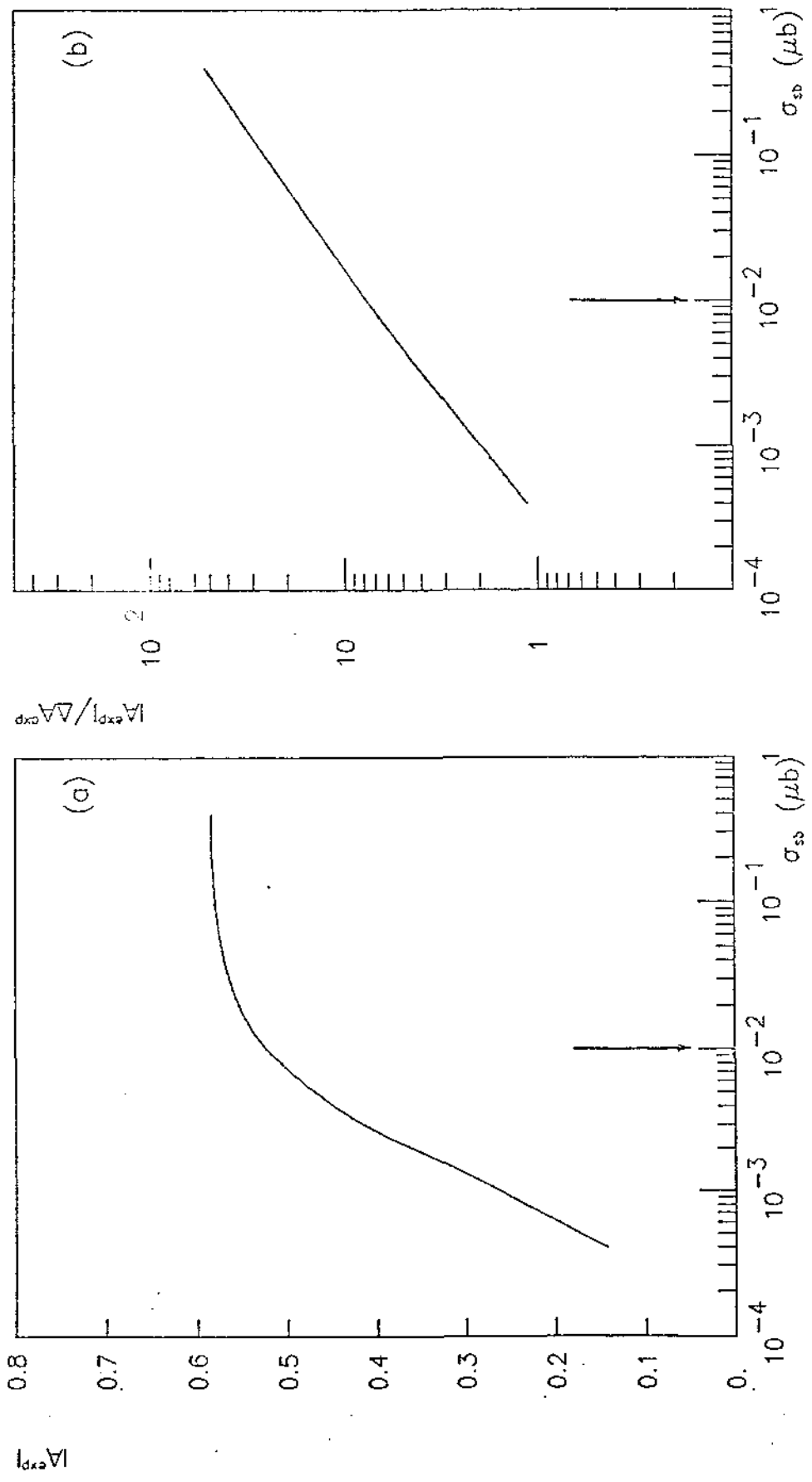


FIG. 30

Top ($m=25$ GeV), $p_T=11-14$ GeV/c

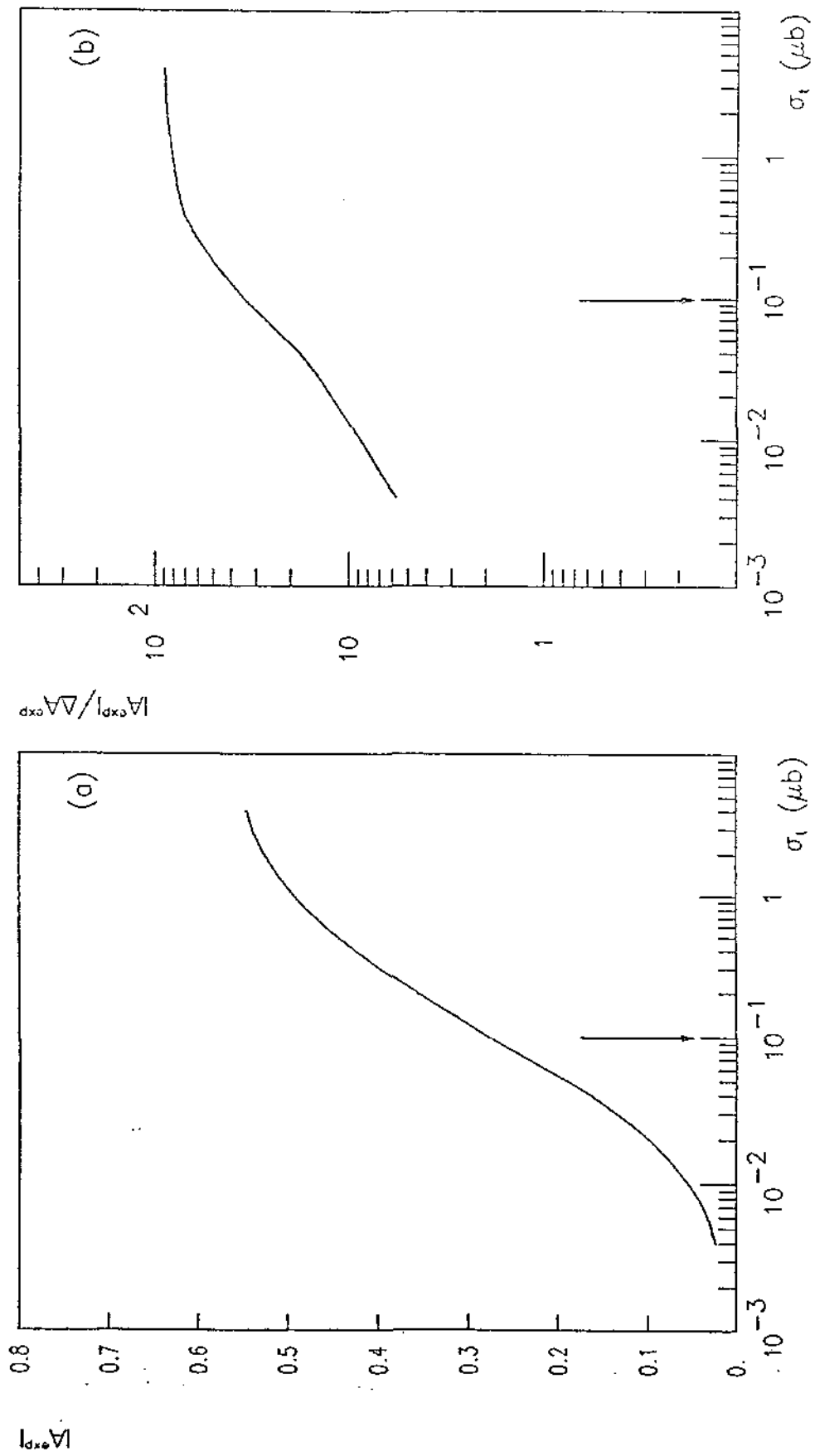


FIG. 31

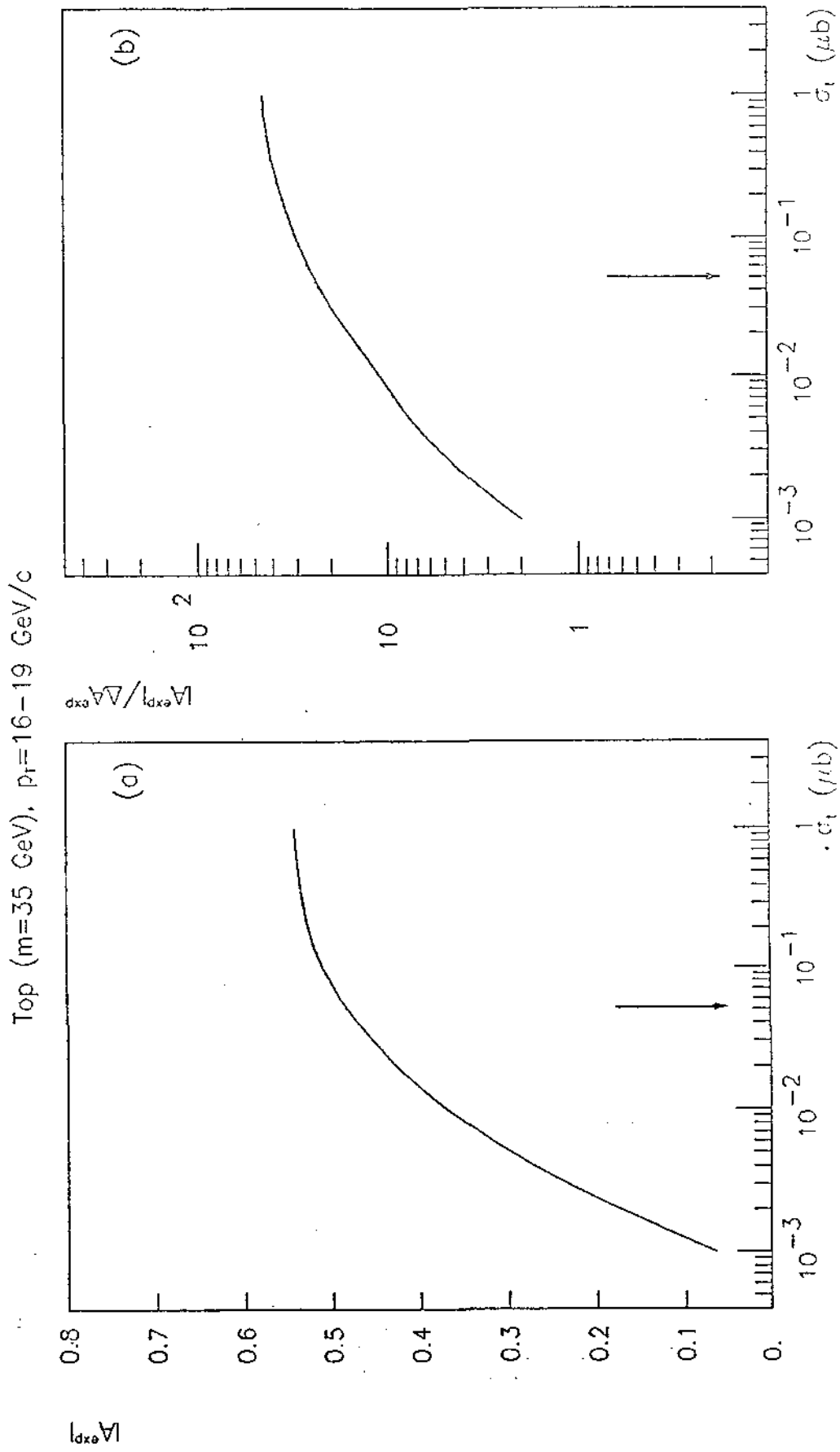


FIG. 3.

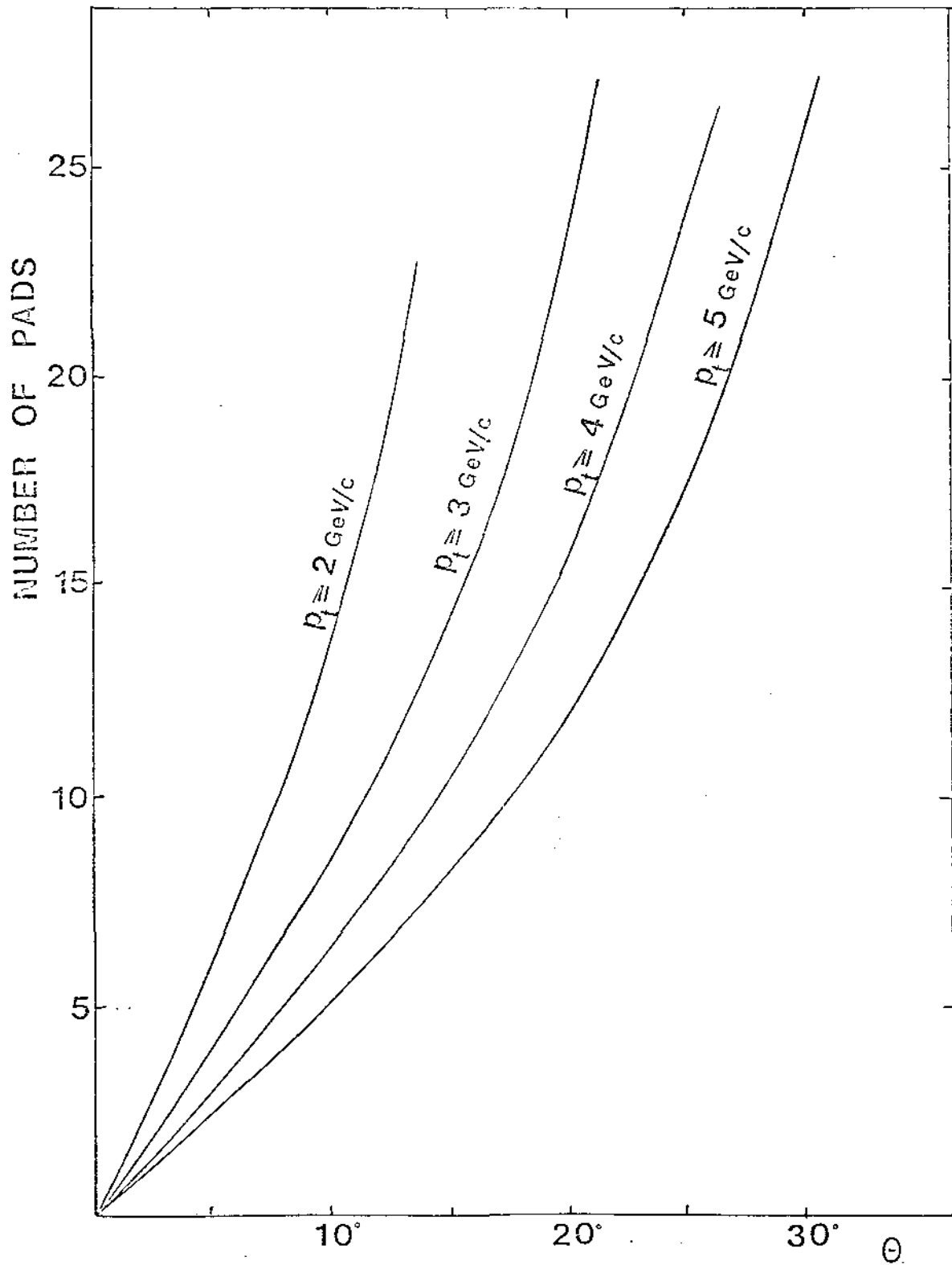


FIG. 33

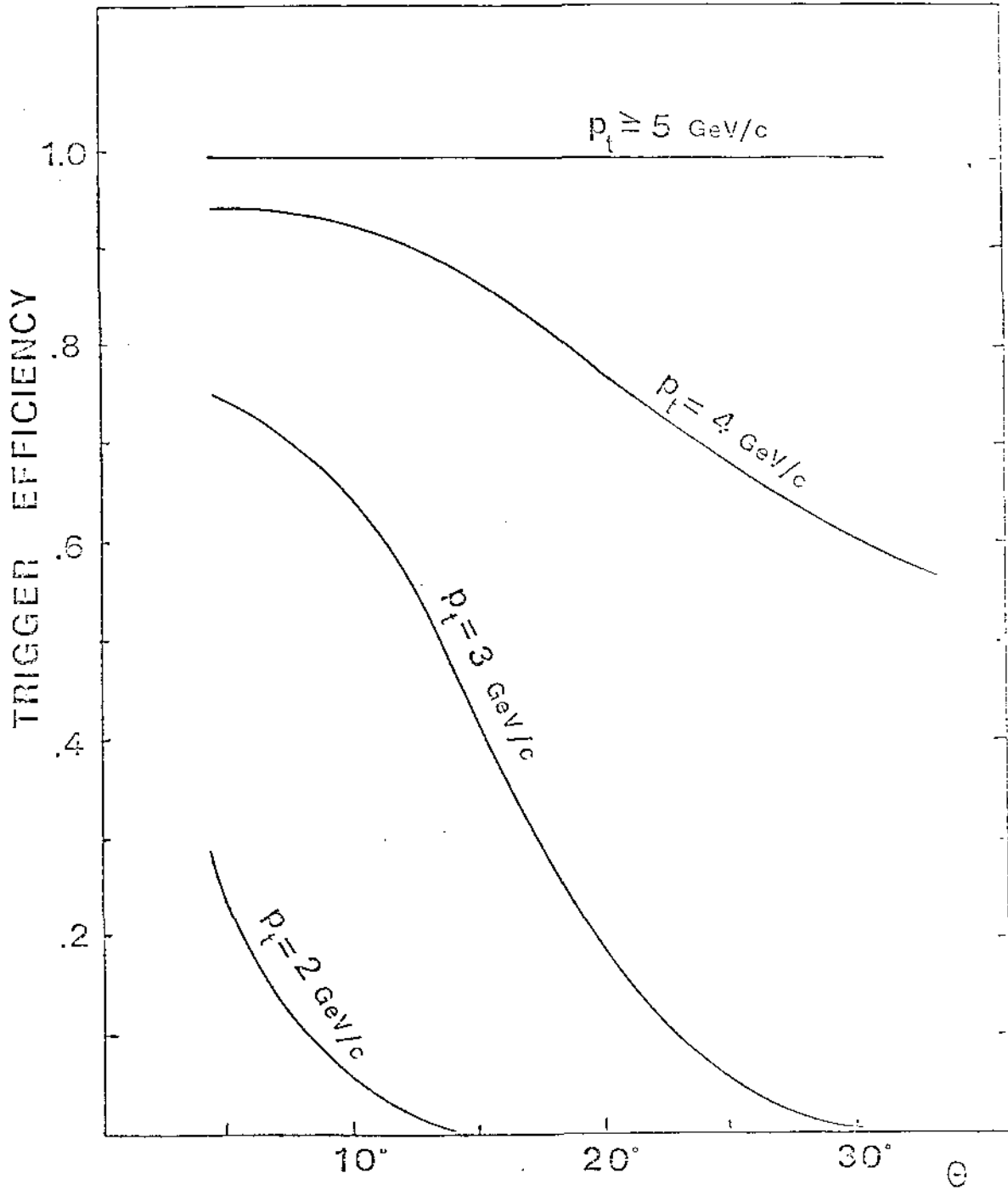


FIG. 34

- III-8. "The problem of new heavy flavours: top and superbeauty"
Proc. of the XXI Course of the Ettore Majorana
International School of Subnuclear Physics: "How far
are we from the Gauge Forces" (Plenum Press Inc.,
New York-London), Erice, August 4-13, 1983.

3 - 14 August 1983

8 - THE PROBLEM OF NEW HEAVY FLAVORS:

TOP AND SUPERBEAUTY

A. Zichichi

Cern
 Geneva
 Switzerland

1. INTRODUCTION: FROM PAST KNOWLEDGE TO FUTURE POSSIBILITIES

The present status of our knowledge on quarks and leptons may be summarized as follows:

Families:	1st	2nd	3rd
Quarks:	$\begin{pmatrix} u \\ d \end{pmatrix}$	$\begin{pmatrix} c \\ s \end{pmatrix}$	$\begin{pmatrix} ? \\ b \end{pmatrix}$
Leptons	$\begin{pmatrix} \nu_e \\ e \end{pmatrix}$	$\begin{pmatrix} \nu_\mu \\ \mu \end{pmatrix}$	$\begin{pmatrix} \nu_\tau \\ \tau \end{pmatrix}$

There are very good reasons to believe that our knowledge is far from being complete and thus the search for new heavy flavors and the study of their family structure is one of the key problems in Sub-nuclear Physics.

Let me quote two "theoretical" arguments in favor of further needs of new quarks. The ABJ anomaly cancellation requires that the number of leptons be equal to the number of quarks. This means that a sixth quark is needed. Its natural location would be the up-like member of the 3rd family, i.e. the "top" quark.

According to Supersymmetry, a very heavy quark with a mass in the few $10^2 \text{GeV}/c^2$ range is needed in order to produce radiatively (see Figure 1) a gluino with a mass such as to avoid a conflict with existing lower limits[1]. None of the presently known quarks (s, c and b) is heavy enough for this purpose.

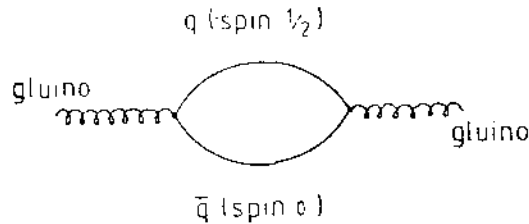


Fig. 1. The diagram illustrates how a gluino can acquire a mass from radiative processes, where a spin $\frac{1}{2}$ quark and a spin 0 antiquark are virtually produced. The quark mass must be in the $10^2 \text{ GeV}/c^2$ range, in order to allow a gluino mass of the order of a few GeV/c^2 .

Apart from these theoretical arguments we should not underestimate that Nature has often provided physicists with more regularities than needed (for example the equality between the proton and the electron charges, which took more than three decades to be understood).

We propose to consider the ratio between the masses of the known heavy quarks as a limit for the regularity in their masses. There are good reasons[2] to consider the strange quark heavy enough to be used in our argument.

At present we know that:

- i) $(m_c/m_s) \cong (1.8/0.5) \cong 3.5 \cong 4$;
- ii) $(m_b/m_s) \cong (5.5/0.5) \cong 11 \cong 10$.

Suppose that (i) and (ii) are of general validity, i.e.:

$$(m_c/m_s) = [m(\text{uplike quark})/m(\text{downlikequark})] = 4, \quad (1)$$

and

$$(m_m/m_s) = [m(\text{family } N+1)/m(\text{family } N)] = 10. \quad (2)$$

We ignore the 1st family (u, d) because of its very light mass. On the other hand, the ratios (1) and (2) would not be inconsistent with the various models used to derive the quark masses from bound states.

The validity of (1) and (2) would allow to conclude that the "top" mass is in the $20 \text{ GeV}/c^2$ range. This is too light for Supersymmetric models to avoid a gluino mass in conflict with experimental data. On the other hand, Supersymmetry tells us that the maximum number of flavors, n_f , allowed in order to have a consistent theory

(for example: the unification limit not above the Planck mass) is $n_f=8$. This means that the maximum number of families is 4. In the theories that ignore Supersymmetry, the asymptotic freedom is lost if $n_f > 16$.

What is not forbidden, in Nature, does take place. Thus, the message from Supersymmetry is twofold:

- i) four families of quarks are allowed;
- ii) quarks heavier than (d, u, s, c, b and t) are needed.

Formulas (1) and (2) tell us that the 4th family would have the heavy masses wanted by Supersymmetry. In fact, using (2), the heavy down-like quark (called, in the following, "superbeauty" or sb) would have a mass in the 50 GeV/c² range:

$$m(\text{down-heavy}) = m(\text{"superbeauty"}) \approx 10 \times 5.5 \approx 55 \text{ GeV}/c^2,$$

and, using (1), the heavy up-like quark would have a mass in the 200 GeV/c² range:

$$m(\text{up-heavy}) = m(\text{"supertruth"}) \approx 55 \times 4 \approx 220 \text{ GeV}/c^2.$$

The up-like quark of the 4th family should be called "supertruth". In fact, this very heavy mass is wanted by Supersymmetry; moreover, if Supersymmetry is a good theory, the 4th family should really be the last of the quark families, ever to be discovered.

The four families are shown in the next graph, where the main objectives of this first part of my talk are indicated by the dotted circles.

Families:	1st	2nd	3rd	4th
Quarks:	$\begin{pmatrix} u \\ d \end{pmatrix}$	$\begin{pmatrix} c \\ s \end{pmatrix}$	$\begin{pmatrix} t \\ b \end{pmatrix}$	$\begin{pmatrix} u_H \\ d_H \end{pmatrix}$
Leptons:	$\begin{pmatrix} \nu_e \\ e \end{pmatrix}$	$\begin{pmatrix} \nu_\mu \\ \mu \end{pmatrix}$	$\begin{pmatrix} \nu_\tau \\ \tau \end{pmatrix}$	$\begin{pmatrix} \nu_H \\ L_H \end{pmatrix}$

Let us come to a key question: are "top" and "superbeauty" accessible to (pp̄) Collider energies? If yes, how can they be detected?

Many methods have been suggested:

- i) detection of a hidden state with the study of the invariant mass of the lepton pairs;
- ii) detection of an open state with the identification of hadronic decay channels;

- iii) study of multilepton events;
- iv) study of the inclusive transverse momentum spectrum of the leptons from semileptonic decays;
- v) study of the transverse dilepton (i, ν) and jets masses.

All of these methods present, in various degrees, experimental problems related to small production cross sections, low global branching ratios, high background levels, poor experimental resolution of the quantities needed to be measured. Moreover, most of them have big troubles in being able to identify the up-like or down-like nature of the new flavors.

We present here a new method to observe the production of heavy mass states, either up-like ("top") or down-like ("superbeauty") which is based on the "Leading" baryon production mechanism, extended to the heaviest baryon and antibaryon states. In fact, due to this production mechanism, a charge asymmetry of the leptons, originating from these heavy flavors can be observed in a selected region of the phase space. Moreover, this asymmetry will show an energy dependence characteristic of the masses of the decaying states.

More precisely, the "top" baryonic state will decay semileptonically into ℓ^+ and produce a positive asymmetry in the outgoing proton rapidity hemisphere

$$A_P = (\ell^+ - \ell^-) / (\ell^+ + \ell^-) = \text{positive.}$$

The "anti-top" antibaryonic state will produce a negative asymmetry in the outgoing antiproton rapidity hemisphere

$$A_{\bar{P}} = (\ell^+ - \ell^-) / (\ell^+ + \ell^-) = \text{negative.}$$

The signs of these asymmetries will be reversed for the "superbeauty" case.

The energy range where to measure the ℓ^\pm asymmetry, and the separation between the maxima, depend on the parent-daughter mass difference in the decay of the two new flavors. Extending the validity of the generalized Cabibbo mixing (GCM) to the 4th family, the mass differences in the superbeauty and top decays would be:

$$\Delta m = m(\text{top}) - m(\text{beauty}) \approx 20 \text{ GeV}/c^2,$$

$$\Delta m = m(\text{superbeauty}) - m(\text{top}) \approx 30 \text{ GeV}/c^2.$$

The ℓ^\pm transverse momentum spectra associated with "top" and "superbeauty" will be quite different because:

$$m(\text{"top"}) \approx 25 \text{ GeV}/c^2,$$

$$m(\text{"superbeauty"}) \approx 55 \text{ GeV}/c^2,$$

thus the Asymmetry will change sign with increasing lepton energy. Figure 2 shows the main trend of the measurement we propose. Notice that this GCM condition, if not valid, would not spoil our method. It would only shift the energy spectrum of e^- from superbeauty decay to higher values.

As we will see in the following, the amplitude of the effect depends on:

- i) production cross sections;
- ii) production and decay, angular and momentum distributions;
- iii) branching ratios into semileptonic channels;
- iv) luminosity;
- v) acceptance and rejection power of the experimental set-up designed to observe the leptons produced by these "new" flavors decay.

2. A BRIEF REVIEW OF HEAVY FLAVORS PRODUCTION IN HADRONIC MACHINES

How to look for "top" and "superbeauty" at the $(p\bar{p})$ Collider, is a problem analogous to "charm" and "beauty" in hadronic machines and,

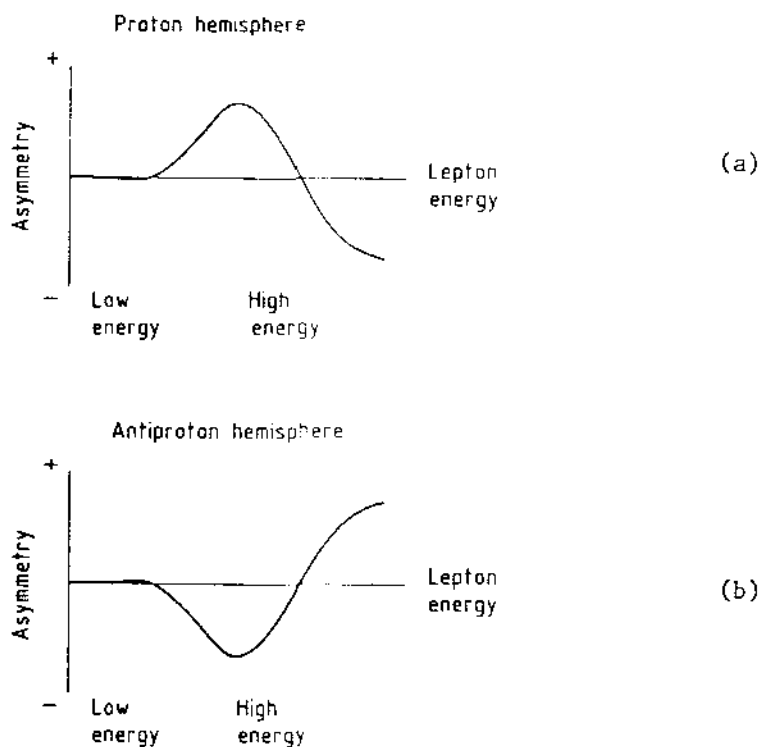


Fig. 2. Main trend of the electron charge Asymmetry in the proton hemisphere (a) and in the antiproton hemisphere (b).

in particular, at the ISR. It is probably instructive to review, very briefly, the main steps in this field.

2.1. Production Cross Sections

The theoretical predictions for the charm production cross section and the experimental findings are shown in Table 1.

If we were to believe in the string model or in the statistical thermodynamical model, or in the first QCD attempts (fusion model), the conclusion should have been that the production and observation of "charm" is out of question in hadronic machines.

Only recently QCD models (flavor excitation) came nearer to experimental findings. In Figure 3 all the experimental data are shown and compared with the various steps in the QCD models. Notice that neither $\ln(s)$ nor $\ln^2(s)$ are compatible with the observed threshold behavior.

2.2. The "Leading" Effect

A result which was theoretically unpredicted is the "Leading" effect which shows up in the production of heavy flavors.

A detailed study of (pp) interactions at the ISR showed that the Λ_c^+ is produced in a "Leading" way[7].

After this experimental result was obtained, a series of theoretical proposals were presented, to account for the "Leading" Λ_c^+ production. The longitudinal momentum distribution[7] for Λ_c^+ was in fact found at the ISR to be:

$$(d\sigma/d|x|) \sim (1 - |x|)^\alpha \quad \text{with } \alpha = 0.40 \pm 0.25.$$

Table 1. Charm Cross Section at ISR Energies ($\sigma_\pi = 10^2 \text{mb}$).

String model	: 10^{-10}	$\times \sigma_\pi$
Fermi-Hagedorn	: 10^{-5}	$\times \sigma_\pi$
QCD (Fusion)	: 10^{-4}	$\times \sigma_\pi$
QCD (Flavor excitation)	: $10^{-2}-10^{-3}$	$\times \sigma_\pi$
Experimentally	: $\approx 10^{-2}$	$\times \sigma_\pi$

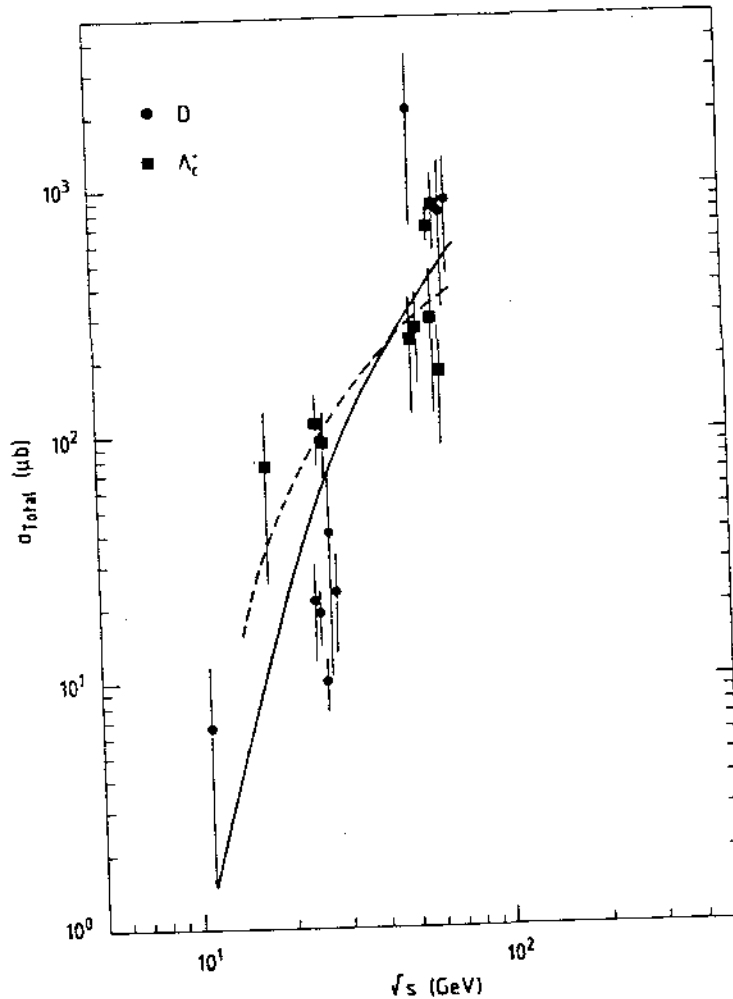


Fig. 3. Cross sections expected on the basis of gluon and quark fusion models ($gg + c\bar{c}$ and $q\bar{q} + c\bar{c}$ curves). Other QCD models are also shown. The data are taken from 3, 4, 5 and 6.

The results are shown in Figure 4a. The charmed meson production[8] was on the other hand measured to be "non-Leading", i.e.

$$E(d\sigma/d|x|) \approx (1 - |x|)^\alpha \quad \text{with } \alpha \approx 3.$$

This can be "a posteriori" qualitatively understood in terms of the Λ_c^+ obtained by a recombination of the spectator c-quark with a valence (ud) pair in the proton; while the \bar{D} production is given by the recombination of the spectator \bar{c} -quark with a most one valence quark[9,10].

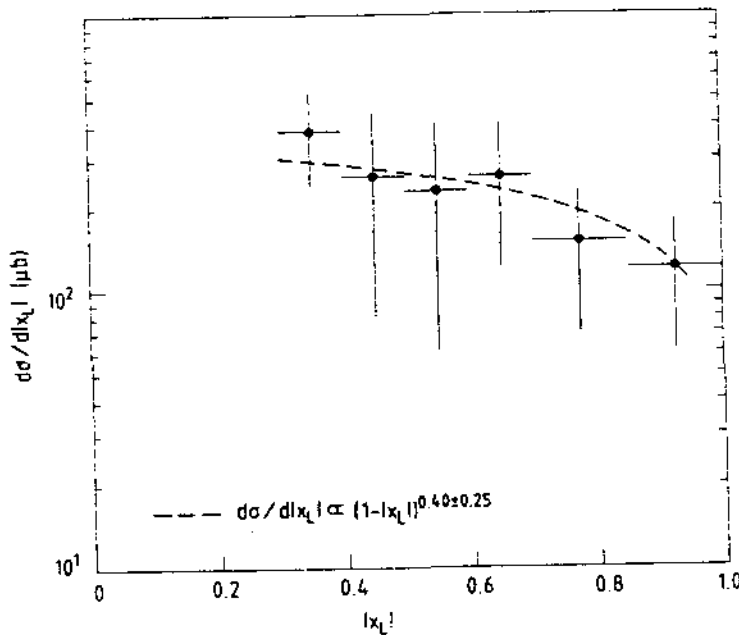


Fig. 4a. Experimental longitudinal momentum distribution of Λ_c^+ .

Figure 4b shows the qualitative behavior, as a function of the quark mass, of the quantity (Leading/Total), which will be defined in section 5.4 as the ratio between the inclusive cross-section for producing leading baryons in one hemisphere and the total cross-section for producing $(q\bar{q})$ pairs. This figure shows that, at least at the ISR energies, the "Leading" production increases with increasing quark mass.

A more complete summary of charm production in purely hadronic interactions is reported in the Table 2. There is no model which can fit all measured quantities.

2.3. Further Comments

For those who have strong faith on QCD it could be interesting to extend our review. In fact the photoproduction was considered a simpler case for QCD. Therefore its predictions should have been in agreement with experimental findings.

A summary of QCD problems in photoproduction physics is as follows:

- a) large photoproduction cross sections of the Heavy Flavors are impossible to be predicted by perturbative QCD;
- b) the p_T dependence of inelastic $(c\bar{c})$, for open and hidden states, cannot be accounted for by QCD;
- c) the A -dependence cannot be A^1 .

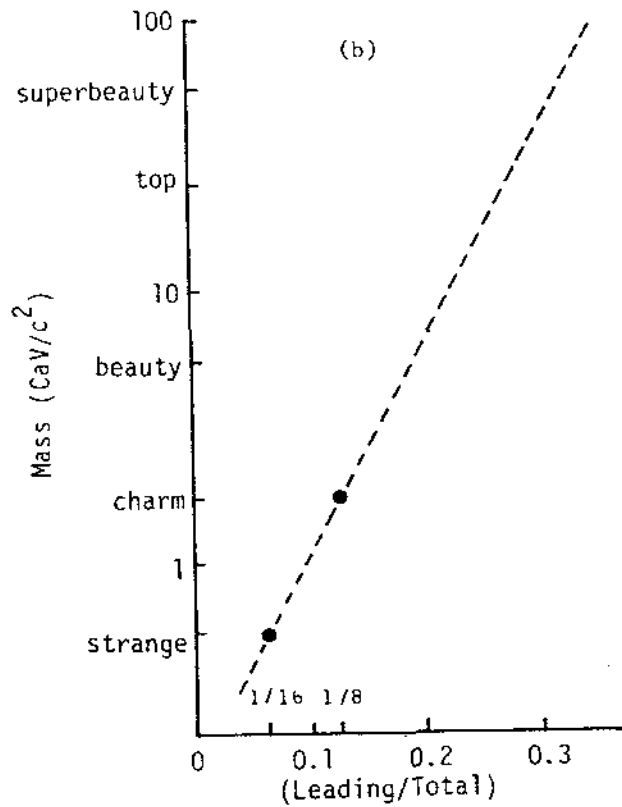


Fig. 4b. Qualitative behavior of the quantity (Leading/Total) as a function of the quark mass, at $\sqrt{s} = 62$ GeV.

Table 2.

	Experiment	Models		
		Diffractive	Flavor excitation	Fusion
Leading effect	Yes	Yes	Yes	No
Threshold behavior	Steeper than $\ln^2 s$	$\ln s$	Steeper than $\ln^2 s$	\gg Steeper than $\ln^2 s$
Mass dependence	?	$1/m^2$	Stronger than $1/m^2$	\gg Stronger than $1/m^2$
Cross section	Large	Large	Large	Small
A^α dependence	$\alpha < 2/3^*$	$\alpha = 2/3$	$\alpha = 1$	$\alpha = \dots$

*The p_T dependence is derived from data on strangeness.

2.4. Conclusions

The conclusion of this short review on the "charm" flavor production in (pp) interactions is therefore:

- i) the cross section values found are at least an order of magnitude above the "theoretical" predictions of perturbative QCD;
- ii) the x-distribution for Λ_c^+ , i.e. the "Leading" effect, was theoretically unpredicted;
- iii) with "new" models (essentially flavor excitation[11,10] and non-perturbative QCD)[9] both cross sections values and x-distributions can be "theoretically" derived.

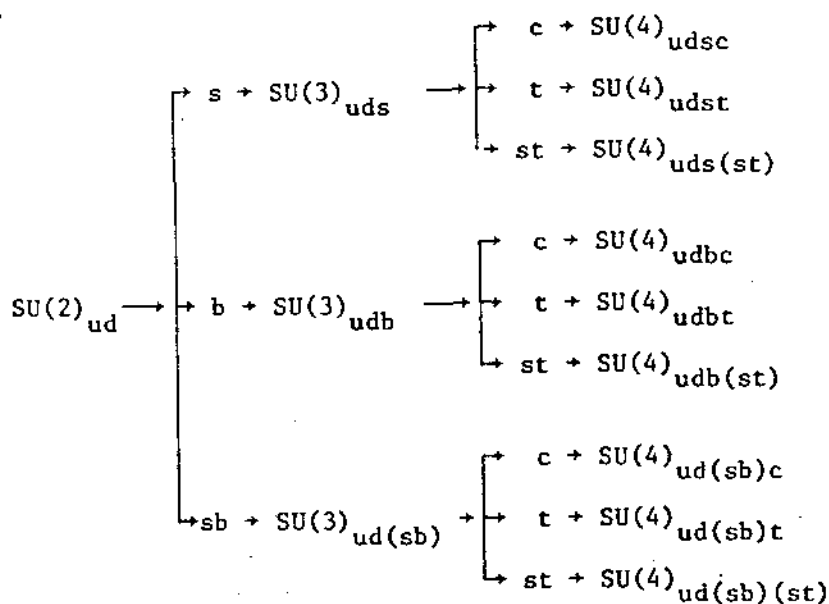
All this should be quite a warning for QCD prediction on Heavy Flavors production at extreme energies such as those of the (pp) CERN Collider.

3.2. EXPECTED NEW HEAVY FLAVORED STATES

The main purpose of this section is to call attention on the enormous number of new states which are expected on the basis of the old and new flavors.

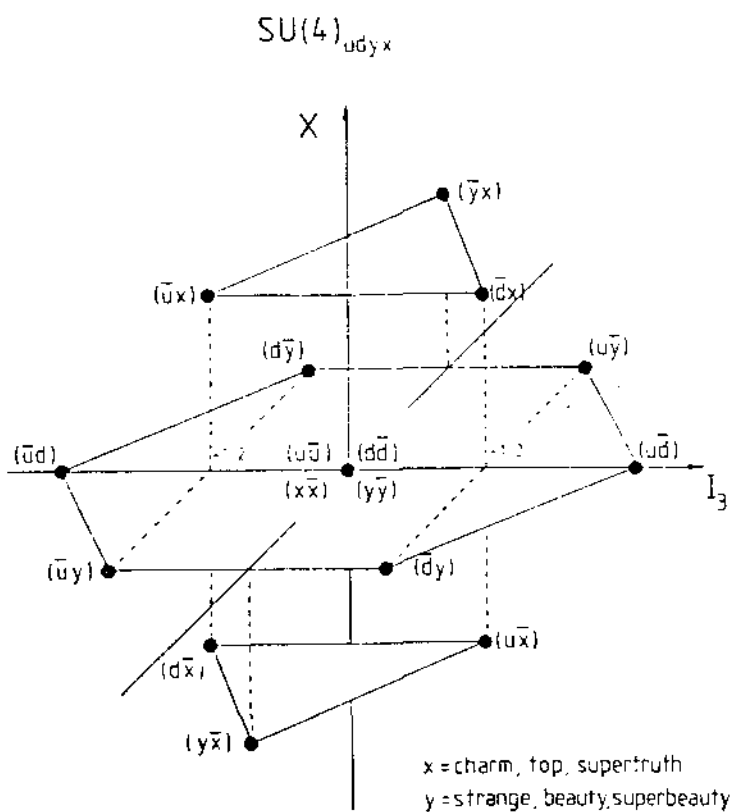
3.1. Examples from Previous Experience with $SU(3)_{uds}$ and $SU(4)_{udsc}$

The following graph illustrates what could indeed happen.



With 3 flavors (u, d and s) the famous $SU(3)_{uds}$ came out. It could be that "beauty" will produce another $SU(3)_{udb}$. The advent of the "charm" with four flavors (udsc) produced $SU(4)_{udsc}$. On the other hand with the "top" there are two possible $SU(4)$: $SU(4)_{udst}$ and $SU(4)_{udbt}$.

Despite the large mass differences among the various flavors, it could be that Nature will provide, as usual, more regularities than wanted. The above global symmetry groups for the structure of the various possible particle states could eventually show up, even if not expected.



$J^P = 0^-$ and $J^P = 1^-$ MESONS (2x16 STATES)

Fig. 5. The $SU(4)_f$ mesonic multiplets for $J^P = 0^-$; the same multiplet structure repeats for $J^P = 1^-$. "x" represents the quarks with electric charge $+2/3$, "y" the quarks with electric charge $-1/3$. Each of the possible $udyx$ combinations should produce an $SU(4)_f$. The quark composition for each state is indicated in parenthesis.

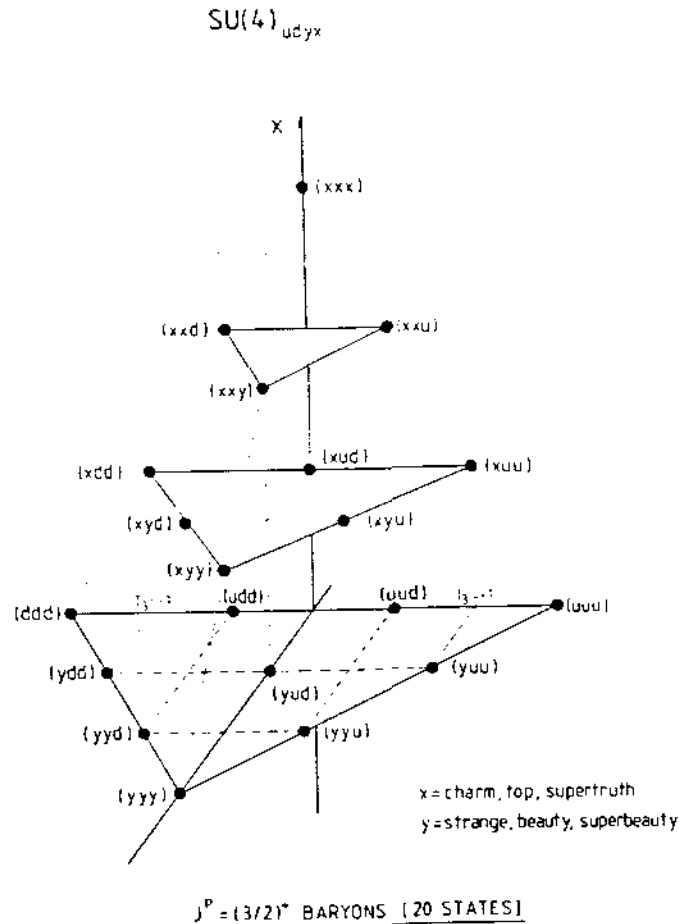


Fig. 7. Showing the structure of the expected baryonic $J^P = 3/2^+$ $SU(4)_f$ 20-plets.

If we enlarge the symmetries to the intrinsic spins the multitude of states increases further. These are indicated, for the first 3 flavors (u, d and s), in the Tables 3 and 4, respectively for the mesons and for the baryons in $SU(6)$.

An example of how the multitude of the states goes with the mass is shown in Figures 8a and 8b, where the masses of the particles run from few GeV/c^2 up to $60 \text{ GeV}/c^2$.

Table 3. SU(6) Mesonic Supermultiplets

SU(6)	SU(3) _f	J ^{PC}	Particle states	Number of states
[(35 ⊕ 1) ⊗ 1]; (L=0)	8 ⊕ 1	0 ⁻⁺	π, K, η, η'	36
	8 ⊕ 1	1 ⁻⁻	ρ, K*, ω, φ	
	8 ⊕ 1	1 ^{+−}	B, Q _{1,2} , ..., ?	
[(35 ⊕ 1) ⊗ 3]; (L=1)	8 ⊕ 1	0 ⁺⁺	S, χ, S*, ε	108
	8 ⊕ 1	1 ⁺⁺	A ₁ , Q _{1,2} , D, E	
	8 ⊕ 1	1 ⁺⁺	A ₁ , Q _{1,2} , D, E	
	8 ⊕ 1	2 ⁺⁺	A ₂ , K**, f, f'	

Table 4. Baryons in SU(6) Supermultiplets

[Su(6), L ^P]	SU(3) _f	J ^P	Standard names of particle states
(56, 0 ⁺)	8	1/2 ⁺	N, Λ, Σ, Ξ ⁻
	10	3/2 ⁺	N*, Λ*, Ξ*, Ω ⁻
	1	1/2 ⁻	Repeat singlet
	8	1/2 ⁻	Repeat octet
	10	1/2 ⁻	Repeat decuplet
(70, 1 ⁻)	1	3/2 ⁻	Repeat singlet
	8	3/2 ⁻	Repeat octet
	10	3/2 ⁻	Repeat decuplet
	8	1/2 ⁻	Repeat octet
	8	3/2 ⁻	Repeat octet
	8	5/2 ⁻	Repeat octet

Repeat means that the quantum numbers (isospin and strangeness) of the states are identical to the "octet" and "decuplet" already known for the 56-case.

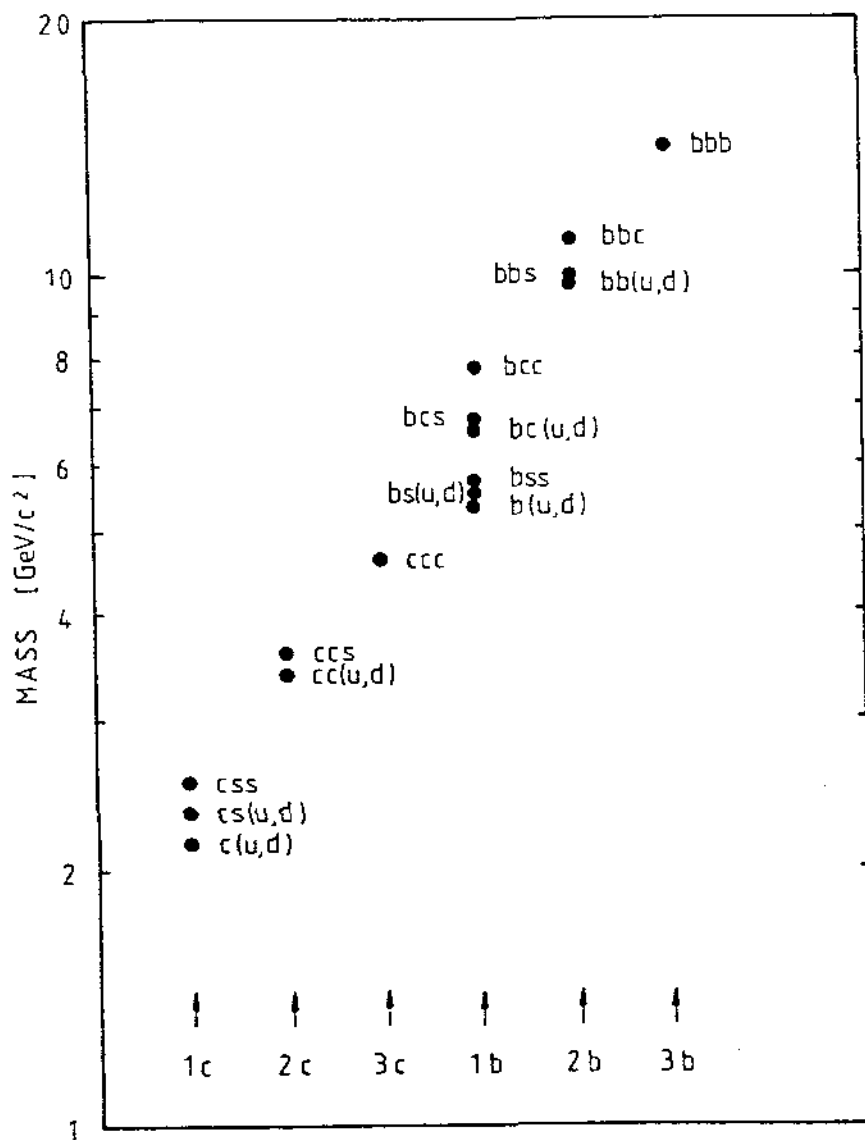


Fig. 8a. The figure shows the mass ranges of the baryon states with: (a) from 1 to 3 charm or beauty quarks; (b) from 1 to 3 top quarks.

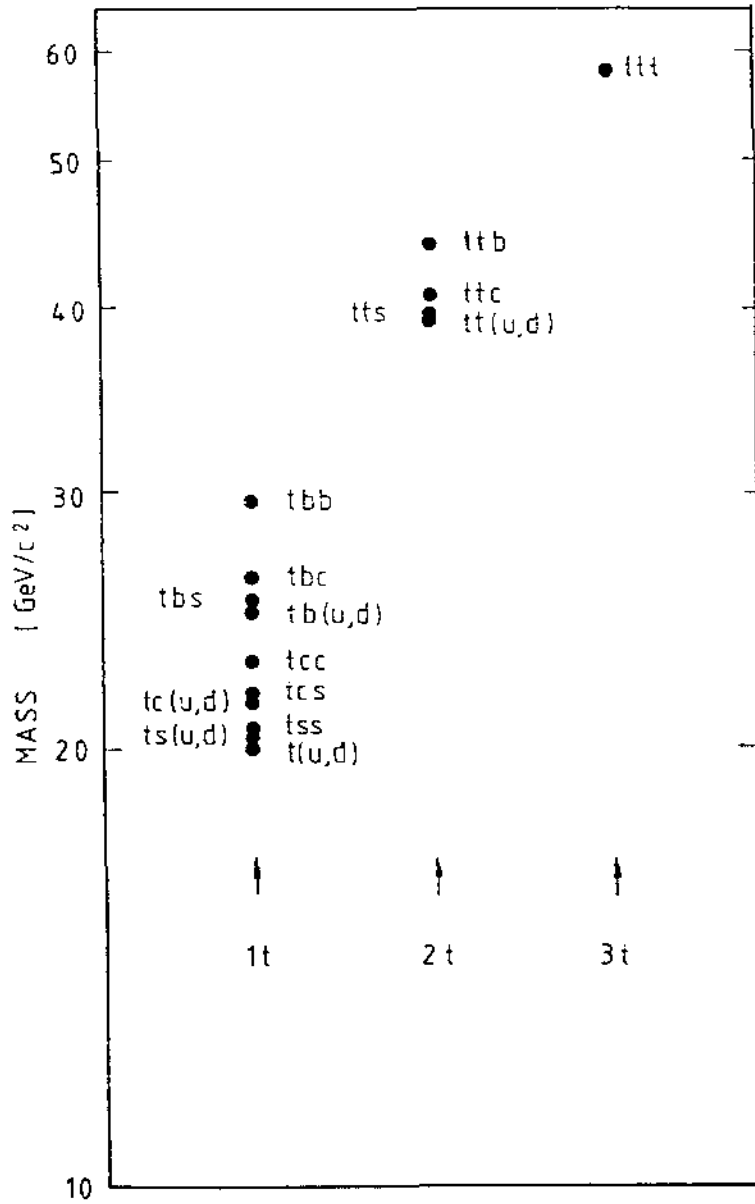


Fig. 8b. The figure shows the mass ranges of the baryon states with: (a) from 1 to 3 charm or beauty quarks; (b) from 1 to 3 top quarks.

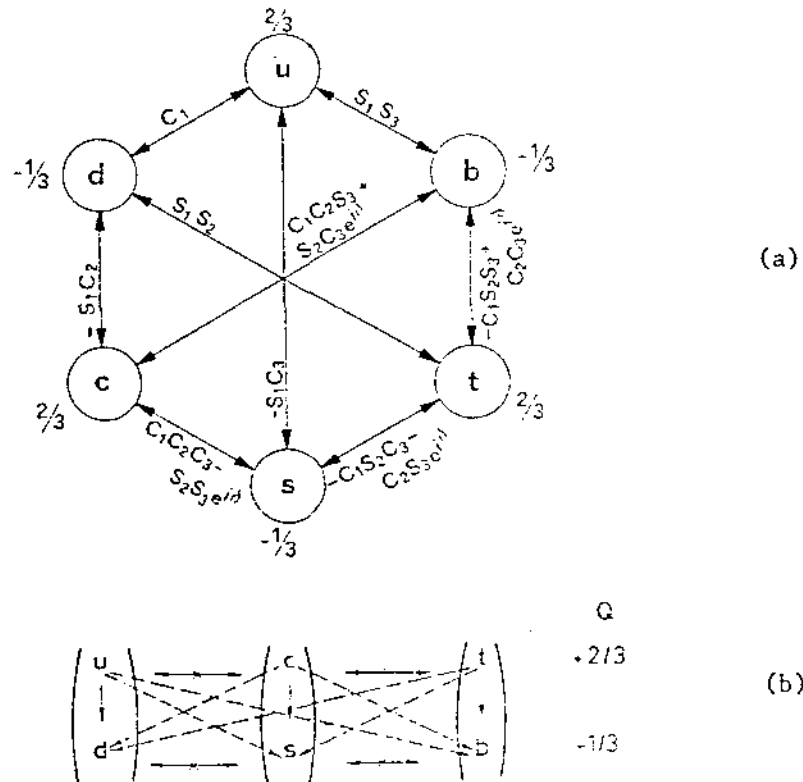


Fig. 9. (a) The six quark mixing with CP violation. $S_i = \sin\theta_i$, $C_i = \cos\theta_i$. (b) Transitions among the various i states. The Cabibbo mixing opens the dashed channels. The horizontal transitions are forbidden for any value of the mixing angle. Allowed neutral currents are: $u\bar{u}$, $c\bar{c}$, $t\bar{t}$, $d\bar{d}$, $s\bar{s}$ and $b\bar{b}$.

3.2. Note on the Semi-Leptonic Decay Modes: Generalized Cabibbo Mixing

A fact of Nature is that the matrix which relates the down-like "weak" flavors "Cabibbo mixed"

$$\begin{pmatrix} d \\ c \\ s \\ b \end{pmatrix}$$

to the "strong" flavors

$$\begin{pmatrix} d \\ s \\ b \end{pmatrix}$$

is approximately a unit matrix

$$\begin{pmatrix} d \\ c \\ s \\ b \end{pmatrix} \cong \begin{pmatrix} 1 & 0 & 0 \\ 0 & 1 & 0 \\ 0 & 0 & 1 \end{pmatrix} \begin{pmatrix} d \\ s \\ b \end{pmatrix}$$

as shown in Figures 9a and 9b.

In order to extend the generalized Cabibbo mixing to the 4th Family, we make the following extrapolations:

- i) all the generalized Cabibbo angles, even those coming from the existence of the 4th family are small;
- ii) the flavor-changing neutral currents are forbidden to any order of family;
- ii) the amplitude for the transition from family N to family $N-\alpha$ has a coefficient

$$\prod_{i=1, \alpha} (\sin \theta_i)$$

As a consequence, the Cabibbo-favored decay chains of flavors c, b, t and sb are:

$$\begin{aligned} c &\rightarrow s \\ b &\rightarrow c \rightarrow s \\ t &\rightarrow b \rightarrow c \rightarrow s \\ sb &\rightarrow t \rightarrow b \rightarrow c \rightarrow s. \end{aligned}$$

All we need to know is the charge sign of the lepton in a transition from an "up-like" to a "down-like" flavor and viceversa. This can be summarized as follows:

$$\begin{array}{cccc} \begin{pmatrix} u \\ d \end{pmatrix} & \begin{pmatrix} c \\ s \end{pmatrix} & \begin{pmatrix} t \\ b \end{pmatrix} & \begin{pmatrix} st \\ sb \end{pmatrix} \\ \Downarrow & \Downarrow & \Downarrow & \Downarrow \\ \begin{pmatrix} 1 \\ 2 \end{pmatrix} & \begin{pmatrix} 3 \\ 4 \end{pmatrix} & \begin{pmatrix} 5 \\ 6 \end{pmatrix} & \begin{pmatrix} 7 \\ 8 \end{pmatrix} \end{array} \quad \begin{array}{l} \leftarrow \text{ODD (= UP-LIKE) QUARKS} \\ \leftarrow \text{EVEN (= DOWN-LIKE) QUARKS} \end{array}$$

with the charge formula written as:

$$Q = (1/3 + f_1)/2$$

with:

$$f_i = +1 \text{ for odd quarks } (i = 1, 3, 5, 7)$$

$$f_i = -1 \text{ for even quarks } (i = 2, 4, 6, 8).$$

From this follows the electric charge sign of the lepton in the semileptonic decay of the flavor:

ODD \longrightarrow EVEN (UP-LIKE \longrightarrow DOWN-LIKE)

TRANSITION \implies POSITIVE LEPTON

EVEN \longrightarrow ODD (DOWN-LIKE UP-LIKE) TRANSITION \implies

\implies NEGATIVE LEPTON

As will be seen in the Figure 15, a sequence $t \rightarrow b \rightarrow c \rightarrow s$ will be accompanied by the semileptonic series giving rise to $e^+ \rightarrow e^- \rightarrow e^+$. For the antiquark sequence $\bar{t} \rightarrow \bar{b} \rightarrow \bar{c} \rightarrow \bar{s}$, the charges will be reversed ($e^- \rightarrow e^+ \rightarrow e^-$). These results are straightforward consequences of the previous table.

4. CROSS SECTION ESTIMATES: HOW TO GO FROM STRANGENESS TO CHARM, BEAUTY, TOP AND SUPERBEAUTY

Now comes a key question: once we know the "strange" and "charm" cross sections, is it possible to predict the heavier flavors (c, b, t or sb) cross sections in hadronic collisions?

Simple arguments bring to the conclusion that:

$$\sigma(m) \sim (1/m^2) \times f(s/m^2). \quad (3)$$

In fact, the only quantities which enter in the problem of producing a (q \bar{q}) pair, having at disposal the total energy \sqrt{s} , are the quark mass, m , and the total energy, \sqrt{s} .

Formula (3) is based on dimensional and scaling arguments:

- Dimension says that: $\sigma \sim (1/m^2)$;
- Scaling says that the two quantities m^2 and s are such that nothing changes if their ratio (s/m^2) is kept constant; the ratio (s/m^2) is the dimensionless quantity needed if no other scale should remain in the game.

The basic formula is therefore:

$$\sigma_i[(\sqrt{s})_{pp} = E_i] = (m_j/m_i)^2 \times \sigma_j[(\sqrt{s})_{pp} = E_j = (m_j/m_i)E_i] \quad (4)$$

where:

σ_i, σ_j are the production cross sections,

m_i, m_j are the masses,

E_i, E_j are the energies,

at which flavors f_i and f_j are produced.

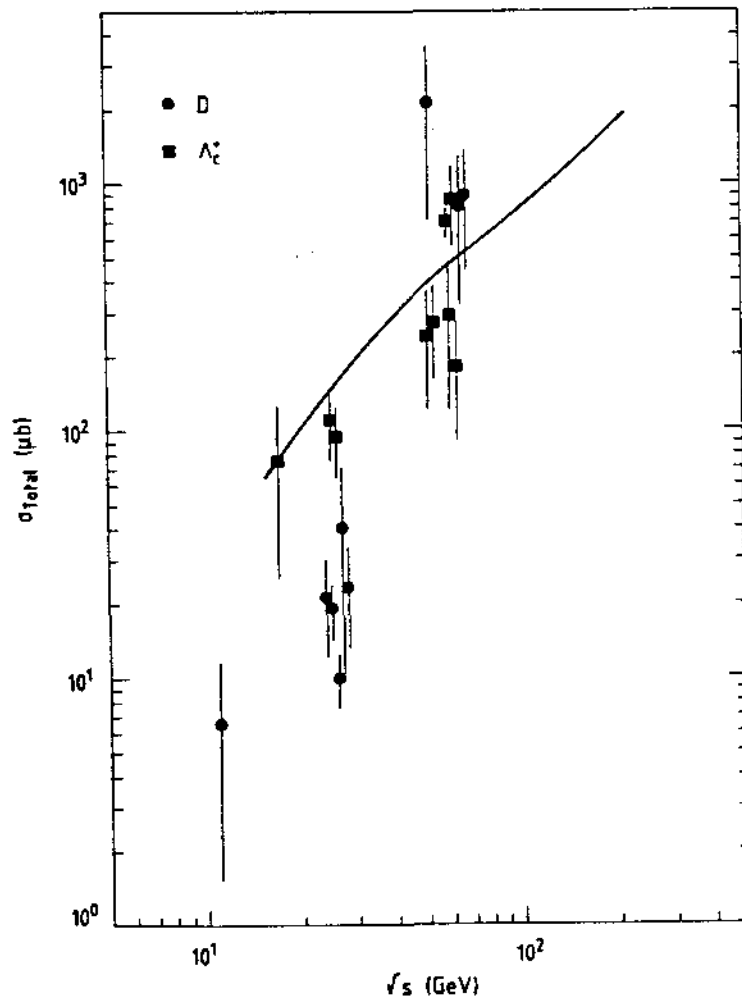


Fig. 10. Charm cross section derived from strange cross section following formula (4).

The results are shown in Figures 10-13, where we have used:

- i) the strangeness data to predict c, b, t and sb;
- ii) the "charm" data to predict b, t and sb;
- iii) the "beauty" data to predict t and sb.

Finally, for completeness, we also report the most recent QCD predictions of references 10 and 9 (Figure 14).

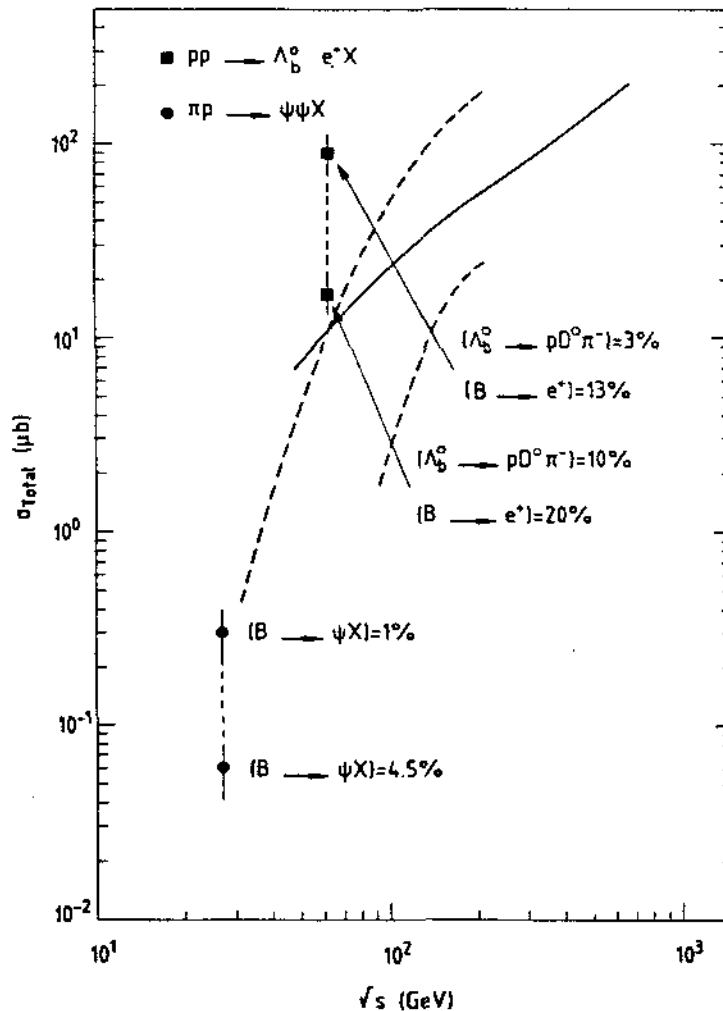


Fig. 11. Beauty cross section derived from strange (full line) and charm (dashed lines - notice the width due to the experimental uncertainties) cross sections following formula (4). The data are taken from references 12 and 13.

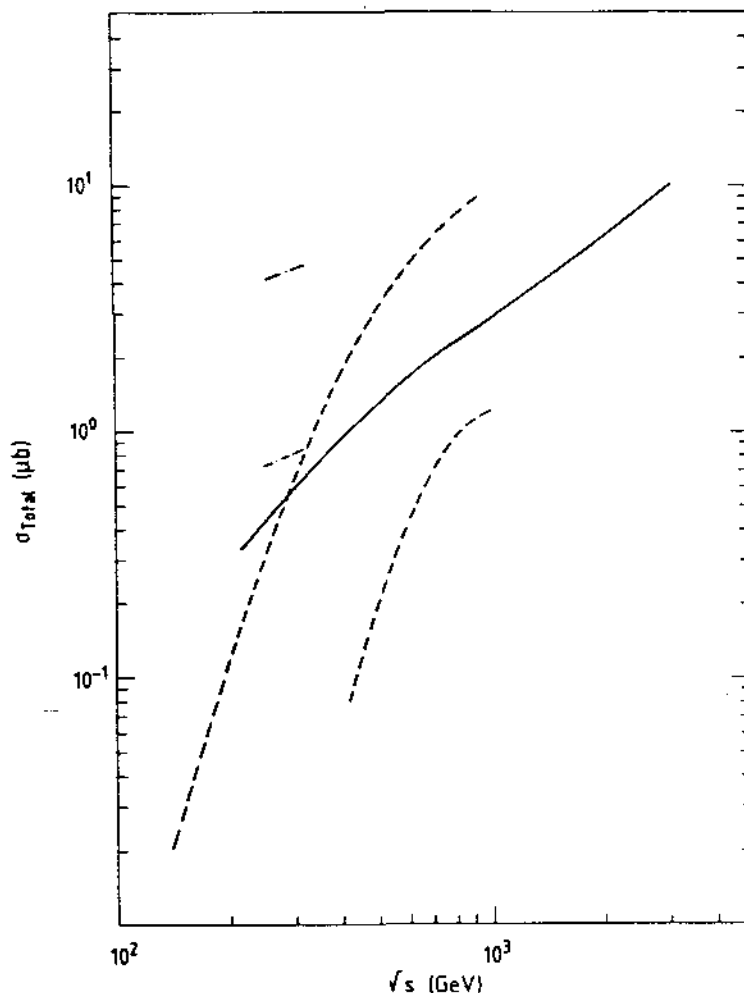


Fig. 12. Top cross section derived from strange (full line), charm (dashed lines) and beauty (dash/dotted lines) cross sections following formula (4).

5. THE STUDY OF THE LEPTON CHARGE ASYMMETRY AND ITS ENERGY DEPENDENCE AS A WAY TO DETECT THE HEAVIEST FLAVORED STATES (BARYONIC AND ANTI-BARYONIC) AT THE ($p\bar{p}$) COLLIDER

The leptonic decay chains, following the generalized Cabibbo dominance, for the various flavors c , b , t , sb , are shown in Figure 15.

Once a particle-antiparticle pair has been produced, on the average the number of positive and negative leptons from its decay is equal. However we will discuss under which conditions an asymmetry in the number of positive and negative leptons can be observed, due

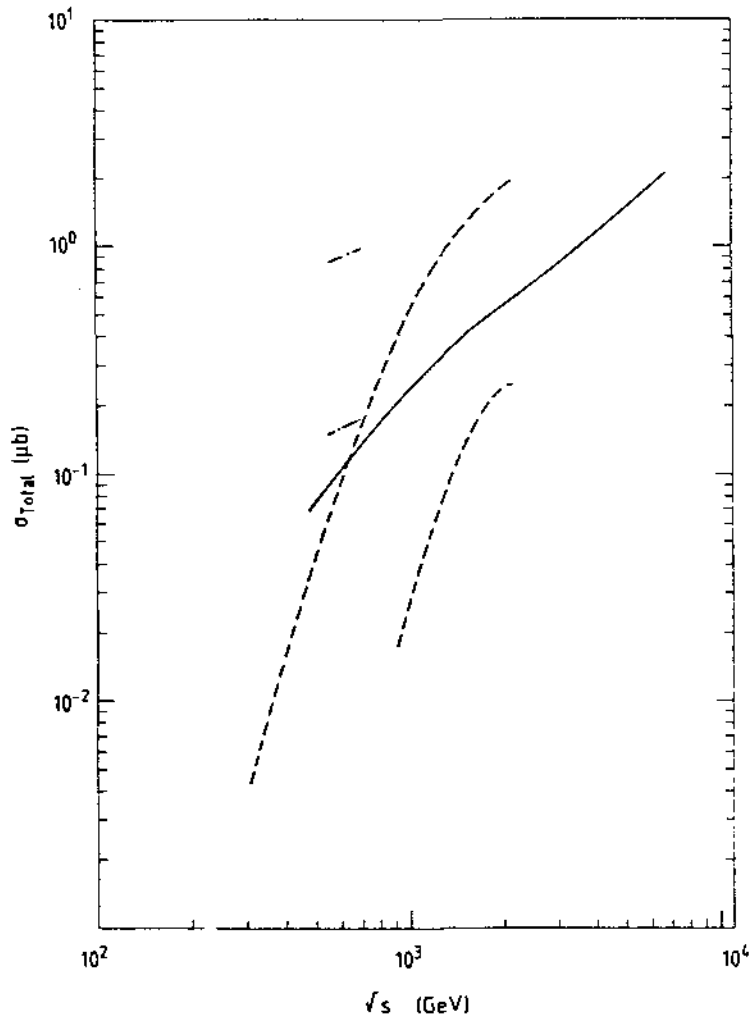


Fig. 13. Superbeauty cross section derived from strange (full line), charm (dashed line) and beauty (dash/point lines) cross sections following formula (4).

to the different longitudinal momentum production distribution for baryons and mesons, and to the dependence of the lepton p_T spectra from the product particle mass.

Let us define the Asymmetry parameters as

$$A^\circ(p_T, \theta_{\text{cut}}) = \frac{N(\ell^+) - N(\ell^-)}{N(\ell^+) + N(\ell^-)} \quad (5)$$

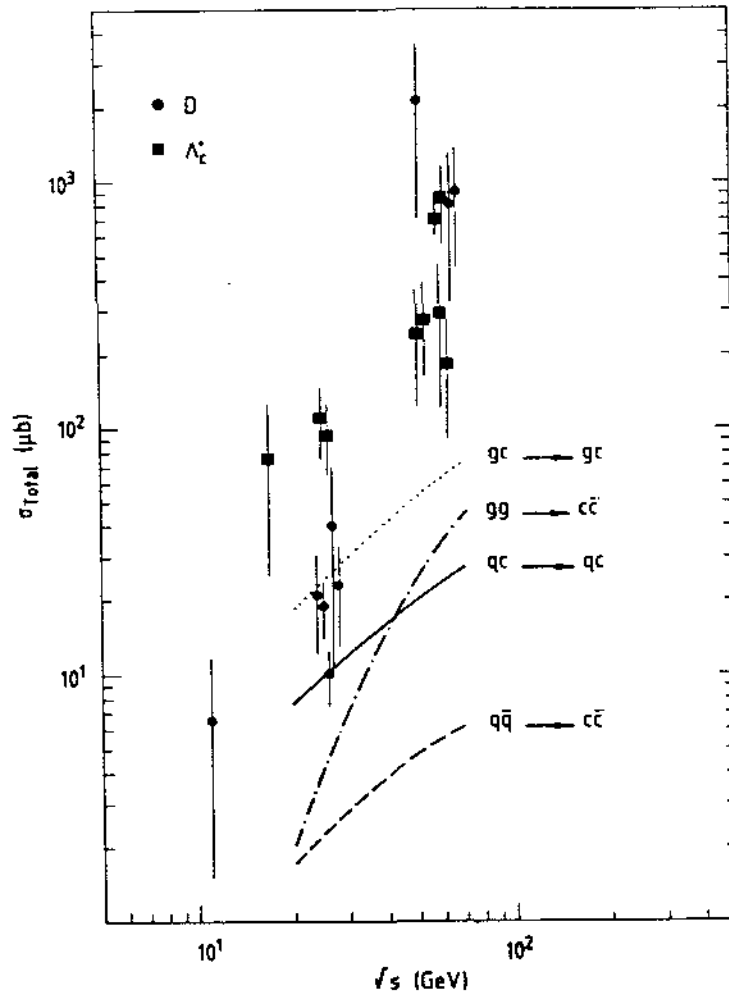


Fig. 14. Non perturbative QCD predictions (dashed line) and flavor excitation perturbative QCD predictions (full line) for charm hadroproduction.

where $N(\ell^+) \equiv N(\ell^+; p_T, \theta_{cut})$ and $N(\ell^-) \equiv N(\ell^-; p_T, \theta_{cut})$ are the number of positive and negative leptons produced in the angular range $0^\circ < \theta < \theta_{cut}$ and with transverse momentum p_T .

The number of positive leptons ℓ^+ is expressed by

$$N(\ell^+) = L[n_{sb}(\ell^+) + n_t(\ell^+) + n_b(\ell^+) + n_c(\ell^+)]$$

where L is the total integrated luminosity and $n_f(\ell^+)$ (with $f = sb, t, b, c$) is the contribution from the direct production of sb, t, b, c states.

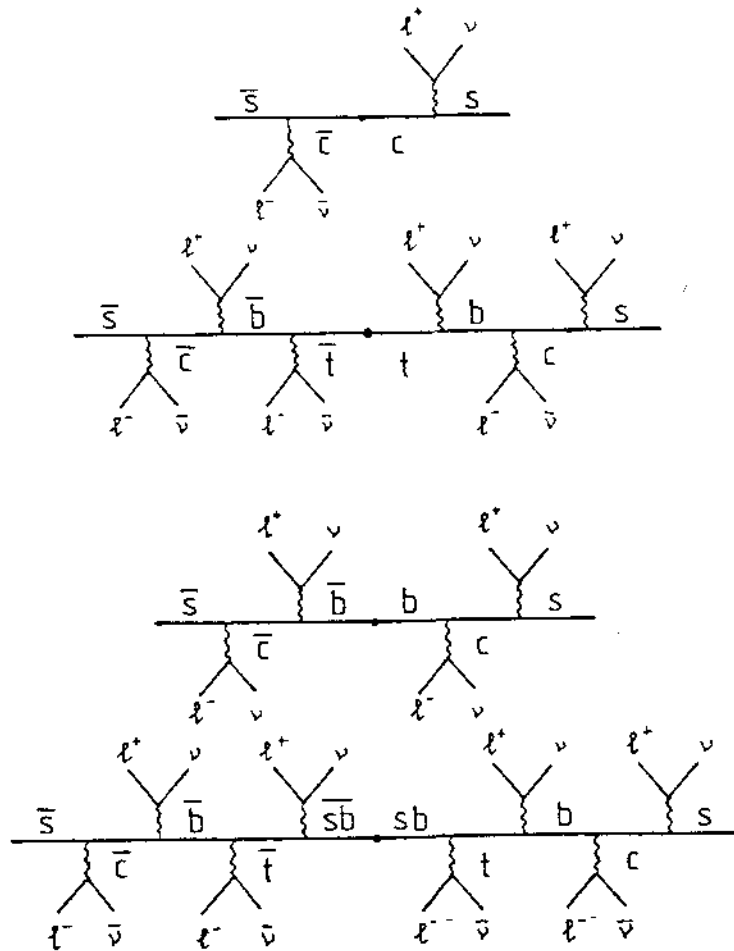


Fig. 15. Diagram illustrating all the possible electric charge signs of the electrons originating from the semileptonic decay of the quarks c, b, t and sb.

Analogously the number of negative leptons is given by

$$N(l^-) = L[(n_{sb}(l^-) + n_t(l^-) + n_b(l^-) + n_c(l^-))].$$

The leptons originated by the decay of the various flavors and antiflavors are summarized in Tables 4 and 5.

In order to write down explicitly $n_f(l^+)$ let us define:

- 1) $\sigma_f^T \equiv$ total cross section for the production of open (f, \bar{f}) pairs;

- ii) $\rho_{Mf}, \rho_{\bar{M}f}, \rho_{Bf}, \rho_{\bar{B}f} \equiv$ ratio between, the inclusive cross-section for producing ($M =$ meson, $\bar{M} =$ antimeson, $B =$ baryon, $\bar{B} =$ antibaryon) states, and the total cross section σ_f^T ;
- iii) $BR_{Mf'}, BR_{\bar{M}f'}, BR_{Bf'}, BR_{\bar{B}f'} \equiv$ semileptonic branching ratio of the various states with flavor f' ($f' = c, b, t, sb$);
- iv) $\epsilon_{Mf}(\ell_f^\pm), \epsilon_{\bar{M}f}(\ell_f^\pm), \epsilon_{Bf}(\ell_f^\pm), \epsilon_{\bar{B}f}(\ell_f^\pm) \equiv$ acceptance for ℓ^\pm from the leptonic decay of the flavor f' produced in the decay chain of the state with flavor f . This acceptance is a function of the lepton p_T and of the cut in $\theta < \theta_{cut}$ applied to the lepton polar angle.

Accordingly we have, for the case of "superbeauty":

$$n_{sb}(\ell^+) = \sigma_{sb}^T \left\{ \sigma_{Msb} \left[BR_{Mt} \epsilon_{Msb}(\ell_t^+) + BR_{Mc} \epsilon_{Msb}(\ell_c^+) \right] + \rho_{\bar{M}sb} \left[BR_{\bar{M}sb} \epsilon_{\bar{M}sb}(\ell_{sb}^+) + BR_{\bar{M}b} \epsilon_{\bar{M}sb}(\ell_b^+) \right] + \rho_{Bsb} \left[BR_{Bt} \epsilon_{Bsb}(\ell_t^+) + BR_{Bc} \epsilon_{Bsb}(\ell_c^+) \right] + \rho_{\bar{B}sb} \left[BR_{\bar{B}sb} \epsilon_{\bar{B}sb}(\ell_{sb}^+) + BR_{\bar{B}b} \epsilon_{\bar{B}sb}(\ell_b^+) \right] \right\}$$

and

$$n_{sb}(\ell^-) = \sigma_{sb}^T \left\{ \rho_{\bar{M}sb} \left[BR_{\bar{M}t} \epsilon_{\bar{M}sb}(\ell_t^-) + BR_{\bar{M}c} \epsilon_{\bar{M}sb}(\ell_c^-) \right] + \rho_{Msb} \left[BR_{Msb} \epsilon_{Msb}(\ell_{sb}^-) + BR_{Mb} \epsilon_{Msb}(\ell_b^-) \right] + \rho_{\bar{B}sb} \left[BR_{\bar{B}t} \epsilon_{\bar{B}sb}(\ell_t^-) + BR_{\bar{B}c} \epsilon_{\bar{B}sb}(\ell_c^-) \right] + \rho_{Bsb} \left[BR_{Bsb} \epsilon_{Bsb}(\ell_{sb}^-) + BR_{Bb} \epsilon_{Bsb}(\ell_b^-) \right] \right\} .$$

Table 4

Flavor	Decays producing ℓ^+	Decays producing ℓ^-
sb	$sb \rightarrow t + b + \ell^+$	$sb \rightarrow t + \ell^-$
	$sb \rightarrow t + b + c + s + \ell^+$	$sb \rightarrow t + b + c + \ell^-$
t	$t \rightarrow b + \ell^+$	$t \rightarrow b + c + \ell^-$
	$t \rightarrow b + c + s + \ell^+$	
b	$b \rightarrow c + s + \ell^+$	$b \rightarrow c + \ell^-$
c	$c \rightarrow s + \ell^+$	

Table 5

Antiflavor	Decays producing ℓ^+	Decays producing ℓ^-
$\bar{s}\bar{b}$	$\bar{s}\bar{b} \rightarrow \bar{t} + \ell^+$ $\bar{s}\bar{b} \rightarrow \bar{t} + \bar{b} + \bar{c} + \ell^+$	$\bar{s}\bar{b} \rightarrow \bar{t} + \bar{b} + \ell^-$ $\bar{s}\bar{b} \rightarrow \bar{t} + \bar{b} + \bar{c} + \bar{s} + \ell^-$
\bar{t}	$\bar{t} \rightarrow \bar{b} + \bar{c} + \ell^+$	$\bar{t} + \bar{b} + \ell^-$ $\bar{t} + \bar{b} + \bar{c} + \bar{s} + \ell^-$
\bar{b}	$\bar{b} \rightarrow \bar{c} + \ell^+$	$\bar{b} + \bar{c} + \bar{s} + \ell^-$
\bar{c}		$\bar{c} + \bar{s} + \ell^-$

The analogous expressions for $n_s(\ell^+)$, $n_b(\ell^+)$, $n_c(\ell^+)$ can be easily derived and are not reported here.

From the above formulas it can be seen that in order to evaluate the Asymmetry parameter A° one needs to know:

- i) the total cross section $\Rightarrow \sigma^T$;
- ii) the decay branching ratios $\Rightarrow BR$;
- iii) the production distribution of the baryons or mesons states $\Rightarrow \epsilon$;
- iv) the relative fraction of baryons and mesons $\Rightarrow \rho$;
- v) the lepton distribution in the decays $\Rightarrow \epsilon$.

We will now discuss in some detail the assumptions we made for these quantities.

5.1. The Total Cross Sections

We will extrapolate the total cross sections for the heavy flavors at the (pp) Collider energy, $\sqrt{s} = 540$ GeV, using formula (4) and starting from the strangeness cross section. Using the known masses for "charm" and "beauty" baryons and mesons, and the values:

$$m_t = 25 \text{ GeV}/c^2, \quad m_{sb} = 55 \text{ GeV}/c^2,$$

for the "top" and "superbeauty" particles, one obtains:

$$\sigma_c \approx 2000 \text{ } \mu\text{b}, \quad (6a)$$

$$\sigma_b \approx 140 \text{ } \mu\text{b}, \quad (6b)$$

$$\sigma_t \approx 1.5 \text{ } \mu\text{b}, \quad (6c)$$

$$\sigma_{sb} \approx 0.15 \text{ } \mu\text{b}. \quad (6d)$$

Other estimates, from perturbative QCD, will however be taken into account when discussing the results. It will be shown that, under some conditions, even these very low cross sections ($\sigma_b \approx 10\mu\text{b}$ and $\sigma_c \approx 0.1\mu\text{b}$) [14] give rise to a measurable Asymmetry.

5.2. The Decay Branching Ratios

Recent data from CLEO[15] give for the semileptonic branching ratio of the "beauty" mesons:

$$(M_b \rightarrow \ell^+) / (M_b \rightarrow \text{all}) \approx 0.13.$$

In our Monte Carlo we assume the known semileptonic branching ratios for "charm":

$$(D \rightarrow \ell^+) / (D \rightarrow \text{all}) \approx 0.085,$$

$$(\Lambda_c^+ \rightarrow \ell^+) / (\Lambda_c^+ \rightarrow \text{all}) \approx 0.045.$$

and the conservative value of 0.1 for all other heavier particles.

5.3. The Production Distributions of Baryon and Meson States

The study of the reactions:

$$pp \rightarrow D + e^- + \text{anything},$$

$$pp \rightarrow \Lambda_c^+ + e^- + \text{anything},$$

$$pp \rightarrow \Lambda_b^0 + e^+ + \text{anything},$$

at the ISR, indicate that in baryon-baryon collisions the heavy flavored baryons are produced according to a rather flat x-distribution:

$$(d\sigma/dx) \approx \text{const.},$$

while the heavy flavored mesons are produced with softer x-distribution of the type:

$$E(d\sigma/d|x|) \approx (1 - |x|)^3.$$

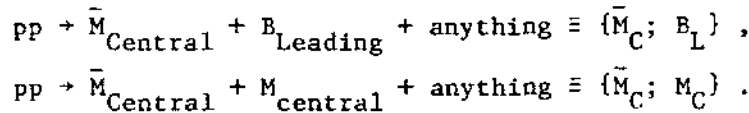
These distributions will be assumed all along the following discussion, together with the p_T dependence:

$$(d\sigma/dp_T) \approx p_T \exp(-2.5 p_T)$$

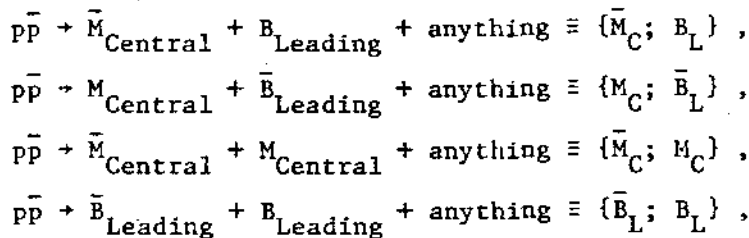
observed at the ISR in the production of heavy flavors[16,17].

5.4. The Relative Yield of Mesons and Baryons

From the data on strangeness production at the ISR, it can be assumed that, in (pp) collisions the following reactions dominate



In (p \bar{p}) collisions, due to the anti-baryonic nature of the p hemisphere, the following reactions can take place:



In this case, the ratio of the inclusive cross sections for producing the four classes of particles \bar{M}_C , M_C , \bar{B}_L and B_L and the total cross sections are:

$$\begin{aligned} \rho_M &= \left[\sigma\{M_C; \bar{B}_L\} + \sigma\{\bar{M}_C; M_C\} \right] / \sigma^T , \\ \rho_{\bar{M}} &= \left[\sigma\{\bar{M}_C; B_L\} + \sigma\{M_C; M_C\} \right] / \sigma^T , \\ \rho_B &= \left[\sigma\{\bar{M}_C; B_L\} + \sigma\{\bar{B}_L; B_L\} \right] / \sigma^T , \\ \rho_{\bar{B}} &= \left[\sigma\{M_C; \bar{B}_L\} + \sigma\{B_L; B_L\} \right] / \sigma^T , \end{aligned}$$

with

$$\sigma^T = \sigma\{\bar{M}_C; B_L\} + \sigma\{M_C; \bar{B}_L\} + \sigma\{\bar{M}_C; M_C\} + \sigma\{\bar{B}_L; B_L\} .$$

Defining the ratio:

$$\text{Leading/Total} = \rho_B$$

the four inclusive cross sections can be written as:

$$\begin{aligned} \rho_B &= \rho_{\bar{B}} = (\text{Leading/Total}) , \\ \rho_M &= \rho_{\bar{M}} = [1 - (\text{Leading/Total})] . \end{aligned}$$

At ISR, in each hemisphere, the ratio (Leading/Total) is $\sim 1/16$ for strangeness and $\sim 1/8$ for "charm". In our discussion we will study the behavior of A° as a function of (Leading/Total).

5.5. The Lepton Decay Distributions

The data from CLEO[18] show that in the semileptonic decay of "beauty" mesons, M_b , the magnitude of the mass recoiling with respect to the leptons is very near to the D mass:

$$M_b \rightarrow X + \ell, \quad \text{with } M_X - M_D \approx 2.0 \text{ GeV}/c^2.$$

Moreover, the mean charged multiplicity of the decay is 3.5, where the D contributes with 2.5 charged particles on average. We can conclude that, even at values of the mass as high as the mass of the M_b , the semileptonic decay proceeds via a 3-body decay. On the contrary, the mean charged multiplicity in the hadronic decays of the M_b mesons is 6.3, i.e. the hadronic decay of the M_b produces, on average, one D plus four charged particles plus two neutral particles:

$$M_b \rightarrow D + 6\text{-bodies}.$$

In the following we will consider two possibilities:

- i) the total multiplicity of all decays is 3: this is the worst case for the Asymmetry A° ;
- ii) the total multiplicity of all semileptonic decay is 3 and the decay is $K_{\ell 3}$ -like for mesons and phase-space for baryons, while the total multiplicity of all the hadronic decays have the known values for "charm" and "beauty" (.3 for "charm", . charm + 6 for "beauty"), and, for "top" and "superbeauty", the same multiplicity as "beauty". It should be noted that this is already a conservative hypothesis, since the hadronic decays of "top" and "superbeauty" can be expected to produce more particles than "beauty". Higher values of multiplicity would produce higher values for the asymmetry.

5.6. Estimates of the Asymmetry A°

In order to estimate the Asymmetry A° , we have restricted our study to the case of electrons and positrons.

The detection acceptances ϵ have been evaluated by means of a Monte Carlo simulation, with the conditions set in the previous section and for 5 values of θ_{cut} ($\theta_{\text{cut}} = 10^\circ, 20^\circ, 30^\circ, 40^\circ$ and 90°).

Figures from 16a to 16t show the e^\pm acceptances for $\theta_{\text{cut}} = 30^\circ$ and model (ii) of section 5.5 for baryons, mesons and antimésons. The acceptances for e^\pm originated by the decay of antibaryons are, of course, negligible.

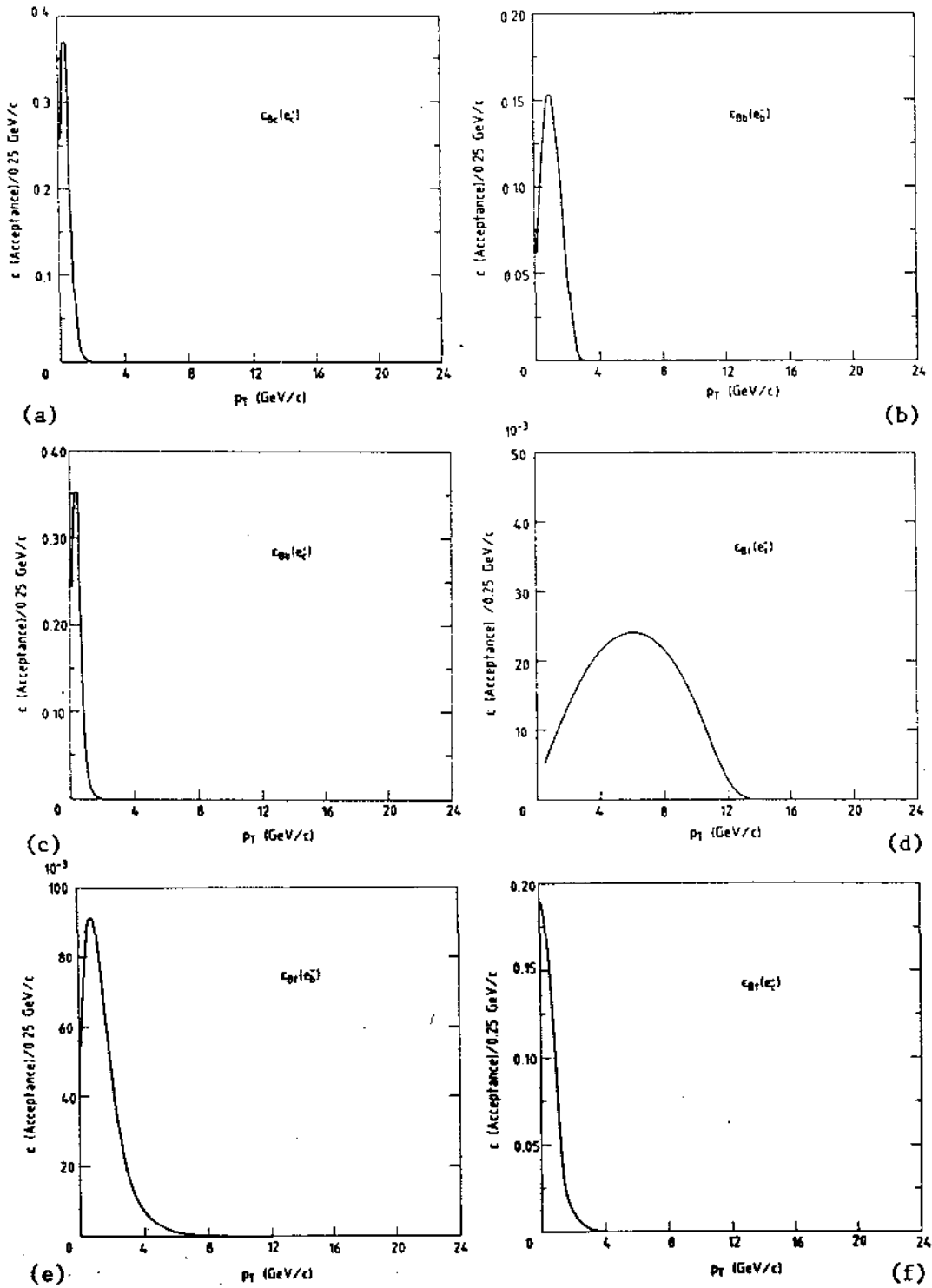


Fig. 16. (a) to (f): Acceptances ϵ for the various states and decay chains.

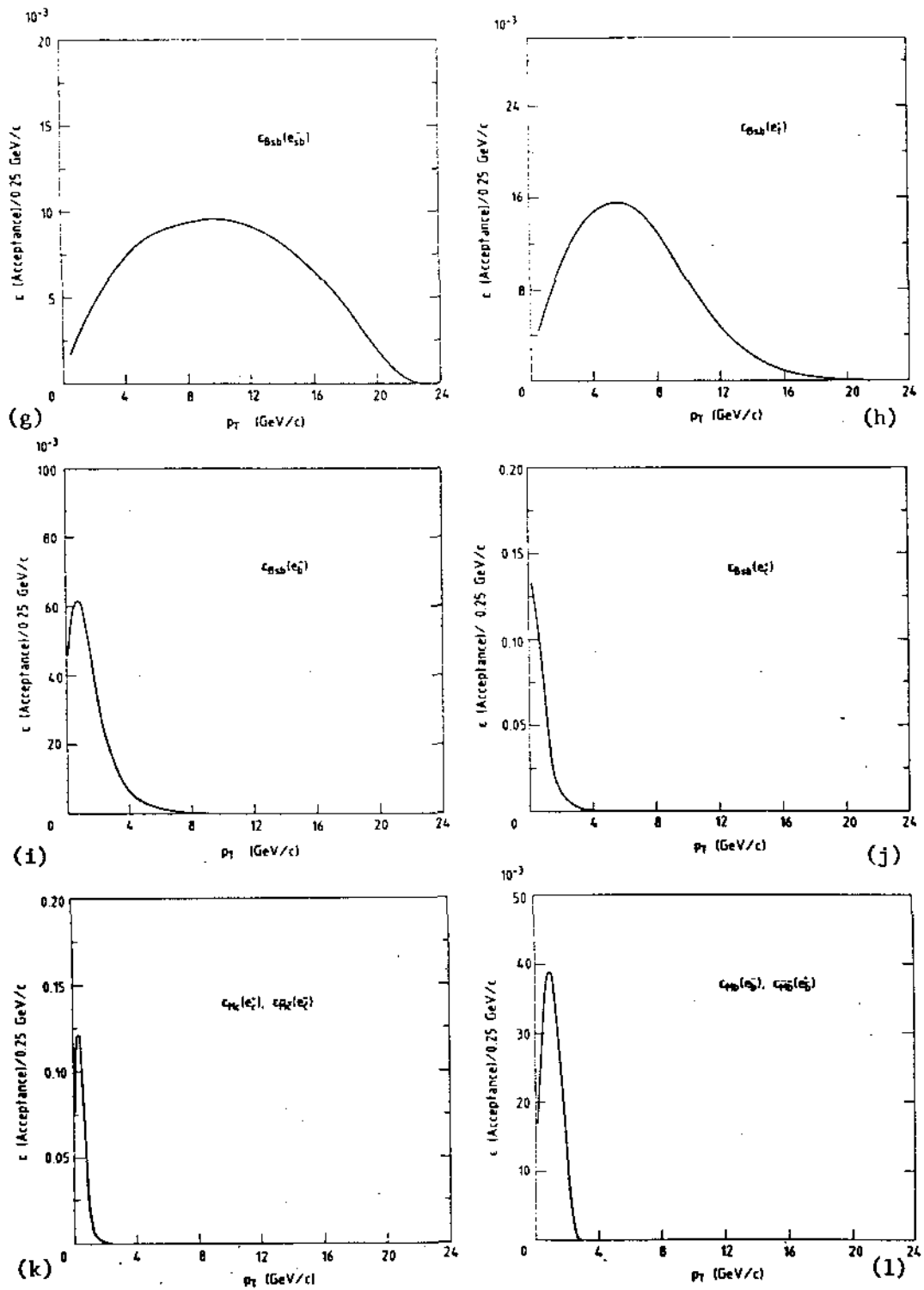


Fig. 16. (g) to (l): Acceptances ϵ for the various states and decay chains.

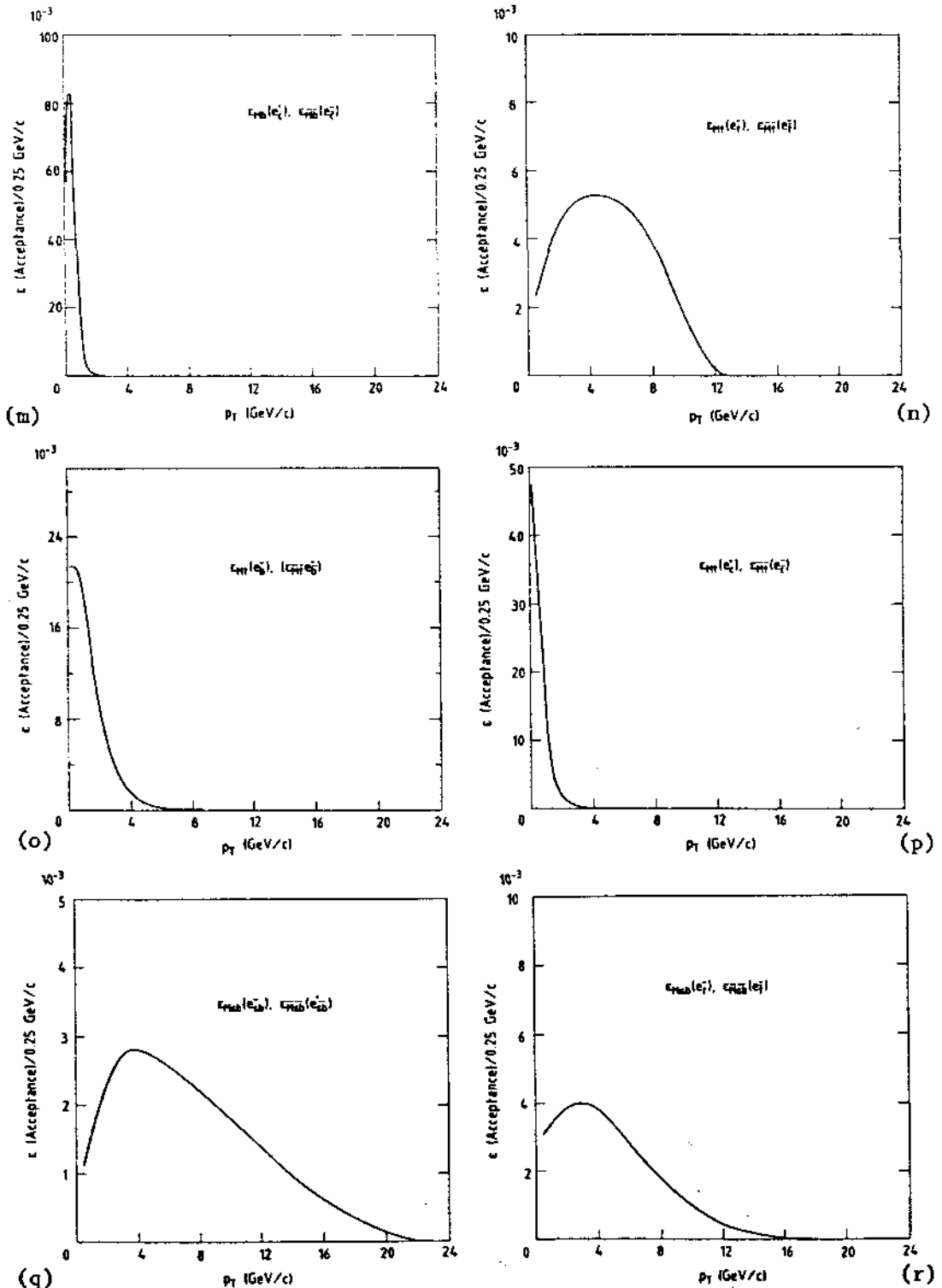


Fig. 16. (m) to (r): Acceptances ϵ for the various states and decay chains.

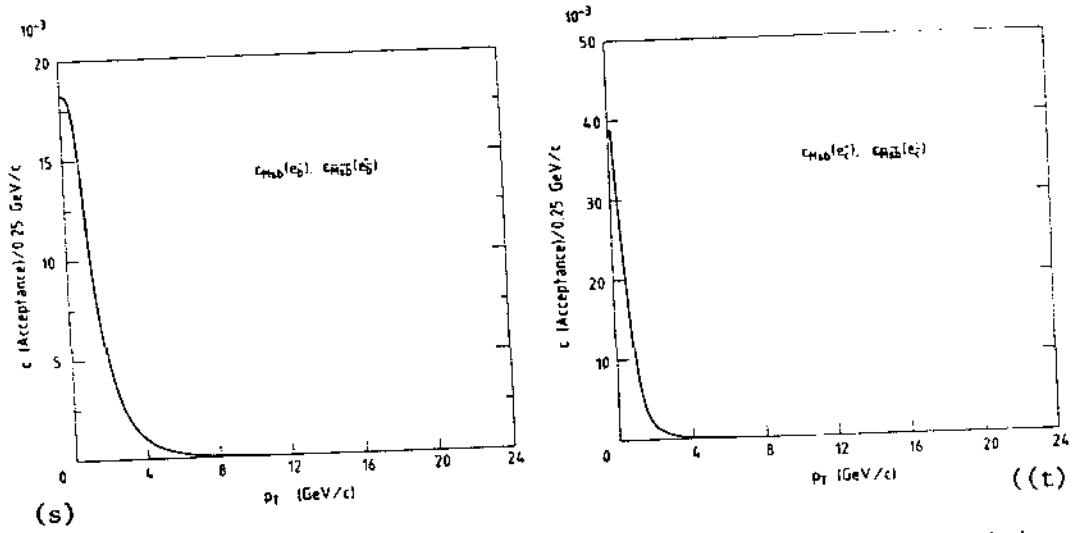


Fig. 16. (s) to (t): Acceptances ϵ for the various states and decay chains.

Figure 17 shows the behavior of $A^{\circ}(p_T, 30^{\circ})$, for (Leading/Total) = 0.25 and model (ii) of section 5.5. There are two main peaks, one positive around $p_T = 10$ GeV/c, due to the "top" baryon decay into e^+ , and one negative around $p_T = 19$ GeV/c, due to "superbeauty" baryon decay into e^- .

It is interesting to note that the separation between the two peaks depends only on the mass differences in the semileptonic decays of "superbeauty" and "top" states.

In fact in the 3-body semileptonic decay the transverse momentum spectrum of the electrons or positrons scales with $p_T/\Delta m$ where Δm is the difference between the parent mass and mass of the hadronic particle produced in the decay. This is shown in Figure 18 where the normalized $p_T/\Delta m$ spectra of the electrons and positrons produced in the decays:

- i) $\Lambda_{sb}^0 \rightarrow \Lambda_c^+ e^- \bar{\nu}$;
- ii) $\Lambda_c^+ \rightarrow \Lambda_b^0 e^+ \nu$;
- iii) $\Lambda_b^0 \rightarrow \Lambda_c^+ e^- \bar{\nu}$;
- iv) $\Lambda_c^+ \rightarrow \Lambda_s^0 e^+ \nu$;

are reported.

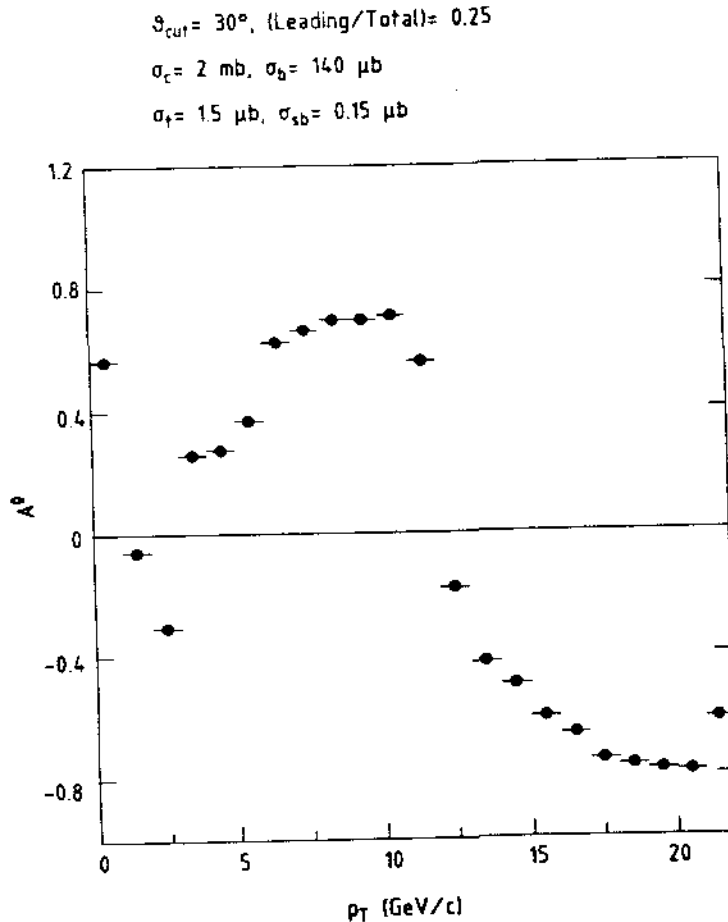


Fig. 17. Plot of $A^0(p_T, \theta_{\text{cut}} = 30^\circ)$ as a function of p_T . The values assumed for the cross sections and for (Leading/Total) are indicated in the figure.

The mass differences Δm have the following values:

- i) $\Delta m = m(\Lambda_{sb}^0) - m(\Lambda_t^+) \approx 30 \text{ GeV}/c^2$ for the "sb" baryon decay;
- ii) $\Delta m = m(\Lambda_t^+) - m(\Lambda_b^0) \approx 19.5 \text{ GeV}/c^2$ for the "t" baryon decay;
- iii) $\Delta m = m(\Lambda_b^0) - m(\Lambda_c^+) \approx 3.2 \text{ GeV}/c^2$ for the "b" baryon decay;
- iv) $\Delta m = m(\Lambda_c^+) - m(\Lambda_s^0) \approx 1.2 \text{ GeV}/c^2$ for the "c" baryon decay;

Figures 19a, b and 20a, b show the amplitude of the two peaks as a function of θ_{cut} and (Leading/Total) for: a) model (i) of section 5.5 (all 3-body decays) and: b) model (ii) of section 5.5 (greater multiplicity for the hadronic decays).

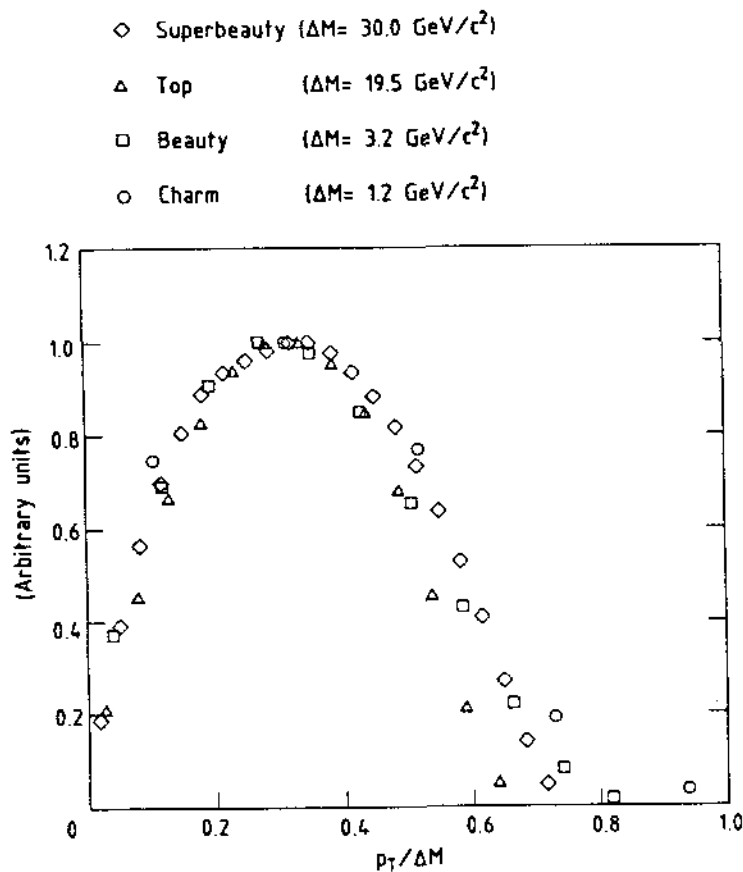


Fig. 18. Normalized $(p_T/\Delta M)$ spectra of the electrons from the decays: $\Lambda_{sb}^0 \rightarrow \Lambda_t^+ e^- \bar{\nu}$; $\Lambda_t^+ \rightarrow \Lambda_b^0 e^+ \nu$; $\Lambda_b^0 \rightarrow \Lambda_c^+ e^- \bar{\nu}$; $\Lambda_c^+ \rightarrow \Lambda_{sb}^0 e^+ \nu$. The Δm values relative to the four decays are indicated in the figure.

5.7. Background Evaluation

In what has been described so far, the background contamination in the sample of prompt e^+ and e^- has not been considered. It is mainly due to:

- i) the misidentification of charged and neutral hadrons in the experimental apparatus;
- ii) the prompt e^+ or e^- production from sources other than open heavy flavor states.

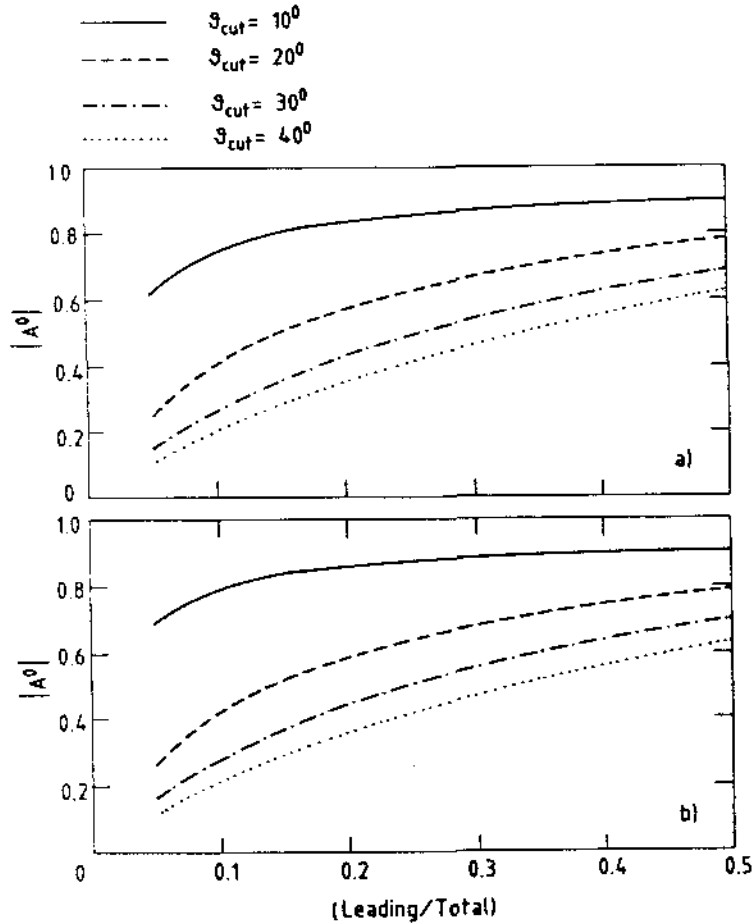


Fig. 19. Plot of $A^0(p_T = 10 \text{ GeV}/c, \theta_{\text{cut}})$ ("top" peak) as a function of (Leading/Total) for different values of θ_{cut} , and using: a) model (i) of section 5.5, and b) model (ii) of section 5.5.

The contribution (i) can be derived by extrapolating, above $p_T \approx 10 \text{ GeV}/c$ the inclusive pion cross section as measured by the UAI experiment[19], using the fit to their data:

$$E(d^3\sigma/dp^3) = A \times p_0^n / (p_0 + p_T)^n \quad (7)$$

with $A = 0.46 \pm 0.10 \text{ mb}^2 c^2 \text{ GeV}^{-2}$, $p_0 = 1.3 \pm 0.18 \text{ GeV} c^{-1}$ and $n = 9.14 \pm 0.77$.

Formula (7) is relative only to charged pions (averaged over the two charges) and is given in unit of rapidity. We have assumed the contribution to the background due to the neutral pions to be 0.2 of

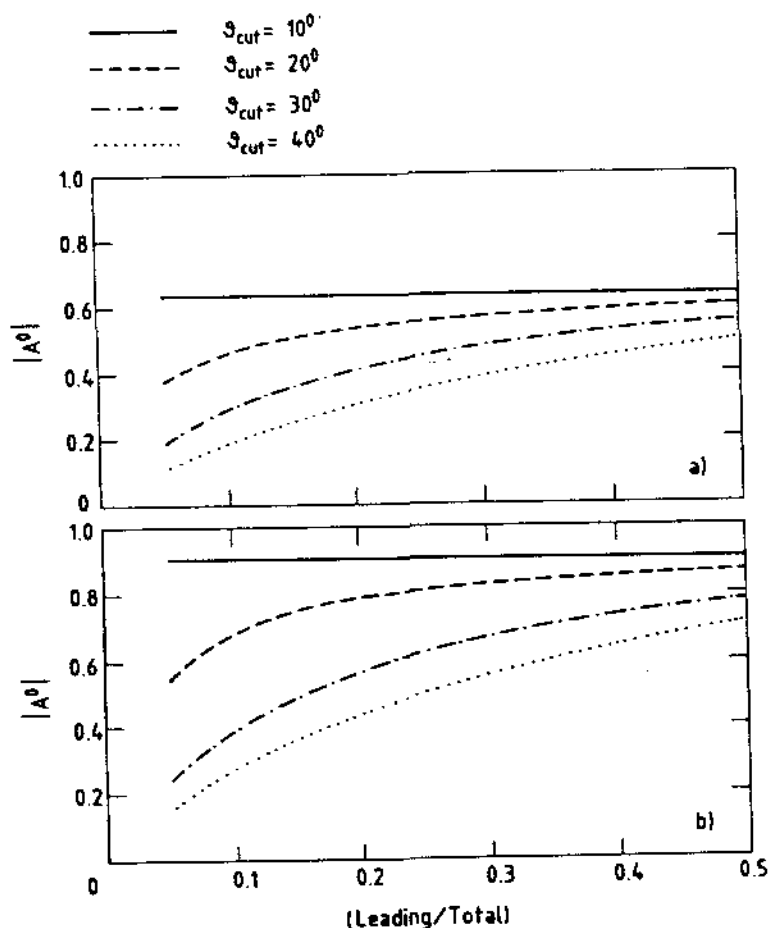


Fig. 20. Plot of $A^0(p_T = 19 \text{ GeV}/c, \theta_{\text{cut}})$ ("superbeauty" peak) as a function of (Leading/Total) for different values of θ_{cut} , and using: a) model (i) of section 5.5, and b) model (ii) of section 5.5.

the cross section (7). The rapidity interval over which we integrated the background depends on the θ_{cut} :

$$\begin{aligned} \theta_{\text{cut}} = 90^\circ &\Rightarrow \Delta y \approx 4.0, \\ \theta_{\text{cut}} = 40^\circ &\Rightarrow \Delta y \approx 3.0, \\ \theta_{\text{cut}} = 30^\circ &\Rightarrow \Delta y \approx 2.7, \\ \theta_{\text{cut}} = 20^\circ &\Rightarrow \Delta y \approx 2.3, \\ \theta_{\text{cut}} = 10^\circ &\Rightarrow \Delta y \approx 1.5. \end{aligned}$$

The extrapolated background rates should be multiplied by a reduction factor representing the rejection of the background from source (i) in the experimental apparatus.

Concerning the prompt electron background (ii), we assume, as a first approximation, that it would be negligible when compared with the contribution (i).

5.8. Estimate of the Asymmetry Parameter Inclusive of Background

Due to the background sources described in the previous section, the experimental Asymmetry parameter is given by:

$$A^{\text{exp}}(p_T, \theta_{\text{cut}}) = \frac{[N(e^+) + N_{\text{bg}}(e^+)] - [N(e^-) + N_{\text{bg}}(e^-)]}{[N(e^+) + N_{\text{bg}}(e^+)] + [N(e^-) + N_{\text{bg}}(e^-)]}$$

where $N_{\text{bg}}(e^\pm)$ is the number of background positrons or electrons. A^{exp} can then be expressed as a function of A° and of the Signal-to-Background ratio defined as:

$$\frac{\text{Signal}}{\text{Background}} \equiv \frac{N(e^\pm)}{N_{\text{bg}}(e^\pm)}$$

by assuming $N_{\text{bg}}(e^+) = N_{\text{bg}}(e^-) = N_{\text{bg}}(e)$ and by substituting, in turns, in the above equation of A^{exp} , the expression of $N(e^-)$ and $N(e^+)$ derived from the definition of A° . The result is:

$$A^{\text{exp}} = \frac{A^\circ}{1 + \frac{1 + A^\circ}{N(e^+)/N_{\text{bg}}(e)}}, \quad \text{for } A^\circ > 0 ;$$

$$A^{\text{exp}} = \frac{A^\circ}{1 + \frac{1 - A^\circ}{N(e^-)/N_{\text{bg}}(e)}}, \quad \text{for } A^\circ < 0 ;$$

Figure 21 shows the quantity A^{exp} plotted as a function of the Signal/Background ratio for various values of A° . The results can be expressed with curves of constant A^{exp} as function of (rejection power) versus (cross section for "top" and "superbeauty" production), for different θ_{cut} , (Leading/Total) and decay models (Figures 22 to 31).

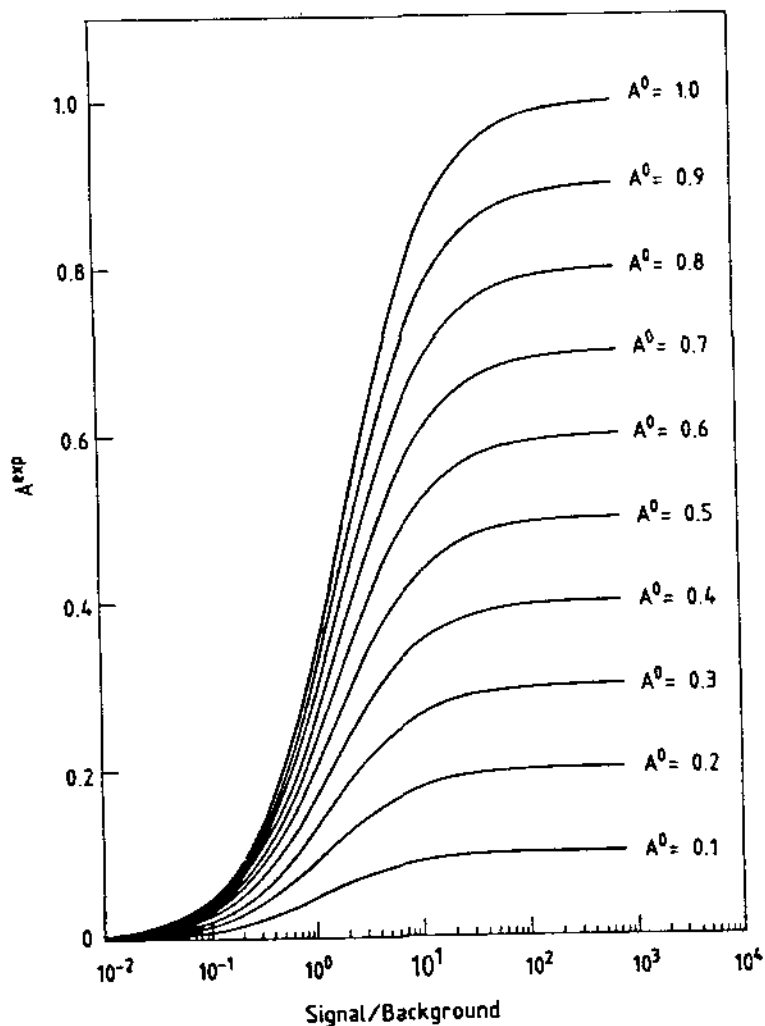


Fig. 21. The curves give the behavior of A^{exp} as a function of Signal/Background, for different values of A^0 .

The Table 6 summarizes results given in Figures 22 to 31, for two values of the total cross section. They show the rejection powers needed to obtain $A^{\text{exp}} > 0.3$ or $A^{\text{exp}} < -0.3$, i.e. a reasonably high value for the Asymmetry, at the "top" and "superbeauty" peaks respectively. It can be seen that, with a rejection power of the order of 10^{-3} , a large range of θ_{cut} , (Leading/Total) and cross section values are accessible.

Table 6

$P_T = 10 \text{ GeV}$						
Cross section estimates						
θ_{cut}	(Leading/ Total)	$\sigma_t = 1.5 \mu\text{b}$		$\sigma_t = 0.1 \mu\text{b}$		
		$\sigma_{\text{sb}} = 0.15 \mu\text{b}$		$\sigma_{\text{sb}} = 0.01 \mu\text{b}$		
		(formula (9))		(perturbative QCD)		
		Model (i)	Model (ii)	Model (i)	Model (ii)	
10°	0.1	3.0	3.5	0.2	0.3	
	0.25	10.0	12.0	0.6	0.7	
	0.5	15.0	18.0	1.0	1.3	
20°	0.1	1.3	1.5	0.1	0.1	
	0.25	8.0	9.0	0.5	0.6	
	0.5	20.0	23.0	1.0	1.2	
30°	0.1	-	-	-	-	
	0.25	6.0	7.0	0.4	0.4	
	0.5	19.0	22.0	1.0	1.2	
40°	0.1	-	-	-	-	
	0.25	3.5	4.8	0.3	0.3	
	0.5	17.0	21.0	1.0	1.1	
$P_T = 19 \text{ GeV/c}$						
10°	0.1	0.4	1.0	0.02	0.1	
	0.25	0.9	2.5	0.1	0.2	
	0.5	1.7	4.5	0.1	0.3	
20°	0.1	2.5	5.5	0.2	0.4	
	0.25	10.0	20.0	0.5	1.0	
	0.5	25.0	50.0	1.3	2.2	
30°	0.1	-	2.2	-	0.2	
	0.25	9.0	25.0	0.6	1.1	
	0.5	23.0	45.0	1.6	2.0	
40°	0.1	-	-	-	-	
	0.25	4.0	19.0	0.3	1.0	
	0.5	20.0	40.0	1.5	2.0	

Rejection power in units of 10^{-3} .

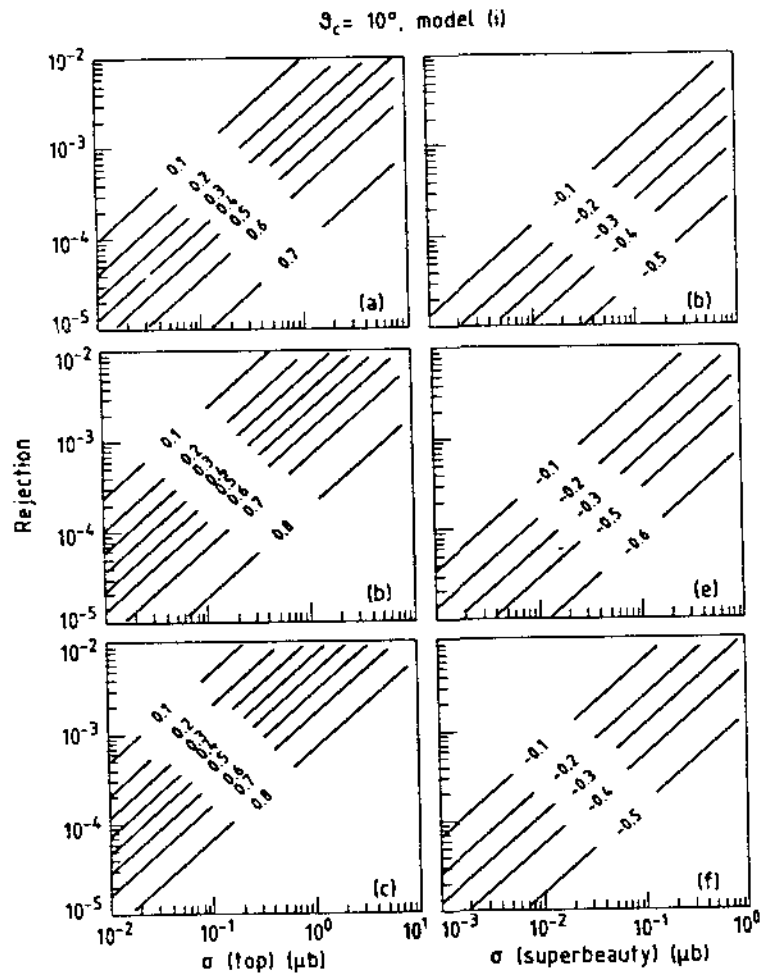


Fig. 22. Curves of constant A^{exp} , in the plot (rejection power) versus (cross section for "top" or "superbeauty") for $\theta_{\text{cut}} = 10^\circ$ and for model (i). Plots (a), (b) and (c) refers to $p_T = 10$ GeV/c ("top" peak), plots (d), (e) and (f) refers to $p_T = 19$ GeV/c ("superbeauty" peak). Plots (a) and (d) are obtained with (Leading/Total) = 0.1, plots (b) and (e) with (Leading/Total) = 0.25, plots (c) and (f) with (Leading/Total) = 0.5.

5.9. A Detailed Case

As an example of what can be obtained experimentally in terms of the Asymmetry A^{exp} , let us fix in a reasonable way some of the parameters. We take (as in Figures 29b and e):

- i) (Leading/Total) = 0.25;
- ii) $\theta_{\text{cut}} = 30^\circ$;
- iii) decay model (ii).

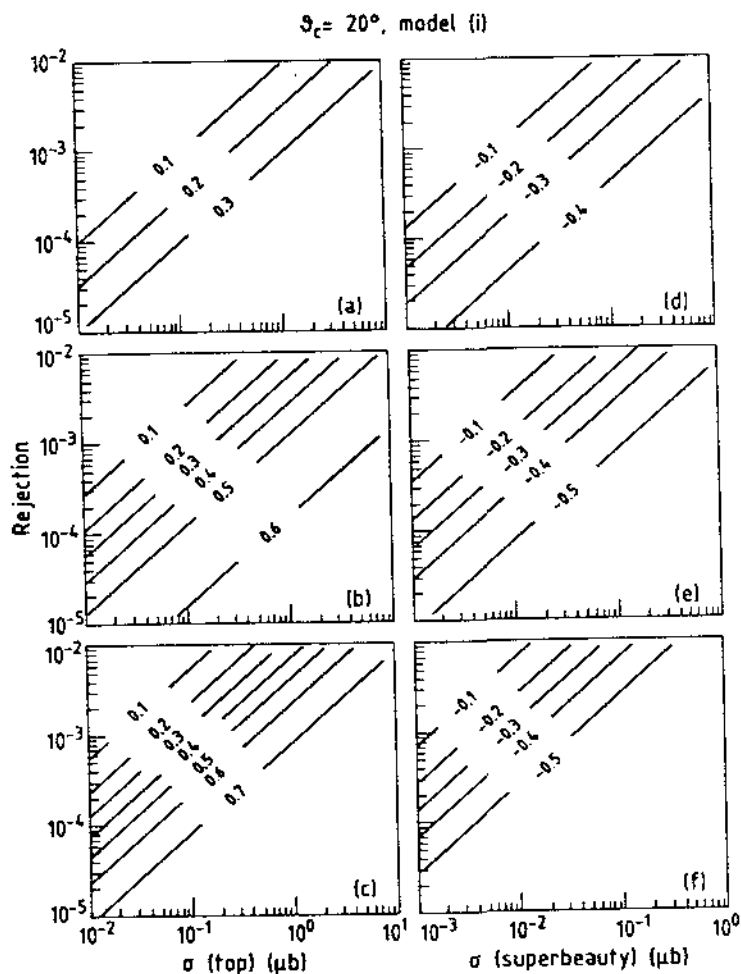


Fig. 23. As Figure 22 but for $\theta_{\text{cut}} = 20^\circ$ and model (1).

Moreover, in order to have an estimate for the experimental errors on A^{exp} , we assume a total integrated luminosity $L = 300 \text{ nb}^{-1}$ (foreseen for 1983 at the CERN (pp) Collider).

Figures 32a and 32b show the plot of A^{exp} as a function of p_T , for a rejection power of 10^{-3} and for the two cross section estimates: as in section 5.1 (formula (6)) and as from perturbative QCD ($\sigma_t : \sigma_{\text{sb}} = 10:1$), respectively. The errors are purely statistic.

Figures 33a and 33b show the expected number of produced electrons as a function of p_T , with the same two assumptions for the total cross sections. Superimposed is the expected background, as defined in section 5.7, and with a rejection factor of 10^{-3} .

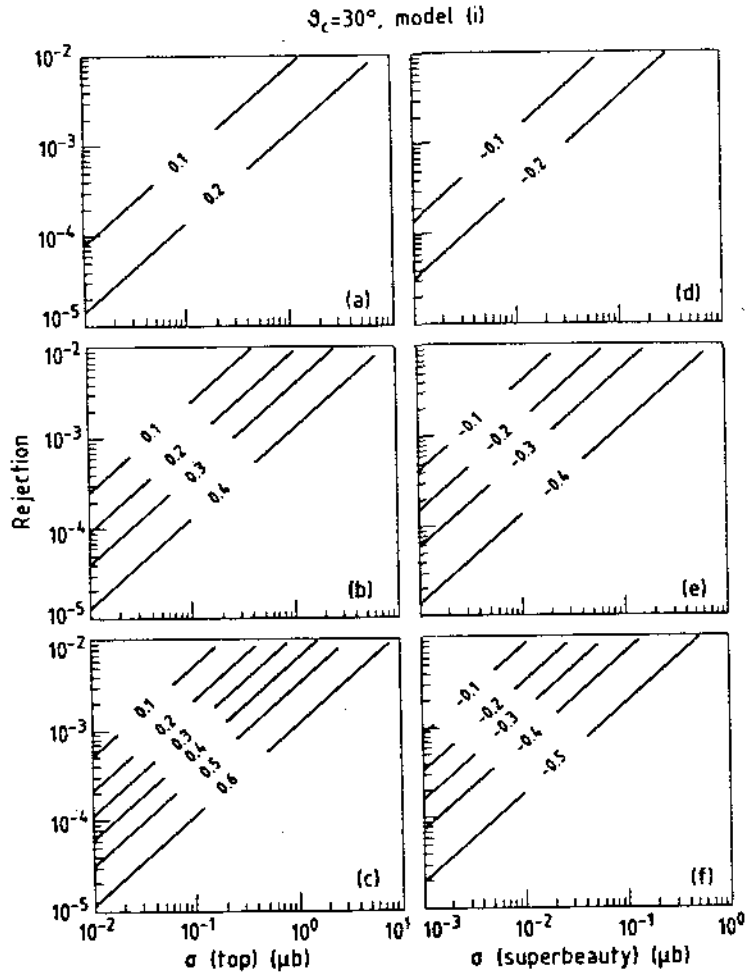


Fig. 24. As Figure 22 but for $\theta_{\text{cut}} = 30^\circ$ and model (i).

It could be that the rejection factor needed is much less than 10^{-3} . In fact, a very heavy state (such as Λ_t^+ or Λ_{sb}^0) decaying semi-leptonically, may have the hadronic "jet" recoiling against the lepton pair. The study of the hadronic pattern associated with the (e^-) could be of such an help in the selection of good events, that a rejection power much below 10^{-3} could be sufficient. For example, an order of magnitude improvement would mean that the data which, at present, are quoted with a rejection of order 10^{-3} (Figures 22-34), would reach the level of 10^{-4} . In this case, all our expectations would be scaled by this factor.

For completeness, let us mention that, at present, the (e/π) ratio in the p_T range above ~ 20 GeV is not known at the ($p\bar{p}$) Collider.

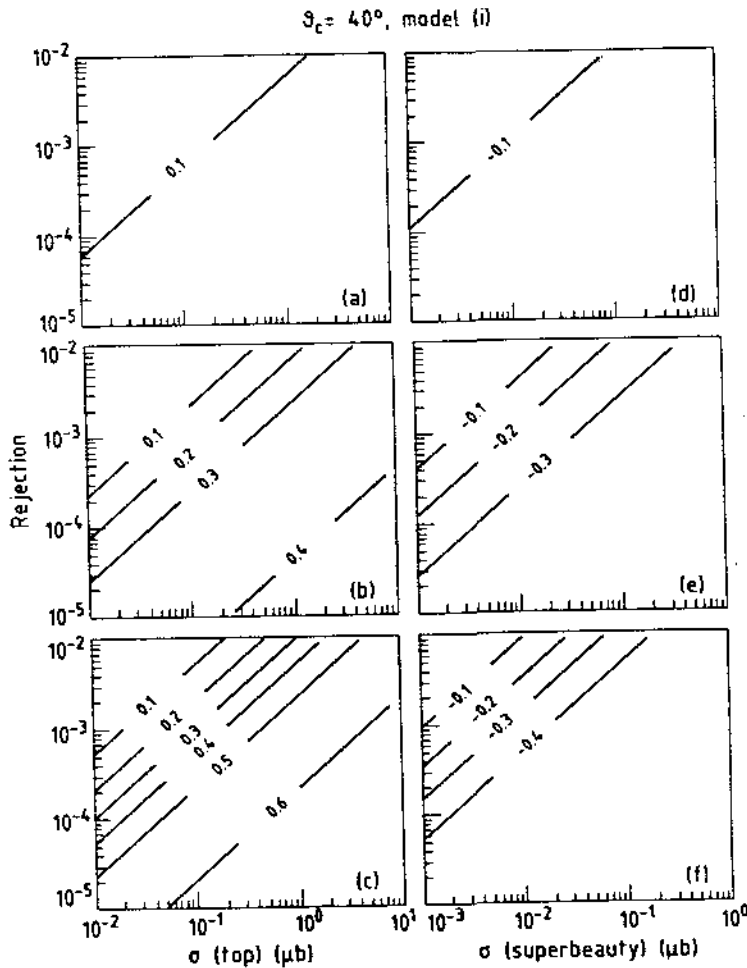


Fig. 25. As Figure 22 but for $\theta_{\text{cut}} = 40^\circ$ and model (i).

In order to compute the statistical significance of the observed effect, it is convenient to integrate A^{exp} over the p_T ranges:

- i) $7 < p_T < 12$ GeV/c, corresponding to the "top" region;
- ii) $14 < p_T < 23$ GeV/c, corresponding to the "superbeauty" region.

This is equivalent to the experimental procedure of fitting the data to reduce the statistical errors on the single points.

Figures 34a and 34b show the number of standard deviations that can be obtained in the measurement of A^{exp} , respectively in the "top" and in the "superbeauty" regions, as function of the total cross sections σ_t and σ_{sb} , in the same conditions specified above. The 90% confidence level in the measurement is also shown. These results show that, especially in the "top" case, a high statistical significance can be reached with a moderate rejection power, even if the total cross section for "top" production is as low as $0.1 \mu\text{b}$, i.e. the value predicted by QCD.

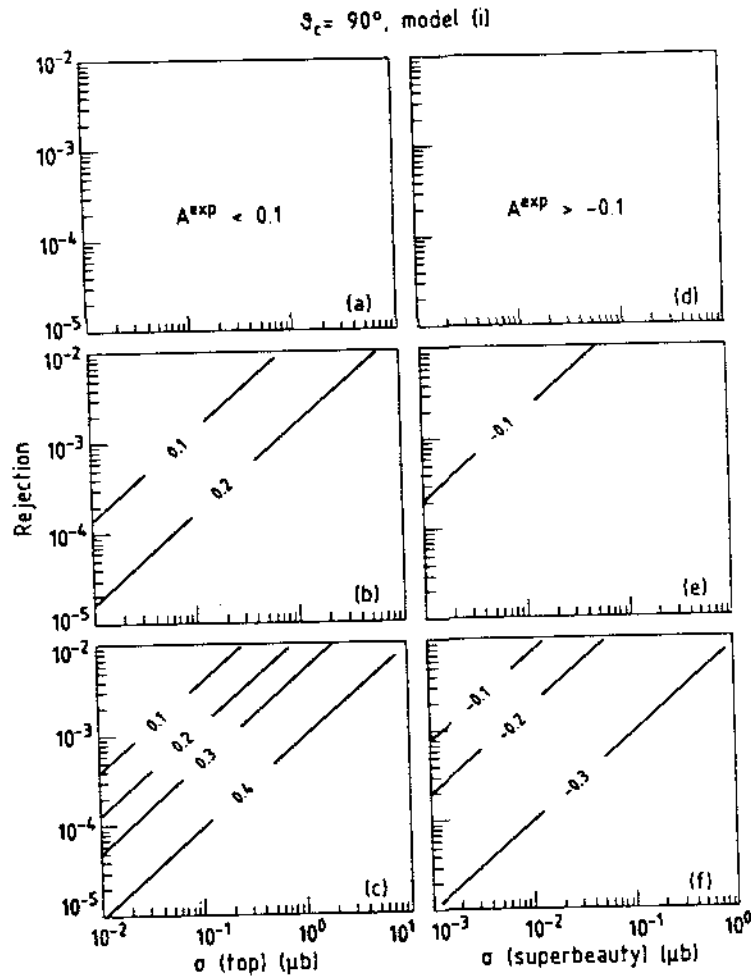


Fig. 26. As Figure 22 but for $\theta_{\text{cut}} = 90^\circ$ and model (i).

In Figure 35, the behavior of the ratio (Signal/Background) as a function of the total cross section for "top" and "superbeauty" and for different values of the rejection power, is shown.

6. COMPARISON WITH PRELIMINARY DATA FROM CERN ($p\bar{p}$) COLLIDER

As a first step in the study of the heavy-quark physics using the ($p\bar{p}$) Collider, we propose to compare our predictions with the data already available from the ($p\bar{p}$) Collider.

In their search for electron candidates, the UAI Collaboration finds 16 events with an isolated electron [20]. Five of these events are attributed to W^- decay, whilst the remaining 11 are characterized by a "jet activity" in the azimuthal region opposite the isolated

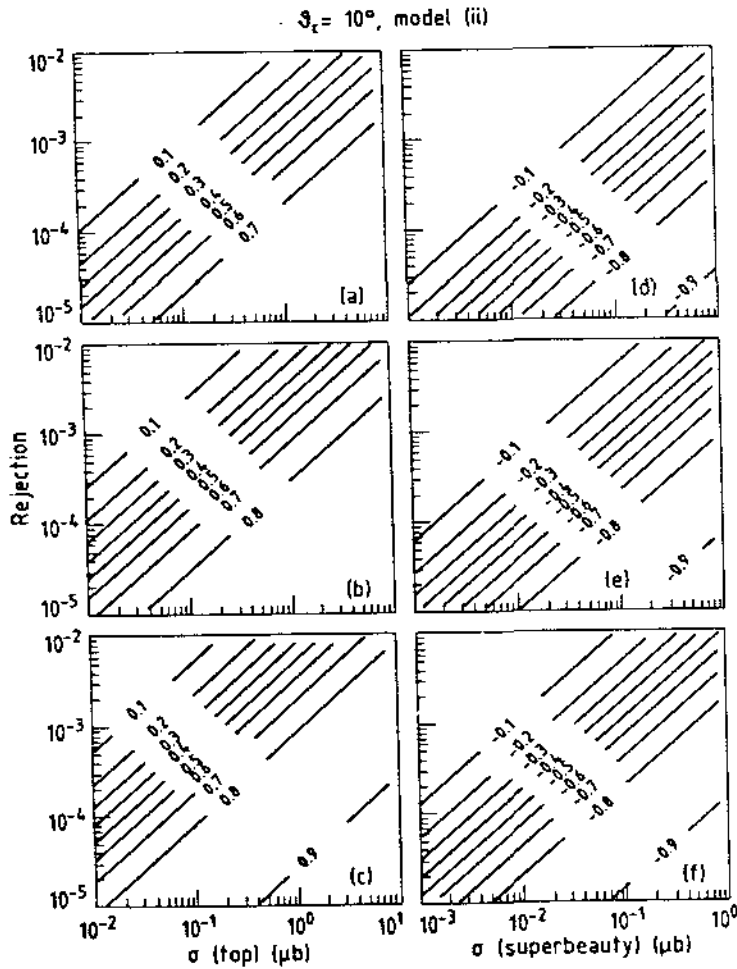


Fig. 27. As Figure 22 but for $\theta_{\text{cut}} = 10^\circ$ and model (ii).

electron. The events correspond to a total integrated luminosity of $L = 20 \text{ nb}^{-1}$.

According to the Monte Carlo discussed in detail in the previous section, the acceptance for electrons originating from "superbeauty" decays in the phase-space region defined by the UA1 data ($p_T > 15 \text{ GeV}/c$ and, for the polar angle, $25^\circ < \theta < 155^\circ$) is, for baryon and antibaryon decays,

$$\epsilon_B(e^\pm) = 0.08 ,$$

and the meson and antimeson decays

$$\epsilon_M(e^\pm) = 0.12 .$$

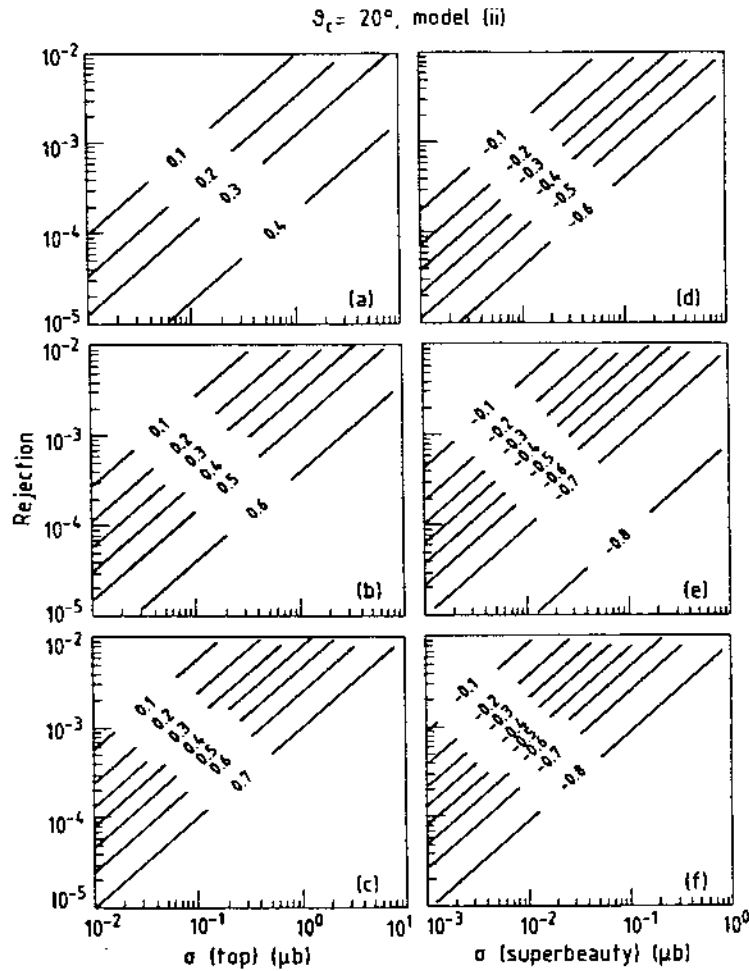


Fig. 28. As Figure 22 but for $\theta_{\text{cut}} = 20^\circ$ and model (ii).

We can therefore use the approximation

$$\epsilon(e^\pm) = \epsilon_B(e^\pm) = \epsilon_M(e^\pm) = 0.1 .$$

Since the heavy flavors are produced in pairs, the total efficiency for seeing at least one electron from the leptonic decay of "superbeauty" is

$$\epsilon_T(e^\pm) = 2 \times \epsilon(e^\pm) = 0.2 ,$$

where we have assumed equal semileptonic branching ratios for baryon and meson decays.

The request for "jet activity" opposite in azimuth to the electron gives rise to another acceptance factor, $\epsilon_T(\text{jet})$, which we

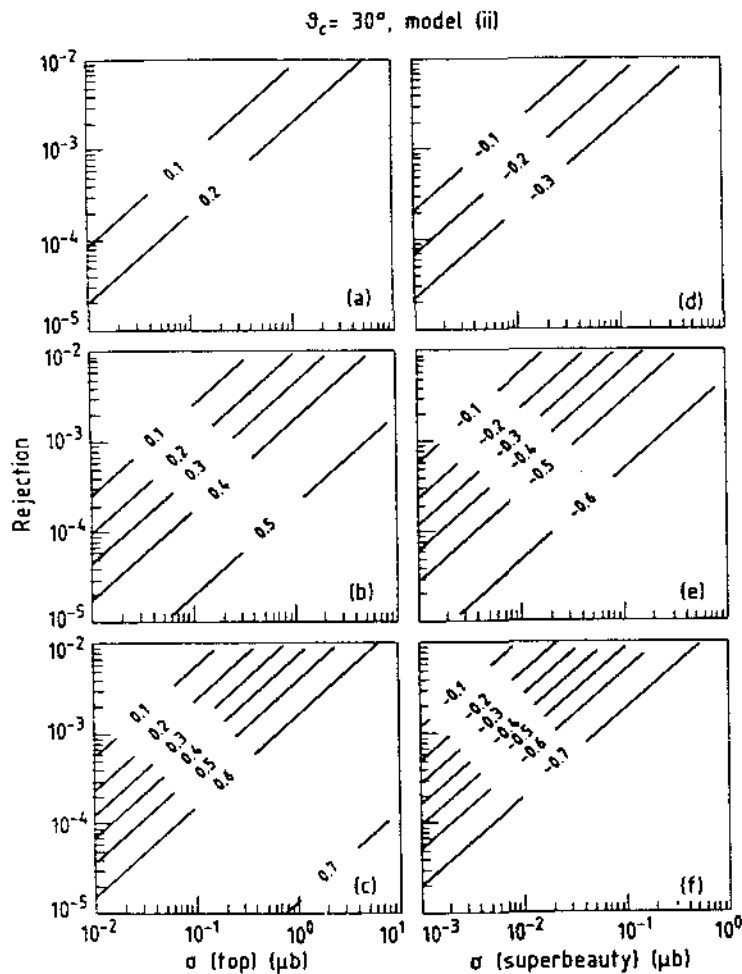


Fig. 29. As Figure 22 but for $\theta_{\text{cut}} = 30^\circ$ and model (ii).

can derive by analyzing the hadronic pattern of the "superbeauty" semileptonic decays predicted by our Monte Carlo, according to the "jet" definition outlined by the UA1 Collaboration, i.e.

- i) all particles with $p_T > 2.5 \text{ GeV}/c$ are associated with a jet if their separation in phase-space is

$$\Delta R = \sqrt{(\Delta\phi)^2 + (\Delta\eta)^2} < 1 ,$$

with $\Delta\phi$ in radians and $\eta (= \text{pseudorapidity}) = -\ln(\text{tg}\theta/2)$;

- ii) all other particles are associated with the jet defined as in point (i), if they satisfy the conditions

p_T relative to the jet $< 1 \text{ GeV}/c$,
 θ^T relative to the jet $< 45^\circ$;

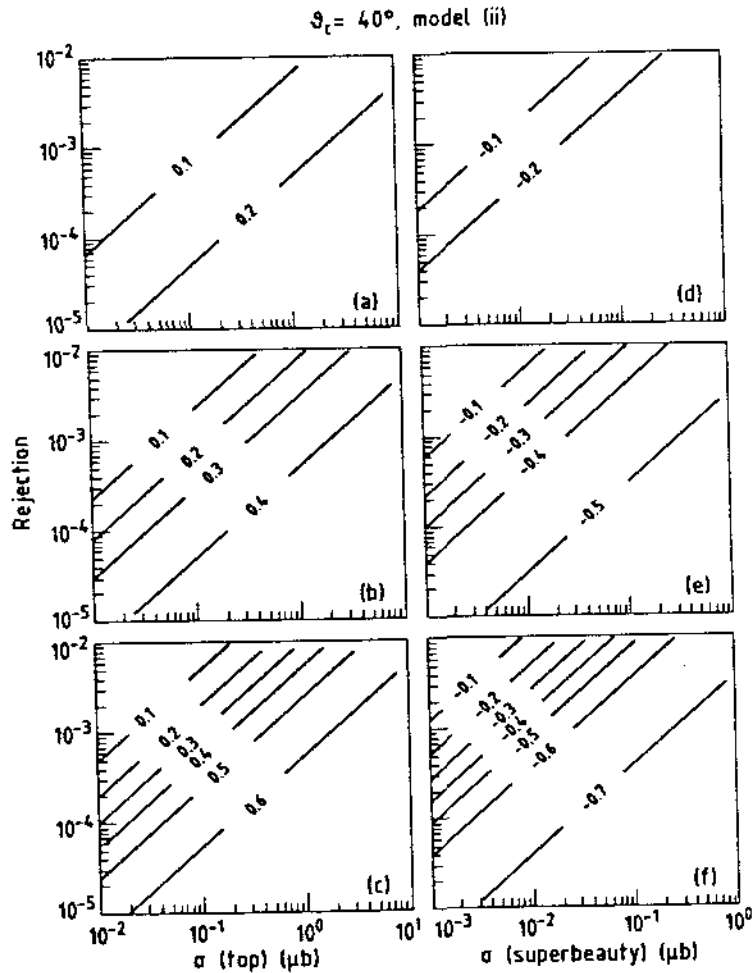


Fig. 30. As Figure 22 but for $\theta_{\text{cut}} = 40^\circ$ and model (ii).

iii) the total transverse energy of the jet must be greater than 10 GeV.

The result is

$$\epsilon_T(\text{jet}) \approx 70\%.$$

On the other hand, as shown in Figure 36, the condition that the jet is opposite in azimuth to the electron within $\Delta\phi = 30^\circ$ is nearly always satisfied.

The number of electrons from "superbeauty" semileptonic decays in the UA1 electron sample is therefore given by

$$N(e^\pm) = \sigma_{\text{sb}} \times \text{BR} \times L \times \epsilon_T(e^\pm) \times \epsilon_T(\text{jet}), \quad (8)$$

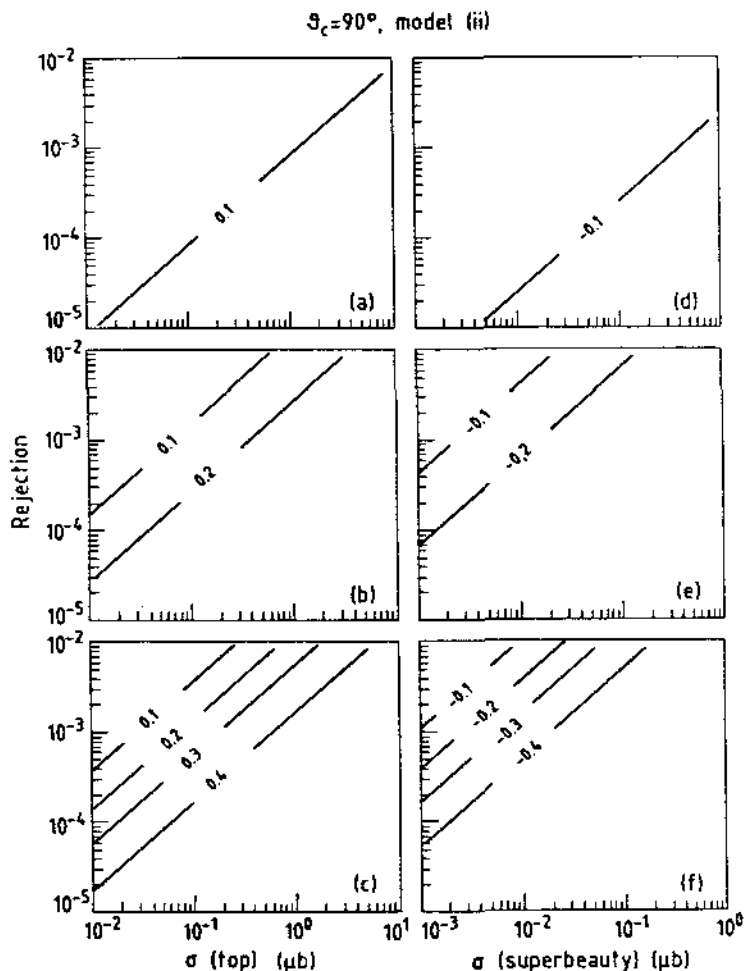


Fig. 31. As Figure 22 but for $\theta_{\text{cut}} = 90^\circ$ and model (ii).

where BR is the semileptonic branching ratio of the "superbeauty" state, taken to be $BR \approx 0.15$, and σ_{sb} is the cross section for the production of "superbeauty" particle states at the (pp) Collider; the other symbols have already been defined. The UAl results show that $N(e^-) = 11 \pm 3$.

Note that in Equation (8) the efficiencies for the electron trigger have not been taken into account. They are as follows:

- 1) The efficiency for detecting "isolated" electrons, i.e. with no other particles with $p_T > 2 \text{ GeV}/c$ in a 20° cone around the electron direction. Here the risk is in the random vetoing, otherwise the efficiency for genuine events is very high. From UAl data[20] it is possible to deduce the upper limit for random vetoing: it must be below 75%, and it could, in fact, be almost zero.

$\theta_{\text{cut}} = 30^\circ$, (Leading/Total) = 0.25
 $\sigma_c = 2 \text{ mb}$, $\sigma_b = 140 \mu\text{b}$
 $\sigma_\tau = 1.5 \mu\text{b}$, $\sigma_{\text{nb}} = 0.15 \mu\text{b}$

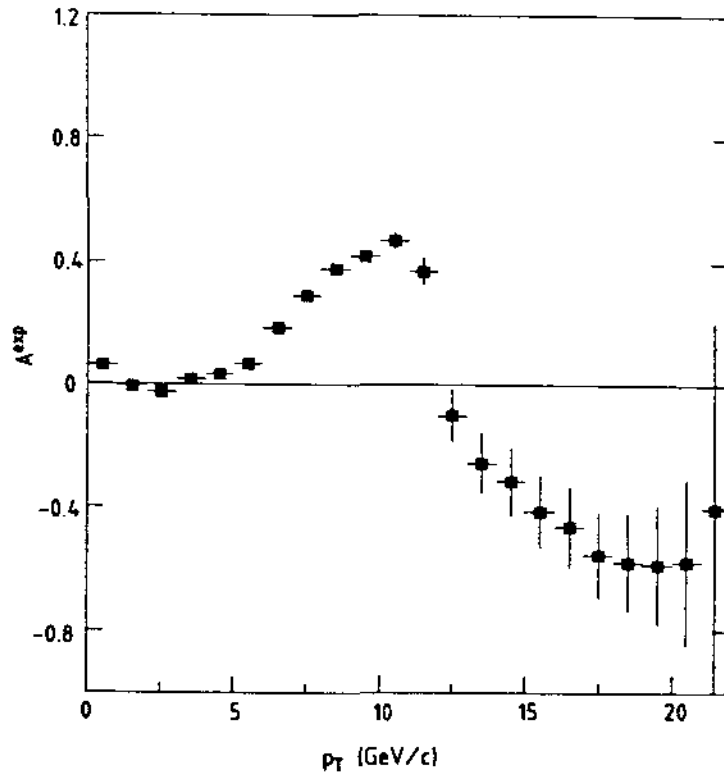


Fig. 32a. Plot of A^{exp} as a function of p_T , for a total Luminosity $L = 300 \text{ nb}^{-1}$, a rejection power of 10^{-3} , $\theta_{\text{cut}} = 30^\circ$ and (Leading/Total) = 0.25, using the cross section estimates. (a) from formula (6); (b) from perturbative QCD. The errors are statistical.

- ii) The efficiency of the energy cut $E_T > 15 \text{ GeV/c}$ owing to the finite resolution of the electromagnetic shower detectors (EMSDs). This efficiency can be evaluated to be $> 95\%$, using the quoted EMSDs energy resolution ($\Delta E/E = 0.15/\sqrt{E}$).

Figure 37a shows the cross-section corresponding to the (11 ± 3) events observed. Notice that the "experimental" finding of UAI falls in a remarkable range of agreement with the crude extrapolation from "charm" and QCD.

Going further, we have compared the p_T distributions of the (e^\pm) from the UAI with that from our Monte Carlo simulation. This is

$$\theta_{\text{cut}} = 30^\circ, (\text{Leading/Total}) = 0.25$$

$$\sigma_c = 2 \text{ mb}, \sigma_b = 10 \mu\text{b}$$

$$\sigma_t = 0.1 \mu\text{b}, \sigma_{\text{sb}} = 0.01 \mu\text{b}$$

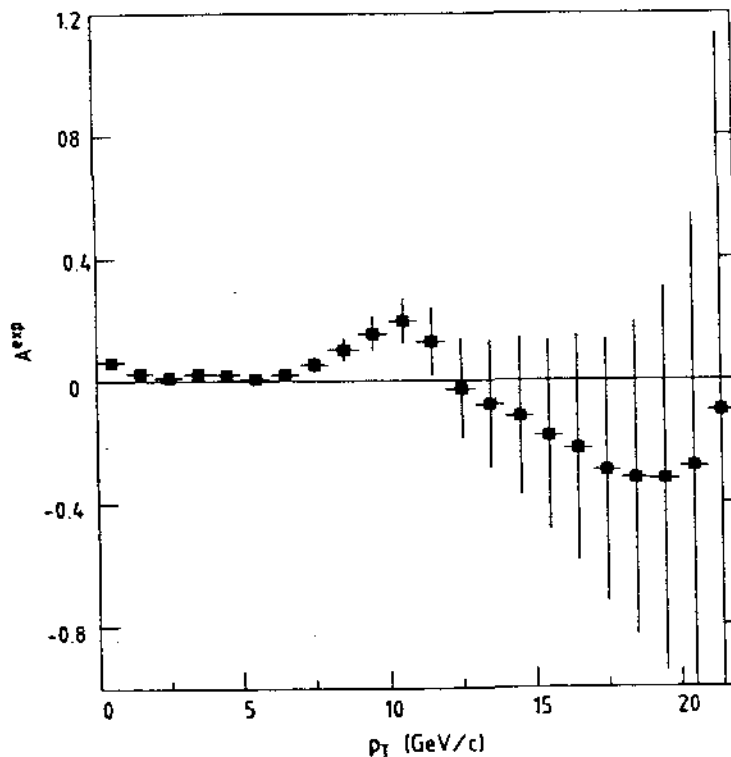


Fig. 32b. Plot of A^{exp} as a function of p_T , for a total Luminosity $L = 300 \text{ nb}^{-1}$, a rejection power of 10^{-3} , $\theta_{\text{cut}} = 30^\circ$ and $(\text{Leading/Total}) = 0.25$, using the cross section estimates. (a) from formula (6); (b) from perturbative QCD. The errors are statistical.

shown in Figure 38, where the Monte Carlo expectations are obtained using different values for the parameter b in the "superbeauty" production process

$$d\sigma/dp_T = p_T \exp(-bp_T).$$

Data and Monte Carlo distributions are normalized to the total number of events with $p_T > 15 \text{ GeV}/c$.

A value of $b \approx 0.20 \text{ GeV}^{-1}c$, i.e. a mean value for the production average transverse momentum $\langle p_T \rangle$ of the order of $10 \text{ GeV}/c$, fits the UA1 data quite well. This value for b is much smaller than the value ($b = 2.5$) which we found in our study of "charm" production at the

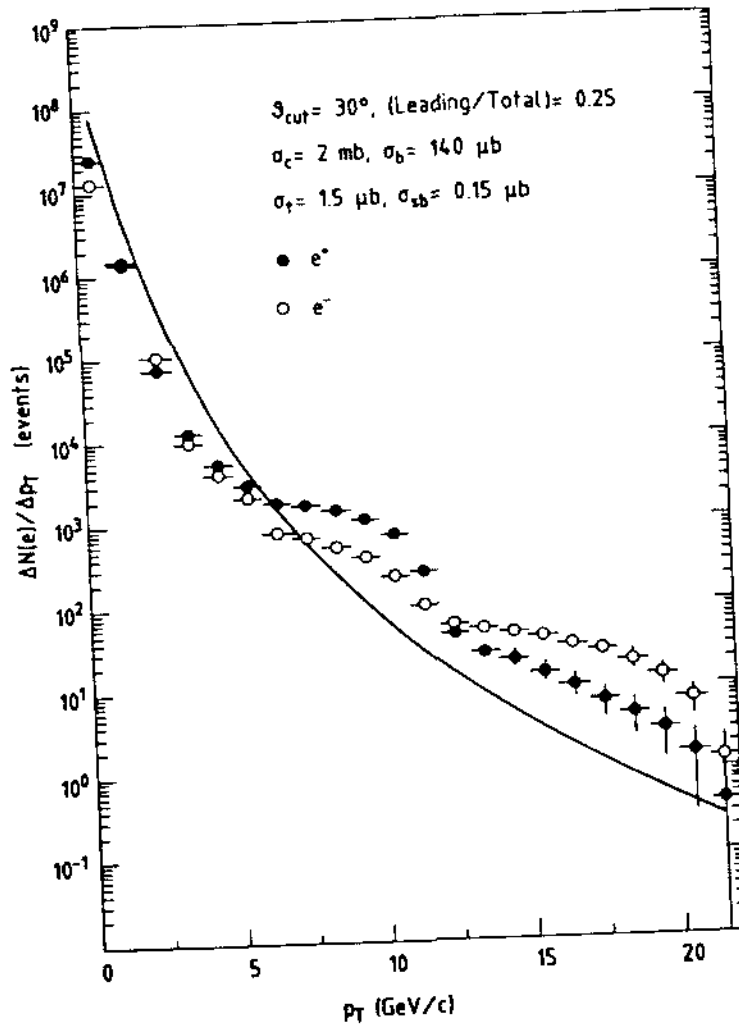


Fig. 33a. Expected number of produced electrons as a function of p_T with the same assumptions as in Figure 29, and the two cross section estimates: (a) from formula (6); (b) from perturbative QCD. The errors are statistical.

ISR[4,16]. However, it should be noticed that here we are dealing with the production of a flavor much heavier than "charm". The value $b = 0.2$ is in good agreement with the prescription $\langle p_T^2 \rangle \approx m^2/4$ (m is the quark mass) used by Odorico[10] to compute the "charm" production properties from flavor excitation.

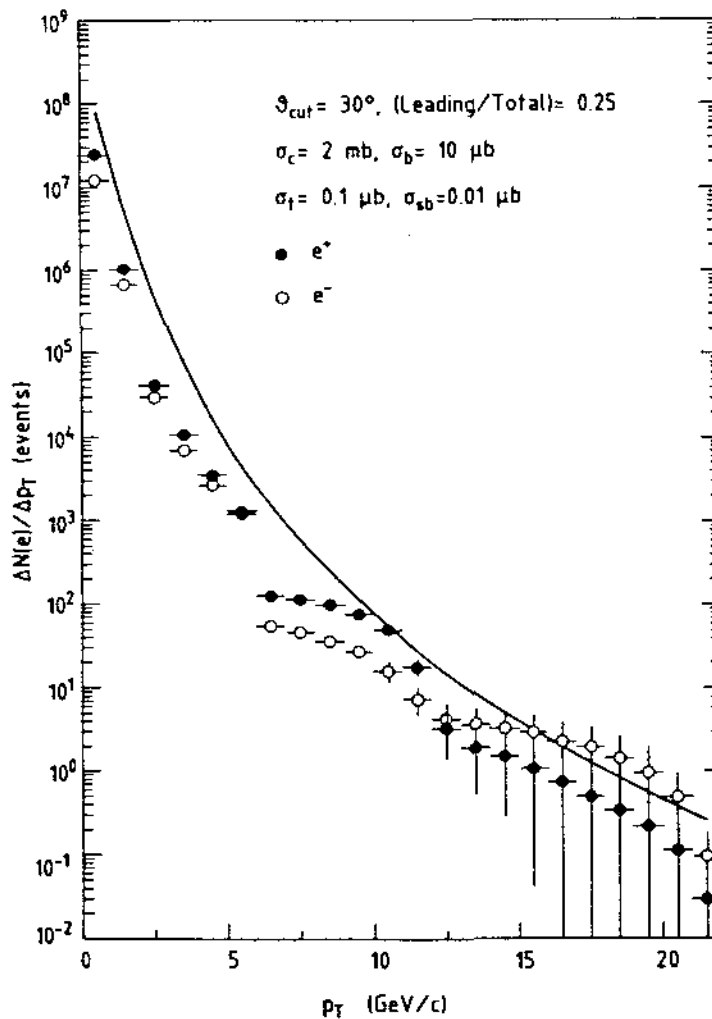


Fig. 33b. Expected number of produced electrons as a function of p_T with the same assumptions as in Figure 29, and the two cross section estimates: (a) from formula (6); (b) from perturbative QCD. The errors are statistical.

The efficiency for detecting electrons with $p_T > 15 \text{ GeV}/c$ in the Monte Carlo simulation does not change very much for $b > 0.2$, as shown in Figure 39. Thus the total "superbeauty" cross-section derived by Equation (8) holds, within $\pm 30\%$, even with this very low but expected value of b .

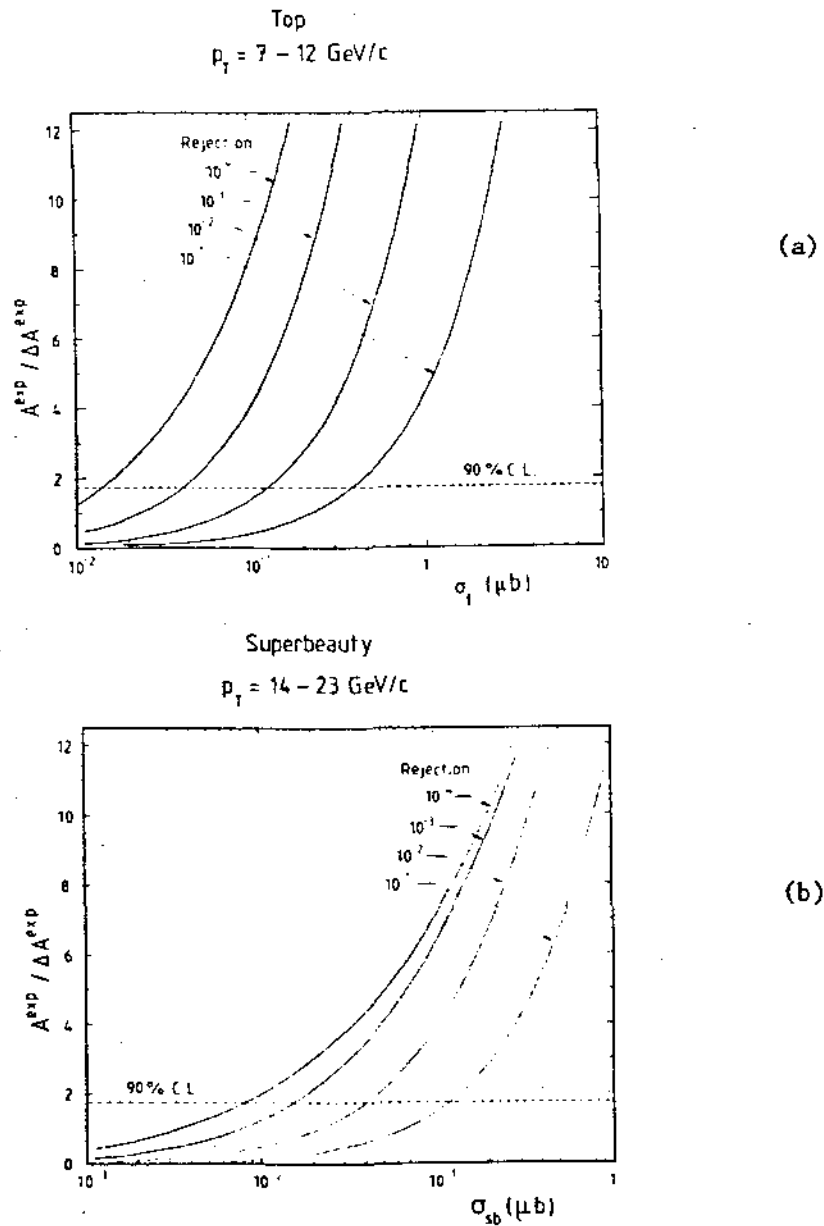


Fig. 34. The statistical significance of the measurement of A^{exp} ($A^{\text{exp}}/\Delta A^{\text{exp}}$), is shown, for a total luminosity of $L = 300 \text{ nb}^{-1}$. $\theta_{\text{cut}} = 30^\circ$ and $(\text{Leading/Total}) = 0.25$, and for the two p_T ranges: (a) $p_T = 7-12 \text{ GeV/c}$; (b) $p_T = 14-23 \text{ GeV/c}$.

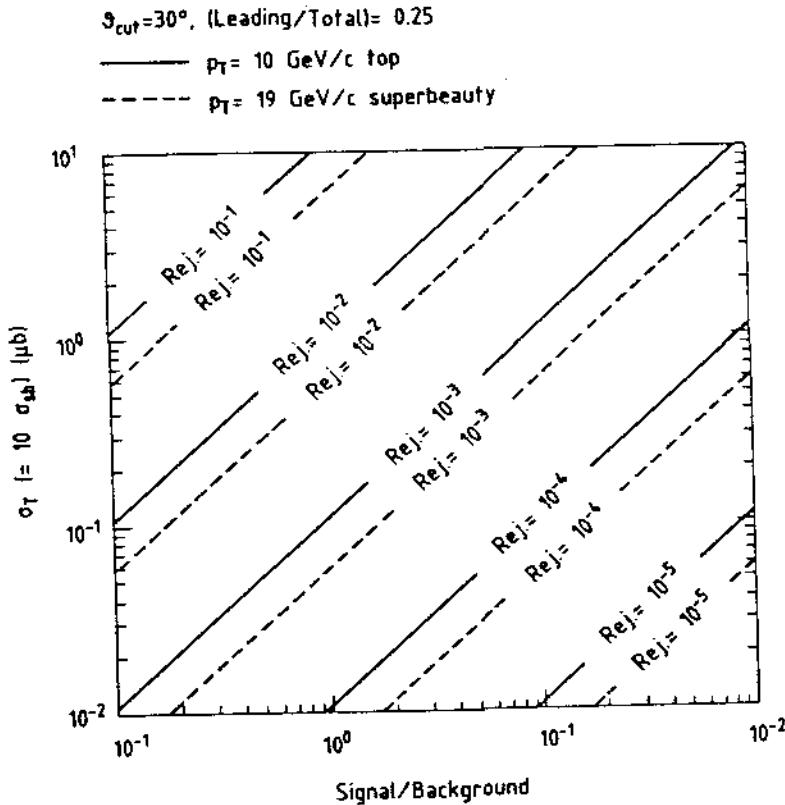


Fig. 35. Correspondence between rejection power and signal-to-background ratio (Signal/Background) as function of total cross section for "top" and "superbeauty" production, and at the two p_T values: 10 GeV/c and 19 GeV/c.

As mentioned above, the "down-like" nature of the observed (11 ± 3) events cannot be established in a direct way. It is based on a chain of self-consistent arguments. Let us give up the mass ratio (1) which binds the "top" flavor to be in the 25 GeV/c² range. If we repeat the analysis without this constraint, the (11 ± 3) events can be reinterpreted as the "up-like" signature with the "top" flavor mass 30 GeV/c² above the beauty flavor. The value of the cross-section would in this case be as shown in Figure 37b.

A sequence of arguments based on known facts and on simple hypotheses, extrapolated to the CERN (pp) Collider energies, allow us to conclude that the (11 ± 3) events observed by the UAl Collaboration and consisting each of a single (e^\pm) accompanied by a jet activity in the opposite hemisphere, correspond to a value of the cross-section expected for the production of a very heavy flavored state, in the 55 GeV/c² mass range. Moreover, the observed transverse momentum spectrum of the (e^\pm) follows the expectations for the semileptonic decay of a very massive state, again in the 55 GeV/c² mass range.

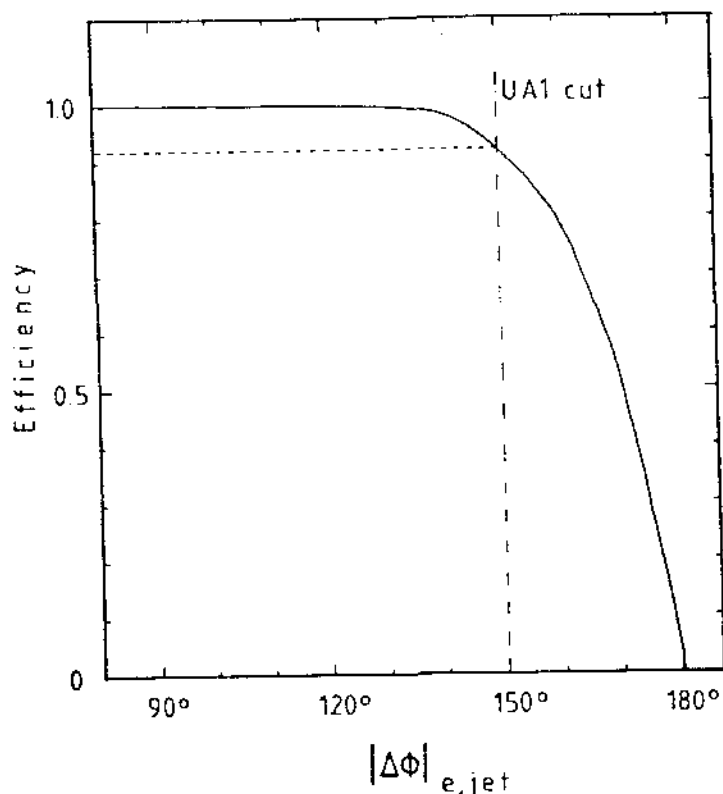


Fig. 36. Efficiency versus the cut value in the difference of azimuth $|\Delta\phi|$ between the electron and the hadronic jet in "superbeauty" decay, as derived from the Monte Carlo simulation.

It should, however, be noticed that the identification of the "down-like" nature of the heavy-flavored state is based on a series of hypotheses which produce the correct $\Delta m \approx 30 \text{ GeV}/c^2$ for the (e^-) transverse momentum spectrum, and the correct magnitude for the cross-section. If we were to ignore the cross-section and the quark mass ratios which allow us to predict the masses of the 4th family, the only parameter left to fit the observed (e^-) transverse momentum spectrum would be the value $\Delta m \approx 30 \text{ GeV}/c^2$. In this case the conservative interpretation of the UA1 results would be a "top" with a mass $30 \text{ GeV}/c^2$ above the "beauty".

This shows the importance of our proposal to study in detail the production of new heavy flavors at the CERN (pp) Collider by measuring the (e^+/e^-) asymmetry. In fact, the sign of the asymmetry allows the identification of the "up-like" or "down-like" nature of the heavy-flavored state in a direct and unambiguous way. Moreover, the

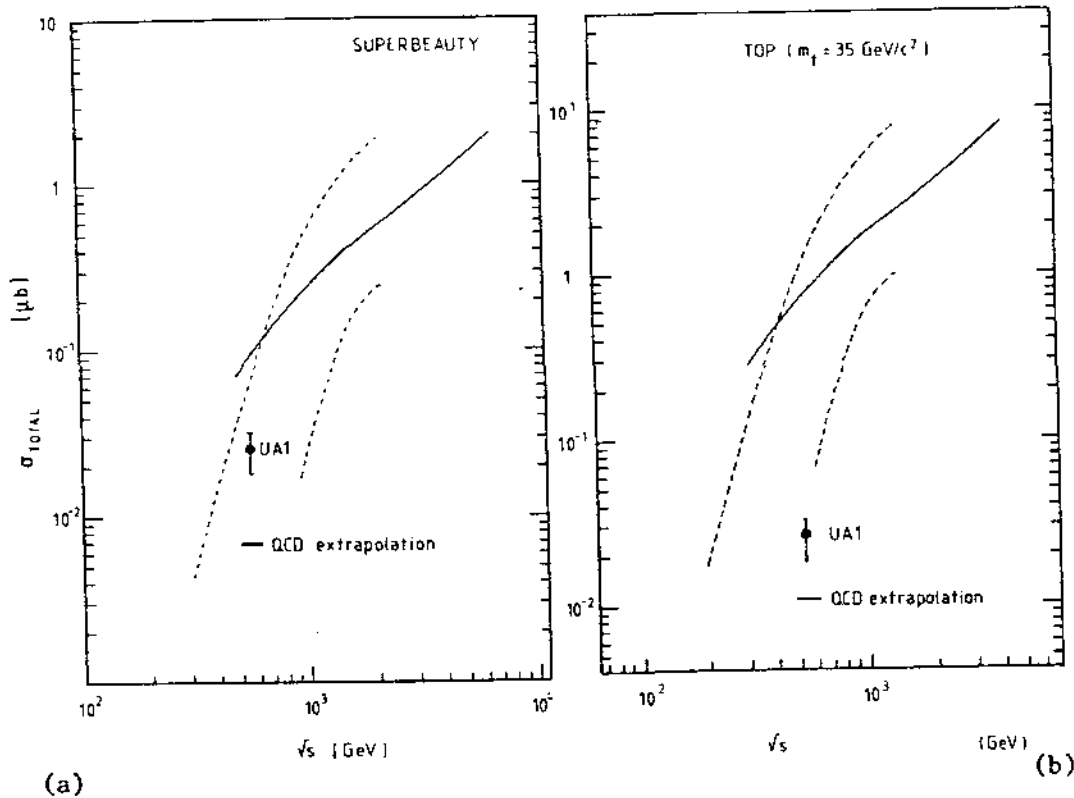


Fig. 37. Comparison between the UA1 results and the cross-sections for: (a) superbeauty ($m_{sb} = 55 \text{ GeV}/c^2$); (b) top ($m_t = 35 \text{ GeV}/c^2$); derived from strange (full line) and charm (dashed lines) cross-sections following formula (4).

(e^+/e^-) energy dependence of the asymmetry enables us to establish the correct sequence of

"down-like" \leftrightarrow "up-like"

decay chains for the new heavy flavors, and their mass difference.

7. CONCLUSIONS

The following conclusions are in order:

- 1) Past experience says: do not take too seriously the "theoretical" QCD predictions; many things still do not fit between theory and experiments. In particular, neither the large "charm" cross sections, nor the "Leading" effect were predicted.

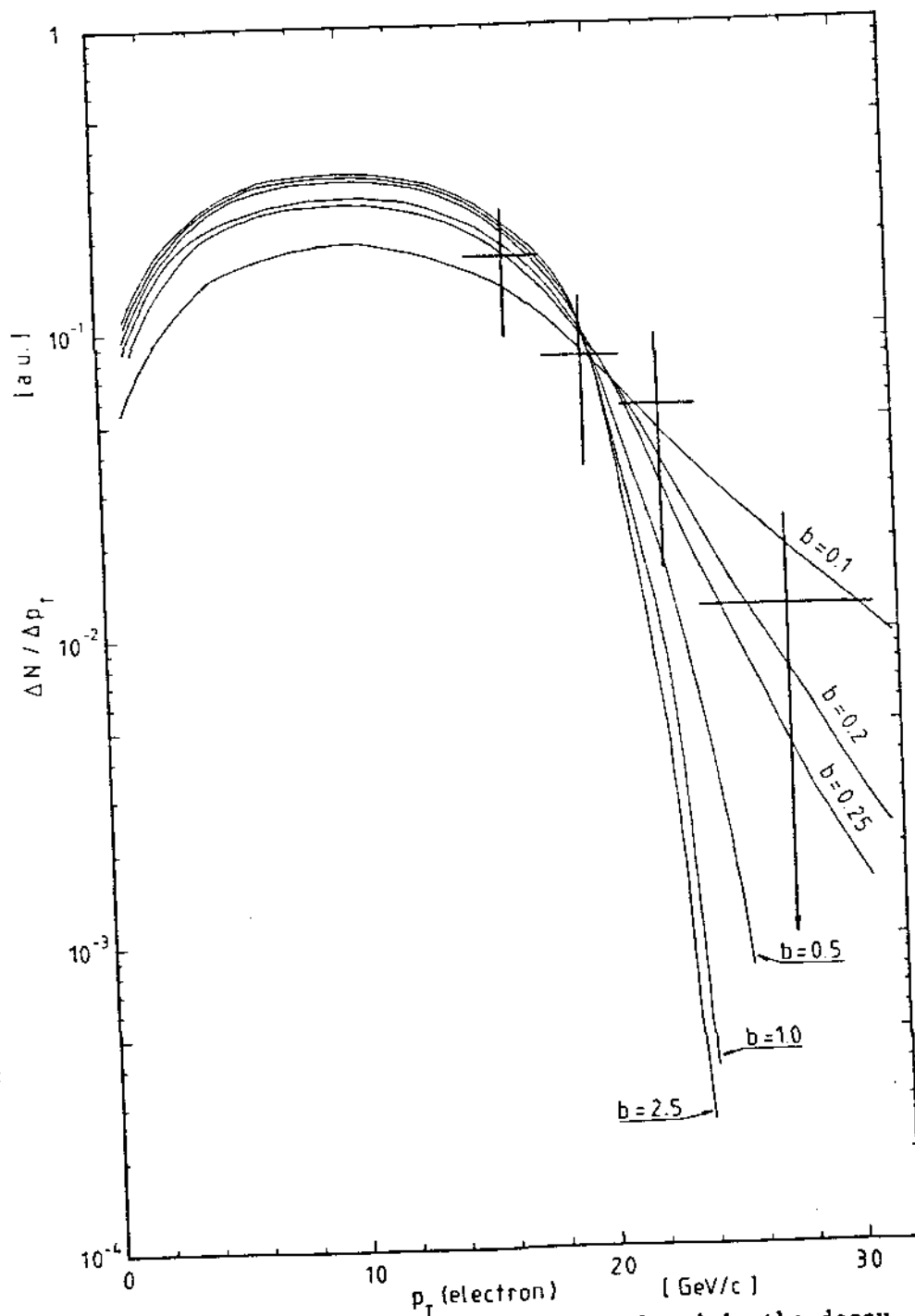


Fig. 38. p_T spectra of the electrons produced in the decay $(sb) \rightarrow tev$, for different $(d\sigma/dp_T) \propto p_T \exp(-bp_T)$ production distributions of the parent T (sb) particle, and comparison with UA1 data. The normalization is for $p_T > 15$ GeV/c.

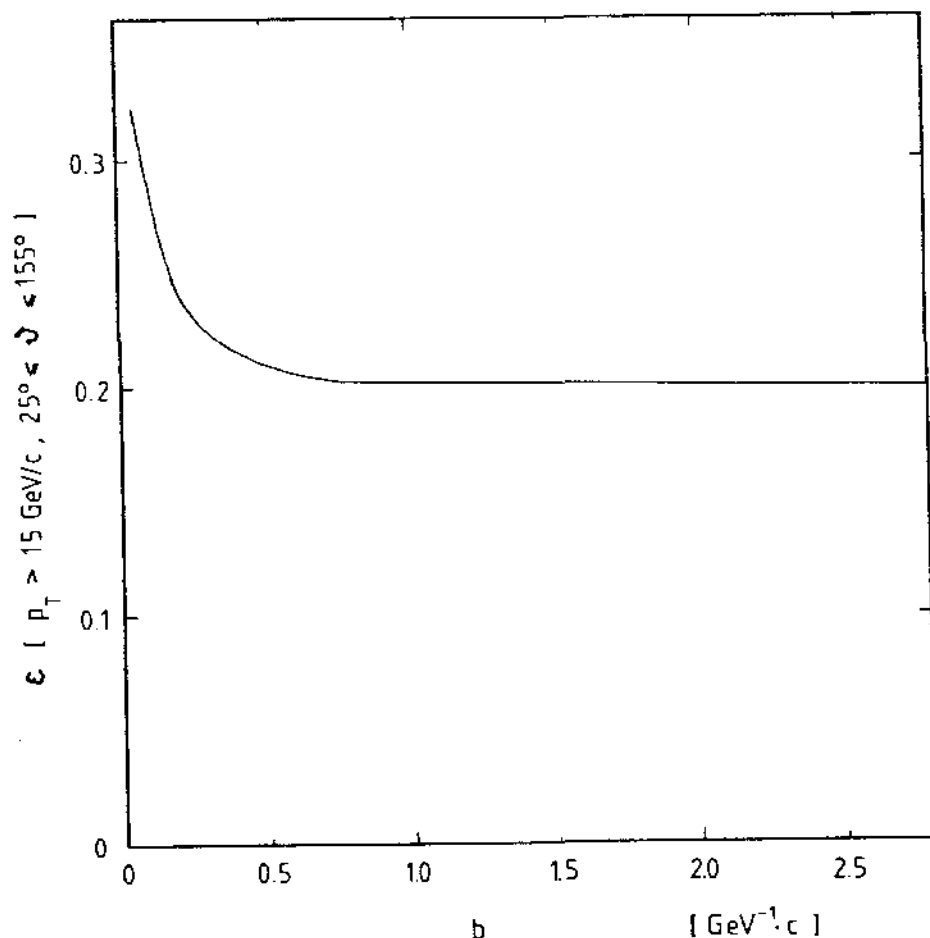


Fig. 39. Efficiency of the Monte Carlo simulation for the UA1 electron selection, as a function of the exponent parameter b in the parent (sb) p_T production distribution.

- ii) A detailed study of the production mechanism of heavy flavors at the ISR is important in order to make reasonable extrapolations to the (pp) Collider energy.
- iii) The number of "new" states with heavy flavors is very large. If their production cross sections follow the simple extrapolation proposed by us, the CERN (pp) Collider would be a quasi-factory for these new states. The problem is to have the instrumentation able to detect their existence.
- iv) The study of the electron-positron asymmetry and of its energy dependence is of the utmost importance at the (pp) Collider. If the "Leading" effect follows the same trend as "charm" at the ISR, this asymmetry is expected to be detectable, even if the production cross sections of the heavy flavored states would follow the QCD predictions.

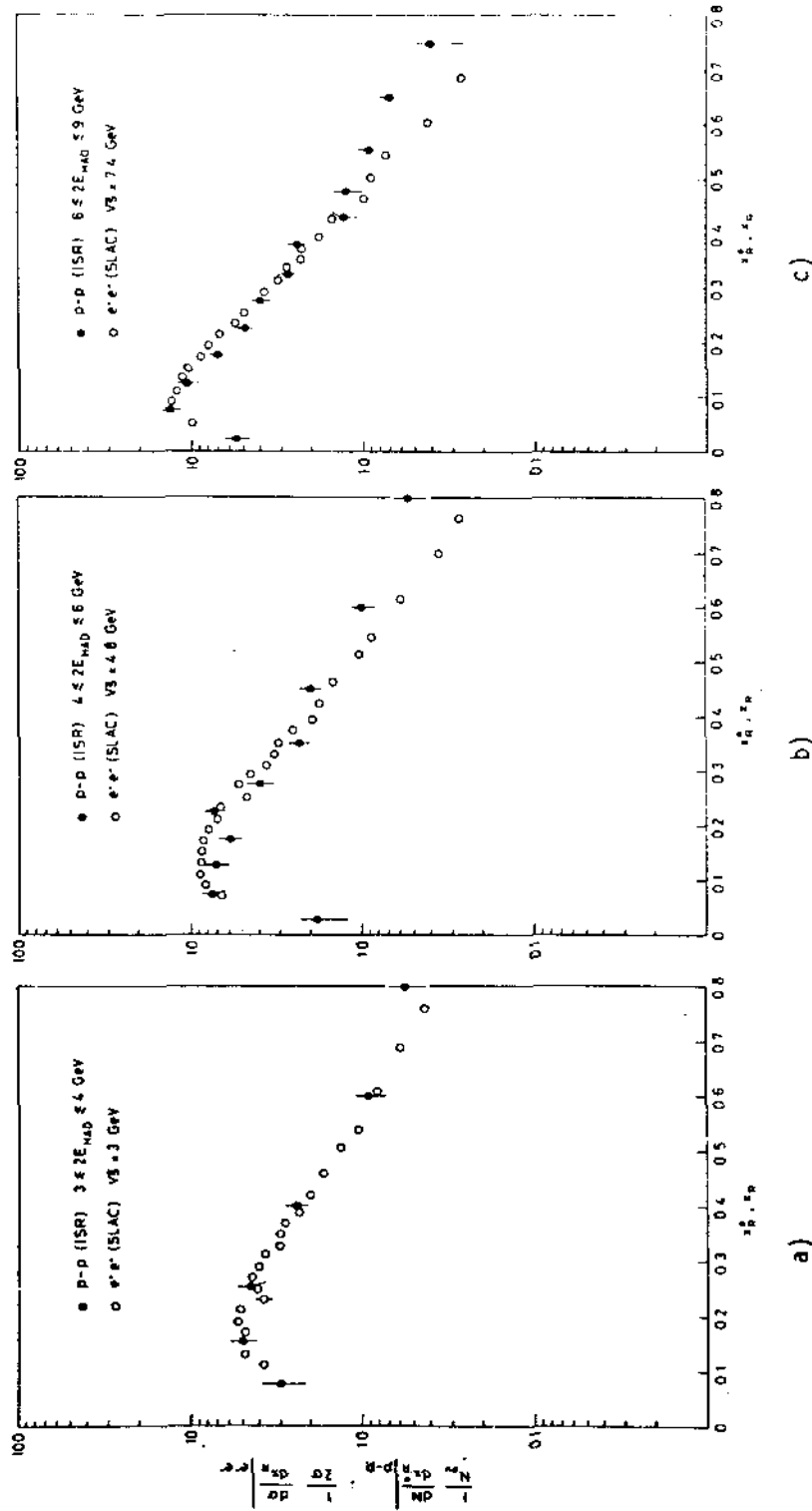


Fig. 40. The inclusive single-particle fractional momentum distributions $(1/N_{ev}) (dN_{track}/dx^*)$ for data taken at $(\sqrt{s})_{pp} = 30$ GeV and for three intervals of $2E_{had}$: (a) $(3 \leq 2E_{had} \leq 4)$ GeV; (b) $(4 \leq 2E_{had} \leq 6)$ GeV; (c) $(6 \leq 2E_{had} \leq 9)$ GeV. Also shown are data from SPEAR at $(\sqrt{s})_{e^+e^-} = 3, 4.8$ and 7.4 GeV.

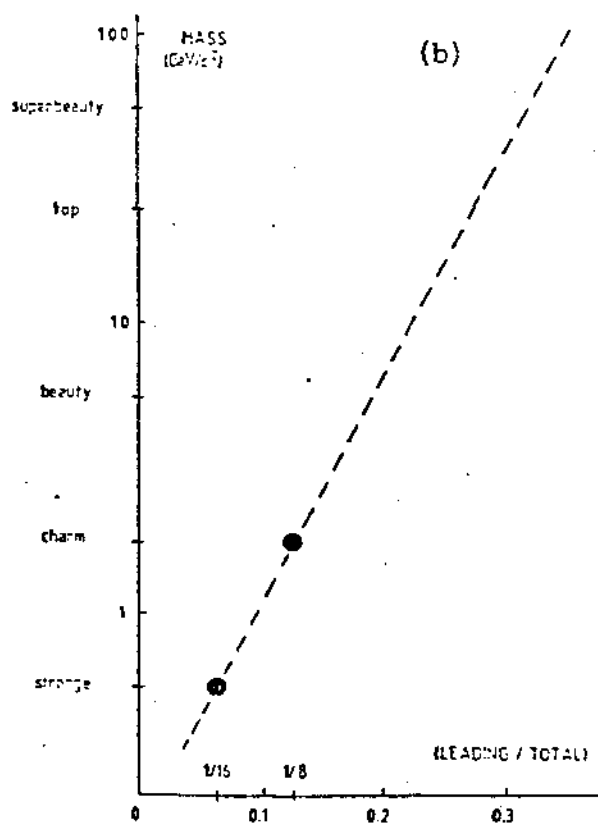
The study of the electron asymmetry and of its energy dependence is not less important than the searches for the Z^0 and the W^- . Finding the Z^0 and the W^- would tell us nothing about one of the most crucial problems of Subnuclear Physics: the families problem.

A detailed study of the electron asymmetry allows to investigate the presence, in a mass range so far unaccessible to any other machines, of the new flavors up-like ("top") and down-like ("super-beauty"), and to determine their mass relation.

REFERENCES

1. S. Ferrara, private communication.
2. A. Martin, The masses of the Heavy Flavoured Hadrons, CERN, Preprint TH-3314 (1982).
3. M. Basile et al., Nuovo Cimento, 63A:230 (1981).
4. M. Basile et al., Nuovo Cimento, 65A:457 (1981).
5. M. Basile et al., Nuovo Cimento, 67A:40 (1982).
6. D. Drijard et al., Phys.Lett., 85B:452 (1979); K. Giboni et al., Phys.Lett., 85B:437 (1979); W. Lockman et al., Phys.Lett., 85B:443 (1979); J. Eickmeyer et al., XX ICHEP (Madison, 1981); D. Drijard et al., Phys.Lett., 81B:250 (1979); P. F. Jacques et al., Phys.Rev., D21:1206 (1980); P. Coteus et al., Phys.Rev.Lett., 42:1438 (1979); A. Soukas et al., Phys.Rev.Lett., 44:564 (1980); A. E. Asratyan et al., Phys.Lett., 74B:497 (1978); P. Alibrant et al., Phys.Lett., 74B:134 (1978); T. Hansl et al., Phys.Lett., 74B:139 (1978); A. Bosetti et al., Phys.Lett., 74B:143 (1978); M. Fritze et al., Phys.Lett., 96B:427 (1980); D. Jonker et al., Phys.Lett., 96B:435 (1980); H. Abramowicz et al., CERN Preprint CERN-EP/82-17 (1982); M. Aguilar-Benitez et al., CERN Preprint CERN-EP/81-131 (1981); T. Aziz et al., Nuclear Phys., B199:424 (1982); J. Sandweiss et al., Phys.Rev.Lett., 44:1104 (1980).
7. M. Basile et al., Lett.Nuovo Cimento, 30:487 (1981).
8. M. Basile et al., Lett.Nuovo Cimento, 33:33 (1982).
9. F. Halzen, W. Y. Keung and D. M. Scott, Madison Report MAD/PH/63 (1982).
10. R. Odorico, Phys.Lett., 107B:231 (1981).
11. V. Barger, F. Halzen and W. Y. Keung, Phys.Rev., D24:1428 (1981).
12. M. Basile et al., Nuovo Cimento, 65A:391 (1981).
13. J. Badier et al., XXI Intern. Conf. on High Energy Physics, Paris, 1982.
14. F. Halzen, Rapp. Talk XXI Intern. Conf. on High Energy Physics, Paris, 1982.
15. K. Chadwick et al., Preprint CLNS/82/546 (1982).
16. M. Basile et al., Lett.Nuovo Cimento, 30:481 (1981).
17. M. Basile et al., Lett.Nuovo Cimento, 33:17 (1982).

18. L. Olsen, Monriond Workshop on New Flavours, Les Arcs, France, 1982.
19. UA2 Collaboration, Phys.Lett., B118:203 (1982).
20. G. Arnison et al., UA1 Collaboration, Preprint CERN-EP/83-13 (1983).



III-9. "A study of possible new heavy-flavour production at the
CERN ($p\bar{p}$) Collider"
Lettere al Nuovo Cimento, vol.37, p.255, June 18, 1983.

9 - A Study of Possible New Heavy-Flavour Production at the CERN ($p\bar{p}$) Collider.

M. BASILE, J. BERBIERS, G. BONVICINI, G. CARA ROMEO, L. CIFARELLI, A. CONTIN, M. CURATOLO, G. D'ALI, C. DEL PAPA, B. ESPOSITO, P. GIUSTI, T. MASSAM, R. NANIA, F. PALMONARI, G. SARTORELLI, G. SUSINNO, L. VOTANO and A. ZICHICHI

CERN - Geneva, Switzerland

Istituto di Fisica dell'Università - Bologna, Italia

Istituto Nazionale di Fisica Nucleare - Sezione di Bologna, Italia

Istituto Nazionale di Fisica Nucleare, Laboratori Nazionali di Frascati - Frascati, Italia

(ricevuto il 25 Marzo 1983)

PCAS. 13.90. - Other topics in specific reactions and phenomenology of elementary particles.

Summary. - In this paper, we review briefly the main hypotheses and extrapolations used to predict the observability of new heavy flavours at the CERN ($p\bar{p}$) collider. Some results from this study are compared with the first experimental data on the production of high- p_T electrons accompanied by hadronic « jets » at the ($p\bar{p}$) collider, as observed by the UA1 collaboration. These events could, in fact, be the signature of the semi-leptonic decay of a very massive new heavy-flavoured state. Its « downlike » or « uplike » nature cannot be established in a direct and unambiguous way. More sophisticated measurements are needed as discussed in detail in a previous paper.

Introduction. We have already emphasized the important role that the CERN ($p\bar{p}$) Collider might have as a machine to produce very heavy flavours⁽¹⁾. So far, in the ($p\bar{p}$) Collider exploitation, the emphasis has been concentrated in the search for the intermediate vector bosons W^\pm and Z^0 . However, the discovery of these theoretically expected particles sheds no light on either of the two crucial and totally unresolved problems of subnuclear physics: the family and the hierarchy.

This is why more attention should be devoted to the problem of what the ($p\bar{p}$)

(¹) M. BASILE, J. BERBIERS, G. BONVICINI, G. CARA ROMEO, L. CIFARELLI, A. CONTIN, M. CURATOLO, G. D'ALI, C. DEL PAPA, B. ESPOSITO, P. GIUSTI, T. MASSAM, R. NANIA, F. PALMONARI, G. SARTORELLI, G. SUSINNO, L. VOTANO and A. ZICHICHI: *New flavours: experiment vs. theory. From charm to the 4th family*, in *III Topical Workshop on Proton-Antiproton Collider Physics, Rome, January 12-14, 1983* (to be published).

collider could do in the heavy-flavour domain. In fact, the search for new flavours compares very well with the physics of the electroweak gauge bosons.

We have already discussed in detail ⁽¹⁾ a method to detect new heavy flavours with a direct and unambiguous identification of their «uplike» or «downlike» nature, via the (e^+/e^-) asymmetry measurement.

Here, we propose an approach to the heavy flavours at the $(p\bar{p})$ collider which shows the importance of the asymmetry method. This approach is based on known facts and on few simple hypotheses. Facts and hypotheses are then extrapolated to $(p\bar{p})$ collider energies.

Our estimates are compared with the UA1 data ⁽²⁾, i.e. their eleven events showing an isolated (e^\pm) accompanied by a hadronic jet.

The facts. The facts are that

1) the heavy flavours Λ_c^+ and Λ_b^0 are produced at ISR energies in a «leading» way ⁽³⁾, i.e.

$$(1) \quad d\sigma/dx \propto (1-x)^\alpha,$$

with $\alpha \sim 1$;

2) the «heavy»-quark masses are in the following ratios ⁽⁴⁾:

$$(2a) \quad m_c/m_s \simeq 3.5,$$

$$(3a) \quad m_b/m_s \simeq 11;$$

3) there are good reasons to believe ⁽⁴⁾ that the «strange»-quark mass, m_s , is heavy enough to behave like a heavy flavour, such as «charm» and «beauty»;

4) the cross-sections for the heavy flavours «strange» (s), «charm» (c) and «beauty» (b) are measured up to the ISR energies, even if with large uncertainties (c and b);

5) all generalized Cabibbo angles, measured so far, are either small or compatible with being small.

The hypotheses. The hypotheses are

1)

$$(2b) \quad \frac{m_c}{m_s} = \frac{m(\text{uplike})}{m(\text{downlike})};$$

2)

$$(3b) \quad \frac{m_b}{m_s} = \frac{m(\text{family } N+1)}{m(\text{family } N)};$$

3a) the cross-sections for production of heavy flavours are mainly dictated by dimensionality and scaling:

⁽¹⁾ G. ARNISON *et al.* (UA1 COLLABORATION): preprint CERN-EP/83-13 (1983).

⁽²⁾ M. BASILE, G. CARA ROMEO, L. CIFARELLI, A. CONTI, G. D'ALI, P. DI CESARE, B. ESPOSITO, P. GIUSTI, T. MASSAM, F. PALMONARI, G. SARTORELLI, G. VALENTI and A. ZICHICHI: *Lett. Nuovo Cimento*, **30**, 487 (1981); *Nuovo Cimento A*, **65**, 421 (1981).

⁽³⁾ A. MARTIN: preprint CERN TH-3314 (1982).

dimensionality says

$$\sigma \propto (1/m_i)^2,$$

scaling says

$$\sigma \propto f(\sqrt{s}/m_i);$$

therefore

$$(4) \quad \sigma \propto (1/m_i)^2 f(\sqrt{s}/m_i),$$

which means that the knowledge of the cross-section for the production of a heavy flavour having mass m_i at energy $(\sqrt{s})_i$, allows us to know the cross-section of a heavier flavour having mass m_j at the scaled energy $(\sqrt{s})_j$, according to

$$(5) \quad \sigma_j[(\sqrt{s})_j = (m_j/m_i) \times (\sqrt{s})_i] = \sigma_i[(\sqrt{s})_i] \times (m_i/m_j)^2;$$

3b) the cross-sections for heavy-flavour production can be predicted by QCD ^(*);

4) the generalized Cabibbo angles, even those coming from the existence of the 4th family, are small, and the Δ flavour changing Δ neutral currents are forbidden to any order of family. The amplitude for a transition from family N to family $(N \pm \alpha)$ has a coefficient

$$\prod_{i=1, \alpha} \sin \theta_i;$$

this implies that the dominant transitions are those between neighbouring families.

The extrapolations. The extrapolations are

1a) the Δ leading Δ phenomenon holds for the production of heavy flavours at the collider energies;

1b) the Δ leading Δ phenomenon is also present in the decay of the heavy-flavoured states;

$$2) \quad \frac{m_c}{m_s} \simeq 3.5 \simeq \frac{m(\text{uplike})}{m(\text{downlike})} = 4;$$

$$3) \quad \frac{m_b}{m_s} \simeq 11 \simeq \frac{m(\text{family } N+1)}{m(\text{family } N)} = 11;$$

4a) the cross-sections measured for $\Delta s \Delta$ and $\Delta c \Delta$ at lower energies can be extrapolated to the $(p\bar{p})$ collider energy, by using formula (5);

4b) the cross-sections calculated by using QCD ^(*) can be extrapolated, by using formula (5), to very heavy masses at the $(p\bar{p})$ collider energies.

The consequences. The consequences are the following:

1a) The Δ leading Δ phenomenon in the production of heavy-flavoured states at the $(p\bar{p})$ collider, produces an (e^+/e^-) asymmetry which changes sign from the proton

(*) R. ODORICO: preprint IFUB 82/3 (1982).

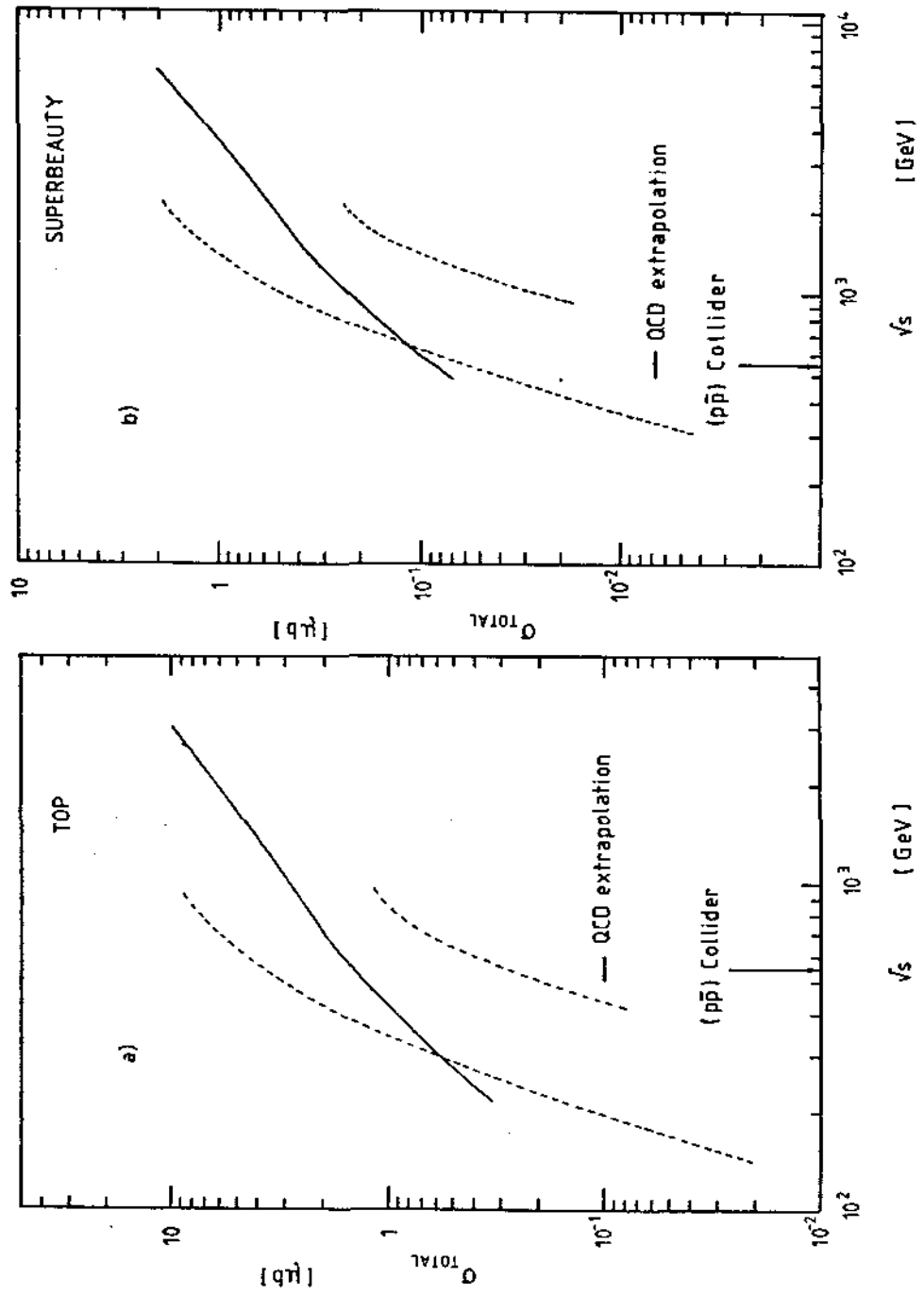


Fig. 1. - (a) and (b) cross-sections derived from strange charm and charm cross-sections (dashed lines—notice the width due to the experimental uncertainties) following formula (5).

to the antiproton hemisphere and is (c^+/e^-) energy dependent. Notice that the asymmetry method allows the «uplike» or «downlike» nature of the new heavy flavours to be distinguished in a direct way.

This effect has already been discussed in detail elsewhere⁽¹⁾.

1b) The «leading» phenomenon in the semi-leptonic decay of a heavy-flavoured state, produces a very specific pattern: the heavy-quark side of the decay state has a depressed «hadronization» and it recoils against the weak intermediate boson, i.e. against the $(e\nu)$ pair.

2) The mass of the «top» quark is expected to be in the 25 GeV/c² range. This mass value is important because it determines the energy available in the decay from a heavier quark.

3) The mass of the first member of the 4th family, «downlike», (called «superbeauty»)⁽¹⁾ is in the 55 GeV/c² range. We will, therefore, take $\Delta m \approx 30$ GeV/c² as the typical mass difference in the decay of «superbeauty» into «top».

4) The values of the cross-sections for «top» and «superbeauty» are given, respectively, in fig. 1a) and b) as extrapolations from «s» and from «c». It is interesting to note that these two ways of getting cross-section information in the $(p\bar{p})$ collider range are not in violent disagreement. Furthermore, the QCD expectation is within the «charm» extrapolated range of uncertainty in the «superbeauty» case.

Comparison with preliminary data from the CERN $(p\bar{p})$ collider. As a first step in the study of the heavy-quark physics using the $(p\bar{p})$ collider, we propose to compare our predictions with the data already available from the $(p\bar{p})$ collider.

In their search for electron candidates, the UA1 collaboration finds 16 events with an isolated electron⁽²⁾. Five of these events are attributed to W^\pm decay, while the remaining 11 are characterized by a «jet activity» in the azimuthal region opposite to the isolated electron. The events correspond to a total integrated luminosity of $L = 20 \text{ nb}^{-1}$.

According to the Monte Carlo program discussed in detail in a previous paper⁽¹⁾, the acceptance for electrons originated by «superbeauty» decays in the phase-space region defined by the UA1 data ($p_T > 15$ GeV/c and, for the polar angle, $25^\circ < \theta < 155^\circ$) is, for baryon and antibaryon decays,

$$\varepsilon_B(e^\pm) = 0.08$$

and, for meson and antimeson decays,

$$\varepsilon_M(e^\pm) = 0.12.$$

We can, therefore, use the approximation

$$\varepsilon(e^\pm) = \varepsilon_B(e^\pm) = \varepsilon_M(e^\pm) = 0.1.$$

Since the heavy flavours are produced in pairs, the total efficiency to see at least one electron from the semi-leptonic decay of «superbeauty» is

$$\varepsilon_T(e^\pm) = 2 \times \varepsilon(e^\pm) = 0.2,$$

where we have assumed equal semi-leptonic branching ratios for baryon and meson decays.

The request of «jet activity» opposite in azimuth to the electron, gives rise to another acceptance factor, $\varepsilon_{\tau}(\text{jet})$, which we can derive by analysing the hadronic pattern of the «superbeauty» semi-leptonic decays predicted by our Monte Carlo simulation, according to the «jet» definition outlined by the UA1 collaboration, i.e.

i) all particles with $p_{\tau} > 2.5 \text{ GeV}/c$ are associated to a jet, if their separation in phase space is

$$\Delta R = \sqrt{(\Delta\varphi)^2 + (\Delta\eta)^2} < 1$$

with $\Delta\varphi$ in radians and η (= pseudorapidity) = $-\ln(\tan \theta/2)$;

ii) all other particles are associated to the jet defined as in point i), if they satisfy the conditions

$$p_{\tau} \text{ relative to the jet} < 1 \text{ GeV}/c,$$

$$\theta \text{ relative to the jet} < 45^\circ;$$

iii) the total transverse energy of the jet must be greater than 10 GeV.

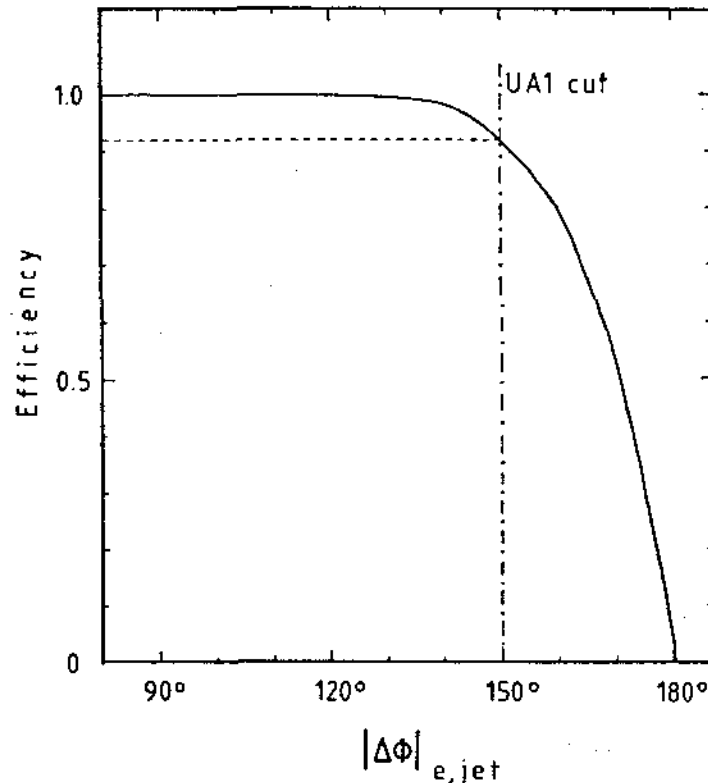


Fig. 2. - Efficiency vs. the cut value in the difference of azimuth $|\Delta\varphi|$ between the electron and the hadronic jet in «superbeauty» decay, as derived from the Monte Carlo simulation.

The result is

$$\epsilon_T(\text{jet}) \simeq 70\%.$$

On the other hand, as shown in fig. 2, the condition that the jet is opposite in azimuth to the electron within $\Delta\phi = 30^\circ$, is nearly always satisfied.

The number of electrons from *superbeauty* semi-leptonic decays in the UA1 electron sample is, therefore, given by

$$(6) \quad N(e^\pm) = \sigma_{sb} \times \text{BR} \times L \times \epsilon_T(e^\pm) \times \epsilon_T(\text{jet}),$$

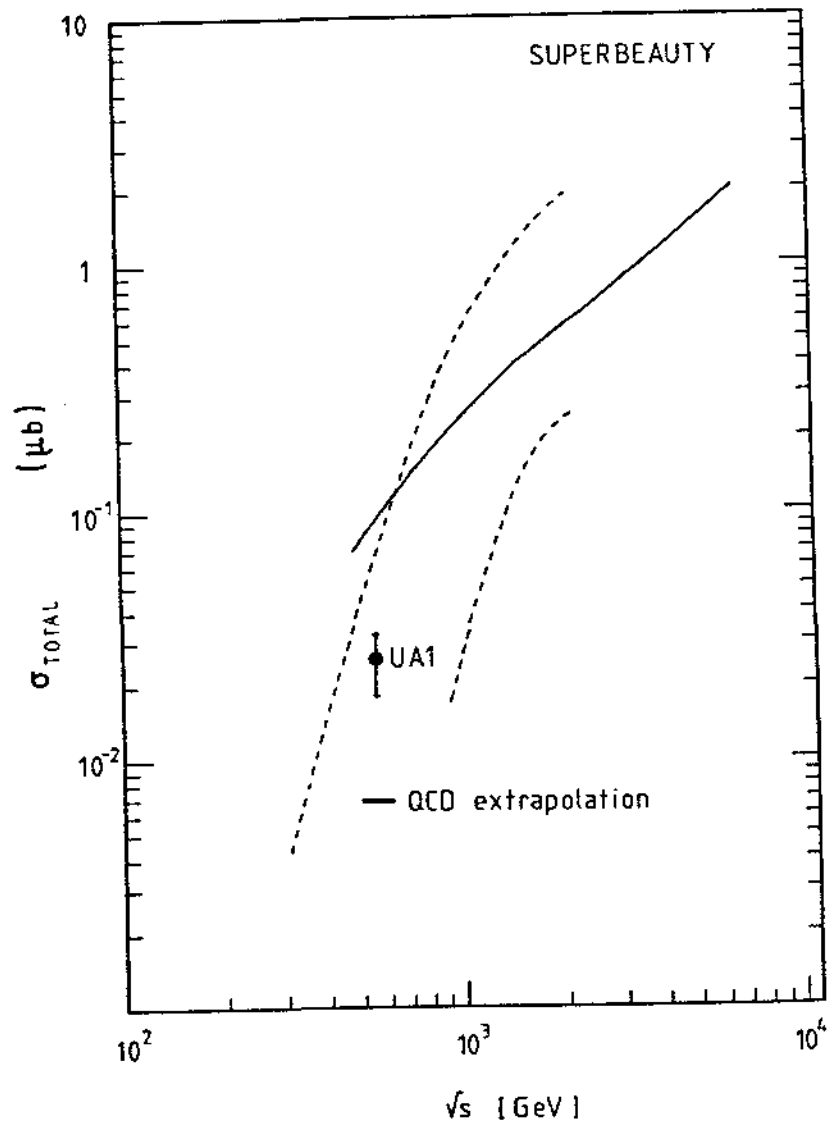


Fig. 3. - Where the cross-section evaluated from the UA1 data falls.

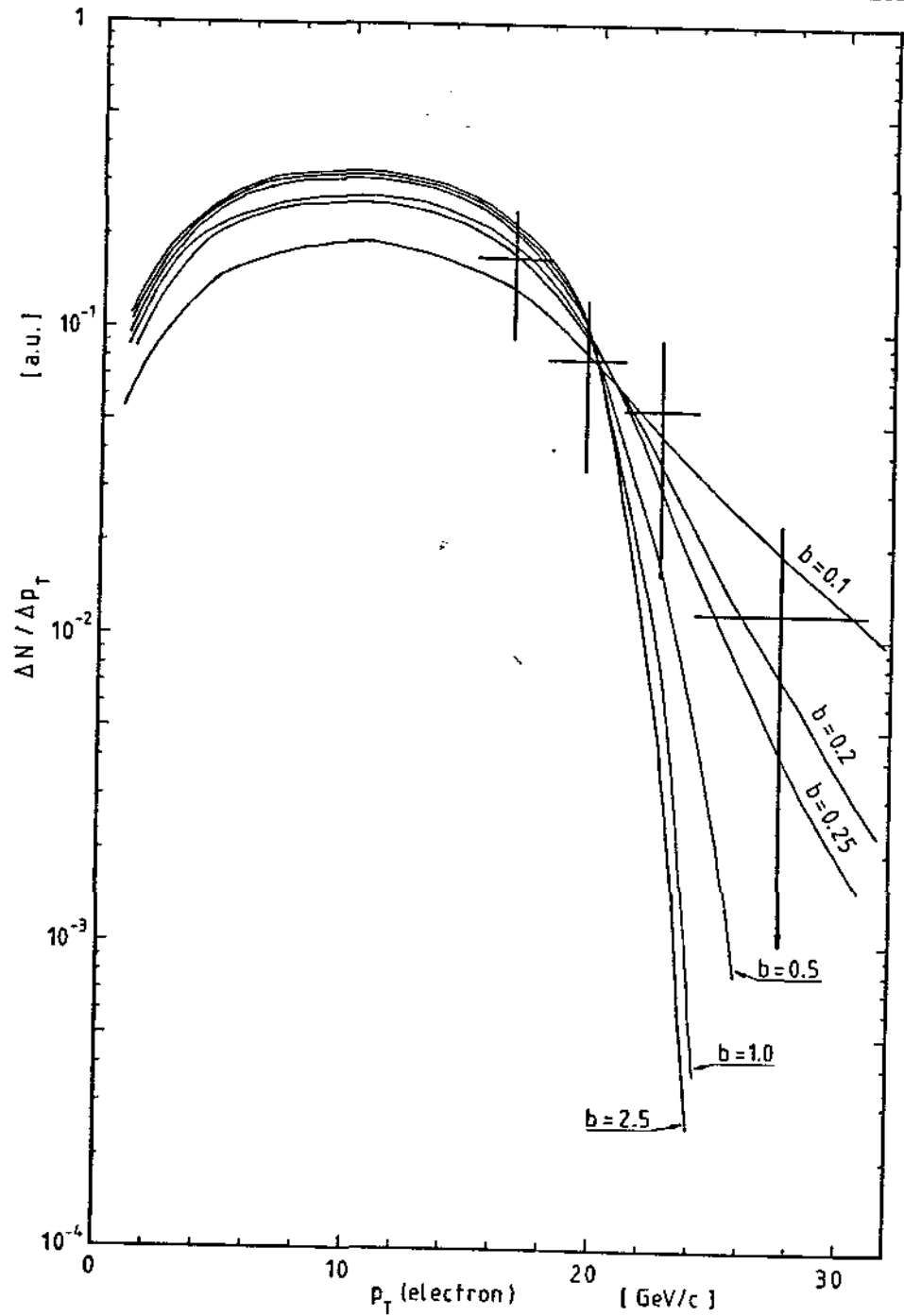


Fig. 4. - p_T spectra of the electrons produced in the decay $(sb) \rightarrow tev$, for different $(d\sigma/dp_T) \propto p_T \exp(-bp_T)$ production distributions of the parent (sb) particle, and comparison with UA1 data. The normalization is for $p_T > 15$ GeV/c.

where BR is the semi-leptonic branching ratio of the «superbeauty» state⁽¹⁾, taken to be $BR \approx 0.15$, σ_{sb} is the cross-section for the production of «superbeauty» particle states at the (p \bar{p}) collider, and the other symbols have already been defined.

From the UA1 it results: $N(e^\pm) = 11 \pm 3$.

Note that, in (6), the efficiencies for the electron trigger have not been taken into account. They are as follows:

i) The efficiency for detecting «isolated» electrons, i.e. with no other particles with $p_T > 2$ GeV/c in a 20° cone around the electron direction. Here the risk is in the random vetoing, otherwise the efficiency for genuine events is very high. From UA1 data⁽²⁾ it is possible to deduce the upper limit for random vetoing: it must be below 75%, and it could be, in fact, practically zero.

ii) The efficiency of the energy cut $E_T > 15$ GeV/c, due to the finite resolution of the EMSDs. This efficiency can be evaluated to be $> 95\%$, by using the quoted EMSD energy resolution ($\Delta E/E = 0.15/\sqrt{E}$).

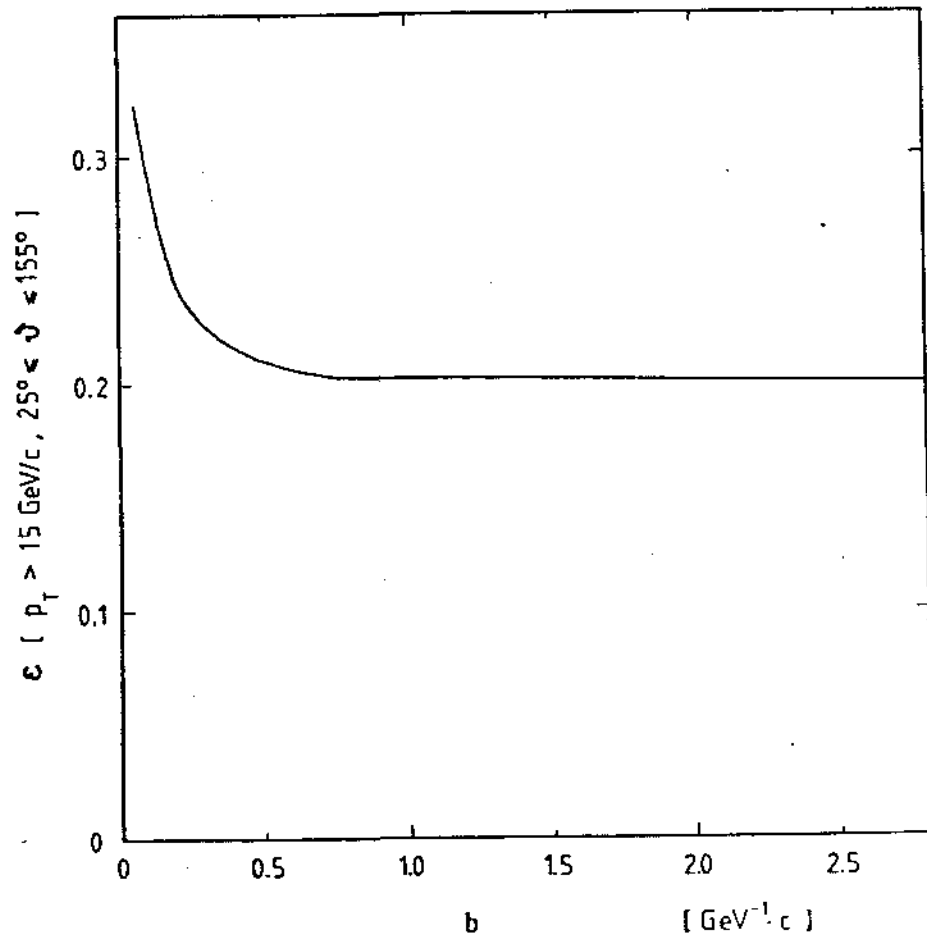


Fig. 5. - Efficiency of the Monte Carlo simulation for the UA1 electron selection, as a function of the exponent parameter b in the parent (sb) p_T production distribution.

Figure 3 shows the cross-section corresponding to the (11 ± 3) events observed. Notice that the « experimental » finding of UA1 falls in a remarkable range of agreement with the crude extrapolations from « charm » and QCD.

Going further, we have compared the p_T distributions of the (e^\pm) from UA1 with that from our Monte Carlo simulation. This is shown in fig. 4, where the Monte Carlo expectations are obtained using different values for the parameter b in the « super-beauty » production process:

$$d\sigma/dp_T \propto p_T \exp[-bp_T].$$

Data and Monte Carlo distributions are normalized to the total number of events $p_T > 15 \text{ GeV}/c$.

A value of $b \simeq 0.20 \text{ (GeV)}^{-1}/c$, i.e. a mean value for the production average transverse momentum, $\langle p_T \rangle$, of the order of $10 \text{ GeV}/c$, fits the UA1 data quite well. This value for b is much smaller than the value ($b = 2.5$) which we found in our study of « charm » production at the ISR⁽⁴⁾. However, it should be noticed that we are dealing here with the production of a flavour much heavier than « charm ». The value $b = 0.2$ is in good agreement with the prescription $\langle p_T^2 \rangle \simeq m^2/4$ (m is the quark mass) used by ODRAGO⁽⁵⁾ to compute the « charm » production properties from flavour excitation.

The efficiency for detecting electrons with $p_T > 15 \text{ GeV}/c$ in the Monte Carlo simulation does not change very much for $b > 0.2$, as shown in fig. 5. Thus the total « superbeauty » cross-section, derived by formula (6), holds, within $\pm 30\%$, even with this very low, but expected, value of b .

As mentioned above the « downlike » nature of the observed (11 ± 3) events cannot be established in a direct way. It is based on a chain of self-consistent arguments. Let us give up the ratio (2b) which binds the « top » flavour to be in the 25 GeV range. If we repeat the analysis without this constraint the (11 ± 3) events can be reinterpreted as the « uplike » signature, with the « top » flavour mass 30 GeV above the « beauty » flavour. The value of the cross-section would in this case be as shown in fig. 6.

Conclusions. A sequence of arguments based on known facts, and on simple hypotheses, extrapolated to the CERN ($p\bar{p}$) Collider energies, allow us to conclude that the (11 ± 3) events observed by the UA1 collaboration and consisting each of a single (e^\pm) accompanied by a jet activity in the opposite hemisphere, correspond to a value of the cross-section expected for the production of a very-heavy-flavoured state, in the $55 \text{ GeV}/c^2$ mass range. Moreover, the observed p_T spectrum of the (e^\pm) follows the expectations for the semi-leptonic decay of a very massive state, again in the $55 \text{ GeV}/c^2$ mass range.

It should, however, be noticed that the identification of the « downlike » nature of the heavy-flavoured state is based on a series of hypotheses which produce the

(⁴) M. BASILE, G. CARA ROMEO, L. CIFARELLI, A. CONTIN, G. D'ALÌ, P. DI CESARE, B. ESPOSITO, P. GIUSTI, T. MASSAM, F. PALMONARI, G. SARTORELLI, G. VALENTI and A. ZICHICHI: *Lett. Nuovo Cimento*, **30**, 481 (1981); M. BASILE, G. CARA ROMEO, L. CIFARELLI, A. CONTIN, G. D'ALÌ, P. DI CESARE, B. ESPOSITO, P. GIUSTI, T. MASSAM, R. NANIA, F. PALMONARI, G. SARTORELLI, G. VALENTI and A. ZICHICHI: *Lett. Nuovo Cimento*, **33**, 17 (1982).

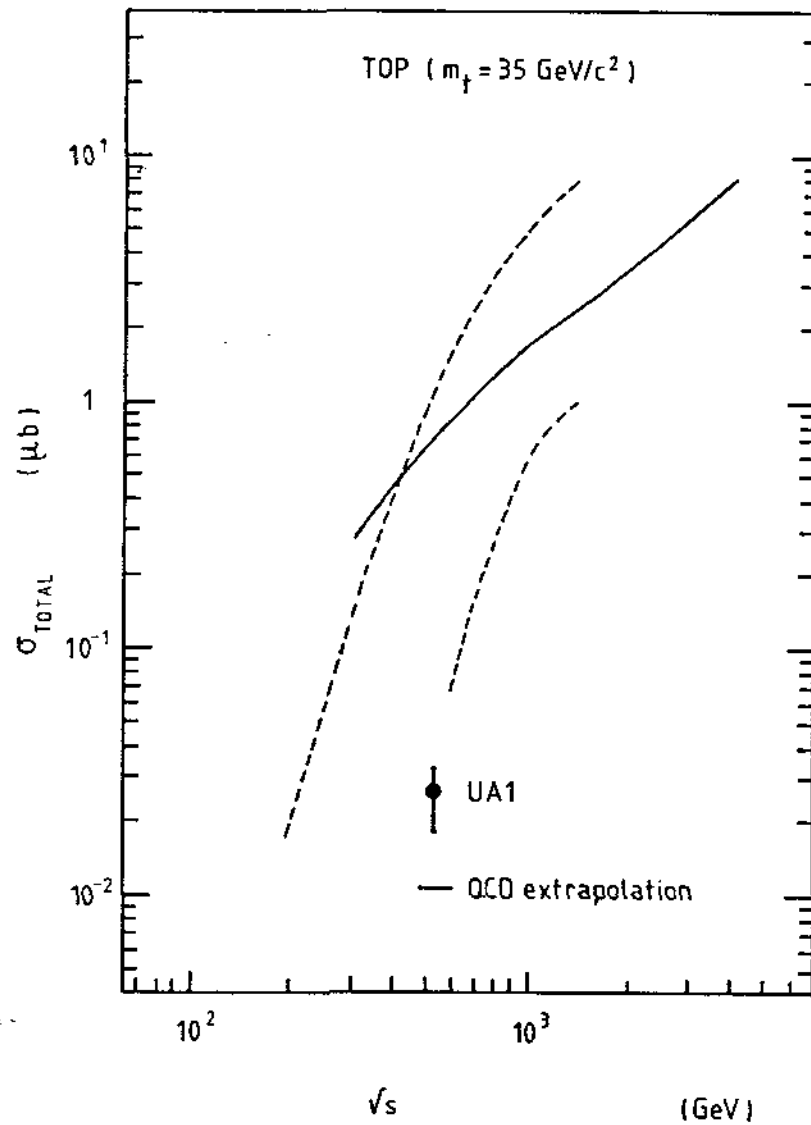


Fig. 6. - Comparison between the cross-section evaluated from the UA1 data, and the cross-sections derived from 'strange' (full line) and 'charm' (dashed lines) following formula (5) and using for 'top' the mass value $m_t = 35 \text{ GeV}/c^2$.

correct $\Delta m \approx 30 \text{ GeV}/c^2$ for the (e^\pm) transverse-momentum spectrum observed, and the correct magnitude for the cross-section. If we were to ignore the cross-section and the quark mass ratios which allows us to predict the masses of the 4th family, the only parameter left to fit the observed (e^\pm) transverse-momentum spectrum, would be the value $\Delta m \approx 30 \text{ GeV}/c^2$. In this case the conservative interpretation of the UA1 results would be a 'top' with a mass $30 \text{ GeV}/c^2$ above the 'beauty'.

This shows the importance of our proposal⁽¹⁾ to study in detail the production of new heavy flavours at the CERN ($p\bar{p}$) collider, by measuring the (c^+/c^-) asymmetry. In fact, the sign of the asymmetry allows the identification of the « uplike » or « downlike » nature of the heavy-flavoured state in a direct and unambiguous way. Moreover, the (c^+/c^-) energy dependence of the asymmetry allows us to establish the correct sequence of

« downlike » \rightarrow « uplike »

decay chains for the new heavy flavours, and their mass difference.

CERN
SERVICE D'INFORMATION
SCIENTIFIQUE

M. BASILE, *et al.*
18 Giugno 1983
Lettere al Nuovo Cimento
Serie 2, Vol. 37, pag. 255-266

III-10. "New flavours: experiment versus theory.
From charm to the 4th family"
Proc. of the 3rd Topical Workshop on Proton-Antiproton
Collider Physics (CERN-83-04),
Roma, January 12-14, 1983.

10- NEW FLAVOURS: EXPERIMENT VERSUS THEORY. FROM CHARM TO THE 4TH FAMILY.

M. Basile, J. Berbiers, G. Bonvicini, G. Cara Romeo, L. Cifarelli,
 A. Contin, M. Curatolo, G. D'Ali, C. Del Papa, B. Esposito,
 P. Giusti, T. Massam, R. Nania, G. Natale, F. Palmonari,
 G. Sartorelli, M. Spinetti, G. Susinno, L. Votano and A. Zichichi

CERN, Geneva, Switzerland

Istituto di Fisica dell'Università di Bologna, Italy

Istituto Nazionale di Fisica Nucleare, Bologna, Italy

Istituto Nazionale di Fisica Nucleare, LNF, Frascati, Italy

(Presented by A. Zichichi)

ABSTRACT

A new method of searching for heavy flavours "up-like" and "down-like" in hadronic interactions at the CERN $p\bar{p}$ Collider is proposed. The method is based on the measurement of the e^\pm asymmetry in the proton and antiproton hemispheres. The amplitude of the asymmetry depends on the "leading" production of baryons and antibaryons -- the sign on the "up-like" or "down-like" nature of the heavy flavour carried by the baryonic states. A detailed study of cross-section estimates, production and decay distributions, and detection acceptances, shows that the effect looks measurable at the CERN $p\bar{p}$ Collider.

1. INTRODUCTION

The problem of searching for heavy flavours at the CERN $p\bar{p}$ Collider is, needless to say, of the utmost importance. At this meeting you have heard a lot about Z^0 and W^\pm : in this case the cross-section evaluations are easy. Moreover, their "expected" masses are well known. The Z^0 and W^\pm will play a crucial role in our understanding of the electroweak forces. If Z^0 and W^\pm are found at the expected masses, we can conclude that the heavy bosons expected as manifestations of the broken local gauge symmetry indeed exist.

This discovery will, however, shed no light on the other two key problems of subnuclear physics: the family, and the hierarchy.

Presented at the "3rd Topical Workshop on
 Proton Antiproton Collider Physics",
 Roma, January 12-14, 1983.

Finding the "top" will allow us to conclude that the 3rd family does exist, and that it looks like the other two. Studying the 4th family will open a new way towards the understanding of the families structure. The four families are shown in the next graph. The main objectives of the present paper are indicated by the dotted circles:

$$\begin{array}{cccc}
 \text{1st} & \text{2nd} & \text{3rd} & \text{4th} \\
 \begin{pmatrix} u \\ d \end{pmatrix} & \begin{pmatrix} c \\ s \end{pmatrix} & \begin{pmatrix} \textcircled{t} \\ b \end{pmatrix} & \begin{pmatrix} u_H \\ \textcircled{d_H} \end{pmatrix} \\
 \\
 \begin{pmatrix} \nu_e \\ e \end{pmatrix} & \begin{pmatrix} \nu_\mu \\ \mu \end{pmatrix} & \begin{pmatrix} \nu_\tau \\ \tau \end{pmatrix} & \begin{pmatrix} \nu_H \\ L_H \end{pmatrix}
 \end{array}$$

Let me say a few words about these objectives. The reason for a 3rd family in the quark world came from the PC violation (six quarks are needed), and the Adler-Bell-Jackiw (ABJ) anomaly cancellation (the number of leptons should be equal to the number of quarks). In the 3rd family, there is a missing quark: the "top". (We propose continuing to call it "top": the "truth" should be the last quark ever to exist).

There is an interesting problem in SuperSymmetry (SUSY). A very heavy quark is needed so as to avoid a conflict with the existing lower limits in the gluino mass [1]. This quark should have a mass in the few $10^2 \text{ GeV}/c^2$ range, in order to produce radiatively (see Fig. 1) a few GeV/c^2 mass for the gluino. The existing quarks (s, b, and c) are not heavy enough for this purpose.

On the other hand, nature has often provided physicists with more regularities than are needed. For example, the equality between the proton and the electron charges, which it took more than three decades to understand.

We propose to consider the ratio between the masses of the known heavy quarks as a limit for the regularity in their masses. There are good reasons [2] for considering the strange quark to be heavy enough to be used in our argument.

At present we know that

$$\text{i) } (m_c/m_s) \cong (1.8/0.5) \cong 3.5 \cong 4 ;$$

$$\text{ii) } (m_b/m_s) \cong (5.5/0.5) \cong 11 \cong 10 .$$

Suppose that (i) and (ii) are of general validity, i.e.

$$(m_c/m_s) = [m(\text{up-like quark})/m(\text{down-like quark})] = 4 , \quad (1)$$

and

$$(m_b/m_s) = [m(\text{family } N+1)/m(\text{family } N)] = 10 . \quad (2)$$

We ignore the 1st family (u,d) because of its very light mass. The validity of Eqs. (1) and (2) would allow us to conclude that the "top" mass is in the 20 GeV/c² range. This is too light for supersymmetric models to avoid a gluino mass in conflict with experimental data. On the other hand, SUSY tells us that the maximum number of flavours n_f allowed in order to have a consistent theory (for example: the unification limit not above the Planck mass) is $n_f = 8$. This means that the maximum number of families is four. In the theories that ignore SUSY, the asymptotic freedom is lost if $n_f > 16$.

What is not forbidden in nature, does take place. Thus the message from SUSY is twofold:

- i) four families of quarks are allowed;
- ii) quarks heavier than (d, u, s, c, b, and t) are needed.

Equations (1) and (2) tell us that the 4th family would have the heavy masses required by SUSY. In fact, using Eq. (2), the heavy down-like quark [called, in the following, "superbeauty" or (sb)] would have a mass in the 50 GeV/c² range:

$$m(\text{down-heavy}) = m(\text{"superbeauty"}) \cong 10 \times 5.5 = 55 \text{ GeV/c}^2 ,$$

and, using Eq. (1), the heavy up-like quark would have a mass in the 200 GeV/c² range:

$$m(\text{up-heavy}) = m(\text{"supertruth"}) \cong 55 \times 4 = 220 \text{ GeV/c}^2 .$$

The up-like quark of the 4th family should be called "supertruth". In fact, this very heavy mass is required by SUSY; moreover, if SUSY is

a good theory, the 4th family should really be the last of the quark families ever to be discovered.

Now comes a key question: If "top" and "superbeauty" are accessible to $p\bar{p}$ Collider energies, how can they be detected? In order to answer this question we need to discuss:

- i) production cross-sections;
- ii) angular and momentum distributions of the production and the decay;
- iii) branching ratios into semileptonic channels;
- iv) luminosity;
- v) rejection power of the experimental set-up designed to observe the leptons produced by the decay of these "new" flavours.

We will concentrate our search in the semileptonic decay channels. Moreover, we will restrict the leptons only to e^\pm , and the search only to the asymmetry produced by these e^\pm .

More precisely, the "top" baryonic state will decay semileptonically into e^+ and produce a positive asymmetry in the outgoing proton rapidity hemisphere:

$$A_p = (e^+ - e^-)/(e^+ + e^-) = \text{positive} .$$

The "anti-top" antibaryonic state will produce a negative asymmetry in the outgoing antiproton rapidity hemisphere

$$A_{\bar{p}} = (e^+ - e^-)/(e^+ + e^-) = \text{negative} .$$

The signs of these asymmetries will be reversed for the "superbeauty" case.

The e^\pm transverse momentum spectra associated with "top" and "superbeauty" will be quite different because

$$\begin{aligned} m(\text{"top"}) &\cong 25 \text{ GeV}/c^2 , \\ m(\text{"superbeauty"}) &\cong 55 \text{ GeV}/c^2 . \end{aligned}$$

Thus the asymmetry will change sign with increasing electron energy. Figure 2 shows the main trend of the measurement we propose. This will be discussed in detail in Section 5.

The energy range where the e^{\pm} asymmetry has to be measured, and the separation between the maxima, depend on the mass difference Δm between the two new flavours:

$$\Delta m = m(\text{"superbeauty"}) - m(\text{"top"}) .$$

As we will see in Section 5, the amplitude of the effect depends on the production cross-sections, production and decay distributions, branching ratios, luminosity, and acceptance and rejection power of the experimental apparatus.

The matter is of great relevance: Can hadronic machines compete with (e^+e^-) rings in searching for new particle states? Note, for example, that the PETRA e^+e^- Collider has already established lower limits for a "top"-like flavour, a down-like flavour, and a possible new lepton -- all these limits being at about $19 \text{ GeV}/c^2$ [3].

2. A BRIEF REVIEW OF HEAVY-FLAVOUR PRODUCTION IN HADRONIC MACHINES

How to look for "top" and "superbeauty" at the CERN $p\bar{p}$ Collider is a problem analogous to "charm" and "beauty" in hadron machines, and in particular at the CERN ISR. It is probably instructive to review, very briefly, the main steps in this field.

2.1 Production cross-sections

The theoretical predictions for the charm production cross-section and the experimental findings are shown in the following Table 1.

Table 1

Theoretical predictions for the charm cross-section at ISR energies as a function of $\sigma(\pi)$.

The cross-section value experimentally found is indicated for comparison.

String model	: 10^{-10}	} $\times \sigma_{\pi}^{*})$
Fermi-Hagedorn	: 10^{-5}	
QCD (fusion)	: 10^{-4}	
QCD (flavour excitation)	: $10^{-2} - 10^{-3}$	
Experimentally	: $\sim 10^{-2}$	

*) $\sigma_{\pi} \approx 10^2 \text{ mb}$.

If we were to believe in the string model or in the statistical thermodynamical model, or in the first QCD attempts (fusion model), the conclusion should have been that the production and observation of "charm" is out of the question in hadron machines.

Only recently, QCD models (flavour excitation) came nearer to experimental findings. In Fig. 3 all the experimental data [4] are shown and compared with the various steps in the QCD models. Notice that neither $\ln(s)$ nor $\ln^2(s)$ are compatible with the observed threshold behaviour.

2.2 The "leading" effect

A result which was unpredicted by theory is the "leading" effect which shows up in the production of heavy flavours.

A detailed study of (pp) interactions at the ISR showed that the Λ_c^+ is produced in a "leading" way [5].

After this experimental result was obtained, a series of theoretical proposals were presented, to account for the "leading" Λ_c^+ production. The longitudinal momentum distribution [5] for Λ_c^+ was, in fact, found at the ISR to be

$$(d\sigma/d|x|) \sim (1 - |x|)^\alpha, \quad \text{with } \alpha = 0.40 \pm 0.25 .$$

The results are shown in Fig. 4. The charmed-meson production [6] was, on the other hand, measured to be "non-leading", i.e.

$$E(d\sigma/d|x|) \sim (1 - |x|)^\alpha, \quad \text{with } \alpha \approx 3 .$$

This can be *a posteriori* qualitatively understood in terms of the Λ_c^+ obtained by a recombination of the spectator c-quark with a valence (ud) pair in the proton, whilst the \bar{D} production is given by the recombination of the spectator \bar{c} -quark with at most one valence quark [7,8].

A more complete summary of charm production in purely hadronic interactions is reported in Table 2. There is no model which can fit all measured quantities.

Table 2
Experimental findings versus theoretical predictions
for various heavy-flavour production properties

	Experiment	Models		
		Diffraction	Flavour excitation	Fusion
Leading effect	Yes	Yes	Yes	No
Threshold behaviour	Steeper than $\ln^2 s$	$\ln s$	Steeper than $\ln^2 s$	\gg steeper than $\ln^2 s$
Mass dependence	?	$1/m^2$	Stronger than $1/m^2$	\gg stronger than $1/m^2$
Cross-section	Large	Large	Large	Small
A^α dependence	$\alpha < 2/3$ *)	$\alpha = 2/3$	$\alpha = 1$	$\alpha = \dots$

*) The p_T dependence is derived from data on strangeness.

2.3 Further comments

For the benefit of those who have strong faith in QCD, it could be interesting to extend our review. In fact the photoproduction was considered a simpler case for QCD. Therefore its predictions should have been in agreement with experimental findings.

A summary of QCD problems in photoproduction physics is as follows:

- a) it is impossible to predict large photoproduction cross-sections of the heavy flavours by means of perturbative QCD;
- b) the p_T dependence of inelastic ($c\bar{c}$), for open and hidden states cannot be accounted for by QCD;
- c) the A -dependence cannot be A^1 . (Perturbative QCD predicts A^1 .)

2.4 Conclusions

The conclusion of this short review on the "charm" flavour production in (pp) interactions is therefore as follows:

- i) the cross-section values found are at least an order of magnitude above the "theoretical" predictions of perturbative QCD;
- ii) the x -distribution for Λ_c^+ , i.e. the "leading" effect, was theoretically unpredicted;

iii) with "new" models (essentially flavour excitation [8,9] and non-perturbative QCD [7]), both cross-section values and x-distributions can be "theoretically" derived.

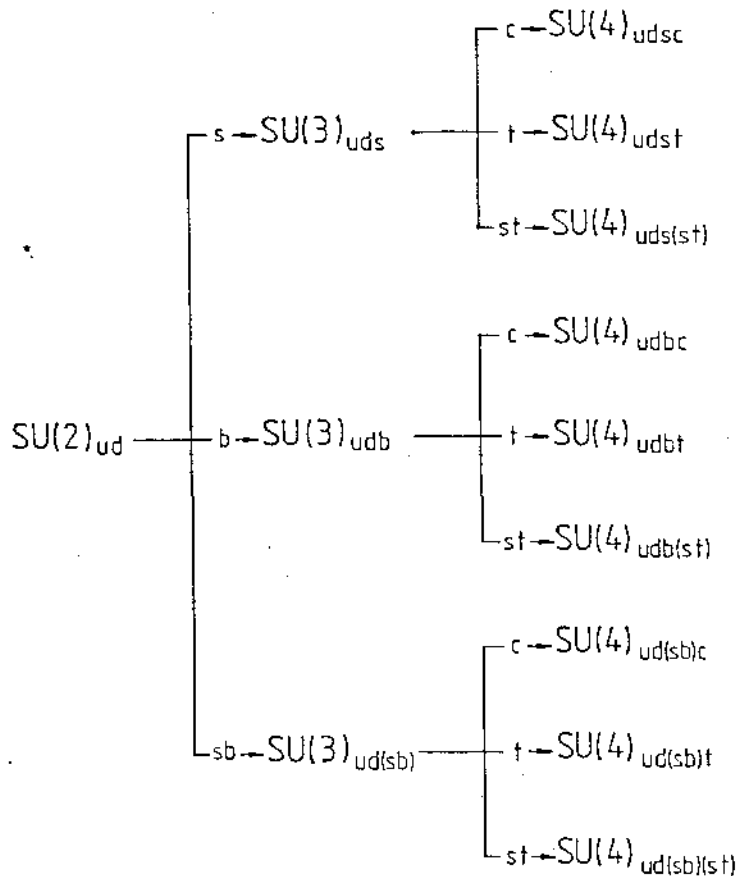
All this should be quite a warning for QCD prediction on heavy-flavour production at extreme energies such as those of the CERN $p\bar{p}$ Collider.

3. EXPECTED NEW HEAVY-FLAVOUR STATES

The main purpose of this section is to call attention to the enormous number of new states which are expected on the basis of the old and new flavours. In order to attempt to give order to the vast multitude of states, we will limit ourselves to the possibility that they will follow the global symmetries already known with (udsc).

3.1 Examples from previous experience with $SU(3)_{uds}$ and $SU(4)_{udsc}$

The following graph illustrates what could indeed happen.



With three flavours (u, d, and s) the famous $SU(3)_{uds}$ came out. It could be that "beauty" will produce another $SU(3)_{udb}$. The advent of the "charm" with four flavours (udsc) produced $SU(4)_{udsc}$. On the other hand, with the "top" there are two possible $SU(4)$: $SU(4)_{udst}$ and $SU(4)_{udbt}$.

Despite the large mass differences amongst the various flavours, it could be that nature will provide, as usual, more regularities than are required. The above global symmetry groups for the structure of the various possible particle states could eventually show up, even if not expected.

If "superbeauty" was there, we would have even a larger set of $SU(3)$ and $SU(4)$ states and, in addition, all combinations of purely singlet states such as s, c, b, t, and (sb).

Examples of $SU(4)$ structures using u, d, s, c, b, t, superbeauty (sb), and supertruth (st) are presented in Figs. 5 to 7. They include mesonic and baryonic states.

If we enlarge the symmetries to the Lorentz spins and angular momenta amongst quarks, the multitude of states increases further. These are indicated, for the first three flavours (u, d, and s) in Tables 3 and 4 for the mesons and for the baryons in $SU(6)$, respectively.

Table 3
SU(6) mesonic multiplets

SU(6)	$SU(3)_f$	J^{PC}	Particle states	Number of states
$[(35 \oplus 1) \otimes 1]; (L = 0)$	$8 \oplus 1$	0^{-+}	π, K, η, η'	36
	$8 \oplus 1$	1^{--}	ρ, K^*, ω, ϕ	
$[(35 \oplus 1) \otimes 3]; (L = 1)$	$8 \oplus 1$	1^{+-}	$B, Q_{1,2} \dots ?$	108
	$8 \oplus 1$	0^{++}	S, χ, S^*, ϵ	
	$8 \oplus 1$	1^{++}	$A_1, Q_{1,2}, D, E$	
	$8 \oplus 1$	2^{++}	A, K^{**}, f, f'	

Table 4
Baryons in SU(6) multiplets

$[SU(6), L^P]$	$SU(3)_f$	J^P	Standard names of particle states
$(56, 0^+)$	8	$1/2^+$	N, Λ , Σ , Ξ^-
	10	$3/2^+$	N^* , Σ^* , Ξ^* , Ω^-
$(70, 1^-)$	1	$1/2^-$	Repeat singlet
	8	$1/2^-$	Repeat octet
	10	$1/2^-$	Repeat decuplet
	1	$3/2^-$	Repeat singlet
	8	$3/2^-$	Repeat octet
	10	$3/2^-$	Repeat decuplet
	8	$1/2^-$	Repeat octet
	8	$3/2^-$	Repeat octet
8	$5/2^-$	Repeat octet	

[Repeat means that the quantum numbers (isospin and strangeness) of the states are identical to the "octet" and "decuplet" already known for the 56-case.]

An example of how the multitude of the states goes with the mass is shown in Figs. 8a and 8b, where the masses of the particles run from a few GeV/c^2 to $60 \text{ GeV}/c^2$.

3.2 Note on the semileptonic decay modes: Cabibbo dominance

A fact of nature is that the matrix which relates the down-like "weak" flavours "Cabibbo mixed",

$$\begin{pmatrix} d_c \\ s_c \\ b_c \end{pmatrix},$$

to the "strong" flavours

$$\begin{pmatrix} d \\ s \\ b \end{pmatrix},$$

is approximately a unit matrix

$$\begin{pmatrix} d_c \\ s_c \\ b_c \end{pmatrix} \approx \begin{pmatrix} 1 & 0 & 0 \\ 0 & 1 & 0 \\ 0 & 0 & 1 \end{pmatrix} \begin{pmatrix} d \\ s \\ b \end{pmatrix}$$

We will now follow the expected generalized Cabibbo dominance in the decay of the flavoured quark, as illustrated in Figs. 9a and 9b. All that we need is the charge sign of the lepton in a transition from an "up-like" to a "down-like" flavour. This is summarized in Table 5.

Table 5

How to compute the electric charge sign of the leptons (e^\pm or μ^\pm) produced in the semileptonic decays of quarks

$\begin{pmatrix} u \\ d \end{pmatrix}$	$\begin{pmatrix} c \\ s \end{pmatrix}$	$\begin{pmatrix} t \\ b \end{pmatrix}$	$\begin{pmatrix} st \\ sb \end{pmatrix}$	
↓	↓	↓	↓	
$\begin{pmatrix} 1 \\ 2 \end{pmatrix}$	$\begin{pmatrix} 3 \\ 4 \end{pmatrix}$	$\begin{pmatrix} 5 \\ 6 \end{pmatrix}$	$\begin{pmatrix} 7 \\ 8 \end{pmatrix}$	← ODD (= UP-LIKE) QUARKS ← EVEN (= DOWN-LIKE) QUARKS
The charge formula can be written as:				
$Q = (1/3 + f_i)/2$,				
with.				
$f_i = +1$ for odd quarks ($i = 1, 3, 5, 7$),				
$f_i = -1$ for even quarks ($i = 2, 4, 6, 8$).				
From this follows the electric charge sign of the lepton in the semileptonic decay of the flavour:				
ODD → EVEN (UP-LIKE → DOWN-LIKE) TRANSITION ⇒ POSITIVE LEPTON				
EVEN → ODD (DOWN-LIKE → UP-LIKE) TRANSITION ⇒ NEGATIVE LEPTON				

As will be seen in Figs. 10, a sequence $t \rightarrow b \rightarrow c \rightarrow s$ will be accompanied by the semileptonic series giving rise to $e^+ + e^- \rightarrow e^+$. For the antiquark sequence $\bar{t} \rightarrow \bar{b} \rightarrow \bar{c} \rightarrow \bar{s}$, the charges will be reversed ($e^- \rightarrow e^+ \rightarrow e^-$). These results are straightforward consequences of the previous table.

4. CROSS-SECTION ESTIMATES: HOW TO GO FROM STRANGENESS TO CHARM, BEAUTY, TOP, AND SUPERBEAUTY

Now comes a key question: Once we know the "strange" and "charm" cross-sections, is it possible to predict the heavier flavour [c, b, t, or (sb)] cross-sections in hadronic collisions?

Simple arguments bring us to the conclusion that

$$\sigma(m) \sim (1/m^2) \times f(s/m^2) . \quad (3)$$

In fact, the only quantities which enter in the problem of producing a (q \bar{q}) pair, having at disposal the total energy \sqrt{s} , are the quark mass m and the total energy \sqrt{s} .

Formula (3) is based on dimensional and scaling arguments:

Dimension says that: $\sigma \sim (1/m^2)$.

Scaling says that the two quantities m^2 and s are such that nothing changes if their ratio (s/m^2) is kept constant; the ratio (s/m^2) is the dimensionless quantity needed if no other scale would remain in the game.

The basic formula is therefore:

$$\sigma_i [(\sqrt{s})_{pp} = E_i] = (m_j/m_i)^2 \times \sigma_j [(\sqrt{s})_{pp} = E_j = (m_j/m_i)E_i] , \quad (4)$$

where

σ_i, σ_j are the production cross-sections,
 m_i, m_j are the masses,
 E_i, E_j are the energies

at which flavours f_i and f_j are produced.

The results are shown in Figs. 11 to 14, where we have used

- i) the strangeness data to predict c, b, t, and (sb);
- ii) the "charm" data to predict b, t, and (sb);
- iii) the "beauty" data to predict t and (sb).

Finally, for completeness, we also report the most recent QCD predictions of [7] and [8] (Fig. 15).

5. THE STUDY OF THE LEPTON CHARGE ASYMMETRY AND ITS ENERGY DEPENDENCE
AS A WAY OF DETECTING THE HEAVIEST FLAVOURED STATES
(BARYONIC AND ANTIBARYONIC) AT THE CERN $p\bar{p}$ COLLIDER

Many possibilities have been suggested for detecting the production of the heaviest flavours at the $p\bar{p}$ Collider. They are summarized in Table 6, together with their main difficulties.

Table 6

Summary of the various experimental methods which can be used for detecting the production of heavy flavours at the CERN $p\bar{p}$ Collider, together with their main difficulties

States to be observed	Method	Problems with the method
Hidden	Invariant mass ($\ell^+\ell^-$) pairs	Low cross-sections and low branching ratios
Open	Invariant mass of the decay products	Low branching ratios for exclusive channels, and high combinatorial background due to the high multiplicity of the event
	Study of multilepton events	Low cross-sections due to the multiple branching ratios involved
	Study of inclusive lepton p_T spectra	Need for a high rejection power against hadron background

Here we present a new method of observing the production of heavy mass states, either up-like ("top") or down-like ("superbeauty"), which is based on the "leading" baryon effect production mechanism, extended to the heaviest baryon and antibaryon states. In fact, owing to this production mechanism, a charge asymmetry of the leptons originating from these heavy flavours can be observed in a selected region of the phase space. Moreover, this asymmetry will show an energy dependence characteristic of the masses of the decaying states.

5.1 Definition of the asymmetry parameter A^0

Figure 10 shows the leptonic decay chains, following the generalized Cabibbo dominance, for the various flavours c, b, t, (sb).

Once a particle-antiparticle pair has been produced, the number of positive and negative leptons from its decay is on the average, equal. However, in the following we will discuss under which conditions we can observe an asymmetry in the number of positive and negative leptons, which is due to the different longitudinal momentum production distribution for baryons and mesons and to the dependence of the lepton p_T spectra from the product particle mass.

Let us define the asymmetry parameter as

$$A^0(p_T, \theta_{\text{cut}}) = \frac{N(\ell^+) - N(\ell^-)}{N(\ell^+) + N(\ell^-)}, \quad (5)$$

where $N(\ell^+) \equiv N(\ell^+; p_T, \theta_{\text{cut}})$ and $N(\ell^-) \equiv N(\ell^-; p_T, \theta_{\text{cut}})$ are the number of positive and negative leptons produced in the angular range $0^\circ < \theta < \theta_{\text{cut}}$ and with transverse momentum p_T .

The number of positive leptons ℓ^+ is expressed by

$$N(\ell^+) = L [n_{sb}(\ell^+) + n_t(\ell^+) + n_b(\ell^+) + n_c(\ell^+)],$$

where L is the total integrated luminosity and $n_f(\ell^+)$ [with $f = (sb), t, b, c$] is the contribution from the direct production of (sb), t, b, c states.

Analogously the number of negative leptons is given by

$$N(\ell^-) = L [n_{sb}(\ell^-) + n_t(\ell^-) + n_b(\ell^-) + n_c(\ell^-)].$$

The leptons originated by the decay of the various flavours and anti-flavours are summarized in Tables 7a and 7b.

Table 7

All the heavy-flavour (a) and heavy-antiflavour (b) decay chains producing ℓ^+ and ℓ^-

a)

Flavour	Decays producing ℓ^+	Decays producing ℓ^-
sb	$sb \rightarrow t \rightarrow b + \ell^+$ $sb \rightarrow t \rightarrow b \rightarrow c \rightarrow s + \ell^+$	$sb \rightarrow t + \ell^-$ $sb \rightarrow t \rightarrow b \rightarrow c \rightarrow \ell^-$
t	$t \rightarrow b + \ell^+$ $t \rightarrow b \rightarrow c \rightarrow s + \ell^+$	$t \rightarrow b \rightarrow c + \ell^-$
b	$b \rightarrow c \rightarrow s + \ell^+$	$b \rightarrow c \rightarrow \ell^-$
c	$c \rightarrow s + \ell^+$	

b)

Antiflavour	Decays producing ℓ^+	Decays producing ℓ^-
\overline{sb}	$\overline{sb} \rightarrow \overline{t} + \ell^+$ $\overline{sb} \rightarrow \overline{t} \rightarrow \overline{b} \rightarrow \overline{c} + \ell^+$	$\overline{sb} \rightarrow \overline{t} \rightarrow \overline{b} + \ell^-$ $\overline{sb} \rightarrow \overline{t} \rightarrow \overline{b} \rightarrow \overline{c} \rightarrow \overline{s} + \ell^-$
\overline{t}	$\overline{t} \rightarrow \overline{b} \rightarrow \overline{c} + \ell^+$	$\overline{t} \rightarrow \overline{b} + \ell^-$ $\overline{t} \rightarrow \overline{b} \rightarrow \overline{c} \rightarrow \overline{s} + \ell^-$
\overline{b}	$\overline{b} \rightarrow \overline{c} + \ell^+$	$\overline{b} \rightarrow \overline{c} \rightarrow \overline{s} + \ell^-$
\overline{c}		$\overline{c} \rightarrow \overline{s} + \ell^-$

In order to write down explicitly $n_f(\ell^+)$, let us define the following:

- i) σ_f^{tot} : total cross-section for the production of open (f, \overline{f})-pairs;
- ii) $\rho_{M\overline{f}}, \rho_{\overline{M}f}, \rho_{Bf}, \rho_{\overline{B}\overline{f}}$: ratios between the inclusive cross-section for producing ($M = \text{meson}, \overline{M} = \text{antimeson}, B = \text{baryon}, \overline{B} = \text{antibaryon}$) states, and the total cross-section σ_f^{tot} ;
- iii) $BR_{Mf'}, BR_{\overline{M}\overline{f}'}, BR_{Bf'}, BR_{\overline{B}\overline{f}'}$: semileptonic branching ratios of the various states with flavour f' [$f' = c, b, t, (sb)$];

- iv) $\epsilon_{Mf}(\ell_f^\pm)$, $\epsilon_{\bar{M}\bar{f}}(\ell_{\bar{f}}^\pm)$, $\epsilon_{Bf}(\ell_f^\pm)$, $\epsilon_{\bar{B}\bar{f}}(\ell_{\bar{f}}^\pm)$: acceptance for ℓ^\pm from the leptonic decay of the flavour f' produced in the decay chain of the state with flavour f . This acceptance is a function of the lepton p_T and of the cut in $\theta < \theta_{\text{cut}}$ applied to the lepton polar angle.

Accordingly, we have for the case of "superbeauty":

$$n_{sb}(\ell^+) = \sigma_{sb}^{\text{tot}} \left\{ \rho_{Msb} \left[BR_{Mt} \epsilon_{Msb}(\ell_t^+) + BR_{Mc} \epsilon_{Msb}(\ell_c^+) \right] \right. \\ + \rho_{\bar{M}\bar{s}\bar{b}} \left[BR_{\bar{M}\bar{s}\bar{b}} \epsilon_{\bar{M}\bar{s}\bar{b}}(\ell_{\bar{s}\bar{b}}^+) + BR_{\bar{M}\bar{b}} \epsilon_{\bar{M}\bar{s}\bar{b}}(\ell_{\bar{b}}^+) \right] \\ + \rho_{Bsb} \left[BR_{Bt} \epsilon_{Bsb}(\ell_t^+) + BR_{Bc} \epsilon_{Bsb}(\ell_c^+) \right] \\ \left. + \rho_{\bar{B}\bar{s}\bar{b}} \left[BR_{\bar{B}\bar{s}\bar{b}} \epsilon_{\bar{B}\bar{s}\bar{b}}(\ell_{\bar{s}\bar{b}}^+) + BR_{\bar{B}\bar{b}} \epsilon_{\bar{B}\bar{s}\bar{b}}(\ell_{\bar{b}}^+) \right] \right\}$$

and

$$n_{sb}(\ell^-) = \sigma_{sb}^{\text{tot}} \left\{ \rho_{\bar{M}\bar{s}\bar{b}} \left[BR_{\bar{M}\bar{t}} \epsilon_{\bar{M}\bar{s}\bar{b}}(\ell_{\bar{t}}^-) + BR_{\bar{M}\bar{c}} \epsilon_{\bar{M}\bar{s}\bar{b}}(\ell_{\bar{c}}^-) \right] \right. \\ + \rho_{Msb} \left[BR_{Msb} \epsilon_{Msb}(\ell_{sb}^-) + BR_{Mb} \epsilon_{Msb}(\ell_b^-) \right] \\ + \rho_{\bar{B}\bar{s}\bar{b}} \left[BR_{\bar{B}\bar{t}} \epsilon_{\bar{B}\bar{s}\bar{b}}(\ell_{\bar{t}}^-) + BR_{\bar{B}\bar{b}} \epsilon_{\bar{B}\bar{s}\bar{b}}(\ell_{\bar{b}}^-) \right] \\ \left. + \rho_{Bsb} \left[BR_{Bsb} \epsilon_{Bsb}(\ell_{sb}^-) + BR_{Bb} \epsilon_{Bsb}(\ell_b^-) \right] \right\}.$$

The analogous expressions for $n_c(\ell^+)$, $n_b(\ell^+)$, and $n_c(\ell^-)$ can be easily derived and are not reported here.

From the above formulas it can be seen that in order to evaluate the asymmetry parameter A^0 , one needs to know:

- i) the total cross-section: σ^{tot} ;
- ii) the decay branching ratios: BR;
- iii) the efficiency relative to the production distributions of the baryon or meson states and to the lepton distributions in the decays: ϵ ;
- iv) the relative fraction of baryons and mesons: ρ .

We will now discuss in some detail the assumptions we made for these quantities.

5.2 The total cross-sections

We will extrapolate the total cross-sections for the heavy flavours at the CERN $p\bar{p}$ Collider energies using formula (4) and starting from the strangeness cross-section. Using the known masses for "charm" and "beauty" baryons and mesons, and the values:

$$m_t = 25 \text{ GeV}/c^2 ,$$

$$m_{sb} = 55 \text{ GeV}/c^2 ,$$

for the "top" and "superbeauty" particles, we obtain

$$\sigma_c \approx 2000 \text{ } \mu\text{b} , \quad (6a)$$

$$\sigma_b \approx 140 \text{ } \mu\text{b} , \quad (6b)$$

$$\sigma_t \approx 1.5 \text{ } \mu\text{b} , \quad (6c)$$

$$\sigma_{sb} \approx 0.15 \text{ } \mu\text{b} . \quad (6d)$$

Other estimates, from perturbative QCD, will however be taken into account when discussing the results. It will be shown that, under some conditions, even these very low cross-sections ($\sigma_b \approx 10 \text{ } \mu\text{b}$ and $\sigma_t \approx 0.1 \text{ } \mu\text{b}$ [12]) give rise to a measurable asymmetry.

5.3 The decay branching ratio

Recent data from CLEO [13] give for the semileptonic branching ratio of the "beauty" mesons:

$$(M_b \rightarrow \ell^\pm) / (M_b \rightarrow \text{all}) \approx 0.13 .$$

For quark masses greater than the "beauty" mass, the semileptonic branching ratio should be even greater, approaching the value 0.16 which is expected from the quark colours and leptons counting.

In our Monte Carlo simulation we assume the known semileptonic branching ratios for "charm":

$$(D \rightarrow \ell^\pm) / (D \rightarrow \text{all}) \approx 0.085 ,$$

$$(\Lambda_c^+ \rightarrow \ell^\pm) / (\Lambda_c^+ \rightarrow \text{all}) \approx 0.045 ,$$

and the conservative value of 0.1 for all other heavier particles.

5.4 The production distributions of baryon and meson states

The study of the reactions

$$pp \rightarrow D + e^+ + \text{anything} ,$$

$$pp \rightarrow \Lambda_c^+ + e^- + \text{anything} ,$$

$$pp \rightarrow \Lambda_b^0 + e^+ + \text{anything} ,$$

at the ISR indicate that in baryon-baryon collisions the heavy-flavoured baryons are produced according to a rather flat x-distribution:

$$(d\sigma/dx) \sim \text{const} ,$$

whilst the heavy-flavoured mesons are produced with softer x-distribution of the type

$$E(d\sigma/d|x|) \sim (1 - |x|)^3 .$$

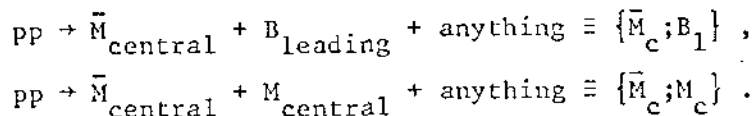
These distributions will be assumed all through the following discussion, together with the p_T dependence

$$(d\sigma/dp_T) \sim p_T \exp(-2.5 p_T)$$

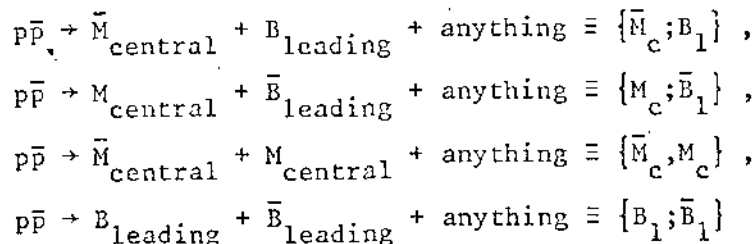
observed at the ISR in the production of heavy flavours [14].

5.5 The relative yield of mesons and baryons

From the data on strangeness production at the ISR it can be assumed that, in (pp) collisions, the following reactions dominate



In (p \bar{p}) collisions, because of the antibaryonic nature of the \bar{p} hemisphere, the following reactions can take place:



In this case, the ratio of the inclusive cross-sections for producing the four classes of particles M_c , \bar{M}_c , B_1 , and \bar{B}_1 , and the total cross-sections are

$$\begin{aligned} \rho_M &= [\sigma\{M_c; \bar{B}_1\} + \sigma\{M_c; \bar{M}_c\}]/\sigma^{\text{tot}} , \\ \rho_{\bar{M}} &= [\sigma\{\bar{M}_c; B_1\} + \sigma\{\bar{M}_c; M_c\}]/\sigma^{\text{tot}} , \\ \rho_B &= [\sigma\{\bar{M}_c; B_1\} + \sigma\{B_1; \bar{B}_1\}]/\sigma^{\text{tot}} , \\ \rho_{\bar{B}} &= [\sigma\{M_c; \bar{B}_1\} + \sigma\{B_1; \bar{B}_1\}]/\sigma^{\text{tot}} ; \end{aligned}$$

with:

$$\sigma^{\text{tot}} = \sigma\{\bar{M}_c; B_1\} + \sigma\{M_c; \bar{B}_1\} + \sigma\{\bar{M}_c; M_c\} + \sigma\{B_1; \bar{B}_1\} .$$

Defining the ratio

$$\text{leading/total} = \rho_B ,$$

the four ratios ρ can be written as:

$$\rho_B = \rho_{\bar{B}} = (\text{leading/total})$$

$$\rho_M = \rho_{\bar{M}} = [1 - (\text{leading/total})] .$$

At the ISR, in each hemisphere the ratio (leading/total) is $\sim 1/16$ for strangeness and $\sim 1/8$ for "charm". In our discussion we will study the behaviour of Λ^0 as a function of (leading/total).

5.6 The lepton decay distributions

The data from CLEO [15] show that the semileptonic decay of "beauty" mesons M_b , the magnitude of the mass recoiling with respect to the leptons is very near to the D mass:

$$M_b \rightarrow X \nu, \quad \text{with } M_X \sim M_D \approx 2.0 \text{ GeV}/c^2 .$$

Moreover, the mean charged multiplicity of the decay is 3.5, where the D contributes with 2.5 charged particles on the average. We can conclude that, even at values of the mass as high as the mass of the M_b , the semileptonic decay proceeds via a three-body decay. On the contrary, the mean charged multiplicity in the hadronic decays of the M_b mesons is 6.3, i.e. the hadronic decay of the M_b produces, on the average, one D plus four charged particles plus two neutral particles:

$$M_b \rightarrow D + 6 \text{ bodies} .$$

In the following we will consider two possibilities:

- i) the total multiplicity of all decays is 3: this is the worst case for the asymmetry Λ^0 ;
- ii) the total multiplicity of all semileptonic decays is 3 and the decay is $K_{\ell 3}$ -like for mesons and phase-space for baryons, whilst the total multiplicities of all the hadronic decays have the known values for

"charm" and "beauty" (~ 3 for "charm", $\sim \text{charm} + 6$ for "beauty"), and, for "top" and "superbeauty", the same multiplicity as for "beauty". It should be noted that this is already a conservative hypothesis, since the hadronic decays of "top" and "superbeauty" can be expected to produce more particles than "beauty". Higher values of multiplicity would produce higher values for the asymmetry.

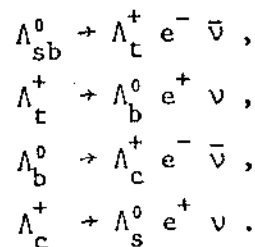
5.7 Estimates of the asymmetry A^0

The detection acceptances ϵ have been evaluated by means of a Monte Carlo simulation, with the conditions set in the previous sections and for five values of θ_{cut} ($\theta_{\text{cut}} = 10^\circ, 20^\circ, 30^\circ, 40^\circ, \text{ and } 90^\circ$).

Figures 16a to 16t show the e^\pm acceptances in the baryon hemisphere for $\theta_{\text{cut}} = 30^\circ$ and model (ii) of subsection 5.6 for baryons, mesons, and antimessons. The acceptances for e^\pm in the baryon hemisphere originated by the decay of antibaryons, produced mainly in the antibaryon hemisphere because of the "leading" effect, are, of course, negligible.

Figure 17 shows the behaviour of $A^0(p_T, 30^\circ)$, for (leading/total) = 0.25 and model (ii) of subsection 5.6. There are two main peaks: one positive around $p_T = 10$ GeV/c, due to the "top" baryon decay into e^+ ; and one negative around $p_T = 19$ GeV/c, due to "superbeauty" baryon decay into e^- .

It is interesting to note that the separation between the two peaks depends only on the mass difference between the "superbeauty" and the "top" states. In fact, in the three-body semileptonic decay the transverse momentum spectrum of the electrons or positrons scales with $p_T/\Delta m$, where Δm is the difference between the parent mass and the mass of the hadronic particle produced in the decay. This is shown in Fig. 18, where the normalized $p_T/\Delta m$ spectra of the electrons and positrons produced in the following reactions are reported:



The mass differences Δm have the following values:

- i) $\Delta m = m(\Lambda_{sb}^0) - m(\Lambda_t^+) \approx 30 \text{ GeV}/c^2$ for the "sb" baryon decay;
- ii) $\Delta m = m(\Lambda_t^+) - m(\Lambda_b^0) \approx 19.5 \text{ GeV}/c^2$ for the "t" baryon decay;
- iii) $\Delta m = m(\Lambda_b^0) - m(\Lambda_c^+) \approx 3.2 \text{ GeV}/c^2$ for the "b" baryon decay;
- iv) $\Delta m = m(\Lambda_c^+) - m(\Lambda_s^0) \approx 1.2 \text{ GeV}/c$ for the "c" baryon decay;

Figures 19a,b and 20a,b show the amplitude of the two peaks as a function of θ_{cut} and (leading/total) for: a) model (i) of subsection 5.6 (all three-body decays); and b) model (ii) of subsection 5.6 (greater multiplicity for the hadronic decays).

5.8 Background evaluation

In what has been described so far, the background contamination in the sample of prompt e^+ and e^- has not been considered. It is mainly due to:

- i) the misidentification of charged and neutral hadrons in the experimental apparatus;
- ii) the prompt e^+ or e^- production from sources other than open heavy-flavour states.

The contribution (i) can be derived by extrapolating, above $p_T \approx 10 \text{ GeV}/c$, the inclusive pion cross-section as measured by the UAL experiment [16], using the fit to their data:

$$E(d\sigma^3/dp^3) = A \times p_0^n / (p_0 + p_T)^n, \quad (7)$$

with $A = 0.46 \pm 0.10 \text{ mb}^2 \text{ c}^2 \text{ GeV}^{-2}$, $p_0 = 1.3 \pm 0.18 \text{ GeV c}^{-1}$ and $n = 9.14 \pm 0.77$.

Formula (7) is relative only to charged pions (averaged over the two charges) and is given in units of rapidity. We have assumed the contribution to the background due to the neutral pions to be ~ 0.2 of the cross-section (7). The rapidity interval over which we integrated the background depends on the θ_{cut} :

$$\begin{aligned}
 \theta_{\text{cut}} &= 90^\circ, & \Delta y &\approx 4.0, \\
 \theta_{\text{cut}} &= 40^\circ, & \Delta y &\approx 3.0, \\
 \theta_{\text{cut}} &= 30^\circ, & \Delta y &\approx 2.7, \\
 \theta_{\text{cut}} &= 20^\circ, & \Delta y &\approx 2.3, \\
 \theta_{\text{cut}} &= 10^\circ, & \Delta y &\approx 1.5.
 \end{aligned}$$

The extrapolated background rates should be multiplied by a reduction factor representing the rejection of the background from source (i).

Concerning the prompt electron background (ii), we assume, as a first approximation, that it would be negligible when compared with the contribution (i).

5.9 Estimate of the asymmetry parameter inclusive of background

Owing to the background sources described in the previous section, the experimental asymmetry parameter is given by:

$$A^{\text{exp}}(p_T, \theta_{\text{cut}}) = \frac{[N(e^+) + N_{\text{bg}}(e^+)] - [N(e^-) + N_{\text{bg}}(e^-)]}{[N(e^+) + N_{\text{bg}}(e^+)] + [N(e^-) + N_{\text{bg}}(e^-)]} \quad (8)$$

where $N_{\text{bg}}(e^\pm)$ is the number of background positrons or electrons; A^{exp} can then be expressed as a function of A^0 and of the signal-to-background ratio. In fact

$$\frac{\text{signal}}{\text{background}} = \frac{N(e^\pm)}{N_{\text{bg}}(e^\pm)};$$

assuming $N_{\text{bg}}(e^+) = N_{\text{bg}}(e^-) = N_{\text{bg}}(e)$ and substituting in Eq. (8) the expressions for $N(e^-)$ and $N(e^+)$ derived from the definition of A^0 , the result would be

$$A^{\text{exp}} = \frac{A^0}{1 + \{(1 + A^0)/[N(e^+)/N_{\text{bg}}(e)]\}}, \quad \text{for } A^0 > 0;$$

$$A^{\text{exp}} = \frac{A^0}{1 + \{(1 - A^0)/[N(e^-)/N_{\text{bg}}(e)]\}}, \quad \text{for } A^0 < 0.$$

Figure 21 shows the quantity A^{exp} plotted as a function of the signal-to-background ratio for various values of A^0 . The results can be

expressed with curves of constant A^{exp} as a function of (rejection power) versus (cross-section for "top" and "superbeauty" production), for different θ_{cut} leading/total, and decay models (Figs. 22 to 31).

Tables 8a,b summarize the results given in Figs. 22 to 31 for two values of the total cross-section. They show the rejection powers needed to obtain $A^{\text{exp}} > 0.3$ or $A^{\text{exp}} < -0.3$, i.e. a reasonably high value for the asymmetry, at the "top" and "superbeauty" peaks respectively. It can be seen that, with a rejection power of the order of 10^{-3} , a large range of θ_{cut} , leading/total, and cross-section values are accessible.

Table 8

Rejection power, in units of 10^{-3} ,
needed to obtain $A^{\text{exp}} = 0.3$ in the "top" region (a),
and $A^{\text{exp}} = -0.3$ in the "superbeauty" region (b),
for various values of θ_{cut} and leading/total

a)

$p_T = 10 \text{ GeV/c (top)}$					
θ_{cut}	(leading/total)	Cross-section estimates			
		[Formula (6)]		(perturbative QCD)	
		$\sigma_t = 1.5 \mu\text{b}$ $\sigma_{\text{sb}} = 0.15 \mu\text{b}$		$\sigma_t = 0.1 \mu\text{b}$ $\sigma_{\text{sb}} = 0.01 \mu\text{b}$	
		Model (i)	Model (ii)	Model (i)	Model (ii)
10°	0.1	3.0	3.5	0.2	0.3
	0.25	10.0	12.0	0.6	0.7
	0.5	15.0	18.0	1.0	1.3
20°	0.1	1.3	1.5	0.1	0.1
	0.25	8.0	9.0	0.5	0.6
	0.5	20.0	23.0	1.0	1.2
30°	0.1	-	-	-	-
	0.25	6.0	7.0	0.4	0.4
	0.5	19.0	22.0	1.0	1.2
40°	0.1	-	-	-	-
	0.25	3.5	4.8	0.3	0.3
	0.5	17.0	21.0	1.0	1.1

b)

$p_T = 19 \text{ GeV/c}$ (superbeauty)					
θ_{cut}	(leading/total)	Cross-section estimates			
		[formula (6)]		(perturbative QCD)	
		$\sigma_t = 1.5 \text{ } \mu\text{b}$ $\sigma_{\text{sb}} = 0.15 \text{ } \mu\text{b}$		$\sigma_t = 0.1 \text{ } \mu\text{b}$ $\sigma_{\text{sb}} = 0.01 \text{ } \mu\text{b}$	
		Model (i)	Model (ii)	Model (i)	Model (ii)
10°	0.1	0.4	1.0	0.02	0.1
	0.25	0.9	2.5	0.1	0.2
	0.5	1.7	4.5	0.1	0.3
20°	0.1	2.5	5.5	0.2	0.4
	0.25	10.0	20.0	0.5	1.0
	0.5	1.7	4.5	0.1	0.3
30°	0.1	-	2.2	-	0.2
	0.25	9.0	25.0	0.6	1.1
	0.5	23.0	45.0	1.6	2.0
40°	0.1	-	-	-	-
	0.25	4.0	19.0	0.3	1.0
	0.5	20.0	40.0	1.5	2.0

5.10 Conclusions

As an example of what can be obtained experimentally in terms of the asymmetry A^{exp} , let us fix some of the parameters in a reasonable way. We take (as in Figs. 29b and 29e):

- i) (leading/total) = 0.25,
- ii) $\theta_{\text{cut}} = 30^\circ$,
- iii) decay model (ii).

Moreover, in order to have an estimate for the experimental errors on A^{exp} , we assume a total integrated luminosity $L = 300 \text{ nb}^{-1}$ (foreseen for 1983 at the CERN $p\bar{p}$ Collider).

Figures 32a,b show the plot of A^{exp} as a function of p_T , for a rejection power of 10^{-3} and for the two cross-section estimates: as in

subsection 5.2 [formula (6)] and as from perturbative QCD ($\sigma_t : \sigma_{sb} = 10:1$), respectively. The errors are purely statistical.

Figures 33a,b show the expected number of produced electrons as a function of p_T , with the same two assumptions for the total cross-sections. Superimposed is the expected background, as defined in subsection 5.8, and with a rejection factor of 10^{-3} .

It could be that the rejection factor needed is much less than 10^{-3} . In fact, a very heavy state (such as Λ_t^+ or Λ_{sb}^0) decaying semileptonically may have the hadronic "jet" recoiling against the lepton pair. The study of the hadronic pattern associated with the (e^\pm) could be of such a help in the selection of good events that a rejection power much below 10^{-3} would be sufficient. For example, an order-of-magnitude improvement would mean that the data which, at present, are quoted with a rejection of order 10^{-3} (Figs. 22-34), would reach the level of 10^{-4} . In this case, all our expectations would be scaled by this factor.

For completeness, let us mention that, at present, the (e/π) ratio in the p_T range above ~ 20 GeV is not known at the CERN $p\bar{p}$ Collider.

In order to compute the statistical significance of the observed effect, it is convenient to integrate Λ^{exp} over the p_T ranges:

- i) $7 \leq p_T \leq 12$ GeV/c, corresponding to the "top" region;
- ii) $14 \leq p_T \leq 23$ GeV/c, corresponding to the "superbeauty" region.

This is equivalent to the experimental procedure of fitting the data to reduce the statistical errors on the single points.

Figures 34a,b show the number of standard deviations that can be obtained in the measurement of Λ^{exp} , in the "top" and in the "superbeauty" regions, respectively, as a function of the total cross-sections σ_t and σ_{sb} and in the same conditions as those specified above. The 90% confidence level in the measurement is also indicated. These results show that especially in the "top" case, a high statistical significance can be reached with a moderate rejection power, even if the total cross-section for "top" production is as low as 0.1 pb, i.e. the value predicted by QCD.

Figure 35 shows the behaviour of the ratio (signal/background) as a function of the total cross-section for "top" and "superbeauty" and for different values of the rejection power.

6. CONCLUDING REMARKS

The following conclusions are in order.

- i) Past experience says: do not take the "theoretical" QCD predictions too seriously; many things still do not fit between theory and experiments. In particular, neither the large "charm" cross-sections, nor the "leading" effect were predicted.
- ii) A detailed study of the production mechanism of heavy flavours at the ISR is important in order to make reasonable extrapolations to the $p\bar{p}$ Collider energy.
- iii) The number of "new" states with heavy flavours is very large. If their production cross-sections follow the simple extrapolation proposed by us, the CERN $p\bar{p}$ Collider would be a quasi-factory for these new states. The problem is to have the instrumentation that is able to detect their existence.
- iv) The study of the electron-positron asymmetry and of its energy dependence is of the utmost importance at the $p\bar{p}$ Collider. If the "leading" effect follows the same trend as "charm" at the ISR, this asymmetry is expected to be detectable, even if the production cross-sections of the heavy-flavoured states would follow the QCD predictions.

The study of the electron asymmetry and of its energy dependence is not less important than the searches for the Z^0 and the W^\pm . Finding the Z^0 and the W^\pm would tell us nothing about one of the most crucial problems of subnuclear physics: the families.

A detailed study of the electron asymmetry allows us to investigate the presence, in a mass range so far inaccessible to any other machine, of the new flavours, up-like ("top") and down-like ("superbeauty"), and to determine their mass relation.

- v) What we will be able to do at the CERN $p\bar{p}$ Collider is going to be very important for establishing if hadronic colliders can compete with (e^+e^-) colliders.

REFERENCES

- [1] S. Ferrara, private communication.
- [2] A. Martin, preprint CERN TH-3314 (1982).
- [3] P. Söding, private communication.
- [4] M. Basile et al., Nuovo Cimento 63A (1981) 230.
 M. Basile et al., Nuovo Cimento 65A (1981) 457.
 M. Basile et al., Nuovo Cimento 67A (1982) 40.
 D. Drijard et al., Phys. Lett. 85B (1979) 452.
 K. Giboni et al., Phys. Lett. 85B (1979) 437.
 W. Lockman et al., Phys. Lett. 85B (1979) 443.
 J. Eickmeyer et al., 20th Int. Conf. on High-Energy Physics, Madison, 1981 (American Institute of Physics, New York, 1981), p. 193.
 D. Drijard et al., Phys. Lett. 81B (1979) 250.
 P.F. Jacques et al., Phys. Rev. D 21 (1980) 1206.
 P. Coteus et al., Phys. Rev. Lett. 42 (1979) 1438.
 A. Soukas et al., Phys. Rev. Lett. 44 (1980) 564.
 A.E. Asratyan et al., Phys. Lett. 74B (1978) 497.
 P. Alibrant et al., Phys. Lett. 74B (1978) 134.
 T. Hansl et al., Phys. Lett. 74B (1978) 139.
 A. Bosetti et al., Phys. Lett. 74B (1978) 143.
 M. Fritze et al., Phys. Lett. 96B (1980) 427.
 D. Jonker et al., Phys. Lett. 96B (1980) 435.
 H. Abramowicz et al., preprint CERN-EP/82-17 (1982).
 M. Aguilar-Benitez et al., preprint CERN-EP/82-17 (1982).
 T. Aziz et al., Nucl. Phys. B199 (1982) 424.
 J. Sandweiss et al., Phys. Rev. Lett. 44 (1980) 1104.
- [5] M. Basile et al., Nuovo Cimento Lett. 30 (1981) 487.
- [6] M. Basile et al., Nuovo Cimento Lett. 33 (1982) 33.
- [7] F. Halzen, W.Y. Keung and D.M. Scott, Madison report MAD/PH/63 (1982).
- [8] R. Odorico, Phys. Lett. 107B (1981) 231.
- [9] V. Barger, F. Halzen and W.Y. Keung, Phys. Rev. D 24 (1981) 1428.
- [10] M. Basile et al., Nuovo Cimento 65A (1981) 391.

- [11] J. Badier et al., preprint CERN-EP/82-67 (1982).
- [12] F. Halzen, Rapporteur talk, 21st Int. Conf. on High-Energy Physics, Paris, 1982 [J. Phys. (France) 43, C3-381 (1982)].
- [13] K. Chadwick et al., preprint CLNS/82/546.
- [14] M. Basile et al., Nuovo Cimento Lett. 30 (1981) 481.
M. Basile et al., Nuovo Cimento Lett. 33 (1982) 17.
- [15] S.L. Olsen, Moriond Workshop on New Flavours, Les Arcs, 1982 (Editions Frontières, Dreux, France, 1982), p. 147.
- [16] G. Arnison et al., UAl Collaboration, preprint CERN-EP/82-171 (1982).

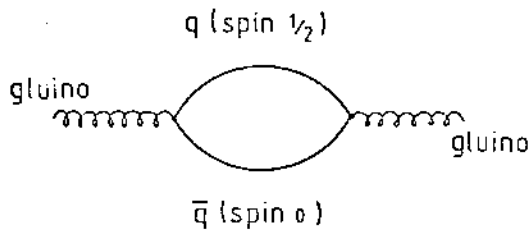


Fig. 1 The diagram illustrates how a gluino can acquire a mass from radiative processes, where a spin $1/2$ quark and a spin 0 anti-quark are virtually produced. The quark mass must be in the 10^2 GeV/ c^2 range, in order to allow a gluino mass of the order of a few GeV/ c^2 .

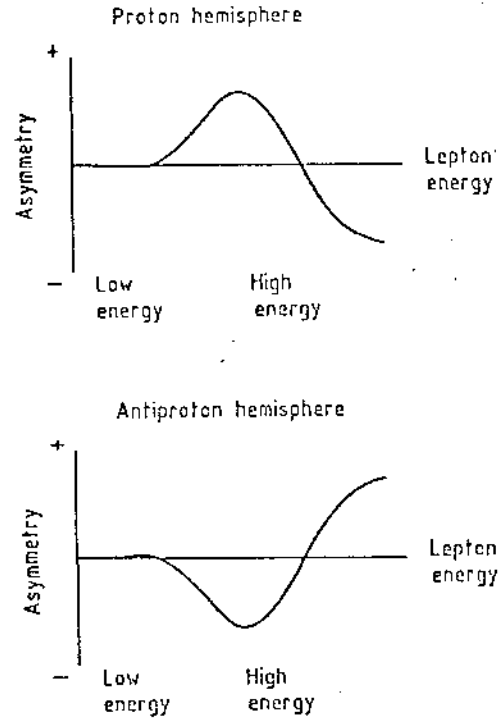


Fig. 2 Main trend of the electron charge asymmetry in the proton hemisphere (a) and in the anti-proton hemisphere (b).

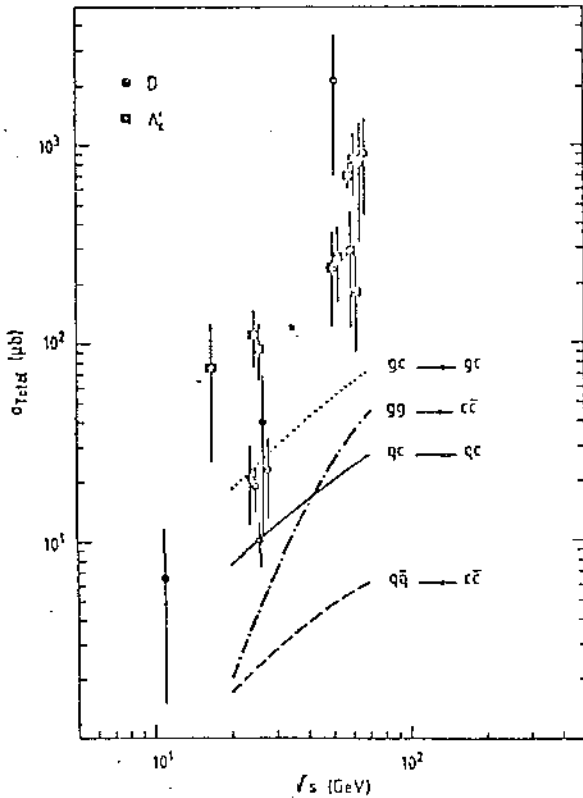


Fig. 3 Cross-sections expected on the basis of gluon and quark fusion models ($gg \rightarrow c\bar{c}$ and $q\bar{q} \rightarrow c\bar{c}$ curves). Other QCD models are also shown. The data are taken from Ref. 4.

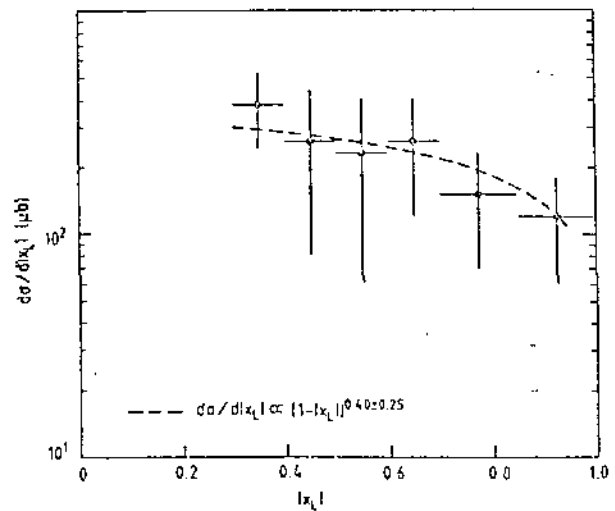


Fig. 4 Experimental longitudinal momentum distribution of Λ_c^+ .

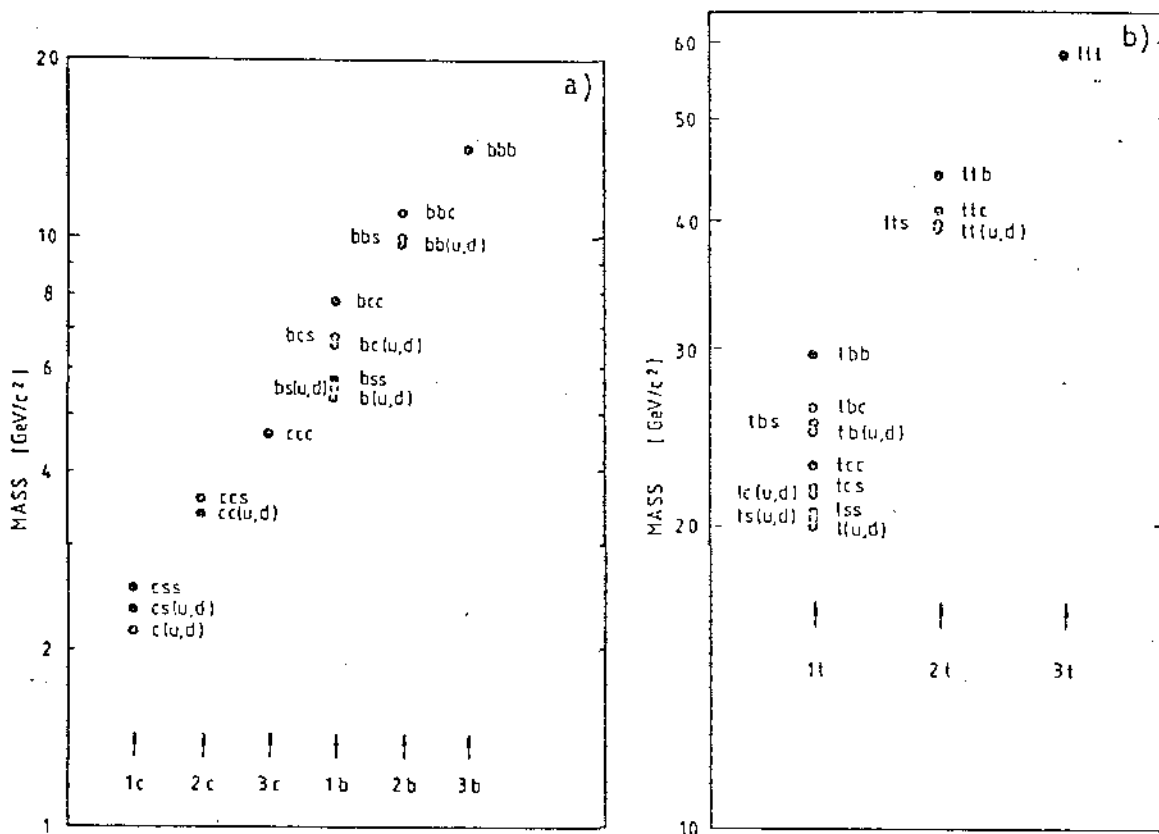


Fig. 8 The mass ranges of the baryon states with: a) from one to three charm or beauty quarks; b) from one to three top quarks.

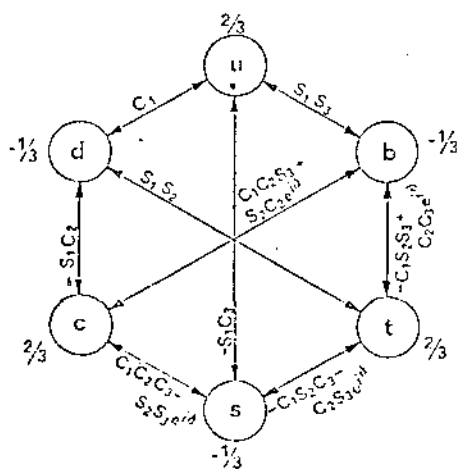


Fig. 9a The six-quark mixing with CP violation. $S_i = \sin \theta_i$, $C_i = \cos \theta_i$.

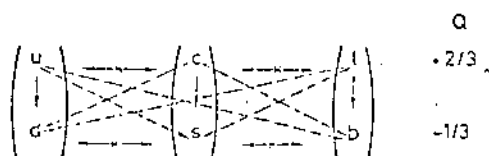


Fig. 9b Transitions among the various states. The Cabibbo mixing opens the dashed channels. The horizontal transitions are forbidden for any value of the mixing angle. Allowed neutral currents are: $u\bar{u}$, $c\bar{c}$, $t\bar{t}$, $d\bar{d}$, $s\bar{s}$, and $b\bar{b}$.

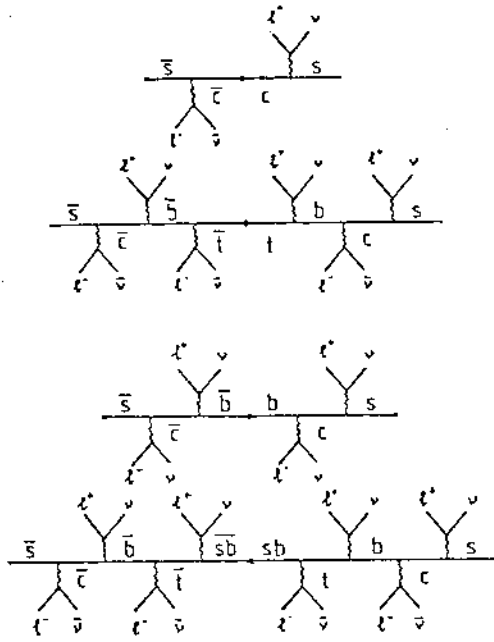


Fig. 10 Diagram illustrating all the possible electric charge signs of the electrons originating from the semi-leptonic decay of the quarks c , b , t , and (sb) , and for the antiquarks \bar{c} , \bar{b} , \bar{t} , and $(\bar{s}\bar{b})$.

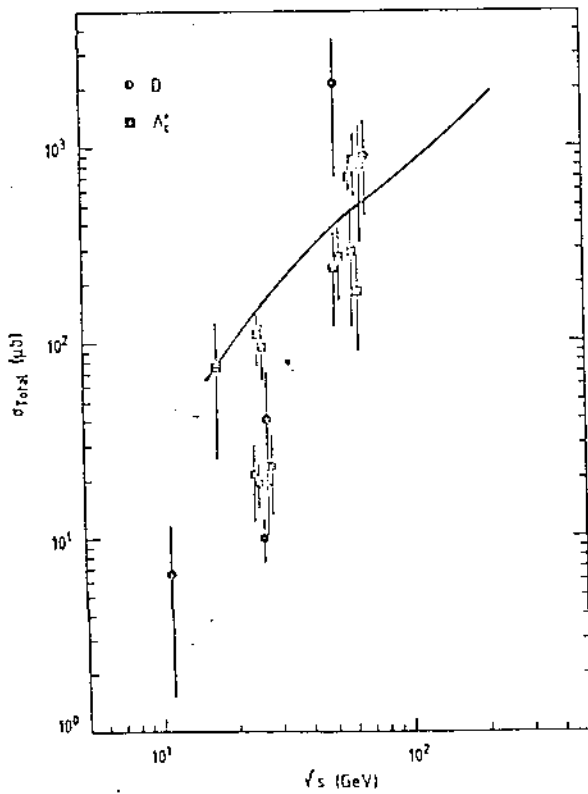


Fig. 11 Charm cross-section derived from strange cross-section following formula (4).

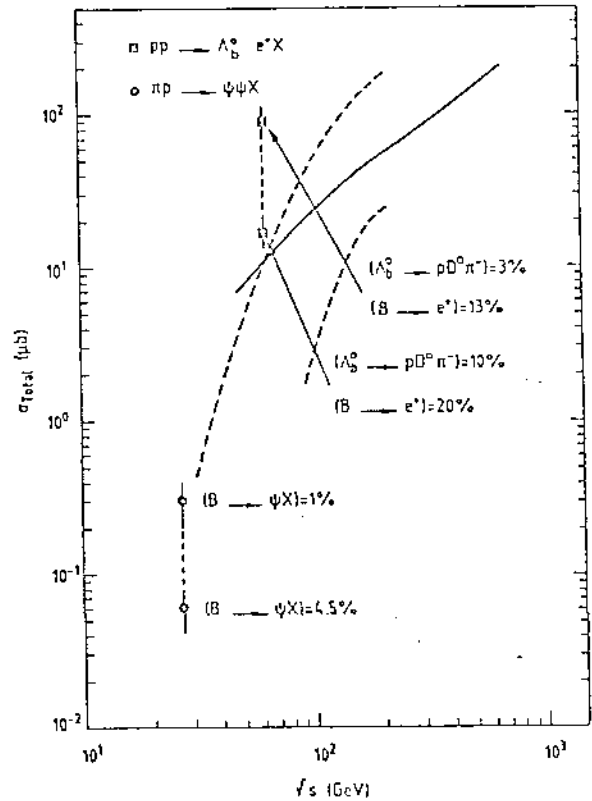


Fig. 12 Beauty cross-section derived from strange (full line) and charm (dashed lines - notice the width due to the experimental uncertainties) cross-sections following formula (4). The data are taken from Refs. 10 and 11.

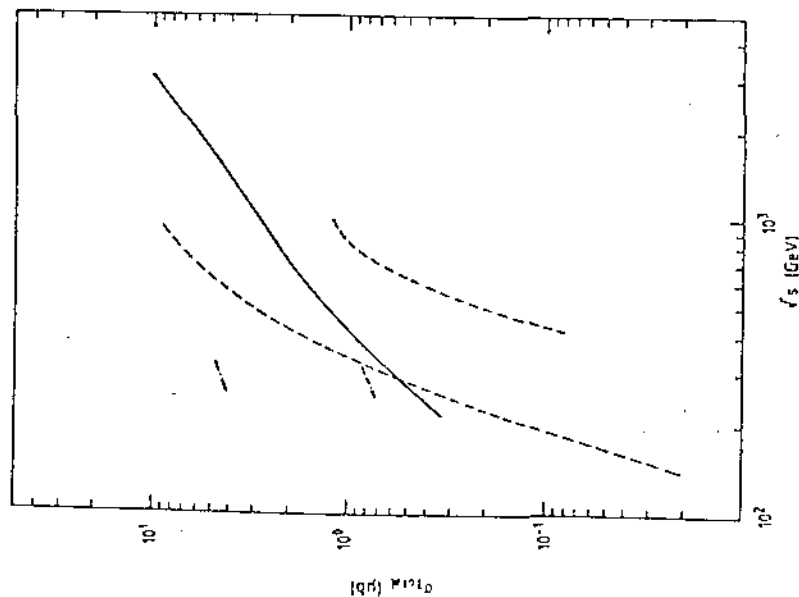


Fig. 13 Top cross-section derived from strange (full line), charm (dashed lines) and beauty (dash-dotted lines) cross-sections following formula (4).

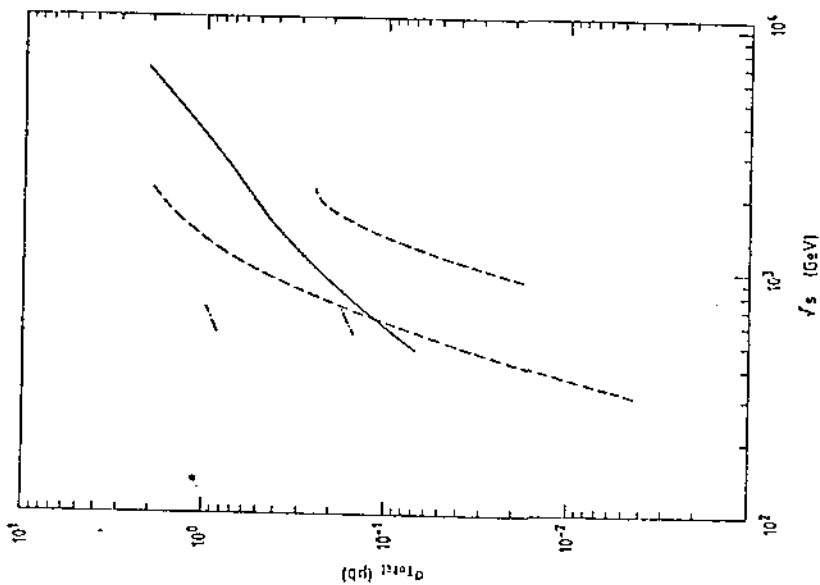


Fig. 14 Superbeauty cross-section derived from strange (full line), charm (dashed lines) and beauty (dash-dotted lines) cross-sections following formula (4).

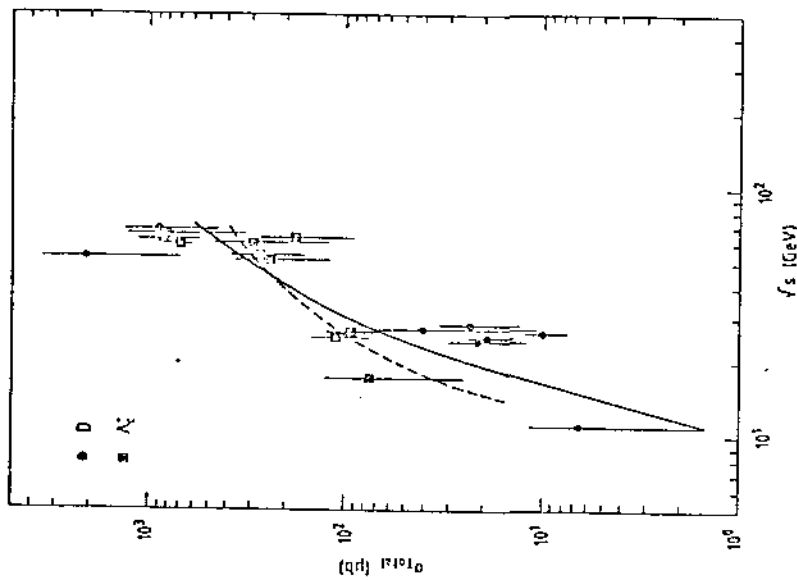


Fig. 15 Non-perturbative QCD predictions (dashed line) and flavour excitation perturbative QCD predictions (full line) for charm hadroproduction.

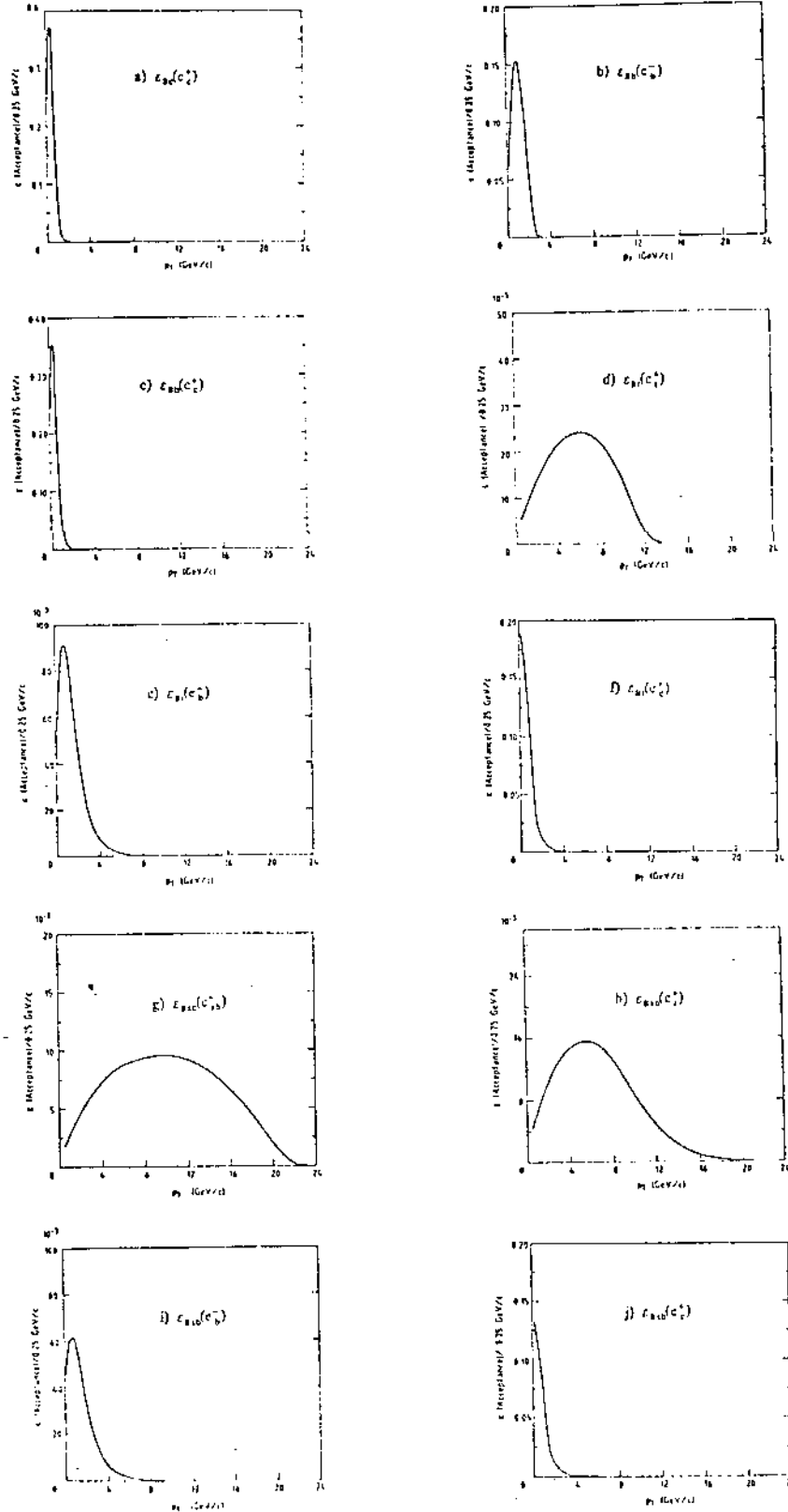


Fig. 16 (a) to (j): Acceptances ϵ relative to baryons for the various decay chains.

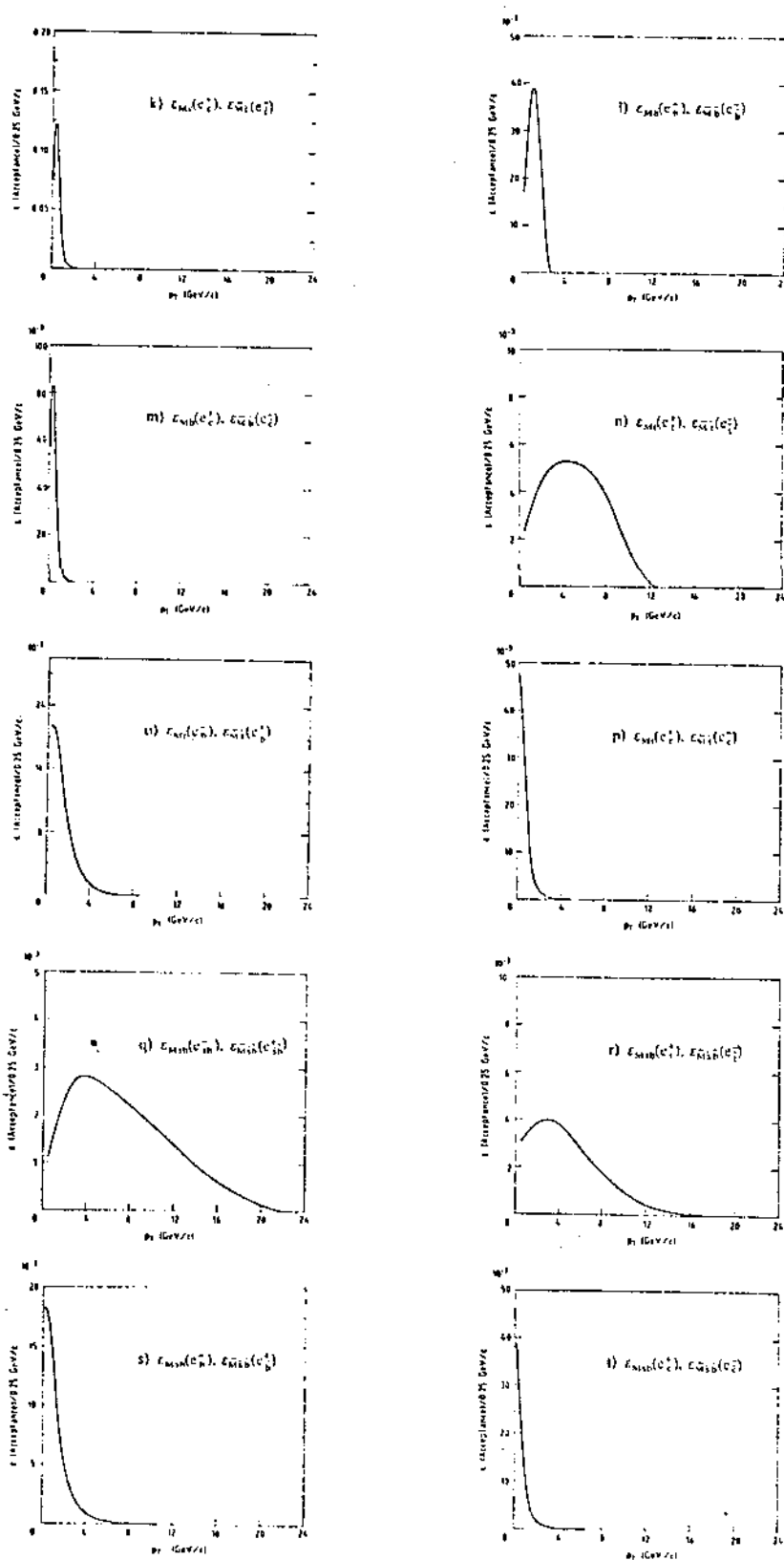


Fig. 16 (k) to (t): Acceptances ϵ relative to mesons and antimemesons for the various decay chains.

$\theta_{cut} = 30^\circ$, (Leading/Total) = 0.25

$\sigma_c = 2$ mb, $\sigma_b = 14.0$ μ b

$\sigma_t = 1.5$ μ b, $\sigma_{cb} = 0.15$ μ b

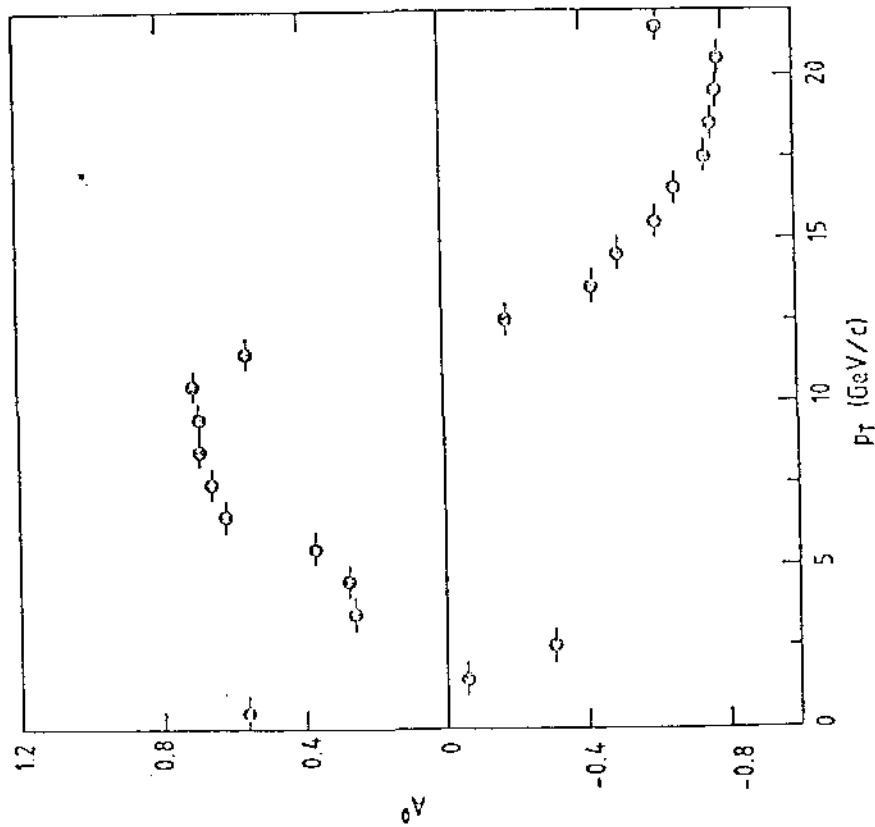


Fig. 17 Plot of $A^0(p_T, \theta_{cut} = 30^\circ)$ as a function of p_T . The values assumed for the cross-sections and for (leading/total) are indicated in the figure.

- ◇ Superbeauty ($\Delta M = 30.0$ GeV/ c^2)
- △ Top ($\Delta M = 19.5$ GeV/ c^2)
- Beauty ($\Delta M = 3.2$ GeV/ c^2)
- Charm ($\Delta M = 1.2$ GeV/ c^2)

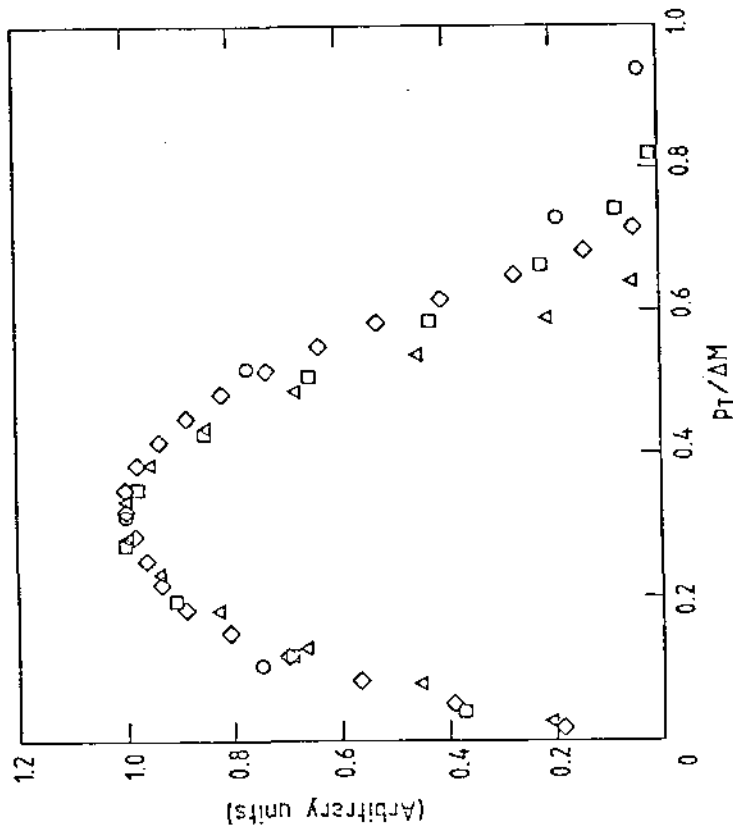


Fig. 18 Normalized $(p_T/\Delta M)$ spectra of the electrons from the decays: $\Lambda_{cb}^0 \rightarrow \Lambda_c^+ e^- \bar{\nu}$; $\Lambda_c^+ \rightarrow \Lambda_b^0 e^+ \nu$; $\Lambda_b^0 \rightarrow \Lambda_c^+ e^- \bar{\nu}$; $\Lambda_c^+ \rightarrow \Lambda_b^0 e^+ \nu$. The ΔM values relative to the four decays are indicated in the figure.

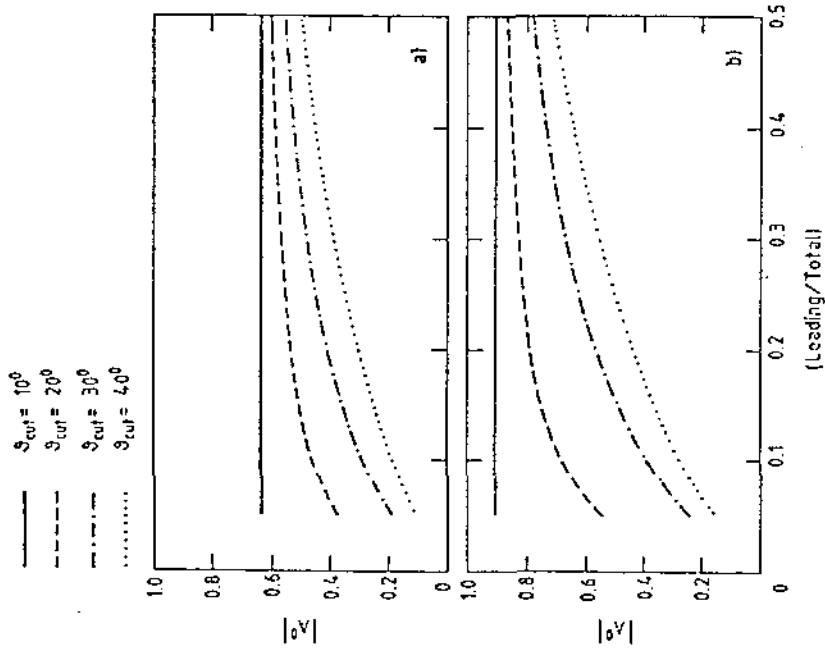


Fig. 19 Plot of $A^0(p_T = 10 \text{ GeV}/c, \theta_{\text{cut}})$ ("top" peak) as a function of (leading/total) for different values of θ_{cut} , and using: a) model (i) of subsection 5.6; and b) model (ii) of subsection 5.6.

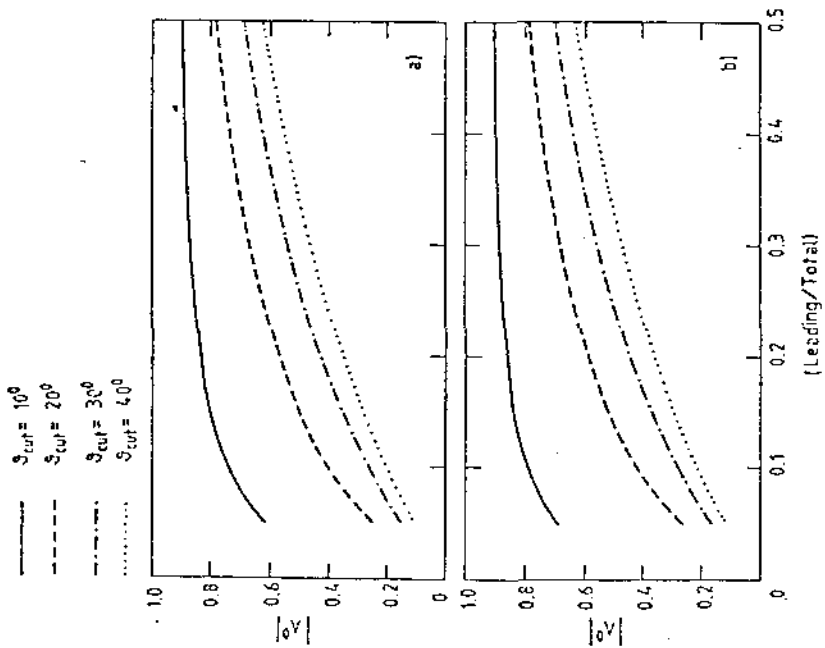


Fig. 20 Plot of $A^0(p_T = 19 \text{ GeV}/c, \theta_{\text{cut}})$ ("super-beauty" peak) as a function of (leading/total) for different values of θ_{cut} , and using: a) model (i) of subsection 5.6, and b) model (ii) of subsection 5.6.

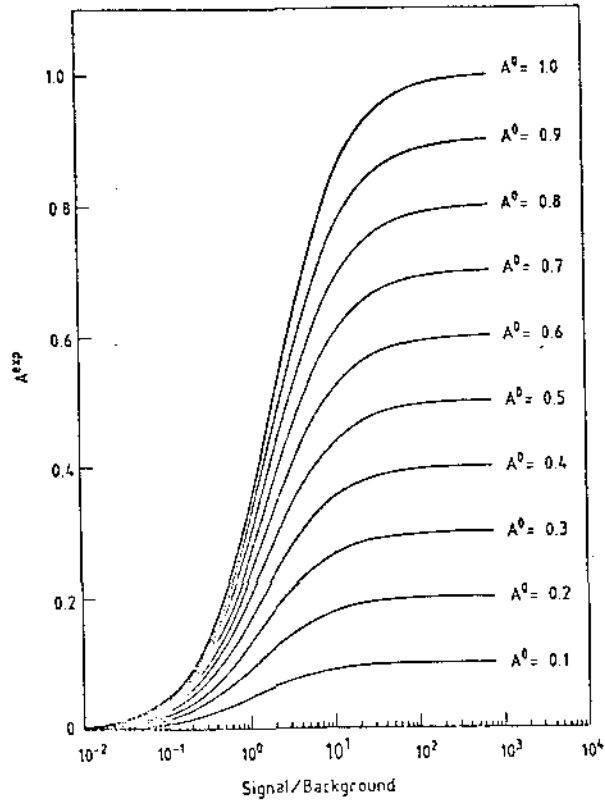


Fig. 21 The curves give the behaviour of A^{exp} as a function of signal/background, for different values of A^0 .

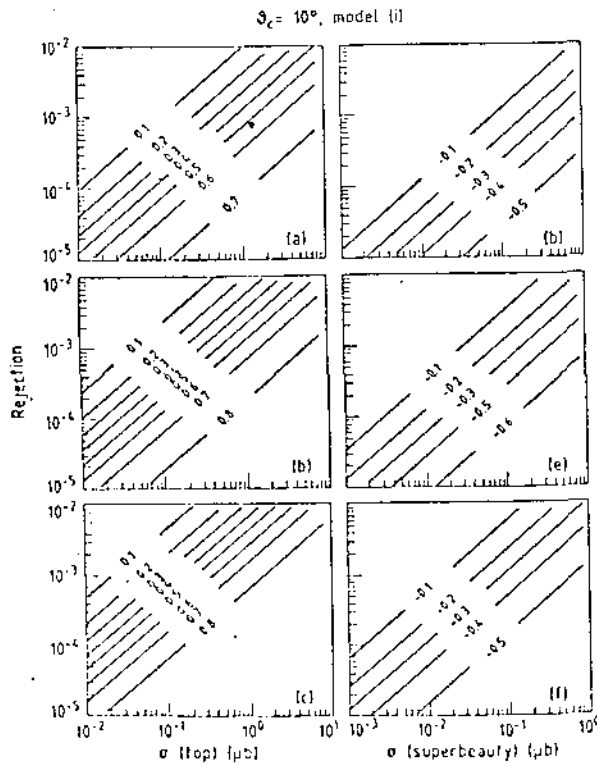


Fig. 22 Curves of constant A^{exp} , in the plot (rejection power) versus (cross-section for "top" or "superbeauty") for $\theta_{\text{cut}} = 10^\circ$ and for model (i). Plots (a), (b), and (c) refer to $p_T = 10$ GeV/c ("top" peak); plots (d), (e), and (f) refer to $p_T = 19$ GeV/c ("superbeauty" peak). Plots (a) and (d) are obtained with (leading/total) = 0.1; plots (b) and (e) with (leading/total) = 0.25; plots (c) and (f) with (leading/total) = 0.5.

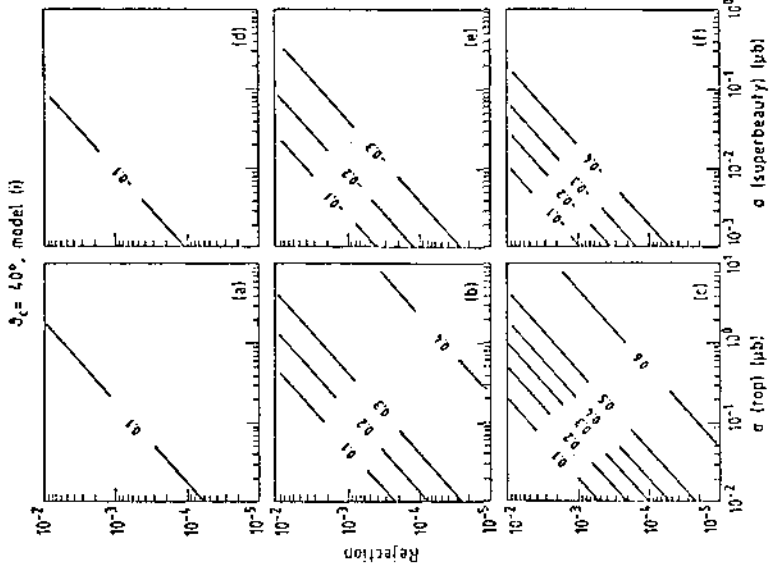


Fig. 23 As Fig. 22 but for $\theta_{cut} = 20^\circ$ and model (i).

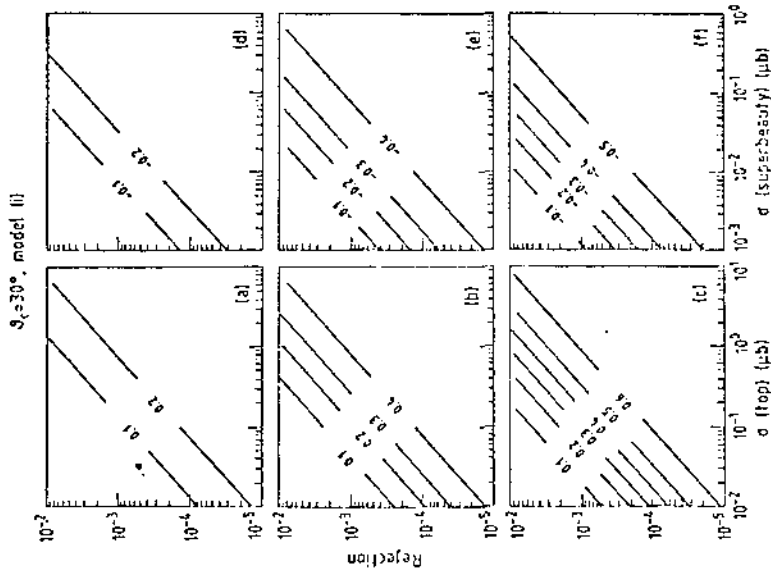


Fig. 24 As Fig. 22 but for $\theta_{cut} = 30^\circ$ and model (i).

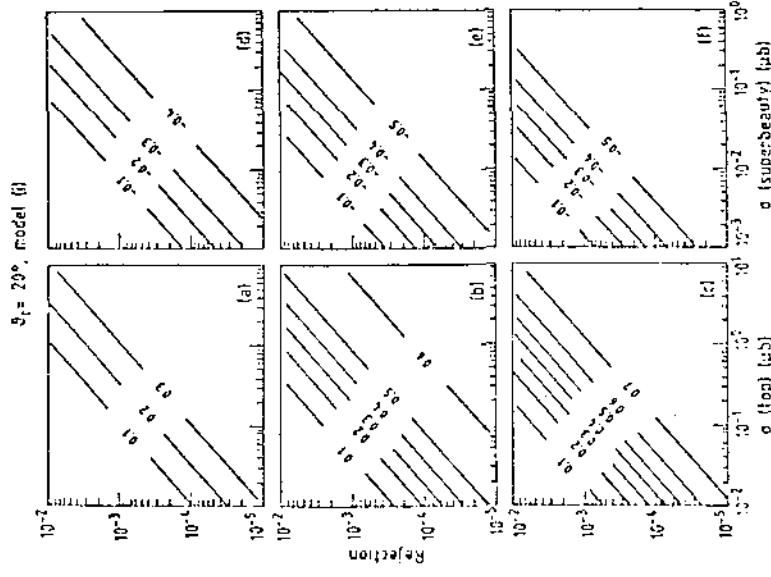


Fig. 25 As Fig. 22 but for $\theta_{cut} = 40^\circ$ and model (i).

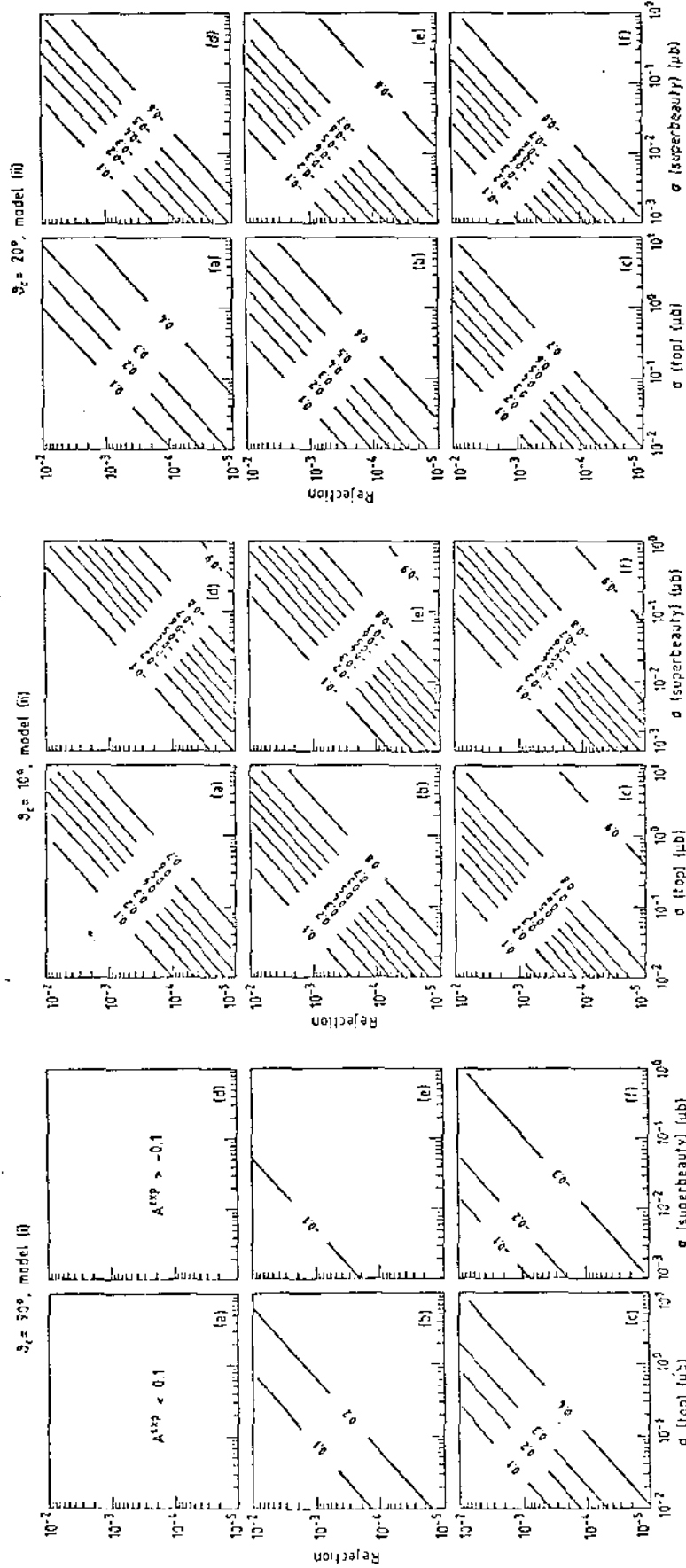


Fig. 26 As Fig. 22 but for $\theta_{cut} = 90^\circ$ and model (i).

Fig. 27 As Fig. 22 but for $\theta_{cut} = 10^\circ$ and model (ii).

Fig. 28 As Fig. 22 but for $\theta_{cut} = 20^\circ$ and model (ii).

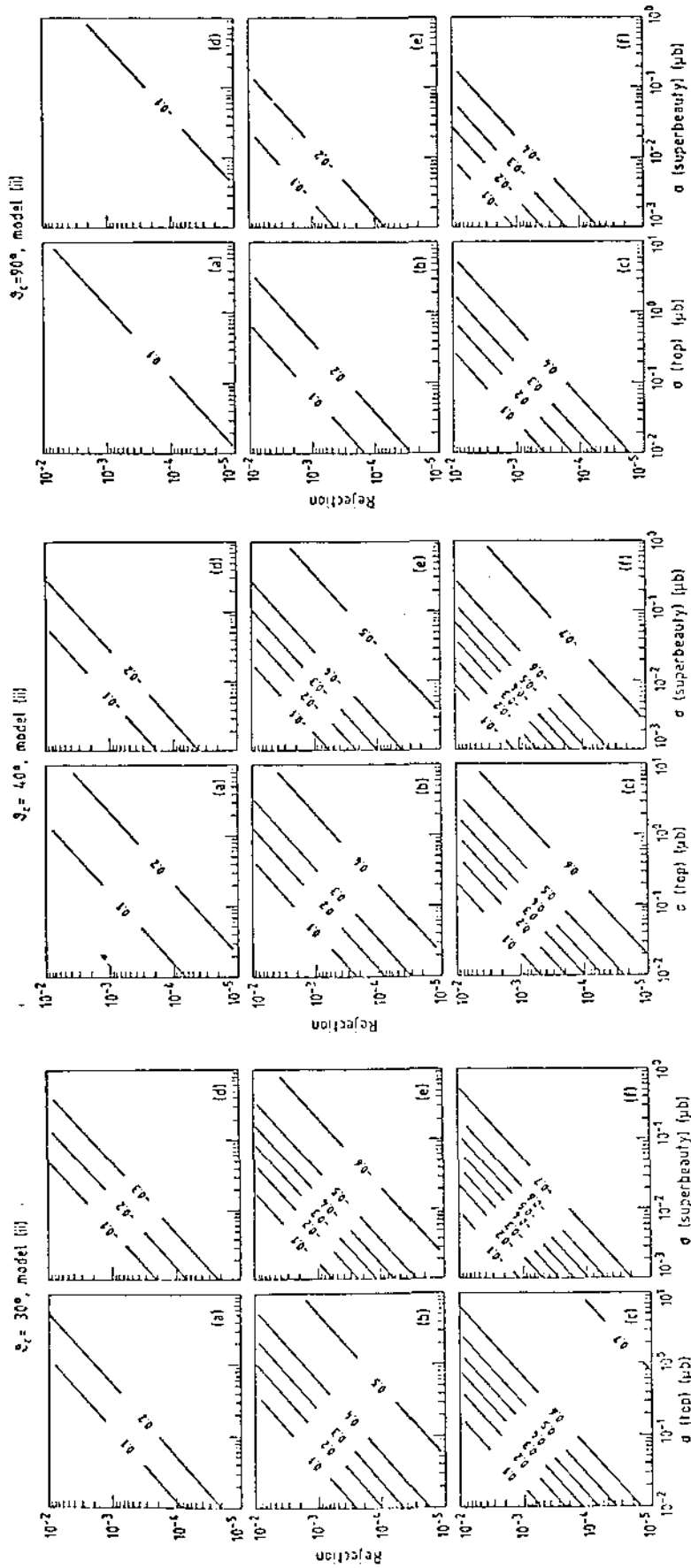


Fig. 29 As Fig. 22 but for $\theta_{cut} = 30^\circ$ and model (ii).

Fig. 30 As Fig. 22 but for $\theta_{cut} = 40^\circ$ and model (ii).

Fig. 31 As Fig. 22 but for $\theta_{cut} = 90^\circ$ and model (ii).

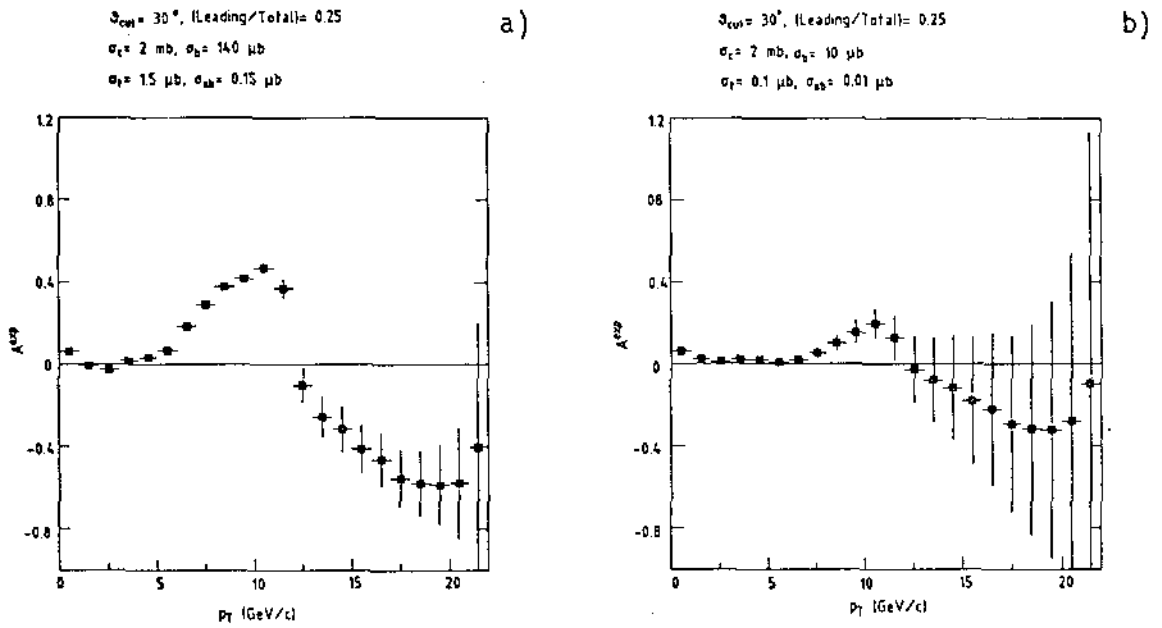


Fig. 32 Plot of A^{exp} as a function of p_T , for a total luminosity $L = 300 \text{ nb}^{-1}$, a rejection power of 10^{-3} , $\theta_{\text{cut}} = 30^\circ$, and (leading/total) = 0.25, using the cross-section estimates: a) from formula (4); b) from perturbative QCD. The errors are statistical.

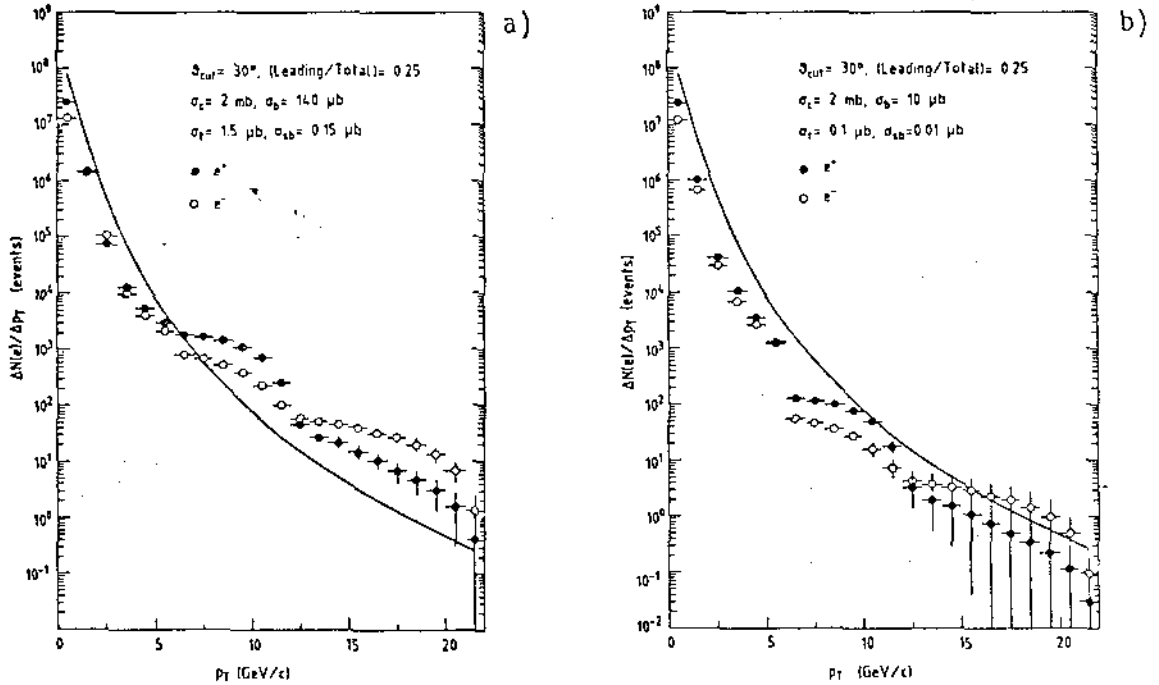


Fig. 33 Expected number of produced electrons as a function of p_T with the same assumptions as in Fig. 29, and the two cross-section estimates: a) from formula (4); b) from perturbative QCD. The errors are statistical. The solid line represents the background, as computed in subsection 5.8, multiplied by a rejection factor of 10^{-3} .

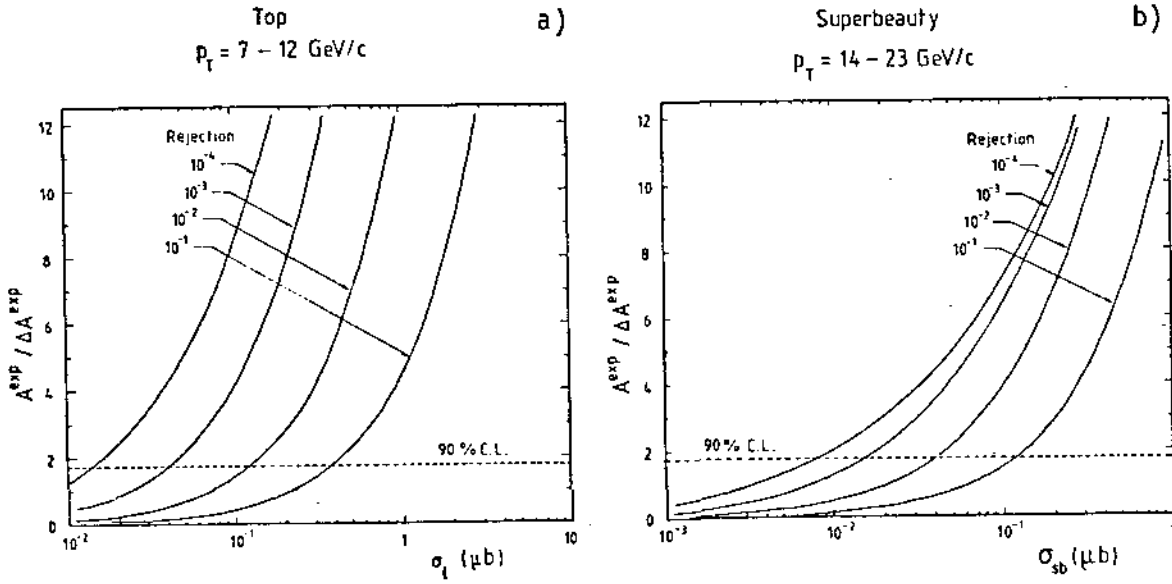


Fig. 34 The statistical significance of the measurement of A^{exp} ($A^{\text{exp}}/\Delta A^{\text{exp}}$) is shown, for a total luminosity of $L = 300 \text{ nb}^{-1}$, $\theta_{\text{cut}} = 30^\circ$ and (leading/total) = 0.25, and for the two p_T ranges: a) $p_T = 7-12 \text{ GeV/c}$; b) $p_T = 14-23 \text{ GeV/c}$.

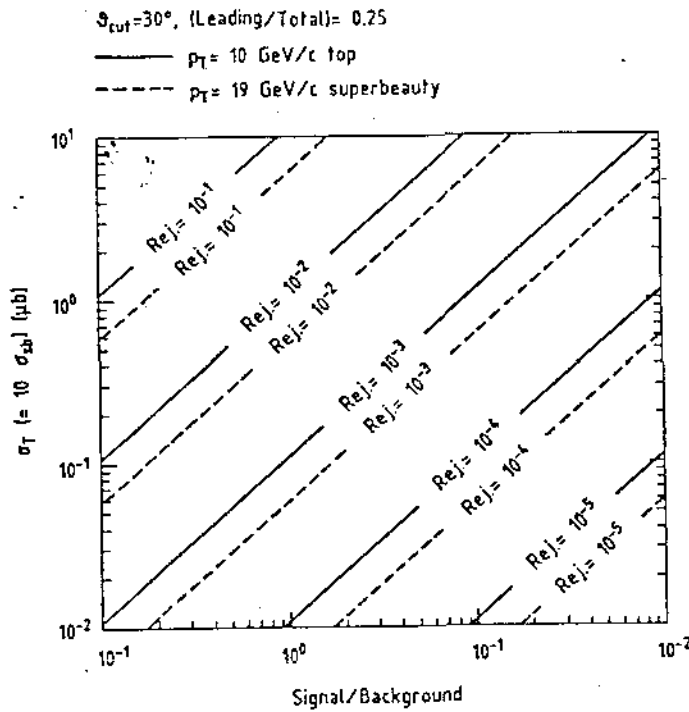


Fig. 35 Correspondence between rejection power and signal/background as function of the total cross-section for "top" and "superbeauty" production, and at the two p_T values: 10 GeV/c and 19 GeV/c.

III- 11. "Search for open top at the CERN ($p\bar{p}$) Collider"
Il Nuovo Cimento, vol.68A, p.65. March 1, 1982.

11 - Search for Open «Top» at the CERN (p \bar{p}) Collider.

M. BASILE, G. BONVICINI, G. CARA ROMEO, L. CIFARELLI,
 A. CONTIN, M. CURATOLO, G. D'ALÍ, P. DI CESARE, B. ESPOSITO,
 P. GIUSTI, T. MASSAM, R. NANIA, F. PALMONARI, A. PETROSINO,
 V. ROSSI, G. SARTORELLI, M. SPINETTI, G. SUSINNO,
 L. VOTANO and A. ZICHICHI

CERN - Geneva, Switzerland

Istituto di Fisica dell'Università - Bologna, Italia

Istituto Nazionale di Fisica Nucleare - Bologna, Italia

Istituto Nazionale di Fisica Nucleare - Laboratori Nazionali di Frascati, Italia

(ricevuto il 9 Dicembre 1981)

Summary. — A new method of observing the production of open «top» baryonic states at the CERN (p \bar{p}) Collider is presented. It is based on the «leading» production mechanism, extended to the heaviest-flavoured baryon and antibaryon states, and on the charge asymmetry of the leptons originating from their semi-leptonic decays.

1. - Introduction.

The purpose of this study is to investigate the observability of open «top» states at the CERN (p \bar{p}) Collider.

The guideline comes from our recent ISR results on heavy-flavour production at $\sqrt{s} = 62$ GeV. Evidence was found for both the charm baryon Λ_c^+ and the beauty baryon Λ_b^0 in the reactions^(1,2)

$$(1) \quad pp \rightarrow e^- + \Lambda_c^+ + \text{anything}$$

(¹) M. BASILE, G. CARA ROMEO, L. CIFARELLI, A. CONTIN, G. D'ALÍ, P. DI CESARE, B. ESPOSITO, P. GIUSTI, T. MASSAM, R. NANIA, F. PALMONARI, G. SARTORELLI, G. VALENTI and A. ZICHICHI: *Nuovo Cimento A*, **63**, 230 (1981).

(²) M. BASILE, G. BONVICINI, G. CARA ROMEO, L. CIFARELLI, A. CONTIN, G. D'ALÍ,

and

$$(2) \quad pp \rightarrow e^+ + \Lambda_b^0 + \text{anything},$$

where the electron (positron) originated from the semi-leptonic decay of the associated antilavoured state. Moreover, it was established that these Λ baryons were produced in a «leading» way, *i.e.* with an approximately flat $x_L (= 2p_L/\sqrt{s})$ distribution^(3,4) in association with an antimeson produced «centrally», *i.e.* with an $E(d\sigma/dx_L) \propto (1-x_L)^2$ behaviour.

On the other hand, we have also measured the longitudinal-momentum distribution of the D mesons observed in the same experiment⁽⁵⁾. This appears to be compatible with a rather «central» production mechanism, both for the meson and the associated antimeson.

These results suggest that, in high-energy (pp) collisions, heavy-flavoured baryons are produced in a «leading» way, in association with a «central» antilavoured meson, whilst in the case of meson-antimeson pairs both mesons are produced «centrally».

In this paper we will extrapolate our findings to the search for particles with open «top» in (p \bar{p}) interactions at $\sqrt{s} = 540$ GeV. Notice that, according to the above-specified heavy-flavour production mechanism, in (p \bar{p}) interactions we should also observe «leading» antibaryons in association with «central» mesons, and «leading» antibaryons in association with «leading» baryons.

2. - How to detect an open t-state.

One possibility of detecting an open t-state in (p \bar{p}) interactions would be via the detection of its hadronic decay. However, since the multiplicity increases when going from the energy of the CERN Intersecting Storage Rings (ISR)

P. DI CESARE, B. ESPOSITO, P. GIUSTI, T. MASSAM, R. NANIA, F. PALMONARI, G. SARTORELLI, G. VALENTI and A. ZICHICHI: *Lett. Nuovo Cimento*, **31**, 97 (1981).

(3) M. BASILE, G. CARA ROMEO, L. CIFARELLI, A. CONTIN, G. D'ALÍ, P. DI CESARE, B. ESPOSITO, P. GIUSTI, T. MASSAM, F. PALMONARI, G. SARTORELLI, G. VALENTI and A. ZICHICHI: *Lett. Nuovo Cimento*, **30**, 487 (1981).

(4) M. BASILE, G. BONVICINI, G. CARA ROMEO, L. CIFARELLI, A. CONTIN, G. D'ALÍ, P. DI CESARE, B. ESPOSITO, P. GIUSTI, T. MASSAM, R. NANIA, F. PALMONARI, G. SARTORELLI, G. VALENTI and A. ZICHICHI: *Nuovo Cimento A*, **65**, 408 (1981).

(5) M. BASILE, G. CARA ROMEO, L. CIFARELLI, A. CONTIN, G. D'ALÍ, P. DI CESARE, B. ESPOSITO, P. GIUSTI, T. MASSAM, R. NANIA, F. PALMONARI, G. SARTORELLI, G. VALENTI and A. ZICHICHI: *Lett. Nuovo Cimento*, **33**, 33 (1982).

to that of the Collider (*), an invariant-mass analysis applied to the (p \bar{p}) final state would be very difficult because of the amplification of the combinatorial background. Moreover, the detection of the decay chain $t \rightarrow b \rightarrow c \rightarrow s$, where first a b-state then a c-state are identified, would involve a prohibitively small branching ratio (of the order of 10^{-6}).

Another approach would be to take advantage of the sizable branching ratio ($\approx 10\%$) of the semi-leptonic decay of the heavy-flavour states. In this study we will show that the «leading» production of heavy-flavoured baryons and their semi-leptonic decay provides a tool for disentangling the production of the «top» quark from the large physical background.

(*) M. BASILE, G. CARA ROMEO, L. CIFARELLI, A. CONTIN, G. D'ALÍ, P. DI CESARE, B. ESPOSITO, P. GIUSTI, T. MASSAM, R. NANIA, F. PALMONARI, A. PETROSINO, V. ROSSI, G. SARTORELLI, M. SPINETTI, G. SUSINNO, G. VALENTI, L. VOTANO and A. ZICHICHI: *A prediction for the total charge multiplicity in hadronic interactions at extreme high energies*, preprint CERN-EP/81-147 (1981).

(?) G. ARNISON, A. ASTBURY, B. AUBERT, C. BACCI, R. BERNABEI, A. BÉZAGUET, R. BOCK, M. CALVETTI, P. CATZ, S. CENTRO, F. CERADINI, B. CHERTOK, J. CIBOROWSKI, S. CITTOLIN, A. M. CNOPS, C. COCHET, J. COLAS, M. CORDEN, D. DALLMAN, S. D'ANGELO, M. DEBEER, M. DELLA NEGRA, M. DEMOULIN, D. DENEGRI, D. DiBITONTO, L. DOBRZYNSKI, J. D. DOWELL, M. EDWARDS, K. EGGERT, E. EISENHANDLER, N. ELLIS, P. ERHARD, H. FAISSNER, G. FONTAINE, J. P. FOURNIER, R. FREY, R. FRÜHWIRTH, J. GARVEY, S. GEER, C. GHESQUIÈRE, P. GHEZ, K. L. GIBONI, W. R. GIBSON, Y. GIRAUD-HERAUD, A. GIVERNAUD, A. GONIDEC, G. GRAYER, P. GUTIERREZ, R. HAIDAN, T. HANSL-KOZANECKA, W. J. HAYNES, L. O. HERTZBERGER, C. HODGES, D. HOFFMANN, H. HOFFMANN, D. J. HOLTHUIZEN, R. J. HOMER, A. HONMA, W. JANK, P. I. P. KALMUS, V. KARIMÁKI, R. KEELER, I. KENYON, A. KERNAN, R. KINNUNEN, H. KOWALSKI, W. KOZANECKI, D. KRYN, F. LACAVA, J. P. LAUGIER, J. P. LEES, H. LEHMANN, R. LEUCHS, A. LÉVÊQUE, D. LINGLIN, E. LOCCI, G. MAURIN, T. McMAHON, J. P. MENDIBURU, M. N. MINARD, M. MORICCA, H. MUIRHEAD, F. MULLER, Y. MURAKI, A. K. NANDI, L. NAUMANN, A. NORTON, A. ORKIN-LECOURTOIS, L. PAOLUZI, M. PERNICKA, G. PETRUCCI, G. PIANO MORTARI, M. PIMIÁ, A. PLACCI, P. QUERU, E. RADERMACHER, H. REITHLER, J. RICH, M. RIJSENBECK, C. ROBERTS, C. RUBBIA, B. SADOULET, G. SAJOT, G. SALVI, G. SALVINI, J. SASS, J. SAUDRAIX, A. SAVOY-NAVARRO, G. SCHANZ, D. SCHINZEL, W. SCOTT, T. P. SHAH, M. SPIRO, J. STRAUSS, K. SUMOROK, C. TAO, G. THOMPSON, E. TSCHESLOG, J. TUOMINIEMI, H. VERWEIJ, J. P. VIALLE, J. VRANA, V. VUILLEMIN, H. WAHL, P. WATKINS, J. WILSON, M. YVERT and E. ZURFLUH: *Some observations on the first events seen at the CERN proton-antiproton collider*, preprint CERN/EP 81-155 (1981).

(*) K. ALPGÅRD, R. E. ANSORGE, B. ÅSMAN, S. BERGLUNG, K. BERKELMAN, D. BERTRAND, K. BÖCKMANN, C. N. BOOTH, C. BUFFAM, L. BUROW, P. CARLSON, J. R. CARTER, J.-L. CHEVALLEY, B. ECKART, G. EKSPONG, J.-P. FABRE, K. A. FRENCH, J. GAUDAEN, M. GIJSEN, K. VON HOLT, R. HOSPES, D. JOHNSON, K. JON-ÅND, TH. KOKOTT, R. MACKENZIE, M. N. MAGGS, R. MEINKE, TH. MÜLLER, H. MULKENS, D. J. MUNDAY, A. ODIAN, M. ROSENBERG, J. G. RUSHBROOKE, H. SAARIKKO, T. SAARIKKO, F. TRIANTIS, CH. WALCK, C. P. WARD, D. R. WARD, G. WEBER, A. R. WEIDBERG, T. O. WHITE, G. WILQUET and N. YAMDAGNI: *First results on complete events from p \bar{p} collisions at the c.m. energy of 540 GeV*, preprint CERN/EP 81-152 (1981); *Charged particle multiplicities at the CERN SPS collider*, preprint CERN/EP 81-153 (1981).

In the following, $B_{i(\bar{i})}$ and $M_{i(\bar{i})}$ indicate, respectively, the heavy-flavoured baryon (antibaryon) and meson (antimeson) states.

As mentioned before, the associated heavy-flavour production in $(p\bar{p})$ interactions would consist of the following components:

$$\begin{aligned} & [(B_t)_{\text{leading}}(B_{\bar{t}})_{\text{leading}}], \\ & [(B_t)_{\text{leading}}(M_{\bar{t}})_{\text{central}}], \\ & [(B_{\bar{t}})_{\text{leading}}(M_t)_{\text{central}}], \\ & [(M_t)_{\text{central}}(M_{\bar{t}})_{\text{central}}]. \end{aligned}$$

We have assumed that the production of $B_i B_{\bar{i}}$ pairs, in which both the B_i and the $B_{\bar{i}}$ are « central », is significantly depressed.

Let us consider, for simplicity, only the leptons in the outgoing-proton rapidity hemisphere. For the outgoing-antiproton rapidity hemisphere, the same results will apply if the electric-charge sign of the leptons is reversed.

The number of positive leptons l^+ is expressed by

$$(3) \quad N(l^+) = LR[n_t(l^+) + n_b(l^+) + n_c(l^+)],$$

where L is the total integrated luminosity, R is the semi-leptonic branching ratio (assumed to be equal for all flavoured states) and $n_f(l^+)$ ($f = t, b, c$) are the contributions from the direct production of top, beauty and charm states according to the diagrams shown in fig. 1a)-f):

$$(3a) \quad n_t(l^+) = \sigma(B_t B_{\bar{t}})[\varepsilon_{B_t}(l^+) + \varepsilon_{B_t}(l_{bc}^+) + \varepsilon_{M_t}(l_{bb}^+)] + \\ + \sigma(M_t M_{\bar{t}})[\varepsilon_{M_t}(l^+) + \varepsilon_{M_t}(l_{bc}^+) + \varepsilon_{M_t}(l_{bb}^+)] + \sigma(M_t B_{\bar{t}})[\varepsilon_{M_t}(l^+) + \varepsilon_{M_t}(l_{bc}^+) + \varepsilon_{B_{\bar{t}}}(l_{bb}^+)] + \\ + \sigma(B_t M_{\bar{t}})[\varepsilon_{B_t}(l^+) + \varepsilon_{B_t}(l_{bc}^+) + \varepsilon_{M_{\bar{t}}}(l_{bb}^+)],$$

$$(3b) \quad n_b(l^+) = \sigma(B_b B_{\bar{b}})[\varepsilon_{B_b}(l_{bc}^+) + \varepsilon_{B_{\bar{b}}}(l_b^+)] + \\ + \sigma(M_b M_{\bar{b}})[\varepsilon_{M_b}(l_{bc}^+) + \varepsilon_{M_{\bar{b}}}(l_b^+)] + \sigma(M_b B_{\bar{b}})[\varepsilon_{M_b}(l_{bc}^+) + \varepsilon_{B_{\bar{b}}}(l_b^+)] + \\ + \sigma(B_b M_{\bar{b}})[\varepsilon_{B_b}(l_{bc}^+) + \varepsilon_{M_{\bar{b}}}(l_b^+)],$$

$$(3c) \quad n_c(l^+) = \sigma(B_c B_{\bar{c}})[\varepsilon_{B_c}(l_c^+)] + \sigma(M_c M_{\bar{c}})[\varepsilon_{M_c}(l_c^+)] + \\ + \sigma(M_c B_{\bar{c}})[\varepsilon_{M_c}(l_c^+)] + \sigma(B_c M_{\bar{c}})[\varepsilon_{B_c}(l_c^+)].$$

The σ factors are the cross-sections for $B_i B_{\bar{i}}$, $M_i M_{\bar{i}}$ and $M_{i(\bar{i})} B_{i(\bar{i})}$ production, and the ε factors are the detection efficiencies, in a given phase-space region $\Delta\Omega$, for the l^+ originating from $B_{i(\bar{i})}$ or $M_{i(\bar{i})}$ decay. The subscript to l^+ indicates the various possible decay chains. For instance, l_{bc}^+ refers to the decay $t \rightarrow b \rightarrow c \rightarrow l^+$.

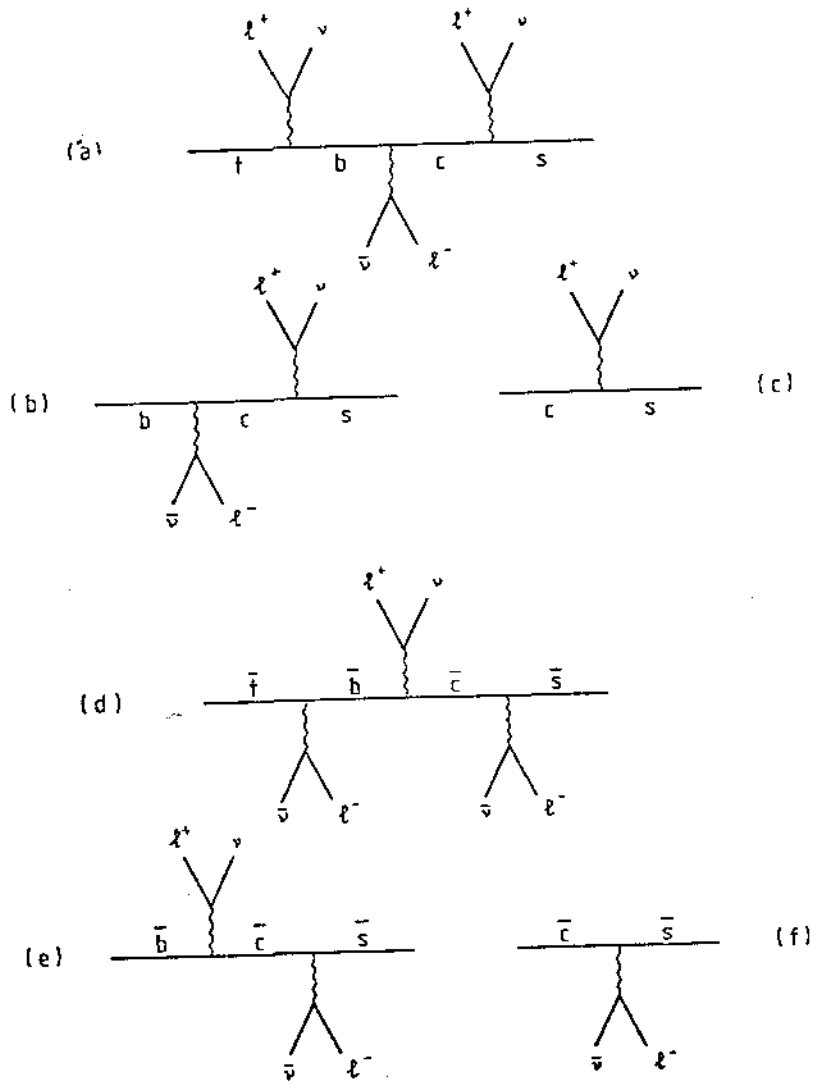


Fig. 1. - Diagrams illustrating all the possible electric-charge signs of the leptons originating from semi-leptonic decays of the chains $t \rightarrow b \rightarrow c \rightarrow s$ (a), $b \rightarrow c \rightarrow s$ (b), $c \rightarrow s$ (c), $\bar{t} \rightarrow \bar{b} \rightarrow \bar{c} \rightarrow \bar{s}$ (d), $\bar{b} \rightarrow \bar{c} \rightarrow \bar{s}$ (e) and $\bar{c} \rightarrow \bar{s}$ (f).

Analogously, the number of t^- in the proton hemisphere is given by

$$(4) \quad N(t^-) = LR[n_t(t^-) + n_b(t^-) + n_c(t^-)],$$

where, according to the diagrams shown in fig. 1a)-f),

$$(4a) \quad n_t(t^-) = \sigma(B_t B_{\bar{t}})[\varepsilon_{B_t}(t_{tb}^-) + \varepsilon_{B_{\bar{t}}}(t_{\bar{t}}^-) + \varepsilon_{B_{\bar{t}}}(t_{\bar{t}\bar{c}}^-)] + \\ + \sigma(M_t M_{\bar{t}})[\varepsilon_{M_t}(t_{tb}^-) + \varepsilon_{M_{\bar{t}}}(t_{\bar{t}}^-) + \varepsilon_{M_{\bar{t}}}(t_{\bar{t}\bar{c}}^-)] + \sigma(M_t B_{\bar{t}})[\varepsilon_{M_t}(t_{tb}^-) + \varepsilon_{B_{\bar{t}}}(t_{\bar{t}}^-) + \varepsilon_{B_{\bar{t}}}(t_{\bar{t}\bar{c}}^-)] + \\ + \sigma(B_t M_{\bar{t}})[\varepsilon_{B_t}(t_{tb}^-) + \varepsilon_{M_{\bar{t}}}(t_{\bar{t}}^-) + \varepsilon_{M_{\bar{t}}}(t_{\bar{t}\bar{c}}^-)],$$

$$(4b) \quad n_b(t^-) = \sigma(B_b B_{\bar{b}})[\varepsilon_{B_b}(t_b^-) + \varepsilon_{B_{\bar{b}}}(t_{\bar{b}\bar{c}}^-)] + \\ + \sigma(M_b M_{\bar{b}})[\varepsilon_{M_b}(t_b^-) + \varepsilon_{M_{\bar{b}}}(t_{\bar{b}\bar{c}}^-)] + \sigma(M_b B_{\bar{b}})[\varepsilon_{M_b}(t_b^-) + \varepsilon_{B_{\bar{b}}}(t_{\bar{b}\bar{c}}^-)] + \\ + \sigma(B_b M_{\bar{b}})[\varepsilon_{B_b}(t_b^-) + \varepsilon_{M_{\bar{b}}}(t_{\bar{b}\bar{c}}^-)],$$

$$(4c) \quad n_c(t^-) = \sigma(B_c B_{\bar{c}})[\varepsilon_{B_c}(t_c^-)] + \sigma(M_c M_{\bar{c}})[\varepsilon_{M_c}(t_c^-)] + \\ + \sigma(M_c B_{\bar{c}})[\varepsilon_{M_c}(t_c^-)] + \sigma(B_c M_{\bar{c}})[\varepsilon_{M_c}(t_c^-)].$$

Finally, let us define the « asymmetry » ratio

$$(5) \quad A^0 = \frac{N(t^+) - N(t^-)}{N(t^+) + N(t^-)}.$$

From our previous statements on $B_{t\bar{b}}$ and $M_{t\bar{b}}$ production distributions in a suitable forward region of the outgoing-proton rapidity hemisphere, we expect that the quantity A^0 will be a good tool for looking for a possible open « top » signal.

3. - Estimate of the « asymmetry » ratio A^0 .

In order to estimate the value of the « asymmetry » ratio A^0 , the following quantities are needed.

i) *The cross-sections values.* We have assumed $\sigma_c = 250 \mu\text{b}$ for the total charm cross-section in the ISR energy range, a value which is consistent with our measurements (^{1,9,10}), and a factor of 3 increase of this cross-section at the

(⁹) M. BASILE, G. CARA ROMEO, L. CIFARELLI, A. CONTIN, G. D'ALÍ, P. DI CESARE, B. ESPOSITO, P. GIUSTI, T. MASSAM, R. NANIA, F. PALMONARI, G. SARTORELLI, G. VALENTI and A. ZICHICHI: *Nuovo Cimento A*, **65**, 457 (1981).

(¹⁰) M. BASILE, G. CARA ROMEO, L. CIFARELLI, A. CONTIN, G. D'ALÍ, P. DI CESARE, B. ESPOSITO, P. GIUSTI, T. MASSAM, R. NANIA, F. PALMONARI, G. SARTORELLI, G. VALENTI and A. ZICHICHI: *Nuovo Cimento A*, **67**, 40 (1982).

(p \bar{p}) Collider energy. We have then assumed that the heavy-flavour cross-sections scale as the inverse ratio of the quark masses squared⁽¹¹⁾:

$$\sigma_b/\sigma_c = m_c^2/m_b^2,$$

and

$$\sigma_s/\sigma_b = m_b^2/m_s^2.$$

For the «top» quark, we assumed a mass $m_t = 25 \text{ GeV}/c^2$. The cross-

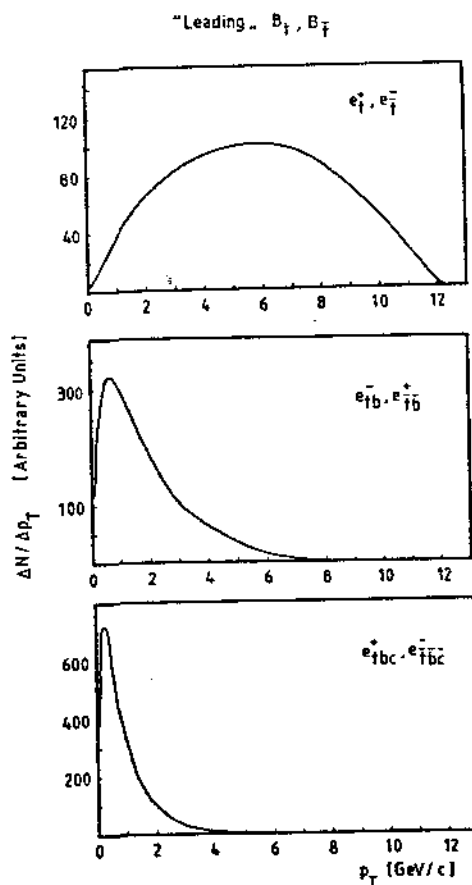


Fig. 2. - Transverse-momentum spectra of the leptons originating from the decay of t (\bar{t}) «leading» baryon states, obtained as described in the text.

⁽¹¹⁾ A. MARTIN: preprint CERN Th. 2980 (1980), and private communication.

section values at $\sqrt{s} = 540$ GeV are, therefore,

$$\sigma_c = 750 \mu\text{b}, \quad \sigma_b = 75 \mu\text{b} \quad \text{and} \quad \sigma_t = 3 \mu\text{b}.$$

We also used, for all flavours, the hypothesis

$$\sigma(B_i B_j) = \sigma(M_i M_j) = \sigma(M_i B_j) = \sigma(M_j B_i) = \sigma_i/4.$$

ii) *The semi-leptonic branching ratio.* We have assumed the branching ratio of the semi-leptonic decay into a given lepton to be 10% for all heavy-flavoured states.

iii) *The detection efficiency ϵ .* The detection efficiencies ϵ have been evaluated with a Monte Carlo simulation. The heavy-flavour state and its associated

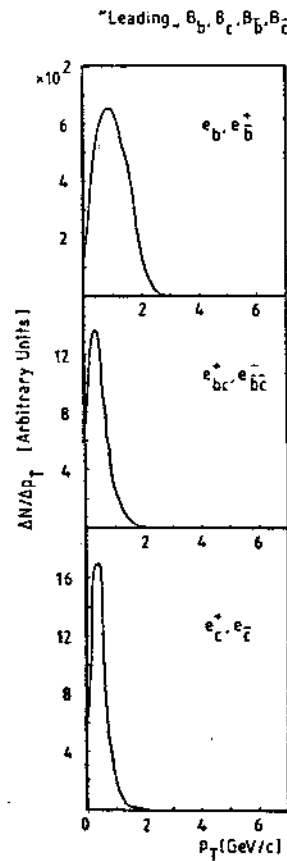


Fig. 3. - Same as fig. 2, but for b (\bar{b}), c (\bar{c}) + leading + baryon states.

antistate were assumed to be produced in an uncorrelated way. The generation was based on a flat- x_L distribution ($d\sigma/dx_L = \text{const}$) for baryons and on a central- x_L distribution [$E(d\sigma/dx_L) \propto (1-x_L)^2$] for mesons. The p_T dependence was assumed to be $(1/p_T)(d\sigma/dp_T) \propto \exp[-2.5p_T]$ for all flavours.

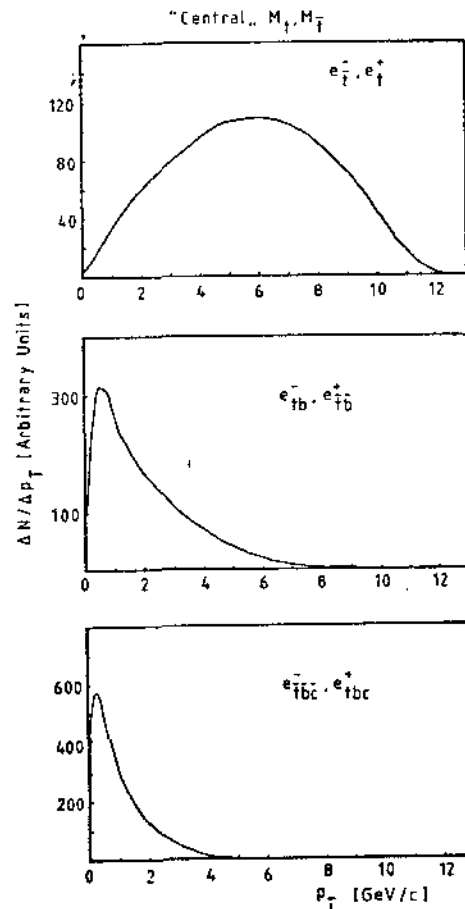


Fig. 4. - Same as fig. 2, but for t (\bar{t}) *central* meson states.

For each flavour the semi-leptonic decay was simulated by using a K_{t_1} decay matrix. The p_T spectra from the various decays are shown in fig. 2-5. The choice of the phase-space region $\Delta\Omega$, defined by the conditions

$$\theta < 30^\circ \quad \text{and} \quad p_T > 5 \text{ GeV}/c,$$

was determined as a compromise between the efficiency for t^+ originating via

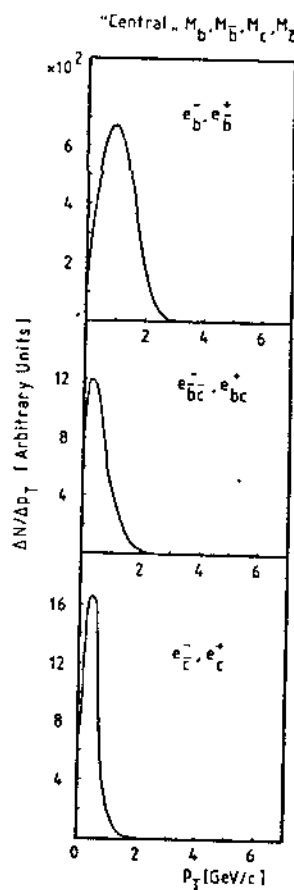


Fig. 5. - Same as fig. 2, but for b (\bar{b}), c (\bar{c}) «central» meson states.

the direct decay $t \rightarrow t^+$ of the «top»-flavoured baryons and the rejection of leptons from different sources. The detection efficiencies for the leptons originating from the various sources are summarized in table I.

The results of our analysis are the following:

$$N(t^+) = L(7.59 \cdot 10^{-2} \mu\text{b}),$$

$$N(t^-) = L(1.95 \cdot 10^{-2} \mu\text{b}),$$

$$A^0 = \frac{N(t^+) - N(t^-)}{N(t^+) + N(t^-)} = 0.59.$$

Notice that this value corresponds to the ratio $N(t^+)/N(t^-) = 3.90$.

SEARCH FOR OPEN «TOP» AT THE CERN (pp) COLLIDER

75

TABLE I. - The t^{\pm} detection efficiencies for $\theta < 30^{\circ}$ and $p_T > 5$ GeV/c in the proton rapidity hemisphere (see corresponding equations in column 3).

$\epsilon_{B_t}(t^+)$:	$4.2 \cdot 10^{-1}$	$\epsilon_{B_t}(t^+)$:	0	(3a)
$\epsilon_{B_c}(t_{bc}^+)$:	$1.3 \cdot 10^{-3}$	$\epsilon_{B_c}(t_{bc}^+)$:	0	(3a)
$\epsilon_{B_b}(t_{bc}^+)$:	$< 10^{-4}$	$\epsilon_{B_b}(t_{bc}^+)$:	0	(3b)
$\epsilon_{B_c}(t_c^+)$:	~ 0	$\epsilon_{B_c}(t_c^+)$:	0	(3c)
$\epsilon_{B_t}(t_{tb}^-)$:	$4.5 \cdot 10^{-2}$	$\epsilon_{B_t}(t_{tb}^-)$:	0	(4a)
$\epsilon_{B_c}(t_{bc}^-)$:	$< 10^{-4}$	$\epsilon_{B_c}(t_{bc}^-)$:	0	(4a)
$\epsilon_{B_b}(t_b^-)$:	$< 10^{-4}$	$\epsilon_{B_b}(t_b^-)$:	0	(4b)
$\epsilon_{B_c}(t_c^-)$:	~ 0	$\epsilon_{B_c}(t_c^-)$:	0	(4c)
$\epsilon_{M_t}(t^+)$:	$7.6 \cdot 10^{-2}$	$\epsilon_{M_t}(t^+)$:	$7.4 \cdot 10^{-3}$	(3a)
$\epsilon_{M_c}(t_{bc}^+)$:	$1.3 \cdot 10^{-3}$	$\epsilon_{M_c}(t_{bc}^+)$:	$7.4 \cdot 10^{-3}$	(3a)
$\epsilon_{M_b}(t_{bc}^+)$:	~ 0	$\epsilon_{M_b}(t_{bc}^+)$:	~ 0	(3b)
$\epsilon_{M_c}(t_c^+)$:	~ 0	$\epsilon_{M_c}(t_c^+)$:	~ 0	(3c)
$\epsilon_{M_t}(t_{tb}^-)$:	$7.4 \cdot 10^{-3}$	$\epsilon_{M_t}(t_{tb}^-)$:	$7.6 \cdot 10^{-3}$	(4a)
$\epsilon_{M_c}(t_{bc}^-)$:	~ 0	$\epsilon_{M_c}(t_{bc}^-)$:	$1.3 \cdot 10^{-3}$	(4a)
$\epsilon_{M_b}(t_b^-)$:	~ 0	$\epsilon_{M_b}(t_b^-)$:	~ 0	(4b)
		$\epsilon_{M_c}(t_c^-)$:	~ 0	(4c)

We have also evaluated the «asymmetry» ratio A° , using a different extrapolation for σ_b and σ_t , assuming

$$\sigma_b = \sigma_c/m_b^2 \quad \text{and} \quad \sigma_t = \sigma_c/m_t^2.$$

This leads to

$$\sigma_b = 30 \mu\text{b} \quad \text{and} \quad \sigma_t \simeq 1 \mu\text{b}$$

at $\sqrt{s} = 540$ GeV, with $\sigma_c = 750 \mu\text{b}$.

In these conditions we get

$$N(t^+) = L(2.53 \cdot 10^{-3} \mu\text{b}),$$

$$N(t^-) = L(6.50 \cdot 10^{-3} \mu\text{b}),$$

$$A^{\circ} = \frac{N(t^+) - N(t^-)}{N(t^+) + N(t^-)} = 0.59.$$

The «asymmetry» ratio A° does not depend on the cross-section extrapolations, because the detection efficiencies for leptons from beauty and charm are negligible in the phase-space region specified in point iii). However, the value

of the «top» production cross-section will be important for determining the integrated luminosity needed to reach a given statistical significance on the measurement of A^0 and for determining, as will be discussed in sect. 5, the rejection power of the apparatus needed to obtain a given signal-to-background ratio.

4. - Background evaluation.

In what has been described so far, the background contamination in the sample of prompt t^+ and t^- has not been considered. It is mainly due to

i) the misidentification of charged and neutral hadrons in the experimental apparatus,

ii) the prompt t^+ or t^- production from sources other than open heavy-flavour states.

An attempt was made to evaluate the contribution i). To derive the pion production in $(p\bar{p})$ interactions at $\sqrt{s} = 540$ GeV, we have used a parametrization of the single-pion cross-section measured at the ISR ⁽¹²⁾:

$$E(d^3\sigma/dp^3) = A \exp[-Bp_T] + C \frac{(1-x_T)^p}{(p_T^2 + F)^4},$$

where $x_T = 2p_T/\sqrt{s}$.

A further conservative hypothesis was made by including a p_T^{-4} term in the expression for $E(d^3\sigma/dp^3)$, for $p_T > 7$ GeV ⁽¹³⁾.

The extrapolated π rate, in the phase-space region defined in sect. 3 ($\theta < 30^\circ$, $p_T > 5$ GeV/c), should be multiplied by a reduction factor representing the achievable rejection of background source i) in the experimental apparatus.

As regard the prompt lepton background ii), we assume, as a first approximation, that it would be negligible when compared with the contribution i).

⁽¹²⁾ B. ALPER, H. BÖGGILD, P. BOOTH, F. BULOS, L. J. CARROLL, G. DAMGAARD, G. VON DARDEL, B. DUFF, K. H. HANSEN, F. HEYMANN, J. N. JACKSON, G. JARLSKOG, L. JÖNSSON, A. KLOVNING, L. LEISTAM, E. LILLETUN, E. LOHSE, G. LYNCH, G. MANNING, K. POTTER, M. PRENTICE, P. SHARP, S. SHARROCK, S. ØLGAARD-NIELSEN, D. QUARRIE and J. M. WEISS: *Nucl. Phys. B*, **100**, 237 (1975).

⁽¹³⁾ C. KOURKOUNELIS, L. K. RESVANIS, T. A. FILIPPAS, E. FOKITIS, A. M. CNOPS, S. IWATA, R. B. PALMER, D. C. RAHN, P. REHAK, I. STUMER, G. W. FABJAN, T. FIELDS, D. LISSAUER, I. MANNELLI, P. MOUZOURAKIS, A. NAPPI, W. J. WILLIS and M. GOLDBERG: *Phys. Lett. B*, **84**, 271 (1979).

5. - Estimate of the «asymmetry» ratio A^0 in experimental conditions.

In the presence of background, the experimental «asymmetry» ratio is given by

$$A^{exp} = \frac{[N(t^+) + N_{bg}(t^+)] - [N(t^-) + N_{bg}(t^-)]}{[N(t^+) + N_{bg}(t^+)] + [N(t^-) + N_{bg}(t^-)]}$$

Assuming $N_{bg}(t^+) = N_{bg}(t^-) = N_{bg}(t)$, and expressing $N(t^-)$ as

$$N(t^+)[(1 - A^0)/(1 + A^0)]$$

according to eq. (5), we have

$$(6) \quad A^{exp} = \frac{A^0}{1 + (1 + A^0)/[N(t^+)/N_{bg}(t)]}$$

The quantity A^{exp} is plotted in fig. 6 as a function of the signal-to-background ratio

$$S/B = N(t^+)/N_{bg}(t)$$

Notice that A^{exp} is substantially different from 0 as soon as S/B is greater than 1. However, from eq. (6) it is clear that in order to keep the value of A^{exp}

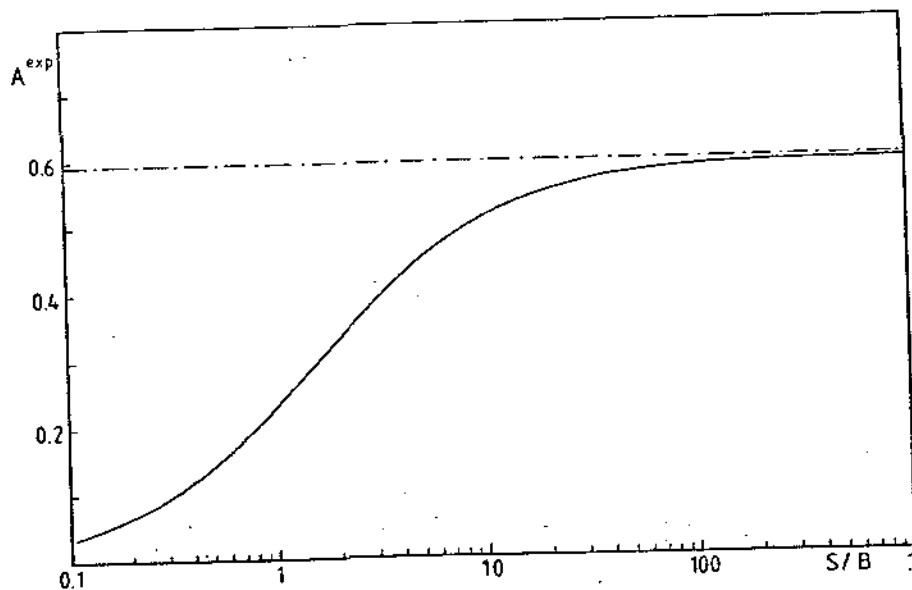


Fig. 6. - Behaviour of the experimental «asymmetry» A^{exp} , as a function of $S/B = N(t^+)/N_{bg}(t)$.

constant, *i.e.* independent of the « top » production cross-section σ_t , the rejection power of the apparatus must increase linearly with decreasing σ_t .

On the basis of the background estimate, computed as specified in sect. 4, and for the range of σ_t considered, we have

$$1 < S/B < 10$$

for a rejection against charged and neutral hadron background ranging from 10^{-3} to 10^{-4} .

6. — Conclusions.

The above studies show a new way to investigate the production of the « top » flavour at the (p \bar{p}) Collider. They are based on the measurement of an excess of t^+ on the proton side and of an excess of t^- on the antiproton side, both asymmetries being due to the semi-leptonic decays of the « top » baryon and the « antitop » antibaryon, each produced in a « leading » way.

The main parameters for the observation of this effect are the background level (estimated on the basis of our knowledge) and the cross-section values for the production of the leading baryons.

With the previously specified assumptions, and by assuming a luminosity between 10^{28} and 10^{29} cm $^{-2}$ s $^{-1}$, a few hundred hours of running would be sufficient for determining the value of A^{top} with a precision of a few percent, thus establishing clear evidence for (or against) the production of « leading » t -flavoured baryon (antibaryon) states.

● RIASSUNTO

Si presenta un nuovo metodo per studiare la produzione di particelle con « top » in interazioni (p \bar{p}) al Collider del CERN. Tale metodo si basa sul meccanismo di produzione « leading » esteso agli stati barionici e antibarionici dotati del piú pesante « flavour », e sull'asimmetria di carica dei leptoni originati dal loro decadimento semileptonico.

Поиск открытой « вершины » на (p \bar{p}) пучках в ЦЕРНе.

Резюме (*). — Предлагается новый метод наблюдения рождения барионных состояний на (p \bar{p}) пучках в ЦЕРНе. Этот метод основан на механизме рождения « лидирующей » частицы, обобщенном на наиболее тяжелые барионные и антибарионные состояния с ароматом, и на зарядовой асимметрии лептонов, образованных из их полуплептонных распадов.

(*). *Переведено редакцией.*

IV - CONCLUSIONS

IV. CONCLUSIONS

We summarize the main points which have been raised during the several formal and informal discussions (Open Committee meetings and direct interactions with Referees).

IV.1 - The cross-sections for Heavy Flavour production.

We have shown that using very simple assumptions, "dimensionality" and "scaling", it is possible to compute: "charm" cross-sections as predicted by "strangeness", and "beauty" cross-sections as predicted by "strangeness" and "charm". The experimental data support the validity of our simple assumptions (see figures on pages 33,34). On the other hand QCD has failed so far to account for the experimental results obtained in the field of Heavy Flavour production. For example, Table II in page 43 shows that three models are needed to account for the "charm" data. Each model can fit a set of data, but fails in some others.

It has been said that our simple hypotheses produce predictions that are one or two orders of magnitude above some QCD models. This is true, but irrelevant. In fact, the same QCD models fail to predict known facts, such as the "leading" effect. If QCD were like QED, it should be able to "predict" the "leading" effect: this is a phenomenon we have studied in all processes (Nuovo Cimento 66A, 129, 1981) and found to dominate particle production, no matter if the interaction is weak, electromagnetic or strong (Nuovo Cimento Letters 32, 321, 1981), provided there is a quark in the initial state, and no matter if the energy is low (ISR) or high (Collider). Our group has proved that the data on multiparticle production obtained at the CERN Collider show that the "leading" baryon effect does not decrease with energy (Nuovo Cimento Letters 38, 359, 1983, Nuovo Cimento Letters 41, 298, 1984 and figures on page 303).

As the problem of QCD cross-sections for Heavy Flavour production has been emphasized by some Committee's members, it is worth spelling out clearly what was the status of QCD theoretical predictions for charm production, at ISR energies, before the experimental results:

$$\left. \begin{array}{l} \text{String model} \quad : 10^{-10} \times \sigma_{\pi} \\ \text{Fermi-Hagedorn: } 10^{-5} \quad " \\ \text{QCD (fusion)} \quad : 10^{-4} \quad " \end{array} \right\} \text{Experimental results: } 10^{-2} \times \sigma_{\pi}$$

with $\sigma_{\pi} = 10^2$ mb. The other QCD models attempting to reproduce $10^{-2} \times \sigma_{\pi}$ came later.

The conclusion is therefore as follows:

- i) the cross-section values found were at least two orders of magnitude above the "theoretical" predictions of perturbative QCD;
- ii) the x-distribution for Λ_c^+ , i.e. the "leading" effect, was theoretically unpredicted.

For the benefit of those who have strong faith in QCD, it could be interesting to recall few more facts:

- a) it was impossible to predict large photoproduction cross-sections of heavy flavours by means of perturbative QCD;
- b) the p_T dependence of inelastic ($c\bar{c}$), for open and hidden states, could not be accounted for by QCD;
- c) the A-dependence could not be A^1 (perturbative QCD predicted A^1 .)

It should not be forgotten that photoproduction was considered a simpler case for QCD, compared to (pp). Therefore its predictions should have been in agreement with experimental findings, without any need of further complications to be introduced.

IV.2 - The ratio of "leading" versus total cross-sections.

The "leading" effect is a quark recombination phenomenon. In (e^+e^-) machines it shows up when the heavy flavour mass is near threshold (see figures on pages 343, 344, 345). On the other hand at the ISR energies, Λ_c^+ and Λ_b^0 production seems to be as leading as Λ_s^0 production (see figures on pages 45, 46, 47). These hints suggest that the "quark recombination" effect is present even for large values of the new flavour mass. In our simulation programs we have spanned the ratio Leading/Total (L/T) from 25% to as low as 5% and the results are shown in pages 67, 68.

IV.3 - Three-body versus more than three-body decays of the Heavy Flavours.

All experimental results known so far support the point that the semileptonic decay of a heavy flavour is dominated by a 3-body decay (see figure on page 41). This is perfectly consistent with the fact that the simple quark transition (up like \leftrightarrow down like) is the most physically plausible model. The hadron multiplicity which will accompany the decay-quark line is coming as a result of the "hadronization". The vertex is therefore a 3-body process (see diagram on page 40a). Nevertheless we have (at the request of a Referee) calculated what would happen if the 4-body decay would dominate (see work III-3, page 235). The asymmetry is still there. Its p_T dependence is less sharp (see figure on page 257). However it should not be forgotten that the 4-body decay of a heavy flavoured baryon is a physically unacceptable model.

IV.4 - Lepton-jet physics and UA1 hermeticity.

In our discussion with UA1 and with the Research Director (R. Klapish) we have pointed out that LAA provides UA1 with a far better hermeticity than at present (see figure on page 75). In addition the hermeticity provided by LAA is "magnetized" and

this is a very important element to reject low momentum particles. This rejection is needed in order to handle the new ACOL luminosity.

It has been said that, if it was for UA1 only, the hermeticity could be provided at far less expenses and furthermore that our LAA does not make the best use of the available space. We have worked for 5 months and produced 7 different versions of possible set-ups to be coupled with UA1, before reaching the final result. Drafting a few lines on a piece of paper cannot be compared with an accurate work by a group of dedicated physicists. We confirm that LAA, as it stands now, makes use of the available space around UA1 in the cheapest and physically most efficient way.

IV.5 - The phenomenology in addition to the Heavy Flavour Physics

The scientific interest of a proposal has two motivations.

One is based on theoretically sound predictions, the other on new phenomena to be discovered. The soundest theoretical predictions for the CERN Collider were the masses and the cross-sections for W^+ and Z^0 . Next follow the high q^2 QCD calculations for jet cross-section. The leading production mechanism for old and new Heavy Flavours is not theoretically predictable. The only possibility is to do experiments, using an experimental set-up as powerful as possible. In designing this new set-up, it is physically reasonable to use known facts (see the examples quoted above) and to make simple extrapolations. If these extrapolations can be checked at lower energies and with lighter Heavy Flavours (for example: s,c,b), this should add confidence in the domain of the unknown. One of us was student of the great Patrick Blackett. He was used to say that it is important to know what the theorists are thinking, but this should be a guide to design experiments where the theoretically expected phenomena are to be considered as the "background" for the unexpected. In our proposal the "background asymmetry" is a crucial QCD test. The ability to trigger with ACOL, and the high detection power for muons, in the forward angular range of the

proposed set-up, are essential ingredients for new physics to be searched for, apart from all physics arguments presented to justify the installation of a powerful muon detector in conjunction with UA1.

IV.6 - Note on past experience with Committees

Experimental set-ups should be justified in terms of their potential ability to discover new phenomena. If, in order to be approved by Committees, firm theoretical predictions were needed, we would reach the conclusion that only QED experiments should be approved.

QCD experiments should not be supported: in fact, QCD is far from being a well established theory. Asymptotic freedom is theoretically proved, but confinement is still to be demonstrated. To follow the line that, only well established theoretical predictions are worth being checked experimentally, means to stop the searches for Higgs, gluinos, photinos, gravitinos and all supersymmetric partners of the known particles. The experiments on the existence of the "excited vacuum" in Heavy Ions collisions should be stopped. There should be no support for neutrino oscillations, for $(B\bar{B})$ oscillations. The above is just to quote a few examples along the Committees logic. On the other hand, a well established theory is not worth being checked. The conclusion is: no support for experimental physics.

One of us, during the closed SPSC meeting (CERN - 19 March 1986), recalled some of his past experience with Committees. It is probably worth to put this on record.

1 - At Frascati, a fine energy scan with (e^+e^-) machines was considered to be physically unsound. Theoretical explanation: a new meson in the GeV mass range must have a width in the hundred MeV range. We wanted to be scheduled for a fine scan and to push the ADONE energy above the 3 GeV limit. If we were allowed to do this, the Ψ would have been discovered at ADONE.

2 - Our proposal to search for a new "heavy lepton" via the method of $(e\mu)$ acoplanar pairs was considered "science fiction". If we would have received the wanted support, the τ lepton

would have been discovered at Frascati.

3 - When the study of the $(p\bar{p})$ annihilation into lepton pairs, (e^+e^-) and $(\mu^+\mu^-)$, was completed, we proposed to investigate the inelastic production of lepton pairs in hadronic interactions. The proposal was not approved because we were told that we had already proved that the "elastic" channel was depressed by a factor 500 with respect to the "point-like" expectations. If allowed to go on, we would have discovered the J, here at CERN.

4 - Our proposal to build for ISR physics a "2 π magnet", in order to study 90° physics, was rejected because a great physicist, still alive, said: "There is no physics at 90 degrees".

5 - When SLAC discovered the DIS effect, we proposed to do the experiment at the CERN PS, using protons instead of leptons as primary incident particles. The proposal was supported by Sergio Fubini, but opposed by other theorists; one of them said "If the proton behaves like a lepton, I will resign from theoretical physics". We have demonstrated, 15 years later, that some basic features measured in DIS using leptons (electrons, muons, neutrinos) are identical to those obtained using protons (instead of leptons) as primary particles. In fact, the proton behaves as a lepton not at the 1% level, but at the 50% level. The lepton-like features of hadron physics is by far more important than could, most optimistically, be hoped (Nuovo Cimento 79A, 1, 1984). This lepton-like feature is based on the "leading" effect, which, as mentioned earlier, is present in all interactions involving at least a hadron (Nuovo Cimento 66A, 129, 1981 and Nuovo Cimento Letters 32, 321, 1981). As mentioned in the text (see work III.4, page 282), we have analysed the Collider data on multiplicity correlations (Nuovo Cimento Letters 38, 359 1983) and charged particle multiplicity distribution (Nuovo Cimento Letters 41, 298, 1984). This analysis shows that the "leading" proton effect is, at Collider energies, as strong as it is at ISR energies. On the other hand the "leading" Heavy Flavour production has been discovered at the ISR, but no data exist at the CERN Collider, and it is physically sound to assume that the "leading" effect for Heavy Flavours is also present at Collider energies.

In addition to the above "direct" experience, we could quote a few other facts. For example, the famous Fitch-Cronin experiment was not proposed as a check of CP violation, but as a check on the reported evidence for an "anomalous" regeneration in hydrogen. The "anomalous" regeneration was not there, but CP violation was. If the experiment would have been proposed as a check of CP, probably it would have been rejected. The Committee approved the proposal on the basis of a "wrong" result.

When the "two neutrinos" experiments started to be discussed, a famous theorist (still alive) said : "One neutrino is enough. Nature cannot be so stupid to need two neutrinos".

The recollection of these experiences with Committees could suggest that sometimes physicists should be allowed to follow their intuition, even if deprived from any theoretical support.